# POLYUNSATURATED FATTY ACIDS AND THEIR EPOXIDE METABOLITES IN NEURAL AGING

By

Morteza Sarparast

# A DISSERTATION

Submitted to
Michigan State University
in partial fulfillment of the requirements
for the degree of

Chemistry – Doctor of Philosophy

2023

#### **ABSTRACT**

In this dissertation, we explored the role of polyunsaturated fatty acid (PUFA) metabolites in neurodegeneration, Alzheimer's disease (AD), and aging, using *Caenorhabditis elegans* (*C. elegans*) as a model organism. Our investigation focused on the impact of cytochrome P450 (CYP) and epoxide hydrolase (EH) metabolic pathways on ferroptosis-mediated neurodegeneration, the relationship between oxylipins and AD pathology, and the influence of CYP-EH metabolites on lifespan, healthspan, and reproduction.

We discovered that dihomo gamma linolenic acid (DGLA), a specific  $\omega$ -6 PUFA, triggers ferroptosis-mediated neurodegeneration in dopaminergic neurons. This neurodegenerative effect occurs when DGLA is metabolized into dihydroxyeicosadienoic acid (DHED) via the action of CYP and EH enzymes. Our mechanistic study showed that it is the DHED metabolite that drives the neurodegenerative process, highlighting the critical role of CYP-EH-mediated PUFA metabolism in ferroptosis regulation. Consequently, this study identifies EH as a potential novel therapeutic target for addressing ferroptosis-related diseases and underscores the importance of understanding PUFA metabolism in the development of innovative treatment strategies.

We further uncovered an intricate relationship between oxylipins, A $\beta$ , and tau in neurodegeneration, demonstrating that A $\beta$  and/or tau expression in *C. elegans* disrupts the oxylipin profile. EH inhibition alleviated the ensuing neurodegeneration, likely through elevating the epoxy-to-hydroxy ratio of various CYP-EH metabolites. This study established a link between A $\beta$  and/or tau expression and CYP-EH metabolites, highlighting the potential therapeutic implications of epoxide hydrolase inhibition in AD.

Lastly, we investigated the impact of pharmacological inhibition and genetic knock out of EH on the lifespan, healthspan, and reproductive capabilities of *C. elegans* and analyzed the

corresponding alterations in oxylipin profiles. While the lifespan and reproduction remained unchanged in wild-type worms treated with the epoxide hydrolase inhibitor, AUDA, the genetic knockout of either *ceeh-1* or *ceeh-2* significantly shortened the lifespan and decreased egg production capacity. Although we identified significant changes in CYP-EH metabolites across experimental groups, the specific metabolites responsible for these effects remain elusive, mainly due to experimental challenges in testing a large number of compounds with possible synergistic effects during aging. Conventional techniques, such as agar plates, are limited by the difficulties in manual phenotypic and lifespan analyses, as well as in maintaining age-synchronized worms due to time-consuming progeny elimination processes. We discussed potential solutions, including high-throughput assays and microfluidic devices, to study the effect of numerous compounds on aging. However, we recognized that current techniques, like the use of 5-fluoro-2-deoxyuridine (FUDR) and PDMS-based microfluidic systems, present limitations that could interfere with the study of CYP-EH metabolites.

Overall, this dissertation sheds light on the complex relationship between dietary PUFAs, their metabolites, and neurodegenerative diseases. It highlights the potential therapeutic value of targeting specific CYP-EH metabolites and sets the stage for future research in understanding their role in aging and neurodegeneration using the *C. elegans* model.

Copyright by MORTEZA SARPARAST 2023 NULLIUS IN VERBA

#### ACKNOWLEDGMENTS

I am deeply grateful to my loving mother (Reyhan) and father (Kioumars), for their unwavering love, encouragement, and support throughout this journey. Your sacrifices have been invaluable in helping me achieve my goals.

I would also like to extend my heartfelt thanks to Dr. Sing Lee and Dr. Jamie Alan for kindly accepting me into their lab, putting a lot of effort into my transition to a new field of research, engaging in daily conversations with me, and teaching me valuable lessons beyond science. I appreciate Dr. Babak Borhan for his support and assistance not only in my research but also in addressing the challenges I faced during my time at MSU. Additionally, I am grateful to Dr. Heedeok for his support and guidance as a member of my committee.

I would like to thank my current and previous lambastes: Devon, Derek, Elham, Jennifer, Tommy, Chris, Sara, Leslie, and Christin. Your camaraderie and collaboration have made my time in the lab enjoyable and enriching. A special thanks to Heather for her invaluable assistance.

I want to extend my deepest gratitude to my friends who have been pillars of support and companionship in this journey. Foremost, I would like to especially thank Mohammad (Saied) and Mona for their resolute support and encouragement. Other cherished individuals include Farzam, Fatemeh (Mola), Mk, Mahmood (MJC), Aria, Fali, Ali Nik, Akbar, Reza, Hadi, and many others. The camaraderie and encouragement I received from you all have been instrumental in making this journey possible, and I am eternally grateful for your presence in my life.

Finally, I cannot forget to express my gratitude to my cat, Snickers, who has been a valuable and cherished companion throughout this journey. Snickers' unwavering affection and presence have provided me with emotional support, and the moments we shared brought joy and comfort during challenging times. Thank you, Snickers, for being there for me.

# TABLE OF CONTENTS

LIST OF ABBREVIATIONS	. viii
Chapter 1. CYTOCHROME P450 METABOLISM OF POLYUNSATURATED FATTY ACIDS AND NEURODEGENERATION	1
BIBLIOGRAPHY	
Chapter 2. DIHYDROXY-METABOLITES OF DIHOMO-GAMMA-LINOLENIC ACID DRIVE FERROPTOSIS-MEDIATED NEURODEGENERATION	87
BIBLIOGRAPHY	110
Chapter 3. EXPLORING THE ROLE OF CYP-EH METABOLITES IN AB AND TAU-INDUCED NEURODEGENERATION: INSIGHTS FROM CAENORHABDITIS ELEGANS	120
BIBLIOGRAPHY	147
<b>Chapter 4.</b> PHARMACOLOGICAL INHIBITION VS GENETIC KNOCKOUT OF EPOXIDE HYDROLASE; A FUTURE DIRECTION IN STUDYING AGING AND PUFA	
METABOLITES RELATION	
BIBLIOGRAPHY	200
APPENDIX 1: SUPPORTING INFORMATION FOR CHAPTER 2	218
APPENDIX 2: SUPPORTING INFORMATION FOR CHAPTER 3	288
APPENDIX 3: SUPPORTING INFORMATION FOR CHAPTER 4	317

# LIST OF ABBREVIATIONS

17,18-Epoxyeicosatetraenoic acid
14,15-Epoxyeicosatetraenoic acid
11,12-Epoxyeicosatetraenoic acid
8,9-Epoxyeicosatetraenoic acid
5,6-Epoxyeicosatetraenoic acid
17,18-Dihydroxyeicosatetraenoic acid
14,15-Dihydroxyeicosatetraenoic acid
11,12-Dihydroxyeicosatetraenoic acid
8,9-Dihydroxyeicosatetraenoic acid
5,6-Dihydroxyeicosatetraenoic acid
12,13-Epoxyoctadecamonoenoic acid
9,10-Epoxyoctadecamonoenoic acid
12,13-Dihydroxyoctadecamonoenoic acid
9,10-Dihydroxyoctadecamonoenoic acid
14,15-Epoxyeicosatrienoic acid
11,12-Epoxyeicosatrienoic acid
8,9-Epoxyeicosatrienoic acid
5,6-Epoxyeicosatrienoic acid
14,15-Dihydroxyeicosatrienoic acid
11,12-Dihydroxyeicosatrienoic acid
8,9-Dihydroxyeicosatrienoic acid
5,6-Dihydroxyeicosatrienoic acid

14.15 EED	14.15 Europeiron dinaria arid
14,15-EED	14,15-Epoxyeicosadienoic acid
11,12-EED	11,12-Epoxyeicosadienoic acid
8,9-EED	8,9-Epoxyeicosadienoic acid
14,15-DHED	14,15-Dihydroxyeicosadienoic acid
11,12-DHED	11,12-Dihydroxyeicosadienoic acid
8,9-DHED	8,9-Dihydroxyeicosadienoic acid
15,16-EpODE	15,16-Epoxyoctadecadienoic acid
12,13-EpODE	12,13-Epoxyoctadecadienoic acid
9,10-EpODE	9,10-Epoxyoctadecadienoic acid
15,16-DiHODE	15,16-Dihydroxyoctadecadienoic acid
12,13-DiHODE	12,13-Dihydroxyoctadecadienoic acid
9,10-DiHODE	9,10-Dihydroxyoctadecadienoic acid
13-HODE	13-Hydroxyoctadecadienoic acid
9-HODE	9-Hydroxyoctadecadienoic acid
20-НЕТЕ	20-Hydroxyeicosatetraenoic acid
19-НЕТЕ	19-Hydroxyeicosatetraenoic acid
15-HETE	15-Hydroxyeicosatetraenoic acid
12-НЕТЕ	12-Hydroxyeicosatetraenoic acid
9-HETE	9-Hydroxyeicosatetraenoic acid
8-НЕТЕ	8-Hydroxyeicosatetraenoic acid
5-HETE	5-Hydroxyeicosatetraenoic acid
15(S)-HETE	15(S)-Hydroxyeicosatetraenoic acid
20-НЕРЕ	20-Hydroxyeicosapentaenoic acid

18-HEPE 18-Hydroxyeicosapentaenoic acid

15-HEPE 15-Hydroxyeicosapentaenoic acid

12-HEPE 12-Hydroxyeicosapentaenoic acid

8-HEPE 8-Hydroxyeicosapentaenoic acid

5-HEPE 5-Hydroxyeicosapentaenoic acid

5-HT 5-Hydroxytryptamine (Serotonin)

LA Linoleic Acid

DGLA Dihomo-gamma-linolenic Acid

AA Arachidonic Acid

α-LA Alpha-Linolenic Acid

EPA Eicosapentaenoic Acid

DGA Docosahexaenoic Acid

CYP Cytochrome P450 Enzyme

EH Epoxide Hydrolase Enzyme

C. elegans Caenorhabditis elegans

CEEH Caenorhabditis elegans Epoxide Hydrolase

Aβ Amyloid Beta

 $\quad \omega \qquad \qquad Omega$ 

HPLC high-performance liquid chromatography

# **Chapter 1.** CYTOCHROME P450 METABOLISM OF POLYUNSATURATED FATTY ACIDS AND NEURODEGENERATION

#### **ABSTRACT**

Due to the aging population in the world, neurodegenerative diseases have become a serious public health issue that greatly impacts patients' quality of life and adds a huge economic burden. Even after decades of research, there is no effective curative treatment for neurodegenerative diseases. Polyunsaturated fatty acids (PUFAs) have become an emerging dietary medical intervention for health maintenance and treatment of diseases including neurodegenerative diseases. Recent research demonstrated that the oxidized metabolites, particularly the cytochrome P450 (CYP) metabolites, of PUFAs are beneficial to several neurodegenerative diseases including Alzheimer disease and Parkinson's disease, however, the mechanism(s) remains unclear. The endogenous levels of CYP metabolites are greatly affected by our diet, endogenous synthesis, and the downstream metabolism. While the activity of omega-3 (ω-3) CYP PUFA metabolites and omega-6 (ω-6) CYP PUFA metabolites largely overlapped, the ω-3 CYP PUFA metabolites are more active in general. In this review, we will briefly summarize recent findings regarding the biosynthesis and metabolism of CYP PUFA metabolites. We will also discuss the potential mechanism(s) of CYP PUFA metabolites on neurodegeneration, which will ultimately improve our understanding of how PUFAs affect neurodegeneration and may identify potential drug targets for neurodegenerative diseases.

# 1. Introduction

Neurodegenerative diseases (NDs) are affected by both genetic and environmental factors suggesting that there are likely multiple etiologies for these diseases <sup>1,2</sup>. In addition, the prevalence of NDs correlates well with age<sup>3</sup>. According to the United Nations, the population over the age of 65 is expected to increase from approximately 9% (2019) to roughly 20% by 2050. With this demographic change, a coinciding increased incidence of age-related NDs is expected in the near future <sup>4</sup>. Despite decades of effort, no curative treatment has been developed for these diseases, and almost all medication interventions are aimed at reducing the symptoms. Perhaps the primary reason for the lack of treatments for ND is that no consistent underlying mechanism(s) for ND pathologies has been identified. Human genetic studies revealed several genes responsible for NDs, such as Apolipoprotein E (APOE), which has been extensively reviewed and is not the focus of this review <sup>4,5</sup>. On the other hand, numerous studies revealed that environmental factors or a complex interaction between environmental and genetic factors result in slow and sustained dysfunctions in the nervous system during aging and could be major causes for NDs. Among the environmental factors, exposure to pesticides and trace metals, head injuries, lifestyle and diet, are deemed to be most significant factors contributing to NDs <sup>6</sup>. Interestingly, one pathway that appears to be influential in the aging process, but remains to be fully explored, is the metabolism of PUFAs. In this review paper, we focus primarily on dietary factors, specifically, the relationship between cytochrome P450 (CYP) metabolism of polyunsaturated fatty acids (PUFAs) and age-associated NDs <sup>1,2</sup>.

In mammals,  $\omega$ -3 PUFAs cannot be synthesized endogenously; therefore, they must be obtained from dietary sources <sup>7</sup>. PUFAs are suspected to play significant roles in neural function,

due to their abundance in neural tissues. Arachidonic acid (AA) and docosahexaenoic acid (DHA) are the two most abundant PUFAs within the nervous system, and together comprise roughly 35% of the lipid content in brain tissue  $^8$ . It has been demonstrated that dietary PUFA intake can be beneficial for neurodevelopment and attenuating neurodegeneration  $^9$ . The cohort Rotterdam study, which assessed a cohort on 5,289 subjects aged 55 and older, showed an association between PUFA intake and reduced incidence of PD  $^{10}$ . In rodents fed a diet deficient in  $\omega$ -3 PUFAs, dramatic decreases in brain PUFA content was observed, which was also accompanied with a decrease in the number of dopaminergic neurons in the substantia nigra  $^{11}$ . Manipulating the PUFA composition of the cell membrane has been demonstrated to change the function and/or signaling of a variety of receptors including cholinergic, dopaminergic, and GABAergic receptors  $^{12}$ , while the detailed mechanism remains largely unknown. The endogenous level of PUFAs greatly affected the composition of their downstream metabolites *in vivo*. Therefore, it has been suggested that the downstream metabolites may be responsible for the action of  $\omega$ -3 and  $\omega$ -6 PUFAs in neurons.

PUFAs are metabolized by three main oxidative pathways which include (i) lipoxygenase (LOX), (ii) cyclooxygenase (COX), and (iii) cytochrome P450 (CYP) pathways to produce different oxidized lipid mediators called oxylipins <sup>13</sup>. Generally, ω-6 PUFA oxylipins tend to be proinflammatory while ω-3 PUFA oxylipins are considered anti-inflammatory and pro-resolving. Oxylipins are regulators in physiological processes in various tissues including neuron <sup>13</sup>. AA oxylipins such as lipoxin A4, as well as prostaglandin D2 and E2, have shown neuroprotective properties <sup>13</sup>. The pro-resolving mediators derived from DHA such as protectin D1, as well as resolvin D1 and D2 seem to inhibit age-related memory decline and protect the brain from cell injury and death <sup>13,14</sup>. Furthermore, the oxylipins generated by COX and LOX, such as

prostaglandin and leukotrienes, respectively, tend to be pro-inflammatory and exert excitatory effects on neurons. On the other hand, Ep-PUFAs oxylipins generated by CYP enzymes seem to produce the opposite effects, and have neuroprotective, anti-hypertensive, and analgesic effects  $^{13,15,16}$ . The activity of  $\omega$ -3 Ep-PUFA and  $\omega$ -6 Ep-PUFA are largely overlapped and the  $\omega$ -3 Ep-PUFA are generally more active than  $\omega$ -6 Ep-PUFA. The beneficial properties of Ep-PUFAs appear to be when Ep-PUFAs are converted to their corresponding diols by soluble epoxy hydrolase (sEH) $^{17}$ , which will be discussed later in this review. As more research has accumulated, CYP metabolites of PUFAs have been suggested to be a key class of Ep-PUFAs that affect neurodegeneration. Inhibition of sEH, the enzyme largely responsible for the degradation of CYP PUFA metabolites, has been shown to be beneficial in Alzheimer disease and Parkinson's disease

Additionally, there is evidence that inhibition or genetic knock-out of sEH can protect the dopaminergic neurons in the mouse brain against neurotoxins  $^{19}$ . Even though there is controversy in randomized clinical trials regarding the effects of  $\omega$ -3 PUFAs in AD, most of observational studies have shown the beneficial effects of  $\omega$ -3 intake on reducing the incidence of AD  $^{9,13,18}$ . Additionally, the oxylipin profiles of blood serum in AD subjects shows around 20% higher levels of dihydroxyeicosatrienoic acid (which is the product of the sEH metabolism of the epoxymetabolite of AA) compared to the elderly individuals that were cognitively healthy  $^{20}$ . Therefore, sEH is an important enzyme in PUFA metabolism and a lucrative drug target  $^{21}$ . However, the mechanism of action of the CYP PUFA metabolites remains largely unknown. The endogenous level of CYP PUFA metabolites is not only affected by their metabolism but is also greatly affected by the endogenous level of their PUFA precursors as well as their uptake by diet  $^{22,23}$ . Therefore, in this review, we will 1) describe the biosynthesis and metabolism of PUFAs and downstream

CYP metabolites and the role of biosynthesis and metabolism of PUFAs in neurodegeneration; 2) highlight the key CYP and EH enzymes present in CNS; and 3) elaborate on potential mechanism(s) of action of CYP PUFA metabolites in neuroinflammation and corresponding neurodegeneration.

# 2. Neurodegeneration: a brief overview

Neurons have an incredibly high respiratory rate due to the presence of highly active processes such as vesicle trafficking, neurotransmitter synthesis, protein synthesis, molecular/ion transport, etc., and thus generate a great deal of oxidative stress<sup>1,24</sup>. This further necessitates a high demand of energy for the maintenance of redox homeostasis and organelle and protein quality control <sup>1,24</sup>. Chronic and excessive perturbations in these metabolic pathways can cause neurodegeneration. Figure 1 displays common neuronal pathways that are disturbed in neurodegenerative diseases <sup>1,25</sup>. These pathways are mostly interdependent. For instance, chronic neuroinflammation can lead to protein accumulation, ER stress, mitochondria dysfunction, uncontrolled oxidative stress, axonal transport impairment, and apoptosis, which are detrimental to neurons, leading to NDs <sup>26,27</sup>. The major ND pathologies include, but are not limited to protein misfolding, synaptic dystrophy, changes in neurotransmitter production, an increased oxidative stress response, and neuron loss <sup>2,28–30</sup>. In addition, reduction in brain volume is often observed (in both grey and white matter), along with increased lesions in white matter and dysfunction of the blood–brain barrier (BBB) <sup>28</sup>. While the mechanisms that are involved in the pathology of NDs are pertinent to this review, the details are not included here, as they has been extensively discussed in other reviews <sup>1,24,25</sup>. Our focus here is to review and discuss how CYP metabolism of PUFAs is potentially involved in neurodegeneration.

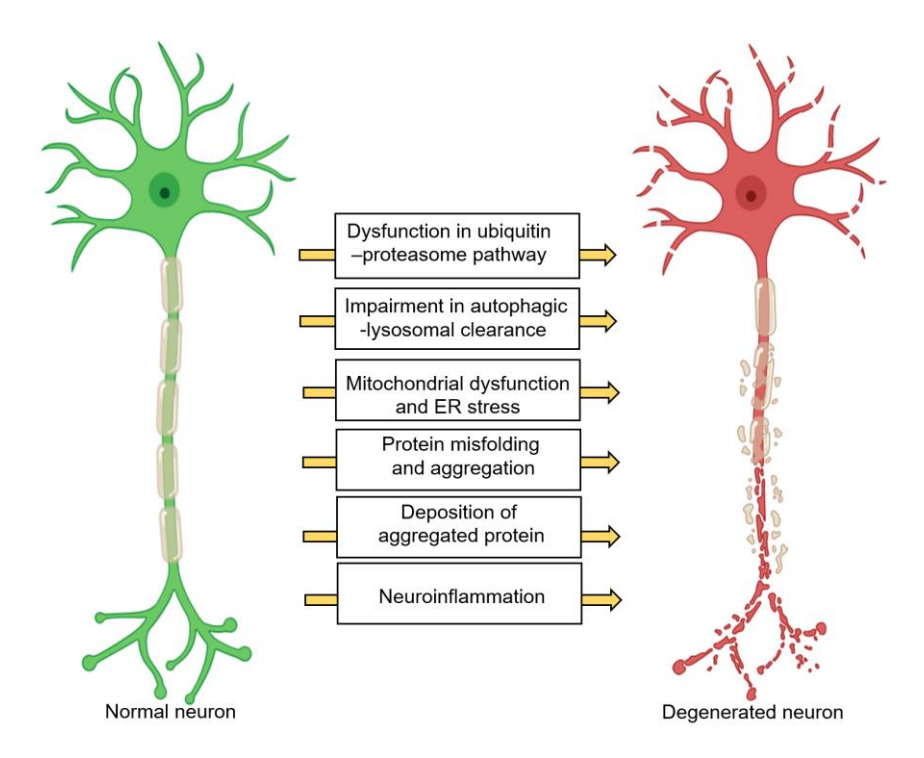


**Figure 1.** Common neuronal pathways that are changed in different neurodegenerative diseases (1) Dysfunction in the ubiquitin—proteasome pathway increases the intracellular misfolded, damaged, or unneeded protein. (2) Dysfunction in the autophagy—lysosomal pathway triggers the accumulation of pathogenic protein aggregates and damaged mitochondria. (3) Mitochondria dysfunction causes dysfunction and uncontrolled release of reactive oxygen species. (4) ER stress occurs when the homeostatic protein folding and trafficking in the cell is overwhelmed or unbalanced, leading to UPR. (5) Transcellular propagation and seeding of protein aggregates cause disease progression. (6) The aggregation of misfolded proteins contributes to toxicity. (7) A chronic neuroinflammatory state can lead to protein accumulation, ER stress, mitochondria dysfunction, uncontrolled oxidative stress, and axonal transport impairment. Abbreviations- ER: endoplasmic reticulum, UPR: unfolded protein response.

#### 3. Overview of PUFAs

Polyunsaturated fatty acids (PUFAs) are long-chain fatty acids comprising of at least two carbon-carbon double bonds that play crucial roles in a variety of physiological processes. The endogenous level of w-3 and  $\omega$  -6 PUFAs significantly modulates the *in vivo* level of their downstream metabolites, particularly the CYP PUFA metabolites <sup>31,32</sup>. In mammals, small quantities of PUFAs can be synthesized endogenously, and the rest are obtained from diet. An overview of these two factors influencing the biological level of PUFAs, and thus their downstream metabolism is presented in this section.

#### 3.1. Biosynthesis of PUFAs and neurodegenerative diseases

The major steps in PUFA biosynthesis in organisms are: (i) elongation, by elongase enzymes; and (ii) desaturation by desaturase enzymes  $^{7,33}$ . Some metazoans, such as *Caenorhabditis elegans*, are capable of endogenous production of  $\omega$ -6 and  $\omega$ -3 PUFAs through the conversion of  $\omega$ -9 monounsaturated oleic acid (OA) to  $\omega$ -6 linoleic acid (LA) via a  $\Delta$ 12 desaturase, and then further conversion of  $\omega$ -6 PUFAs to  $\omega$ -3 PUFAs via  $\Delta$ 15 ( $\omega$ -3) desaturase  $^{34}$ . These animals do not require dietary sources of PUFAs. Vertebrates however do not have genes encoding functional  $\Delta$ 12 and  $\omega$ -3 desaturase enzymes, and thus cannot endogenously synthesize PUFAs from OA  $^{35}$ . Despite this, vertebrates do have the ability to use LA and  $\square$ -linoleic acid (ALA), which must be obtained from the diet, as precursors for the biosynthesis of the other  $\omega$ -6 and  $\omega$ -3 PUFAs, respectively, through desaturation and elongation  $^{7,33}$ . The conventional enzymatic pathway that produces these PUFAs is depicted in (Figure 2A).

Although humans only synthesize a small amount of PUFAs, recent studies revived that fatty acid desaturases (FADS) in humans play an important role in modulating endogenous levels of different PUFAs. A genome-wide genotyping study conducted by Ameur *et al.* revealed two common haplotypes of the *fads* gene: (i) haplotype D that can drive more active conversion in PUFAs, and (ii) the less active haplotype A  $^{36}$ . People homozygous for the D type have higher levels of ARA (43%) and DHA (24 %) as well as greater plasma lipid levels compared to those who are homozygous for haplotype A  $^{36}$ . Several studies have shown the association between breastfeeding and child brain development, as a *fads* gene variant can control the PUFA composition of breast milk  $^{37-40}$ . Furthermore, from rare human studies, a very low level of  $\Delta 6$  desaturase was found in patients with Sjögren-Larsson syndrome, which is characterized by neurological, skin, and eye problems  $^{41}$ . A single-nucleotide polymorphism (SNP) in FADS2 was also discovered to be associated with the

occurrence of attention-deficit/hyperactivity disorder (ADHD), mostly hypothesized to result from abnormal regulation of dopamine at the neural synapse 42. Most of these rare studies can be considered as preliminary data, and replication in a larger population, and consideration of other PUFA metabolic genes such as ELO is required. In addition to human studies, mouse models with genetic defects in FADS1 and FADS2 have been conducted <sup>43,44</sup>. The fads1 knockout mice failed to thrive and died before reaching 12 weeks of age. These mice also exhibited perturbed immune cell homeostasis and severe inflammatory problems. Dietary supplementation with AA prolonged the lifespan of these mice to levels comparable to wild-type mice <sup>43</sup>. Surprisingly, deletion of the fads2 gene in mice did not show significant impairment in their lifespan and viability, but rather only resulted in male and female sterility and increased bleeding time 44. Brown and colleagues selectively knocked down fads1 in adult hyperlipidemic mice to determine the key role of endogenous biosynthesis of AA and Eicosapentaenoic acid (EPA) in inflammatory disease progression and liver X receptor signaling <sup>45</sup>. Thus, variability in gene expression may be one of the key factors impacting PUFA downstream metabolism by controlling the fads gene. Considering this idea, researchers studying the effects of PUFA supplementation should consider genetic effects in the specific population under study, which might be the reason for inconsistency in the clinical and epidemiology studies that have been done so far regarding PUFA effects on human health and disease.

# 3.2. Dietary PUFA

Although humans have both desaturase and elongase enzymes, the conversion/biosynthesis of PUFAs is quite limited in humans. Because of this, PUFA blood and tissue levels are modulated by dietary intakes  $^{7,46}$ . Hence, there is great interest surrounding the potential benefits of supplementation, and  $\omega$ -3 PUFAs are one of the most consumed dietary supplements  $^7$ . The main sources of fatty acids are different among countries, and mainly controlled by food availability,

economy, and culture [7,39]. ω-3 PUFAs mostly originate from specific plant (or modified plant),

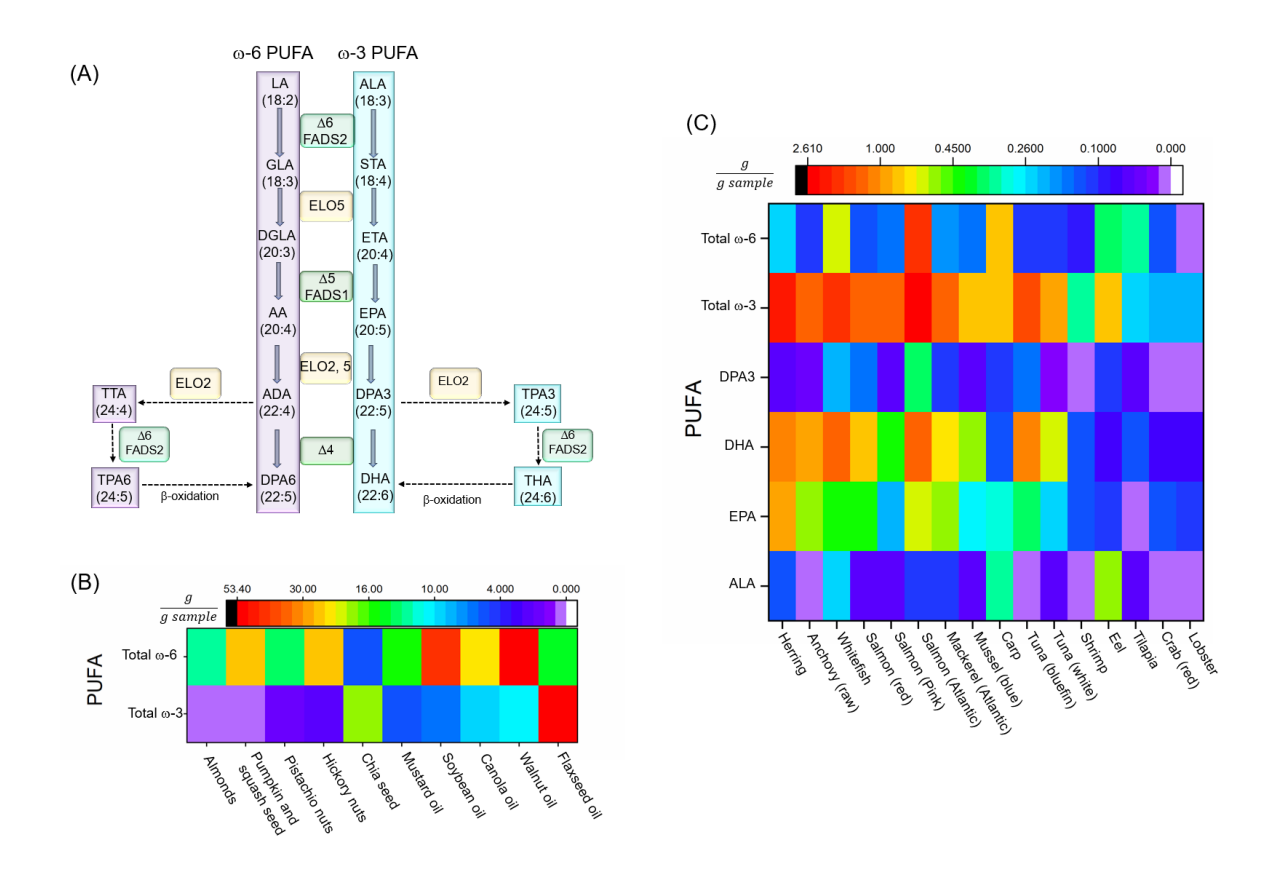


**Figure 2.** (A) PUFA biosysnthesis pathways. (B) Common vegtable oil or seeds. The total ω-PUFA content is almost exclusively ALA, with little to no EPA, DHA, and DPA3 [47]. (C) PUFA amounts in different fish and seefood (all are cooked or baked unless otherwise mentioned) [47]. LA:Linolec acid, GLA:Gamma-linolenic acid, DGLA:Dihomo gamma-linolenic acid, AA:Arachidonic acid, AD: drenic acid, TTA:Tetracosatetraenoic acid, TPA6:Tetracosapentenoic acid (ω-6), DPA6:Docosapentaenoic acid(ω-6), ALA:a-Linoic Acid, STA:Stearidonic acid, ETA:Eicosatrienoic acid, EPA:Eicosapentaenoic acid, DPA3:Docosapentaenoic acid (ω-3), TPA3: Tetracosapentenoic acid (ω-3), THA:Tetracosahexaenoic acid, DHA Docosahexaenoic acid D:Desaturase, ELO: Elongase, FADS 1:Fatty Acid Desaturase 2, FADS2:Fatty Acid Desaturase 2.

algal, marine, and single-cell sources. While plants such as nuts some seeds, and vegetable oil are the primary source of ALA (Figure 2B), marines are the main source of EPA, DHA, and docosapentaenoic acid ( $\omega$ -3) (DPA3) (Figure 2C) <sup>47</sup>. Dietary supplementation studies show a controversy in randomized clinical trials regarding the effects of PUFAs on neurodegeneration which can be due to the genetic variability, different lifestyle and habits in population under study, as well as presence of additive prescribed by these PUFA supplementation <sup>46</sup>. Also, these studies

in humans demonstrate a causal relationship between the dietary lipid ratio supplementation of  $\omega$ -3 and  $\omega$ -6 PUFAs and NDs such as AD and PD which is beyond the scope of this review<sup>6,10,46,48,49</sup>.

# 4. CYP: a key monooxygenase enzyme in PUFAs metabolism

PUFAs are mainly metabolized through three oxidative pathways: (i) lipoxygenases (LOX), (ii) cyclooxygenases (COX), and (iii) cytochrome P450 (CYP) pathways (Figure 3A) to produce many lipids signaling molecules called oxylipins <sup>50–52</sup>. Most of these mono-oxygenated lipid metabolites are key lipid mediators in physiological processes in mammals. Research on the lipoxygenase and cyclooxygenase pathways and neurodegeneration has been extensively reviewed <sup>52,53</sup>; thus, are not the focus of this review. In this section, we will summarize the recent findings on a CYP pathway of PUFAs and the effects of CYP selectivity on mammalian physiology.

#### 4.1 Characteristics of CYP

CYP are heme-thiolate proteins primarily involved in syntheses and metabolisms of many xenobiotic and endogenous biological molecules such as steroid hormones, fatty acids, cholesterol, drugs, vitamin D, etc. via oxidation <sup>54</sup>. CYPs in general contain a signature residue sequence of FXXGXbXXCXG, in which Xb is a basic residue and the cysteine is located at the axial position to the heme, and a Soret peak at 450 nm when a carbon monoxide binds to the Fe(II) of the heme group <sup>55,56</sup>. Note that there are some other proteins with the same heme group, axial cysteine residue, similar Soret peak in presence of CO, as well as some related catalytic properties such as some peroxidases and nitric oxide synthases, but they are not considered CYP enzymes. The 3D structures of these proteins also differentiate them from CYP enzymes, which share the same folding <sup>57,58</sup>.

The human genome project has identified 57 genes expressing different CYP enzymes, which are grouped into 18 families (43 sub-families) based on the amino acid sequence homology <sup>59,60</sup>. Thus, each CYP enzyme is named by a number representing the family and a letter indicating the subfamily, followed by a second number specific for an individual CYP enzyme (e.g., CYP2J2). In contrast to prokaryotes that have soluble CYP enzymes, in mammals CYPs are primarily membrane-associated proteins located either on endoplasmic reticulum (ER) or mitochondria membranes <sup>61,62</sup>. The catalytic domain of these enzymes is partially immersed in the membrane and can move along the membrane surface. The active site connection to both the cytosolic environment and the membrane through networks of access channels allows them to interact with substrates in either compartment <sup>62</sup>. Of the 57 human CYP enzymes, 50 are located on the ER and are usually involved in xenobiotic metabolism (i.e., drugs and environmental pollutants), while the rest are located in the mitochondria membrane and are generally engaged in the metabolism/biosynthesis of endogenous molecules <sup>63</sup>. Even though these enzymes are mostly expressed in the liver, they can be also expressed in many other tissues including, but not limited to, the kidney, brain, intestinal mucosa, skin, and lung <sup>64</sup>.

# 4.2 Catalytic function and mechanism of CYP

Historically, the first CYP enzyme was described by Klingenberg and Garfinkel as an unknown pigment that binds carbon monoxide in its reduced form and produces a Soret absorption peak at 450 nm <sup>65,66</sup>. This unknown pigment was then identified as a new cytochrome by Omura *et al.* <sup>55</sup>. About ten years later, in 1979, Benhamou and colleagues further confirmed this observation by studying the inhibitory effect of AA administration on metabolizing the hepatic drug by CYP enzymes in mice <sup>67</sup>.

CYPs catalyze a large variety of reactions including oxidation of heteroatoms, heteroatom dealkylation, C–C bond cleavage, desaturation, ring formation, aryl ring couplings, and rearrangements of oxygenated molecules <sup>68–70</sup>. The monooxygenase activity of CYPs has been discussed thoroughly elsewhere <sup>71–73</sup>, and therefore we will only provide a brief description here. Figure 3B shows the monooxygenase mechanism of CYPs, related to its epoxygenase activity, in 7 steps: 1) Before binding of the substrate to the CYP protein, there is an equilibrium between the hexa- and pentacoordinate Fe(III); substrate binding to the CYP enzymes shifts the equilibrium in favor of pentacoordinate; 2) an electron will transfer to this complex either directly from NADPH or through a redox protein partner, to reduce Fe (III) to Fe (II). Note that this step is critical for substrate oxidation, as the diatom oxygen cannot bind to Fe (III); 3) oxygen binds to the Fe(II); 4) the next electron is either transferred directly from NAD(P)H or through a redox protein partner; 5) two subsequent protonations occur; 6) the complex gets deprotonated by releasing a water molecule, which results in an iron-oxo complex; 7) finally, the oxygen atom is transferred to the substrate and results in an oxidized products <sup>71–73</sup>.

#### 4.3 Major CYP responsible for PUFA metabolism

CYPs can metabolize PUFAs to produce either Ep-PUFAs (epoxygenase activity) or hydroxy-PUFAs (with hydroxylase activity). The final product depends on the specific CYP enzyme as well as the type of PUFA substrate. In general, the regio/stereo selectivity, catalytic properties, and structure of each CYP enzyme might be significantly determined by a B-C loop in their structure, controlling the type of reaction and prevalence of a specific regio/stereoisomer product <sup>56,74,75</sup>.

In this section we discuss the major CYPs and their products when  $\omega$ -3 and  $\omega$ -6 PUFAs are substrates.

#### 4.3.1 Regio- and stereo- selective epoxidation by major CYPs

In the case of AA, the main CYPs that generate Ep-PUFAs are CYP2B, 2C, and 2J subfamilies (known as AA epoxygenase), while 1A, 4A, and 4F subfamilies produce the majority of ω and ω-1 hydroxylated AA (known as AA hydroxylase) (Figure 3A) <sup>76</sup>. Both CYPs families are regio- and stereo-selective 77,78. For instance, CYP2C and 2J subfamilies can convert AA into four regioisomers of epoxyeicosatrienoic acids (EETs) depending on which double bond is involved in oxygen insertion, which results in 5,6-EET, 8,9-EET, 11,12-EET, and 14,15-EET. Each of the EET products can be either the R,S- or the S,R stereoisomer <sup>77,78</sup>. This regio- and the stereoselectivity of EETs is CYP isoform-specific. For instance, while CYP2C8 in humans can metabolize AA with high regio/stereo selectivity to 14,15- and 11,12-EET (with ratio of 1.3:1 and more than 80% optical purity (OP) of R,S enantiomers), CYP2C9 shows very low regio- and stereoselectivity <sup>79,80</sup>. CYP2J2 is not regioselective as it produces all four regioisomers of EETs in which 8,9- and 11,12-EET are largely a racemic mixture, and 14,15 -EET is mainly in the form of 14(R), 15(S)-EET (OP $\approx$ 76%)<sup>81</sup>. CYP2C23, which is the main CYP involving in AA epoxidation in the rat kidney, generates 8,9-, 11,12- and 14,15-EET in a ratio of 1:2:0.7 with high stereoselectivity (OP  $\approx$  95, 85 and 75%, respectively) 82. Likewise, CYP2C44 in mice results in the same products <sup>83</sup>. Figure 3C displays the regioselectivity of different CYPs and the relative amount of each regioisomer.

Even though the CYPs subfamilies involving in LA metabolism have not yet been meticulously examined, the available studies propose that all CYP isoforms can metabolize LA, with high efficiency. For instance, CYP2C9 is known as the main LA epoxygenase in the human liver and generates both 9,10- and 12,13-epoxyoctadecamonoenic acids (EpOMEs) <sup>84</sup>. Other AA metabolizing CYP isoforms that can also accept LA as a substrate are CYP2C8 and -19; CYP2J2,

-3, -5, and -9; CYP1A2; and CYP3A4 <sup>85–87</sup>. It is worth mentioning that the same CYP isoform can have different preferential to whether act as epoxygenase or hydroxylase when the substrate is changing from AA to LA. For example, while human CYP2E1 has primarily hydroxylase activity with AA, it is a major LA epoxygenase <sup>87</sup>.

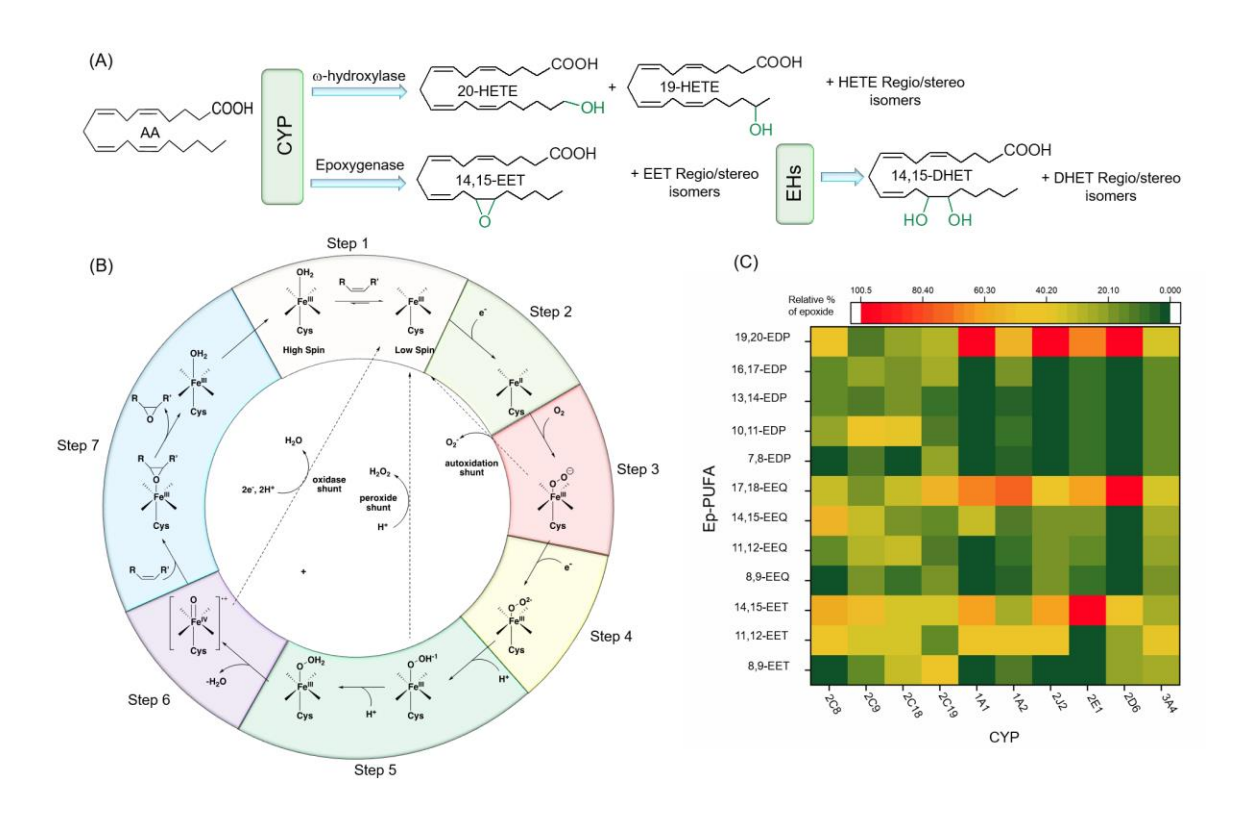


**Figure 3**. A) CYP hydroxylase and epoxygenase activity on AA, as well as EHs epoxy hydrolase products of EETs. B) CYP mechanism of function for monoxygenase activity. C) Regioselectivity in epoxygenase activity of different CYP adapted from [88]. Note that all EETs and HETEs (except 20-HETE) can be present either as the R- or S-enantiomers.AA:Arachidonic acid, CYP:Cytochrome P450 EET:Epoxyeicosatrienoic acid EEQ:Epoxyeicosatetraenoic acids, EDP:Epoxy docosapentaenoic acids HETE:Hydroxyeicosatetraenoic acid DHET:Dihydroxyeicosatrienoic acids, EHs:Epoxy hydrolase.

Like LA, EPA and DHA have been shown to be effective alternative substrate for CYPs isoforms in human, rat and mouse <sup>22</sup>. For example, the human isoforms CYP2C8, 9, 18, and 19, as well as CYP2J2 can epoxidize both EPA and DHA<sup>88,89</sup>. Moreover, the catalytic activity of CYP2C isoforms for EPA and DHA is almost the same as for AA, while CYP2J2 displays 9 and 2 times higher rates in metabolizing EPA and DHA, respectively, compared to AA<sup>88,90</sup>. Also, these

epoxygenase enzymes have different regioselectivity for EPA and DHA  $^{88,90,91}$ . For instance, while CYP2C23 metabolizes AA to 8,9-, 11,12-,and 14,15-EET in a ratio of about 1:2:0.6, the epoxidation of EPA by CYP2C23 results in 17,18-, 14,15-, 11,12- and 8,9- epoxy eicosatetraenoic acids (EEQs) in a ratio of about 6:1:1:1 $^{90,91}$ . Also, while human CYP2C8 produces mainly 11,12- and 14,15-EET with AA as a substrate, it produces exclusively a terminal w-3 PUFA epoxide with  $\omega$ -3 PUFAs as a substrate, such as 17,18-EEQ with EPA, and 19,20- epoxy docosapentaenoic acid (19,20-EDPs) with DHA  $^{88,90,91}$ . However, very low regioselectivity has been reported for other CYP2C isoforms toward EPA and DHA  $^{22,89}$ . Also, as mentioned earlier, CYP2J2 has a very lower regioselectivity toward AA. However, it has high regioselectivity is towards  $\omega$ -3 PUFAs, while preferentially generating terminal  $\omega$ -3 PUFA epoxides  $^{88,90}$ . Furthermore, it should be noted that CYP2J2 and all CYP2C isoforms, except CYP2C8, exhibits high stereoselectivity in favor of producing the R,S-enantiomers of 17,18-EEQ and 19,20-EDP  $^{91,92}$ .

# 4.3.2 Regio- and stereo- selective hydroxylation of PUFAs by CYPs

Like epoxygenase activity, CYPs also hydroxylates in a regio-selective manner. CYP4A and 4F subfamilies hydroxylate AA at the terminal methyl group to produce 20-hydroxyeicosatetraenoic acid (20-HETE) as the major product, and 19-HETE as the minor product. Specifically, 20-and 19-HETE can be generated by human CYP4A11, rat CYP4A1, and mouse CYP4A12A, in a ratio of 90:10, 93:7, and 87:13, respectively <sup>93–95</sup>. CYP4F isoforms such as CYP4F2, CYP4F3A ,and CYP4F3B are more regioselective than CYP4A in ω hydroxylation <sup>96</sup>. On the other hand, the CYP1A1, CYP1A2, and CYP 2E1 show mainly ω-1 hydroxylase activity on AA, yielding 19-HETE as the predominant product, and 16-, 17-HETE (CYP1A1 and CYP1A2) and 18-HETE (CYP2E1) as minor products, and 20-HETE is not produced <sup>22,76</sup>. Interestingly, CYP2J9 is in the rare CYP2J subfamily that almost exclusively generates the 19-

HETE from of AA , while the other members in the subfamily such as human CYP2J2 and rat CYP2J3 have mainly epoxygenase activity on AA, and CYP2J9 displays very low ( $\omega$ -1)-hydroxylase activity on AA<sup>81,96,97</sup>. CYP4A1, which is the main PUFA hydroxylase in rats can metabolize LA at the same rate as AA, and generates 18- and 17-hydroxy octadecadienoic acids (HODE) in a ratio of 3:1 <sup>94</sup>. Likewise, human CYP4A11 has shown hydroxylase activity on LA <sup>87,98</sup>.

EPA and DHA can also be effectively hydroxylated by CYP hydroxylases such as human CYP4A11, CYP4F2, CYP4F3A and -B, as well as mouse CYP4A12, and rat CYP4A195,96,99,100. Again, when the substrate of these CYPs changes from AA to EPA or DHA, the regioselectivity as well as reactivity is altered. For instance, while CYP4A1 hydroxylates AA (generating mainly 20- and 19-HETE), it epoxidizes and hydroxylates EPA to produce predominantly 17,18-EEQ (68%) and 19-HEPE (31%) 94,100,101. Furthermore, when DHA is a substrate, the CYP4A1 exclusively produces the epoxidized product: 19,20-EDP <sup>88,92</sup>. Likewise, CYP4A12A can function exclusively as  $\omega/(\omega-1)$ -hydroxylase with AA producing 20- and 19-HETE in a ratio of 8:2 and can metabolize EPA exclusively to 17,18-EEQ with a minor amount of 20- and 19-HEPE 95. The same trend in shifting from a hydroxylase to an epoxygenase by changing the substrate from AA to EPA and DHA is observed in CYP2E1<sup>88,90</sup>. Note that the change in catalytic preference from ω to (ω-1)-hydroxylase activity of CYPs has also been observed. For instance, by changing the substrate from AA to EPA and DHA the ratio of  $\omega$  to  $(\omega-1)$ -hydroxylase of CYP4A1 shifts from 4:1 to 1:3 and 1:2, respectively <sup>96</sup>. Considering CYP4F subfamilies, CYP4F3A and CYP4F3B display higher catalytic activity for AA and DHA compared to EPA, while CYP4F2 has a higher preference for hydroxylating DHA compared to AA and EPA <sup>96</sup>. CYP4F8 and CYP4F12 mainly function as (ωn)-hydroxylases, with AA producing 18- and 19-HETE, and producing 17,18-EEQ and 19,20-EDP

as the main products of EPA and DHA, respectively  $^{102}$ . CYP2U1 is another CYP isoforms that is expressed in the brain, which mainly acts as a  $\omega$ -hydroxylase for ALA, AA, EPA, and DHA  $^{103,104}$ .

The regio- and stereo- selectivity of CYP enzymes ultimately affects the physiology because numerous studies have suggested that the biological activity of Ep-PUFAs is controlled by the regio-/stereoselectivity of the target receptors, which will be discussed in the following paragraphs (Section 4.4).

# 4.3.3. Physiological functions of regio/stereoisomers of CYP products: Ep-PUFAs and hydroxy-PUFAs

The regio- and stereo- selectivity of CYP enzymes ultimately could alter their effects on mammalian physiology because numerous studies have suggested that the biological activity of Ep-PUFAs is regio/stereo selective and will be briefly summarized in this section. The specific effects of CYP PUFA metabolites on neurodegeneration will be discussed in Section 7.

An earlier study regarding the regioselective effects of EET by Node *et. al.* demonstrated that 11,12-EET exerts significant anti-inflammatory effects by inhibiting the TNF- $\alpha$ -induced vascular cell adhesion molecule–1 (VCAM-1) expression, while 14,15-EET is inactive in this process  $^{105}$ . In addition, peroxisome proliferator-activated receptor-  $\alpha$  (PPAR $\alpha$ ), which plays an important role in inflammation, can only be activated by 8,9-EET, and 11,12-EET, but not 14,15-EET  $^{106}$ . Besides,  $\omega$ -6 Ep-PUFAs, the  $\omega$ -3 Ep-PUFAs also affect physiological process regioselectivity. For example, EDPs alleviate nociception response in rodent inflammatory pain model with a relative potency of 13,14- EDPs > 16,17- EDPs > 19,20- EDPs  $^{107}$ . The biological effects on mammals are also stereospecific. For instance, Ding *et al.* found that a Gs-coupled receptor on the membrane of endothelial cells responds to 11(R),12(S)-EET, but not 11(S),12(R)-EET, which mediates protein kinase A (PKA)-dependent translocation and activation of transient receptor

potential (TRP) C6 channels <sup>108</sup>. Over last decades, several studies have shown that the Ep-PUFAs are likely acted stereospecifically <sup>100,109–111</sup>. In addition to Ep-PUFAs, stereo- and regio- isomers of hydroxy-PUFAs have different biological functions <sup>22,112–115</sup>.

Overall, these studies show the significance of regio- and stereochemistry in the physiological effects of Ep- and hydroxy-PUFAs. One of the main challenges in investigating the regio-/stereo-isomers of PUFA metabolites is obtaining significant quantities of pure regioisomers and their antipodes. Chemical epoxidation is neither chemo-selective nor enantioselective, and purification process of positional isomers and enantiomers is a tedious process<sup>116</sup>. While enzymatic epoxidation seems to be an effective way to generate single enantiomers, using a chemical inversion process is inevitable to access the corresponding enantiomers. Besides, this method is non-diversifiable and cannot be utilized in synthesizing the corresponding analogues <sup>116,117</sup>. Thus, progress in synthetic routes to achieve large quantities of specific regio-/stereoisomers with high purity is the key to improve our understanding of these isomers and the mechanism of their function.

# 4.4. CYP enzymes in the central nervous system

The first evaluation of CYP in the brain was done in 1977 by Sasame and coworkers <sup>118</sup>. They found 30 pmol/mg of CYP enzymes in rat brain, which was approximately 3% of the corresponding level in liver, with 30 times lower activity <sup>118</sup>. Since then, many efforts have been done to identify different CYP enzymes, their activity, as well as expression patterns within the brain. To date, 41 of 57 CYP enzymes are identified in various brain regions <sup>119</sup>. Studies on CYP enzyme expression and function in the brain revealed some remarkable information. CYPs can be found in both glial cells and neurons either in the cell bodies or throughout the cell processes. For instance, isoforms such as CYP2E1, 1A1, 3A, and 2B, are mostly expressed in neurons, while others like CYP2D6 are predominately expressed in both glial and neuron cells <sup>120,121</sup>. CYP

enzyme expression in the brain is heterogeneous among different parts of brain due to the presence of various cell types with different needs and functionality <sup>119</sup>. Also, some CYP enzyme levels in specific neurons are even greater than their counterparts in hepatocytes. For example, CYP46A1, which regulates the cholesterol homeostasis in the brain, and CYP2D6, which is involved in biosynthesis of serotonin and dopamine, are mainly expressed in the brain <sup>122,123</sup>. Even though CYP enzymes (especially 2C, 2J, and 4A) can potentially be highly influential in the brain function through their monooxygenase activity in PUFAs metabolism, which will be discussed later, they are also key factors in hormone, cholesterol, endocannabinoids, and neurotransmitter metabolism <sup>18,124</sup>. Therefore, these enzymes can affect neuronal activity and homeostasis through other mechanisms (Figure 4). For instance, CYP2D6 expressed in brain is involved in metabolism of endogenous neural compounds such as catecholamines, and can metabolize drugs and inactivate neurotoxins such as 1-methyl-4-phenyl-1,2,3,6-tet-rahydropyridine (MPTP) and 1-methyl-4phenylpyridinium (MPP+). Therefore, low activity of this enzyme can result in neuronal hypofunction, especially in dopaminergic neurons. Mann et al. demonstrated that CYP2D6 levels increase with age, however in PD patients, this enzyme is expressed 40% lower compared to a healthy brain <sup>125</sup>. Lower levels of this enzyme in PD patients may reduce their ability to inactivate PD-causing neurotoxins. Also, CYP46 and CYP27 seems to be important in AD and Huntington disease, probably due to their role in the brain cholesterol homeostasis and metabolism <sup>126–128</sup>. In addition, genetic variations in CYP19 and CYP2J2 have been associated with enhanced susceptibility AD <sup>129,130</sup>. The rs890293 variant of CYP2J2, which results in a CYP2J2 enzyme with reduced function, has been shown to be associated with late-onset AD in the Chinese Han population <sup>131</sup>. These data suggest a possible role of Ep-PUFAs, DH-PUFAs or H-PUFAs in neuroprotection and reduced risk of AD, as CYP2J2 is one of the key isoforms of CYP responsible

for Ep-PUFAs metabolism. There are extensive studies on the CYP enzymes effects in neuronal function and homeostasis, which is beyond the scope of this paper, and we are only focusing on the role they have in Ep-PUFAs or dihydroxy-PUFAs metabolism.

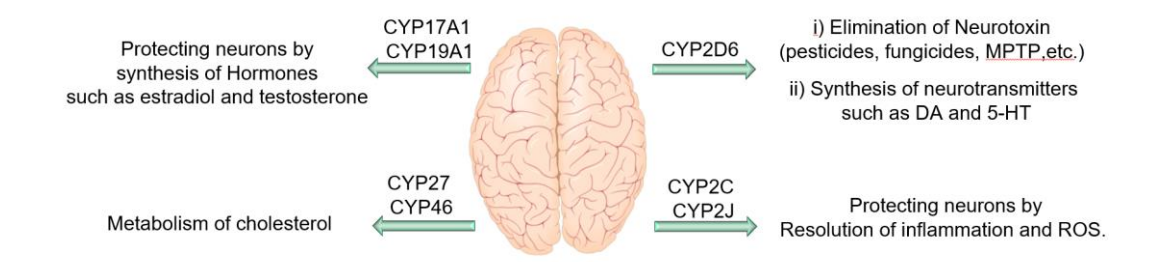


**Figure 4.** CYPs are protective in neurodegenerative diseases. MPTP:(1-methyl-4-phenyl-1,2,3,6-tetrahydropyridine) DA:dopamine, 5-HT: 5-hydroxytryptamine (or serotonin), ROS: reactive oxygen species.

#### 5. EH: Epoxy hydrolase, a critical member in Ep-PUFA metabolism

The epoxide is a three-membered heterocycle that has unfavorable bond angles and a polarized C-O bond leading to significant electrophilic activity <sup>132</sup>. Thus, epoxides could covalently react with a nucleophile and cause a wide range of biological and pathological effects. For instance, styrene epoxide derivatives can be attacked by nucleophilic exocyclic amino groups of nucleotides or N7 moiety of purines causing DNA adducts and mutations <sup>133,134</sup>. There is extensive evidence confirming the potential of some epoxides, particularly Ep-PUFAs, to act as secondary messengers involved in the initiation of different physiological pathways. Epoxide hydrolases (EHs) catalyze the hydrolysis of both endogenous and exogenous epoxides, resulting in corresponding 1,2-diol compounds <sup>135</sup>. Therefore, EHs are involved in detoxification and regulating signaling molecule metabolism by hydrolyzing epoxides and modulating their endogenous levels.

The EHs can be detected in both prokaryotes and eukaryotes. There are seven different EHs identified in mammals (i) Microsomal epoxide hydrolase (mEH, EPHX1), (ii) Soluble epoxide hydrolase (sEH, EPHX2), (iii) epoxide hydrolase 3 (EH3, EPHX3), (iv) epoxide hydrolase 4 (EH4,

EPHX4), (v) hepoxilin hydrolase, (vi) leukotriene A4 (LTA4) hydrolase, and (vii) cholesterol epoxide hydrolase  $^{136-141}$ . The sEH, mEH, EH3, and EH4 enzymes can be considered as EPHX subfamilies, which are members of  $\alpha/\beta$ -fold hydrolases superfamily, comprising of eight antiparallel β-strands as the core domain connected together by  $\alpha$ -helices that are interrupted by an adjustable lid domain. The other three enzymes can be categorized in different families due to their different catalytic mechanisms and substrate preferences that are well reviewed elsewhere and will not be discussed further  $^{136,137,139}$ . Note that paternally expressed gene 1 (peg1)/mesoderm-specific transcript (MEST) gene (peg1/MEST) is another candidate that might be considered an EH due to its considerable sequence similarity to  $\alpha/\beta$  hydrolases. However, its enzymatic function is currently unknown  $^{142}$ . Thus, we are using EH to refer to sEH, mEH, EH3, and EH4 in this review, unless otherwise mentioned.

#### 5.1 Characteristics of the main EH enzymes

Among the EHs, mEH is the first identified mammalian EH, which is encoded by the EPHX1 gene and has a primary structure of 455 amino acids  $^{143,144}$ . This membrane-bound enzyme is attached to the surface of the ER or the plasma membrane by its N-terminal membrane anchor  $^{145,146}$ . The mEH also has an N-terminal extension that wraps around the protein and holds the lid domain down to the  $\alpha/\beta$  hydrolase fold  $^{147,148}$ . The localization of N-terminal in the membrane is a mechanism by which the C terminal region with epoxide hydrolase activity faces towards the cytosol on ER membranes, and on the plasma is exposed to the extracellular medium. The mEH and CYP enzymes are both type I membrane-bound proteins, and there is evidence of close proximity of CYP and mEH in the endoplasmic reticulum  $^{149}$ , suggesting possible physical interaction. Interestingly, when mEH dissociates from the membrane and is found in the blood, this is considered a preneoplastic antigen, a marker for tissue damage including cancer  $^{150}$ .

The sEH on the other hand, can selectively hydrolyze lipid epoxides with a high catalytic rate, while having an unknown role in xenobiotic metabolism in the liver <sup>140</sup>. Human sEH, encoded by EPHX2, is a 62 kDa homodimeric enzyme, located in the intracellular environment (cytosol and peroxisomes) <sup>140</sup>. Each monomer has two regions: a C-terminal region with epoxide hydroxylase activity, and a N-terminal region with phosphatase activity, which are linked together by a proline-rich linker (Figure 5A) <sup>151</sup>. Both mEH and sEH are widely found in different tissues with the highest levels found in the liver, and their expression as well as specific activity can be altered by tissue, sex, and age <sup>140,152</sup>.

Both EH3 and EH4 are predicted to be single-pass type II membrane proteins and possess N-terminal membrane anchors based on their amino acid sequences, yet these properties need to be experimentally confirmed. EH3 and EH4 have 45% homology in their sequence and were originally named as  $\alpha/\beta$  hydrolase domain containing protein 9 (ABHD9) and protein7 (ABHD7), but were renamed after studies done by Arand's group showed that epoxide hydrolase activity toward epoxy octadecenoic acids (EpOMEs) and EETs <sup>153,154</sup>. However, their specific *in vivo* function is still under investigation. EH3 is a 41 kDa (360 residue) protein encoded by EPHX3 gene, and its microsomal properties have been identified by a related gene in insect cells <sup>154</sup>.

EH3 expression is generally low compared to mEH and sEH. Isolated mRNA from a representative set of mouse organs revealed the lowest expression in liver and kidney, while the highest expression was observed in skin, stomach, lung, and tongue <sup>154</sup>. This expression pattern suggests a potential function of EH3 in barrier formation, which is supported by a recent study showing high turnover hydrolyzing activity toward a skin-related epoxide involved in a key step of water permeability barrier formation in the outer epidermis <sup>155</sup>. EH3 is also involved in leukotoxin metabolism to mediate acute respiratory distress syndrome (ARDS) <sup>156</sup>.

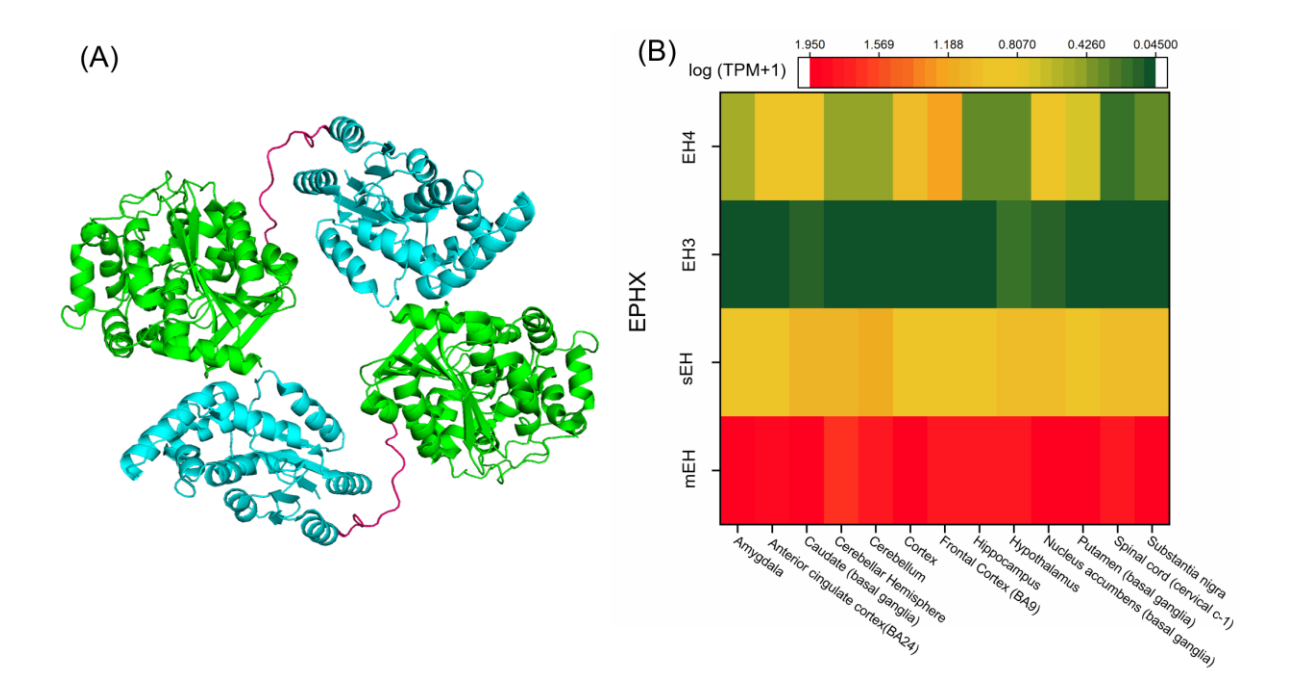


**Figure 5.** A) Crystal structure of the sEH dimer (PDB accession code 1S8O [151] The sEH monomer is composed of two globular regions representing the a/b tertiary structure and a short proline-rich linker (pink) connects the C-terminal of one monomer to the N-terminal region of another. The catalytic site with epoxide hydrolase activity is located within the C-terminal region, whereas N-terminal region possesses phosphatase activity. B) EH distribution in human brain based on mRNA expression. Expression values are shown as a median of TPM (Transcripts Per Million), calculated from a gene model with isoforms collapsed to a single gene with no other normalization (https://www.gtexportal.org/home/gene/EPHX).

In addition, several studies identified the epigenetic silencing of EH3 in different types of cancers. For instance, hypermethylation of EH3 is associated with prostate cancer relapse <sup>157</sup>, and has been observed in human colorectal carcinomas <sup>158</sup>, gastric cancers <sup>159</sup>, as well as malignant melanomas <sup>160</sup>.

EH4 is a 42 kDa (362 residue) protein encoded by EPHX4 gene located on chromosome 1p22.1. As already mentioned, like other mEH and sEH, both EH3 and 4 possess an aspartate nucleophile, distinguishing them from other ABHD proteins that have either a serine or cysteine as nucleophile residue in the catalytic triad, placing them in the EH family<sup>153,154</sup>. EH4 expression is much higher in the brain compared to other tissues <sup>142</sup>. EH4 has been recognized as a target gene for the zinc finger protein 217, an important oncogene that is over amplified and overexpressed in

a variety of human tumors <sup>161</sup>. In addition, hypermethylated EH4 has been found in human colorectal cancer. Thus, EH4 is associated with the pathogenesis of some cancers <sup>162</sup>. In general, very little is known about EH4 substrate spectrum and enzymatic function. However, the presence of a nucleophilic aspartate in the catalytic triad (that distinguishes EH3 and 4 from other ABHDs), and high homology with two EHs in *C. elegans* <sup>17</sup>, suggest the potential for EH4 to be an active EH with important physiological activity in the brain <sup>153</sup>.

#### 5.2. Catalytic function and mechanism of EHs

The major function of EH is to hydroxylate xenobiotic epoxides and Ep-PUFAs (Figure 3A). The catalytic activity of EHs can be described in three steps, with the contribution of four amino acids, which are involved in transforming the epoxide to a diol <sup>135</sup>. In the first step, the epoxide enters through the L-shaped hydrophobic tunnel with the nucleophilic aspartate in the center and it is stabilized there by van der Walls and hydrogen bonding with the hydrophobic pocket and two tyrosines, respectively. The second step is the formation of an ester intermediate, in which the nucleophilic aspartate and polarizing tyrosines are involved. In this step, the oxygen of the epoxide is polarized by hydrogen bonds between OH group of two tyrosine residues. At the same time, the carboxylate of Asp (a nucleophilic amino acid), which is opposite of the tyrosine residues, gets orientated and activated by other amino acids in the active site including His and an acidic residue (Asp in sEH and Glu in mEH) adjacent to the nucleophilic Asp. Then, the activated nucleophilic Asp attacks the electrophilic carbon of the epoxide resulting in a hydroxyl acylated-enzyme intermediate. The third step is diol formation. When the intermediate is formed in the second step, the His orients and then the charge relay system between the Glu/Asp and His, activates the His to facilitate hydrolysis of the acylated intermediate, forming the corresponding 1,2-diol product. Table 1 shows the different residues in the catalytic triad of mEH, sEH, EH3, and EH4. Besides

these highly conserved regions, the amino acid sequences and the N-terminal region are largely different among different EHs, probably due to their different origin in evolutionary pathways.

**Tables 1.** Different residues in the catalytic triad of mEH, sEH, EH3, and EH4 and their function

EH type	Polarizing Residues	nucleophilic residue	Involve in orientation and activation of nucleophilic residues
mEH	Tyr299 Tyr374	Asp226	His 431 Glu 404
sEH	Tyr383 Tyr466	Asp335	His 524 Asp 496
ЕН3	Tyr220 Tyr281	Asp173	His 337 Asp307
Eh4	Tyr216 Tyr281	Asp 169	His 336 Asp307

Tyr: Tyrosine, Asp: Aspartic acid, Glu: Glutamic acid His: Histidine

# 5.3 Major EHs responsible for Ep-PUFA metabolism

sEH is the main enzyme that degrades Ep-PUFAs, but other EHs also play a role in Ep-PUFA metabolism [85]. mEH can selectively hydrolase arene and cyclic epoxides, is involved in xenobiotic metabolism, and catalyzes the epoxidation of a wide and still growing range of substrates <sup>152</sup>. It was reported that expression of mEH in specific neuronal populations suggests a previously unnoticed role in processing endogenous substrates. Zeldin *et al.* reported that mEH hydrolyzes EET with up to an 8-fold lower Km than sEH <sup>163,164</sup>. However, the catalytic efficacy (*kcat*/Km) of mEH is still five- to 50-fold lower than that of sEH for all EET regioisomers. The regio-selectivity of the two enzymes, based on the catalytic efficacies, was 11,12-EET>8,9-EET=14,15-EET>5,6-EET for mEH and 14,15-EET=11,12-EET>8,9-EET>5,6-EET for sEH <sup>165</sup>.

Considering role of EH3 in the Ep-PUFA metabolism, an *in vitro* study using EETs as substrates demonstrated that EH3 has high catalytic efficacy in the range of sEH as well as the highest specific activity reported thus far among EHs. These data suggest that even low expression of EH3 would be enough for a high concentration of EETs produced in cell <sup>154</sup>. On the other hand, the substrate spectrum of EH4 is unknown, mainly because it has not shown enzymatic activity on

any of the substrates tested so far. The lack of turnover could be due to the expression of a misfolded protein, because EH4 is potentially membrane bound, complicating recombinant expression. Therefore, epoxy hydrolase activity is still speculative in the case of EH4.

#### 5.4 EHs in the brain

In this section the different EHs and their distribution along with potential application are discussed.

#### 5.4.1. mEH in the brain

In the brain, mEH is highly expressed in epithelial cells, especially in cerebral blood vessels and the choroid plexus that form the blood brain barrier, where mEH might be mainly involved in detoxification and protecting CNS. This enzyme is also found in smooth muscle cells and specific neuronal cells including, but not limited to, cerebellar granule cells, central amygdala neurons, striatal neurons, hippocampal pyramidal neurons, and in some of astrocytes <sup>152,166</sup>. Figure 5B shows the distribution of EHs in different region of human brain using mRNA expression techniques. The role of mEH in neurological disorders is a subject of intense interest in the field of pathophysiology-related EPHX1 due to its high expression in the brain <sup>152</sup>. In support of this, Lui et al. identified high expression of mEH in the hippocampus and in the cortex of AD patients <sup>165</sup>. They also found that exposure to β-amyloid aggregation could induce mEH overexpression in astrocytes in primary hippocampal glial culture. Over expression of mEH has also been observed in the rat hippocampus and entorhinal cortex when the animals were treated with trimethyl-tin, an environmental neurotoxic agent, further supporting the role of mEH in the pathogenesis of neurodegeneration and neurotoxicity 165. Generic ablation of mEH in mice treated with methamphetamine (METH) caused a decreased in synaptosomal DA uptake in the striatum, while

enhancing the extracellular DA levels in the nucleus accumbens compared to the wild-type mice, suggesting that mEH is a potential therapeutic target for drug addiction treatment <sup>167</sup>. In addition, increased levels of mEH have been found in human brain tumor cells, further supporting the pivotal role of mEH in brain-related pathogenesis <sup>168</sup>.

Although the role of mEH xenobiotic metabolism has been extensively studied, its distribution suggests a possible endogenous role <sup>169,170</sup>. Even though mEH possesses low catalytic activity towards Ep-PUFAs, high levels of mEH expression in specific brain regions and neurons, as well as evidence for substrate channeling between mEH and CYP on ER, suggests that mEH contributes to Ep-PUFA hydrolysis in the brain <sup>166,171,172</sup>. For instance, tracking of dihydroxyeicosatrienoic acids (DHET) regioisomers formation in freshly isolated mouse brain hippocampal cells of WT, mEH<sup>-/-</sup>, and sEH<sup>-/-</sup> mice revealed substantial mEH-dependent EET turnover when cells were treated with AA. Furthermore, hippocampal cells treated with ACU, a selective sEH inhibitor, could still hydrolyze EETs to their dihydroxy product, further supporting a possible role of mEH in the brain Ep-PUFAs metabolism <sup>165</sup>. In short, while mEH activity in hydrolyzing Ep-PUFAs is well studied, its role in neuronal signaling and hemostasis is mostly unknown.

### 5.4.2. sEH in the brain

sEH is expressed in different brain regions (Figure 5B) and in multiple cell types such as astrocytes, endothelial cells, oligodendrocytes, and neural cell bodies <sup>173,174</sup>. sEH expression in microglia cells has not yet been well characterized; however, Huang *et al.* found sEH expressed in the BV2 microglial murine cell line <sup>175</sup>. They also found that genetic ablation or pharmaceutical inhibition of sEH can attenuate microglia activation, suggesting a significant role in neuroinflammation <sup>175</sup>. Consistent with this study, researchers have revealed a role for sEH in different neuroinflammatory and neurodegenerative pathogenesis involving microglia, astrocytes,

and neurons by its contribution to Ep-PUFA metabolism <sup>21,176,177</sup>, which will be discussed later. Furthermore, sEH is critical to pathways related to axonal growth in neurons as well as neuronal development, mainly through its Ep-PUFA hydrolyzing activity <sup>178</sup>. Taken together, these data point to sEH as a potent therapeutic target known for investigating the effect of Ep-PUFAs downstream in neuronal activity and maintenance.

#### 5.4.3. EH3 and other EHs in the brain

Expression of EH3 is very low in almost all tissues including the brain. However, the stomach, skin, and lung are organs with the highest EH3 levels, suggesting that EH3 might be mostly involved in barrier formation <sup>154,155</sup>. Hoopes *et al.* used EH3 knockout mice to track the EH3 function *in vivo* <sup>179</sup>. Interestingly, they found no difference in endogenous epoxide:diol ratios (such as EETs:DHETs or EpOME:DiHOME ratios) in different tissues compared to wild-type tissues. In addition, EH3 ablation had no effect on the mRNA levels of CYP epoxygenase, and the EH3<sup>-/-</sup> mice exhibited a similar inflammatory response to LPS compared to WT mice. Also, no overt phenotype, i.e., no significant change in weight, and anatomical normality of organs, and reproductive capacity, was observed in the EH3<sup>-/-</sup> mice <sup>179</sup>. Therefore, sEH and mEH are predominant enzymes involved in diol formation. In contrast to EH3, EH4 is expressed mainly in the brain, with the highest expression in the neocortex and hippocampus (Figure 5B). Like EH3, there is a very low expression of EH4 in the liver and intestine <sup>180</sup>.

## 5.5. Possible physiological roles of dihydroxy-PUFAs

Dihydroxy-PUFAs generated by EHs possess higher polarity compared to their Ep-PUFA precursors. Thus, they mainly accumulate in the extracellular fluid and are generally considered to have little to no activity <sup>23</sup>. However, several studies suggest a possible physiologically function

of the PUFA diols generated by EHs. For instance, an early study from Moghaddam et al. showed that dihydroxy octadecenoate, an EH product of leutotoxin (epoxy octadecenoate) is toxic cells <sup>156</sup>. In addition, Weintraub et al. demonstrated that preincubation of 14,15-DHET, and 11,12-DHET can augment both the magnitude and duration of inflammation-induced relaxation in pig porcine coronary arteries <sup>181</sup>. Oltman *et al.* showed that the DHET regioisomers were as potent as (or, in the case of 11,12-DHET, more potent than) their parent EETs in vasodilation of dog canine coronary arterioles <sup>182</sup>. Larsen et al. also found that DHETs can modulates vasomotor tone in the resistance vessels of the human heart and can induce vasodilation via a BK<sub>Ca</sub> channel-mediated mechanism <sup>183</sup>. In addition, Abukhashim et al. observed that while 11,12-EETs can modulate cAMP production, the corresponding 11,12-DHET metabolite can function as a negative controller to limit cAMP production in HEK293 cells <sup>184</sup>. Another study found 14,15-DHET can act as an endogenous activator of PPARa 185,186 Sisemor et al. found that DiHOMEs can disrupt mitochondrial function, specifically through activation of the mitochondrial permeability transition <sup>187</sup>. Consistent with this Moran *et al.* showed an inhibitory effect of DiHOMEs on the mitochondria respiratory chain in a regioselective way, as 12,13-DiHOME is approximately 4-fold more potent than 9,10-DiHOME <sup>188</sup>. A study by Stanford et al. also demonstrated that 12,13-DiHOME, a lipokine produced by brown adipose tissue, increases fatty acid uptake in muscle<sup>189</sup>. Interestingly, Kundu et al. also reported that DHETs are essential to monocyte chemoattractant protein-1 (MCP-1) dependent chemotaxis, suggesting a proinflammatory role<sup>190</sup>. Furthermore, different studies showed the presence of dihydroxy-PUFA in human urine or plasma, and these levels correspond to various diseases. For instance, glucuronic acid conjugates DiHOME was found in the urine of children with generalized peroxisomal disorders. Also, a blood serum analysis of AD patients showed about 20% higher levels of all four DHET species compared to healthy

individuals <sup>20</sup>. Also, individuals with type 2 diabetes and AD showed higher levels of 14, 15-dihydroxy eicosatetraenoic acid (14,15-DiHETE)(66%), and 17, 18-DiHETE (29%) compared to type 2 diabetes patients with healthy cognitive function, with no difference in DHET species between these two group <sup>20</sup>. These studies suggest potential biological effects of dihydroxy-PUFAs, which need to be elucidated.

## 6. CYP PUFA metabolism and the nervous system.

The brain has high capacity for de novo synthesis of the Ep-PUFAs from their parent PUFAs by CYP enzymes, which can act on neuronal cells, and the resulting Ep-PUFAs are rapidly degraded by EHs such as sEH191,192. While the CYP pathway seems to be the dominant route of production of Ep-PUFAs in brain, they can be also transported to the brain by cellular uptake <sup>193,194</sup>. The major elimination pathway of Ep-PUFAs is their hydrolysis by EHs to more polar 1,2diols, whereas spontaneous hydration, beta oxidation, chain elongation, and reincorporation into the phospholipids are also potential mechanisms to maintain the homeostasis of Ep-PUFA<sup>192</sup>. Note that each of the PUFA elimination pathways can have their own biological functions, which has yet to be fully understood <sup>190</sup>. For example, incorporation of Ep-PUFA into lipid bilayers might not eliminate their biological activity as studies demonstrated the activity of membrane bound Ep-PUFAs such as EETs<sup>194</sup>. Furthermore, the regioselectivity of both the CYP and sEH can potentially control the concentration of specific Ep-PUFAs in tissues and brain. For instance, the concentration of 7,8-EpDPE, which is not a preferred substrate of sEH, is almost 30 times higher than other regioisomers in the brain and the spinal cord of rats <sup>107</sup>. The Ep-PUFAs can also be further oxidized P450 or bind to fatty acid binding protein (FABP) <sup>192</sup>.

Besides, several studies demonstrated that the brain oxylipins might be amenable to the dietary lipid content  $^{14}$ . For instance,  $\omega$ -3 PUFA (EPA and DHA) supplementation enhances the level of

EPA-derived and DHA-derived CYP metabolites and decreases AA CYP metabolites in the brain of mice  $^{195,196}$ . Ostermann *et al.* found that an  $\omega$ -3 PUFA enriched with EPA and DHA reduced Ep-PUFAs and the ratio of epoxy- to dihydroxy-PUFA, revealing higher sEH activity  $^{197}$ . Rey *et al.* also observed that dietary  $\omega$ -3 PUFAs supplementation promotes synthesis of pro-resolving oxylipins in the mouse hippocampus  $^{198}$ . Moreover, feeding rat with  $\omega$ -6 PUFA (LA) could increase the oxylipin metabolites of AA and LA and reduce EPA-derived oxylipins in the brain cerebral cortex of animal  $^{199}$ ; while LA deficient diet decreases LPS-induced proinflammatory PGE2 formation in rat brain  $^{200}$ . Note that, even though the dietary PUFAs effect on brain FAs composition has been well-studied, oxylipin profiles do not necessarily reflect tissue precursor PUFA composition  $^{201-203}$ . For example, the high DHA to AA ratio in CNS system does not necessarily lead to high levels of DHA-derived oxylipins in the CNS.

# 7. Epoxy PUFAs and neuroinflammation

Neuroinflammation is a complex process required for homeostasis maintenance in the CNS including clearance of cellular debris,  $\beta$ -amyloid plaques, and glial scars that if unmitigated can result in chronic inflammation, leading to neural pathogenesis <sup>204,205</sup>. Neuroinflammation also contributes to neurodevelopment, immune conditioning against infections, as well as clearance of damaged tissues upon injury <sup>204</sup>. Microglia and astrocytes are the main cells involved in the neuroinflammatory response <sup>206</sup>. Activated microglia produce pro- and anti-inflammatory cytokines such as interleukins  $1\beta$  and 6 (IL- $1\beta$  and IL-6), tumor necrosis factor alpha (TNF $\alpha$ ), interferons  $\alpha$  and  $\gamma$  (IFN- $\alpha$  and IFN- $\gamma$ ), chemokines like IL-8, and Macrophage Inflammatory Proteins  $1\alpha$  and  $1\beta$  (MIP- $1\alpha$ , MIP- $1\beta$ ), neurotrophins such as brain-derived neurotrophic factor (BDNF) and nerve growth factor (NGF), growth factors such as fibroblast growth factors (FGFs) and transforming growth factor  $\beta$  (TGF- $\beta$ ), ROS and RNS, inflammatory markers such as serum

amyloid P and C-reactive protein, along with proteases and complement system proteins<sup>204,206,207</sup>. Perivascular macrophages and endothelia cells also play a significant role in the interpretation and propagation of inflammatory signals within the CNS. Even though the neuroinflammatory response aspires to remove an injury or insult, when resolution fails it becomes a chronic condition, and chronic inflammation is related to numerous major disease states <sup>26</sup>. Thus, neuroinflammation can cause or exacerbate the pathogenesis of NDs such as the PD, AD, depression, etc. <sup>26,205,208</sup>. In this section we focused on recent discoveries about the role(s) of Ep-PUFAs, which regulate acute and chronic neuroinflammation.

### 7.1. Acute neuroinflammation

A promising therapeutic potential of Ep-PUFAs is mitigating neuroinflammation caused by acute nervous system damaged such as seizures, brain trauma, and ischemic and hemorrhagic strokes <sup>206,209,210</sup>. The neural loss or damage resulting from these insults activates the resident immune cells including microglia and astrocytes to repair the injured tissues. However, uncontrolled activation can result in chronic damage as observed in other organ systems <sup>26,205,208</sup>. The neuroinflammation can be controlled by either suppressing the expression and release of proinflammatory mediators such as iNOS, Iba1, TNF-a, or increase anti-inflammatory cytokines including IL-10 by polarized microglia, which is greatly affected by endogenous Ep-PUFAs, in particular EETs [136,138,139]. Several studies have shown that deletion or inhibition of sEH induces production of anti-inflammatory cytokines such as IL-10, while reducing proinflammatory mediators including lipopolysaccharide (LPS) and IFN-γ and decreasing TNF-a localization and circulation <sup>176,211,212</sup>.

Several studies in mice with pharmacologically-induced seizures suggest a possible contribution of Ep-PUFAs in neuroinflammatory suppression. Inceoglu *et al.* has shown that

genetic knockout or pharmaceutical inhibition of sEH attenuated seizures generated by GABA receptor antagonists such as picrotoxin and pentylenetetrazole <sup>16</sup>. However, slight or no effect of sEH inhibition was observed in cases of seizures induced by 4-aminopyridine as a potassium channel blocker. Vito et al. reported that coadministration of an sEH inhibitor and diazepam can of seizures lethality protect against the progression tonic and induced tetramethylenedisulfotetramine in a mouse model <sup>213</sup>. In addition, Huang et al. observed increased levels of both sEH and proinflammatory cytokines including IL-1β and IL-6 in the hippocampus of mice who underwent pilocarpine-induced seizures, further suggesting a potential relationship between sEH and seizures <sup>214</sup>. Using double immunofluorescence labeling they indicated that astrocytes are the major source of sEH in the hippocampus (subfields of dentate gyrus, CA1, CA3, and dentate gyrus). This result suggested that alternation of sEH in the hippocampus may contribute to the observed significant astrogliosis in response to seizures. Finally, it has been shown that inhibition of sEH suppresses pilocarpine-induced seizures and increases the seizureinduction threshold [141]. Similarly, suppression of neuro-inflammation caused by cortical impact injury as a model of traumatic brain injury (TBI) has been also observed by deletion or inhibition of sEH <sup>175</sup>.

The TBI leads to an induction of CYPs, and increased level of PUFAs (especially AA and DHA), leading to a dynamic change of Ep-PUFA, and an upregulation of sEH in the injured brain <sup>215</sup>. Hung *et al.* found that higher levels of EETs and an increased ratio of EET to DHET in the injured brain of sEH KO mice and ones treated with AUDA (an sEH inhibitor), suppressed inflammatory responses <sup>175</sup>. sEH deletion was shown to reduce BBB permeability, brain edema, neural apoptosis, and death. These changes were associated with significantly reduced EETs degradation, inflammatory mediator expression, microglial/macrophage activation, and IFN-γ-

induced NO production. Also, treatment of primary microglial cultures with a sEH inhibitor attenuated LPS- or IFN-γ-stimulated NO production, and decreased LPS- or IFN-γ-induced p38 MAPK and NF-κB signaling, and the effects were abolished by co-administration with a 14,15-EET antagonist (14,15-EEZE) <sup>175</sup>. This result suggested that 14,15-EET could be a major mediator of sEH inhibition. Several studies have shown that 14,15-EET can induce secretion of vascular endothelial growth factor (VEGF) and BDNF to protect the existing neurons during inflammation <sup>176,216</sup>. Apart from the protective effects of EETs through their actions on auxiliary cells, EETs can directly impact neurons, for instance, by enhancing their neurite outgrowth <sup>178,217</sup>[123,143]. In addition, both genetic ablation and pharmacological inhibition of sEH could attenuate the functional and historical deficits in cerebral Ischemia by vascular and neural protection <sup>218,219</sup>. These effects suggest that sEH inhibition and increased Ep-PUFAs may reduce CNS injury both by reducing the inflammatory response in resident immune cells and by direct neuroprotective effects on the neurons through modulation of the endogenous level of beneficial Ep-PUFAs.

## 7.2. Chronic neuroinflammation

The acute neuroinflammatory response caused by glial cell activation leads to repair of damaged areas of the brain and spinal cord. However, if the neuroinflammatory response is persistent and is dysregulated, the acute neuroinflammation shifts to harmful chronic neuroinflammation <sup>26,205,208</sup>. Chronic activation of glial cells, which leads to the chronic neuroinflammatory state, leads to protein accumulation, ER stress, mitochondria dysfunction, uncontrolled oxidative stress, axonal transport impairment, and apoptosis. Thus, causes detrimental impacts on neuronal function and can lead to NDs such AD, PD, amyotrophic lateral sclerosis, and neuropsychiatric disorders including schizophrenia and depression<sup>26,27</sup>.

### 7.2.1. Alzheimer disease

AD is a gradual degenerative brain disease, mostly involving the hippocampus and neocortex, which are associated with progressive memory disorders and cognitive dysfunction, as well as psychiatric symptoms <sup>3,220,221</sup>. Two main pathological characteristics of AD are aggregates of tau protein inside neurons, and extracellular senile plaques due to depositions of amyloid-β (Aβ) protein fibrils <sup>222</sup>. Moreover, the Aβ in soluble form is extensively studied as one of major causes of the pathogenesis of AD, primarily by inducing mitochondrial dysfunction <sup>223,224</sup>. It has been shown that the blocking endogenous EET production by a selective epoxygenase inhibitor, MS-PPOH, aggravated the effect of Aβ in astrocyte mitochondrial dysfunction, whereas pretreatment of primary hippocampal astrocyte culture with exogenous 11,12-EET or 14,15-EET prevented Aβinduced mitochondrial depolarization and fragmentation <sup>225</sup>. In another study done by same group, Sarkar et al. found that Aβ causes a significant decrease in the level of both DHETs and EETs in microsomes isolated from the rat cerebral cortex in a region- and cell-specific manner, which was suggested to be due to a decrease in CYP activity after Aβ exposure <sup>226</sup>. However, another study demonstrated an increased level of AA-derived EETs in the hippocampus of human amyloid precursor protein (hAPP) expressing mice, suggesting increased activity of CYP or a decreased level of sEH <sup>227</sup>. In addition, different studies showed an increase in the level of DHET in AD patients. For instance, a blood serum analysis of the AD subjects showed higher levels of all four DHET species: 5,6- DHET (15% higher), 8,9-DHET (23% higher), 11,12 DHET (18% higher), and 14,15-DHET (18% higher) compared to healthy individuals <sup>20</sup>. Also, sEH is upregulated in multiple transgenic AD mouse models as well as in human AD brains in many studies <sup>168,228</sup>. Thus, the contradictory results regarding the EET and DHET levels may be due to the difference in experimental design and the models used.

In a further effort to study the effects of EHs in AD, Lee et al. found an upregulation of sEH in the brain and predominantly in hippocampal astrocytes in a murine model of early-onset Alzheimer (APP/PS1 Tg) with severe AD-impaired pathology <sup>229</sup>. Genetic deletion of sEH in APP/PS1 Tg mice, could result in decreased Aβ plaque formation, increasing astrogliosis in the brain, higher production of anti-inflammatory cytokines, and increased activity of two different transcription factors, nuclear factor kappa-light-chain-enhancer of activated B cells (NF-κB, and nuclear factor of activated T cells (NFAT) . The APP/PS1 Tg/sEH--- mice also had improved memory formation, spatial learning, and nesting building ability <sup>229</sup>. These data suggest a pivotal role of sEH in the regulation of neuroinflammation in AD pathology. A study by Gosh et al. also found a significant upregulation of sEH in a β-amyloid mouse model (5xFAD) and in postmortem human AD brain samples. The oxylipin analysis in transgenic 5xFAD mice showed a drastic reduction in Ep-PUFAs, in particular EDP and EETs. Orally administrated TPPU, a potent sEH inhibitor in the 5xFAD mice reinstated the Ep-PUFA levels and reversed astrocyte and microglia reactivity as well as immune pathway dysregulation <sup>228</sup>. Consistent with this result, another study examined administration of three structurally different sEH inhibitors in two AD mouse models (5XFAD and SAMP8, paradigms of early-onset and late-onset AD) <sup>230</sup>. They found a reduction in gene expression and brain protein levels of proinflammatory cytokines including tumor necrosis factor $-\alpha$  (TNF- $\alpha$ ), IL-1 $\beta$ , C-C motif ligand 3(CCL3), in both mouse models. They also observed an overall decrease in ER stress and oxidative stress when AD mouse models were treated with inhibitors, though the magnitude of the effect was different among the inhibitors <sup>230</sup>. These data reveal that the biological outcomes observed were not due to off-target effects related to a specific sEH inhibitor. These studies could well support the potential therapeutic effects of sEH inhibition in regulating neuroinflammation, and reducing tau hyperphosphorylation pathology, amyloid

plaques formation, ER stress, oxidative stress, and reducing cognitive impairment. However, the detailed mechanism underlying sEH-mediated regulation of AD pathologies such as  $A\beta$  formation and clearance demands more investigation.

While the role of mEH in AD is still unknown, the level of mEH expression is likely regulated during brain insults, causing a significant upregulation of the enzyme. For instance, high levels of mEH expression is found in activated astrocytes in epileptic tissue and around  $\beta$ -amyloid plaques in brain tissue of patients with AD symptoms <sup>168</sup>.

### 7.2.2. Parkinson disease

Parkinson's disease (PD) is the second most frequent neurodegenerative disease after AD  $^{231}$ . Although the precise pathogenesis of PD remains unknown, loss or dysfunction of dopaminergic neurons in the substantia nigra (SN) pars compacta (SNpc) and deposition of accumulation of misfolded  $\alpha$ -synuclein in intra-cytoplasmic inclusions called Lewy bodies (LBs) are considered as hallmarks of PD  $^{231,232}$ . In addition, enhanced levels of inflammatory mediators including IL-1 $\beta$ , IFN- $\gamma$ , and TNF- $\alpha$  are evident in various studies with PD models  $^{231,232}$ . To date, there are no pharmaceutical curative treatments approved by the FDA  $^{232}$ .

MPTP is a precursor compound for the mitochondrial complex I inhibitor 1-methyl-4-phenylpyridinium (MPP+) that induces neurotoxicity including dopaminergic loss or dysfunction (such as, loss of tyrosine hydrolase-positive (TH+) cells, loss of dopamine transporter (DAT), and increased oxidative stress and ER stress). Several studies also confirmed that overexpression of sEH in the striatum is accompanied by MPTP treatment, while sEH ablation protects neurons against MPTP-induced neurotoxicity in the mouse striatum. Qin *et al.* showed that administration of MPTP to mice causes a dramatic loss in the TH+ neurons, while sEH is upregulated in the substantia nigra. Interestingly, genetic knockout of sEH or treatment with a sEH inhibitor, and to

a lesser extent 14,15-EET, could attenuate the neurotoxicity induced by MPTP  $^{233}$ . Ren *et al.* also demonstrated that MPTP-induced neurotoxicity in the striatum and substantia nigra was attenuated after subsequent repeated oral administration of TPPU  $^{19}$ . Furthermore, by *in vitro* study they found that TPPU has a therapeutic effect directly on induced pluripotent stem cells (iPSC) with a parkin RBR E3 ubiquitin protein ligase (PARK2) mutation, by suppressing the increase in caspase-3 cleavage, thereby reducing apoptosis in dopaminergic neurons  $^{19}$ . In addition to these studies, several other studies have shown that the sEH expression positively correlates with phosphorylation of  $\alpha$ -synuclein in the striatum, which further supports a role for sEH and EpPUFAs in the pathogenesis of neurological disorders such as PD and shows promising potential for sEH as a biomarker for PD diagnosis  $^{234,235}$ 

## 7.3. Potential molecular targets of Ep-PUFAs in the nervous system

Ep-PUFAs such as EETs are involved in inflammation through multiple mechanisms as demonstrated in animal models and tissues. However, no specific receptors for Ep-PUFAs have been identified yet. Therefore, a mechanistic study of Ep-PUFAs is difficult. Over the years, it has been shown that EETs initiate their anti-inflammatory effects through NF-κB, which is a transcription factor with significant roles in cell survival, immune responses, and inflammation. Several studies showed that an increased activity of CYP2J2 and/or EETs can reduce inflammation by suppressing the degradation of  $I\kappa B\alpha$ , an endogenous NF-κB inhibitor, and thus reducing the activation of NF-κB and inflammation. For instance, NF- $\alpha$  induced nuclear translocation of NF-κB in endothelial cells by preventing  $I\kappa B\alpha$  degradation through inhibition of  $I\kappa B$  kinase (IKK) activity  $^{105}$ . However, the IKK and  $I\kappa B\alpha$  regulation is intricate, and more research is needed to elucidate how EETs and other EpFAs regulate the activity of NF-κB. Decades of studies indicate that the mechanism of action of EETs and other Ep-PUFAs is through a direct interaction with

peroxisome proliferator-activated receptor (PPAR), a putative membrane-bound G protein-coupled receptor (GPCR), and ion channels such as transient receptor potential TRP channels (Figure 6A) <sup>174,194</sup>. Below, we will discuss several potential targets for Ep-PUFAs in regulating the neuronal function and neuroinflammation.

### 7.3.1. PPARs

PPARs are involved in regulating FAs and glucose metabolism, cellular proliferation, and differentiation, as well as inflammation <sup>236,237</sup>. In this regard, a variety of PUFAs and their oxidized metabolites (epoxy- or hydroxy-PUFA) are potential ligand that can bind to PPARs <sup>238</sup>. Studies have demonstrated that PUFAs bind to PPAR isoforms in the μM range, while oxidized metabolites of PUFAs can activate PPARs at nM level<sup>239,240</sup>. These data suggest that the endogenous PPAR ligands may be the oxidized metabolites of PUFAs.

An *in vitro* study showed that lipopolysaccharide (LPS)-induced inflammation in astrocytes downregulates CYP2J3 and CYP2C11, which are the major CYPs to produce Ep-PUFAs. Interestingly, inhibition of NF- $\kappa$ B restores expression of CYP2J3 and has a limited effect on CYP2C11, suggesting that additional regulatory mechanisms are involved in CYP2C11 regulation during LPS-induced inflammation <sup>241</sup>. One of the alternative mechanisms might be PPAR  $\alpha$  pathways. PPAR $\alpha$  is one of the three ligand-activated transcription factors of PPARs, a subfamily of the nuclear receptor superfamily <sup>242</sup>.

Several studies demonstrated that PPAR- $\alpha$  agonists down-regulate CYP2C11 which is a major CYP involved in the production of Ep-PUFAs. This result suggested that PPAR- $\alpha$  agonist could

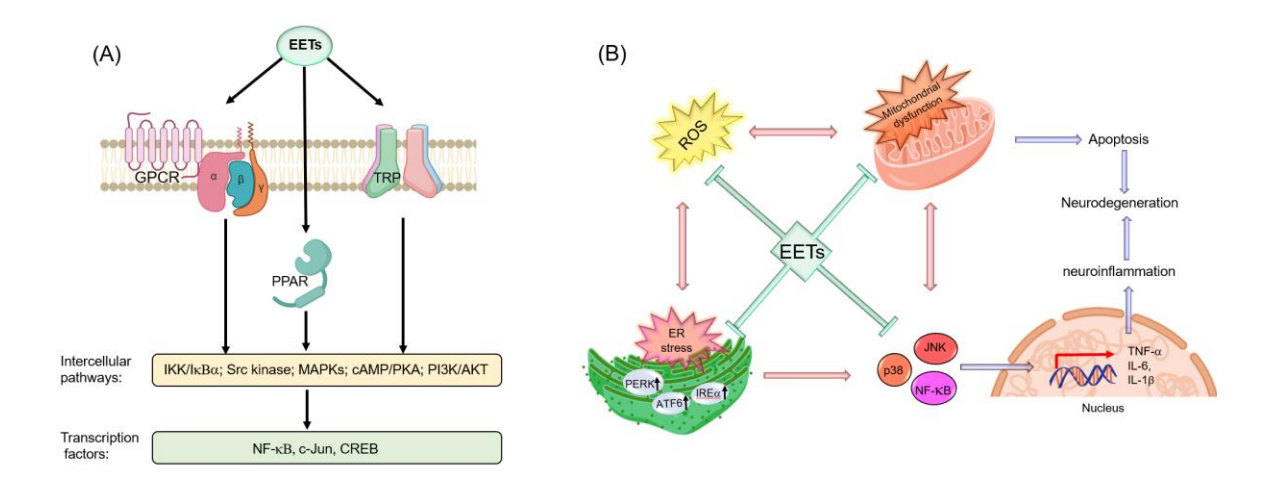


**Figure 6.** A) Mechanisms of action of EETs through three main EETs cellular targets. Verity of EET functions occur through PPAR-, TRP-, and GPCR-dependent mechanism, which activates intercellular pathways that modulate transcription factors in the target cell; B) The possible anti-inflammatory mechanism of EETs. EETs: epoxyeicosatrienoic acids, PPAR: peroxisome proliferator-activated receptor, TRP: transient receptor potential channel, GPCR: G protein-coupled receptor; ROS: reactive oxygen species; IRE1α:inositol-requiring enzyme, PERK: protein kinase R-like endoplasmic reticulum kinase, and ATF6: activating transcription factor 6. Figure is in some parts created with biorender.com.

affects neuroinflammation through modulating the endogenous level of Ep-PUFAs  $^{243-245}$ . On the other hand, Wary *et al.* demonstrated that overexpression of human CYP2J2 in HEK293 cells has inductive effects on all three subfamilies of PPAR (i.e., PPAR $\alpha$ , - $\beta$ / $\delta$ , and - $\gamma$ ) reporter gene activity  $^{106}$ . Furthermore, IL-1 $\beta$ -induced NF- $\kappa$ B reporter activity was significantly inhibited in cells expressing the specific combination of CYP2J2 and PPAR $\alpha$ . They also found that the 8,9-EET, and 11,12-EET, but not 14,15-EET could activate PPAR $\alpha$   $^{106}$ . Consistent with the Node *et al.* found that 11,12-EET has anti-inflammatory effects, and suggested PPAR $\alpha$  as an anti-inflammatory target for 11,12-EET and CYP2J2  $^{105}$ . Liu *et al.* also found that treating endothelial cells either by EETs or AUDA increases the anti-inflammatory response, and further treatment by GW9662, a PPAR $\gamma$  inhibitor, significantly abolished the EET-mediated anti-inflammatory effect, potentially by preventing I $\kappa$ B degradation abolished the EET-mediated anti-inflammatory effect, PPAR. For instance, PPAR activation may also be possible, as 17,18-EEQ inhibits tumor necrosis factor  $\alpha$ -induced inflammation in human bronchi, which is sensitive to PPAR $\gamma$  inhibition  $^{247}$ . These

studies suggest that PPARs could be potential receptor targets for Ep-PUFAs in regulating the inflammatory response. However, how PPAR activation could mediate the effects of EETs is still unclear, mainly because some of the early sEH inhibitors could also cause PPAR $\alpha$  activation through off-target effects  $^{248}$ .

### 7.3.2. TRP channels

Transient receptor potential channels are non-selective cationic channels, which can control various cellular functions <sup>249</sup>. These channels, upon activation, depolarize the cell, which leads to activation or inactivation of specific voltage-gated ion channels and Ca<sup>2+</sup> homeostasis. TRP channels, especially TRP vanilloid (TRPV), TRP ankyrin (TRPA), and TRP canonical (TRPC) are highly expressed in the brain, and play significant roles in brain development, synaptic transmission, neurogenesis, and neuroinflammation by regulating neuronal and glial functions <sup>250–253</sup>. The molecular mechanism of TRP channel regulation is yet to be elucidated, however, several findings suggested that their activity are modulated by various PUFA metabolites, in particular Ep-PUFAs <sup>249,254</sup>.

Several studies indicated different Ep-PUFAs as potential ligands for TRP channels. Watanabe *et al.* found that 5,6-EET activates TRPV4 in murine endothelial cells to induce hyperpolarization <sup>255</sup>. Vriens *et al.* also implicated 5,6-EET, 8,9-EET as direct TRPV4 agonists by studying mouse aortic endothelial cells. They also showed that pharmaceutical modulation of CYP2C9 induced robust Ca<sup>2+</sup> responses by TRPV4 stimuli such as AA and cell swelling, while CYP2C9 inhibition abolished the response to stimuli. None of these effects were observed in TRPV4<sup>-/-</sup> mice <sup>256</sup>. In addition, some studies have shown that 11,12-EET can stimulate TRPV4 in cerebral artery smooth muscle cells leading to hyperpolarization, an increase in the BKCa on the glial cell membrane, and a regulation of neurovascular coupling <sup>257,258</sup>. Furthermore, using *in vivo* 

screening in a transgenic *C. elegans* model expressing rat TRPV4, Caires *et al.* indicated that 17,18-EEQ is necessary for the function of this channel<sup>259</sup>. Also, genetic ablation and diet supplementation revealed a decrease in TRPV4 activity when PUFAs and related eicosanoid levels were reduced <sup>259</sup>.

Interestingly, studies found that EETs can bind to multiple TRP channels independent of Ca<sup>2+</sup> signaling <sup>260,261</sup>. For instance, even though 5,6 EET can activate TRPV4 in colonic afferents and potentially cause visceral hyperalgesia, it acts as a TRPA1 activator and causes a TRPV4independent Ca<sup>2+</sup> transients in the lumbar DRG neurons L4 and L5 <sup>262–264</sup>. Sisignano et al. also observed an increase in 5,6-EET levels of the dorsal spinal cord and dorsal root ganglia (DRG) during capsaicin-induced nociception<sup>264</sup>. They also found that 5,6-EET treatment can induce a calcium flux in cultured DRG neurons, while this treatment has no effect in TRPA1 negative cells <sup>264</sup>. Brenneis et al. found that 8,9-EET can significantly increase the amplitude of Allyl isothiocyanate- (AITC) induced calcium increases in cultured DRG neurons through activation and sensitization of TRPA1 channels 265. Liu et al. demonstrated that sEH inhibition of aortic vascular smooth muscle cells with 8-HUDE can increase vascular tone, calcium flux, and upregulation of TRPC1 and C6 <sup>266</sup>. Interestingly, another study by Fleming et al. showed that 11,12-EET enhances intracellular translocation of activated TPRC6 channels to the plasma membrane, indicating a possible connection to hyperpolarization <sup>267</sup>. 11,12 EET was also reported to activate a TRPV4-TRPC1-BKCa complex in smooth muscle cells <sup>268</sup>, but it remains to be shown whether such channel complexes also exist in neurons. These studies reveal the complexity of how Ep-PUFAs affect TRP channels with multiple possible mechanisms, which depends on the compound, tissue tested, and receptor expression.

#### 7.3.3 GPCRs

G-protein coupled receptors (GPCRs) such as chemokine receptors, eicosanoid receptors, histamine receptors, and adenosine receptors are the largest family of membrane-bound proteins, and of more than 370 identified non-sensory GPCRs, about 90% are expressed in the brain <sup>269,270</sup>. The role of GPCRs in the brain includes, but is not limited to, appetite, mood, inflammation, pain, synaptic transmission, as well as cognition <sup>271</sup>. Also, these receptors are involved in the pathogenesis of several neurodegenerative diseases such as AD, PD, and HD <sup>269,270,272</sup>. A more comprehensive discussion on the GPCRs involved in the pathogenesis neuroinflammation and neurodegeneration is covered in related reviews <sup>272–274</sup>.

Even after decades of research, the GPCRs for Ep-PUFAs have yet to be identified. In this regard, Wong *et al.* identified a specific high affinity binding site for 14,15-EET through a series of studies on guinea pig mononuclear (GPM) and human monocyte (U937) cells <sup>275–277</sup>. These studies revealed that the potential binding site of 14,15-EET is saturable and regio- and stereoselective a highest affinity for 14(R), 15(S)-EET compared to other enantiomers. The binding is also sensitive to protease treatment, which indicates that the target is a protein, and is associated with a receptor that can be down regulated by an increase in intracellular cAMP and activation of a protein kinase A signal transduction mechanism, which is consistent with the mechanism of action of GPCRs for other prostanoids <sup>275–277</sup>. Interestingly, elevated levels of cAMP, associated with the PKA activation, are able to inhibit NF-kB, exerting anti-inflammatory activity. Therefore, this pathway may explain the anti-inflammatory activity of EETs <sup>278</sup>. In addition, Chen *et al.* also demonstrated that EETs, in particular 14,15-EETs, can stimulate membrane-associated activities through activation of Src and initiation of a tyrosine kinase phosphorylation cascade <sup>279</sup>. Snyder *et al.* also demonstrated that a 14, 15 EET analog coupled with silica beads, which can only act on

the cell surface, completely retained its ability to inhibit cAMP-stimulated aromatase activity. These data further support possible GPCR targets for 14,15 EETs <sup>280</sup>. Behm *et al.* suggest that EETs may function as an endogenous GPCR antagonist, which can cause anti-inflammatory actions by direct inhibition of thromboxane receptors <sup>281</sup>. However, even after decades of research, researchers have yet to find a specific high affinity GPCR for 14, 15 EETs using an array of isolated tissue/cell biochemical assays and GPCRs screening <sup>281,282</sup>.

Besides 14,15-EETs, the other regioisomers of EETs, 11,12-EET, has been also extensively studied with the hope of identifying a GPCR <sup>108,283–285</sup>. It should be mentioned that in all these studies, non-neural cells were used as target cells, implying that this observation might not be applicable to neuronal cells, as the cell type used can be a key factor to determine the type of GPCR activation by EETs. Bearing these in mind, Mule *et al.* used CA1 pyramidal cells (PCs) in the mouse hippocampus and demonstrated that the 11,12 EET mediated opening of a G protein-coupled inwardly-rectifying potassium (GIRK) channel through the activation of Gi/o proteins, introducing a new EETs-dependent cellular pathway, which remains to be elucidated<sup>286</sup>. The activation of Gi/o proteins corroborates other studies suggesting that EETs are potential target for the μ-opioid receptor, a GPCR system mainly linked to Gi/o proteins <sup>287,288</sup>.

## 7.3.4. Endoplasmic reticulum (ER)

ER stress occurs when the homeostatic protein folding and trafficking in the cell is overwhelmed or unbalanced, leading to the unfolded protein response (UPR) and often to apoptosis <sup>177</sup>. The failure of ER adaptive capacity, which is a hallmark of several neuroinflammatory disorders such as PD and AD, can be induced by different factors including, but not limited to, neurotoxins, unfolded and misfolded proteins, mitochondrial ROS, and high glucose as in diabetes <sup>289–291</sup>. ER stress intersects with many different inflammatory and stress

signaling pathways, such as the NF $\kappa$ B pathway, and thus the therapeutic mechanism(s) of action of Ep-PUFAs may be related to their interactions with the molecular constituents therein <sup>292</sup>. Several studies have shown the effects of Ep-PUFAs on the phosphorylation state of the key ER stress proteins including inositol-requiring enzyme (IRE1 $\alpha$ ), protein kinase R-like endoplasmic reticulum kinase (PERK) and activating transcription factor 6 (ATF6) (Figure 6B). For instance, Bettaiab *et al.* observed that a high fat diet (HFD)- and chemical-induced ER stress increased sEH expression. Meanwhile, sEH ablation or its pharmacological inhibition attenuated this stress by decreasing the phosphorylation of IRE1 $\alpha$ , PERK, and ATF6 <sup>293</sup>. In addition, Ren *et al.* found that administration of TPPU or sEH deletion suppressed these markers in the striatum of MPTP-treated mice <sup>19</sup>.

Even though the actual mechanism behind the Ep-PUFAs effects on the ER stress pathway remains to be revealed, there are several points of evidence. EETs may act partly through the PI3K/Akt pathway. For instance Dhanasekaran *et al.* demonstrated that treatment of HL-1 cardiac muscle cells and HL-1 cardiac muscle cells with 14,15-EETs under hypoxia/reoxygenation conditions increased AKT phosphorylation PIP3 level, indicating that EETs can act at least partly through the PI3K/AKT pathway<sup>294</sup>. ER-stress suppression through AKT activation prevents apoptosis by upregulating apoptotic protein inhibitor family proteins such as XIAP, cIAP-2, and mitochondrial Bcl-2 <sup>295–297</sup>. Ep-PUFAs can also acts through JNK and p38 MAPK pathways. Inceoglu *et al.* observed that kinase mediators of neuropathic pain, p38, and JNK can be effectively blocked by inhibition of sEH <sup>298</sup>. Despite this evidence, the direct interaction between Ep-PUFAs and the ER has not yet been reported. Thus, a better understanding of the nature of involvement of Ep-PUFAs on ER stress can lead to new therapeutic strategies to reduce the incidence of neuroinflammatory disorders.

#### 7.3.5 Mitochondria

In an effort to find the underlying mechanisms of age-associated neurodegeneration, the main hypothesis is impairment in protein quality control systems and protein accumulation  $^{1,221}$ . An alternative mechanism that recently emerged is the loss of mitochondrial function and uncontrolled production of ROS leading to neurodegeneration, particularly in PD and AD development. For instance, it has been shown that age-related mitochondrial dysfunction affects both expression and processing of amyloid- $\beta$  protein precursor (A $\beta$ PP), which initiates the A $\beta$  accumulation, the primary hallmark of ADs  $^{299}$ . Also, there is evidence of disruption in mitophagy (a selective and programmed degradation of damaged mitochondria by autophagy) by aging, leading to an increase in the damaged mitochondrion, which can also contribute to age-related neurodegeneration  $^{299,300}$ . Mitochondrial dysfunction has been well documented in AD and PD  $^{1,2,299-301}$ .

Recent studies have revealed the promising potential of Ep-PUFAs in rescuing mitochondrial function in various models <sup>302,303</sup>. For instance, Samokhvalov *et al.* indicates that 14,15-EET can protect mitochondrial functions in starvation-induced injury, probably through regulation of the autophagic response <sup>304</sup>. Katragadda *et al.* also found that exogenous supplementation of 14,15-EET protects mitochondrial function and reduced cellular stress in isolated rat cardiomyocytes and H9c2 cells, which is suggested to be through the mitoK<sup>+</sup> channel-dependent pathway that preserves mitochondrial membrane potential under cellular stress <sup>305</sup>. Wang *et al.* also demonstrated that 14,15-EET can protect cortical neurons from apoptosis in oxygen–glucose deprivation (OGD) condition by elevating mitochondrial biogenesis, and acts through activation of PGC-1α and NRF-1 mediated by cAMP response element-binding protein (CREB) <sup>303</sup>.

EETs have also been shown to preserve mitochondrial function through mitigating the uncontrolled release of ROS and decreasing ER response (Figure 6B). All of these attenuate

cellular damages accompanied by neuroinflammatory pathology <sup>302,306,307</sup>. EETs have been shown to induce some cellular mechanisms to buffer free radicals, hence protecting sub-cellular organelles from oxidative damage <sup>193,308</sup>. Liu *et al.* indicated that 11,12-EET-pretreatment of carcinoma cells can attenuate the ROS-mediated mitochondrial dysfunction through induction of antioxidant proteins superoxide dismutase and catalase, thereby mitigating different major apoptotic pathways such as activation of p38 MAP kinase, c-Jun NH2-terminal kinase, as well as caspase-3 and -9 <sup>309</sup>. Qu *et al.* also found an anti-apoptotic effect of 14, 15-EET in cerebral microvascular smooth muscle cells under OGD conditions by reducing the free radical level through the JNK/c-Jun and mTOR signaling pathways <sup>310</sup>. Nevertheless, the specific signaling pathways the result in direct effect of EETs on mitochondrial function and ROS level in glia and neuronal cells is still unknown.

# 8. C. elegans and neurodegeneration

Caenorhabditis elegans (*C. elegans*) possess exceptional features such as well-annotated genome, genetically malleable, short lifespan, simple anatomy, transparency, as well as low cost and easy maintenance, making this nematode as a promising animal model to study different biological process. Table 2 compares the *C. elegans* nematode with *fat-1* mice model with regards to neurodegeneration study.

**Table 2.** comparison between *C. elegans* and mice for neurodegeneration study

Animal		Price (per	Maintenance	Neuron	Neurodegeneration	PUFA	Interference
Model	Lifespan	animal)		analysis	study	metabolism	
			Needs	Needs	Mostly needs to be	Needs	Other PUFA oxygenase
M	1-3 years	\$225	animal care	surgery	induced	supplementation	(LOX*, COX**)
9-12							
	2-3	\$10	Easy	Transpare	Both inducing and	Make all PUFA de	NO homologue of LOX or
	weeks		culturing	nt	ageing	novo /Genetically	COX has been found
						malleable	

<sup>\*</sup>LOX: Lipoxygenase enzyme \*\* Cyclooxygenase Enzyme

Besides the general advantages, there are several other features that make C. elegans an excellent animal model to study neurodegeneration, in particular those related to the CYP-EH metabolites and neurodegeneration. 1) About 60-80% of genes in C. elegans possess human orthologues, and around 42% of human disease genes have orthologues in this nematode 311. Furthermore, various biological signaling pathways in humans, including aging pathways, are evolutionarily conserved from C. elegans <sup>312</sup>, making this nematode a promising biological model to study different age-related biological processes. 2) C. elegans can synthesize a wide spectrum of ω-3 and ω-6 PUFAs de novo, which have to intake from their diets<sup>34</sup>. The worms also can synthesize a vast majority of CYP450 metabolites (including Ep-PUFAs), and express various mammalian counterparts CYP450 34,313; while other pathways within the arachidonic cascade are not found in C. elegans (based on our BLAST search at WormBase.org) which facilitate the investigation of Ep-PUFA metabolism with minimum interference. 3) Hermaphrodite C. elegans has a nervous system containing 302 neurons, including GABAergic, glutamatergic, and aminergic such as dopaminergic (DAergic), serotonergic, and cholinergic neurons, with great similarity in neuron signaling to human <sup>314</sup>; These nematodes are also a well-established model organism for AD and aging studies<sup>315</sup>. Multiple aging, neurodegeneration, and disease targets such as TDP-43 have been identified or confirmed in C. elegans, and the results are translatable to mammalian models and likely humans<sup>315–319</sup>. Last but not least, the absence of inflammatory cells, microglia, and astrocytes in C. elegans will allow us to illustrate the relation between aging and PUFA metabolites independent of inflammation. Taking all these into account, C. elegans is an ideal model system for this proof-of-concept project and makes it possible to apply the finding of this project to more complex mammalian models and humans in the future.

# 9. Ferroptosis and neurodegeneration

Ferroptosis is a recently discovered form of iron-dependent cell death, distinct from other types of cell death such as apoptosis and necrosis. This process primarily involves three key metabolic pathways related to thiol, lipid, and iron, which result in iron-dependent lipid peroxidation generation and ultimately lead to cell death  $^{320,321}$ . The initial theoretical idea of ferroptosis may have developed from nutrient (in particular cysteine) depletion-induced cancer cell death and "oxytosis"  $^{322-325}$ . In 2003, Erastin was discovered to be lethal when combined with the expression of the engineered mutant RAS oncogene in human foreskin fibroblasts (BJeLR cells)  $^{326}$ . However, subsequent research has not found enough targets for cell death induced by Erastin  $^{327}$ . In 2008, RAS-selective lethal small molecules (RSL)-3 and RSL-5 were identified as synthetic compounds that selectively killed BJeLR cells through a non-apoptotic mechanism  $^{328}$ . It was only in 2012 that this form of cell death was termed ferroptosis, and it was revealed that Erastin inhibits cystine uptake by the cystine/glutamate antiporter (system  $X_c$ ), leading to cell death  $^{329}$ . Figure 7 summarizes the timeline of ferroptosis research.

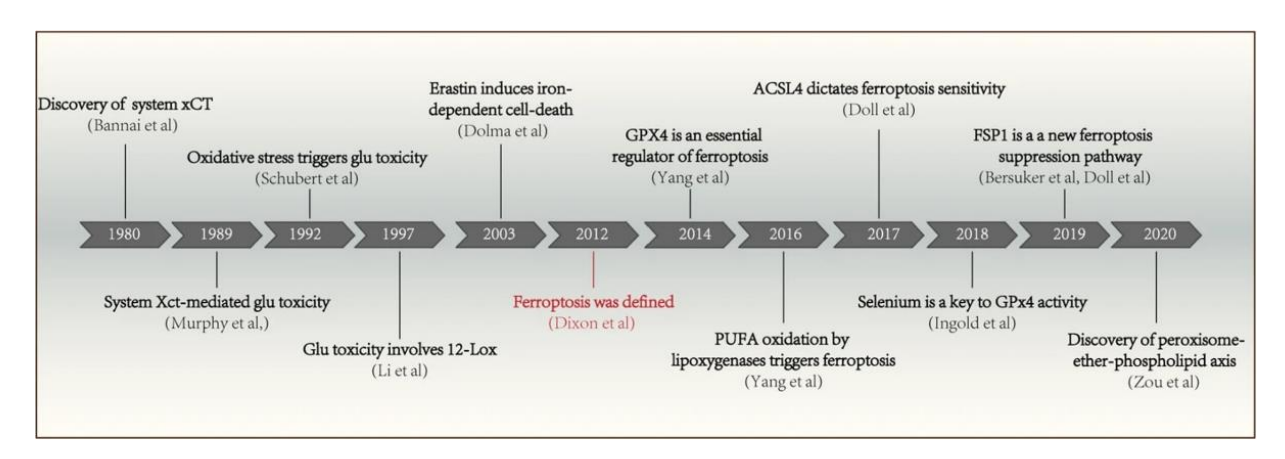


**Figure 7.** The timeline of ferroptosis research. Taken form Ref [320]

While the entire mechanism of ferroptosis is yet to be understood, two main factors seem to be highly involved in ferroptosis: (i) Iron accumulation, and (ii) lipid peroxidation. Traditional ferroptosis activators, such as Erastin and RSL3, have been found to increase intracellular iron accumulation by inhibiting the antioxidant system <sup>329</sup>. This excess iron can directly produce a large amount of reactive oxygen species (ROS) through the Fenton reaction, subsequently leading to increased oxidative damage <sup>329</sup>. Moreover, the interplay between systemic and local cellular iron regulation influences ferroptosis sensitivity <sup>320</sup>. Several studies also found that targeting genes associated with iron overload or utilizing iron-chelating agents can effectively inhibit cell death induced by ferroptosis <sup>320,321,330–334</sup>. The reason behind the exclusive ability of iron, as opposed to other metals like zinc, which also generate reactive oxygen species (ROS) via the Fenton reaction, to induce ferroptosis remains uncertain <sup>321,335</sup>. A potential explanation is that an overload of iron triggers particular downstream effectors that play a role in carrying out ferroptosis following the creation of lipid ROS.

Lipid peroxidation of PUFA serves as the catalyst for initiating ferroptosis <sup>336,337</sup>. Lipid peroxides, primarily lipid hydroperoxides (L-OOH), possess the capacity to inflict damage upon the lipid bilayer of the plasma membrane<sup>334</sup>. The physical properties of lipid bilayers are significantly altered by membrane lipid peroxidation, leading to ion gradient disruption, reduced membrane fluidity, decelerated lateral diffusion, heightened membrane permeability, and the loss of ionic homeostasis <sup>334,338–340</sup>. Thus, Oxidized PUFA fragments are speculated to damage membranes and release toxic reactive fragments into cells, possibly disrupting other cellular processes <sup>341,342</sup>. It is worth mentioning that while the main hypothesis of lipid peroxidation in ferroptosis is related to the plasma membrane, peroxidation of PUFA can also happen in other subcellular locations like mitochondria, endoplasmic reticulum (that contains the largest pool of lipids in cells), and lysosomes<sup>341</sup>. Also, the vulnerability of each organelle to lipid peroxidation

may be different because of differences in lipid compositions, iron storage, GSH level, GPX localization.

Overall, while iron regulation and lipid peroxidation have found to be two major contributors in ferroptosis, further investigation is required to get better insight into the upstream and downstream of ferroptosis induced cell death. In this regard, several different ferroptosis inducer and inhibitors have been found that could be used to further understand the ferroptosis through in vitro and in vivo analysis (**Table 3**)

**Table 3.** Different classes of ferroptosis inducers and inhibitors. Adapted from Ref 341.

	Class	Characteristics	Impact on Ferroptosis	Compound Examples			
Ferroptosis Inducers	1	Inhibition Of system X <sub>c</sub>	Prevents cystine import, causes GSH depletion and loss Of GPX4 activity	Erastin, PE, IKE, Other erastin analogs, sulfasalazine, sorafenib, glutamate			
	2	Direct inhibition Of GPX4	Covalently interacts with GPX4 and inhibits its enzymatic activity	RSL3, ML162, DPI compounds			
	3	Depletion of GPX4 protein and CoQ10	Depletes GPX4 protein and simultaneously causes depletion of CoQ10 via SQS-mevalonate athwa	FIN56 and CIL56			
	4	Induction of lipid peroxidation	Oxidizes iron, drives lipid peroxidation and indirect inactivation Of GPX4	FIN02			
	Others	BSO, DP12, cisplatin, cysteinase, statins, ferric ammonium citrate, trigonelline, CC14, silica-based nanoparticles, nonthermal plasma					
Ferroptosis Inhibitors	1	Iron chelators	Deplete iron and prevent iron-dependent lipid peroxidation	Deferoxamine, cyclipirox, deferiprone			
	2	Lipophilic antioxidants	Prevent lipid peroxidation	Vitamin E, BHT, Fer-l, liproxstatin-l, XJB-5131, CoQ10			
	3	D.PUFAs	Prevents initiation and propagation of lipid eroxidation	D <sub>4</sub> -Aarachidonic acid, D <sub>10</sub> -Docosahexaenoic acid			
	4	LOX inhibitors	Inactivate LOX and block LOX- induced lipid peroxidation	CDC, baicalein, PD-146176, AA-861, zileuton			
	Others	glutaminolysis inhibitors, cycloheximides beta-mercaptoethanol, dopamine, selenium, vildagliptin.					

Abbreviations: BSO, buthionine sulfoximine; CCl4, carbon tetrachloride; CIL56, caspase-independent lethal 56; CoQ10, coenzyme Q10; DPI, divehydroxytoluene; cal inhibitor; FIN56, ferroptosis inducer 56; FIN02, ferroptosis inducer endoperoxide; GPX4, glutathione peroxidase 4; GSH, glutathione; IKE, imidazole ketone erastin; ML162, Molecular Libraries 162; PE, piperazine Erastin; RSL3, RAS-selective lethal 3; SQS, squalene synthase, AA, arachidonic acid; BHT, butylated hydroxytoluene; D-PUFA, deuterated polyunsaturated fatty acid; per-I, ferrostatin-l; LOX, lipoxygenase

## 10. Future Directions

PUFAs are an emerging class of dietary components that play a critical role in aging and neurodegeneration. However, the effect and the underlying mechanism of PUFAs on neurodegeneration remains largely unknown. In this review, we discussed that downstream CYP

PUFA metabolites, whose endogenous levels are greatly affected by diet, are largely beneficial for neurodegenerative diseases. Studies have shown that the anti-inflammatory effects of CYP PUFA metabolites, particularly Ep-PUFAs, could alleviate neuroinflammation, which is beneficial in neurodegenerative diseases. Ep-PUFAs enhance the production of anti-inflammatory cytokines and decrease the production of pro-inflammatory cytokines in murine models of Alzheimer disease and Parkinson's diseases. While the beneficial effects of Ep-PUFAs in NDs have been well established with inhibition of sEH, which hydrolyzes endogenous Ep-PUFAs, the molecular mechanisms have not been solved. As discussed above, there are several proposed molecular mechanisms through which Ep-PUFAs modulate neurodegeneration. Understanding the molecular signaling mechanism of Ep-PUFAs in neurodegeneration could help us to design a better diet for the aging population and could identify potential new therapeutic targets for neurodegenerative diseases.

Studying the molecular mechanisms of neurodegeneration is difficult, due to their complexity and lack of a translatable *in vitro* model. As discussed, it becomes even more challenging with Ep-PUFAs because their protein target has yet to be identified. To date, a better way to study neurodegeneration remains animal models; however, these models are expensive and low throughput. Fortunately, due to the recent development of novel genetic models including *C. elegans* and Zebrafish, our understanding of the mechanism of neurodegeneration can be greatly accelerated. Both *C. elegans* and Zebrafish are highly homologous to humans, and most of the disease-causing genes in humans have the orthologues in both *C. elegans* and Zebrafish. These models will facilitate the investigation of the molecular mechanism(s) driving neurodegeneration. Our laboratory is currently studying the mechanism of CYP PUFA metabolism in neurodegeneration using *C. elegans* as a biological model.

As we discussed, there is an unmet need to develop novel therapies for neurodegenerative diseases. In this review, we have shown that sEH could be a novel target for Alzheimer disease and Parkinson's disease. However, there are challenges in developing sEH inhibitors to treat NDs. Although the sEH inhibitors used in the murine model can cross the blood brain barrier (BBB), they require further optimization to better cross the BBB with improved physical properties for formulation. Ep-PUFAs are a class of CYP PUFA metabolites that contains both  $\omega$ -3 and  $\omega$ -6 Ep-PUFAs. However, in the reported studies, the active Ep-PUFAs have yet to be identified. Since the endogenous levels of  $\omega$ -3 and  $\omega$ -6 Ep-PUFA are greatly impacted by the diet, the beneficial effects of an sEH inhibitor for NDs may be greatly impacted by patient diets. Therefore, an alternate approach for developing a new therapy for neurodegenerative diseases would be designing a mimic of the active Ep-PUFAs that would not be affected by diet or  $\omega$ -3 supplementation. All in all, CYP PUFA metabolism is an exciting pathway for research in neurodegeneration, and more research is needed to better understand the mechanism(s) behind the effects of CYP PUFA metabolites in neurodegeneration.

#### **BIBLIOGRAPHY**

- (1) Gan, L.; Cookson, M. R.; Petrucelli, L.; La Spada, A. R. Converging Pathways in Neurodegeneration, from Genetics to Mechanisms. *Nat. Neurosci.* **2018**, *21* (10), 1300–1309. https://doi.org/10.1038/s41593-018-0237-7.
- (2) Bishop, N. A.; Lu, T.; Yankner, B. A. Neural Mechanisms of Ageing and Cognitive Decline. *Nature* **2010**, *464* (7288), 529–535. https://doi.org/10.1038/nature08983.
- (3) Hou, Y.; Dan, X.; Babbar, M.; Wei, Y.; Hasselbalch, S. G.; Croteau, D. L.; Bohr, V. A. Ageing as a Risk Factor for Neurodegenerative Disease. *Nat. Rev. Neurol.* **2019**, *15* (10), 565–581. https://doi.org/10.1038/s41582-019-0244-7.
- (4) Migliore, L.; Coppedè, F. Genetics, Environmental Factors and the Emerging Role of Epigenetics in Neurodegenerative Diseases. *Mutat. Res.* **2009**, *667* (1–2), 82–97. https://doi.org/10.1016/j.mrfmmm.2008.10.011.
- (5) Coppedè, F.; Mancuso, M.; Siciliano, G.; Migliore, L.; Murri, L. Genes and the Environment in Neurodegeneration. *Biosci. Rep.* **2006**, *26* (5), 341–367. https://doi.org/10.1007/s10540-006-9028-6.
- (6) Moore, K.; Hughes, C. F.; Ward, M.; Hoey, L.; McNulty, H. Diet, Nutrition and the Ageing Brain: Current Evidence and New Directions. *Proc. Nutr. Soc.* **2018**, 77 (2), 152–163. https://doi.org/10.1017/s0029665117004177.
- (7) Shahidi, F.; Ambigaipalan, P. Omega-3 Polyunsaturated Fatty Acids and Their Health Benefits. *Annu. Rev. Food Sci. Technol.* **2018**, *9*, 345–381. https://doi.org/10.1146/annurevfood-111317-095850.
- (8) Bishop-Bailey, D.; Thomson, S.; Askari, A.; Faulkner, A.; Wheeler-Jones, C. Lipid-Metabolizing CYPs in the Regulation and Dysregulation of Metabolism. *Annu. Rev. Nutr.* **2014**, *34* (1), 261–279. https://doi.org/10.1146/annurev-nutr-071813-105747.
- (9) Wall, R.; Ross, R. P.; Fitzgerald, G. F.; Stanton, C. Fatty Acids from Fish: The Anti-Inflammatory Potential of Long-Chain Omega-3 Fatty Acids. *Nutr. Rev.* **2010**, *68* (5), 280–289. https://doi.org/10.1111/j.1753-4887.2010.00287.x.
- (10) de Lau, L. M. L.; Bornebroek, M.; Witteman, J. C. M.; Hofman, A.; Koudstaal, P. J.; Breteler, M. M. B. Dietary Fatty Acids and the Risk of Parkinson Disease: The Rotterdam Study. *Neurology* **2005**, *64* (12), 2040–2045. https://doi.org/10.1212/01.WNL.0000166038.67153.9F.
- (11) Cardoso, H. D.; dos Santos Junior, E. F.; de Santana, D. F.; Gonçalves-Pimentel, C.; Angelim, M. K.; Isaac, A. R.; Lagranha, C. J.; Guedes, R. C. A.; Beltrão, E. I.; Morya, E.; Rodrigues, M. C. A.; Andrade-da-Costa, B. L. da S. Omega-3 Deficiency and Neurodegeneration in the Substantia Nigra: Involvement of Increased Nitric Oxide Production and Reduced BDNF Expression. *Biochim. Biophys. Acta* 2014, 1840 (6), 1902–1912. https://doi.org/10.1016/j.bbagen.2013.12.023.

- (12) Healy-Stoffel, M.; Levant, B. N-3 (Omega-3) Fatty Acids: Effects on Brain Dopamine Systems and Potential Role in the Etiology and Treatment of Neuropsychiatric Disorders. *CNS Neurol. Disord. Drug Targets* **2018**, *17* (3), 216–232. https://doi.org/10.2174/1871527317666180412153612.
- (13) Bazinet, R. P.; Layé, S. Polyunsaturated Fatty Acids and Their Metabolites in Brain Function and Disease. *Nat. Rev. Neurosci.* **2014**, *15* (12), 771–785. https://doi.org/10.1038/nrn3820.
- (14) Ferdouse, A.; Leng, S.; Winter, T.; Aukema, H. M. The Brain Oxylipin Profile Is Resistant to Modulation by Dietary N-6 and n-3 Polyunsaturated Fatty Acids in Male and Female Rats. *Lipids* **2019**, *54* (1), 67–80. https://doi.org/10.1002/lipd.12122.
- (15) Freitas, H. R.; Isaac, A. R.; Malcher-Lopes, R.; Diaz, B. L.; Trevenzoli, I. H.; De Melo Reis, R. A. Polyunsaturated Fatty Acids and Endocannabinoids in Health and Disease. *Nutr. Neurosci.* **2018**, *21* (10), 695–714. https://doi.org/10.1080/1028415x.2017.1347373.
- (16) Inceoglu, B.; Zolkowska, D.; Yoo, H. J.; Wagner, K. M.; Yang, J.; Hackett, E.; Hwang, S. H.; Lee, K. S. S.; Rogawski, M. A.; Morisseau, C.; Hammock, B. D. Epoxy Fatty Acids and Inhibition of the Soluble Epoxide Hydrolase Selectively Modulate GABA Mediated Neurotransmission to Delay Onset of Seizures. *PLoS One* **2013**, 8 (12), e80922. https://doi.org/10.1371/journal.pone.0080922.
- (17) Harris, T. R.; Aronov, P. A.; Jones, P. D.; Tanaka, H.; Arand, M.; Hammock, B. D. Identification of Two Epoxide Hydrolases in Caenorhabditis Elegans That Metabolize Mammalian Lipid Signaling Molecules. *Arch. Biochem. Biophys.* **2008**, *472* (2), 139–149. https://doi.org/10.1016/j.abb.2008.01.016.
- (18) Navarro-Mabarak, C.; Camacho-Carranza, R.; Espinosa-Aguirre, J. J. Cytochrome P450 in the Central Nervous System as a Therapeutic Target in Neurodegenerative Diseases. *Drug Metab. Rev.* **2018**, *50* (2), 95–108. https://doi.org/10.1080/03602532.2018.1439502.
- (19) Ren, Q.; Ma, M.; Yang, J.; Nonaka, R.; Yamaguchi, A.; Ishikawa, K.-I.; Kobayashi, K.; Murayama, S.; Hwang, S. H.; Saiki, S.; Akamatsu, W.; Hattori, N.; Hammock, B. D.; Hashimoto, K. Soluble Epoxide Hydrolase Plays a Key Role in the Pathogenesis of Parkinson's Disease. *Proc. Natl. Acad. Sci. U. S. A.* **2018**, *115* (25), E5815–E5823. https://doi.org/10.1073/pnas.1802179115.
- (20) Morris, J. K.; Piccolo, B. D.; John, C. S.; Green, Z. D.; Thyfault, J. P.; Adams, S. H. Oxylipin Profiling of Alzheimer's Disease in Nondiabetic and Type 2 Diabetic Elderly. *Metabolites* **2019**, *9* (9), 177. https://doi.org/10.3390/metabo9090177.
- (21) Wagner, K.; Vito, S.; Inceoglu, B.; Hammock, B. D. The Role of Long Chain Fatty Acids and Their Epoxide Metabolites in Nociceptive Signaling. *Prostaglandins Other Lipid Mediat.* **2014**, *113–115*, 2–12. https://doi.org/10.1016/j.prostaglandins.2014.09.001.
- (22) Konkel, A.; Schunck, W.-H. Role of Cytochrome P450 Enzymes in the Bioactivation of Polyunsaturated Fatty Acids. *Biochim. Biophys. Acta* **2011**, *1814* (1), 210–222. https://doi.org/10.1016/j.bbapap.2010.09.009.

- (23) Spector, A. A.; Kim, H.-Y. Cytochrome P450 Epoxygenase Pathway of Polyunsaturated Fatty Acid Metabolism. *Biochim. Biophys. Acta* **2015**, *1851* (4), 356–365. https://doi.org/10.1016/j.bbalip.2014.07.020.
- (24) Soto, C.; Pritzkow, S. Protein Misfolding, Aggregation, and Conformational Strains in Neurodegenerative Diseases. *Nat. Neurosci.* **2018**, *21* (10), 1332–1340. https://doi.org/10.1038/s41593-018-0235-9.
- (25) Dugger, B. N.; Dickson, D. W. Pathology of Neurodegenerative Diseases. *Cold Spring Harb. Perspect. Biol.* **2017**, *9* (7), a028035. https://doi.org/10.1101/cshperspect.a028035.
- (26) Franceschi, C.; Campisi, J. Chronic Inflammation (Inflammaging) and Its Potential Contribution to Age-Associated Diseases. *J. Gerontol. A Biol. Sci. Med. Sci.* **2014**, *69 Suppl I* (Suppl 1), S4-9. https://doi.org/10.1093/gerona/glu057.
- (27) Guzman-Martinez, L.; Maccioni, R. B.; Andrade, V.; Navarrete, L. P.; Pastor, M. G.; Ramos-Escobar, N. Neuroinflammation as a Common Feature of Neurodegenerative Disorders. *Front. Pharmacol.* **2019**, *10*, 1008. https://doi.org/10.3389/fphar.2019.01008.
- (28) Peters, R. Ageing and the Brain. *Postgrad. Med. J.* **2006**, 82 (964), 84–88. https://doi.org/10.1136/pgmj.2005.036665.
- (29) Svennerholm, L.; Boström, K.; Jungbjer, B. Changes in Weight and Compositions of Major Membrane Components of Human Brain during the Span of Adult Human Life of Swedes. *Acta Neuropathol.* **1997**, *94* (4), 345–352. https://doi.org/10.1007/s004010050717.
- (30) Elobeid, A.; Libard, S.; Leino, M.; Popova, S. N.; Alafuzoff, I. Altered Proteins in the Aging Brain. *J. Neuropathol. Exp. Neurol.* **2016**, 75 (4), 316–325. https://doi.org/10.1093/jnen/nlw002.
- (31) Naoe, S.; Tsugawa, H.; Takahashi, M.; Ikeda, K.; Arita, M. Characterization of Lipid Profiles after Dietary Intake of Polyunsaturated Fatty Acids Using Integrated Untargeted and Targeted Lipidomics. *Metabolites* **2019**, *9* (10), 241. https://doi.org/10.3390/metabo9100241.
- (32) Ferdouse, A.; Leng, S.; Winter, T.; Aukema, H. M. Dietary N-6 and n-3 PUFA Alter the Free Oxylipin Profile Differently in Male and Female Rat Hearts. *Br. J. Nutr.* **2019**, *122* (3), 252–261. https://doi.org/10.1017/S0007114519001211.
- (33) Monroig, Ó.; Tocher, D. R.; Navarro, J. C. Biosynthesis of Polyunsaturated Fatty Acids in Marine Invertebrates: Recent Advances in Molecular Mechanisms. *Mar. Drugs* **2013**, *11* (10), 3998–4018. https://doi.org/10.3390/md11103998.
- (34) Mokoena, N. Z.; Sebolai, O. M.; Albertyn, J.; Pohl, C. H. Synthesis and Function of Fatty Acids and Oxylipins, with a Focus on Caenorhabditis Elegans. *Prostaglandins Other Lipid Mediat.* **2020**, *148* (106426), 106426. https://doi.org/10.1016/j.prostaglandins.2020.106426.

- (35) Nakamura, M. T.; Nara, T. Y. Structure, Function, and Dietary Regulation of Delta6, Delta5, and Delta9 Desaturases. *Annu. Rev. Nutr.* **2004**, *24* (1), 345–376. https://doi.org/10.1146/annurev.nutr.24.121803.063211.
- (36) Ameur, A.; Enroth, S.; Johansson, A.; Zaboli, G.; Igl, W.; Johansson, A. C. V.; Rivas, M. A.; Daly, M. J.; Schmitz, G.; Hicks, A. A.; Meitinger, T.; Feuk, L.; van Duijn, C.; Oostra, B.; Pramstaller, P. P.; Rudan, I.; Wright, A. F.; Wilson, J. F.; Campbell, H.; Gyllensten, U. Genetic Adaptation of Fatty-Acid Metabolism: A Human-Specific Haplotype Increasing the Biosynthesis of Long-Chain Omega-3 and Omega-6 Fatty Acids. *Am. J. Hum. Genet.* **2012**, *90* (5), 809–820. https://doi.org/10.1016/j.ajhg.2012.03.014.
- (37) Koletzko, B.; Reischl, E.; Tanjung, C.; Gonzalez-Casanova, I.; Ramakrishnan, U.; Meldrum, S.; Simmer, K.; Heinrich, J.; Demmelmair, H. FADS1 and FADS2 Polymorphisms Modulate Fatty Acid Metabolism and Dietary Impact on Health. *Annu. Rev. Nutr.* **2019**, *39* (1), 21–44. https://doi.org/10.1146/annurev-nutr-082018-124250.
- (38) Steer, C. D.; Davey Smith, G.; Emmett, P. M.; Hibbeln, J. R.; Golding, J. FADS2 Polymorphisms Modify the Effect of Breastfeeding on Child IQ. *PLoS One* **2010**, *5* (7), e11570. https://doi.org/10.1371/journal.pone.0011570.
- (39) Moltó-Puigmartí, C.; Plat, J.; Mensink, R. P.; Müller, A.; Jansen, E.; Zeegers, M. P.; Thijs, C. FADS1 FADS2 Gene Variants Modify the Association between Fish Intake and the Docosahexaenoic Acid Proportions in Human Milk. *Am. J. Clin. Nutr.* **2010**, *91* (5), 1368–1376. https://doi.org/10.3945/ajcn.2009.28789.
- (40) Xie, L.; Innis, S. M. Genetic Variants of the FADS1 FADS2 Gene Cluster Are Associated with Altered (n-6) and (n-3) Essential Fatty Acids in Plasma and Erythrocyte Phospholipids in Women during Pregnancy and in Breast Milk during Lactation. *J. Nutr.* **2008**, *138* (11), 2222–2228. https://doi.org/10.3945/jn.108.096156.
- (41) Hernell, O.; Holmgren, G.; Jagell, S. F.; Johnson, S. B.; Holman, R. T. Suspected Faulty Essential Fatty Acid Metabolism in Sjögren-Larsson Syndrome. *Pediatr. Res.* **1982**, *16* (1), 45–49. https://doi.org/10.1203/00006450-198201001-00009.
- (42) Brookes, K. J.; Chen, W.; Xu, X.; Taylor, E.; Asherson, P. Association of Fatty Acid Desaturase Genes with Attention-Deficit/Hyperactivity Disorder. *Biol. Psychiatry* **2006**, *60* (10), 1053–1061. https://doi.org/10.1016/j.biopsych.2006.04.025.
- (43) Fan, Y.-Y.; Monk, J. M.; Hou, T. Y.; Callway, E.; Vincent, L.; Weeks, B.; Yang, P.; Chapkin, R. S. Characterization of an Arachidonic Acid-Deficient (Fads1 Knockout) Mouse Model. *J. Lipid Res.* **2012**, *53* (7), 1287–1295. https://doi.org/10.1194/jlr.M024216.
- (44) Stoffel, W.; Holz, B.; Jenke, B.; Binczek, E.; Günter, R. H.; Kiss, C.; Karakesisoglou, I.; Thevis, M.; Weber, A.-A.; Arnhold, S.; Addicks, K. Delta6-Desaturase (FADS2) Deficiency Unveils the Role of Omega3- and Omega6-Polyunsaturated Fatty Acids. *EMBO J.* **2008**, 27 (17), 2281–2292. https://doi.org/10.1038/emboj.2008.156.

- (45) Gromovsky, A. D.; Schugar, R. C.; Brown, A. L.; Helsley, R. N.; Burrows, A. C.; Ferguson, D.; Zhang, R.; Sansbury, B. E.; Lee, R. G.; Morton, R. E.; Allende, D. S.; Parks, J. S.; Spite, M.; Brown, J. M. Δ-5 Fatty Acid Desaturase FADS1 Impacts Metabolic Disease by Balancing Proinflammatory and Proresolving Lipid Mediators. *Arterioscler. Thromb. Vasc. Biol.* 2018, 38 (1), 218–231. https://doi.org/10.1161/ATVBAHA.117.309660.
- (46) Ghasemi Fard, S.; Wang, F.; Sinclair, A. J.; Elliott, G.; Turchini, G. M. How Does High DHA Fish Oil Affect Health? A Systematic Review of Evidence. *Crit. Rev. Food Sci. Nutr.* **2019**, 59 (11), 1684–1727. https://doi.org/10.1080/10408398.2018.1425978.
- (47) Verdier, P.; Beare-Rogers, J. L. The Canadian Nutrient File. J. Can. Diet. Assoc. 1984, 45 (1), 52–55.
- (48) Avallone, R.; Vitale, G.; Bertolotti, M. Omega-3 Fatty Acids and Neurodegenerative Diseases: New Evidence in Clinical Trials. *Int. J. Mol. Sci.* **2019**, *20* (17), 4256. https://doi.org/10.3390/ijms20174256.
- (49) Morris, M. C.; Evans, D. A.; Bienias, J. L.; Tangney, C. C.; Bennett, D. A.; Wilson, R. S.; Aggarwal, N.; Schneider, J. Consumption of Fish and N-3 Fatty Acids and Risk of Incident Alzheimer Disease. *Arch. Neurol.* **2003**, *60* (7), 940–946. https://doi.org/10.1001/archneur.60.7.940.
- (50) Tapiero, H.; Ba, G. N.; Couvreur, P.; Tew, K. D. Polyunsaturated Fatty Acids (PUFA) and Eicosanoids in Human Health and Pathologies. *Biomed. Pharmacother.* **2002**, *56* (5), 215–222. https://doi.org/10.1016/s0753-3322(02)00193-2.
- (51) Christie, W. W.; Harwood, J. L. Oxidation of Polyunsaturated Fatty Acids to Produce Lipid Mediators. *Essays Biochem.* **2020**. https://doi.org/10.1042/EBC20190082.
- (52) de Bus, I.; Witkamp, R.; Zuilhof, H.; Albada, B.; Balvers, M. The Role of N-3 PUFA-Derived Fatty Acid Derivatives and Their Oxygenated Metabolites in the Modulation of Inflammation. *Prostaglandins Other Lipid Mediat.* **2019**, *144* (106351), 106351. https://doi.org/10.1016/j.prostaglandins.2019.106351.
- (53) Czapski, G. A.; Czubowicz, K.; Strosznajder, J. B.; Strosznajder, R. P. The Lipoxygenases: Their Regulation and Implication in Alzheimer's Disease. *Neurochem. Res.* **2016**, *41* (1–2), 243–257. https://doi.org/10.1007/s11064-015-1776-x.
- (54) Li, Z.; Jiang, Y.; Guengerich, F. P.; Ma, L.; Li, S.; Zhang, W. Engineering Cytochrome P450 Enzyme Systems for Biomedical and Biotechnological Applications. *J. Biol. Chem.* **2020**, 295 (3), 833–849. https://doi.org/10.1074/jbc.REV119.008758.
- (55) Omura, T.; Sato, R. A New Cytochrome in Liver Microsomes. *J. Biol. Chem.* **1962**, 237, 1375–1376.
- (56) Guengerich, F. P.; Waterman, M. R.; Egli, M. Recent Structural Insights into Cytochrome P450 Function. *Trends Pharmacol. Sci.* **2016**, *37* (8), 625–640. https://doi.org/10.1016/j.tips.2016.05.006.

- (57) Crane, B. R.; Arvai, A. S.; Ghosh, D. K.; Wu, C.; Getzoff, E. D.; Stuehr, D. J.; Tainer, J. A. Structure of Nitric Oxide Synthase Oxygenase Dimer with Pterin and Substrate. *Science* **1998**, 279 (5359), 2121–2126. https://doi.org/10.1126/science.279.5359.2121.
- (58) Sundaramoorthy, M.; Terner, J.; Poulos, T. L. The Crystal Structure of Chloroperoxidase: A Heme Peroxidase-Cytochrome P450 Functional Hybrid. *J. Inorg. Biochem.* **1995**, *59* (2–3), 427. https://doi.org/10.1016/0162-0134(95)97523-s.
- (59) Ingelman-Sundberg, M. The Human Genome Project and Novel Aspects of Cytochrome P450 Research. *Toxicol. Appl. Pharmacol.* **2005**, 207 (2 Suppl), 52–56. https://doi.org/10.1016/j.taap.2005.01.030.
- (60) Nelson, D. R. The Cytochrome P450 Homepage. *Hum. Genomics* **2009**, *4* (1), 59–65. https://doi.org/10.1186/1479-7364-4-1-59.
- (61) Black, S. D. Membrane Topology of the Mammalian P450 Cytochromes. *FASEB J.* **1992**, *6* (2), 680–685. https://doi.org/10.1096/fasebj.6.2.1537456.
- (62) Šrejber, M.; Navrátilová, V.; Paloncýová, M.; Bazgier, V.; Berka, K.; Anzenbacher, P.; Otyepka, M. Membrane-Attached Mammalian Cytochromes P450: An Overview of the Membrane's Effects on Structure, Drug Binding, and Interactions with Redox Partners. *J. Inorg. Biochem.* **2018**, *183*, 117–136. https://doi.org/10.1016/j.jinorgbio.2018.03.002.
- (63) Guengerich, F. P. Human Cytochrome P450 Enzymes. In *Cytochrome P450*; Springer International Publishing: Cham, 2015; pp 523–785. https://doi.org/10.1007/978-3-319-12108-6 9.
- (64) Preissner, S. C.; Hoffmann, M. F.; Preissner, R.; Dunkel, M.; Gewiess, A.; Preissner, S. Polymorphic Cytochrome P450 Enzymes (CYPs) and Their Role in Personalized Therapy. *PLoS One* **2013**, 8 (12), e82562. https://doi.org/10.1371/journal.pone.0082562.
- (65) Klingenberg, M. Pigments of Rat Liver Microsomes. *Arch. Biochem. Biophys.* **1958**, *75* (2), 376–386. https://doi.org/10.1016/0003-9861(58)90436-3.
- (66) Garfinkel, D. Studies on Pig Liver Microsomes. I. Enzymic and Pigment Composition of Different Microsomal Fractions. *Arch. Biochem. Biophys.* **1958**, 77 (2), 493–509. https://doi.org/10.1016/0003-9861(58)90095-x.
- (67) Pessayre, D.; Mazel, P.; Descatoire, V.; Rogier, E.; Feldmann, G.; Benhamou, J. P. Inhibition of Hepatic Drug-Metabolizing Enzymes by Arachidonic Acid. *Xenobiotica* **1979**, *9* (5), 301–310. https://doi.org/10.3109/00498257909038733.
- (68) Ortiz de Montellano, P. R. Substrate Oxidation by Cytochrome P450 Enzymes. In *Cytochrome P450*; Springer International Publishing: Cham, 2015; pp 111–176. https://doi.org/10.1007/978-3-319-12108-6\_4.

- (69) Guengerich, F. P. Common and Uncommon Cytochrome P450 Reactions Related to Metabolism and Chemical Toxicity. *Chem. Res. Toxicol.* **2001**, *14* (6), 611–650. https://doi.org/10.1021/tx0002583.
- (70) Isin, E. M.; Guengerich, F. P. Complex Reactions Catalyzed by Cytochrome P450 Enzymes. *Biochim. Biophys. Acta* **2007**, *1770* (3), 314–329. https://doi.org/10.1016/j.bbagen.2006.07.003.
- (71) Guengerich, F. P. Mechanisms of Cytochrome P450-Catalyzed Oxidations. *ACS Catal.* **2018**, 8 (12), 10964–10976. https://doi.org/10.1021/acscatal.8b03401.
- (72) Meunier, B.; de Visser, S. P.; Shaik, S. Mechanism of Oxidation Reactions Catalyzed by Cytochrome P450 Enzymes. *Chem. Rev.* **2004**, *104* (9), 3947–3980. https://doi.org/10.1021/cr020443g.
- (73) Denisov, I. G.; Makris, T. M.; Sligar, S. G.; Schlichting, I. Structure and Chemistry of Cytochrome P450. *Chem. Rev.* **2005**, *105* (6), 2253–2277. https://doi.org/10.1021/cr0307143.
- (74) Xu, L.-H.; Fushinobu, S.; Ikeda, H.; Wakagi, T.; Shoun, H. Crystal Structures of Cytochrome P450 105P1 from Streptomyces Avermitilis: Conformational Flexibility and Histidine Ligation State. *J. Bacteriol.* **2009**, *191* (4), 1211–1219. https://doi.org/10.1128/JB.01276-08.
- (75) Xu, L.-H.; Du, Y.-L. Rational and Semi-Rational Engineering of Cytochrome P450s for Biotechnological Applications. *Synth. Syst. Biotechnol.* **2018**, *3* (4), 283–290. https://doi.org/10.1016/j.synbio.2018.10.001.
- (76) Shoieb, S. M.; El-Ghiaty, M. A.; Alqahtani, M. A.; El-Kadi, A. O. S. Cytochrome P450-Derived Eicosanoids and Inflammation in Liver Diseases. *Prostaglandins Other Lipid Mediat.* **2020**, *147* (106400), 106400. https://doi.org/10.1016/j.prostaglandins.2019.106400.
- (77) El-Sherbeni, A. A.; Aboutabl, M. E.; Zordoky, B. N. M.; Anwar-Mohamed, A.; El-Kadi, A. O. S. Determination of the Dominant Arachidonic Acid Cytochrome P450 Monooxygenases in Rat Heart, Lung, Kidney, and Liver: Protein Expression and Metabolite Kinetics. *AAPS J.* **2013**, *15* (1), 112–122. https://doi.org/10.1208/s12248-012-9425-7.
- (78) Isobe, Y.; Itagaki, M.; Ito, Y.; Naoe, S.; Kojima, K.; Ikeguchi, M.; Arita, M. Comprehensive Analysis of the Mouse Cytochrome P450 Family Responsible for Omega-3 Epoxidation of Eicosapentaenoic Acid. *Sci. Rep.* **2018**, *8* (1). https://doi.org/10.1038/s41598-018-26325-4.
- (79) Zeldin, D. C.; DuBois, R. N.; Falck, J. R.; Capdevila, J. H. Molecular Cloning, Expression and Characterization of an Endogenous Human Cytochrome P450 Arachidonic Acid Epoxygenase Isoform. *Arch. Biochem. Biophys.* **1995**, *322* (1), 76–86. https://doi.org/10.1006/abbi.1995.1438.
- (80) Daikh, B. E.; Lasker, J. M.; Raucy, J. L.; Koop, D. R. Regio- and Stereoselective Epoxidation of Arachidonic Acid by Human Cytochromes P450 2C8 and 2C9. *J. Pharmacol. Exp. Ther.* **1994**, *271* (3), 1427–1433.

- (81) Wu, S.; Moomaw, C. R.; Tomer, K. B.; Falck, J. R.; Zeldin, D. C. Molecular Cloning and Expression of CYP2J2, a Human Cytochrome P450 Arachidonic Acid Epoxygenase Highly Expressed in Heart. *J. Biol. Chem.* **1996**, 271 (7), 3460–3468. https://doi.org/10.1074/jbc.271.7.3460.
- (82) Karara, A.; Makita, K.; Jacobson, H. R.; Falck, J. R.; Guengerich, F. P.; DuBois, R. N.; Capdevila, J. H. Molecular Cloning, Expression, and Enzymatic Characterization of the Rat Kidney Cytochrome P-450 Arachidonic Acid Epoxygenase. *J. Biol. Chem.* **1993**, 268 (18), 13565–13570.
- (83) DeLozier, T. C.; Tsao, C.-C.; Coulter, S. J.; Foley, J.; Bradbury, J. A.; Zeldin, D. C.; Goldstein, J. A. CYP2C44, a New Murine CYP2C That Metabolizes Arachidonic Acid to Unique Stereospecific Products. *J. Pharmacol. Exp. Ther.* **2004**, *310* (3), 845–854. https://doi.org/10.1124/jpet.104.067819.
- (84) Draper, A. J.; Hammock, B. D. Identification of CYP2C9 as a Human Liver Microsomal Linoleic Acid Epoxygenase. *Arch. Biochem. Biophys.* **2000**, *376* (1), 199–205. https://doi.org/10.1006/abbi.2000.1705.
- (85) Bylund, J.; Kunz, T.; Valmsen, K.; Oliw, E. H. Cytochromes P450 with Bisallylic Hydroxylation Activity on Arachidonic and Linoleic Acids Studied with Human Recombinant Enzymes and with Human and Rat Liver Microsomes. *J. Pharmacol. Exp. Ther.* **1998**, 284 (1), 51–60.
- (86) Daikh, B. E.; Laethem, R. M.; Koop, D. R. Stereoselective Epoxidation of Arachidonic Acid by Cytochrome P-450s 2CAA and 2C2. *J. Pharmacol. Exp. Ther.* **1994**, 269 (3), 1130–1135.
- (87) Moran, J. H.; Mitchell, L. A.; Bradbury, J. A.; Qu, W.; Zeldin, D. C.; Schnellmann, R. G.; Grant, D. F. Analysis of the Cytotoxic Properties of Linoleic Acid Metabolites Produced by Renal and Hepatic P450s. *Toxicol. Appl. Pharmacol.* **2000**, *168* (3), 268–279. https://doi.org/10.1006/taap.2000.9053.
- (88) Fer, M.; Dréano, Y.; Lucas, D.; Corcos, L.; Salaün, J.-P.; Berthou, F.; Amet, Y. Metabolism of Eicosapentaenoic and Docosahexaenoic Acids by Recombinant Human Cytochromes P450. *Arch. Biochem. Biophys.* **2008**, *471* (2), 116–125. https://doi.org/10.1016/j.abb.2008.01.002.
- (89) Westphal, C.; Konkel, A.; Schunck, W.-H. Cytochrome P450 Enzymes in the Bioactivation of Polyunsaturated Fatty Acids and Their Role in Cardiovascular Disease. *Adv. Exp. Med. Biol.* **2015**, *851*, 151–187. https://doi.org/10.1007/978-3-319-16009-2\_6.
- (90) Arnold, C.; Markovic, M.; Blossey, K.; Wallukat, G.; Fischer, R.; Dechend, R.; Konkel, A.; von Schacky, C.; Luft, F. C.; Muller, D. N.; Rothe, M.; Schunck, W.-H. Arachidonic Acid-Metabolizing Cytochrome P450 Enzymes Are Targets of ω-3 Fatty Acids. *J. Biol. Chem.* 2010, 285 (43), 32720–32733. https://doi.org/10.1074/jbc.m110.118406.
- (91) Barbosa-Sicard, E.; Markovic, M.; Honeck, H.; Christ, B.; Muller, D. N.; Schunck, W.-H. Eicosapentaenoic Acid Metabolism by Cytochrome P450 Enzymes of the CYP2C Subfamily.

- *Biochem. Biophys. Res. Commun.* **2005**, *329* (4), 1275–1281. https://doi.org/10.1016/j.bbrc.2005.02.103.
- (92) Lucas, D.; Goulitquer, S.; Marienhagen, J.; Fer, M.; Dreano, Y.; Schwaneberg, U.; Amet, Y.; Corcos, L. Stereoselective Epoxidation of the Last Double Bond of Polyunsaturated Fatty Acids by Human Cytochromes P450. *J. Lipid Res.* **2010**, *51* (5), 1125–1133. https://doi.org/10.1194/jlr.M003061.
- (93) Gainer, J. V.; Bellamine, A.; Dawson, E. P.; Womble, K. E.; Grant, S. W.; Wang, Y.; Cupples, L. A.; Guo, C.-Y.; Demissie, S.; O'Donnell, C. J.; Brown, N. J.; Waterman, M. R.; Capdevila, J. H. Functional Variant of CYP4A11 20-Hydroxyeicosatetraenoic Acid Synthase Is Associated with Essential Hypertension. *Circulation* **2005**, *111* (1), 63–69. https://doi.org/10.1161/01.CIR.0000151309.82473.59.
- (94) Nguyen, X.; Wang, M.-H.; Reddy, K. M.; Falck, J. R.; Schwartzman, M. L. Kinetic Profile of the Rat CYP4A Isoforms: Arachidonic Acid Metabolism and Isoform-Specific Inhibitors. *Am. J. Physiol. Regul. Integr. Comp. Physiol.* **1999**, 276 (6), R1691–R1700. https://doi.org/10.1152/ajpregu.1999.276.6.R1691.
- (95) Muller, D. N.; Schmidt, C.; Barbosa-Sicard, E.; Wellner, M.; Gross, V.; Hercule, H.; Markovic, M.; Honeck, H.; Luft, F. C.; Schunck, W.-H. Mouse Cyp4a Isoforms: Enzymatic Properties, Gender- and Strain-Specific Expression, and Role in Renal 20-Hydroxyeicosatetraenoic Acid Formation. *Biochem. J.* **2007**, *403* (1), 109–118. https://doi.org/10.1042/BJ20061328.
- (96) Fer, M.; Corcos, L.; Dréano, Y.; Plée-Gautier, E.; Salaün, J.-P.; Berthou, F.; Amet, Y. Cytochromes P450 from Family 4 Are the Main Omega Hydroxylating Enzymes in Humans: CYP4F3B Is the Prominent Player in PUFA Metabolism. *J. Lipid Res.* **2008**, *49* (11), 2379–2389. https://doi.org/10.1194/jlr.M800199-JLR200.
- (97) Wu, S.; Chen, W.; Murphy, E.; Gabel, S.; Tomer, K. B.; Foley, J.; Steenbergen, C.; Falck, J. R.; Moomaw, C. R.; Zeldin, D. C. Molecular Cloning, Expression, and Functional Significance of a Cytochrome P450 Highly Expressed in Rat Heart Myocytes. *J. Biol. Chem.* **1997**, 272 (19), 12551–12559. https://doi.org/10.1074/jbc.272.19.12551.
- (98) Adas, F.; Salaün, J. P.; Berthou, F.; Picart, D.; Simon, B.; Amet, Y. Requirement for Omega and (Omega;-1)-Hydroxylations of Fatty Acids by Human Cytochromes P450 2E1 and 4A11. *J. Lipid Res.* **1999**, *40* (11), 1990–1997.
- (99) Harmon, S. D.; Fang, X.; Kaduce, T. L.; Hu, S.; Raj Gopal, V.; Falck, J. R.; Spector, A. A. Oxygenation of Omega-3 Fatty Acids by Human Cytochrome P450 4F3B: Effect on 20-Hydroxyeicosatetraenoic Acid Production. *Prostaglandins Leukot. Essent. Fatty Acids* **2006**, 75 (3), 169–177. https://doi.org/10.1016/j.plefa.2006.05.005.
- (100) Lauterbach, B.; Barbosa-Sicard, E.; Wang, M.-H.; Honeck, H.; Kärgel, E.; Theuer, J.; Schwartzman, M. L.; Haller, H.; Luft, F. C.; Gollasch, M.; Schunck, W.-H. Cytochrome P450-Dependent Eicosapentaenoic Acid Metabolites Are Novel BK Channel Activators. *Hypertension* **2002**, *39* (2 Pt 2), 609–613. https://doi.org/10.1161/hy0202.103293.

- (101) Schwarz, D.; Kisselev, P.; Ericksen, S. S.; Szklarz, G. D.; Chernogolov, A.; Honeck, H.; Schunck, W.-H.; Roots, I. Arachidonic and Eicosapentaenoic Acid Metabolism by Human CYP1A1: Highly Stereoselective Formation of 17(R),18(S)-Epoxyeicosatetraenoic Acid. *Biochem. Pharmacol.* **2004**, *67* (8), 1445–1457. https://doi.org/10.1016/j.bcp.2003.12.023.
- (102) Stark, K.; Wongsud, B.; Burman, R.; Oliw, E. H. Oxygenation of Polyunsaturated Long Chain Fatty Acids by Recombinant CYP4F8 and CYP4F12 and Catalytic Importance of Tyr-125 and Gly-328 of CYP4F8. *Arch. Biochem. Biophys.* **2005**, *441* (2), 174–181. https://doi.org/10.1016/j.abb.2005.07.003.
- (103) Chuang, S. S.; Helvig, C.; Taimi, M.; Ramshaw, H. A.; Collop, A. H.; Amad, M.; White, J. A.; Petkovich, M.; Jones, G.; Korczak, B. CYP2U1, a Novel Human Thymus- and Brain-Specific Cytochrome P450, Catalyzes Omega- and (Omega-1)-Hydroxylation of Fatty Acids. *J. Biol. Chem.* **2004**, 279 (8), 6305–6314. https://doi.org/10.1074/jbc.M311830200.
- (104) Karlgren, M.; Backlund, M.; Johansson, I.; Oscarson, M.; Ingelman-Sundberg, M. Characterization and Tissue Distribution of a Novel Human Cytochrome P450-CYP2U1. *Biochem. Biophys. Res. Commun.* **2004**, *315* (3), 679–685. https://doi.org/10.1016/j.bbrc.2004.01.110.
- (105) Node, K.; Huo, Y.; Ruan, X.; Yang, B.; Spiecker, M.; Ley, K.; Zeldin, D. C.; Liao, J. K. Anti-Inflammatory Properties of Cytochrome P450 Epoxygenase-Derived Eicosanoids. *Science* **1999**, 285 (5431), 1276–1279. https://doi.org/10.1126/science.285.5431.1276.
- (106) Wray, J. A.; Sugden, M. C.; Zeldin, D. C.; Greenwood, G. K.; Samsuddin, S.; Miller-Degraff, L.; Bradbury, J. A.; Holness, M. J.; Warner, T. D.; Bishop-Bailey, D. The Epoxygenases CYP2J2 Activates the Nuclear Receptor PPARalpha in Vitro and in Vivo. *PLoS One* **2009**, *4* (10), e7421. https://doi.org/10.1371/journal.pone.0007421.
- (107) Morisseau, C.; Inceoglu, B.; Schmelzer, K.; Tsai, H.-J.; Jinks, S. L.; Hegedus, C. M.; Hammock, B. D. Naturally Occurring Monoepoxides of Eicosapentaenoic Acid and Docosahexaenoic Acid Are Bioactive Antihyperalgesic Lipids. *J. Lipid Res.* **2010**, *51* (12), 3481–3490. https://doi.org/10.1194/jlr.M006007.
- (108) Ding, Y.; Frömel, T.; Popp, R.; Falck, J. R.; Schunck, W.-H.; Fleming, I. The Biological Actions of 11,12-Epoxyeicosatrienoic Acid in Endothelial Cells Are Specific to the R/S-Enantiomer and Require the G(s) Protein. *J. Pharmacol. Exp. Ther.* **2014**, *350* (1), 14–21. https://doi.org/10.1124/jpet.114.214254.
- (109) Zou, A. P.; Fleming, J. T.; Falck, J. R.; Jacobs, E. R.; Gebremedhin, D.; Harder, D. R.; Roman, R. J. Stereospecific Effects of Epoxyeicosatrienoic Acids on Renal Vascular Tone and K(+)-Channel Activity. *Am. J. Physiol.* **1996**, *270* (5 Pt 2), F822-32. https://doi.org/10.1152/ajprenal.1996.270.5.F822.
- (110) Falck, J. R.; Krishna, U. M.; Reddy, Y. K.; Kumar, P. S.; Reddy, K. M.; Hittner, S. B.; Deeter, C.; Sharma, K. K.; Gauthier, K. M.; Campbell, W. B. Comparison of Vasodilatory Properties of 14,15-EET Analogs: Structural Requirements for Dilation. *Am. J. Physiol. Heart Circ. Physiol.* **2003**, 284 (1), H337-49. https://doi.org/10.1152/ajpheart.00831.2001.

- (111) Fitzpatrick, F. A.; Ennis, M. D.; Baze, M. E.; Wynalda, M. A.; McGee, J. E.; Liggett, W. F. Inhibition of Cyclooxygenase Activity and Platelet Aggregation by Epoxyeicosatrienoic Acids. Influence of Stereochemistry. *J. Biol. Chem.* **1986**, *261* (32), 15334–15338.
- (112) Carroll, M. A.; Balazy, M.; Margiotta, P.; Huang, D. D.; Falck, J. R.; McGiff, J. C. Cytochrome P-450-Dependent HETEs: Profile of Biological Activity and Stimulation by Vasoactive Peptides. *Am. J. Physiol.* **1996**, *271* (4 Pt 2), R863-9. https://doi.org/10.1152/ajpregu.1996.271.4.R863.
- (113) Cheng, J.; Ou, J.-S.; Singh, H.; Falck, J. R.; Narsimhaswamy, D.; Pritchard, K. A., Jr; Schwartzman, M. L. 20-Hydroxyeicosatetraenoic Acid Causes Endothelial Dysfunction via ENOS Uncoupling. *Am. J. Physiol. Heart Circ. Physiol.* **2008**, *294* (2), H1018-26. https://doi.org/10.1152/ajpheart.01172.2007.
- (114) Alonso-Galicia, M.; Falck, J. R.; Reddy, K. M.; Roman, R. J. 20-HETE Agonists and Antagonists in the Renal Circulation. *Am. J. Physiol.* **1999**, 277 (5 Pt 2), F790-6. https://doi.org/10.1152/ajprenal.1999.277.5.F790.
- (115) Shoieb, S. M.; El-Sherbeni, A. A.; El-Kadi, A. O. S. Identification of 19-(S/R)Hydroxyeicosatetraenoic Acid as the First Endogenous Noncompetitive Inhibitor of Cytochrome P450 1B1 with Enantioselective Activity. *Drug Metab. Dispos.* **2019**, *47* (2), 67–70. https://doi.org/10.1124/dmd.118.084657.
- (116) Cinelli, M. A.; Lee, K. S. S. Asymmetric Total Synthesis of 19,20-Epoxydocosapentaenoic Acid, a Bioactive Metabolite of Docosahexaenoic Acid. *J. Org. Chem.* **2019**, *84* (23), 15362–15372. https://doi.org/10.1021/acs.joc.9b02378.
- (117) Cinelli, M. A.; Yang, J.; Scharmen, A.; Woodman, J.; Karchalla, L. M.; Lee, K. S. S. Enzymatic Synthesis and Chemical Inversion Provide Both Enantiomers of Bioactive Epoxydocosapentaenoic Acids. *J. Lipid Res.* **2018**, *59* (11), 2237–2252. https://doi.org/10.1194/jlr.D089136.
- (118) Sasame, H. A.; Ames, M. M.; Nelson, S. D. Cytochrome P-450 and NADPH Cytochrome c Reductase in Rat Brain: Formation of Catechols and Reactive Catechol Metabolites. *Biochem. Biophys. Res. Commun.* **1977**, 78 (3), 919–926. https://doi.org/10.1016/0006-291x(77)90510-1.
- (119) Dutheil, F.; Beaune, P.; Loriot, M.-A. Xenobiotic Metabolizing Enzymes in the Central Nervous System: Contribution of Cytochrome P450 Enzymes in Normal and Pathological Human Brain. *Biochimie* **2008**, *90* (3), 426–436. https://doi.org/10.1016/j.biochi.2007.10.007.
- (120) Dutheil, F.; Dauchy, S.; Diry, M.; Sazdovitch, V.; Cloarec, O.; Mellottée, L.; Bièche, I.; Ingelman-Sundberg, M.; Flinois, J.-P.; de Waziers, I.; Beaune, P.; Declèves, X.; Duyckaerts, C.; Loriot, M.-A. Xenobiotic-Metabolizing Enzymes and Transporters in the Normal Human Brain: Regional and Cellular Mapping as a Basis for Putative Roles in Cerebral Function. *Drug Metab. Dispos.* **2009**, *37* (7), 1528–1538. https://doi.org/10.1124/dmd.109.027011.

- (121) Miksys, S.; Tyndale, R. F. Cytochrome P450-Mediated Drug Metabolism in the Brain. *J. Psychiatry Neurosci.* **2013**, *38* (3), 152–163. https://doi.org/10.1503/jpn.120133.
- (122) Petrov, A. M.; Pikuleva, I. A. Cholesterol 24-Hydroxylation by CYP46A1: Benefits of Modulation for Brain Diseases. *Neurotherapeutics* **2019**, *16* (3), 635–648. https://doi.org/10.1007/s13311-019-00731-6.
- (123) Cheng, J.; Zhen, Y.; Miksys, S.; Beyoğlu, D.; Krausz, K. W.; Tyndale, R. F.; Yu, A.; Idle, J. R.; Gonzalez, F. J. Potential Role of CYP2D6 in the Central Nervous System. *Xenobiotica* **2013**, *43* (11), 973–984. https://doi.org/10.3109/00498254.2013.791410.
- (124) Guengerich, F. P. Cytochrome P450 and Chemical Toxicology. *Chem. Res. Toxicol.* **2008**, 21 (1), 70–83. https://doi.org/10.1021/tx700079z.
- (125) Mann, A.; Miksys, S. L.; Gaedigk, A.; Kish, S. J.; Mash, D. C.; Tyndale, R. F. The Neuroprotective Enzyme CYP2D6 Increases in the Brain with Age and Is Lower in Parkinson's Disease Patients. *Neurobiol. Aging* **2012**, *33* (9), 2160–2171. https://doi.org/10.1016/j.neurobiolaging.2011.08.014.
- (126) Garcia, A. N. M.; Muniz, M. T. C.; Souza e Silva, H. R.; da Silva, H. A.; Athayde-Junior, L. Cyp46 Polymorphisms in Alzheimer's Disease: A Review. *J. Mol. Neurosci.* **2009**, *39* (3), 342–345. https://doi.org/10.1007/s12031-009-9227-2.
- (127) Boussicault, L.; Alves, S.; Lamazière, A.; Planques, A.; Heck, N.; Moumné, L.; Despres, G.; Bolte, S.; Hu, A.; Pagès, C.; Galvan, L.; Piguet, F.; Aubourg, P.; Cartier, N.; Caboche, J.; Betuing, S. CYP46A1, the Rate-Limiting Enzyme for Cholesterol Degradation, Is Neuroprotective in Huntington's Disease. *Brain* **2016**, *139* (Pt 3), 953–970. https://doi.org/10.1093/brain/awv384.
- (128) Brown, J., 3rd; Theisler, C.; Silberman, S.; Magnuson, D.; Gottardi-Littell, N.; Lee, J. M.; Yager, D.; Crowley, J.; Sambamurti, K.; Rahman, M. M.; Reiss, A. B.; Eckman, C. B.; Wolozin, B. Differential Expression of Cholesterol Hydroxylases in Alzheimer's Disease. *J. Biol. Chem.* **2004**, 279 (33), 34674–34681. https://doi.org/10.1074/jbc.M402324200.
- (129) Huang, R.; Poduslo, S. E. CYP19 Haplotypes Increase Risk for Alzheimer's Disease. *J. Med. Genet.* **2006**, *43* (8), e42. https://doi.org/10.1136/jmg.2005.039461.
- (130) Solanki, M.; Pointon, A.; Jones, B.; Herbert, K. Cytochrome P450 2J2: Potential Role in Drug Metabolism and Cardiotoxicity. *Drug Metab. Dispos.* **2018**, *46* (8), 1053–1065. https://doi.org/10.1124/dmd.117.078964.
- (131) Yan, H.; Kong, Y.; He, B.; Huang, M.; Li, J.; Zheng, J.; Liang, L.; Bi, J.; Zhao, S.; Shi, L. CYP2J2 Rs890293 Polymorphism Is Associated with Susceptibility to Alzheimer's Disease in the Chinese Han Population. *Neurosci. Lett.* **2015**, *593*, 56–60. https://doi.org/10.1016/j.neulet.2015.03.024.
- (132) Parker, R. E.; Isaacs, N. S. Mechanisms of Epoxide Reactions. *Chem. Rev.* **1959**, *59* (4), 737–799. https://doi.org/10.1021/cr50028a006.

- (133) Arand, M.; Cronin, A.; Oesch, F.; Mowbray, S. L.; Jones, T. A. The Telltale Structures of Epoxide Hydrolases. *Drug Metab. Rev.* **2003**, *35* (4), 365–383. https://doi.org/10.1081/DMR-120026498.
- (134) Moore, M. M.; Pottenger, L. H.; House-Knight, T. Critical Review of Styrene Genotoxicity Focused on the Mutagenicity/Clastogenicity Literature and Using Current Organization of Economic Cooperation and Development Guidance. *Environ. Mol. Mutagen.* **2019**, *60* (7), 624–663. https://doi.org/10.1002/em.22278.
- (135) Morisseau, C.; Hammock, B. D. Epoxide Hydrolases: Mechanisms, Inhibitor Designs, and Biological Roles. *Annu. Rev. Pharmacol. Toxicol.* **2005**, *45* (1), 311–333. https://doi.org/10.1146/annurev.pharmtox.45.120403.095920.
- (136) Sevanian, A.; McLeod, L. L. Catalytic Properties and Inhibition of Hepatic Cholesterol-Epoxide Hydrolase. *J. Biol. Chem.* **1986**, *261* (1), 54–59.
- (137) Haeggström, J. Z.; Tholander, F.; Wetterholm, A. Structure and Catalytic Mechanisms of Leukotriene A4 Hydrolase. *Prostaglandins Other Lipid Mediat.* **2007**, *83* (3), 198–202. https://doi.org/10.1016/j.prostaglandins.2007.01.006.
- (138) Pace-Asciak, C. R.; Lee, W. S. Purification of Hepoxilin Epoxide Hydrolase from Rat Liver. *J. Biol. Chem.* **1989**, *264* (16), 9310–9313.
- (139) Nigam, S.; Zafiriou, M.-P.; Deva, R.; Ciccoli, R.; Roux-Van der Merwe, R. Structure, Biochemistry and Biology of Hepoxilins: An Update. *FEBS J.* **2007**, *274* (14), 3503–3512. https://doi.org/10.1111/j.1742-4658.2007.05910.x.
- (140) Harris, T. R.; Hammock, B. D. Soluble Epoxide Hydrolase: Gene Structure, Expression and Deletion. *Gene* **2013**, *526* (2), 61–74. https://doi.org/10.1016/j.gene.2013.05.008.
- (141) Morisseau, C.; Hammock, B. D. Epoxide Hydrolases: Mechanisms, Inhibitor Designs, and Biological Roles. *ChemInform* **2005**, *36* (39). https://doi.org/10.1002/chin.200539226.
- (142) Decker, M.; Arand, M.; Cronin, A. Mammalian Epoxide Hydrolases in Xenobiotic Metabolism and Signalling. *Arch. Toxicol.* **2009**, *83* (4), 297–318. https://doi.org/10.1007/s00204-009-0416-0.
- (143) Oesch, F. Purification and Specificity of a Human Microsomal Epoxide Hydratase. *Biochem. J.* **1974**, *139* (1), 77–88. https://doi.org/10.1042/bj1390077.
- (144) Porter, T. D.; Beck, T. W.; Kasper, C. B. Complementary DNA and Amino Acid Sequence of Rat Liver Microsomal, Xenobiotic Epoxide Hydrolase. *Arch. Biochem. Biophys.* **1986**, 248 (1), 121–129. https://doi.org/10.1016/0003-9861(86)90408-x.
- (145) Holler, R.; Arand, M.; Mecky, A.; Oesch, F.; Friedberg, T. Erratum to "the Membrane Anchor of Microsomal Epoxide Hydrolase from Human, Rat, and Rabbit Displays an Unexpected Membrane Topology" [Biochem. Biophys. Res. Commun. 236 (1997) 754–759].

- *Biochem. Biophys. Res. Commun.* **2003**, *306* (3), 797. https://doi.org/10.1016/s0006-291x(03)01031-3.
- (146) Friedberg, T.; Löllmann, B.; Becker, R.; Holler, R.; Oesch, F. The Microsomal Epoxide Hydrolase Has a Single Membrane Signal Anchor Sequence Which Is Dispensable for the Catalytic Activity of This Protein. *Biochem. J.* **1994**, *303* ( *Pt 3*), 967–972. https://doi.org/10.1042/bj3030967.
- (147) Zou, J.; Hallberg, B. M.; Bergfors, T.; Oesch, F.; Arand, M.; Mowbray, S. L.; Jones, T. A. Structure of Aspergillus Niger Epoxide Hydrolase at 1.8 Å Resolution: Implications for the Structure and Function of the Mammalian Microsomal Class of Epoxide Hydrolases. *Structure* **2000**, 8 (2), 111–122. https://doi.org/10.1016/s0969-2126(00)00087-3.
- (148) Arand, M.; Hemmer, H.; Dürk, H.; Baratti, J.; Archelas, A.; Furstoss, R.; Oesch, F. Cloning and Molecular Characterization of a Soluble Epoxide Hydrolase from Aspergillus Niger That Is Related to Mammalian Microsomal Epoxide Hydrolase. *Biochem. J.* **1999**, *344 Pt 1*, 273–280. https://doi.org/10.1042/0264-6021:3440273.
- (149) Orjuela Leon, A. C.; Marwosky, A.; Arand, M. Evidence for a Complex Formation between CYP2J5 and MEH in Living Cells by FRET Analysis of Membrane Protein Interaction in the Endoplasmic Reticulum (FAMPIR). *Arch. Toxicol.* **2017**, *91* (11), 3561–3570. https://doi.org/10.1007/s00204-017-2072-0.
- (150) Hammock, B. D.; Loury, D. N.; Moody, D. E.; Ruebner, B.; Baselt, R.; Milam, K. M.; Volberding, P.; Ketterman, A.; Talcott, R. A Methodology for the Analysis of the Preneoplastic Antigen. *Carcinogenesis* **1984**, *5* (11), 1467–1473. https://doi.org/10.1093/carcin/5.11.1467.
- (151) Gomez, G. A.; Morisseau, C.; Hammock, B. D.; Christianson, D. W. Structure of Human Epoxide Hydrolase Reveals Mechanistic Inferences on Bifunctional Catalysis in Epoxide and Phosphate Ester Hydrolysis. *Biochemistry* **2004**, *43* (16), 4716–4723. https://doi.org/10.1021/bi036189j.
- (152) Václavíková, R.; Hughes, D. J.; Souček, P. Microsomal Epoxide Hydrolase 1 (EPHX1): Gene, Structure, Function, and Role in Human Disease. *Gene* **2015**, *571* (1), 1–8. https://doi.org/10.1016/j.gene.2015.07.071.
- (153) Lord, C. C.; Thomas, G.; Brown, J. M. Mammalian Alpha Beta Hydrolase Domain (ABHD) Proteins: Lipid Metabolizing Enzymes at the Interface of Cell Signaling and Energy Metabolism. *Biochim. Biophys. Acta* **2013**, *1831* (4), 792–802. https://doi.org/10.1016/j.bbalip.2013.01.002.
- (154) Decker, M.; Adamska, M.; Cronin, A.; Di Giallonardo, F.; Burgener, J.; Marowsky, A.; Falck, J. R.; Morisseau, C.; Hammock, B. D.; Gruzdev, A.; Zeldin, D. C.; Arand, M. EH3 (ABHD9): The First Member of a New Epoxide Hydrolase Family with High Activity for Fatty Acid Epoxides. *J. Lipid Res.* **2012**, *53* (10), 2038–2045. https://doi.org/10.1194/jlr.M024448.

- (155) Yamanashi, H.; Boeglin, W. E.; Morisseau, C.; Davis, R. W.; Sulikowski, G. A.; Hammock, B. D.; Brash, A. R. Catalytic Activities of Mammalian Epoxide Hydrolases with Cis and Trans Fatty Acid Epoxides Relevant to Skin Barrier Function. *J. Lipid Res.* **2018**, *59* (4), 684–695. https://doi.org/10.1194/jlr.M082701.
- (156) Moghaddam, M. F.; Grant, D. F.; Cheek, J. M.; Greene, J. F.; Williamson, K. C.; Hammock, B. D. Bioactivation of Leukotoxins to Their Toxic Diols by Epoxide Hydrolase. *Nat. Med.* **1997**, *3* (5), 562–566. https://doi.org/10.1038/nm0597-562.
- (157) Cottrell, S.; Jung, K.; Kristiansen, G.; Eltze, E.; Semjonow, A.; Ittmann, M.; Hartmann, A.; Stamey, T.; Haefliger, C.; Weiss, G. Discovery and Validation of 3 Novel DNA Methylation Markers of Prostate Cancer Prognosis. *J. Urol.* **2007**, *177* (5), 1753–1758. https://doi.org/10.1016/j.juro.2007.01.010.
- (158) Oster, B.; Thorsen, K.; Lamy, P.; Wojdacz, T. K.; Hansen, L. L.; Birkenkamp-Demtröder, K.; Sørensen, K. D.; Laurberg, S.; Orntoft, T. F.; Andersen, C. L. Identification and Validation of Highly Frequent CpG Island Hypermethylation in Colorectal Adenomas and Carcinomas. *Int. J. Cancer* 2011, 129 (12), 2855–2866. https://doi.org/10.1002/ijc.25951.
- (159) Yamashita, S.; Tsujino, Y.; Moriguchi, K.; Tatematsu, M.; Ushijima, T. Chemical Genomic Screening for Methylation-Silenced Genes in Gastric Cancer Cell Lines Using 5-Aza-2'-Deoxycytidine Treatment and Oligonucleotide Microarray. *Cancer Sci.* **2006**, *97* (1), 64–71. https://doi.org/10.1111/j.1349-7006.2006.00136.x.
- (160) Furuta, J.; Nobeyama, Y.; Umebayashi, Y.; Otsuka, F.; Kikuchi, K.; Ushijima, T. Silencing of Peroxiredoxin 2 and Aberrant Methylation of 33 CpG Islands in Putative Promoter Regions in Human Malignant Melanomas. *Cancer Res.* **2006**, *66* (12), 6080–6086. https://doi.org/10.1158/0008-5472.CAN-06-0157.
- (161) Krig, S. R.; Jin, V. X.; Bieda, M. C.; O'Geen, H.; Yaswen, P.; Green, R.; Farnham, P. J. Identification of Genes Directly Regulated by the Oncogene ZNF217 Using Chromatin Immunoprecipitation (ChIP)-Chip Assays. *J. Biol. Chem.* **2007**, 282 (13), 9703–9712. https://doi.org/10.1074/jbc.M611752200.
- (162) Schnekenburger, M.; Diederich, M. Epigenetics Offer New Horizons for Colorectal Cancer Prevention. *Curr. Colorectal Cancer Rep.* **2012**, 8 (1), 66–81. https://doi.org/10.1007/s11888-011-0116-z.
- (163) Oliw, E. H.; Guengerich, F. P.; Oates, J. A. Oxygenation of Arachidonic Acid by Hepatic Monooxygenases. Isolation and Metabolism of Four Epoxide Intermediates. *J. Biol. Chem.* **1982**, 257 (7), 3771–3781.
- (164) Zeldin, D. C.; Wei, S.; Falck, J. R.; Hammock, B. D.; Snapper, J. R.; Capdevila, J. H. Metabolism of Epoxyeicosatrienoic Acids by Cytosolic Epoxide Hydrolase: Substrate Structural Determinants of Asymmetric Catalysis. *Arch. Biochem. Biophys.* **1995**, *316* (1), 443–451. https://doi.org/10.1006/abbi.1995.1059.

- (165) Marowsky, A.; Burgener, J.; Falck, J. R.; Fritschy, J.-M.; Arand, M. Distribution of Soluble and Microsomal Epoxide Hydrolase in the Mouse Brain and Its Contribution to Cerebral Epoxyeicosatrienoic Acid Metabolism. *Neuroscience* **2009**, *163* (2), 646–661. https://doi.org/10.1016/j.neuroscience.2009.06.033.
- (166) Armstrong, R. N.; Cassidy, C. S. New Structural and Chemical Insight into the Catalytic Mechanism of Epoxide Hydrolases. *Drug Metab. Rev.* **2000**, *32* (3–4), 327–338. https://doi.org/10.1081/dmr-100102337.
- (167) Farin, F. M.; Omiecinski, C. J. Regiospecific Expression of Cytochrome P-450s and Microsomal Epoxide Hydrolase in Human Brain Tissue. *J. Toxicol. Environ. Health* **1993**, 40 (2–3), 317–335. https://doi.org/10.1080/15287399309531797.
- (168) Liu, M.; Sun, A.; Shin, E.-J.; Liu, X.; Kim, S.-G.; Runyons, C. R.; Markesbery, W.; Kim, H.-C.; Bing, G. Expression of Microsomal Epoxide Hydrolase Is Elevated in Alzheimer's Hippocampus and Induced by Exogenous Beta-Amyloid and Trimethyl-Tin. *Eur. J. Neurosci.* **2006**, *23* (8), 2027–2034. https://doi.org/10.1111/j.1460-9568.2006.04724.x.
- (169) Shin, E.-J.; Bing, G.; Chae, J. S.; Kim, T. W.; Bach, J.-H.; Park, D. H.; Yamada, K.; Nabeshima, T.; Kim, H.-C. Role of Microsomal Epoxide Hydrolase in Methamphetamine-Induced Drug Dependence in Mice. *J. Neurosci. Res.* **2009**, *87* (16), 3679–3686. https://doi.org/10.1002/jnr.22166.
- (170) Kessler, R.; Hamou, M. F.; Albertoni, M.; de Tribolet, N.; Arand, M.; Van Meir, E. G. Identification of the Putative Brain Tumor Antigen BF7/GE2 as the (de)Toxifying Enzyme Microsomal Epoxide Hydrolase. *Cancer Res.* **2000**, *60* (5), 1403–1409.
- (171) Rawal, S.; Morisseau, C.; Hammock, B. D.; Shivachar, A. C. Differential Subcellular Distribution and Colocalization of the Microsomal and Soluble Epoxide Hydrolases in Cultured Neonatal Rat Brain Cortical Astrocytes. *J. Neurosci. Res.* **2009**, *87* (1), 218–227. https://doi.org/10.1002/jnr.21827.
- (172) Kohn, M. C.; Melnick, R. L. Physiological Modeling of Butadiene Disposition in Mice and Rats. *Chem. Biol. Interact.* **2001**, *135–136*, 285–301. https://doi.org/10.1016/s0009-2797(01)00176-4.
- (173) Sura, P.; Sura, R.; Enayetallah, A. E.; Grant, D. F. Distribution and Expression of Soluble Epoxide Hydrolase in Human Brain. *J. Histochem. Cytochem.* **2008**, *56* (6), 551–559. https://doi.org/10.1369/jhc.2008.950659.
- (174) Atone, J.; Wagner, K.; Hashimoto, K.; Hammock, B. D. Cytochrome P450 Derived Epoxidized Fatty Acids as a Therapeutic Tool against Neuroinflammatory Diseases. *Prostaglandins Other Lipid Mediat.* **2020**, *147* (106385), 106385. https://doi.org/10.1016/j.prostaglandins.2019.106385.
- (175) Hung, T.-H.; Shyue, S.-K.; Wu, C.-H.; Chen, C.-C.; Lin, C.-C.; Chang, C.-F.; Chen, S.-F. Deletion or Inhibition of Soluble Epoxide Hydrolase Protects against Brain Damage and

- Reduces Microglia-Mediated Neuroinflammation in Traumatic Brain Injury. *Oncotarget* **2017**, *8* (61), 103236–103260. https://doi.org/10.18632/oncotarget.21139.
- (176) Zhang, Y.; Hong, G.; Lee, K. S. S.; Hammock, B. D.; Gebremedhin, D.; Harder, D. R.; Koehler, R. C.; Sapirstein, A. Inhibition of Soluble Epoxide Hydrolase Augments Astrocyte Release of Vascular Endothelial Growth Factor and Neuronal Recovery after Oxygen-Glucose Deprivation. *J. Neurochem.* **2017**, *140* (5), 814–825. https://doi.org/10.1111/jnc.13933.
- (177) Wagner, K. M.; McReynolds, C. B.; Schmidt, W. K.; Hammock, B. D. Soluble Epoxide Hydrolase as a Therapeutic Target for Pain, Inflammatory and Neurodegenerative Diseases. *Pharmacol. Ther.* **2017**, *180*, 62–76. https://doi.org/10.1016/j.pharmthera.2017.06.006.
- (178) Abdu, E.; Bruun, D. A.; Yang, D.; Yang, J.; Inceoglu, B.; Hammock, B. D.; Alkayed, N. J.; Lein, P. J. Epoxyeicosatrienoic Acids Enhance Axonal Growth in Primary Sensory and Cortical Neuronal Cell Cultures. *J. Neurochem.* **2011**, *117* (4), 632–642. https://doi.org/10.1111/j.1471-4159.2010.07139.x.
- (179) Hoopes, S. L.; Gruzdev, A.; Edin, M. L.; Graves, J. P.; Bradbury, J. A.; Flake, G. P.; Lih, F. B.; DeGraff, L. M.; Zeldin, D. C. Generation and Characterization of Epoxide Hydrolase 3 (EPHX3)-Deficient Mice. *PLoS One* **2017**, *12* (4), e0175348. https://doi.org/10.1371/journal.pone.0175348.
- (180) Marowsky, A.; Arand, M. Mammalian Epoxide Hydrolases. In *Comprehensive Toxicology*; Elsevier, 2018; pp 308–325. https://doi.org/10.1016/b978-0-12-801238-3.95622-8.
- (181) Weintraub, N. L.; Fang, X.; Kaduce, T. L.; VanRollins, M.; Chatterjee, P.; Spector, A. A. Potentiation of Endothelium-Dependent Relaxation by Epoxyeicosatrienoic Acids. *Circ. Res.* **1997**, *81* (2), 258–267. https://doi.org/10.1161/01.res.81.2.258.
- (182) Oltman, C. L.; Weintraub, N. L.; VanRollins, M.; Dellsperger, K. C. Epoxyeicosatrienoic Acids and Dihydroxyeicosatrienoic Acids Are Potent Vasodilators in the Canine Coronary Microcirculation. *Circ. Res.* **1998**, *83* (9), 932–939. https://doi.org/10.1161/01.res.83.9.932.
- (183) Larsen, B. T.; Miura, H.; Hatoum, O. A.; Campbell, W. B.; Hammock, B. D.; Zeldin, D. C.; Falck, J. R.; Gutterman, D. D. Epoxyeicosatrienoic and Dihydroxyeicosatrienoic Acids Dilate Human Coronary Arterioles via BK(Ca) Channels: Implications for Soluble Epoxide Hydrolase Inhibition. *Am. J. Physiol. Heart Circ. Physiol.* **2006**, *290* (2), H491-9. https://doi.org/10.1152/ajpheart.00927.2005.
- (184) Abukhashim, M.; Wiebe, G. J.; Seubert, J. M. Regulation of Forskolin-Induced CAMP Production by Cytochrome P450 Epoxygenase Metabolites of Arachidonic Acid in HEK293 Cells. *Cell Biol. Toxicol.* **2011**, 27 (5), 321–332. https://doi.org/10.1007/s10565-011-9190-x.
- (185) Fang, X.; Hu, S.; Xu, B.; Snyder, G. D.; Harmon, S.; Yao, J.; Liu, Y.; Sangras, B.; Falck, J. R.; Weintraub, N. L.; Spector, A. A. 14,15-Dihydroxyeicosatrienoic Acid Activates

- Peroxisome Proliferator-Activated Receptor-Alpha. *Am. J. Physiol. Heart Circ. Physiol.* **2006**, 290 (1), H55-63. https://doi.org/10.1152/ajpheart.00427.2005.
- (186) Ng, V. Y.; Huang, Y.; Reddy, L. M.; Falck, J. R.; Lin, E. T.; Kroetz, D. L. Cytochrome P450 Eicosanoids Are Activators of Peroxisome Proliferator-Activated Receptor Alpha. *Drug Metab. Dispos.* **2007**, *35* (7), 1126–1134. https://doi.org/10.1124/dmd.106.013839.
- (187) Schepmann, H. G.; Pang, J.; Matsuda, S. P. Cloning and Characterization of Ginkgo Biloba Levopimaradiene Synthase Which Catalyzes the First Committed Step in Ginkgolide Biosynthesis. *Arch. Biochem. Biophys.* **2001**, *392* (2), 263–269. https://doi.org/10.1006/abbi.2001.2438.
- (188) Moran, J. H.; Mon, T.; Hendrickson, T. L.; Mitchell, L. A.; Grant, D. F. Defining Mechanisms of Toxicity for Linoleic Acid Monoepoxides and Diols in Sf-21 Cells. *Chem. Res. Toxicol.* **2001**, *14* (4), 431–437. https://doi.org/10.1021/tx0002000.
- (189) Stanford, K. I.; Lynes, M. D.; Takahashi, H.; Baer, L. A.; Arts, P. J.; May, F. J.; Lehnig, A. C.; Middelbeek, R. J. W.; Richard, J. J.; So, K.; Chen, E. Y.; Gao, F.; Narain, N. R.; Distefano, G.; Shettigar, V. K.; Hirshman, M. F.; Ziolo, M. T.; Kiebish, M. A.; Tseng, Y.-H.; Coen, P. M.; Goodyear, L. J. 12,13-DiHOME: An Exercise-Induced Lipokine That Increases Skeletal Muscle Fatty Acid Uptake. *Cell Metab.* **2018**, 27 (5), 1111-1120.e3. https://doi.org/10.1016/j.cmet.2018.03.020.
- (190) Kundu, S.; Roome, T.; Bhattacharjee, A.; Carnevale, K. A.; Yakubenko, V. P.; Zhang, R.; Hwang, S. H.; Hammock, B. D.; Cathcart, M. K. Metabolic Products of Soluble Epoxide Hydrolase Are Essential for Monocyte Chemotaxis to MCP-1 in Vitro and in Vivo. *J. Lipid Res.* **2013**, *54* (2), 436–447. https://doi.org/10.1194/jlr.M031914.
- (191) Wagner, K.; Inceoglu, B.; Hammock, B. D. Soluble Epoxide Hydrolase Inhibition, Epoxygenated Fatty Acids and Nociception. *Prostaglandins Other Lipid Mediat.* **2011**, *96* (1–4), 76–83. https://doi.org/10.1016/j.prostaglandins.2011.08.001.
- (192) Spector, A. A. Arachidonic Acid Cytochrome P450 Epoxygenase Pathway. *J. Lipid Res.* **2009**, *50 Suppl* (Supplement), S52-6. https://doi.org/10.1194/jlr.R800038-JLR200.
- (193) Iliff, J. J.; Jia, J.; Nelson, J.; Goyagi, T.; Klaus, J.; Alkayed, N. J. Epoxyeicosanoid Signaling in CNS Function and Disease. *Prostaglandins Other Lipid Mediat.* **2010**, *91* (3–4), 68–84. https://doi.org/10.1016/j.prostaglandins.2009.06.004.
- (194) Spector, A. A.; Norris, A. W. Action of Epoxyeicosatrienoic Acids on Cellular Function. *Am. J. Physiol. Cell Physiol.* **2007**, 292 (3), C996-1012. https://doi.org/10.1152/ajpcell.00402.2006.
- (195) Hashimoto, M.; Katakura, M.; Tanabe, Y.; Al Mamun, A.; Inoue, T.; Hossain, S.; Arita, M.; Shido, O. N-3 Fatty Acids Effectively Improve the Reference Memory-Related Learning Ability Associated with Increased Brain Docosahexaenoic Acid-Derived Docosanoids in Aged Rats. *Biochim. Biophys. Acta* **2015**, *1851* (2), 203–209. https://doi.org/10.1016/j.bbalip.2014.10.009.

- (196) Ostermann, A. I.; Waindok, P.; Schmidt, M. J.; Chiu, C.-Y.; Smyl, C.; Rohwer, N.; Weylandt, K.-H.; Schebb, N. H. Modulation of the Endogenous Omega-3 Fatty Acid and Oxylipin Profile in Vivo-A Comparison of the Fat-1 Transgenic Mouse with C57BL/6 Wildtype Mice on an Omega-3 Fatty Acid Enriched Diet. *PLoS One* **2017**, *12* (9), e0184470. https://doi.org/10.1371/journal.pone.0184470.
- (197) Ostermann, A. I.; Reutzel, M.; Hartung, N.; Franke, N.; Kutzner, L.; Schoenfeld, K.; Weylandt, K.-H.; Eckert, G. P.; Schebb, N. H. A Diet Rich in Omega-3 Fatty Acids Enhances Expression of Soluble Epoxide Hydrolase in Murine Brain. *Prostaglandins Other Lipid Mediat.* **2017**, *133*, 79–87. https://doi.org/10.1016/j.prostaglandins.2017.06.001.
- (198) Rey, C.; Delpech, J. C.; Madore, C.; Nadjar, A.; Greenhalgh, A. D.; Amadieu, C.; Aubert, A.; Pallet, V.; Vaysse, C.; Layé, S.; Joffre, C. Dietary N-3 Long Chain PUFA Supplementation Promotes a pro-Resolving Oxylipin Profile in the Brain. *Brain Behav. Immun.* **2019**, *76*, 17–27. https://doi.org/10.1016/j.bbi.2018.07.025.
- (199) Taha, A. Y.; Hennebelle, M.; Yang, J.; Zamora, D.; Rapoport, S. I.; Hammock, B. D.; Ramsden, C. E. Regulation of Rat Plasma and Cerebral Cortex Oxylipin Concentrations with Increasing Levels of Dietary Linoleic Acid. *Prostaglandins Leukot. Essent. Fatty Acids* **2018**, *138*, 71–80. https://doi.org/10.1016/j.plefa.2016.05.004.
- (200) Taha, A. Y.; Blanchard, H. C.; Cheon, Y.; Ramadan, E.; Chen, M.; Chang, L.; Rapoport, S. I. Dietary Linoleic Acid Lowering Reduces Lipopolysaccharide-Induced Increase in Brain Arachidonic Acid Metabolism. *Mol. Neurobiol.* **2017**, *54* (6), 4303–4315. https://doi.org/10.1007/s12035-016-9968-1.
- (201) Leng, S.; Winter, T.; Aukema, H. M. Dietary LA and Sex Effects on Oxylipin Profiles in Rat Kidney, Liver, and Serum Differ from Their Effects on PUFAs. *J. Lipid Res.* **2017**, *58* (8), 1702–1712. https://doi.org/10.1194/jlr.m078097.
- (202) Leng, S.; Winter, T.; Aukema, H. M. Dietary ALA, EPA and DHA Have Distinct Effects on Oxylipin Profiles in Female and Male Rat Kidney, Liver and Serum. *J. Nutr. Biochem.* **2018**, *57*, 228–237. https://doi.org/10.1016/j.jnutbio.2018.04.002.
- (203) Mendonça, A. M.; Cayer, L. G. J.; Pauls, S. D.; Winter, T.; Leng, S.; Taylor, C. G.; Zahradka, P.; Aukema, H. M. Distinct Effects of Dietary ALA, EPA and DHA on Rat Adipose Oxylipins Vary by Depot Location and Sex. *Prostaglandins Leukot. Essent. Fatty Acids* **2018**, *129*, 13–24. https://doi.org/10.1016/j.plefa.2017.12.004.
- (204) Sochocka, M.; Diniz, B. S.; Leszek, J. Inflammatory Response in the CNS: Friend or Foe? *Mol. Neurobiol.* **2017**, *54* (10), 8071–8089. https://doi.org/10.1007/s12035-016-0297-1.
- (205) Heneka, M. T.; Carson, M. J.; El Khoury, J.; Landreth, G. E.; Brosseron, F.; Feinstein, D. L.; Jacobs, A. H.; Wyss-Coray, T.; Vitorica, J.; Ransohoff, R. M.; Herrup, K.; Frautschy, S. A.; Finsen, B.; Brown, G. C.; Verkhratsky, A.; Yamanaka, K.; Koistinaho, J.; Latz, E.; Halle, A.; Petzold, G. C.; Town, T.; Morgan, D.; Shinohara, M. L.; Perry, V. H.; Holmes, C.; Bazan, N. G.; Brooks, D. J.; Hunot, S.; Joseph, B.; Deigendesch, N.; Garaschuk, O.; Boddeke, E.; Dinarello, C. A.; Breitner, J. C.; Cole, G. M.; Golenbock, D. T.; Kummer, M. P.

- Neuroinflammation in Alzheimer's Disease. *Lancet Neurol.* **2015**, *14* (4), 388–405. https://doi.org/10.1016/S1474-4422(15)70016-5.
- (206) Simon, D. W.; McGeachy, M. J.; Bayır, H.; Clark, R. S. B.; Loane, D. J.; Kochanek, P. M. The Far-Reaching Scope of Neuroinflammation after Traumatic Brain Injury. *Nat. Rev. Neurol.* **2017**, *13* (3), 171–191. https://doi.org/10.1038/nrneurol.2017.13.
- (207) Zhang, J.-M.; An, J. Cytokines, Inflammation, and Pain. *Int. Anesthesiol. Clin.* **2007**, *45* (2), 27–37. https://doi.org/10.1097/AIA.0b013e318034194e.
- (208) Wang, Q.; Liu, Y.; Zhou, J. Neuroinflammation in Parkinson's Disease and Its Potential as Therapeutic Target. *Transl. Neurodegener.* **2015**, *4* (1), 19. https://doi.org/10.1186/s40035-015-0042-0.
- (209) Kodani, S. D.; Morisseau, C. Role of Epoxy-Fatty Acids and Epoxide Hydrolases in the Pathology of Neuro-Inflammation. *Biochimie* **2019**, *159*, 59–65. https://doi.org/10.1016/j.biochi.2019.01.020.
- (210) Vezzani, A.; Balosso, S.; Ravizza, T. Neuroinflammatory Pathways as Treatment Targets and Biomarkers in Epilepsy. *Nat. Rev. Neurol.* **2019**, *15* (8), 459–472. https://doi.org/10.1038/s41582-019-0217-x.
- (211) Taguchi, N.; Nakayama, S.; Tanaka, M. Single Administration of Soluble Epoxide Hydrolase Inhibitor Suppresses Neuroinflammation and Improves Neuronal Damage after Cardiac Arrest in Mice. *Neurosci. Res.* **2016**, *111*, 56–63. https://doi.org/10.1016/j.neures.2016.05.002.
- (212) Pallàs, M.; Vázquez, S.; Sanfeliu, C.; Galdeano, C.; Griñán-Ferré, C. Soluble Epoxide Hydrolase Inhibition to Face Neuroinflammation in Parkinson's Disease: A New Therapeutic Strategy. *Biomolecules* **2020**, *10* (5), 703. https://doi.org/10.3390/biom10050703.
- (213) Vito, S. T.; Austin, A. T.; Banks, C. N.; Inceoglu, B.; Bruun, D. A.; Zolkowska, D.; Tancredi, D. J.; Rogawski, M. A.; Hammock, B. D.; Lein, P. J. Post-Exposure Administration of Diazepam Combined with Soluble Epoxide Hydrolase Inhibition Stops Seizures and Modulates Neuroinflammation in a Murine Model of Acute TETS Intoxication. *Toxicol. Appl. Pharmacol.* **2014**, *281* (2), 185–194. https://doi.org/10.1016/j.taap.2014.10.001.
- (214) Hung, Y.-W.; Hung, S.-W.; Wu, Y.-C.; Wong, L.-K.; Lai, M.-T.; Shih, Y.-H.; Lee, T.-S.; Lin, Y.-Y. Soluble Epoxide Hydrolase Activity Regulates Inflammatory Responses and Seizure Generation in Two Mouse Models of Temporal Lobe Epilepsy. *Brain Behav. Immun.* **2015**, *43*, 118–129. https://doi.org/10.1016/j.bbi.2014.07.016.
- (215) Birnie, M.; Morrison, R.; Camara, R.; Strauss, K. I. Temporal Changes of Cytochrome P450 (Cyp) and Eicosanoid-Related Gene Expression in the Rat Brain after Traumatic Brain Injury. *BMC Genomics* **2013**, *14*, 303. https://doi.org/10.1186/1471-2164-14-303.
- (216) Yuan, L.; Liu, J.; Dong, R.; Zhu, J.; Tao, C.; Zheng, R.; Zhu, S. 14,15-Epoxyeicosatrienoic Acid Promotes Production of Brain Derived Neurotrophic Factor from Astrocytes and Exerts

- Neuroprotective Effects during Ischaemic Injury. *Neuropathol. Appl. Neurobiol.* **2016**, 42 (7), 607–620. https://doi.org/10.1111/nan.12291.
- (217) Oguro, A.; Inoue, T.; Kudoh, S. N.; Imaoka, S. 14,15-Epoxyeicosatrienoic Acid Produced by Cytochrome P450s Enhances Neurite Outgrowth of PC12 and Rat Hippocampal Neuronal Cells. *Pharmacol. Res. Perspect.* **2018**, *6* (5), e00428. https://doi.org/10.1002/prp2.428.
- (218) Simpkins, A. N.; Rudic, R. D.; Schreihofer, D. A.; Roy, S.; Manhiani, M.; Tsai, H.-J.; Hammock, B. D.; Imig, J. D. Soluble Epoxide Inhibition Is Protective against Cerebral Ischemia via Vascular and Neural Protection. *Am. J. Pathol.* **2009**, *174* (6), 2086–2095. https://doi.org/10.2353/ajpath.2009.080544.
- (219) Zhang, W.; Otsuka, T.; Sugo, N.; Ardeshiri, A.; Alhadid, Y. K.; Iliff, J. J.; DeBarber, A. E.; Koop, D. R.; Alkayed, N. J. Soluble Epoxide Hydrolase Gene Deletion Is Protective against Experimental Cerebral Ischemia. *Stroke* **2008**, *39* (7), 2073–2078. https://doi.org/10.1161/STROKEAHA.107.508325.
- (220) Reitz, C.; Mayeux, R. Alzheimer Disease: Epidemiology, Diagnostic Criteria, Risk Factors and Biomarkers. *Biochem. Pharmacol.* **2014**, 88 (4), 640–651. https://doi.org/10.1016/j.bcp.2013.12.024.
- (221) Tönnies, E.; Trushina, E. Oxidative Stress, Synaptic Dysfunction, and Alzheimer's Disease. J. Alzheimers. Dis. 2017, 57 (4), 1105–1121. https://doi.org/10.3233/JAD-161088.
- (222) Tarasoff-Conway, J. M.; Carare, R. O.; Osorio, R. S.; Glodzik, L.; Butler, T.; Fieremans, E.; Axel, L.; Rusinek, H.; Nicholson, C.; Zlokovic, B. V.; Frangione, B.; Blennow, K.; Ménard, J.; Zetterberg, H.; Wisniewski, T.; de Leon, M. J. Clearance Systems in the Brain-Implications for Alzheimer Disease. *Nat. Rev. Neurol.* **2015**, *11* (8), 457–470. https://doi.org/10.1038/nrneurol.2015.119.
- (223) Casley, C. S.; Land, J. M.; Sharpe, M. A.; Clark, J. B.; Duchen, M. R.; Canevari, L. Beta-Amyloid Fragment 25-35 Causes Mitochondrial Dysfunction in Primary Cortical Neurons. *Neurobiol. Dis.* **2002**, *10* (3), 258–267. https://doi.org/10.1006/nbdi.2002.0516.
- (224) Van Giau, V.; An, S. S. A.; Hulme, J. P. Mitochondrial Therapeutic Interventions in Alzheimer's Disease. *J. Neurol. Sci.* **2018**, *395*, 62–70. https://doi.org/10.1016/j.jns.2018.09.033.
- (225) Sarkar, P.; Zaja, I.; Bienengraeber, M.; Rarick, K. R.; Terashvili, M.; Canfield, S.; Falck, J. R.; Harder, D. R. Epoxyeicosatrienoic Acids Pretreatment Improves Amyloid β-Induced Mitochondrial Dysfunction in Cultured Rat Hippocampal Astrocytes. *Am. J. Physiol. Heart Circ. Physiol.* **2014**, *306* (4), H475-84. https://doi.org/10.1152/ajpheart.00001.2013.
- (226) Sarkar, P.; Narayanan, J.; Harder, D. R. Differential Effect of Amyloid β on the Cytochrome P450 Epoxygenase Activity in Rat Brain. *Neuroscience* **2011**, *194*, 241–249. https://doi.org/10.1016/j.neuroscience.2011.07.058.

- (227) Sanchez-Mejia, R. O.; Newman, J. W.; Toh, S.; Yu, G.-Q.; Zhou, Y.; Halabisky, B.; Cissé, M.; Scearce-Levie, K.; Cheng, I. H.; Gan, L.; Palop, J. J.; Bonventre, J. V.; Mucke, L. Phospholipase A2 Reduction Ameliorates Cognitive Deficits in a Mouse Model of Alzheimer's Disease. *Nat. Neurosci.* **2008**, *11* (11), 1311–1318. https://doi.org/10.1038/nn.2213.
- (228) Ghosh, A.; Comerota, M. E.; Wan, D.; Chen, F.; Propson, N. E.; Hwang, S. H.; Hammock, B. D.; Zheng, H. Epoxy Fatty Acid Dysregulation and Neuroinflammation in Alzheimer's Disease Is Resolved by a Soluble Epoxide Hydrolase Inhibitor. *bioRxiv*, 2020. https://doi.org/10.1101/2020.06.30.180984.
- (229) Lee, H.-T.; Lee, K.-I.; Chen, C.-H.; Lee, T.-S. Genetic Deletion of Soluble Epoxide Hydrolase Delays the Progression of Alzheimer's Disease. *J. Neuroinflammation* **2019**, *16* (1), 267. https://doi.org/10.1186/s12974-019-1635-9.
- (230) Griñán-Ferré, C.; Codony, S.; Pujol, E.; Yang, J.; Leiva, R.; Escolano, C.; Puigoriol-Illamola, D.; Companys-Alemany, J.; Corpas, R.; Sanfeliu, C.; Pérez, B.; Loza, M. I.; Brea, J.; Morisseau, C.; Hammock, B. D.; Vázquez, S.; Pallàs, M.; Galdeano, C. Pharmacological Inhibition of Soluble Epoxide Hydrolase as a New Therapy for Alzheimer's Disease. *Neurotherapeutics* **2020**. https://doi.org/10.1007/s13311-020-00854-1.
- (231) Poewe, W.; Seppi, K.; Tanner, C. M.; Halliday, G. M.; Brundin, P.; Volkmann, J.; Schrag, A.-E.; Lang, A. E. Parkinson Disease. *Nat. Rev. Dis. Primers* **2017**, *3*, 17013. https://doi.org/10.1038/nrdp.2017.13.
- (232) Balestrino, R.; Schapira, A. H. V. Parkinson Disease. *Eur. J. Neurol.* **2020**, *27* (1), 27–42. https://doi.org/10.1111/ene.14108.
- (233) Qin, X.; Wu, Q.; Lin, L.; Sun, A.; Liu, S.; Li, X.; Cao, X.; Gao, T.; Luo, P.; Zhu, X.; Wang, X. Soluble Epoxide Hydrolase Deficiency or Inhibition Attenuates MPTP-Induced Parkinsonism. *Mol. Neurobiol.* **2015**, *52* (1), 187–195. https://doi.org/10.1007/s12035-014-8833-3.
- (234) Huang, H.-J.; Wang, Y.-T.; Lin, H.-C.; Lee, Y.-H.; Lin, A. M.-Y. Soluble Epoxide Hydrolase Inhibition Attenuates MPTP-Induced Neurotoxicity in the Nigrostriatal Dopaminergic System: Involvement of α-Synuclein Aggregation and ER Stress. *Mol. Neurobiol.* **2018**, *55* (1), 138–144. https://doi.org/10.1007/s12035-017-0726-9.
- (235) Borlongan, C. V. Fatty Acid Chemical Mediator Provides Insights into the Pathology and Treatment of Parkinson's Disease. *Proc. Natl. Acad. Sci. U. S. A.* **2018**, *115* (25), 6322–6324. https://doi.org/10.1073/pnas.1807276115.
- (236) Bishop-Bailey, D.; Bystrom, J. Emerging Roles of Peroxisome Proliferator-Activated Receptor-Beta/Delta in Inflammation. *Pharmacol. Ther.* **2009**, *124* (2), 141–150. https://doi.org/10.1016/j.pharmthera.2009.06.011.

- (237) Moraes, L. A.; Piqueras, L.; Bishop-Bailey, D. Peroxisome Proliferator-Activated Receptors and Inflammation. *Pharmacol. Ther.* **2006**, *110* (3), 371–385. https://doi.org/10.1016/j.pharmthera.2005.08.007.
- (238) Bishop-Bailey, D.; Wray, J. Peroxisome Proliferator-Activated Receptors: A Critical Review on Endogenous Pathways for Ligand Generation. *Prostaglandins Other Lipid Mediat.* **2003**, *71* (1–2), 1–22. https://doi.org/10.1016/s0090-6980(03)00003-0.
- (239) Cowart, L. A.; Wei, S.; Hsu, M.-H.; Johnson, E. F.; Krishna, M. U.; Falck, J. R.; Capdevila, J. H. The CYP4A Isoforms Hydroxylate Epoxyeicosatrienoic Acids to Form High Affinity Peroxisome Proliferator-Activated Receptor Ligands. *J. Biol. Chem.* **2002**, 277 (38), 35105–35112. https://doi.org/10.1074/jbc.M201575200.
- (240) Khan, S. A.; Vanden Heuvel, J. P. Reviews: Current Topicsrole of Nuclear Receptors in the Regulation of Gene Expression by Dietary Fatty Acids (Review). *J. Nutr. Biochem.* **2003**, *14* (10), 554–567. https://doi.org/10.1016/s0955-2863(03)00098-6.
- (241) Navarro-Mabarak, C.; Mitre-Aguilar, I. B.; Camacho-Carranza, R.; Arias, C.; Zentella-Dehesa, A.; Espinosa-Aguirre, J. J. Role of NF-KB in Cytochrome P450 Epoxygenases down-Regulation during an Inflammatory Process in Astrocytes. *Neurochem. Int.* **2019**, *129* (104499), 104499. https://doi.org/10.1016/j.neuint.2019.104499.
- (242) Berger, J.; Moller, D. E. The Mechanisms of Action of PPARs. *Annu. Rev. Med.* **2002**, *53* (1), 409–435. https://doi.org/10.1146/annurev.med.53.082901.104018.
- (243) Večeřa, R.; Zachařová, A.; Orolin, J.; Strojil, J.; Skottová, N.; Anzenbacher, P. Fenofibrate-Induced Decrease of Expression of CYP2C11 and CYP2C6 in Rat. *Biopharm. Drug Dispos.* **2011**, *32* (8), 482–487. https://doi.org/10.1002/bdd.774.
- (244) Shaban, Z.; Soliman, M.; El-Shazly, S.; El-Bohi, K.; Abdelazeez, A.; Kehelo, K.; Kim, H.-S.; Muzandu, K.; Ishizuka, M.; Kazusaka, A.; Fujita, S. AhR and PPARalpha: Antagonistic Effects on CYP2B and CYP3A, and Additive Inhibitory Effects on CYP2C11. *Xenobiotica* **2005**, *35* (1), 51–68. https://doi.org/10.1080/00498250400021804.
- (245) Corton, J. C.; Fan, L. Q.; Brown, S.; Anderson, S. P.; Bocos, C.; Cattley, R. C.; Mode, A.; Gustafsson, J. A. Down-Regulation of Cytochrome P450 2C Family Members and Positive Acute-Phase Response Gene Expression by Peroxisome Proliferator Chemicals. *Mol. Pharmacol.* **1998**, *54* (3), 463–473. https://doi.org/10.1124/mol.54.3.463.
- (246) Liu, Y.; Zhang, Y.; Schmelzer, K.; Lee, T.-S.; Fang, X.; Zhu, Y.; Spector, A. A.; Gill, S.; Morisseau, C.; Hammock, B. D.; Shyy, J. Y.-J. The Antiinflammatory Effect of Laminar Flow: The Role of PPARgamma, Epoxyeicosatrienoic Acids, and Soluble Epoxide Hydrolase. *Proc. Natl. Acad. Sci. U. S. A.* **2005**, *102* (46), 16747–16752. https://doi.org/10.1073/pnas.0508081102.
- (247) Morin, C.; Sirois, M.; Echavé, V.; Albadine, R.; Rousseau, E. 17,18-Epoxyeicosatetraenoic Acid Targets PPARγ and P38 Mitogen-Activated Protein Kinase to Mediate Its Anti-

- Inflammatory Effects in the Lung: Role of Soluble Epoxide Hydrolase. *Am. J. Respir. Cell Mol. Biol.* **2010**, *43* (5), 564–575. https://doi.org/10.1165/rcmb.2009-0155OC.
- (248) Fang, X.; Hu, S.; Watanabe, T.; Weintraub, N. L.; Snyder, G. D.; Yao, J.; Liu, Y.; Shyy, J. Y.-J.; Hammock, B. D.; Spector, A. A. Activation of Peroxisome Proliferator-Activated Receptor Alpha by Substituted Urea-Derived Soluble Epoxide Hydrolase Inhibitors. *J. Pharmacol. Exp. Ther.* **2005**, *314* (1), 260–270. https://doi.org/10.1124/jpet.105.085605.
- (249) Riehle, M.; Tsvetkov, D.; Gohlke, B.-O.; Preissner, R.; Harteneck, C.; Gollasch, M.; Nürnberg, B. Molecular Basis for the Sensitivity of TRP Channels to Polyunsaturated Fatty Acids. *Naunyn. Schmiedebergs. Arch. Pharmacol.* **2018**, *391* (8), 833–846. https://doi.org/10.1007/s00210-018-1507-3.
- (250) Parenti, A.; De Logu, F.; Geppetti, P.; Benemei, S. What Is the Evidence for the Role of TRP Channels in Inflammatory and Immune Cells? *Br. J. Pharmacol.* **2016**, *173* (6), 953–969. https://doi.org/10.1111/bph.13392.
- (251) Nilius, B.; Szallasi, A. Transient Receptor Potential Channels as Drug Targets: From the Science of Basic Research to the Art of Medicine. *Pharmacol. Rev.* **2014**, *66* (3), 676–814. https://doi.org/10.1124/pr.113.008268.
- (252) Vennekens, R.; Menigoz, A.; Nilius, B. TRPs in the Brain. *Rev. Physiol. Biochem. Pharmacol.* **2012**, *163*, 27–64. https://doi.org/10.1007/112\_2012\_8.
- (253) Hardie, R. C. A Brief History of Trp: Commentary and Personal Perspective. *Pflugers Arch.* **2011**, *461* (5), 493–498. https://doi.org/10.1007/s00424-011-0922-9.
- (254) Taberner, F. J.; Fernández-Ballester, G.; Fernández-Carvajal, A.; Ferrer-Montiel, A. TRP Channels Interaction with Lipids and Its Implications in Disease. *Biochim. Biophys. Acta* **2015**, *1848* (9), 1818–1827. https://doi.org/10.1016/j.bbamem.2015.03.022.
- (255) Watanabe, H.; Vriens, J.; Prenen, J.; Droogmans, G.; Voets, T.; Nilius, B. Anandamide and Arachidonic Acid Use Epoxyeicosatrienoic Acids to Activate TRPV4 Channels. *Nature* **2003**, *424* (6947), 434–438. https://doi.org/10.1038/nature01807.
- (256) Vriens, J.; Owsianik, G.; Fisslthaler, B.; Suzuki, M.; Janssens, A.; Voets, T.; Morisseau, C.; Hammock, B. D.; Fleming, I.; Busse, R.; Nilius, B. Modulation of the Ca2 Permeable Cation Channel TRPV4 by Cytochrome P450 Epoxygenases in Vascular Endothelium. *Circ. Res.* **2005**, *97* (9), 908–915. https://doi.org/10.1161/01.RES.0000187474.47805.30.
- (257) Earley, S. Endothelium-Dependent Cerebral Artery Dilation Mediated by Transient Receptor Potential and Ca2+-Activated K+ Channels. *J. Cardiovasc. Pharmacol.* **2011**, *57* (2), 148–153. https://doi.org/10.1097/FJC.0b013e3181f580d9.
- (258) Higashimori, H.; Blanco, V. M.; Tuniki, V. R.; Falck, J. R.; Filosa, J. A. Role of Epoxyeicosatrienoic Acids as Autocrine Metabolites in Glutamate-Mediated K+ Signaling in Perivascular Astrocytes. *Am. J. Physiol. Cell Physiol.* **2010**, *299* (5), C1068-78. https://doi.org/10.1152/ajpcell.00225.2010.

- (259) Caires, R.; Sierra-Valdez, F. J.; Millet, J. R. M.; Herwig, J. D.; Roan, E.; Vásquez, V.; Cordero-Morales, J. F. Omega-3 Fatty Acids Modulate TRPV4 Function through Plasma Membrane Remodeling. *Cell Rep.* **2017**, *21* (1), 246–258. https://doi.org/10.1016/j.celrep.2017.09.029.
- (260) Loot, A. E.; Fleming, I. Cytochrome P450-Derived Epoxyeicosatrienoic Acids and Pulmonary Hypertension: Central Role of Transient Receptor Potential C6 Channels. *J. Cardiovasc. Pharmacol.* **2011**, *57* (2), 140–147. https://doi.org/10.1097/FJC.0b013e3181ed088d.
- (261) Sudhahar, V.; Shaw, S.; Imig, J. Epoxyeicosatrienoic Acid Analogs and Vascular Function. *Curr. Med. Chem.* **2010**, *17* (12), 1181–1190. https://doi.org/10.2174/092986710790827843.
- (262) Brierley, S. M.; Page, A. J.; Hughes, P. A.; Adam, B.; Liebregts, T.; Cooper, N. J.; Holtmann, G.; Liedtke, W.; Blackshaw, L. A. Selective Role for TRPV4 Ion Channels in Visceral Sensory Pathways. *Gastroenterology* **2008**, *134* (7), 2059–2069. https://doi.org/10.1053/j.gastro.2008.01.074.
- (263) Sipe, W. E. B.; Brierley, S. M.; Martin, C. M.; Phillis, B. D.; Cruz, F. B.; Grady, E. F.; Liedtke, W.; Cohen, D. M.; Vanner, S.; Blackshaw, L. A.; Bunnett, N. W. Transient Receptor Potential Vanilloid 4 Mediates Protease Activated Receptor 2-Induced Sensitization of Colonic Afferent Nerves and Visceral Hyperalgesia. *Am. J. Physiol. Gastrointest. Liver Physiol.* **2008**, 294 (5), G1288-98. https://doi.org/10.1152/ajpgi.00002.2008.
- (264) Sisignano, M.; Park, C.-K.; Angioni, C.; Zhang, D. D.; von Hehn, C.; Cobos, E. J.; Ghasemlou, N.; Xu, Z.-Z.; Kumaran, V.; Lu, R.; Grant, A.; Fischer, M. J. M.; Schmidtko, A.; Reeh, P.; Ji, R.-R.; Woolf, C. J.; Geisslinger, G.; Scholich, K.; Brenneis, C. 5,6-EET Is Released upon Neuronal Activity and Induces Mechanical Pain Hypersensitivity via TRPA1 on Central Afferent Terminals. *J. Neurosci.* **2012**, *32* (18), 6364–6372. https://doi.org/10.1523/JNEUROSCI.5793-11.2012.
- (265) Brenneis, C.; Sisignano, M.; Coste, O.; Altenrath, K.; Fischer, M. J.; Angioni, C.; Fleming, I.; Brandes, R. P.; Reeh, P. W.; Woolf, C. J.; Geisslinger, G.; Scholich, K. Soluble Epoxide Hydrolase Limits Mechanical Hyperalgesia during Inflammation. *Mol. Pain* **2011**, *7*, 78. https://doi.org/10.1186/1744-8069-7-78.
- (266) Liu, Y.; Wang, R.; Li, J.; Rao, J.; Li, W.; Falck, J. R.; Manthati, V. L.; Medhora, M.; Jacobs, E. R.; Zhu, D. Stable EET Urea Agonist and Soluble Epoxide Hydrolase Inhibitor Regulate Rat Pulmonary Arteries through TRPCs. *Hypertens. Res.* **2011**, *34* (5), 630–639. https://doi.org/10.1038/hr.2011.5.
- (267) Fleming, I.; Rueben, A.; Popp, R.; Fisslthaler, B.; Schrodt, S.; Sander, A.; Haendeler, J.; Falck, J. R.; Morisseau, C.; Hammock, B. D.; Busse, R. Epoxyeicosatrienoic Acids Regulate Trp Channel Dependent Ca2+ Signaling and Hyperpolarization in Endothelial Cells. *Arterioscler. Thromb. Vasc. Biol.* **2007**, 27 (12), 2612–2618. https://doi.org/10.1161/ATVBAHA.107.152074.

- (268) Ma, Y.; Zhang, P.; Li, J.; Lu, J.; Ge, J.; Zhao, Z.; Ma, X.; Wan, S.; Yao, X.; Shen, B. Epoxyeicosatrienoic Acids Act through TRPV4-TRPC1-KCa1.1 Complex to Induce Smooth Muscle Membrane Hyperpolarization and Relaxation in Human Internal Mammary Arteries. *Biochim. Biophys. Acta* **2015**, *1852* (3), 552–559. https://doi.org/10.1016/j.bbadis.2014.12.010.
- (269) Pierce, K. L.; Premont, R. T.; Lefkowitz, R. J. Seven-Transmembrane Receptors. *Nat. Rev. Mol. Cell Biol.* **2002**, *3* (9), 639–650. https://doi.org/10.1038/nrm908.
- (270) Heng, B. C.; Aubel, D.; Fussenegger, M. An Overview of the Diverse Roles of G-Protein Coupled Receptors (GPCRs) in the Pathophysiology of Various Human Diseases. *Biotechnol. Adv.* **2013**, *31* (8), 1676–1694. https://doi.org/10.1016/j.biotechadv.2013.08.017.
- (271) Vassilatis, D. K.; Hohmann, J. G.; Zeng, H.; Li, F.; Ranchalis, J. E.; Mortrud, M. T.; Brown, A.; Rodriguez, S. S.; Weller, J. R.; Wright, A. C.; Bergmann, J. E.; Gaitanaris, G. A. The G Protein-Coupled Receptor Repertoires of Human and Mouse. *Proc. Natl. Acad. Sci. U. S. A.* **2003**, *100* (8), 4903–4908. https://doi.org/10.1073/pnas.0230374100.
- (272) Guerram, M.; Zhang, L.-Y.; Jiang, Z.-Z. G-Protein Coupled Receptors as Therapeutic Targets for Neurodegenerative and Cerebrovascular Diseases. *Neurochem. Int.* **2016**, *101*, 1–14. https://doi.org/10.1016/j.neuint.2016.09.005.
- (273) Huang, Y.; Todd, N.; Thathiah, A. The Role of GPCRs in Neurodegenerative Diseases: Avenues for Therapeutic Intervention. *Curr. Opin. Pharmacol.* **2017**, *32*, 96–110. https://doi.org/10.1016/j.coph.2017.02.001.
- (274) Zhao, J.; Deng, Y.; Jiang, Z.; Qing, H. G Protein-Coupled Receptors (GPCRs) in Alzheimer's Disease: A Focus on BACE1 Related GPCRs. *Front. Aging Neurosci.* **2016**, 8, 58. https://doi.org/10.3389/fnagi.2016.00058.
- (275) Wong, P. Y.; Lin, K. T.; Yan, Y. T.; Ahern, D.; Iles, J.; Shen, S. Y.; Bhatt, R. K.; Falck, J. R. 14(R),15(S)-Epoxyeicosatrienoic Acid (14(R),15(S)-EET) Receptor in Guinea Pig Mononuclear Cell Membranes. *J. Lipid Mediat.* **1993**, *6* (1–3), 199–208.
- (276) Wong, P. Y.; Lai, P. S.; Shen, S. Y.; Belosludtsev, Y. Y.; Falck, J. R. Post-Receptor Signal Transduction and Regulation of 14(R),15(S)-Epoxyeicosatrienoic Acid (14,15-EET) Binding in U-937 Cells. *J. Lipid Mediat. Cell Signal.* **1997**, *16* (3), 155–169. https://doi.org/10.1016/s0929-7855(97)00005-9.
- (277) Wong, P. Y.; Lai, P. S.; Falck, J. R. Mechanism and Signal Transduction of 14 (R), 15 (S)-Epoxyeicosatrienoic Acid (14,15-EET) Binding in Guinea Pig Monocytes. *Prostaglandins Other Lipid Mediat.* **2000**, 62 (4), 321–333. https://doi.org/10.1016/s0090-6980(00)00079-4.
- (278) Campo, G. M.; Avenoso, A.; D'Ascola, A.; Prestipino, V.; Scuruchi, M.; Nastasi, G.; Calatroni, A.; Campo, S. Protein Kinase a Mediated Anti-Inflammatory Effects Exerted by Adenosine Treatment in Mouse Chondrocytes Stimulated with IL-1β. *Biofactors* **2012**, *38* (6), 429–439. https://doi.org/10.1002/biof.1040.

- (279) Chen, J. K.; Falck, J. R.; Reddy, K. M.; Capdevila, J.; Harris, R. C. Epoxyeicosatrienoic Acids and Their Sulfonimide Derivatives Stimulate Tyrosine Phosphorylation and Induce Mitogenesis in Renal Epithelial Cells. *J. Biol. Chem.* **1998**, *273* (44), 29254–29261. https://doi.org/10.1074/jbc.273.44.29254.
- (280) Snyder, G. D.; Krishna, U. M.; Falck, J. R.; Spector, A. A. Evidence for a Membrane Site of Action for 14,15-EET on Expression of Aromatase in Vascular Smooth Muscle. *Am. J. Physiol. Heart Circ. Physiol.* **2002**, 283 (5), H1936-42. https://doi.org/10.1152/ajpheart.00321.2002.
- (281) Behm, D. J.; Ogbonna, A.; Wu, C.; Burns-Kurtis, C. L.; Douglas, S. A. Epoxyeicosatrienoic Acids Function as Selective, Endogenous Antagonists of Native Thromboxane Receptors: Identification of a Novel Mechanism of Vasodilation. *J. Pharmacol. Exp. Ther.* **2009**, *328* (1), 231–239. https://doi.org/10.1124/jpet.108.145102.
- (282) Liu, X.; Qian, Z.-Y.; Xie, F.; Fan, W.; Nelson, J. W.; Xiao, X.; Kaul, S.; Barnes, A. P.; Alkayed, N. J. Functional Screening for G Protein-Coupled Receptor Targets of 14,15-Epoxyeicosatrienoic Acid. *Prostaglandins Other Lipid Mediat.* **2017**, *132*, 31–40. https://doi.org/10.1016/j.prostaglandins.2016.09.002.
- (283) Li, P. L.; Chen, C. L.; Bortell, R.; Campbell, W. B. 11,12-Epoxyeicosatrienoic Acid Stimulates Endogenous Mono-ADP-Ribosylation in Bovine Coronary Arterial Smooth Muscle. *Circ. Res.* **1999**, *85* (4), 349–356. https://doi.org/10.1161/01.res.85.4.349.
- (284) Fukao, M.; Mason, H. S.; Kenyon, J. L.; Horowitz, B.; Keef, K. D. Regulation of BK(Ca) Channels Expressed in Human Embryonic Kidney 293 Cells by Epoxyeicosatrienoic Acid. *Mol. Pharmacol.* **2001**, *59* (1), 16–23. https://doi.org/10.1124/mol.59.1.16.
- (285) Carroll, M. A.; Doumad, A. B.; Li, J.; Cheng, M. K.; Falck, J. R.; McGiff, J. C. Adenosine2A Receptor Vasodilation of Rat Preglomerular Microvessels Is Mediated by EETs That Activate the CAMP/PKA Pathway. *Am. J. Physiol. Renal Physiol.* **2006**, *291* (1), F155-61. https://doi.org/10.1152/ajprenal.00231.2005.
- (286) Mule, N. K.; Orjuela Leon, A. C.; Falck, J. R.; Arand, M.; Marowsky, A. 11,12 Epoxyeicosatrienoic Acid (11,12 EET) Reduces Excitability and Excitatory Transmission in the Hippocampus. *Neuropharmacology* **2017**, *123*, 310–321. https://doi.org/10.1016/j.neuropharm.2017.05.013.
- (287) Conroy, J. L.; Fang, C.; Gu, J.; Zeitlin, S. O.; Yang, W.; Yang, J.; VanAlstine, M. A.; Nalwalk, J. W.; Albrecht, P. J.; Mazurkiewicz, J. E.; Snyder-Keller, A.; Shan, Z.; Zhang, S.-Z.; Wentland, M. P.; Behr, M.; Knapp, B. I.; Bidlack, J. M.; Zuiderveld, O. P.; Leurs, R.; Ding, X.; Hough, L. B. Opioids Activate Brain Analgesic Circuits through Cytochrome P450/Epoxygenase Signaling. *Nat. Neurosci.* **2010**, *13* (3), 284–286. https://doi.org/10.1038/nn.2497.
- (288) Terashvili, M.; Tseng, L. F.; Wu, H.-E.; Narayanan, J.; Hart, L. M.; Falck, J. R.; Pratt, P. F.; Harder, D. R. Antinociception Produced by 14,15-Epoxyeicosatrienoic Acid Is Mediated by the Activation of Beta-Endorphin and Met-Enkephalin in the Rat Ventrolateral

- Periaqueductal Gray. *J. Pharmacol. Exp. Ther.* **2008**, *326* (2), 614–622. https://doi.org/10.1124/jpet.108.136739.
- (289) Mercado, G.; Castillo, V.; Soto, P.; Sidhu, A. ER Stress and Parkinson's Disease: Pathological Inputs That Converge into the Secretory Pathway. *Brain Res.* **2016**, *1648*, 626–632. https://doi.org/10.1016/j.brainres.2016.04.042.
- (290) Gerakis, Y.; Hetz, C. Emerging Roles of ER Stress in the Etiology and Pathogenesis of Alzheimer's Disease. *FEBS J.* **2018**, 285 (6), 995–1011. https://doi.org/10.1111/febs.14332.
- (291) Santos, L. E.; Ferreira, S. T. Crosstalk between Endoplasmic Reticulum Stress and Brain Inflammation in Alzheimer's Disease. *Neuropharmacology* **2018**, *136*, 350–360. https://doi.org/10.1016/j.neuropharm.2017.11.016.
- (292) Hotamisligil, G. S. Endoplasmic Reticulum Stress and the Inflammatory Basis of Metabolic Disease. *Cell* **2010**, *140* (6), 900–917. https://doi.org/10.1016/j.cell.2010.02.034.
- (293) Bettaieb, A.; Nagata, N.; AbouBechara, D.; Chahed, S.; Morisseau, C.; Hammock, B. D.; Haj, F. G. Soluble Epoxide Hydrolase Deficiency or Inhibition Attenuates Diet-Induced Endoplasmic Reticulum Stress in Liver and Adipose Tissue. *J. Biol. Chem.* **2013**, 288 (20), 14189–14199. https://doi.org/10.1074/jbc.M113.458414.
- (294) Dhanasekaran, A.; Gruenloh, S. K.; Buonaccorsi, J. N.; Zhang, R.; Gross, G. J.; Falck, J. R.; Patel, P. K.; Jacobs, E. R.; Medhora, M. Multiple Antiapoptotic Targets of the PI3K/Akt Survival Pathway Are Activated by Epoxyeicosatrienoic Acids to Protect Cardiomyocytes from Hypoxia/Anoxia. *Am. J. Physiol. Heart Circ. Physiol.* **2008**, 294 (2), H724-35. https://doi.org/10.1152/ajpheart.00979.2007.
- (295) Hu, P.; Han, Z.; Couvillon, A. D.; Exton, J. H. Critical Role of Endogenous Akt/IAPs and MEK1/ERK Pathways in Counteracting Endoplasmic Reticulum Stress-Induced Cell Death. *J. Biol. Chem.* **2004**, *279* (47), 49420–49429. https://doi.org/10.1074/jbc.M407700200.
- (296) Geng, H.-X.; Li, R.-P.; Li, Y.-G.; Wang, X.-Q.; Zhang, L.; Deng, J.-B.; Wang, L.; Deng, J.-X. 14,15-EET Suppresses Neuronal Apoptosis in Ischemia-Reperfusion through the Mitochondrial Pathway. *Neurochem. Res.* **2017**, *42* (10), 2841–2849. https://doi.org/10.1007/s11064-017-2297-6.
- (297) Rodriguez, D.; Rojas-Rivera, D.; Hetz, C. Integrating Stress Signals at the Endoplasmic Reticulum: The BCL-2 Protein Family Rheostat. *Biochim. Biophys. Acta* **2011**, *1813* (4), 564–574. https://doi.org/10.1016/j.bbamcr.2010.11.012.
- (298) Inceoglu, B.; Bettaieb, A.; Trindade da Silva, C. A.; Lee, K. S. S.; Haj, F. G.; Hammock, B. D. Endoplasmic Reticulum Stress in the Peripheral Nervous System Is a Significant Driver of Neuropathic Pain. *Proc. Natl. Acad. Sci. U. S. A.* **2015**, *112* (29), 9082–9087. https://doi.org/10.1073/pnas.1510137112.

- (299) Swerdlow, R. H.; Burns, J. M.; Khan, S. M. The Alzheimer's Disease Mitochondrial Cascade Hypothesis: Progress and Perspectives. *Biochim. Biophys. Acta* **2014**, *1842* (8), 1219–1231. https://doi.org/10.1016/j.bbadis.2013.09.010.
- (300) Guo, J.; Zhao, X.; Li, Y.; Li, G.; Liu, X. Damage to Dopaminergic Neurons by Oxidative Stress in Parkinson's Disease (Review). *Int. J. Mol. Med.* **2018**. https://doi.org/10.3892/ijmm.2018.3406.
- (301) Eckert, G. P.; Lipka, U.; Muller, W. E. Omega-3 Fatty Acids in Neurodegenerative Diseases: Focus on Mitochondria. *Prostaglandins Leukot. Essent. Fatty Acids* **2013**, 88 (1), 105–114. https://doi.org/10.1016/j.plefa.2012.05.006.
- (302) Inceoglu, B.; Bettaieb, A.; Haj, F. G.; Gomes, A. V.; Hammock, B. D. Modulation of Mitochondrial Dysfunction and Endoplasmic Reticulum Stress Are Key Mechanisms for the Wide-Ranging Actions of Epoxy Fatty Acids and Soluble Epoxide Hydrolase Inhibitors. *Prostaglandins Other Lipid Mediat.* **2017**, *133*, 68–78. https://doi.org/10.1016/j.prostaglandins.2017.08.003.
- (303) Wang, L.; Chen, M.; Yuan, L.; Xiang, Y.; Zheng, R.; Zhu, S. 14,15-EET Promotes Mitochondrial Biogenesis and Protects Cortical Neurons against Oxygen/Glucose Deprivation-Induced Apoptosis. *Biochem. Biophys. Res. Commun.* **2014**, *450* (1), 604–609. https://doi.org/10.1016/j.bbrc.2014.06.022.
- (304) Samokhvalov, V.; Alsaleh, N.; El-Sikhry, H. E.; Jamieson, K. L.; Chen, C. B.; Lopaschuk, D. G.; Carter, C.; Light, P. E.; Manne, R.; Falck, J. R.; Seubert, J. M. Epoxyeicosatrienoic Acids Protect Cardiac Cells during Starvation by Modulating an Autophagic Response. *Cell Death Dis.* **2013**, *4* (10), e885. https://doi.org/10.1038/cddis.2013.418.
- (305) Katragadda, D.; Batchu, S. N.; Cho, W. J.; Chaudhary, K. R.; Falck, J. R.; Seubert, J. M. Epoxyeicosatrienoic Acids Limit Damage to Mitochondrial Function Following Stress in Cardiac Cells. *J. Mol. Cell. Cardiol.* **2009**, *46* (6), 867–875. https://doi.org/10.1016/j.yjmcc.2009.02.028.
- (306) Akao, M.; Ohler, A.; O'Rourke, B.; Marbán, E. Mitochondrial ATP-Sensitive Potassium Channels Inhibit Apoptosis Induced by Oxidative Stress in Cardiac Cells. *Circ. Res.* **2001**, 88 (12), 1267–1275. https://doi.org/10.1161/hh1201.092094.
- (307) Witte, M. E.; Geurts, J. J. G.; de Vries, H. E.; van der Valk, P.; van Horssen, J. Mitochondrial Dysfunction: A Potential Link between Neuroinflammation and Neurodegeneration? *Mitochondrion* **2010**, *10* (5), 411–418. https://doi.org/10.1016/j.mito.2010.05.014.
- (308) Zhang, G.; Kodani, S.; Hammock, B. D. Stabilized Epoxygenated Fatty Acids Regulate Inflammation, Pain, Angiogenesis and Cancer. *Prog. Lipid Res.* **2014**, *53*, 108–123. https://doi.org/10.1016/j.plipres.2013.11.003.
- (309) Liu, L.; Chen, C.; Gong, W.; Li, Y.; Edin, M. L.; Zeldin, D. C.; Wang, D. W. Epoxyeicosatrienoic Acids Attenuate Reactive Oxygen Species Level, Mitochondrial

- Dysfunction, Caspase Activation, and Apoptosis in Carcinoma Cells Treated with Arsenic Trioxide. *J. Pharmacol. Exp. Ther.* **2011**, *339* (2), 451–463. https://doi.org/10.1124/jpet.111.180505.
- (310) Qu, Y.; Liu, Y.; Zhu, Y.; Chen, L.; Sun, W.; Zhu, Y. Epoxyeicosatrienoic Acid Inhibits the Apoptosis of Cerebral Microvascular Smooth Muscle Cells by Oxygen Glucose Deprivation via Targeting the JNK/c-Jun and MTOR Signaling Pathways. *Mol. Cells* **2017**, *40* (11), 837–846. https://doi.org/10.14348/molcells.2017.0084.
- (311) Harris, T. W.; Chen, N.; Cunningham, F.; Tello-Ruiz, M.; Antoshechkin, I.; Bastiani, C.; Bieri, T.; Blasiar, D.; Bradnam, K.; Chan, J.; Chen, C.-K.; Chen, W. J.; Davis, P.; Kenny, E.; Kishore, R.; Lawson, D.; Lee, R.; Muller, H.-M.; Nakamura, C.; Ozersky, P.; Petcherski, A.; Rogers, A.; Sabo, A.; Schwarz, E. M.; Van Auken, K.; Wang, Q.; Durbin, R.; Spieth, J.; Sternberg, P. W.; Stein, L. D. WormBase: A Multi-Species Resource for Nematode Biology and Genomics. *Nucleic Acids Res.* **2004**, *32* (Database issue), D411-7. https://doi.org/10.1093/nar/gkh066.
- (312) Antebi, A. Genetics of Aging in Caenorhabditis Elegans. *PLoS Genet.* **2007**, *3* (9), 1565–1571. https://doi.org/10.1371/journal.pgen.0030129.
- (313) Kulas, J.; Schmidt, C.; Rothe, M.; Schunck, W.-H.; Menzel, R. Cytochrome P450-Dependent Metabolism of Eicosapentaenoic Acid in the Nematode Caenorhabditis Elegans. *Arch. Biochem. Biophys.* **2008**, *472* (1), 65–75. https://doi.org/10.1016/j.abb.2008.02.002.
- (314) Pereira, L.; Kratsios, P.; Serrano-Saiz, E.; Sheftel, H.; Mayo, A. E.; Hall, D. H.; White, J. G.; LeBoeuf, B.; Garcia, L. R.; Alon, U.; Hobert, O. A Cellular and Regulatory Map of the Cholinergic Nervous System of C. Elegans. *Elife* **2015**, *4*. https://doi.org/10.7554/eLife.12432.
- (315) Uno, M.; Nishida, E. Lifespan-Regulating Genes in C. Elegans. *NPJ Aging Mech. Dis.* **2016**, 2 (1), 16010. https://doi.org/10.1038/npjamd.2016.10.
- (316) Liachko, N. F.; Guthrie, C. R.; Kraemer, B. C. Phosphorylation Promotes Neurotoxicity in a Caenorhabditis Elegans Model of TDP-43 Proteinopathy. *J. Neurosci.* **2010**, *30* (48), 16208–16219. https://doi.org/10.1523/JNEUROSCI.2911-10.2010.
- (317) Kraemer, B. C.; Zhang, B.; Leverenz, J. B.; Thomas, J. H.; Trojanowski, J. Q.; Schellenberg, G. D. Neurodegeneration and Defective Neurotransmission in a Caenorhabditis Elegans Model of Tauopathy. *Proc. Natl. Acad. Sci. U. S. A.* **2003**, *100* (17), 9980–9985. https://doi.org/10.1073/pnas.1533448100.
- (318) Griffin, E. F.; Caldwell, K. A.; Caldwell, G. A. Genetic and Pharmacological Discovery for Alzheimer's Disease Using Caenorhabditis Elegans. *ACS Chem. Neurosci.* **2017**, 8 (12), 2596–2606. https://doi.org/10.1021/acschemneuro.7b00361.
- (319) Benbow, S. J.; Strovas, T. J.; Darvas, M.; Saxton, A.; Kraemer, B. C. Synergistic Toxicity between Tau and Amyloid Drives Neuronal Dysfunction and Neurodegeneration in

- Transgenic C. Elegans. *Hum. Mol. Genet.* **2020**, 29 (3), 495–505. https://doi.org/10.1093/hmg/ddz319.
- (320) Yan, H.-F.; Zou, T.; Tuo, Q.-Z.; Xu, S.; Li, H.; Belaidi, A. A.; Lei, P. Ferroptosis: Mechanisms and Links with Diseases. *Signal Transduct. Target. Ther.* **2021**, *6* (1), 49. https://doi.org/10.1038/s41392-020-00428-9.
- (321) Tang, D.; Chen, X.; Kang, R.; Kroemer, G. Ferroptosis: Molecular Mechanisms and Health Implications. *Cell Res.* **2021**, *31* (2), 107–125. https://doi.org/10.1038/s41422-020-00441-1.
- (322) Eagle, H. Nutrition Needs of Mammalian Cells in Tissue Culture. *Science* **1955**, *122* (3168), 501–514. https://doi.org/10.1126/science.122.3168.501.
- (323) Tan, S.; Schubert, D.; Maher, P. Oxytosis: A Novel Form of Programmed Cell Death. *Curr. Top. Med. Chem.* **2001**, *I* (6), 497–506. https://doi.org/10.2174/1568026013394741.
- (324) Davis, J. B.; Maher, P. Protein Kinase C Activation Inhibits Glutamate-Induced Cytotoxicity in a Neuronal Cell Line. *Brain Res.* **1994**, *652* (1), 169–173. https://doi.org/10.1016/0006-8993(94)90334-4.
- (325) Sato, H.; Tamba, M.; Kuriyama-Matsumura, K.; Okuno, S.; Bannai, S. Molecular Cloning and Expression of Human XCT, the Light Chain of Amino Acid Transport System Xc-. *Antioxid. Redox Signal.* **2000**, 2 (4), 665–671. https://doi.org/10.1089/ars.2000.2.4-665.
- (326) Dolma, S.; Lessnick, S. L.; Hahn, W. C.; Stockwell, B. R. Identification of Genotype-Selective Antitumor Agents Using Synthetic Lethal Chemical Screening in Engineered Human Tumor Cells. *Cancer Cell* **2003**, *3* (3), 285–296. https://doi.org/10.1016/s1535-6108(03)00050-3.
- (327) Yagoda, N.; von Rechenberg, M.; Zaganjor, E.; Bauer, A. J.; Yang, W. S.; Fridman, D. J.; Wolpaw, A. J.; Smukste, I.; Peltier, J. M.; Boniface, J. J.; Smith, R.; Lessnick, S. L.; Sahasrabudhe, S.; Stockwell, B. R. RAS-RAF-MEK-Dependent Oxidative Cell Death Involving Voltage-Dependent Anion Channels. *Nature* **2007**, *447* (7146), 864–868. https://doi.org/10.1038/nature05859.
- (328) Yang, W. S.; Stockwell, B. R. Synthetic Lethal Screening Identifies Compounds Activating Iron-Dependent, Nonapoptotic Cell Death in Oncogenic-RAS-Harboring Cancer Cells. *Chem. Biol.* **2008**, *15* (3), 234–245. https://doi.org/10.1016/j.chembiol.2008.02.010.
- (329) Dixon, S. J.; Lemberg, K. M.; Lamprecht, M. R.; Skouta, R.; Zaitsev, E. M.; Gleason, C. E.; Patel, D. N.; Bauer, A. J.; Cantley, A. M.; Yang, W. S.; Morrison, B., 3rd; Stockwell, B. R. Ferroptosis: An Iron-Dependent Form of Nonapoptotic Cell Death. *Cell* **2012**, *149* (5), 1060–1072. https://doi.org/10.1016/j.cell.2012.03.042.
- (330) Hou, W.; Xie, Y.; Song, X.; Sun, X.; Lotze, M. T.; Zeh, H. J., 3rd; Kang, R.; Tang, D. Autophagy Promotes Ferroptosis by Degradation of Ferritin. *Autophagy* **2016**, *12* (8), 1425–1428. https://doi.org/10.1080/15548627.2016.1187366.

- (331) Gao, M.; Monian, P.; Pan, Q.; Zhang, W.; Xiang, J.; Jiang, X. Ferroptosis Is an Autophagic Cell Death Process. *Cell Res.* **2016**, *26* (9), 1021–1032. https://doi.org/10.1038/cr.2016.95.
- (332) Wang, Y.-Q.; Chang, S.-Y.; Wu, Q.; Gou, Y.-J.; Jia, L.; Cui, Y.-M.; Yu, P.; Shi, Z.-H.; Wu, W.-S.; Gao, G.; Chang, Y.-Z. The Protective Role of Mitochondrial Ferritin on Erastin-Induced Ferroptosis. *Front. Aging Neurosci.* **2016**, 8, 308. https://doi.org/10.3389/fnagi.2016.00308.
- (333) Protchenko, O.; Baratz, E.; Jadhav, S.; Li, F.; Shakoury-Elizeh, M.; Gavrilova, O.; Ghosh, M. C.; Cox, J. E.; Maschek, J. A.; Tyurin, V. A.; Tyurina, Y. Y.; Bayir, H.; Aron, A. T.; Chang, C. J.; Kagan, V. E.; Philpott, C. C. Iron Chaperone Poly RC Binding Protein 1 Protects Mouse Liver from Lipid Peroxidation and Steatosis. *Hepatology* **2021**, *73* (3), 1176–1193. https://doi.org/10.1002/hep.31328.
- (334) Reichert, C. O.; de Freitas, F. A.; Sampaio-Silva, J.; Rokita-Rosa, L.; Barros, P. de L.; Levy, D.; Bydlowski, S. P. Ferroptosis Mechanisms Involved in Neurodegenerative Diseases. *Int. J. Mol. Sci.* **2020**, *21* (22), 8765. https://doi.org/10.3390/ijms21228765.
- (335) Ayala, A.; Muñoz, M. F.; Argüelles, S. Lipid Peroxidation: Production, Metabolism, and Signaling Mechanisms of Malondialdehyde and 4-Hydroxy-2-Nonenal. *Oxid. Med. Cell. Longev.* **2014**, 360438. https://doi.org/10.1155/2014/360438.
- (336) Stockwell, B. R.; Friedmann Angeli, J. P.; Bayir, H.; Bush, A. I.; Conrad, M.; Dixon, S. J.; Fulda, S.; Gascón, S.; Hatzios, S. K.; Kagan, V. E.; Noel, K.; Jiang, X.; Linkermann, A.; Murphy, M. E.; Overholtzer, M.; Oyagi, A.; Pagnussat, G. C.; Park, J.; Ran, Q.; Rosenfeld, C. S.; Salnikow, K.; Tang, D.; Torti, F. M.; Torti, S. V.; Toyokuni, S.; Woerpel, K. A.; Zhang, D. D. Ferroptosis: A Regulated Cell Death Nexus Linking Metabolism, Redox Biology, and Disease. *Cell* **2017**, *171* (2), 273–285. https://doi.org/10.1016/j.cell.2017.09.021.
- (337) Stockwell, B. R.; Jiang, X. The Chemistry and Biology of Ferroptosis. *Cell Chem. Biol.* **2020**, 27 (4), 365–375. https://doi.org/10.1016/j.chembiol.2020.03.013.
- (338) Conrad, M.; Pratt, D. A. The Chemical Basis of Ferroptosis. *Nat. Chem. Biol.* **2019**, *15* (12), 1137–1147. https://doi.org/10.1038/s41589-019-0408-1.
- (339) Yang, W. S.; Stockwell, B. R. Ferroptosis: Death by Lipid Peroxidation. *Trends Cell Biol.* **2016**, 26 (3), 165–176. https://doi.org/10.1016/j.tcb.2015.10.014.
- (340) Magtanong, L.; Ko, P. J.; Dixon, S. J. Emerging Roles for Lipids in Non-Apoptotic Cell Death. *Cell Death Differ.* **2016**, *23* (7), 1099–1109. https://doi.org/10.1038/cdd.2016.25.
- (341) Feng, H.; Stockwell, B. R. Unsolved Mysteries: How Does Lipid Peroxidation Cause Ferroptosis? *PLoS Biol.* **2018**, *16* (5), e2006203. https://doi.org/10.1371/journal.pbio.2006203.
- (342) Agmon, E.; Stockwell, B. R. Lipid Homeostasis and Regulated Cell Death. *Curr. Opin. Chem. Biol.* **2017**, *39*, 83–89. https://doi.org/10.1016/j.cbpa.2017.06.002.

## Chapter 2. DIHYDROXY-METABOLITES OF DIHOMO-GAMMA LINOLENIC ACID DRIVE FERROPTOSIS-MEDIATED NEURODEGENERATION

#### **ABSTRACT**

Even after decades of research, the mechanism of neurodegeneration remains understudied, hindering the discovery of effective treatments for neurodegenerative diseases. Recent reports suggest that ferroptosis could be a novel therapeutic target for neurodegenerative diseases. While polyunsaturated fatty acid (PUFA) plays an important role in neurodegeneration and ferroptosis, how PUFAs may trigger these processes remains largely unknown. PUFA metabolites from cytochrome P450 and epoxide hydrolase metabolic pathways may modulate neurodegeneration. Here, we test the hypothesis that specific PUFAs regulate neurodegeneration through the action of their downstream metabolites by affecting ferroptosis. We find that the PUFA, dihomo gamma linolenic acid (DGLA), specifically induces ferroptosis-mediated neurodegeneration in dopaminergic neurons. Using synthetic chemical probes, targeted metabolomics, and genetic DGLA triggers neurodegeneration mutants. show that upon conversion we dihydroxyeicosadienoic acid through the action of CYP-EH, representing a new class of lipid metabolite that induces neurodegeneration via ferroptosis.

### 1. Introduction

By 2050, the projected population older than age 65 is expected to be more than double, reaching over 1.5 billion, and the projected population older than 80 is predicted to triple to 426 million. As aging is a risk factor for neurodegeneration, it is expected that the population with dementia will significantly increase in the near future.<sup>2</sup> However, the mechanisms of neurodegeneration remain unclear, and effective preventative measures and treatment are currently lacking.<sup>3</sup> Therefore, identifying molecular mechanisms underlying neurodegeneration is an unmet medical need. While tauopathy, neuroinflammation, and excitotoxicity may play key roles in neurodegeneration, recent studies provide compelling evidence that ferroptosis could be a new mechanism underlying neurodegeneration.<sup>3–5</sup> Ferroptosis is a non-apoptotic form of regulated cell death that is driven by an increase of iron-dependent lipid peroxidation in the cellular membrane. <sup>4,6</sup> Epidemiological studies showed that patients with Parkinson's disease (PD) or Alzheimer's disease (AD) have elevated iron and lipid peroxide levels in the brain as compared to healthy controls, which is consistent with ferroptosis.<sup>5,7-12</sup> The regulatory mechanism of ferroptosis in brain cells are understudied, although polyunsaturated fatty acids (PUFAs) play a critical role in this process. 13–17

PUFAs are key structural components of plasma membranes and play a critical role in neuronal functions. <sup>18</sup> Generally,  $\omega$ -3 and  $\omega$ -6 PUFAs are two of the major classes of PUFAs present in human diet. <sup>19</sup> Human studies have demonstrated that an increase in plasma  $\omega$ -3/ $\omega$ -6 PUFA ratio decreases the risk of neurodegenerative diseases, including AD and PD. <sup>20–23</sup> Nonetheless, even after decades of epidemiological studies in mammalian and cell-based models, how PUFAs affect neurodegeneration is poorly understood, with reported results that are contradictory. <sup>21,24,25</sup> While most efforts in research have investigated the neuroprotective effects

Although the mechanisms by which  $\omega$ -6 PUFAs mediate biological effects remain undefined, recent studies have demonstrated that  $\omega$ -6 PUFAs metabolites resulting from cytochrome P450 (CYP) enzymes and epoxide hydrolases (EHs) action are key signaling molecules for human physiology. <sup>18,33,34</sup> As such, this study was initiated to test whether specific  $\omega$ -6 PUFAs modulate neurodegeneration via their downstream CYP metabolites and to investigate if ferroptosis plays a role in the observed biology. Because the CYP enzymes and EHs are differentially expressed in tissues and cell types (Table S1), <sup>35–39</sup> and the expression of both enzymes are significantly affected by cell passages, <sup>40–42</sup> it is difficult to pinpoint a specific cell line suitable for our study. Therefore, a whole animal study is necessary to uncover this novel mechanism without worrying metabolites not being generated locally or overlooking critical cell-cell communications facilitated by these lipid metabolites.

To facilitate our study, we took an interdisciplinary approach by combining a simple genetic animal model, an inhibitor of a metabolic enzyme, synthesized lipid metabolites, and targeted metabolomics to systematically investigate the crosstalk between lipid metabolism, neurodegeneration, and ferroptosis. With this approach, we first demonstrate that among five tested PUFAs, only DGLA induces neurodegeneration in select neurons in *C. elegans*, with more

pronounced effects in dopaminergic neurons, and to a lesser extent in glutaminergic neurons, with no observable effects in cholinergic and GABAergic neurons. Furthermore, we demonstrate that the DGLA-induced neurodegeneration is mediated through its downstream CYP- EHs metabolite, dihydroxyeicosadienoic acid (DHED), and ferroptosis is likely the mechanism involved in DHED-induced neurodegeneration.

#### 2. Results

# 2.1. DGLA, but neither $\omega$ -3 nor other $\omega$ -6 PUFAs, induces degeneration specifically in dopaminergic neurons.

Our prior lipidomic analysis shows that C. elegans absorbs exogenous PUFAs. 43,44 To study the effect of dietary PUFAs on neuronal health span, we supplemented *Pdat-1::gfp* worms, in which the dopaminergic neurons are labeled by green fluorescent protein (GFP), with different  $\omega$ -6 PUFAs and eicosapentaenoic acid (20:5n-3, EPA), the most abundant  $\omega$ -3 PUFA in C. *elegans*, <sup>45</sup> and tracked the dopaminergic neurons throughout the worm lifespan using fluorescent imaging (**Figure 1A-C**). Supplementation was done at the larvae stage 4 (L4) when *C. elegans* has a fully developed neuronal system thus enabling the investigation of neurodegeneration independent of neurodevelopment. <sup>46</sup> Among the tested PUFAs, only DGLA induced significant degeneration in the dopaminergic neurons (Figure 1B). Furthermore, DGLA triggered degeneration in dopaminergic neurons in a dose-dependent manner with an EC<sub>50</sub>= 51.4 µM and 31.2 µM at day 1 and day 8 adulthood, respectively (Figure 1D, and S1). We also showed that the vehicle control, ethanol, did not change dopaminergic neurons' health span as compared to the control (Figure S2). In addition, we found that different types of dopaminergic neurons in the hermaphrodite had varying sensitivities to treatment with DGLA, with the ADE neurons (ADE>>>CEP>PDE) being the most impacted (**Figure S3**). Moreover, loss of the GFP signal did

not appear to result from transcriptional repression of the *Pdat-1::GFP* transgene induced by treatment with DGLA, since a similar trend was observed with the *Pcat-2::GFP* transgenic line upon treatment with DGLA (**Figure 1E and F**)). We then examined whether DGLA can induce degeneration in other major types of neurons that play key roles in neurodegenerative diseases including GABAergic, glutaminergic, and cholinergic neurons. Significant neurodegeneration was not observed in GABAergic (*Punc-25::gfp*) and cholinergic neurons (*Punc-17::gfp*) worms supplemented with DGLA (**Figure 1G-J**).

These findings were further confirmed with a lack of significant changes in thrashing assays in *C. elegans* treated with DGLA (**Figure 1K**), which requires cholinergic and GABAergic neurons activity. <sup>47,48</sup> In the case of glutamatergic neurons (*Peat-4::gfp*), treatment with DGLA caused cell loss in glutamatergic neurons only in later stage in the *C. elegans* lifespan compared to the dopaminergic neurons (**Figure 1L and M**). Altogether, our results suggest that the effect of PUFAs on neurodegeneration is structurally specific.

In addition, while previous studies reported that increased lipid peroxidation could induce neurodegeneration<sup>49–53</sup>, our data show that the treatment with the more peroxidizable arachidonic acid and EPA do not trigger neurodegeneration. Furthermore, our results indicate that the effect of DGLA on neurodegeneration is neuron-type selective, warranting future studies that may shine light on the molecular mechanism(s).

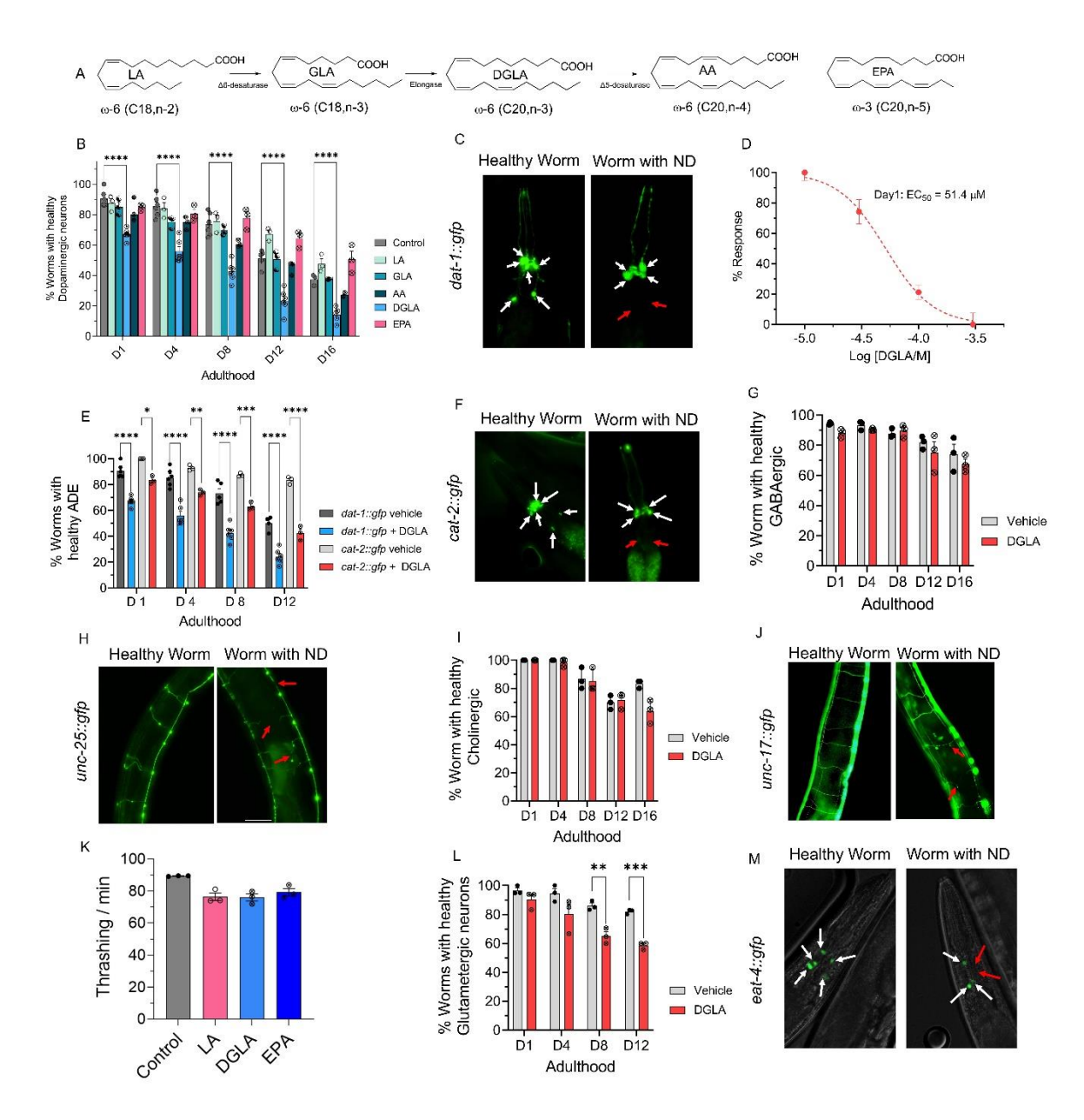


**Figure 1. DGLA, but not other w-3 and w-6 PUFAs, induces degeneration, specifically in dopaminergic neurons.** (**A**) Structure of different w-6 and w-3 PUFAs examined in this study; (**B**) Percentage (%) of worms with healthy dopaminergic neurons for *Pdat-1::gfp* with and without supplementation with 100 mM of different ω-6 and ω-3 PUFAs. (**C**) Fluorescent images of *Pdat-1::gfp* worms with healthy and degenerated dopaminergic neurons (White arrows represent healthy neurons, and red arrows show degenerated/disappeared neurons); (**D**) Dose response curve: the effect of different DGLA concentrations on degeneration of ADE neurons on Day 1 adulthood; (**E**) Comparing the ADE neurons degeneration in *Pdat-1::gfp* and *Pcat-2::gfp* supplemented with 100 mM DGLA; (**F**) Fluorescent images of *Pcat-2::gfp* worms with healthy and degenerated dopaminergic neurons (White arrows represents healthy neurons, and red arrow shows degeneration/disappearance neurons); (**G**) Percentage (%) of worms with healthy GABAergic neurons for *Punc-25::gfp* with and without supplementation with 100 mM DGLA; (**H**) Fluorescence images of *Punc-25::gfp* worm with healthy and degenerated GABAergic neurons (Red arrows show different signs of neurodegeneration including ventral cord break, commissure break and branches); (**I**) Percentage (%) of worms with healthy cholinergic neurons for *Punc-17::gfp* worms with healthy and degenerated cholinergic neurons (Red arrows show different signs of neurodegeneration including ventral cord break, commissure break and branches);

### Figure 1 (cont'd)

(**K**)Thrashing on Day 8 adulthood of wild-type raised on 100 mM of LA, DGLA, and EPA; (**L**) Percentage (%) of worms with healthy glutamatergic neurons with *Peat-4::gfp* with and without supplementation with 100 mM DGLA; (**M**) Fluorescent images of *Peat-4::gfp* worms with healthy and degenerated glutamatergic neurons (White arrows represent healthy neurons, and red arrows show degenerated/disappeared neurons). All supplementations were done at the L4 stage. For all experiments N=3, and about 20 worms were tested on each trial. Two-way analysis of variance (ANOVA), Tukey's multiple comparison test for (B) and (D); and t test for K: \*P  $\leq$  0.05, \*\*P  $\leq$  0.01, \*\*\*P  $\leq$  0.001, \*\*\*P  $\leq$  0.001, non-significant is not shown.

The remaining studies focused on the degeneration of dopaminergic neurons, as was found they are most sensitive to DGLA treatment. Because more robust data were obtained with transgenic *C. elegans Pdat1::gfp*, the rest of our studies were conducted using this strain. Most of the experiments were performed using day 1 and day 8 adults, enabling the determination of acute and chronic effects of DGLA treatment on neurodegeneration. Day 8 worms resemble a middle-aged population of *C. elegans*, thus the effect of DGLA treatment on age-associated neurodegeneration can also be investigated without a significant loss (death) of the tested population, facilitating the throughput of our studies.

### 2.2.DGLA induces neurodegeneration in dopaminergic neurons through ferroptosis

Recent studies show that treatment with DGLA can induce ferroptosis in germ cells and cause sterility in *C. elegans*.<sup>17</sup> To test whether treatment with DGLA induces degeneration in dopaminergic neurons through ferroptosis, *Pdat-1::gfp* expressing worms were co-treated with DGLA and liproxstatin-1 (Lip-1), a radical-trapping antioxidant and ferroptosis inhibitor.<sup>54</sup> While C. *elegans* treated with Lip-1 alone showed no significant effect on age-associated degeneration of dopaminergic neurons as compared to the vehicle control, co-treatment of DGLA with Lip-1 fully rescued the neurodegeneration triggered by DGLA in day 1 adults and largely rescued DGLA-induced neurodegeneration in day 8 adults (**Figure 2A**). Encouraged by these results, we examined neurodegeneration caused by ferroptosis in DGLA-treated worms using pharmacological and genetic approaches. An increase in the labile iron (II) pool and membrane

lipid peroxidation are molecular hallmarks of ferroptosis.<sup>6,55</sup> Therefore, we tested whether treatment with Trolox, a water-soluble form of vitamin E and lipid peroxidation inhibitor, and 2,2'-bipyridine, an iron (II) chelator, alleviates DGLA-induced neurodegeneration. Co-treatment with either Trolox or 2,2'-bipyridine rescued DGLA-induced neurodegeneration, suggesting that both the labile iron (II) pool and membrane lipid peroxidation are involved in DGLA-induced neurodegeneration (**Figure 2B and C**). To specifically investigate whether ferroptosis is involved in DGLA-induced neurodegeneration, was also pursued a genetic approach.

Previous studies have shown that nicotinamide adenine dinucleotide phosphate (NADPH) oxidase (NOX) family of superoxide-producing enzymes (NOX/DUOX) plays a critical role in ferroptosis in mammals and can exacerbate dopaminergic neurotoxicity triggered by ferroptosis inducers.<sup>4,56</sup>

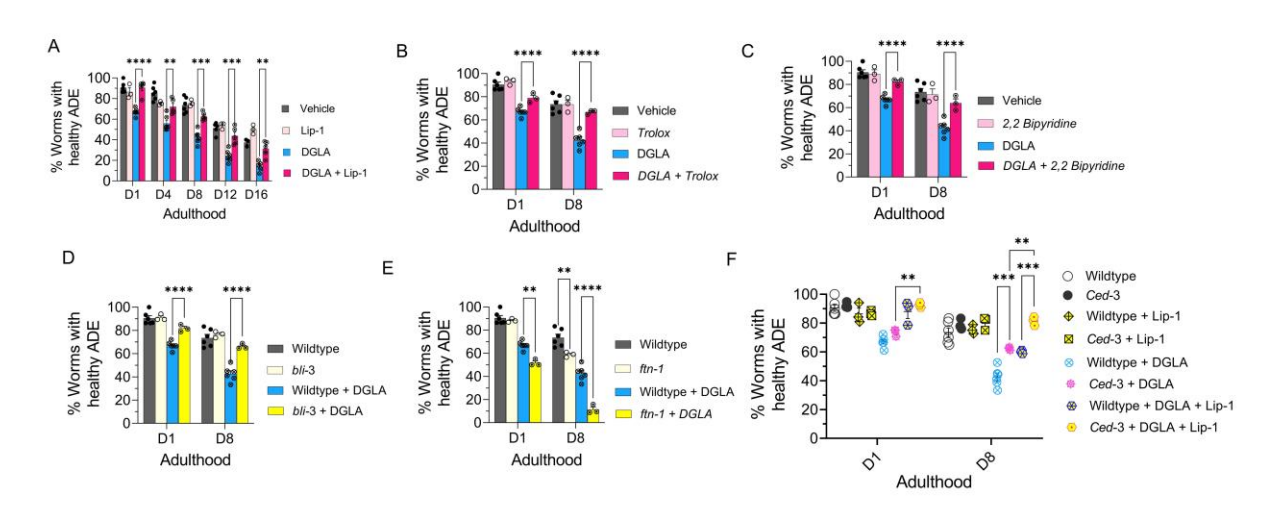


Figure 2. DGLA Induces neurodegeneration in dopaminergic neurons via ferroptosis. (A) Percentage (%) of worms with healthy ADE neurons of worms exposed to 100 mM DGLA  $\pm$  250 mM Liproxstatin-1; (B) Percentage (%) of worms with healthy ADE neurons in wild-type *C. elegans* treated with 100 mM DGLA  $\pm$  500 mM Trolox (vitamin E); (C) Percentage (%) of worms with healthy ADE neurons for *Pdat-1::*gfp worms treated with 100 mM DGLA $\pm$  100 mM 2,2'-bipyridine; (D) Percentage (%) of worms with healthy ADE neurons in *Pdat-1::*gfp and *Pdat-1::*gfp; bli-3 worms treated with 100 mM DGLA; (E) Percentage (%) of worms with healthy ADE neurons for *Pdat-1::*gfp and *Pdat-1::*gfp; ftn-1 worms treated with 100 mM DGLA; (F)Percentage (%) of worms with healthy ADE neurons with *Pdat-1::*gfp and *Pdat-1::*gfp; ced-3 worms treated with 100 mM DGLA  $\pm$  250 mM Liproxstatin-1. All supplementations were done at the L4 stage. A two-way analysis of variance (ANOVA), Tukey's multiple comparison test. \*P  $\leq$  0.05, \*\*P  $\leq$  0.01, \*\*\*P  $\leq$  0.001, \*\*\*P < 0.0001, NS, not significant. DGLA: Dihomo-γ-linolenic acid, LA: Linoleic acid, EPA: eicosapentaenoic acid, Lip-1: Liproxstatin-1.

In addition, ferritin (FTN) is also a key ferroptosis regulatory protein, and genetic knockout of FTN has been shown to sensitize *C. elegans* to ferroptosis. <sup>17,57</sup> To further test whether ferroptosis is involved in DGLA-induced neurodegeneration, two new transgenic C. elegans strains were created by crossing the Pdat-1::gfp with transgenic strains that carry either a loss of function of bli-3 (C. elegans homolog of NOX) mutant or genetic knockout of ftn-1 (Figure 2D, 2E, and S4). Our results indicated that the loss of function bli-3 mutant reduced the degeneration of dopaminergic neurons triggered by DGLA (Figure 2D). Worms with loss of function mutations of BLI-3 attenuated ability to generate reactive oxygen species, thus minimizing lipid peroxidation, and as a result, reduced ferroptosis. 17,58 This result further confirms the pharmacological observation after supplementing worms with the lipophilic antioxidant vitamin E (Trolox), which led to the suppression of neurodegeneration in DGLA-treated worms (**Figure 2B**). Furthermore, genetic knockout of ftn-1 enhanced DGLA-induced neurodegeneration, suggesting that DGLA requires the labile iron (II) pool to exert its effect on dopaminergic neurons (Figure 2E). Our data strongly suggest that DGLA causes degeneration of dopaminergic neurons at least partly through ferroptosis. As illustrated in Figure 2A, while Lip-1 fully rescued DGLA-induced neurodegeneration for day 1 adults, such rescuing effect diminished as C. elegans aged. Furthermore, the EC<sub>50</sub> of DGLA in triggering neurodegeneration for day 1 and day 8 adults is different. Therefore, we hypothesize that chronic treatment of DGLA induces other programmed cell-death pathways, like apoptosis, leading to neurodegeneration.

To test whether DGLA also induces neurodegeneration through apoptosis,<sup>59</sup> an additional transgenic strain was developed. The CED-3 protein, a key enzyme involved in apoptosis, was genetically knocked out in worms in which the dopaminergic neurons were labeled by GFP<sup>17,60</sup> to create transgenic line, *Pdat-1::gfp;ced-3(n717)*. Interestingly, while no significant difference was

observed between Pdat-1::gfp;ced-3(n717) and Pdat-1::gfp worms treated with DGLA at day 1 adulthood, worms that had the ced-3 genetic knockout demonstrated partial rescue from dopaminergic neuron degeneration induced by DGLA (**Figure 2F**) at day 8 of adulthood. Furthermore, the ced-3 knockout worms at day 8 adulthood that were co-treated with Lip-1 were fully rescued from dopaminergic neurodegeneration induced by DGLA (**Figure 2F**). These results could explain the differences observed for day 1 and day 8 worms treated with Lip-1 and DGLA (**Figure 2A**), as well as the differences in the EC<sub>50</sub> of DGLA-induced neurodegeneration between day 1 adults (EC<sub>50</sub> = 51.4  $\mu$ M) and day 8 adults (EC<sub>50</sub> = 31.2  $\mu$ M) (**Figure 1D**). The lower EC<sub>50</sub> for DGLA-induced neurodegeneration for day 8 adults suggests that other neurodegenerative mechanisms (i.e., apoptosis, autophagy) are involved and could either synergize or provide an additive effect with DGLA-induced neurodegeneration. Together, these results suggest that dietary DGLA induces neurodegeneration via ferroptosis in early adulthood and both ferroptosis and additional mechanism(s), such as apoptosis, are induced by DGLA in dopaminergic neurodegeneration in middle-aged C. elegans.

# 2.3. Downstream metabolites of DGLA are key players in neurodegeneration induced by DGLA treatment.

In mammals, DGLA and other PUFAs are mono-oxygenated by cytochrome P450 enzymes (CYPs) to hydroxy- and Ep-PUFAs. Ep-PUFAs are further hydrolyzed by epoxide hydrolases (EHs) to the dihydroxy-PUFAs (**Figure 3A**). Numerous animal and human studies have demonstrated that endogenous levels of CYP and EH metabolites produced from various PUFAs are highly correlated to dietary intake of the corresponding PUFAs, 61–63 in stark contrast to metabolites generated by cyclooxygenases and lipoxygenases, which are less correlated. 64–66 Both epoxy- and dihydroxy-PUFAs are key signaling molecules for mammalian physiology including,

but not limited to, neuroprotection. 18,67,68 Therefore, we hypothesized that DGLA primarily induces ferroptosis-mediated neurodegeneration via its CYP and/or EH metabolites, a previously unexplored area. To test this hypothesis, we first investigated whether the CYP/EH metabolism is involved in DGLA-induced ferroptosis-mediated neurodegeneration by investigating how treatment with DGLA impacts CYP/EH metabolism. Our results indicated that treatment with 100 µM DGLA increased the whole animal endogenous levels of the corresponding epoxyeicosadienoic acid (EED) and dihydroxyeicosadienoic acid (DHED) to ~200 pmol/g and ~800 pmol/g, respectively (regioisomer-dependent **Figure S5**), using our oxylipin analysis (Pourmand et. al, unpublished, see experimental methods in SI). These results were similar to the endogenous levels of EPA CYP/EH metabolites, epoxyeicosatetraenoic acid (EpETEs) and dihydroxyeicosatetraenoic acids (DHETE) which are 50-919 pmol/g and 0-458 pmol/g, respectively (regioisomer-dependent) in intact C. elegans, suggesting that the increased level of EED and DHED is physiologically relevant (Figures 3B and S5). Therefore, we sought to determine whether these downstream metabolites (EED and DHED) are key mediators for neurodegeneration induced by treatment with DGLA. Transgenic C. elegans (Pdat-1::gfp) were co-treated with DGLA and 12-(1-adamantane-1-yl-ureido-) dodecanoic acid (AUDA, 100 µM), an EH inhibitor with selective action to inhibit the function of CEEH1 and CEEH2 (C. elegans EH1 and EH2 isoforms). 69 AUDA treatment increased the level of EED and decreased the DHED in vivo concentration, and fully rescued dopaminergic neurodegeneration induced by DGLA, suggesting that the CYP/EH-derived downstream metabolites of DGLA play a critical role in DGLA-induced neurodegeneration (**Figures 3B, C**).

Nonetheless, these results do not discriminate between AUDA's ability to stabilize the level of EED *in vivo* for the observed rescue, or to block the production of DHED metabolites that result

from inhibiting *C. elegans* EHs (**Figures 3B** and **S6**). To distinguish between the latter two possibilities, we synthesized both EED and DHED and tested their effects in *C. elegans* following the procedures in previous reports.<sup>70–73</sup> Treatment with 100 μM EED at the L4 stage induced a more severe neurodegenerative phenotype than treatment with DGLA at the same concentration in the dopaminergic neurons in all tested ages (**Figure 3D**), with a much lower EC<sub>50</sub> (12.6 μM vs 51.4 μM) as compared to DGLA on day 1 adult (**Figures 3E and 1D**). The same trend was observed in glutamatergic neurons when comparing treatments of EED and DGLA, and similar to DGLA treatment, no significant neurodegeneration was observed in GABAergic and cholinergic neurons after treatment with EED (**Figure S7**).

To test whether the effect of EED is structurally specific, C18:1 epoxyoctadecenoic acid (EpOME), an epoxy-metabolite of LA, and a more peroxidizable C20:4 epoxyeicosatetraenoic acid (EEQ), an epoxy-metabolite of EPA, were examined (Figure 3F) and had no effects on neurodegeneration. These results indicate that the effect of Ep-PUFAs on neurodegeneration is specific to EED, but not other Ep-PUFAs. Similar to the neurodegeneration induced by DGLA, co-treatment with Lip-1 rescued neurodegeneration caused by EED, and Lip-1 was more effective in alleviating EED induced neurodegeneration compared to DGLA-induced neurodegeneration (Figures 3G, H). Furthermore, like DGLA, neuronal degeneration induced by EED was not rescued by a genetic knockout of *ced-3*. Genetic knockout of *ftn-1* escalates the effect of EED in both day 1 and day 8 adult, again suggesting that ferroptosis plays a critical role in EED-induced neurodegeneration (Figures 3I and J).

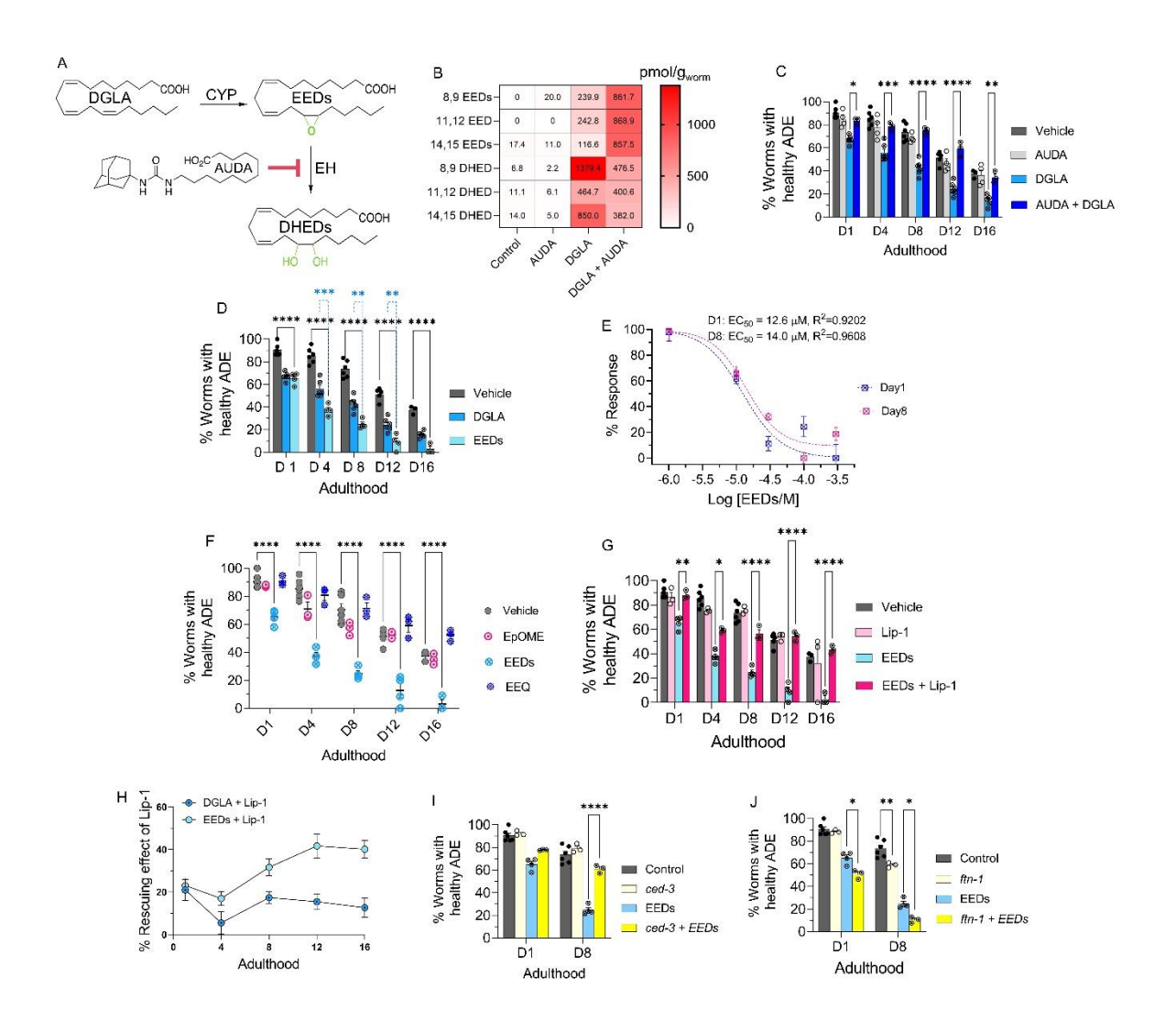


Figure 3. EED, epoxy metabolites downstream of DGLA, induce neurodegeneration by ferroptosis (A) DGLA is metabolized to EED and DHED through the CYP and epoxide hydrolase enzymes, respectively; and AUDA inhibits epoxide hydrolase; (B) Oxylipin profile representing the pmol/g of EED and DHED regioisomers in worms treated with 100 mM of DGLA ± 100 mM AUDA compared to control (C) Percentage (%) of worms with healthy ADE neurons for Pdat-1::gfp treated with 100 mM of DGLA ± 100 mM AUDA; (D) Percentage (%) of worms with healthy ADE neurons for Pdat-1::gfp worms treated with 100 mM DGLA and 100 mM EED; (E) Dose response curve: the effect of different concentration of EED on degeneration of ADE neurons on Day 1 and Day 8 adulthood; (F) Percentage (%) of worms with healthy ADE neurons in Pdat-1::gfp worms treated with 100 mM of different Ep-PUFAs, EpOME, and EEQ; (G) Percentage (%) of worms with healthy ADE neurons of worms treated with 100 mM DGLA  $\pm$  100 mM Liproxstatin-1;(H) Comparison the effect of 250 mM Liproxstatin-1 on *Pdat-1*::*gfp* worms treated with 100 mM of DGLA compared to 100 mM EED;(I) Percentage (%) of worms with healthy ADE neurons with Pdat-1::gfp and Pdat-1::gfp;ced-3 worms treated with 100 mM; (J) Percentage (%) of worms with healthy ADE neurons for Pdat-1::gfp and Pdat-1::gfp; ftn-1 worms treated with 100 mM DGLA; All supplementations were done at the L4 stage. Two-way analysis of variance (ANOVA), Tukey's multiple comparison test. \*P  $\leq$  0.05, \*\*P  $\leq$  0.01, \*\*\* $P \le 0.001$ , \*\*\*\*P < 0.0001, without \* not significant. DGLA: Dihomo- $\gamma$ -linolenic acid, EED: epoxyeicosadienoic acids, DHED: dihydroxyeicosadienoic acids, CYP: Cytochrome P450, EH: epoxide hydrolase, AUDA: 12-(1adamantane-1-yl-ureido-) dodecanoic acid, Lip-1: Liproxstatin-1, EpOME: epoxyoctadecenoic acids; EEQ: epoxyeicosatetraenoic acid.

Our results further suggested that DGLA metabolites are lipid mediators responsible for the effect of DGLA on neurodegeneration. Inhibition of EED hydrolysis using an EH inhibitor (AUDA) resulted in rescue of EED-induced neurodegeneration in *C. elegans* (**Figure 4A**). The oxylipin profile of worms co-treated with EED and AUDA at 100 µM shows that blocking the metabolism of Ep-PUFAs to dihydroxy-PUFAs, specifically EED to DHED with AUDA, stabilizes endogenous levels of Ep-PUFAs including EED, and decreases the *in vivo* levels of dihydroxy-PUFAs and DHED (**Figures 4B and S8**). Altogether, our data further suggests that specific DGLA downstream metabolites, either EED or DHED, are responsible for DGLA-mediated neurodegeneration.

We further tested our hypothesis by supplementing *Pdat-1::gfp* worms with 100 µM of DHED, exhibiting significant neurodegeneration compared to the vehicle control (**Figure 4C**). Intriguingly, co-treatment with AUDA and DHED did not alleviate neurodegeneration induced by DHED, further confirming that DHED is likely the main driver of dopaminergic neurodegeneration in our model (**Figure 4C**). Co-treatment with AUDA alleviated DGLA-induced neurodegeneration likely by blocking the formation of DHED. In addition, co-treatment with Lip-1 and 2,2-bipyridine rescued the neurodegeneration caused by DHED (**Figures 4D**, **and E**). Furthermore, the loss of function *bli-3* mutant also reduced the degeneration of dopaminergic neurons triggered by DHED, and genetic knockout of *ftn-1* augments DHED-induced neurodegeneration (**Figures 4F**, **and G**). Together, these results suggest that the labile iron (II) pool and subsequently ferroptosis are involved in the effect of DHED on dopaminergic neurons. It is noteworthy that we did not observe more severe neurodegeneration induced by DHED as compared to EED supplementation. This effect may be due to the difference in lipid transport mechanism between PUFAs, Epoxy-, and dihydroxy-PUFAs, as suggested by a previous study<sup>74</sup>.

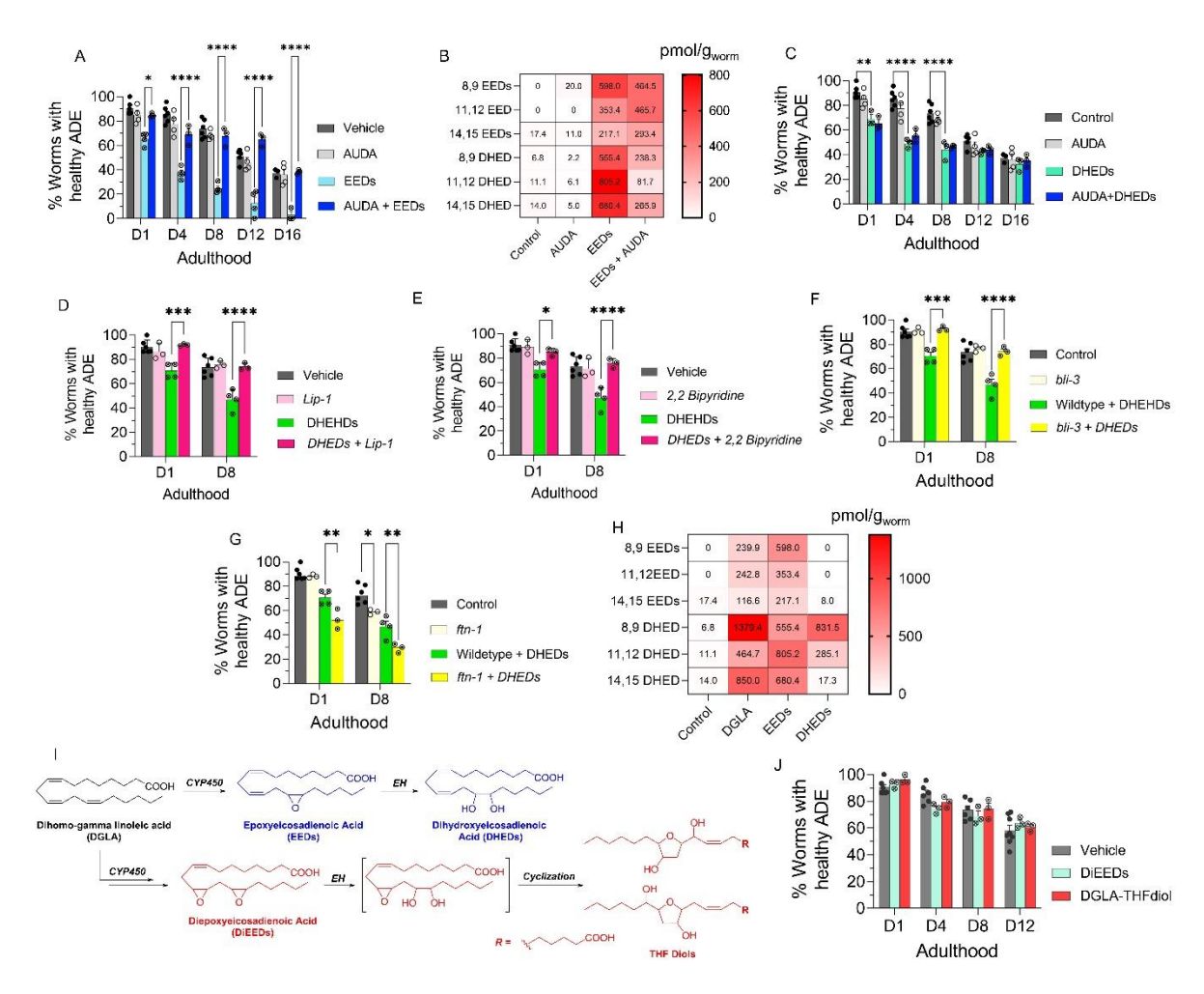


Figure 4. DHEDs, dihydroxy fatty acids downstream of DGLA/EED, are key candidates for neurodegeneration induced by DGLA in dopaminergic neurons (A) Percentage (%) of worms with healthy ADE neurons in Pdat-1::gfp worms treated with 100 mM of EED ± 100 mM AUDA; (B) Oxylipin profile representing pmol/g of EED and DHED regioisomers in worms treated with 100 mM of EED ± 100 mM AUDA compared to control. (C) Percentage (%) of worms with healthy ADE neurons for Pdat-1::gfp treated with 100 mM of DHED ± 100 mM AUDA; (**D**) Percentage (%) of worms with healthy ADE neurons of worms exposed to 100 mM DHED ± 250 mM Liproxstatin-1; (E) Percentage (%) of worms with healthy ADE neurons for *Pdat-1*::gfp worms treated with 100 mM DHEDs ± 100 mM 2,2'-bipyridine; (F) Percentage (%) of worms with healthy ADE neurons for Pdat-1::gfp and Pdat-1::gfp;ftn-1 worms treated with 100 mM DHED; (G) Percentage (%) of worms with healthy ADE neurons in Pdat-1::gfp and Pdat-1::gfp;bli-3 worms treated with 100 mM DEHDs; (H) Oxylipin profile representing the pmol/g of EED and DHED regioisomers in worms treated with 100 mM of DGLA, EED, and DHED compared to control. (I) two possible metabolisms of DGLA through the CYP/EH pathways; the alternative metabolism is that CYP can do two consecutive oxidations (or under oxidative stress) to yield diepoxies EED, which then EH will open one epoxide which under physiological conditions can cyclize to THF diols. (J) Percentage (%) of worms with healthy ADE neurons for Pdat-1::gfp treated with 100 mM of DiEED and 100 mM DGLA-THFdiol. All supplementations were done at the L4 stage. Two-way analysis of variance (ANOVA), Tukey's multiple comparison test. \*P  $\leq$  0.05, \*\*P  $\leq 0.01$ , \*\*\*P  $\leq 0.001$ , \*\*\*\*P < 0.0001, without \* not significant. DGLA: Dihomo- $\gamma$ -linolenic acid, EED: epoxyeicosadienoic acid, DHED: dihydroxyeicosadienoic acid, CYP: Cytochrome P450, EH: epoxide hydrolase, AUDA: 12-(1-adamantane-1-yl-ureido-) dodecanoic acid, DiEED: diepoxyeicosadienoic acid.

hypothesis was confirmed by oxylipin profiling, which showed significantly lower DHED levels (especially for 11,12 and 14,15 DHED) in worms treated with 100 µM DHED as compared to those treated with 100 µM EED or 100 µM DGLA (Figures 4D and S9). While DGLA and EED exhibit a continuous increase in dopaminergic neurodegeneration over their lifespan, DHED exhibited a plateau after day 8, which suggests the presence of a possible mechanism for removal of the offending agent, either by inducing downstream metabolism or activating lipid transport of DHED after chronic treatment. Our data strongly suggest that DGLA/EED induces neurodegeneration through their downstream metabolites. Beyond DHED, there have been a few reports of other downstream CYP-mediated metabolites, namely epoxy-hydroxy-PUFA and diepoxy-PUFAs, which ultimately undergo spontaneous intramolecular cyclization in physiological conditions to form an understudied class of metabolites, the tetrahydrofuran-diols (THF-diols). These THF-diols could be a new class of lipid mediatorsin mammals.<sup>75,76</sup> To examine these potential mediators of biological activity, isomeric vicinal diepoxyeicosenoic acid (DiEEe) and its corresponding THF-diol (DGLA-THF-diol) were synthesized and incubated with the worms (see the experimental section in SI and Figure 4E). However, no significant loss was observed in dopaminergic neurons in worms treated with 100 μM DiEEe and its corresponding THF-diol compared to the vehicle control (Figure 4F). These results strongly suggest that DHED constitutes a novel class of lipid mediators that induces neurodegeneration largely mediated by ferroptosis. In addition, EpETE and EpOME produced from EPA and LA, respectively, showed no effect on neurodegeneration, which further

DHED is not absorbed as well as EED, and thus are not as potent at the same concentration. This

corroborates the effect of DHED on ferroptosis-mediated neurodegeneration is structurally

selective. Furthermore, the results obtained from the treatment with more peroxidizable EPA and

EpETE indicate that the effect of DHED is not due to an increase in peroxidation of the cell membrane, a known mechanism that sensitizes ferroptosis. <sup>15,77–79</sup> As a whole, the results summarized above are contrast with reports on the effect of PUFAs<sup>80–82</sup> or their metabolites, such as lipoxygenase's metabolites, <sup>54,77,81</sup> ether lipids, <sup>83</sup> etc. on ferroptosis.

#### 3. Discussion

Our studies revealed that DHED, CYP-EH metabolite of DGLA, is a novel class of lipid molecules that triggers ferroptosis-mediated degeneration in select neuron types in C. elegans. Our study addresses critical gaps in knowledge in the field of lipid pharmacology, neurodegeneration, and ferroptosis, including how ω-6 PUFAs may trigger neurodegeneration and the identity of endogenous signaling molecules that induces ferroptosis-mediated neuronal cell death. Most research investigates the beneficial effects of ω-3 PUFA supplementation in neurodegenerative diseases, with contradictory findings. <sup>26,27,30</sup> Few studies have tested the effect of ω-6 PUFAs on neurodegeneration.<sup>28</sup> This is of high interest since ω-6 PUFA levels are typically high in western diets. Our findings in C. elegans demonstrate that, unlike other PUFAs, the ω-6 DGLA induces ferroptosis-mediated degeneration specifically in dopaminergic and to a lesser extent in glutaminergic neurons. Recent reports suggest PUFAs play a critical role in ferroptosis and treating cells with PUFAs, their ether-lipid metabolites, and lipoxygenase metabolites, hydroperoxyeicotetraenoic acids, sensitize cells to ferroptosis, but not induce ferroptosis themselves. 54,83 Although synthetic compounds such as erastin, RSL-3, and natural products like α-eleostearic acid have been identified as agents that can induce ferroptosis, the specific endogenous mediators that regulate the upstream pathway of ferroptosis remain unknown,. 13-15,31 Our results indicate that DGLA induces ferroptosis-mediated neuronal death likely through its downstream endogenous CYP-EH metabolites, DHED, and EH plays a critical role in modulating

DGLA-mediated ferroptosis. Our study complements the elegant work showing that DGLA induces ferroptosis in germline and cancer cells.<sup>17</sup> The identification of potential lipid signaling molecules represents a critical first step to investigating the molecular mechanism behind the effects of PUFAs on ferroptosis-mediated neurodegeneration.

Recent reports demonstrated that the expression of soluble EH, an human ortholog of CEEH 1/2, is upregulated in patients with neurodegenerative diseases including Parkinson's disease and Alzheimer's disease and, inhibition of soluble EH is beneficial for neurodegeneration in multiple neurodegenerative diseases animal models. 18,84–87 While the specific role of soluble EH in neurodegeneration is largely unknown, these studies suggested that the epoxy-fatty acids, the substrates of soluble EH, are neuroprotective, and the corresponding downstream EH metabolites dihydroxy-fatty acids have no effect, although a few studies in cell and animal models have showed that these dihydroxy-fatty acids can have detrimental or toxic effects on cells. 88,89 Our results provide an alternate perspective of how neurodegeneration could be regulated endogenously by modulating EH activity to increase ferroptotic metabolites, namely DHED, which has seldom been studied.

Our finding that DHEDs modulate ferroptosis-mediated neurodegeneration challenges the current paradigm in the field. Numerous studies demonstrated that membrane lipid composition and lipid peroxidation are essential for ferroptosis <sup>4,77,90,91</sup>. Supplementation with PUFAs and their metabolites, particularly those metabolites with a higher degree of unsaturation, sensitizes cells to ferroptosis<sup>4</sup>. However, unlike synthetic compounds such as Erastin, RSL-3, etc., these lipid molecules do not trigger ferroptosis, but rather act downstream of ferroptosis pathways by increasing the rate of membrane lipid peroxidation<sup>4,92,93</sup>. This phenomenon is further supported by studies showing that supplementation with a monosaturated fatty acid, such as oleic acid,

desensitizes cells from ferroptosis<sup>78</sup>. In contrast, our results show that a specific  $\omega$ -6 DGLA metabolite, DHED, induces ferroptosis, while other PUFAs (AA and EPA) and EPA metabolites (EEQ), with a higher degree of unsaturation, do not trigger ferroptosis. This observation aligns with a recent study showing that although EPA and AA supplementation are more deleterious in peroxide-induced whole-body oxidative stress, they cannot trigger ferroptotic germline cell death in *C. elegans*<sup>43</sup>.

Our data using Lip-1 supplementation, along with the use of transgenic strains carrying a loss of function ftn-1 mutation, suggests that DHED could trigger lipid peroxidation in the ferroptosis pathway. However, it is unlikely that DHED induces ferroptosis-mediated neurodegeneration by undergoing peroxidation itself, as discussed above, because supplementation with AA, EPA, and EEQ, which are more prone to lipid peroxidation, have minimal or no effects in our neurodegenerative assays. In addition, it has been reported that dihydroxy-PUFAs are unable to incorporate into cell membranes<sup>94</sup>, which suggests that DHEDs have a distinct mechanism for modulating ferroptosis compared to other PUFAs. It is because PUFAs with high degrees of unsaturation can propagate membrane lipid peroxidation during ferroptosis upon incorporation into the cell membrane. Although the exact mechanism underlying DHED induction of ferroptosis-mediated neurodegeneration is largely unknown, and falls beyond the scope of this study, we propose that DHED may interact with potential receptor proteins to activate the upstream ferroptosis pathway, leading to iron-mediated lipid peroxidation. This corroborates our finding from the experiments with Lip-1 and transgenic loss of function ftn-1 strains, which indicate a critical role for lipid peroxidation in DHED-induced neurodegeneration. While DHED has not been extensively studied, 9,10-dihydroxyoctadecenoic acid (DiHOME) and 12,13-DiHOME, which are dihydroxy-metabolites of LA, activate peroxisome proliferatoractivated receptor (PPAR) gamma, and transient receptor potential vanilloid 1 (TRPV1), respectively<sup>95,96</sup>. In addition, 14,15-dihydroxyeicosatrienoic acid, dihydroxy-metabolites of AA, also activate PPAR alpha<sup>97</sup>. All of these proteins have been associated with ferroptosis<sup>98–101</sup>. Therefore, DHEDs could modulate ferroptosis-mediated neurodegeneration by interacting with one of these proteins or similar proteins. Alternatively, although DHED is less likely to be incorporated into the cell membrane, it could still be localized into specific subcellular compartments such as mitochondria, the endoplasmic reticulum (that contains the largest pool of lipids in cells), and lysosomes, where DHED could be peroxidized and propagate lipid peroxidation, leading to ferroptosis <sup>13,54,102–105</sup>. Currently, our laboratory is conducting a variety of genetic experiments to identify potential receptor proteins for DHEDs and synthesizing the deuterated DHEDs to investigate whether DHEDs peroxidation is necessary for their action in ferroptosis-mediated neurodegeneration.

In this study, we employed an approach, which comprised of a simple animal model, an inhibitor of a metabolic enzyme, synthesized lipid metabolites, and targeted metabolomics to systematically investigate the crosstalk between lipid metabolism, neurodegeneration, and ferroptosis in a highly efficient way. We have not only identified the key mediator for ferroptosis-mediated neurodegeneration but have also revealed that DGLA and its metabolites have more pronounced effects on dopaminergic neurons, mild effects on glutaminergic neurons, and no effects on cholinergic and GABAergic neurons in *C. elegans*. Our results complement previous studies by Zille. *et al.*, which showed that different cell types could have distinct regulatory pathways for ferroptosis. While the specific mechanism behind why DGLA and its metabolites, DHED, are more detrimental to dopaminergic neurons remains unknown, Solano Fonseca *et al.* reported a similar vulnerability of different neuron-types in response to biomechanical injury and

suggested that such observation could be due to different physiological regulatory mechanisms between different neuron types.<sup>107</sup> Such neuron type-specific effects triggered by DGLA and DHED warrant future investigation to uncover potential new neurodegeneration mechanisms.

However, investigating ferroptosis to understand differential ferroptosis mechanisms between tissues requires studies being carried out at the system level that is challenging, owing to the lack of appropriate genetic and imaging tools. The genetic malleability of *C. elegans* provides a suitable platform for the study of ferroptosis in a tissue-specific manner. Furthermore, as illustrated in Table S1, most cell lines do not express soluble EH, a human ortholog of CEEHs and studies have demonstrated that different tissues express CYP enzymes and soluble epoxide hydrolase differently.<sup>35–38</sup> Therefore, a whole animal approach is more appropriate for us to explore this novel mechanism and *C. elegans* provides a simple animal model. In addition, the adaptability to high-throughput studies of *C. elegans* allows us quickly to dissect complicated pathways. As such, it is possible to explore how ferroptosis can be regulated differentially by endogenous signaling molecules, such as DHED, between cell-types in an intact organism. Furthermore, the chemical tools developed and utilized for this study lead to the exploration of novel hypotheses that aim to unravel PUFAs effects on organismal physiology, an area that is not only understudied, but also is challenging to execute in mammalian models and humans.

### 4. Conclusion

Oxidized lipid metabolites are key mediators for organismal physiology. Ferroptosis, characterized by an increase of iron-dependent lipid peroxidation, could be a novel mechanism for neurodegeneration. In this study, we reported that exogenous DGLA triggers neurodegeneration predominantly in dopaminergic neurons via its downstream cytochrome P450-epoxide hydrolase (CYP-EH) metabolite, dihydroxyeicosadienoic acid (DHED). The observed neurodegeneration

induced by DGLA/DHED is likely mediated by ferroptosis at the early stages and a combination of ferroptosis and apoptosis after chronic treatment with DGLA/DHED. This study revealed that CYP-EH polyunsaturated fatty acid (PUFA) metabolism is one of the key intrinsic regulatory mechanisms of ferroptosis-mediated neurodegeneration, and EH could be a novel target for ferroptosis-mediated diseases.

#### Acknowledgments

Some nematode strains were provided by the Caenorhabditis Genetics Center, funded by the NIH Office of Research Infrastructure Programs (P40 OD010440). The EM641 *Pcat-2::gfp* strain was a gift from Dr. Scott Emmons. The GA912 *ftn-1(ok3625)* strain was a gift from Dr. David Gems (University College London, London, UK). Funding to K.S.S.L. was provided by the NIGMS R35 GM146983, and Pearl Aldrich Endowment for aging research. J.L.W. was supported by NIH R01 GM133883. K.S.S.L. and J. A. were partially supported by startup funding from Michigan State University. M.S. was partially supported by Pearl Aldrich Endowment for aging research. Funding to T.R was graciously provided by Integrative Pharmacological Sciences Training Grant NIH T32GM142521. We acknowledge the MSU RTSF Mass Spectrometry and Metabolomics Core Facilities for support with oxylipin and lipidomic analysis. We would like to thank Dr. Brian Ackley (University of Kansas) for his advice on the neuronal studies; Dr. Scott Dixon for his comments for this study, as well as Mr. Devon Dattmore, Ms. Leslie Ramirez, and Ms. Heather deFeijter-Rupp (Michigan State University) for their help and assistance.

#### **Supporting Information**

Supporting Information including experimental methods and materials, supplemental figures and table, synthesis and characterization of DGLA metabolites, can be found in **APPENDIX 1.** 

#### **BIBLIOGRAPHY**

- (1) United Nations Department of Economic and Social Affairs. References. In *World Population Ageing 2019*; UN, 2020; pp 37–38. https://doi.org/10.18356/7f55a58e-en.
- (2) Hou, Y.; Dan, X.; Babbar, M.; Wei, Y.; Hasselbalch, S. G.; Croteau, D. L.; Bohr, V. A. Ageing as a Risk Factor for Neurodegenerative Disease. *Nat. Rev. Neurol.* **2019**, *15* (10), 565–581. https://doi.org/10.1038/s41582-019-0244-7.
- (3) Gan, L.; Cookson, M. R.; Petrucelli, L.; La Spada, A. R. Converging Pathways in Neurodegeneration, from Genetics to Mechanisms. *Nat. Neurosci.* **2018**, 21 (10), 1300–1309. https://doi.org/10.1038/s41593-018-0237-7.
- (4) Dixon, S. J.; Lemberg, K. M.; Lamprecht, M. R.; Skouta, R.; Zaitsev, E. M.; Gleason, C. E.; Patel, D. N.; Bauer, A. J.; Cantley, A. M.; Yang, W. S.; Morrison, B., 3rd; Stockwell, B. R. Ferroptosis: An Iron-Dependent Form of Nonapoptotic Cell Death. *Cell* **2012**, *149* (5), 1060–1072. https://doi.org/10.1016/j.cell.2012.03.042.
- (5) Ren, J.-X.; Sun, X.; Yan, X.-L.; Guo, Z.-N.; Yang, Y. Ferroptosis in Neurological Diseases. *Front. Cell. Neurosci.* **2020**, *14*, 218. https://doi.org/10.3389/fncel.2020.00218.
- (6) Dixon, S. J.; Stockwell, B. R. The Hallmarks of Ferroptosis. *Annu. Rev. Cancer Biol.* **2019**, *3* (1), 35–54. https://doi.org/10.1146/annurev-cancerbio-030518-055844.
- (7) Plascencia-Villa, G.; Perry, G. Implication of Ferroptosis Iron-dependent Programmed Cell Death Mechanism in Neurodegeneration. *Alzheimers. Dement.* **2020**, *16* (S3). https://doi.org/10.1002/alz.043978.
- (8) Do Van, B.; Gouel, F.; Jonneaux, A.; Timmerman, K.; Gelé, P.; Pétrault, M.; Bastide, M.; Laloux, C.; Moreau, C.; Bordet, R.; Devos, D.; Devedjian, J.-C. Ferroptosis, a Newly Characterized Form of Cell Death in Parkinson's Disease That Is Regulated by PKC. *Neurobiol. Dis.* **2016**, *94*, 169–178. https://doi.org/10.1016/j.nbd.2016.05.011.
- (9) Nikseresht, S.; Bush, A. I.; Ayton, S. Treating Alzheimer's Disease by Targeting Iron. *Br. J. Pharmacol.* **2019**, *176* (18), 3622–3635. https://doi.org/10.1111/bph.14567.
- (10) Du, L.; Zhao, Z.; Cui, A.; Zhu, Y.; Zhang, L.; Liu, J.; Shi, S.; Fu, C.; Han, X.; Gao, W.; Song, T.; Xie, L.; Wang, L.; Sun, S.; Guo, R.; Ma, G. Increased Iron Deposition on Brain Quantitative Susceptibility Mapping Correlates with Decreased Cognitive Function in Alzheimer's Disease. *ACS Chem. Neurosci.* **2018**, *9* (7), 1849–1857. https://doi.org/10.1021/acschemneuro.8b00194.
- (11) Martin-Bastida, A.; Ward, R. J.; Newbould, R.; Piccini, P.; Sharp, D.; Kabba, C.; Patel, M. C.; Spino, M.; Connelly, J.; Tricta, F.; Crichton, R. R.; Dexter, D. T. Brain Iron Chelation by Deferiprone in a Phase 2 Randomised Double-Blinded Placebo Controlled Clinical Trial in Parkinson's Disease. *Sci. Rep.* **2017**, *7* (1). https://doi.org/10.1038/s41598-017-01402-2.

- (12) Devos, D.; Moreau, C.; Devedjian, J. C.; Kluza, J.; Petrault, M.; Laloux, C.; Jonneaux, A.; Ryckewaert, G.; Garçon, G.; Rouaix, N.; Duhamel, A.; Jissendi, P.; Dujardin, K.; Auger, F.; Ravasi, L.; Hopes, L.; Grolez, G.; Firdaus, W.; Sablonnière, B.; Strubi-Vuillaume, I.; Zahr, N.; Destée, A.; Corvol, J.-C.; Pöltl, D.; Leist, M.; Rose, C.; Defebvre, L.; Marchetti, P.; Cabantchik, Z. I.; Bordet, R. Targeting Chelatable Iron as a Therapeutic Modality in Parkinson's Disease. *Antioxid. Redox Signal.* **2014**, *21* (2), 195–210. https://doi.org/10.1089/ars.2013.5593.
- (13) Feng, H.; Stockwell, B. R. Unsolved Mysteries: How Does Lipid Peroxidation Cause Ferroptosis? *PLoS Biol.* **2018**, *16* (5), e2006203. https://doi.org/10.1371/journal.pbio.2006203.
- (14) Das, U. N. Saturated Fatty Acids, MUFAs and PUFAs Regulate Ferroptosis. *Cell Chem. Biol.* **2019**, *26* (3), 309–311. https://doi.org/10.1016/j.chembiol.2019.03.001.
- (15) Yamada, N.; Karasawa, T.; Kimura, H.; Watanabe, S.; Komada, T.; Kamata, R.; Sampilvanjil, A.; Ito, J.; Nakagawa, K.; Kuwata, H.; Hara, S.; Mizuta, K.; Sakuma, Y.; Sata, N.; Takahashi, M. Ferroptosis Driven by Radical Oxidation of N-6 Polyunsaturated Fatty Acids Mediates Acetaminophen-Induced Acute Liver Failure. *Cell Death Dis.* **2020**, *11* (2), 144. https://doi.org/10.1038/s41419-020-2334-2.
- (16) Agmon, E.; Solon, J.; Bassereau, P.; Stockwell, B. R. Modeling the Effects of Lipid Peroxidation during Ferroptosis on Membrane Properties. *Sci. Rep.* **2018**, 8 (1). https://doi.org/10.1038/s41598-018-23408-0.
- (17) Perez, M. A.; Magtanong, L.; Dixon, S. J.; Watts, J. L. Dietary Lipids Induce Ferroptosis in Caenorhabditiselegans and Human Cancer Cells. *Dev. Cell* **2020**, *54* (4), 447-454.e4. https://doi.org/10.1016/j.devcel.2020.06.019.
- (18) Sarparast, M.; Dattmore, D.; Alan, J.; Lee, K. S. S. Cytochrome P450 Metabolism of Polyunsaturated Fatty Acids and Neurodegeneration. *Nutrients* **2020**, *12* (11), 3523. https://doi.org/10.3390/nu12113523.
- (19) Shahidi, F.; Ambigaipalan, P. Omega-3 Polyunsaturated Fatty Acids and Their Health Benefits. *Annu. Rev. Food Sci. Technol.* **2018**, *9*, 345–381. https://doi.org/10.1146/annurevfood-111317-095850.
- (20) Eriksdotter, M.; Vedin, I.; Falahati, F.; Freund-Levi, Y.; Hjorth, E.; Faxen-Irving, G.; Wahlund, L.-O.; Schultzberg, M.; Basun, H.; Cederholm, T.; Palmblad, J. Plasma Fatty Acid Profiles in Relation to Cognition and Gender in Alzheimer's Disease Patients during Oral Omega-3 Fatty Acid Supplementation: The OmegAD Study. *J. Alzheimers. Dis.* **2015**, *48* (3), 805–812. https://doi.org/10.3233/JAD-150102.
- (21) Jernerén, F.; Cederholm, T.; Refsum, H.; Smith, A. D.; Turner, C.; Palmblad, J.; Eriksdotter, M.; Hjorth, E.; Faxen-Irving, G.; Wahlund, L.-O.; Schultzberg, M.; Basun, H.; Freund-Levi, Y. Homocysteine Status Modifies the Treatment Effect of Omega-3 Fatty Acids on Cognition in a Randomized Clinical Trial in Mild to Moderate Alzheimer's Disease: The OmegAD Study. *J. Alzheimers. Dis.* **2019**, *69* (1), 189–197. https://doi.org/10.3233/JAD-181148.

- (22) Kalmijn, S.; Launer, L. J.; Ott, A.; Witteman, J. C.; Hofman, A.; Breteler, M. M. Dietary Fat Intake and the Risk of Incident Dementia in the Rotterdam Study. *Ann. Neurol.* **1997**, *42* (5), 776–782. https://doi.org/10.1002/ana.410420514.
- (23) Simopoulos, A. P. Importance of the Ratio of Omega-6/Omega-3 Essential Fatty Acids: Evolutionary Aspects. *World Rev. Nutr. Diet.* **2003**, 92, 1–22. https://doi.org/10.1159/000073788.
- (24) Ballenger, J. C. Dietary Patterns and Risk of Dementia: The Three-City Cohort Study. *Year b. psychiatry appl. ment. health* **2009**, 2009, 278–279. https://doi.org/10.1016/s0084-3970(08)79239-9.
- (25) Phillips, M. A.; Childs, C. E.; Calder, P. C.; Rogers, P. J. No Effect of Omega-3 Fatty Acid Supplementation on Cognition and Mood in Individuals with Cognitive Impairment and Probable Alzheimer's Disease: A Randomised Controlled Trial. *Int. J. Mol. Sci.* **2015**, *16* (10), 24600–24613. https://doi.org/10.3390/ijms161024600.
- (26) Lebbadi, M.; Julien, C.; Phivilay, A.; Tremblay, C.; Emond, V.; Kang, J. X.; Calon, F. Endogenous Conversion of Omega-6 into Omega-3 Fatty Acids Improves Neuropathology in an Animal Model of Alzheimer's Disease. *J. Alzheimers. Dis.* **2011**, *27* (4), 853–869. https://doi.org/10.3233/JAD-2011-111010.
- (27) Ajith, T. A. A Recent Update on the Effects of Omega-3 Fatty Acids in Alzheimer's Disease. *Curr. Clin. Pharmacol.* **2018**, *13* (4), 252–260. https://doi.org/10.2174/1574884713666180807145648.
- (28) Ma, Q.-M.; Zhu, C.; Caoili, K.; Frautschy, S. A.; Cole, G. M. The Novel Omega-6 Fatty Acid Docosapentaenoic Acid Positively Modulates Brain Innate Immune Response for Resolving Neuroinflammation at Early and Late Stages of Humanized APOE-based Alzheimer's Disease Models. *Alzheimers. Dement.* **2020**, *16* (S9). https://doi.org/10.1002/alz.044178.
- (29) Simopoulos, A. P. Evolutionary Aspects of Diet and Essential Fatty Acids. *World Rev. Nutr. Diet.* **2001**, 88, 18–27. https://doi.org/10.1159/000059742.
- (30) Blasbalg, T. L.; Hibbeln, J. R.; Ramsden, C. E.; Majchrzak, S. F.; Rawlings, R. R. Changes in Consumption of Omega-3 and Omega-6 Fatty Acids in the United States during the 20th Century. *Am. J. Clin. Nutr.* **2011**, *93* (5), 950–962. https://doi.org/10.3945/ajcn.110.006643.
- (31) Doll, S.; Proneth, B.; Tyurina, Y. Y.; Panzilius, E.; Kobayashi, S.; Ingold, I.; Irmler, M.; Beckers, J.; Aichler, M.; Walch, A.; Prokisch, H.; Trümbach, D.; Mao, G.; Qu, F.; Bayir, H.; Füllekrug, J.; Scheel, C. H.; Wurst, W.; Schick, J. A.; Kagan, V. E.; Angeli, J. P. F.; Conrad, M. ACSL4 Dictates Ferroptosis Sensitivity by Shaping Cellular Lipid Composition. *Nat. Chem. Biol.* **2017**, *13* (1), 91–98. https://doi.org/10.1038/nchembio.2239.
- (32) Deline, M.; Keller, J.; Rothe, M.; Schunck, W.-H.; Menzel, R.; Watts, J. L. Epoxides Derived from Dietary Dihomo-Gamma-Linolenic Acid Induce Germ Cell Death in C. Elegans. *Sci. Rep.* **2015**, *5*, 15417. https://doi.org/10.1038/srep15417.

- (33) Santos, D.; Laila, R. B.; Fleming, I. Role of Cytochrome P450-Derived, Polyunsaturated Fatty Acid Mediators in Diabetes and the Metabolic Syndrome. *Prostaglandins & Other Lipid Mediators* **2020**, *148*.
- (34) Shoieb, S. M.; El-Ghiaty, M. A.; Alqahtani, M. A.; El-Kadi, A. O. S. Cytochrome P450-Derived Eicosanoids and Inflammation in Liver Diseases. *Prostaglandins Other Lipid Mediat.* **2020**, *147*, 106400. https://doi.org/10.1016/j.prostaglandins.2019.106400.
- (35) Enayetallah, A. E.; French, R. A.; Thibodeau, M. S.; Grant, D. F. Distribution of Soluble Epoxide Hydrolase and of Cytochrome P450 2C8, 2C9, and 2J2 in Human Tissues. *J. Histochem. Cytochem.* **2004**, 52 (4), 447–454. https://doi.org/10.1177/002215540405200403.
- (36) Sura, P.; Sura, R.; Enayetallah, A. E.; Grant, D. F. Distribution and Expression of Soluble Epoxide Hydrolase in Human Brain. *J. Histochem. Cytochem.* **2008**, *56* (6), 551–559. https://doi.org/10.1369/jhc.2008.950659.
- (37) Harris, T. R.; Hammock, B. D. Soluble Epoxide Hydrolase: Gene Structure, Expression and Deletion. *Gene* **2013**, *526* (2), 61–74. https://doi.org/10.1016/j.gene.2013.05.008.
- (38) Booth Depaz, I. M.; Toselli, F.; Wilce, P. A.; Gillam, E. M. J. Differential Expression of Cytochrome P450 Enzymes from the CYP2C Subfamily in the Human Brain. *Drug Metab. Dispos.* **2015**, *43* (3), 353–357. https://doi.org/10.1124/dmd.114.061242.
- (39) Karlsson, M.; Zhang, C.; Méar, L.; Zhong, W.; Digre, A.; Katona, B.; Sjöstedt, E.; Butler, L.; Odeberg, J.; Dusart, P.; Edfors, F.; Oksvold, P.; von Feilitzen, K.; Zwahlen, M.; Arif, M.; Altay, O.; Li, X.; Ozcan, M.; Mardinoglu, A.; Fagerberg, L.; Mulder, J.; Luo, Y.; Ponten, F.; Uhlén, M.; Lindskog, C. A Single–Cell Type Transcriptomics Map of Human Tissues. *Sci. Adv.* **2021**, *7* (31). https://doi.org/10.1126/sciadv.abh2169.
- (40) Vierck, J. L.; Dodson, M. V. Interpretation of Cell Culture Phenomena. *Methods Cell Sci.* **2000**, 22 (1), 79–81.
- (41) Fleming, I. Cytochrome P450 Epoxygenases as EDHF Synthase(s). *Pharmacol. Res.* **2004**, 49 (6), 525–533. https://doi.org/10.1016/j.phrs.2003.11.016.
- (42) Pozzi, A.; Macias-Perez, I.; Abair, T.; Wei, S.; Su, Y.; Zent, R.; Falck, J. R.; Capdevila, J. H. Characterization of 5,6- and 8,9-Epoxyeicosatrienoic Acids (5,6- and 8,9-EET) as Potent in Vivo Angiogenic Lipids. *J. Biol. Chem.* **2005**, 280 (29), 27138–27146. https://doi.org/10.1074/jbc.M501730200.
- (43) Perez, M. A.; Clostio, A. J.; Houston, I. R.; Ruiz, J.; Magtanong, L.; Dixon, S. J.; Watts, J. L. Ether Lipid Deficiency Disrupts Lipid Homeostasis Leading to Ferroptosis Sensitivity. *PLoS Genet.* **2022**, *18* (9), e1010436. https://doi.org/10.1371/journal.pgen.1010436.
- (44) Watts, J. L.; Browse, J. Genetic Dissection of Polyunsaturated Fatty Acid Synthesis in Caenorhabditis Elegans. *Proc. Natl. Acad. Sci. U. S. A.* **2002**, 99 (9), 5854–5859. https://doi.org/10.1073/pnas.092064799.

- (45) Watts, J. L. Using Caenorhabditis Elegans to Uncover Conserved Functions of Omega-3 and Omega-6 Fatty Acids. *J. Clin. Med. Res.* **2016**, *5* (2). https://doi.org/10.3390/jcm5020019.
- (46) Pathak, A.; Chatterjee, N.; Sinha, S. Developmental Trajectory of Caenorhabditis Elegans Nervous System Governs Its Structural Organization. *PLoS Comput. Biol.* **2020**, *16* (1), e1007602. https://doi.org/10.1371/journal.pcbi.1007602.
- (47) Gjorgjieva, J.; Biron, D.; Haspel, G. Neurobiology of Caenorhabditis Elegans Locomotion: Where Do We Stand? *Bioscience* **2014**, *64* (6), 476–486. https://doi.org/10.1093/biosci/biu058.
- (48) Altun, Z. F.; Hall, D. H. WormAtlas Hermaphrodite Handbook Nervous System General Description. *WormAtlas* **2005**. https://doi.org/10.3908/wormatlas.1.18.
- (49) Sultana, R.; Perluigi, M.; Butterfield, D. A. Lipid Peroxidation Triggers Neurodegeneration: A Redox Proteomics View into the Alzheimer Disease Brain. *Free Radic. Biol. Med.* **2013**, 62, 157–169. https://doi.org/10.1016/j.freeradbiomed.2012.09.027.
- (50) Praticò, D.; Uryu, K.; Leight, S.; Trojanoswki, J. Q.; Lee, V. M. Increased Lipid Peroxidation Precedes Amyloid Plaque Formation in an Animal Model of Alzheimer Amyloidosis. *J. Neurosci.* **2001**, *21* (12), 4183–4187. https://doi.org/10.1523/jneurosci.21-12-04183.2001.
- (51) Angelova, P. R.; Horrocks, M. H.; Klenerman, D.; Gandhi, S.; Abramov, A. Y.; Shchepinov, M. S. Lipid Peroxidation Is Essential for α-Synuclein-Induced Cell Death. *J. Neurochem.* **2015**, *133* (4), 582–589. https://doi.org/10.1111/jnc.13024.
- (52) Fu, Y.; He, Y.; Phan, K.; Bhatia, S.; Pickford, R.; Wu, P.; Dzamko, N.; Halliday, G. M.; Kim, W. S. Increased Unsaturated Lipids Underlie Lipid Peroxidation in Synucleinopathy Brain. *Acta Neuropathol. Commun.* **2022**, *10* (1), 165. https://doi.org/10.1186/s40478-022-01469-7.
- (53) Galbusera, C.; Facheris, M.; Magni, F.; Galimberti, G.; Sala, G.; Tremolada, L.; Isella, V.; Guerini, F. R.; Appollonio, I.; Galli-Kienle, M.; Ferrarese, C. Increased Susceptibility to Plasma Lipid Peroxidation in Alzheimer Disease Patients. *Curr. Alzheimer Res.* **2004**, *I* (2), 103–109. https://doi.org/10.2174/1567205043332171.
- (54) Friedmann Angeli, J. P.; Schneider, M.; Proneth, B.; Tyurina, Y. Y.; Tyurin, V. A.; Hammond, V. J.; Herbach, N.; Aichler, M.; Walch, A.; Eggenhofer, E.; Basavarajappa, D.; Rådmark, O.; Kobayashi, S.; Seibt, T.; Beck, H.; Neff, F.; Esposito, I.; Wanke, R.; Förster, H.; Yefremova, O.; Heinrichmeyer, M.; Bornkamm, G. W.; Geissler, E. K.; Thomas, S. B.; Stockwell, B. R.; O'Donnell, V. B.; Kagan, V. E.; Schick, J. A.; Conrad, M. Inactivation of the Ferroptosis Regulator Gpx4 Triggers Acute Renal Failure in Mice. *Nat. Cell Biol.* **2014**, *16* (12), 1180–1191. https://doi.org/10.1038/ncb3064.
- (55) Li, J.; Cao, F.; Yin, H.-L.; Huang, Z.-J.; Lin, Z.-T.; Mao, N.; Sun, B.; Wang, G. Ferroptosis: Past, Present and Future. *Cell Death Dis.* **2020**, *11* (2), 88. https://doi.org/10.1038/s41419-020-2298-2.

- (56) Hou, L.; Huang, R.; Sun, F.; Zhang, L.; Wang, Q. NADPH Oxidase Regulates Paraquat and Maneb-Induced Dopaminergic Neurodegeneration through Ferroptosis. *Toxicology* **2019**, *417*, 64–73. https://doi.org/10.1016/j.tox.2019.02.011.
- (57) Chen, X.; Yu, C.; Kang, R.; Tang, D. Iron Metabolism in Ferroptosis. *Front Cell Dev Biol* **2020**, *8*, 590226. https://doi.org/10.3389/fcell.2020.590226.
- (58) Chávez, V.; Mohri-Shiomi, A.; Garsin, D. A. Ce-Duox1/BLI-3 Generates Reactive Oxygen Species as a Protective Innate Immune Mechanism in *Caenorhabditis Elegans*. *Infect. Immun*. **2009**, 77 (11), 4983–4989. https://doi.org/10.1128/iai.00627-09.
- (59) Erekat, N. S. Apoptosis and Its Therapeutic Implications in Neurodegenerative Diseases. *Clin. Anat.* **2022**, *35* (1), 65–78. https://doi.org/10.1002/ca.23792.
- (60) Webster, C. M.; Deline, M. L.; Watts, J. L. Stress Response Pathways Protect Germ Cells from Omega-6 Polyunsaturated Fatty Acid-Mediated Toxicity in Caenorhabditis Elegans. *Dev. Biol.* **2013**, *373* (1), 14–25. https://doi.org/10.1016/j.ydbio.2012.10.002.
- (61) Naoe, S.; Tsugawa, H.; Takahashi, M.; Ikeda, K.; Arita, M. Characterization of Lipid Profiles after Dietary Intake of Polyunsaturated Fatty Acids Using Integrated Untargeted and Targeted Lipidomics. *Metabolites* **2019**, *9* (10), 241. https://doi.org/10.3390/metabo9100241.
- (62) Keenan, A. H.; Pedersen, T. L.; Fillaus, K.; Larson, M. K.; Shearer, G. C.; Newman, J. W. Basal Omega-3 Fatty Acid Status Affects Fatty Acid and Oxylipin Responses to High-Dose N3-HUFA in Healthy Volunteers. *J. Lipid Res.* **2012**, *53* (8), 1662–1669. https://doi.org/10.1194/jlr.P025577.
- (63) Wang, W.; Yang, J.; Nimiya, Y.; Lee, K. S. S.; Sanidad, K.; Qi, W.; Sukamtoh, E.; Park, Y.; Liu, Z.; Zhang, G. ω-3 Polyunsaturated Fatty Acids and Their Cytochrome P450-Derived Metabolites Suppress Colorectal Tumor Development in Mice. *J. Nutr. Biochem.* **2017**, *48*, 29–35. https://doi.org/10.1016/j.jnutbio.2017.06.006.
- (64) Fischer, R.; Konkel, A.; Mehling, H.; Blossey, K.; Gapelyuk, A.; Wessel, N.; von Schacky, C.; Dechend, R.; Muller, D. N.; Rothe, M.; Luft, F. C.; Weylandt, K.; Schunck, W.-H. Dietary Omega-3 Fatty Acids Modulate the Eicosanoid Profile in Man Primarily via the CYP-Epoxygenase Pathway. *J. Lipid Res.* **2014**, *55* (6), 1150–1164. https://doi.org/10.1194/jlr.M047357.
- (65) Schebb, N. H.; Ostermann, A. I.; Yang, J.; Hammock, B. D.; Hahn, A.; Schuchardt, J. P. Comparison of the Effects of Long-Chain Omega-3 Fatty Acid Supplementation on Plasma Levels of Free and Esterified Oxylipins. *Prostaglandins Other Lipid Mediat.* **2014**, *113–115*, 21–29. https://doi.org/10.1016/j.prostaglandins.2014.05.002.
- (66) Schmöcker, C.; Zhang, I.; Kiesler, S.; Kassner, U.; Ostermann, A.; Steinhagen-Thiessen, E.; Schebb, N.; Weylandt, K.-H. Effect of Omega-3 Fatty Acid Supplementation on Oxylipins in a Routine Clinical Setting. *Int. J. Mol. Sci.* **2018**, *19* (1), 180. https://doi.org/10.3390/ijms19010180.

- (67) Morisseau, C.; Hammock, B. D. Impact of Soluble Epoxide Hydrolase and Epoxyeicosanoids on Human Health. *Annu. Rev. Pharmacol. Toxicol.* **2013**, *53*, 37–58. https://doi.org/10.1146/annurev-pharmtox-011112-140244.
- (68) Deng, Y.; Theken, K. N.; Lee, C. R. Cytochrome P450 Epoxygenases, Soluble Epoxide Hydrolase, and the Regulation of Cardiovascular Inflammation. *J. Mol. Cell. Cardiol.* **2010**, 48 (2), 331–341. https://doi.org/10.1016/j.yjmcc.2009.10.022.
- (69) Harris, T. R.; Aronov, P. A.; Jones, P. D.; Tanaka, H.; Arand, M.; Hammock, B. D. Identification of Two Epoxide Hydrolases in Caenorhabditis Elegans That Metabolize Mammalian Lipid Signaling Molecules. *Arch. Biochem. Biophys.* **2008**, *472* (2), 139–149. https://doi.org/10.1016/j.abb.2008.01.016.
- (70) Lee, K. S. S.; Henriksen, N. M.; Ng, C. J.; Yang, J.; Jia, W.; Morisseau, C.; Andaya, A.; Gilson, M. K.; Hammock, B. D. Probing the Orientation of Inhibitor and Epoxy-Eicosatrienoic Acid Binding in the Active Site of Soluble Epoxide Hydrolase. *Arch. Biochem. Biophys.* **2017**, *613*, 1–11. https://doi.org/10.1016/j.abb.2016.10.017.
- (71) Wagner, K.; Lee, K. S. S.; Yang, J.; Hammock, B. D. Epoxy Fatty Acids Mediate Analgesia in Murine Diabetic Neuropathy. *Eur. J. Pain* **2017**, *21* (3), 456–465. https://doi.org/10.1002/ejp.939.
- (72) Cinelli, M. A.; Yang, J.; Scharmen, A.; Woodman, J.; Karchalla, L. M.; Lee, K. S. S. Enzymatic Synthesis and Chemical Inversion Provide Both Enantiomers of Bioactive Epoxydocosapentaenoic Acids. *J. Lipid Res.* **2018**, *59* (11), 2237–2252. https://doi.org/10.1194/jlr.D089136.
- (73) Cinelli, M. A.; Lee, K. S. S. Asymmetric Total Synthesis of 19,20-Epoxydocosapentaenoic Acid, a Bioactive Metabolite of Docosahexaenoic Acid. *J. Org. Chem.* **2019**, *84* (23), 15362–15372. https://doi.org/10.1021/acs.joc.9b02378.
- (74) Fang, X.; Weintraub, N. L.; McCaw, R. B.; Hu, S.; Harmon, S. D.; Rice, J. B.; Hammock, B. D.; Spector, A. A. Effect of Soluble Epoxide Hydrolase Inhibition on Epoxyeicosatrienoic Acid Metabolism in Human Blood Vessels. *Am. J. Physiol. Heart Circ. Physiol.* **2004**, 287 (6), H2412-20. https://doi.org/10.1152/ajpheart.00527.2004.
- (75) Halarnkar, P. P.; Nourooz-Zadeh, J.; Kuwano, E.; Jones, A. D.; Hammock, B. D. Formation of Cyclic Products from the Diepoxide of Long-Chain Fatty Esters by Cytosolic Epoxide Hydrolase. *Arch. Biochem. Biophys.* **1992**, *294* (2), 586–593. https://doi.org/10.1016/0003-9861(92)90729-g.
- (76) Moghaddam, M. Novel Metabolic Pathways for Linoleic and Arachidonic Acid Metabolism. *Biochim. Biophys. Acta Gen. Subj.* **1996**, *1290* (3), 327–339. https://doi.org/10.1016/0304-4165(96)00037-2.
- (77) Yang, W. S.; Kim, K. J.; Gaschler, M. M.; Patel, M.; Shchepinov, M. S.; Stockwell, B. R. Peroxidation of Polyunsaturated Fatty Acids by Lipoxygenases Drives Ferroptosis. *Proc. Natl. Acad. Sci. U. S. A.* **2016**, *113* (34), E4966-75. https://doi.org/10.1073/pnas.1603244113.

- (78) Magtanong, L.; Ko, P.-J.; To, M.; Cao, J. Y.; Forcina, G. C.; Tarangelo, A.; Ward, C. C.; Cho, K.; Patti, G. J.; Nomura, D. K.; Olzmann, J. A.; Dixon, S. J. Exogenous Monounsaturated Fatty Acids Promote a Ferroptosis-Resistant Cell State. *Cell Chem. Biol.* **2019**, *26* (3), 420-432.e9. https://doi.org/10.1016/j.chembiol.2018.11.016.
- (79) Conrad, M.; Pratt, D. A. The Chemical Basis of Ferroptosis. *Nat. Chem. Biol.* **2019**, *15* (12), 1137–1147. https://doi.org/10.1038/s41589-019-0408-1.
- (80) Dierge, E.; Debock, E.; Guilbaud, C.; Corbet, C.; Mignolet, E.; Mignard, L.; Bastien, E.; Dessy, C.; Larondelle, Y.; Feron, O. Peroxidation of N-3 and n-6 Polyunsaturated Fatty Acids in the Acidic Tumor Environment Leads to Ferroptosis-Mediated Anticancer Effects. *Cell Metab.* **2021**, *33* (8), 1701-1715.e5. https://doi.org/10.1016/j.cmet.2021.05.016.
- (81) Kagan, V. E.; Mao, G.; Qu, F.; Angeli, J. P. F.; Doll, S.; Croix, C. S.; Dar, H. H.; Liu, B.; Tyurin, V. A.; Ritov, V. B.; Kapralov, A. A.; Amoscato, A. A.; Jiang, J.; Anthonymuthu, T.; Mohammadyani, D.; Yang, Q.; Proneth, B.; Klein-Seetharaman, J.; Watkins, S.; Bahar, I.; Greenberger, J.; Mallampalli, R. K.; Stockwell, B. R.; Tyurina, Y. Y.; Conrad, M.; Bayır, H. Oxidized Arachidonic and Adrenic PEs Navigate Cells to Ferroptosis. *Nat. Chem. Biol.* **2017**, *13* (1), 81–90. https://doi.org/10.1038/nchembio.2238.
- (82) Lee, J.-Y.; Nam, M.; Son, H. Y.; Hyun, K.; Jang, S. Y.; Kim, J. W.; Kim, M. W.; Jung, Y.; Jang, E.; Yoon, S.-J.; Kim, J.; Kim, J.; Seo, J.; Min, J.-K.; Oh, K.-J.; Han, B.-S.; Kim, W. K.; Bae, K.-H.; Song, J.; Kim, J.; Huh, Y.-M.; Hwang, G.-S.; Lee, E.-W.; Lee, S. C. Polyunsaturated Fatty Acid Biosynthesis Pathway Determines Ferroptosis Sensitivity in Gastric Cancer. *Proc. Natl. Acad. Sci. U. S. A.* **2020**, *117* (51), 32433–32442. https://doi.org/10.1073/pnas.2006828117.
- (83) Zou, Y.; Henry, W. S.; Ricq, E. L.; Graham, E. T.; Phadnis, V. V.; Maretich, P.; Paradkar, S.; Boehnke, N.; Deik, A. A.; Reinhardt, F.; Eaton, J. K.; Ferguson, B.; Wang, W.; Fairman, J.; Keys, H. R.; Dančík, V.; Clish, C. B.; Clemons, P. A.; Hammond, P. T.; Boyer, L. A.; Weinberg, R. A.; Schreiber, S. L. Plasticity of Ether Lipids Promotes Ferroptosis Susceptibility and Evasion. *Nature* **2020**, *585* (7826), 603–608. https://doi.org/10.1038/s41586-020-2732-8.
- (84) Ren, Q.; Ma, M.; Yang, J.; Nonaka, R.; Yamaguchi, A.; Ishikawa, K.-I.; Kobayashi, K.; Murayama, S.; Hwang, S. H.; Saiki, S.; Akamatsu, W.; Hattori, N.; Hammock, B. D.; Hashimoto, K. Soluble Epoxide Hydrolase Plays a Key Role in the Pathogenesis of Parkinson's Disease. *Proc. Natl. Acad. Sci. U. S. A.* **2018**, *115* (25), E5815–E5823. https://doi.org/10.1073/pnas.1802179115.
- (85) Lee, H.-T.; Lee, K.-I.; Chen, C.-H.; Lee, T.-S. Genetic Deletion of Soluble Epoxide Hydrolase Delays the Progression of Alzheimer's Disease. *J. Neuroinflammation* **2019**, *16* (1), 267. https://doi.org/10.1186/s12974-019-1635-9.
- (86) Ghosh, A.; Comerota, M. M.; Wan, D.; Chen, F.; Propson, N. E.; Hwang, S. H.; Hammock, B. D.; Zheng, H. An Epoxide Hydrolase Inhibitor Reduces Neuroinflammation in a Mouse Model of Alzheimer's Disease. *Sci. Transl. Med.* **2020**, *12* (573). https://doi.org/10.1126/scitranslmed.abb1206.

- (87) Griñán-Ferré, C.; Codony, S.; Pujol, E.; Yang, J.; Leiva, R.; Escolano, C.; Puigoriol-Illamola, D.; Companys-Alemany, J.; Corpas, R.; Sanfeliu, C.; Pérez, B.; Loza, M. I.; Brea, J.; Morisseau, C.; Hammock, B. D.; Vázquez, S.; Pallàs, M.; Galdeano, C. Pharmacological Inhibition of Soluble Epoxide Hydrolase as a New Therapy for Alzheimer's Disease. *Neurotherapeutics* **2020**. https://doi.org/10.1007/s13311-020-00854-1.
- (88) Kundu, S.; Roome, T.; Bhattacharjee, A.; Carnevale, K. A.; Yakubenko, V. P.; Zhang, R.; Hwang, S. H.; Hammock, B. D.; Cathcart, M. K. Metabolic Products of Soluble Epoxide Hydrolase Are Essential for Monocyte Chemotaxis to MCP-1 in Vitro and in Vivo. *J. Lipid Res.* **2013**, *54* (2), 436–447. https://doi.org/10.1194/jlr.M031914.
- (89) Hildreth, K.; Kodani, S. D.; Hammock, B. D.; Zhao, L. Cytochrome P450-Derived Linoleic Acid Metabolites EpOMEs and DiHOMEs: A Review of Recent Studies. *J. Nutr. Biochem.* **2020**, 86 (108484), 108484. https://doi.org/10.1016/j.jnutbio.2020.108484.
- (90) Wiernicki, B.; Dubois, H.; Tyurina, Y. Y.; Hassannia, B.; Bayir, H.; Kagan, V. E.; Vandenabeele, P.; Wullaert, A.; Vanden Berghe, T. Excessive Phospholipid Peroxidation Distinguishes Ferroptosis from Other Cell Death Modes Including Pyroptosis. *Cell Death Dis.* **2020**, *11* (10), 922. https://doi.org/10.1038/s41419-020-03118-0.
- (91) Ran, Q.; Liang, H.; Gu, M.; Qi, W.; Walter, C. A.; Roberts, L. J., 2nd; Herman, B.; Richardson, A.; Van Remmen, H. Transgenic Mice Overexpressing Glutathione Peroxidase 4 Are Protected against Oxidative Stress-Induced Apoptosis. *J. Biol. Chem.* **2004**, 279 (53), 55137–55146. https://doi.org/10.1074/jbc.M410387200.
- (92) Shintoku, R.; Takigawa, Y.; Yamada, K.; Kubota, C.; Yoshimoto, Y.; Takeuchi, T.; Koshiishi, I.; Torii, S. Lipoxygenase-Mediated Generation of Lipid Peroxides Enhances Ferroptosis Induced by Erastin and RSL3. *Cancer Sci.* **2017**, *108* (11), 2187–2194. https://doi.org/10.1111/cas.13380.
- (93) Porter, N. A.; Lehman, L. S.; Weber, B. A.; Smith, K. J. Unified Mechanism for Polyunsaturated Fatty Acid Autoxidation. Competition of Peroxy Radical Hydrogen Atom Abstraction, .Beta.-Scission, and Cyclization. *J. Am. Chem. Soc.* **1981**, *103* (21), 6447–6455. https://doi.org/10.1021/ja00411a032.
- (94) VanRollins, M.; Kaduce, T. L.; Knapp, H. R.; Spector, A. A. 14,15-Epoxyeicosatrienoic Acid Metabolism in Endothelial Cells. *J. Lipid Res.* **1993**, *34* (11), 1931–1942. https://doi.org/10.1016/s0022-2275(20)35111-7.
- (95) Lecka-Czernik, B.; Moerman, E. J.; Grant, D. F.; Lehmann, J. M.; Manolagas, S. C.; Jilka, R. L. Divergent Effects of Selective Peroxisome Proliferator-Activated Receptor-Gamma 2 Ligands on Adipocyte versus Osteoblast Differentiation. *Endocrinology* **2002**, *143* (6), 2376–2384. https://doi.org/10.1210/endo.143.6.8834.
- (96) Zimmer, B.; Angioni, C.; Osthues, T.; Toewe, A.; Thomas, D.; Pierre, S. C.; Geisslinger, G.; Scholich, K.; Sisignano, M. The Oxidized Linoleic Acid Metabolite 12,13-DiHOME Mediates Thermal Hyperalgesia during Inflammatory Pain. *Biochim. Biophys. Acta Mol. Cell Biol. Lipids* **2018**, *1863* (7), 669–678. https://doi.org/10.1016/j.bbalip.2018.03.012.

- (97) Fang, X.; Hu, S.; Xu, B.; Snyder, G. D.; Harmon, S.; Yao, J.; Liu, Y.; Sangras, B.; Falck, J. R.; Weintraub, N. L.; Spector, A. A. 14,15-Dihydroxyeicosatrienoic Acid Activates Peroxisome Proliferator-Activated Receptor-Alpha. *Am. J. Physiol. Heart Circ. Physiol.* **2006**, *290* (1), H55-63. https://doi.org/10.1152/ajpheart.00427.2005.
- (98) Venkatesh, D.; O'Brien, N. A.; Zandkarimi, F.; Tong, D. R.; Stokes, M. E.; Dunn, D. E.; Kengmana, E. S.; Aron, A. T.; Klein, A. M.; Csuka, J. M.; Moon, S.-H.; Conrad, M.; Chang, C. J.; Lo, D. C.; D'Alessandro, A.; Prives, C.; Stockwell, B. R. MDM2 and MDMX Promote Ferroptosis by PPARα-Mediated Lipid Remodeling. *Genes Dev.* **2020**, *34* (7–8), 526–543. https://doi.org/10.1101/gad.334219.119.
- (99) Xing, G.; Meng, L.; Cao, S.; Liu, S.; Wu, J.; Li, Q.; Huang, W.; Zhang, L. PPARα Alleviates Iron Overload-Induced Ferroptosis in Mouse Liver. *EMBO Rep.* **2022**, *23* (8), e52280. https://doi.org/10.15252/embr.202052280.
- (100) Duan, C.; Jiao, D.; Wang, H.; Wu, Q.; Men, W.; Yan, H.; Li, C. Activation of the PPARγ Prevents Ferroptosis-Induced Neuronal Loss in Response to Intracerebral Hemorrhage through Synergistic Actions with the Nrf2. *Front. Pharmacol.* **2022**, *13*, 869300. https://doi.org/10.3389/fphar.2022.869300.
- (101) Riegger, J. TRPV1 as an Anti-Ferroptotic Target in Osteoarthritis. *EBioMedicine* **2022**, *84* (104279), 104279. https://doi.org/10.1016/j.ebiom.2022.104279.
- (102) Yang, Y.; Lee, M.; Fairn, G. D. Phospholipid Subcellular Localization and Dynamics. *J. Biol. Chem.* **2018**, 293 (17), 6230–6240. https://doi.org/10.1074/jbc.R117.000582.
- (103) Dixon, S. J.; Patel, D. N.; Welsch, M.; Skouta, R.; Lee, E. D.; Hayano, M.; Thomas, A. G.; Gleason, C. E.; Tatonetti, N. P.; Slusher, B. S.; Stockwell, B. R. Pharmacological Inhibition of Cystine-Glutamate Exchange Induces Endoplasmic Reticulum Stress and Ferroptosis. *Elife* **2014**, *3*, e02523. https://doi.org/10.7554/eLife.02523.
- (104) Gaschler, M. M.; Hu, F.; Feng, H.; Linkermann, A.; Min, W.; Stockwell, B. R. Determination of the Subcellular Localization and Mechanism of Action of Ferrostatins in Suppressing Ferroptosis. *ACS Chem. Biol.* **2018**, *13* (4), 1013–1020. https://doi.org/10.1021/acschembio.8b00199.
- (105) Gan, B. Mitochondrial Regulation of Ferroptosis. *J. Cell Biol.* **2021**, 220 (9). https://doi.org/10.1083/jcb.202105043.
- (106) Zille, M.; Kumar, A.; Kundu, N.; Bourassa, M. W.; Wong, V. S. C.; Willis, D.; Karuppagounder, S. S.; Ratan, R. R. Ferroptosis in Neurons and Cancer Cells Is Similar but Differentially Regulated by Histone Deacetylase Inhibitors. *eNeuro* **2019**, *6* (1), ENEURO.0263-18.2019. https://doi.org/10.1523/ENEURO.0263-18.2019.
- (107) Solano Fonseca, R.; Metang, P.; Egge, N.; Liu, Y.; Zuurbier, K. R.; Sivaprakasam, K.; Shirazi, S.; Chuah, A.; Arneaud, S. L.; Konopka, G.; Qian, D.; Douglas, P. M. Glycolytic Preconditioning in Astrocytes Mitigates Trauma-Induced Neurodegeneration. *Elife* **2021**, *10*. https://doi.org/10.7554/eLife.69438.

Chapter 3. EXPLORING THE ROLE OF CYP-EH METABOLITES IN A $\beta$  AND TAU-INDUCED NEURODEGENERATION: INSIGHTS FROM CAENORHABDITIS ELEGANS

### **ABSTRACT**

This study aims to uncover potent cytochrome P450 (CYP) and epoxide hydrolase (EH) metabolites implicated in AB and/or tau-induced neurodegeneration, independent of neuroinflammation, by utilizing Caenorhabditis elegans (C. elegans) as a model organism. Our research reveals that AB and/or tau expression in C. elegans disrupts the oxylipin profile, and epoxide hydrolase inhibition alleviates the ensuing neurodegeneration, likely through elevating the epoxy-to-hydroxy ratio of various CYP-EH metabolites. These findings emphasize the intriguing relationship between dietary  $\omega$ -3 and  $\omega$ -6 PUFAs and their metabolites, and potentially establishing a link between nutrition, diet, and Alzheimer's disease (AD). (Detailed information on AD and PUFA are discussed in chapter 1) Furthermore, our investigation sheds light on the crucial and captivating role of CYP PUFA metabolites in C. elegans physiology, opening up possibilities for broader implications in mammalian and human contexts.

## 1. Introduction

Alzheimer's disease (AD) is a progressive neurodegenerative disorder characterized by the accumulation of amyloid-beta ( $A\beta$ ) plaques and neurofibrillary tau tangles in the brain<sup>1,2</sup>. The presence of  $A\beta$  and tau remains the hallmarks of AD. While the amyloid cascade hypothesis has dominated the field, the limited efficacy of anti- $A\beta$  therapy suggest a more complex pathogenesis<sup>2–4</sup>. Although tau, or specifically hyperphosphorylated tau, was suggested as an important pathways downstream of  $A\beta$ -induced neurodegeneration, recent studies demonstrated that tau and  $A\beta$  can induce neurodegeneration through different mechanisms and act synergistically in several models <sup>2,5–12</sup>. These data emphasize the potential necessity for treatments addressing multiple facets of AD pathology and the importance of exploring diverse therapeutic targets to tackle the complexities of AD.

The association between lipid mediators and AD presents an intriguing perspective to explore. Lipids and lipid mediators are thought to play a pivotal role in the development and progression of AD, particularly lipid interactions with amyloid-beta (Aβ) and tau proteins .<sup>13–17</sup>. Within the realm of lipid mediators, cytochrome P450 (CYP) and epoxide hydrolase (EH) metabolites, including epoxy-PUFAs (Ep-PUFA), hydroxy-PUFAs and dihydroxy-PUFAs, stand out as essential endogenous lipid signaling molecules with diverse physiological roles <sup>18–21</sup>. The brain possesses a high capacity to make Ep-PUFAs and dihydroxy-PUFAs from their parent PUFAs using CYP and EH enzymes, respectively <sup>18,22–24</sup>. Studies revealed increased levels of proinflammatory lipid mediators, such as HETEs, and decreased pro-resolving oxylipins, like epoxyeicosatrienoic acids (EETs), in the brains of transgenic AD animals compared to their healthy counterparts<sup>25,26</sup>. Furthermore, genetic analyses in humans demonstrated that variations in cytochrome P450 (CYP) isoforms contribute to the risk for AD pathology. Additionally, people

with AD exhibit significantly elevated levels of soluble EH (sEH) in the brain compared to healthy individuals  $^{26-29}$ . In addition, a growing body of evidence shows that inhibiting or genetically knocking out sEH reduces A $\beta$  plaques and phosphorylated tau in the brain, mitigating AD progression in various murine models  $^{26,29,30}$ , further indicating that CYP-EH metabolites play a critical role in AD pathogenesis.

Although the relationship between oxylipins,  $A\beta$ , and tau in the context of AD has been the subject of several studies, much of their reciprocal influence remains poorly understood. This is partly due to the complexity of mammalian nervous systems and lipid metabolism, along with the associated challenges and costs of working with mammalian and human models in aged-associated neurodegeneration. In order to gain a deeper understanding of the interplay between oxylipins, Aβ, and tau, and their impact on age-associated neurodegeneration, a more tractable model organism that can be adapted to high-throughput studies is needed. The nematode Caenorhabditis elegans (C. elegans) offers several advantages in this regard. C. elegans can synthesize a wide range of ω-3 and ω-6 PUFAs de novo, including the CYP-EH metabolites consisting of epoxy- and dihydroxy-PUFAs. <sup>31</sup> Furthermore, these pathways are highly conserved between humans and *C. elegans*. The nematode also possesses a simple nervous system with neuronal signaling similar to humans, making it an excellent model organism for AD and aging research<sup>32,33</sup>. Furthermore, C. elegans share substantial genetic similarity with humans, as approximately 60-80% of its genes have human orthologs, in addition to numerous conserved biological pathways, including those associated with aging<sup>34–38</sup>. Various studies demonstrated that molecular routes, protein targets, and potential drug candidates identified from C. elegans prove effective in mammalian models and are and likely translatable to humans<sup>33,36,39-41</sup> The absence of inflammatory cells, microglia, and astrocytes in C. elegans also allows for the investigation of AB and tau effects on oxylipin profiles

independent of neuroinflammation, 42,43 which allows us to solely study the effect of CYP-EH metabolites on neurons.

In this study, we aimed to investigate the relationship between oxylipins, A $\beta$ , and tau in the context of neurodegeneration using the *C. elegans* model animal. We examined the oxylipin profiles in the presence of A $\beta$  and/or tau expression and their potential role in neurodegenerative processes. Furthermore, we explored the therapeutic potential of epoxide hydrolase inhibition as a means to modulate oxylipin levels, and we examined their impact on A $\beta$  and tau-mediated neurodegeneration. Our findings may provide valuable insights into the complex interplay between oxylipins, A $\beta$ , and tau in Alzheimer's disease and contribute to the development of novel therapeutic strategies targeting multiple facets of AD pathology.

#### 2. Results

To dissect the contribution of tau and A $\beta$  aggregation to AD pathology-related neurotoxicity and neurodegeneration, we used *C. elegans* strains with pan-neuronal expression of human tau and A $\beta$ . Although previous studies have reported the phenotypic response changes in *C. elegans* expressing human tau and A $\beta$ , we aimed to first validate that the strains we used effectively exhibit neurodegeneration and reduced healthspan in our specific experimental conditions. This validation is crucial for ensuring the reliability of our animal model before proceeding with further analyses. Once we confirmed the successful expression of tau and A $\beta$  and their impact on neurodegeneration and healthspan, we then examined the oxylipin profiles of each strain to gain further insights.

## 2.1. Expression of either A $\beta$ 1-42 peptide and/or tau in neurons causes behavioral abnormalities.

To delve into the impact of Aβ or tau expression on neuronal function in C. elegans, we utilized the CL2355 and CK1441 strains, respectively, as well as CK1609 for co-expression of AB and tau <sup>34,44</sup>. Due to temperature dependence of human Aβ and tau gene expression in these strains, we temperature upshifted form 16°C degree to 25°C at L4 stage when the nervous system is fully developed. Therefore, we were able to avoid the possible effects of AB and tau expression on neurodevelopment. We first examined the neuronal function in these transgenic strains using thrashing behavior performed by placing age-synchronized worms in S-basal solution. We found that transgenic worms expressing tau (Tau-Transgenic or Tau-Tg) show significantly less thrashing compared to wildtype worms, while the worm expressing  $A\beta_{1-42}$  ( $A\beta_{1-42}$ -Tg) experienced a mild decline at later ages. These data suggest that there are distinct effects of AB and tau in motor neurons responsible for thrashing (Figure 1A). Co-expression of A $\beta$  and tau (A $\beta_{1-42}$ /Tau-Tg) resulted in a similar trend as the Tau-Tg strain. These finding aligned with the observation in pervious reports<sup>34,44</sup>. Furthermore, the radian locomotion assay, which tracks the worm movement on a solid media rather than in a solution, shows a significant decrease in locomotion behavior in strains expressing A $\beta$  and/or tau compared to wildtype (Figure 1B).

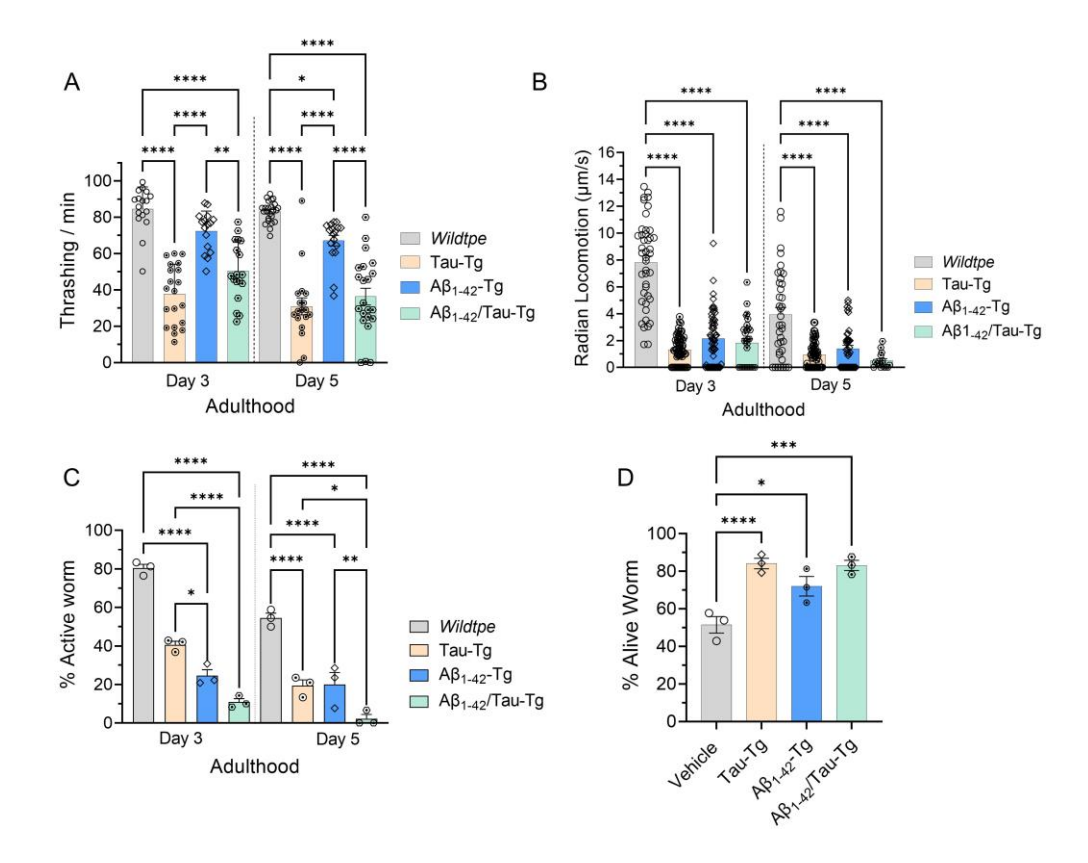


**Figure 1:** Phenotypic assays. (A) Thrashing of 20-25 worms was measured for 30 sec, (B) Radian locomotion (calculated by the distance each worm traveled from the center of seeded plate during 30 mins) was also measured (N=3, and 30-50 worms were used for each trial). (C) A 5-HT assay was conducted by transferring 20-25 age-synchronized worms to a 96-well plate containing 1 mM serotonin/well and scoring the number of active worms (, defined as having at least 1 bends/sec) after 10 minutes; (D) A cold tolerance assay was done by transferring worms from 25°C to 4°C. After 24 hours of cold exposure, the plates were returned to 20-25°C and worms were allowed to recover for 2-4 hours before scoring survival. In all experiments, the worms were grown at 16°C until the L4 stage, and then then transferred and kept at 25°C to induce Aβ and/or tau expression. For the statistical analysis, a one-way analysis of variance (ANOVA) with a Tukey's post-hoc test used; \*P ≤ 0.05, \*\*P ≤ 0.01, \*\*\*\*P ≤ 0.001.

To further assess the effects of A $\beta$  and/or tau expression on *C. elegans* neuronal functions, we performed a serotonin (5-HT) assay. Dysregulation of serotonin signaling has been implicated in various neurological disorders, including Alzheimer's disease and Parkinson's disease. In *C. elegans* serotonin modulates synaptic efficiency in the nervous system and is a major neurotransmitter that is involved in the regulation of behaviors in *C. elegans* including locomotion, egg laying, and olfactory learning<sup>45–48</sup>. Previous studies also demonstrated that 5-HT modulates an enhanced slowing response (Worms recently deprived of food move even more slowly in food)

as an experience dependent behavior in *C. elegans*, linking between the behavioral and the neuronal plasticity<sup>45–47</sup>. Considering these data, we assessed 5-HT hypersensitivity by placing age-synchronized worms in a 1 mM serotonin solution and scoring worms that remained mobile after 10 minutes of exposure<sup>44</sup>. All three transgenic mutants exhibited a significantly higher level of sensitivity (hypersensitivity) to 5-HT compared to wild-type, indicating the neurotoxicity caused by A $\beta$  and/or tau expression in neuronal plasticity and function is at least partially mediated by 5-HT (Figure 1C).

The neurotoxicity of AB and tau was further examined by performing a cold-tolerance assay. In C. elegans, different tissues are involved in cold tolerance including the ASJ and ADL sensory neurons, interneurons, muscle cells, and intestinal cells <sup>49–52</sup>. Even though the exact mechanism is unknown, data suggests that cold tolerance begins with activation of a Ca<sup>2+</sup>dependent endoribonuclease in ASJ and ADL neurons in response to a temperature shift <sup>49,51</sup>. Subsequently, insulin is secreted from the ASJ and binds to insulin receptors in the intestine and neurons<sup>51,52</sup>. This binding initiates a series of signaling cascades. Ultimately, these cascades lead to alterations in Delta 9-desaturase expression<sup>51,53,54</sup>. These cold-induced lipid adjustments are considered to be the key step in cold tolerance<sup>51,53,54</sup>. Previous studies showed that in the absence of signaling from these neurons, worms are resistant to cold temperatures and mutants with broad deficiencies in neuronal signaling broadly, or deficiencies in ASJ signaling in particular, are resistant to colder temperatures <sup>49,55</sup>. To determine whether these transgenic models of neurodegenerative disease display defects in sensory signaling, we assayed their level of cold tolerance. The effects of A $\beta$  and tau in this assay were assessed by raising the temperature to 25 °C and measuring their survival rate after a sudden shift to a cold temperature (4°C). As shown in

Figure 1D, worms expressing  $A\beta$  and/or tau display more cold tolerance compared to the wild type, suggesting a defect in neuronal signaling induced by  $A\beta$  and tau.

## 2.2. Oxylipin analysis alternation upon expression of Aβ and/or tau

Recent studies suggest that CYP-EH PUFA metabolites influence AD progression, including both Aβ and tau-induced neurodegeneration <sup>18,26,29,30</sup>. Nonetheless, a substantial portion of their mutual influence is yet to be elucidated. This can be attributed to the intricacy of mammalian nervous systems and lipid metabolism, as well as the difficulties and expenses associated with utilizing mammalian and human models in age-related neurodegeneration. Given these factors, we aim to achieve a more comprehensive understanding of the interplay among oxylipins, Aβ, and tau, as well as their influence on the observed phenotypic defects upon Aβ and tau expression in C. elegans. To do so, we monitor the oxylipin profile of worms upon expression of A $\beta$  and/or tau. The oxylipin profiles in transgenic C. elegans expressing Aβ and/or tau in neurons were determined by raising worms at 16°C and increasing the temperature to 25°C at the L4 stage. Worms were then maintained at 25°C and collected on day 3 of adulthood when tsevere neuronal dysfunction phenotypes were observed, and the oxylipin analysis was performed using LC/MS-MS, according to previously reported procedure <sup>56</sup> (see the experimental section in SI). Interestingly, all three transgenic worm strains exhibited a change in the oxylipin profile compared to the wildtype (Figure 2A-C and S1). By comparing the oxylipin profiles of Tau-Tg strains with wildtype, we identified several lipid metabolites that are consistently upregulated or downregulated in worms expressing tau compared to WT animals (Figure 2A, and S2). A correlation coefficient analysis for the top 22 compounds with the largest changes in the levels between WT and Tau-Tg worms was performed (Figure 2D). Of these compounds, 14 had a negative correlation coefficient, indicating that their levels tended to decrease in tandem with other

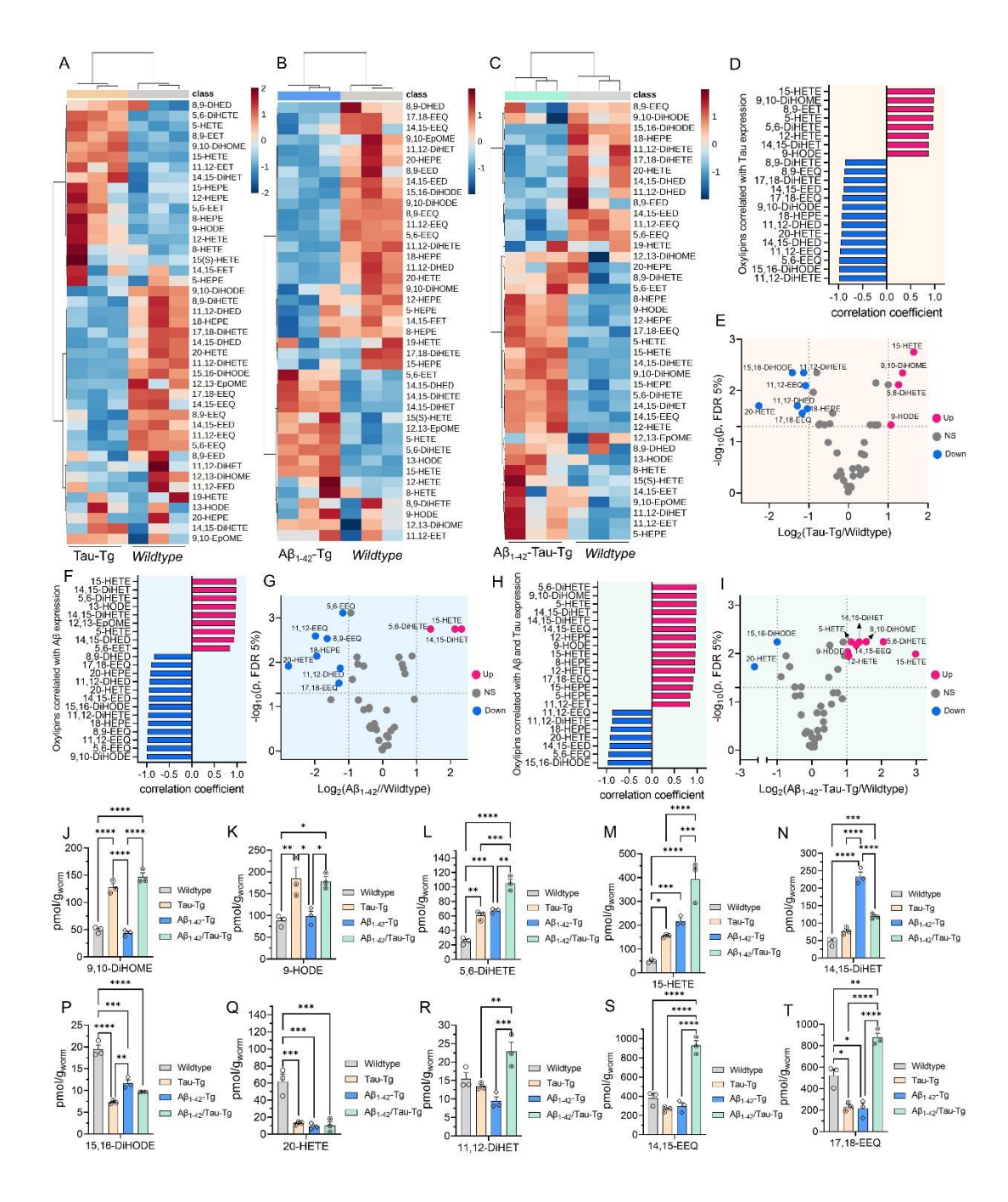


**Figure 2.** Oxylipin analysis of *C. elegans* expressing Aβ and/or tau. (A-C) heatmaps representing the change in different oxylipins in Tau-Tg, Aβ<sub>1-42</sub>-Tg, Aβ<sub>1-42</sub>/Tau-Tg strains, respectively, compared to the wildtype. (D) Oxylipin correlation with tau expression. (E) volcano plot related to the change in oxylipin level upon in Tau-Tg compared to the wildtype strain. (F) Oxylipin correlation with Aβ expression. (G) volcano plot related to change in oxylipin level upon in Aβ<sub>1-42</sub>-Tg compared to the wildtype strain. (H) Oxylipin correlation with co-expression of Aβ and tau. (I) Volcano plot related to change in oxylipin level upon in Aβ<sub>1-42</sub>/Tau-Tg compared to the wildtype. (J-T) Comparison of selected oxylipin level among wildtype, Tau-Tg, Aβ<sub>1-42</sub>-Tg, and Aβ<sub>1-42</sub>/Tau-Tg. In all experiments, worms were grown at 16°C degrees until the L4 stage, then transferred and kept at 25°C. Age-synchronized worms were collected on day 3 for oxylipin analysis. Statistical analysis: (E, G, and H) Multiple unpaired t-test corrected with Benjamini and Hochberg method with FDR=0.05; and (J-T) One-way analysis of variance (ANOVA) with Tukey's post-hoc test was used, where \*P ≤ 0.05, \*\*P ≤ 0.01, \*\*\*P ≤ 0.001, \*\*\*\*P < 0.0001

compounds upon expression of tau. Conversely, 8 compounds had a positive correlation coefficient, indicating that their levels tended to increase together. We used a Student's t-test and fold change analysis to determine which compounds had the largest and most significant changes in Tg-Tau compared to wildtype (Figure S1-S2). The Studen'ts t-test is useful for identifying small yet significant changes in metabolite levels, while the fold change analysis is useful for measuring the magnitude of changes in metabolite levels. We used a volcano plot to visualize and combine these approaches and found a total of 10 oxylipin compounds with the largest changes in levels while still accounting for statistical variability (Figure 2E). Of these compounds 15-HETE, 9-HODE, 9,10-DiHOME, and 5,6-DiHETE had the most significant upregulation, and 20-HETE, 18-HEPE, 17,18 EEQ, 11,12-EEQ, 11,12-DiHETE, 11,12-DHED, and 15,16-DiHODE were the most significantly downregulated in Tau-Tg strain compared to the wildtype.

The strain expressing A $\beta$  also showed changes in several compounds, and the correlation coefficient analysis of the top 22 compounds with the largest changes suggests a coordinated pattern of oxylipin level changes. (Figure 2B, 2F, and S1). The volcano plot reveals that 15-HETE, 5,6-DiHETE, 14,15-DiHET are oxylipins that are largely and significantly upregulated, while 20-HETE, 18-HEPE, 17,18 EEQ, 11,12-EEQ, 8,9-EEQ, 5,6-EEQ, 11,12-DHED are the most significantly downregulated in worms expressing A $\beta$  compared to the wildtype (Figure 2G, S1-S2). Intriguingly, in both the A $\beta$ <sub>1-42</sub>-Tg and Tau-Tg strains 15-HETE and 5,6-DiHETE are those with highest increase, and 20-HETE, 18-HEPE, 17,18 EEQ, 11,12-EEQ, and 11,12-DHED show the great decrease. These compounds may play a more important role in the observed phenotypic features of these two strains.

We further analyzed the oxylipin profile of the strain that simultaneously expressed both  $A\beta_{1-42}$  and tau genes. Similarly, an overall change in the oxylipin profile was observed in the

transgenic worm expressing both  $A\beta$  and tau genes, suggesting that expression of these two genes could regulate pathways related to the oxidative PUFA metabolism (Figures 2C, and S1). The correlation coefficient analysis of the top 22 compounds with the largest changes also supports the idea of coordinated changes in oxylipin levels (Figures 2H, and S1). Furthermore, the volcano plot shows that hat 15-HETE, 12-HETE, 5-HETE, 9-HODE, 14,15-EEQ, 5,6-DiHETE, 14,15-DiHET, and 9,10-DiHOME are the oxylipins that are largely and significantly upregulated, while 20-HETE, and 15,16-DiHODE are the most significantly downregulated in the  $A\beta_{1-42}$ /Tau-Tg strain compared to the wildtype (Figures 2I, S1, and S2). Interestingly, all four oxylipins identified with more than a two-fold increase in the in Tau-tg are were highly increased in the  $A\beta_{1-42}$ /Tau-Tg strain compared to the wildtype strain (Figures 2E, I, and J-M). Similarly, all three oxylipins with at least a 2-fold increase in  $A\beta_{1-42}$ -Tg were also observed in the  $A\beta_{1-42}$ /Tau-Tg strain (Figures 2G, I, and L-N). Furthermore, 15,16-DiHODE, had a two-fold decrease in the Tau-tg strain, and showed a similar decrease in  $A\beta_{1-42}$ /Tau-Tg. Lastly, 20-HETE decreased by more two-fold in all the transgenic strains (Figures 2E, G, I, P, and Q).

It is worth mentioning that several variations were observed in the oxylipin profiles among the A $\beta_{1-42}$ -Tg, Tau-Tg, and A $\beta_{1-42}$ /Tau-Tg strains, highlighting both similarities and differences in their regulatory patterns (Figures 2, and S2 and S3). In comparison between the A $\beta_{1-42}$ -Tg and Tau-Tg strains, several oxylipins exhibit congruent regulatory trends in both strains and some discrepancies were evident (Figures S2 and S3). For instance, 9,10-DiHOME and 9-HODE levels both rise in response to tau expression but remain unchanged by A $\beta$  expression (Figures 2 J and K). Conversely, 14,15-DiHET levels were unchanged in the Tau-Tg strain but were upregulated in A $\beta_{1-42}$ -Tg stain (Figures 2N). These data suggest that A $\beta$  and tau can exert distinct pathological effects on oxylipin metabolism, indicating unique molecular mechanisms underlying the

contribution of oxylipin metabolism to neurodegeneration. Moreover, the oxylipin profile of the  $A\beta_{1-42}$ /Tau-Tg strain displays patterns akin to those observed in either  $A\beta_{1-42}$ -Tg or Tau-Tg, (Figure 2 E, G, and I). However, specific oxylipins show distinct trends (Figures 2, S2, and S3). For example, 11,12-DiHET and 14,15-EEQ levels do not undergo significant alterations upon the expression of A $\beta$  or tau individually, but both are considerably upregulated when both A $\beta$  and tau are expressed concurrently (Figures 2R and S). Additionally, 17,18-EEQ levels exhibit a marked decline in response to  $A\beta$  or tau expression but experience a notable increase in the presence of both Aβ and tau (Figure 2T). These observations suggest a potential synergistic effect of Aβ and tau on CYP-EH metabolism, implying that their combined expression may lead to unique alterations in oxylipin profiles that differ from the effects of either Aβ or tau alone. This synergy could result from the interplay between AB and tau proteins, which might modulate CYP-EH metabolic pathways in a manner that cannot be predicted by examining the individual effects of each protein. Therefore, the combined presence of Aß and tau may induce novel regulatory patterns and potentially unveil new insights into the role of oxylipins in the context of neurodegeneration.

# 2.3. Inhibition of *C. elegans* EH rescues neurodegeneration induced by Aβ and/or tau: phenotypic study.

Our previous research, along with that of others, demonstrated that AUDA (an inhibitor of EH) effectively inhibits epoxide hydrolase in the *C. elegans* animal model  $^{56,57}$ . Thus, to assess the effects of AUDA in our model of AD, age-synchronized worms (wildtype, Tau-Tg and A $\beta_{1-42}$ -Tg, and Ab/Tau-Tg) were grown at 16°C and transferred to on OP50 food containing vehicle or AUDA (100  $\mu$ M) at the L4 stage, followed by a temperature upshift from 16 to 25°C to induce transgene expression (See experimental method in SI). We proceeded to evaluate the rescuing effect of EH

inhibition in these age-synchronized strains by conducting thrashing, radian locomotion, 5-HT, and cold-tolerance assays on days 3 and 5 of adulthood. Worms supplemented with AUDA were compared to the vehicle control to determine the impact of EH inhibition on the aforementioned parameters. We then assessed the rescuing effect of EH inhibition in these age-synchronized strains using thrashing, radian locomotion, 5-HT, and cold-tolerance assays on day 3 and day 5 adulthood in worm supplemented with AUDA compared to the vehicle.

As shown in Figure 3A, expression of A $\beta$  and/or au in in Tau-Tg and A $\beta_{1-42}$ -Tg and A $\beta_{1-42}$ -Tg and addition, treatment with AUDA (inhibits *C. elegans* EH) rescues the neurodegenerative phenotype in the Tau-Tg and A $\beta_{1-42}$ -Tg and A $\beta_{1-42}$ -Tg and A $\beta_{1-42}$ -Tg strains as measured by the thrashing assay. However, no significant change was observed in the strain expressing only A $\beta_{1-42}$ . On the other hand, the results of the locomotion assay were different, as the AUDA treatment was able to significantly improve the radian locomotion score in the A $\beta_{1-42}$ -Tg strain, but not in the Tau-Tg strain (Figure 3B). These results suggest that inhibition of *C. elegans* EH can rescue neurodegenerative phenotypes observed in strains that express A $\beta$  or tau through distinct pathways. Furthermore, while the A $\beta_{1-42}$ -Tau-Tg worms treated with AUDA shows higher scores in our radian locomotion assay compared to the untreated worms, the rescuing effect is not significant in this strain. This result might be due to a more severe locomotion dysfunction in the presence of both A $\beta$  and tau genes, which makes it harder for AUDA to completely rescue this neurodegenerative phenotype.

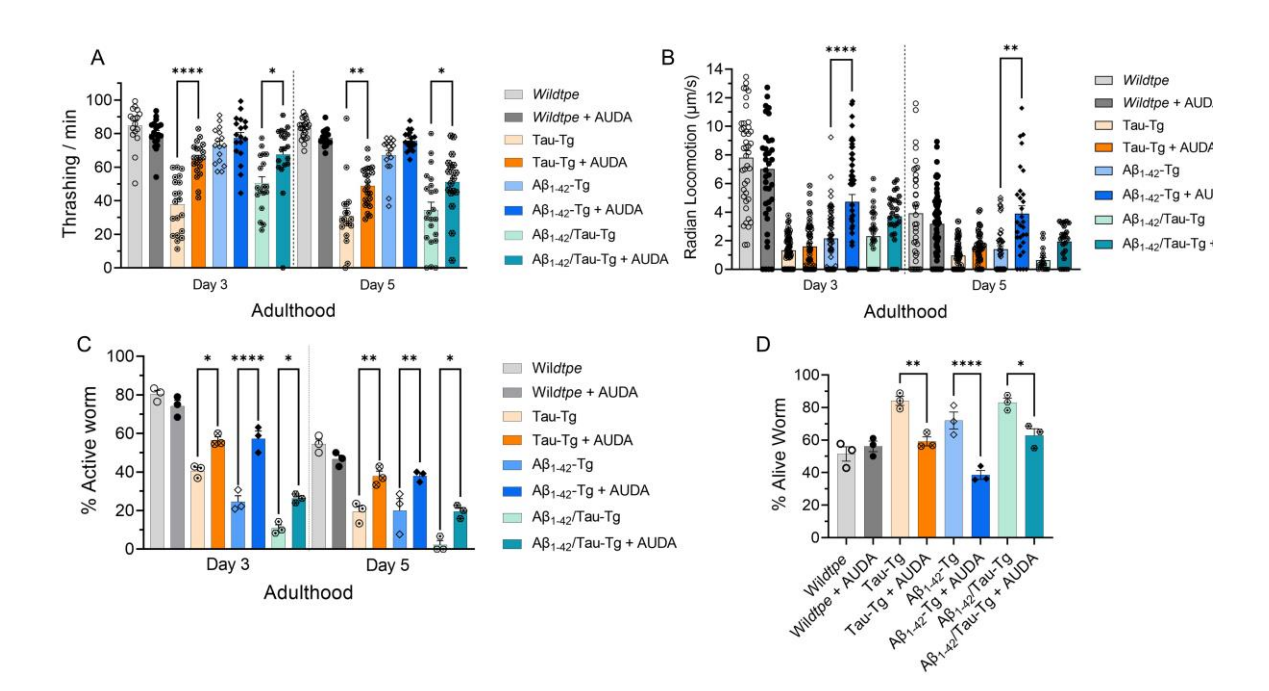


**Figure 3:** An epoxide hydrolase inhibitor, AUDA, rescues some phenotypic effects in strains expressing Aβ and/or tau. (a) Thrashing was measured using 20-25 worms over 30 sec, (b) Radian locomotion was calculated by the distance each worm traveled from the center of the seeded plate over 30 mins (N=3, and 30-50 worms were used for each trial). (c) 5-HT Assay was performed by transferring 20-25 age-synchronized worms to a 96-well plate containing 1 mM serotonin, and scoring the number of active worms (, defined as having at least 1 bends/sec) after 10 minutes; (d) Cold Tolerance was done by transferring worms from 25  $^{0}$ C to 4  $^{0}$ C; 48 hours after cold exposure, plates were returned to 20-25  $^{\circ}$ C, allowing the worms to recover for 2-4 hours before scoring the surviving worms. In all experiments, the worms were grown at 16  $^{\circ}$ C until the L4 stage, then transferred to plates with or without AUDA (100 μM) and kept at 25  $^{0}$ C. On a specific day, phenotypic analyses were performed. For statistical analysis, a one-way analysis of variance (ANOVA) with Tukey's post-hoc test was used. \*P  $\leq$  0.05, \*\*P  $\leq$  0.01, \*\*\*P  $\leq$  0.001, \*\*\*P < 0.0001, non-significant is not shown.

Interestingly, AUDA treatment also rescued the 5-HT hypersensitivity in all three mutant strains, indicating that a CYP-EH pathway is involved in the regulation of serotonin signaling in C. elegans, which is consistent with previous research suggesting a role for this pathway in the modulation of neurotransmitter function, treatment with AUDA reversed the increased cold tolerance in all three mutant strains, bringing their survival rates closer to the wildtype strain (Figure 3D). These findings imply that there may be an interaction between the A $\beta$  and tau pathways and the epoxide hydrolase pathways, which could collectively contribute to the molecular mechanisms underlying the worms' response to environmental stressors.

## 2.4. AUDA affects oxylipin profiles in worms expressing Aβ and/or tau

To further investigate the potential rescuing effects of epoxide hydrolase inhibition, we examined the oxylipin profiles of AD strains treated with AUDA. The oxylipin profile of the AUDA-treated strains revealed several oxylipins that exhibited consistent upregulation or downregulation compared to their non-treated counterparts (Figure 4A). In wildtype worms, AUDA treatment led to decreased levels of both epoxy- and dihydroxy-fatty acid metabolites, with the most pronounced changes observed for EPA and AA derivatives (Figure 4B and S4). This finding is interesting as it suggests that the relationship between epoxide hydrolase activity and oxylipin levels might be more intricate than initially anticipated. Specifically, the assumption is that inhibiting epoxide hydrolase activity would result in an increase in epoxides and a corresponding decrease in diols may not be entirely accurate. This is because there may be other pathways involved in the metabolizing the epoxy- and dihydroxy- fatty acid metabolites, and feedback regulation of other enzymes may also play a role. Additionally, it is important to note that the moderate alterations in the oxylipin profile of wildtype worms treated with AUDA do not impact the phenotypic assays, at least in the assays tested in this study, when compared to untreated wildtype worms (Figure 3). Intriguingly, we found a completely distinct pattern in the tau-Tg strain, where AUDA treatment leads to an upward trajectory of epoxy- and dihydroxy-PUFA metabolites, with the most notable changes associated with elevated levels of EPA-derived epoxides (Figure 4C and S5). All EEQ regioisomers were substantially increased compared to the untreated worms suggesting a crucial role for these oxylipins in the rescuing effect of AUDA in the strains expressing tau. Also, we did not observe a significant alternation in dihydroxy-PUFAs in the presence of AUDA, except for a rise in 15,16-DiHODE.

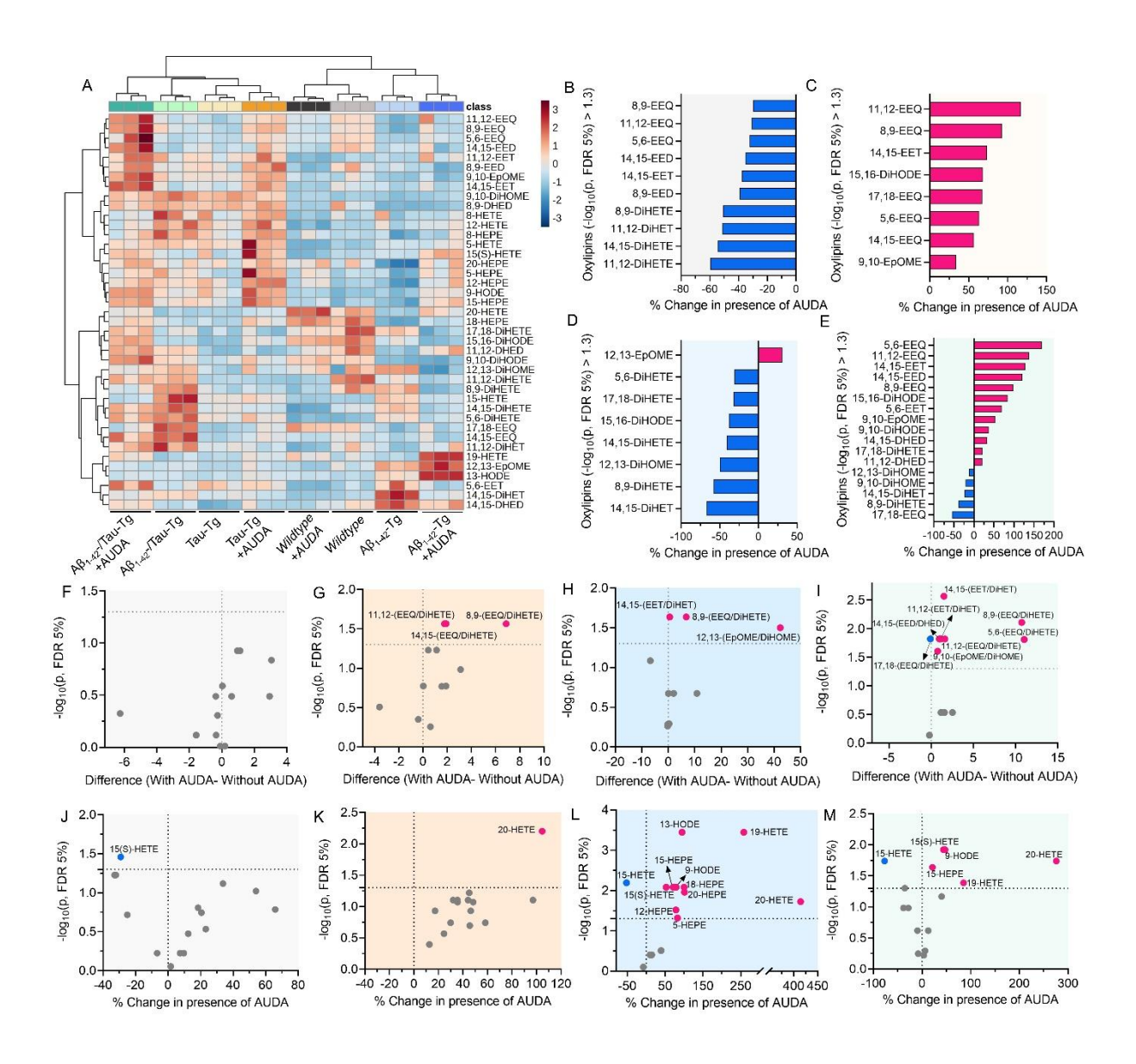


Figure 4: Oxylipin analysis of C. elegans expressing Aβ and/or tau after treatment with AUDA. (A) A heatmap representing the change in different oxylipins in the wildtype, Tau-Tg,  $A\beta_{1-42}$ -Tg, and  $A\beta_{1-42}$ /Tau-Tg strains, with and without AUDA treatment. (B) Epoxy- and dihydroxy-PUFAs with significant changes in the wildtype worm after AUDA treatment. (C) Epoxy- and dihydroxy-PUFAs with significant changes in the Tau-Tg strain after AUDA treatment. (D) Epoxy- and dihydroxy-PUFAs with significant changes in the  $A\beta_{1-42}$ -Tg strain after AUDA treatment. (E) Epoxy- and dihydroxy-PUFAs with a significant change in the  $A\beta_{1-42}/Tau$ -Tg strain after AUDA treatment. (F) Change in the epoxy to dihydroxy ratio in wildtype worm after AUDA treatment. (G) Change in the epoxy to dihydroxy ratio in the Tau-Tg strain after AUDA treatment. (H) Change in the epoxy to dihydroxy ratio in the  $A\beta_{1-42}$ -Tg strain after AUDA treatment. (I) Change in the epoxy to dihydroxy ratio in the Aβ<sub>1-42</sub>/Tau-Tg strain fter AUDA treatment. (J) Change in the hydroxy-PUFAs level in the wildtype worm after AUDA treatment. (K) Change in the hydroxy-PUFAs level in the Tau-Tg strain after AUDA treatment. (L) Change in the hydroxy-PUFA levels in the Aβ<sub>1</sub>-42-Tg strain after AUDA treatment. (M) Change in the hydroxy-PUFA levels in Aβ<sub>1-42</sub>/Tau-Tg strain after AUDA treatment. In all experiments, the worms were grown at 16°C until the L4 stage, and then transferred and kept at 25°C. Age-synchronized worms were collected at day 3 for the oxylipin analysis. Statistical analysis: Multiple unpaired ttest corrected with Benjamini and Hochberg method with FDR=0.05; and \*P  $\leq$  0.05, \*\*P  $\leq$  0.01, \*\*\*P  $\leq$  0.001, \*\*\*\*P < 0.0001.,

EH inhibition using AUDA alters the oxylipin profile of the  $A\beta_{1-42}$ -Tg strain in a completely distinct manner, where the most notable alterations correspond to a reduced concentration of dihydroxy-PUFAs. No substantial increase in Ep-PUFAs was detected, except for 12,13-EpOME (Figure 4C and S6). The distinct changes in the oxylipin profiles fter AUDA treatment in the Tau-Tg and  $A\beta_{1-42}$ -Tg strains highlight the unique role of oxylipins in the context of tau and  $A\beta$ -induced neurodegeneration, suggesting that the underlying mechanisms of neurodegeneration may differ between the two strains.

The greatest number of oxylipin changes was observed in the A $\beta_{1-42}$ /Tau-Tg strain. For instance, the levels of 5,6-EEQ, 8,9-EEQ, and 11,12-EEQ increased, whereas the level of 17,18-EEQ decreased by about fifty percent. Their corresponding diols levels also shifted differently, as 8,9-DiHETE decreased, 5,6- DiHETE and 11,12- DiHETE remained almost the unchanged, andlevels of 17,18-DiHETE increased in presence of AUDA (Figure 4E and S7). Combined with the altered oxylipin profile upon co-expression of Aβ and tau, where levels of both 8,9-EEQ and 11,12-EEQ decreased while 17,18-EEQ increased (Figure 2H), this suggests that these metabolites may have a vital role in the neurodegenerative process and may contribute to the protective effects of AUDA. A similar trend was observed for LA-derived metabolites, where EH inhibition results in elevated levels of 9,10-EpOME and a decrease in its corresponding diol, 9,10-DiHOME, which was increased upon simultaneous expression of Aβ and tau. The other regioisomer only showed a decrease in the dihydroxy metabolite, while the levels of corresponding epoxy metabolite remained unchanged (Figure 4E, 2H, and S7). These findings further substantiate the notion that the neuroprotective effects of AUDA primarily stem from modulation of oxylipin metabolite levels by inhibiting epoxide hydrolase activity, and compensatory mechanisms and other factors may play a role in regulating these oxylipin levels.

To further explore the effects of EH inhibition using AUDA, we analyzed the epoxy to dihydroxy ratio, which is generally considered a marker of sEH inhibition in vivo<sup>59,60</sup>. Wildtype worms treated with AUDA exhibit an overall increase in the epoxy to dihydroxy ratio, although none of the individual metabolites show significant changes (according to the unpaired test with FDR=0.05) (Figure 4F, and S8). In the Tau-Tg strain treated with AUDA, the epoxy to dihydroxy ratio of different metabolites tends to increase, the most significant being 8,9-EEQ/DiHETE, 11,12- EEQ/DiHETE and 14,15- EEQ/DiHETE. These data suggest that these regioisomers may play a pivotal role in the rescuing effect of AUDA on tau-induced neurodegeneration (Figure 4G, and S9). The Aβ<sub>1-42</sub>-Tg strain treated with AUDA showed a general increase in the epoxy-todihydroxy ratio, with the most notable changes related to 8,9-EEQ/DiHETE, 14,15-EET/DiHET, and 12,13-EpOME/DiHOME (Figure 4H, and S10). This finding suggests that the effect of AUDA on the oxylipin profile is somewhat specific to certain metabolites in this strain, and the rescuing effect is through regulation of different downstream pathways. On the other hand, the  $A\beta_{1-42}/Tau$ -Tg strain exhibits a marked enhancement in the level of several epoxy to dihydroxy ratios, including (i) EPA metabolites: 5,6-EEQ/DiHETE, 8,9-EEQ/DiHETE, 11,12-EEQ/DiHETE, (ii) AA-metabolites: 11,12-EET/DiHET, 14,15-EET/DiHET, (iii) DGLA metabolites: 14,15EED/DHED, and (iv) a LA metabolite: 9,10-EpoME/DiHOME (Figure 4I, S11). This result further supports the idea that the general trend in the effect of EH inhibition is increasing epoxy to dihydroxy, however, the genotype of the strain can influence how AUDA affects metabolic pathways. In other words, the response to AUDA treatment depends on the specific molecular pathways involved in the pathology of the strain. Furthermore, a greater number of metabolites showed significant changes in the  $A\beta_{1-42}$ /Tau-Tg treated with AUDA compared to other strains, implying that EH inhibition by AUDA is more effective in modulating oxylipin metabolite levels in strains with higher levels of neurodegeneration. This change might be due to the increased expression of EH in these strains, which amplifies the impact of AUDA treatment. similar trend could be found when comparing  $A\beta_{1-42}$ -Tg and Tau-Tg with wildtype in response to the AUDA. This conclusion is supported by previous research that has reported a correlation between elevated EH expression and neurodegenerative conditions<sup>61–65</sup>.

We also tracked the hydroxy-PUFA levels in all mutants after treatment with AUDA. In wildtype worms, AUDA treatment induced changes in the hydroxy fatty acid levels, with a statistically significant decrease in 15(S)-HETE (according to the unpaired multiple t-test with FDR=0.05) (Figure 4J and S12). The Tau-Tg strain also exhibited alternations in hydroxy-PUFA levels in response to AUDA treatment, with the most significant changes related to an increase in 20-HETE (Figure 4K and S13). While we observed only one hydroxy-PUFA with a significant change in the tau-tg strain in the presence of AUDA, both the  $A\beta_{1-42}$ -Tg and the  $A\beta_{1-42}$ /Tau-Tg strain displayed several hydroxy-PUFAs with altered levels after AUDA treatment (Figure 4L, M, S14, and S15). The levels of 20-HETE, 19-HETE, 15(S)-HETE, 9-HODE, and 15-HEPE consistently increased in both strains, suggesting a possible common mechanism that influences these metabolites. Furthermore, both  $A\beta_{1-42}$ -Tg and  $A\beta_{1-42}$ /Tau-Tg strains experienced a decrease in the 15-HETE level, highlighting another potential overlap in the treatment response among these strains. Additionally, 13-HODE, 12-HEPE, 5-HEPE showed a significant upward pattern exclusively in A $\beta$  strain, which may indicate a unique aspect of the A $\beta_{1-42}$ -Tg strain response to AUDA treatment, which warrants further investigation. These findings emphasize the complex effects of AUDA treatment on hydroxy-PUFA levels and point to possible indirect influences on other enzymatic pathways or feedback regulation mechanisms. Further research is necessary to determine the potential roles of these changes in the rescuing effects of AUDA and to elucidate

the precise mechanisms underlying the observed alterations in hydroxy-PUFA levels in the context of neurodegenerative diseases.

#### 3. Discussion

In this study, we used transgenic *C. elegans* strains expressing human  $A\beta$  and/or tau to investigate their effects on neuronal function and their impact on oxylipin metabolism. We found that worms expressing  $A\beta$  and/or tau exhibited significant differences in neuronal function compared to wild-type animals. In particular,  $A\beta$  and/or tau expression resulted in a decrease in both thrashing and locomotion behavior, indicating a deficiency in locomotor neurons. In addition, transgenic strains were found to have higher levels of serotonin hypersensitivity and more tolerance to downshifts in temperature, suggesting defects in sensory signaling as a result of  $A\beta$  and/or tau expression.

Our oxylipin profiling revealed that several compounds were consistently upregulated or downregulated in worms expressing A $\beta$  or tau compared to wild-type animals. Notably, 15-HETE, and 5,6-DiHETE were significantly upregulated in both strains, while 9-HODE, and 9,10-DiHOME were significantly elevated in the tau strain, and 14,15-DiHETE was significantly upregulated in the A $\beta$  strain. We also found that 20-HETE, 18-HEPE, 17,18-EEQ, 11,12-EEQ, 11,12-DiHED, were significantly downregulated in both A $\beta$  and tau strains, whereas 5,6-EEQ and 8,9-EEQ were only significantly increased in the A $\beta$ <sub>1-42</sub>-Tg strain. Furthermore, 11,12-DiHETE and 9,10-DiHODE are only elevated in the Tau-Tg strain compared to the wildtype. Intriguingly, all oxylipins identified with high upregulation in either the Tau-Tg or A $\beta$ <sub>1-42</sub>-Tg strains are also increased in the A $\beta$ <sub>1-42</sub>/Tau-Tg strain in addition to 14,15-EEQ, 5-HETE, and 12-HETE. Together with different oxylipin downregulation trends in the A $\beta$ <sub>1-42</sub>/Tau-Tg strain, this data suggesst a possible synergic effect of A $\beta$  and tau on CYP-EH related pathways. Notably, some of these oxylipins have been previously implicated in functioning in cellular mechanism either directly or

by activating receptors such as transient receptors, peroxisome proliferator-activated receptors, and G-protein coupled receptors, indicating their pivotal function in inflammation, oxidative stress, apoptosis, autophagy and ferroptosis, which highlighting their potential role in neurodegeneration<sup>18,66–70</sup>. For instance, 9,10-DiHOMEs have been found to cause toxicity by disrupting mitochondrial functions, and 9-HODE contributes to sensitizing the TRPV1 channel in sensory neurons and causing mechanical and thermal hypersensitivity *in vivo*<sup>71–73</sup> Both of these oxylipins levels were significantly elevated in the Tau-Tg and  $A\beta_{1-42}$ /Tau-Tg strains. Furthermore, 5,6-DiHETE was increased in all three mutant strains, and 14,15-DiHETE, which was increased in the  $A\beta_{1-42}$ -Tg and  $A\beta_{1-42}$ /Tau-Tg stains, were also found to be increased in patients with AD.

An increase in sEH, an ortholog of *C. elegans* EH, expression has been observed in the brain of patients with various neurological disorders, including depression <sup>74</sup>, schizophrenia <sup>75</sup>, Parkinson's disease <sup>76</sup>, and recently AD <sup>29,30</sup>. Studies demonstrated that genetic deletion or pharmacological inhibition of sEH can yield beneficial effects in mouse models of these diseases. Specifically, sEH inhibitors exhibited positive outcomes in two distinct AD mouse models, the senescence-accelerated prone mice (SAMP8) and five familial AD (5xFAD) mice, where the inhibitors alleviated cognitive impairment, reduced neuroinflammation, and mitigated key pathological features, such as tau hyperphosphorylation and amyloid burden <sup>29</sup>. Ghosh *et al.* found elevated sEH levels in the brains of AD patients and in an amyloid mouse model of AD, suggesting that sEH blockade can replenish epoxy lipids and counteract neuroinflammation <sup>26</sup>. Treatment of AD mice with a small molecule sEH inhibitor led to restoration of epoxy lipids, a reduction in neuroinflammation and amyloid pathology, and an improvement in cognitive function. In our previous research, we discovered that inhibiting epoxide hydrolase (EH) in *C. elegans* could rescue neurodegeneration induced by ferroptosis <sup>56</sup>.

With this in mind, we sought to explore whether pharmacological inhibition of epoxide hydrolase could offer a protective effect against neurodegeneration in a C. elegans model of AD. We found that administration of an EH inhibitor, AUDA, rescued neuronal function in all three mutant strains, with improvements observed in thrashing and locomotion behavior, as well as reduced serotonin hypersensitivity and increased sensitivity to temperature shifts. Additionally, oxylipin profiling revealed significant changes in the levels of several oxylipins in response to AUDA treatment. These changes were not solely in the direction of increasing Ep-PUFAs and decreasing dihydroxy-PUFA, as one might predict. Thus, we used the epoxy to dihydroxy ratio to further explore the effects of AUDA. Interestingly, while no significant change was found in the epoxy to dihydroxy ratio of wildtype treated with AUDA, the A $\beta_{1-42}$ -Tg strain exhibited a significant increase in 8,9-EEQ/DiHETE, 14,15-EET/DiHET, and 12,13-EpOME/DiHOME rations. The most significant changes in the Tau-Tg strain were related to an increase in different regioisomers of 5,6-, 8,9-, and 11,12-EEQ/DiHETE. The distinct changes in the oxylipin profiles upon AUDA treatment for the Tau-Tg and Aβ<sub>1-42</sub>-Tg strains suggest that the underlying mechanisms of neurodegeneration may differ between the two strains. Overall, AUDA treatment in the Tau-Tg treatment primarily led to increased levels of Ep-PUFAs, in particular EPA-derived epoxides. Meanwhile, treatment with AUDA in the  $A\beta_{1-42}$ -Tg strain resulted in decreased levels of dihydroxy-PUFAs without a significant increase in most Ep-PUFAs. These observations highlight the unique roles of oxylipins in the context of tau and Aβ-induced neurodegeneration, indicating the complexity of their interactions. On the other hand, in the Aβ<sub>1-42</sub>/Tau-Tg strain AUDA treatment led to a significant increase in the epoxy to dihydroxy ratio for several PUFAs, which included the changes observed in the  $A\beta_{1-42}$ -Tg, and Tau-Tg strains. This observation could suggest that the AUDA inhibition of EH is more effective at modulating oxylipin metabolite levels

in strains with higher levels of neurodegeneration. Furthermore, we found an elevated EET to DiHET ratio following AUDA treatment. This intriguing observation echoes findings in several mammalian neurodegeneration studies, where inhibiting soluble EH has successfully mitigated Aβ-induced neurodegeneration and brain tissue damage in mouse models, with elevations in the EET to DiHET ratio <sup>77–79</sup>. This finding further highlights the immense potential of our methodology for delving deeper into the neuroprotective effects of EH inhibitors and the role of oxylipins in neurodegeneration. Also, it paves the way for translating our discoveries in *C. elegans* to mammalian models, opening new avenues for identifying and exploring the significance of key CYP-EH metabolites.

Another interesting finding was related to the change in the hydroxy-PUFA levels after AUDA treatment. For instance, while the levels of 20-HETE significantly decreased after expression of Aβ and/or tau, the AUDA treatment causes a 2-to-4-fold decrease in 20-HETE levels in all transgenic strains. Also, while the 15-HETE levels are increased upon expression of Aβ and/or tau, and treatment with AUDA significantly decreases this hydroxy PUFA level in the Aβ<sub>1-42</sub>-Tg and Aβ<sub>1-42</sub>/Tau-Tg, but not in the Tau-Tg strain. It is also worth mentioning that the hydroxy-PUFAs identified in this study are predominantly produced through three primary pathways in mammals: (i) LOX enzymes, (ii) non-enzymatic oxidation, and (iii) CYP450 enzymes. As there are no LOX homologues in *C. elegans*, the production of these hydroxy-PUFAs is likely driven mainly by non-enzymatic oxidation or CYP450 pathways in this organism<sup>18,80,81</sup>. Previous studies have shown increased levels of oxidative stress upon expression of Aβ and tau<sup>82–84</sup>. Therefore, in a simplified model, a higher level of oxidative stress could result in an overall increase in hydroxy-PUFAs. However, while levels of some compounds, such as 9-HODE, 15-HETE, and 12-HETE, trended upward after Aβ and tau expression, others, like 20-HETE and 18-HEPE, trended

downward. This observation suggests that the changes in hydroxy-PUFA levels may not be solely mediated by oxidative stress but could instead be (i) primarily regulated by enzymatic pathways related to CYP450 or (ii) an unidentified enzyme with lipoxygenase activity, or (iii) due to indirect influences on other enzymatic pathways or feedback regulation mechanisms. Although a decrease in oxidation <sup>85</sup> and, consequently, reduced hydroxy-PUFA levels might be anticipated, our results show otherwise, as most hydroxy-PUFAs with significant changes after AUDA treatment exhibited an increasing trend. These findings emphasize the complex effects of AUDA treatment on hydroxy-PUFA levels and point to possible indirect influences on other enzymatic pathways or feedback regulation mechanisms. Further research is necessary to determine the potential roles of these changes in the rescuing effect of AUDA and to elucidate the precise mechanisms underlying the observed alterations in hydroxy-PUFA levels in the context of neurodegenerative diseases.

This study underscores the significance of using oxylipin analysis for enhancing our comprehension of the impact of  $A\beta$  and/or tau on neurodegeneration, as well as the therapeutic potential of epoxide hydrolase inhibition. A constraint of our research was that we could not use a higher concentration of AUDA, to see where we could reach to the maximum rescuing effect, primarily due to its limited solubility. Our team is currently focused on refining various epoxide hydrolase inhibitors to optimize their properties, including solubility. This approach will enable us to investigate their physiological effects and develop superior therapeutic compounds. Furthermore, several studies, encompassing those carried out by other research groups, have delved into the neurodegeneration induced by amyloid beta and/or tau in specific neurons by scrutinizing neuronal morphology. Although beyond the scope of the present paper, our preliminary data suggest that AUDA may alleviate tau-induced neurodegeneration in glutamatergic neurons (Figure S16). Further research is needed to corroborate these findings and

extend our understanding of the complex interplay between  $A\beta$ , tau, and CYP-EH metabolites in neurodegeneration.

## 4. Conclusion

In conclusion, our study elucidated an intricate relationship between oxylipins,  $A\beta$ , and tau in the context of neurodegeneration using the *C. elegans* model. Our findings highlighted the significance of oxylipin analysis in enhancing our understanding of the impact of  $A\beta$  and tau on neurodegeneration, and the potential therapeutic implications of epoxide hydrolase inhibition. By uncovering the complex interplay between lipid mediators and key pathological hallmarks of Alzheimer's disease, this research contributes valuable insights to the field and paves the way for the development of novel therapeutic strategies targeting multiple aspects of AD pathology. Future studies should build upon these findings to investigate the precise molecular mechanisms underlying the effects of oxylipins on  $A\beta$  and tau-mediated neurodegeneration and to develop targeted interventions that can effectively modulate oxylipin levels to improve the outcomes for individuals affected by Alzheimer's disease.

#### Acknowledgments

Some nematode strains were provided by the Caenorhabditis Genetics Center, funded by the NIH Office of Research Infrastructure Programs (P40 OD010440). Funding to K.S.S.L. and J.K.A. was provided by the NIGMS R03 AG075465, Pearl Aldrich Endowment for aging research and startup funding from Michigan State University. M.S. was partially supported by Pearl Aldrich Endowment for aging research. We acknowledge the MSU RTSF Mass Spectrometry and Metabolomics Core Facilities for support with oxylipin and lipidomic analysis. We would like to thank Mr. Devon Dattmore, Ms. Leslie Ramirez, and Ms. Heather deFeijter-Rupp (Michigan State University) for their help and assistance.

# **Supporting Information**

Supporting Information including experimental methods and materials, supplemental figures and table, is available in **APPENDIX 2**.

#### **BIBLIOGRAPHY**

- (1) Bloom, G. S. Amyloid-β and Tau: The Trigger and Bullet in Alzheimer Disease Pathogenesis. *JAMA Neurol.* **2014**, *71* (4), 505–508.
- (2) Hardy, J.; Selkoe, D. J. The Amyloid Hypothesis of Alzheimer's Disease: Progress and Problems on the Road to Therapeutics. *Science* **2002**, 297 (5580), 353–356.
- (3) Katsenos, A. P.; Davri, A. S.; Simos, Y. V.; Nikas, I. P.; Bekiari, C.; Paschou, S. A.; Peschos, D.; Konitsiotis, S.; Vezyraki, P.; Tsamis, K. I. New Treatment Approaches for Alzheimer's Disease: Preclinical Studies and Clinical Trials Centered on Antidiabetic Drugs. *Expert Opin. Investig. Drugs* **2022**, *31* (1), 105–123.
- (4) Huang, L.-K.; Chao, S.-P.; Hu, C.-J. Clinical Trials of New Drugs for Alzheimer Disease. *J. Biomed. Sci.* **2020**, 27 (1), 18.
- (5) Mattsson-Carlgren, N.; Andersson, E.; Janelidze, S.; Ossenkoppele, R.; Insel, P.; Strandberg, O.; Zetterberg, H.; Rosen, H. J.; Rabinovici, G.; Chai, X.; Blennow, K.; Dage, J. L.; Stomrud, E.; Smith, R.; Palmqvist, S.; Hansson, O. Aβ Deposition Is Associated with Increases in Soluble and Phosphorylated Tau That Precede a Positive Tau PET in Alzheimer's Disease. *Sci. Adv.* **2020**, *6* (16), eaaz2387.
- (6) Rapoport, M.; Dawson, H. N.; Binder, L. I.; Vitek, M. P.; Ferreira, A. Tau Is Essential to Beta -Amyloid-Induced Neurotoxicity. *Proc. Natl. Acad. Sci. U. S. A.* **2002**, *99* (9), 6364–6369.
- (7) Puzzo, D.; Argyrousi, E. K.; Staniszewski, A.; Zhang, H.; Calcagno, E.; Zuccarello, E.; Acquarone, E.; Fa', M.; Li Puma, D. D.; Grassi, C.; D'Adamio, L.; Kanaan, N. M.; Fraser, P. E.; Arancio, O. Tau Is Not Necessary for Amyloid-β-Induced Synaptic and Memory Impairments. *J. Clin. Invest.* **2020**, *130* (9), 4831–4844.
- (8) Kametani, F.; Hasegawa, M. Reconsideration of Amyloid Hypothesis and Tau Hypothesis in Alzheimer's Disease. *Front. Neurosci.* **2018**, *12*. https://doi.org/10.3389/fnins.2018.00025.
- (9) Busche, M. A.; Wegmann, S.; Dujardin, S.; Commins, C.; Schiantarelli, J.; Klickstein, N.; Kamath, T. V.; Carlson, G. A.; Nelken, I.; Hyman, B. T. Tau Impairs Neural Circuits, Dominating Amyloid-β Effects, in Alzheimer Models in Vivo. *Nat. Neurosci.* **2019**, *22* (1), 57–64.
- (10) Benbow, S. J.; Strovas, T. J.; Darvas, M.; Saxton, A.; Kraemer, B. C. Synergistic Toxicity between Tau and Amyloid Drives Neuronal Dysfunction and Neurodegeneration in Transgenic C. Elegans. *Hum. Mol. Genet.* **2020**, *29* (3), 495–505.
- (11) Busche, M. A.; Hyman, B. T. Synergy between Amyloid-β and Tau in Alzheimer's Disease. *Nat. Neurosci.* **2020**, *23* (10), 1183–1193.
- (12) Benbow, S. J.; Strovas, T. J.; Darvas, M.; Saxton, A.; Kraemer, B. C. Synergistic Toxicity between Tau and Amyloid Drives Neuronal Dysfunction and Neurodegeneration in

- Transgenic Caenorhabditis Elegans. *Alzheimers. Dement.* **2020**, *16* (S3). https://doi.org/10.1002/alz.047426.
- (13) Peña-Bautista, C.; Álvarez-Sánchez, L.; Cañada-Martínez, A. J.; Baquero, M.; Cháfer-Pericás, C. Epigenomics and Lipidomics Integration in Alzheimer Disease: Pathways Involved in Early Stages. *Biomedicines* **2021**, *9* (12), 1812.
- (14) Wilson, D. M.; Binder, L. I. Free Fatty Acids Stimulate the Polymerization of Tau and Amyloid Beta Peptides. In Vitro Evidence for a Common Effector of Pathogenesis in Alzheimer's Disease. *Am. J. Pathol.* **1997**, *150* (6), 2181–2195.
- (15) Patil, S.; Chan, C. Palmitic and Stearic Fatty Acids Induce Alzheimer-like Hyperphosphorylation of Tau in Primary Rat Cortical Neurons. *Neurosci. Lett.* **2005**, *384* (3), 288–293.
- (16) Di Natale, G.; Sabatino, G.; Sciacca, M. F. M.; Tosto, R.; Milardi, D.; Pappalardo, G. Aβ and Tau Interact with Metal Ions, Lipid Membranes and Peptide-Based Amyloid Inhibitors: Are These Common Features Relevant in Alzheimer's Disease? *Molecules* **2022**, 27 (16). https://doi.org/10.3390/molecules27165066.
- (17) García-Viñuales, S.; Sciacca, M. F. M.; Lanza, V.; Santoro, A. M.; Grasso, G.; Tundo, G. R.; Sbardella, D.; Coletta, M.; Grasso, G.; La Rosa, C.; Milardi, D. The Interplay between Lipid and Aβ Amyloid Homeostasis in Alzheimer's Disease: Risk Factors and Therapeutic Opportunities. *Chem. Phys. Lipids* **2021**, *236* (105072), 105072.
- (18) Sarparast, M.; Dattmore, D.; Alan, J.; Lee, K. S. S. Cytochrome P450 Metabolism of Polyunsaturated Fatty Acids and Neurodegeneration. *Nutrients* **2020**, *12* (11), 3523.
- (19) Santos, D.; Laila, R. B.; Fleming, I. Role of Cytochrome P450-Derived, Polyunsaturated Fatty Acid Mediators in Diabetes and the Metabolic Syndrome. *Prostaglandins & Other Lipid Mediators* **2020**, *148*.
- (20) Shoieb, S. M.; El-Ghiaty, M. A.; Alqahtani, M. A.; El-Kadi, A. O. S. Cytochrome P450-Derived Eicosanoids and Inflammation in Liver Diseases. *Prostaglandins Other Lipid Mediat.* **2020**, *147*, 106400.
- (21) Favor, O. K.; Chauhan, P. S.; Pourmand, E.; Edwards, A. M.; Wagner, J. G.; Lewandowski, R. P.; Heine, L. K.; Harkema, J. R.; Lee, K. S. S.; Pestka, J. J. Lipidome Modulation by Dietary Omega-3 Polyunsaturated Fatty Acid Supplementation or Selective Soluble Epoxide Hydrolase Inhibition Suppresses Rough LPS-Accelerated Glomerulonephritis in Lupus-Prone Mice. *Front. Immunol.* **2023**, *14*, 1124910.
- (22) Preissner, S. C.; Hoffmann, M. F.; Preissner, R.; Dunkel, M.; Gewiess, A.; Preissner, S. Polymorphic Cytochrome P450 Enzymes (CYPs) and Their Role in Personalized Therapy. *PLoS One* **2013**, *8* (12), e82562.

- (23) Dutheil, F.; Beaune, P.; Loriot, M.-A. Xenobiotic Metabolizing Enzymes in the Central Nervous System: Contribution of Cytochrome P450 Enzymes in Normal and Pathological Human Brain. *Biochimie* **2008**, *90* (3), 426–436.
- (24) Václavíková, R.; Hughes, D. J.; Souček, P. Microsomal Epoxide Hydrolase 1 (EPHX1): Gene, Structure, Function, and Role in Human Disease. *Gene* **2015**, *571* (1), 1–8.
- (25) Shen, Q.; Patten, K. T.; Valenzuela, A.; Lein, P. J.; Taha, A. Y. Probing Changes in Brain Esterified Oxylipin Concentrations during the Early Stages of Pathogenesis in Alzheimer's Disease Transgenic Rats. *Neurosci. Lett.* **2022**, *791* (136921), 136921.
- (26) Ghosh, A.; Comerota, M. M.; Wan, D.; Chen, F.; Propson, N. E.; Hwang, S. H.; Hammock, B. D.; Zheng, H. An Epoxide Hydrolase Inhibitor Reduces Neuroinflammation in a Mouse Model of Alzheimer's Disease. *Sci. Transl. Med.* **2020**, *12* (573). https://doi.org/10.1126/scitranslmed.abb1206.
- (27) Alzheimer's Disease Neuroimaging I. Cyp2c19 Variant Mitigates Alzheimer Disease Pathophysiology in Vivo and Postmortem.
- (28) Yan, H.; Kong, Y.; He, B.; Huang, M.; Li, J.; Zheng, J.; Liang, L.; Bi, J.; Zhao, S.; Shi, L. CYP2J2 Rs890293 Polymorphism Is Associated with Susceptibility to Alzheimer's Disease in the Chinese Han Population. *Neurosci. Lett.* **2015**, *593*, 56–60.
- (29) Griñán-Ferré, C.; Codony, S.; Pujol, E.; Yang, J.; Leiva, R.; Escolano, C.; Puigoriol-Illamola, D.; Companys-Alemany, J.; Corpas, R.; Sanfeliu, C.; Pérez, B.; Loza, M. I.; Brea, J.; Morisseau, C.; Hammock, B. D.; Vázquez, S.; Pallàs, M.; Galdeano, C. Pharmacological Inhibition of Soluble Epoxide Hydrolase as a New Therapy for Alzheimer's Disease. *Neurotherapeutics* **2020**. https://doi.org/10.1007/s13311-020-00854-1.
- (30) Lee, H.-T.; Lee, K.-I.; Chen, C.-H.; Lee, T.-S. Genetic Deletion of Soluble Epoxide Hydrolase Delays the Progression of Alzheimer's Disease. *J. Neuroinflammation* **2019**, *16* (1), 267.
- (31) Mokoena, N. Z.; Sebolai, O. M.; Albertyn, J.; Pohl, C. H. Synthesis and Function of Fatty Acids and Oxylipins, with a Focus on Caenorhabditis Elegans. *Prostaglandins Other Lipid Mediat.* **2020**, *148*, 106426.
- (32) Pereira, L.; Kratsios, P.; Serrano-Saiz, E.; Sheftel, H.; Mayo, A. E.; Hall, D. H.; White, J. G.; LeBoeuf, B.; Garcia, L. R.; Alon, U.; Hobert, O. A Cellular and Regulatory Map of the Cholinergic Nervous System of C. Elegans. *Elife* **2015**, *4*. https://doi.org/10.7554/eLife.12432.
- (33) Uno, M.; Nishida, E. Lifespan-Regulating Genes in C. Elegans. *NPJ Aging Mech. Dis.* **2016**, 2 (1), 16010.
- (34) Kraemer, B. C.; Zhang, B.; Leverenz, J. B.; Thomas, J. H.; Trojanowski, J. Q.; Schellenberg, G. D. Neurodegeneration and Defective Neurotransmission in a Caenorhabditis Elegans Model of Tauopathy. *Proc. Natl. Acad. Sci. U. S. A.* **2003**, *100* (17), 9980–9985.

- (35) Lu, T.; Aron, L.; Zullo, J.; Pan, Y.; Kim, H.; Chen, Y.; Yang, T.-H.; Kim, H.-M.; Drake, D.; Liu, X. S.; Bennett, D. A.; Colaiácovo, M. P.; Yankner, B. A. REST and Stress Resistance in Ageing and Alzheimer's Disease. *Nature* **2014**, *507* (7493), 448–454.
- (36) Griffin, E. F.; Caldwell, K. A.; Caldwell, G. A. Genetic and Pharmacological Discovery for Alzheimer's Disease Using Caenorhabditis Elegans. *ACS Chem. Neurosci.* **2017**, 8 (12), 2596–2606.
- (37) Caldwell, K. A.; Willicott, C. W.; Caldwell, G. A. Modeling Neurodegeneration in Caenorhabditis Elegans. *Dis. Model. Mech.* **2020**, *13* (10). https://doi.org/10.1242/dmm.046110.
- (38) Kraemer, B. C.; Burgess, J. K.; Chen, J. H.; Thomas, J. H.; Schellenberg, G. D. Molecular Pathways That Influence Human Tau-Induced Pathology in Caenorhabditis Elegans. *Hum. Mol. Genet.* **2006**, *15* (9), 1483–1496.
- (39) Liachko, N. F.; Guthrie, C. R.; Kraemer, B. C. Phosphorylation Promotes Neurotoxicity in a Caenorhabditis Elegans Model of TDP-43 Proteinopathy. *J. Neurosci.* **2010**, *30* (48), 16208–16219.
- (40) Knight, A. L.; Yan, X.; Hamamichi, S.; Ajjuri, R. R.; Mazzulli, J. R.; Zhang, M. W.; Daigle, J. G.; Zhang, S.; Borom, A. R.; Roberts, L. R.; Lee, S. K.; DeLeon, S. M.; Viollet-Djelassi, C.; Krainc, D.; O'Donnell, J. M.; Caldwell, K. A.; Caldwell, G. A. The Glycolytic Enzyme, GPI, Is a Functionally Conserved Modifier of Dopaminergic Neurodegeneration in Parkinson's Models. *Cell Metab.* **2014**, *20* (1), 145–157.
- (41) Lublin, A.; Isoda, F.; Patel, H.; Yen, K.; Nguyen, L.; Hajje, D.; Schwartz, M.; Mobbs, C. FDA-Approved Drugs That Protect Mammalian Neurons from Glucose Toxicity Slow Aging Dependent on Cbp and Protect against Proteotoxicity. *PLoS One* **2011**, *6* (11), e27762.
- (42) Kawli, T.; He, F.; Tan, M.-W. It Takes Nerves to Fight Infections: Insights on Neuro-Immune Interactions from C. Elegans. *Dis. Model. Mech.* **2010**, *3* (11–12), 721–731.
- (43) Nagai, J.; Yu, X.; Papouin, T.; Cheong, E.; Freeman, M. R.; Monk, K. R.; Hastings, M. H.; Haydon, P. G.; Rowitch, D.; Shaham, S.; Khakh, B. S. Behaviorally Consequential Astrocytic Regulation of Neural Circuits. *Neuron* **2021**, *109* (4), 576–596.
- (44) Wu, Y.; Wu, Z.; Butko, P.; Christen, Y.; Lambert, M. P.; Klein, W. L.; Link, C. D.; Luo, Y. Amyloid-Beta-Induced Pathological Behaviors Are Suppressed by Ginkgo Biloba Extract EGb 761 and Ginkgolides in Transgenic Caenorhabditis Elegans. *J. Neurosci.* **2006**, *26* (50), 13102–13113.
- (45) Schafer, W. R.; Kenyon, C. J. A Calcium-Channel Homologue Required for Adaptation to Dopamine and Serotonin in Caenorhabditis Elegans. *Nature* **1995**, *375* (6526), 73–78.
- (46) Sawin, E. R.; Ranganathan, R.; Horvitz, H. R. C. Elegans Locomotory Rate Is Modulated by the Environment through a Dopaminergic Pathway and by Experience through a Serotonergic Pathway. *Neuron* **2000**, *26* (3), 619–631.

- (47) Nuttley, W. M.; Atkinson-Leadbeater, K. P.; Van Der Kooy, D. Serotonin Mediates Food-Odor Associative Learning in the Nematode Caenorhabditiselegans. *Proc. Natl. Acad. Sci. U. S. A.* **2002**, *99* (19), 12449–12454.
- (48) Zhang, Y.; Lu, H.; Bargmann, C. I. Pathogenic Bacteria Induce Aversive Olfactory Learning in Caenorhabditis Elegans. *Nature* **2005**, *438* (7065), 179–184.
- (49) Ohta, A.; Ujisawa, T.; Sonoda, S.; Kuhara, A. Light and Pheromone-Sensing Neurons Regulates Cold Habituation through Insulin Signalling in Caenorhabditis Elegans. *Nat. Commun.* **2014**, *5* (1), 4412.
- (50) Sonoda, S.; Ohta, A.; Maruo, A.; Ujisawa, T.; Kuhara, A. Sperm Affects Head Sensory Neuron in Temperature Tolerance of Caenorhabditis Elegans. *Cell Rep.* **2016**, *16* (1), 56–65.
- (51) Ujisawa, T.; Ohta, A.; Ii, T.; Minakuchi, Y.; Toyoda, A.; Ii, M.; Kuhara, A. Endoribonuclease ENDU-2 Regulates Multiple Traits Including Cold Tolerance via Cell Autonomous and Nonautonomous Controls in Caenorhabditis Elegans. *Proc. Natl. Acad. Sci. U. S. A.* **2018**, *115* (35), 8823–8828.
- (52) Takagaki, N.; Ohta, A.; Ohnishi, K.; Minakuchi, Y.; Toyoda, A.; Fujiwara, Y.; Kuhara, A. Mechanoreceptor-Mediated Circuit Regulates Cold Tolerance in Caenorhabditis Elegans. *bioRxiv*, 2019. https://doi.org/10.1101/673863.
- (53) Murray, P.; Hayward, S. A. L.; Govan, G. G.; Gracey, A. Y.; Cossins, A. R. An Explicit Test of the Phospholipid Saturation Hypothesis of Acquired Cold Tolerance in Caenorhabditis Elegans. *Proc. Natl. Acad. Sci. U. S. A.* **2007**, *104* (13), 5489–5494.
- (54) Savory, F. R.; Sait, S. M.; Hope, I. A. DAF-16 and Δ9 Desaturase Genes Promote Cold Tolerance in Long-Lived Caenorhabditis Elegans Age-1 Mutants. *PLoS One* **2011**, *6* (9), e24550.
- (55) Liachko, N. *Cold-tolerance is a fast and easy method to identify neuronal dysfunction in C. elegans*. The WBG. http://wbg.wormbook.org/2016/07/05/cold-tolerance-is-a-fast-and-easy-method-to-identify-neuronal-dysfunction-in-c-elegans/ (accessed 2023-03-22).
- (56) Sarparast, M.; Pourmand, E.; Hinman, J.; Vonarx, D.; Reason, T.; Zhang, F.; Paithankar, S.; Chen, B.; Borhan, B.; Watts, J. L.; Alan, J.; Lee, K. S. S. Dihydroxy-Metabolites of Dihomo-γ-Linolenic Acid Drive Ferroptosis-Mediated Neurodegeneration. *ACS Cent. Sci.* **2023**. https://doi.org/10.1021/acscentsci.3c00052.
- (57) Harris, T. R.; Aronov, P. A.; Jones, P. D.; Tanaka, H.; Arand, M.; Hammock, B. D. Identification of Two Epoxide Hydrolases in Caenorhabditis Elegans That Metabolize Mammalian Lipid Signaling Molecules. *Arch. Biochem. Biophys.* **2008**, *472* (2), 139–149.
- (58) Zhou, Y.; Falck, J. R.; Rothe, M.; Schunck, W.-H.; Menzel, R. Role of CYP Eicosanoids in the Regulation of Pharyngeal Pumping and Food Uptake in Caenorhabditis Elegans. *J. Lipid Res.* **2015**, *56* (11), 2110–2123.

- (59) Inceoglu, B.; Wagner, K.; Schebb, N. H.; Morisseau, C.; Jinks, S. L.; Ulu, A.; Hegedus, C.; Rose, T.; Brosnan, R.; Hammock, B. D. Analgesia Mediated by Soluble Epoxide Hydrolase Inhibitors Is Dependent on CAMP. *Proc. Natl. Acad. Sci. U. S. A.* **2011**, *108* (12), 5093–5097.
- (60) Inceoglu, B.; Zolkowska, D.; Yoo, H. J.; Wagner, K. M.; Yang, J.; Hackett, E.; Hwang, S. H.; Lee, K. S. S.; Rogawski, M. A.; Morisseau, C.; Hammock, B. D. Epoxy Fatty Acids and Inhibition of the Soluble Epoxide Hydrolase Selectively Modulate GABA Mediated Neurotransmission to Delay Onset of Seizures. *PLoS One* **2013**, 8 (12), e80922.
- (61) Ren, Q.; Ma, M.; Ishima, T.; Morisseau, C.; Yang, J.; Wagner, K. M.; Zhang, J.-C.; Yang, C.; Yao, W.; Dong, C.; Han, M.; Hammock, B. D.; Hashimoto, K. Gene Deficiency and Pharmacological Inhibition of Soluble Epoxide Hydrolase Confers Resilience to Repeated Social Defeat Stress Proc. *Natl. Acad. Sci. U. S. A* **2016**, *113*, E1944–E1952.
- (62) Ma, M.; Ren, Q.; Yang, J.; Zhang, K.; Xiong, Z.; Ishima, T.; Pu, Y.; Hwang, S. H.; Toyoshima, M.; Iwayama, Y.; Hisano, Y.; Yoshikawa, T.; Hammock, B. D.; Hashimoto, K. Key Role of Soluble Epoxide Hydrolase in the Neurodevelopmental Disorders of Offspring after Maternal Immune Activation Proc. *Natl. Acad. Sci. U. S. A* **2019**, *116*, 7083–7088.
- (63) Ren, Q.; Ma, M.; Yang, J.; Nonaka, R.; Yamaguchi, A.; Ishikawa, K.-I.; Kobayashi, K.; Murayama, S.; Hwang, S. H.; Saiki, S.; Akamatsu, W.; Hattori, N.; Hammock, B. D.; Hashimoto, K. Soluble Epoxide Hydrolase Plays a Key Role in the Pathogenesis of Parkinson's Disease Proc. *Natl. Acad. Sci. U. S. A* **2018**, *115*, E5815-5823.
- (64) Lee, H.-T.; Chen, K.-I. Genetic Deletion of Soluble Epoxide Hydrolase Delays the Progression of Alzheimer's Disease J. *J. Neuroinflammation* **2019**, *16*.
- (65) Griñán-Ferré, C.; Codony, S.; Pujol, E.; Yang, J.; Leiva, R.; Escolano, C.; Puigoriol-Illamola, D.; Companys-Alemany, J.; Corpas, R.; Sanfeliu, C.; Pérez, B.; Loza, M. I.; Brea, J.; Morisseau, C.; Hammock, B. D.; Vázquez, S.; Pallàs, M.; Galdeano, C.; Codony, S.; Pujol, E.; Yang, J.; Leiva, R.; Escolano, C.; Puigoriol-Illamola, D.; Companys-Alemany, J.; Corpas, R.; Sanfeliu, C.; Pérez, B.; Loza, M. I.; Brea, J.; Morisseau, C.; Hammock, B. D.; Vázquez, S.; Pallàs, M.; Galdeano, C. Pharmacological Inhibition of SGriñán-Ferré C. *Pharmacological Inhibition of SGriñán-Ferré C* 2020.
- (66) Cowart, L. A.; Wei, S.; Hsu, M.-H.; Johnson, E. F.; Krishna, M. U.; Falck, J. R.; Capdevila, J. H. The CYP4A Isoforms Hydroxylate Epoxyeicosatrienoic Acids to Form High Affinity Peroxisome Proliferator-Activated Receptor Ligands. *J. Biol. Chem.* **2002**, *277* (38), 35105–35112.
- (67) Wray, J. A.; Sugden, M. C.; Zeldin, D. C.; Greenwood, G. K.; Samsuddin, S.; Miller-Degraff, L.; Bradbury, J. A.; Holness, M. J.; Warner, T. D.; Bishop-Bailey, D. The Epoxygenases CYP2J2 Activates the Nuclear Receptor PPARalpha in Vitro and in Vivo. *PLoS One* **2009**, *4* (10), e7421.
- (68) Sisignano, M.; Park, C.-K.; Angioni, C.; Zhang, D. D.; von Hehn, C.; Cobos, E. J.; Ghasemlou, N.; Xu, Z.-Z.; Kumaran, V.; Lu, R.; Grant, A.; Fischer, M. J. M.; Schmidtko, A.; Reeh, P.; Ji, R.-R.; Woolf, C. J.; Geisslinger, G.; Scholich, K.; Brenneis, C. 5,6-EET Is

- Released upon Neuronal Activity and Induces Mechanical Pain Hypersensitivity via TRPA1 on Central Afferent Terminals. *J. Neurosci.* **2012**, *32* (18), 6364–6372.
- (69) Liu, Y.; Wang, R.; Li, J.; Rao, J.; Li, W.; Falck, J. R.; Manthati, V. L.; Medhora, M.; Jacobs, E. R.; Zhu, D. Stable EET Urea Agonist and Soluble Epoxide Hydrolase Inhibitor Regulate Rat Pulmonary Arteries through TRPCs. *Hypertens. Res.* **2011**, *34* (5), 630–639.
- (70) Screening for G Protein-Coupled Receptor Targets of 14,15-Epoxyeicosatrienoic Acid. *Prostaglandins Other Lipid Mediat*.
- (71) Patwardhan, A. M.; Akopian, A. N.; Ruparel, N. B.; Diogenes, A.; Weintraub, S. T.; Uhlson, C.; Murphy, R. C.; Hargreaves, K. M. Heat Generates Oxidized Linoleic Acid Metabolites That Activate TRPV1 and Produce Pain in Rodents. *J. Clin. Invest.* **5 2010**, *120* (5), 1617–1626.
- (72) Zimmer, B.; Angioni, C.; Osthues, T.; Toewe, A.; Thomas, D.; Pierre, S. C.; Geisslinger, G.; Scholich, K.; Sisignano, M. The Oxidized Linoleic Acid Metabolite 12,13-DiHOME Mediates Thermal Hyperalgesia during Inflammatory Pain. *Biochim. Biophys. Acta Mol. Cell Biol. Lipids* **2018**, *1863* (7), 669–678.
- (73) Sisignano, M.; Angioni, C.; Park, C.-K.; Meyer Dos Santos, S.; Jordan, H.; Kuzikov, M.; Liu, D.; Zinn, S.; Hohman, S. W.; Schreiber, Y.; Zimmer, B.; Schmidt, M.; Lu, R.; Suo, J.; Zhang, D.-D.; Schäfer, S. M. G.; Hofmann, M.; Yekkirala, A. S.; de Bruin, N.; Parnham, M. J.; Woolf, C. J.; Ji, R.-R.; Scholich, K.; Geisslinger, G. Targeting CYP2J to Reduce Paclitaxel-Induced Peripheral Neuropathic Pain. *Proc. Natl. Acad. Sci. U. S. A.* **2016**, *113* (44), 12544–12549.
- (74) Ren, Q.; Ma, M.; Ishima, T.; Morisseau, C.; Yang, J.; Wagner, K. M.; Zhang, J.-C.; Yang, C.; Yao, W.; Dong, C.; Han, M.; Hammock, B. D.; Hashimoto, K. Gene Deficiency and Pharmacological Inhibition of Soluble Epoxide Hydrolase Confers Resilience to Repeated Social Defeat Stress. *Proc. Natl. Acad. Sci. U. S. A.* **2016**, *113* (13), E1944-52.
- (75) Ma, M.; Ren, Q.; Yang, J.; Zhang, K.; Xiong, Z.; Ishima, T.; Pu, Y.; Hwang, S. H.; Toyoshima, M.; Iwayama, Y.; Hisano, Y.; Yoshikawa, T.; Hammock, B. D.; Hashimoto, K. Key Role of Soluble Epoxide Hydrolase in the Neurodevelopmental Disorders of Offspring after Maternal Immune Activation. *Proc. Natl. Acad. Sci. U. S. A.* **2019**, *116* (14), 7083–7088.
- (76) Ren, Q.; Ma, M.; Yang, J.; Nonaka, R.; Yamaguchi, A.; Ishikawa, K.-I.; Kobayashi, K.; Murayama, S.; Hwang, S. H.; Saiki, S.; Akamatsu, W.; Hattori, N.; Hammock, B. D.; Hashimoto, K. Soluble Epoxide Hydrolase Plays a Key Role in the Pathogenesis of Parkinson's Disease. *Proc. Natl. Acad. Sci. U. S. A.* **2018**, *115* (25), E5815–E5823.
- (77) Hung, T.-H.; Shyue, S.-K.; Wu, C.-H.; Chen, C.-C.; Lin, C.-C.; Chang, C.-F.; Chen, S.-F. Deletion or Inhibition of Soluble Epoxide Hydrolase Protects against Brain Damage and Reduces Microglia-Mediated Neuroinflammation in Traumatic Brain Injury. *Oncotarget* **2017**, *8* (61), 103236–103260.
- (78) Sun, C.-P.; Zhang, X.-Y.; Zhou, J.-J.; Huo, X.-K.; Yu, Z.-L.; Morisseau, C.; Hammock, B. D.; Ma, X.-C. Inhibition of SEH via Stabilizing the Level of EETs Alleviated Alzheimer's

- Disease through GSK3β Signaling Pathway. Food Chem. Toxicol. **2021**, 156 (112516), 112516.
- (79) Hung, Y.-W.; Hung, S.-W.; Wu, Y.-C.; Wong, L.-K.; Lai, M.-T.; Shih, Y.-H.; Lee, T.-S.; Lin, Y.-Y. Soluble Epoxide Hydrolase Activity Regulates Inflammatory Responses and Seizure Generation in Two Mouse Models of Temporal Lobe Epilepsy. *Brain Behav. Immun.* **2015**, *43*, 118–129.
- (80) Bazinet, R. P.; Layé, S. Polyunsaturated Fatty Acids and Their Metabolites in Brain Function and Disease. *Nat. Rev. Neurosci.* **2014**, *15* (12), 771–785.
- (81) Czapski, G. A.; Czubowicz, K.; Strosznajder, J. B.; Strosznajder, R. P. The Lipoxygenases: Their Regulation and Implication in Alzheimer's Disease. *Neurochem. Res.* **2016**, *41* (1–2), 243–257.
- (82) Pluta, R.; Kiś, J.; Januszewski, S.; Jabłoński, M.; Czuczwar, S. J. Cross-Talk between Amyloid, Tau Protein and Free Radicals in Post-Ischemic Brain Neurodegeneration in the Form of Alzheimer's Disease Proteinopathy. *Antioxidants (Basel)* **2022**, *11* (1), 146.
- (83) Cheignon, C.; Tomas, M.; Bonnefont-Rousselot, D.; Faller, P.; Hureau, C.; Collin, F. Oxidative Stress and the Amyloid Beta Peptide in Alzheimer's Disease. *Redox Biol.* **2018**, *14*, 450–464.
- (84) Rhein, V.; Song, X.; Wiesner, A.; Ittner, L. M.; Baysang, G.; Meier, F.; Ozmen, L.; Bluethmann, H.; Dröse, S.; Brandt, U.; Savaskan, E.; Czech, C.; Götz, J.; Eckert, A. Amyloid-Beta and Tau Synergistically Impair the Oxidative Phosphorylation System in Triple Transgenic Alzheimer's Disease Mice. *Proc. Natl. Acad. Sci. U. S. A.* **2009**, *106* (47), 20057–20062.
- (85) Yeh, C.-F.; Chuang, T.-Y.; Hung, Y.-W.; Lan, M.-Y.; Tsai, C.-H.; Huang, H.-X.; Lin, Y.-Y. Soluble Epoxide Hydrolase Inhibition Enhances Anti-Inflammatory and Antioxidative Processes, Modulates Microglia Polarization, and Promotes Recovery after Ischemic Stroke. *Neuropsychiatr. Dis. Treat.* **2019**, *15*, 2927–2941.

**Chapter 4.** PHARMACOLOGICAL INHIBITION VS GENETIC KNOCKOUT OF EPOXIDE HYDROLASE: A FUTURE DIRECTION IN STUDYING AGING AND PUFA METABOLITES RELATION

### **ABSTRACT**

This chapter delves into the effects of epoxide hydrolase (EH) inhibition on the lifespan, healthspan, and reproduction of Caenorhabditis elegans (C. elegans) and examines the corresponding alterations in oxylipin profiles. We investigated pharmacological inhibition using AUDA and genetic knockouts of ceeh-1 and ceeh-2, comparing their effects with vehicle-treated wild-type worms. The egg-laying capacity and oxylipin profiles of these experimental groups were also examined. In order to further explore the potential influence of CYP-EH metabolites on aging and reproduction decline, we employed LC-MS/MS analysis, discussing Ep-PUFA and dihydroxy-PUFAs and their ratios in relation to EH enzyme function. Despite observing complex alterations in various PUFA metabolites and their potential signaling pathways, the specific CYP-EH metabolites responsible for the observed aging phenomena remain to be identified. To address the experimental challenges in manual phenotypic and lifespan analysis, we discuss the use of chemical reproduction inhibitors, such as 5-fluoro-2-deoxyuridine (FUDR), and microfluidic devices for progeny elimination and age-synchronization. This chapter sets the stage for future research in understanding the role of CYP-EH metabolites in aging using the C. elegans model and explores potential techniques to streamline the experimental process.

## 1. Introduction:

## 1.1. Overview on different epoxide hydrolase enzymes

Epoxide hydrolases (EHs) have been found in prokaryotes and eukaryotes ranging from plants to mammals. EHs are enzymes that catalyze the hydrolysis of epoxides, which are three-membered ring organic compounds with oxygen. Epoxide hydrolases play an important role in organismal physiology including both detoxification and homeostasis in the body. They metabolize a variety of natural and synthetic compounds, including drugs, toxins, and hormones; as well as endogenous molecules such as epoxy polyunsaturated fatty acids (Ep-PUFAs) generated by cytochrome P450 enzymes (CYPs)<sup>1,2</sup>. Deficiencies in epoxide hydrolases have been linked to various human diseases including cancer and neurological disorders, implying EHs as potential therapeutic targets<sup>1,3–5</sup>.

Based on genetic analysis in mammal, four different EHs have been identified: microsomal epoxide hydrolase (mEH, EPHX1), soluble epoxide hydrolase (sEH, EPHX2), EH3 (EPHX3), and EH4 (EPHX4) <sup>1,6</sup>. The mEH and sEH enzymes are members of the alpha/beta hydrolase superfamily and share a similar overall structure, with a core domain comprising of eight antiparallel beta-strands connected by alpha-helices and an adjustable lid domain <sup>1,6,7</sup>. Interestingly, mEH and sEH have different substrate specificities and functions <sup>1,7,8</sup>.

Microsomal epoxide hydrolase (mEH) is a membrane-bound enzyme encoded by the EPHX1 gene<sup>9</sup>. EPHX1 is primarily expressed in the liver, although it is also found at lower levels in other tissues such as the brain, skin, lung, and gastrointestinal tract<sup>10</sup>. One of the primary functions of EPHX1 is to detoxify the body by converting epoxide containing xenobiotic substrates into corresponding more polar 1,2-diol metabolites, which can then be eliminated from the body<sup>11</sup>. This metabolism helps to protect cells against genotoxic and cytotoxic compounds. However,

EPHX1 can also activate certain carcinogens by converting them into reactive metabolites that can cause DNA damage and potentially lead to cancer<sup>12–14</sup>. In addition to its detoxification function, EPHX1 has been shown to play a role in several organ-specific physiological responses. For example, EPHX1 regulates the metabolism of steroid hormones such as glucocorticoids (involved in stress response), androgens (involved in male sexual development and function), and estrogens (involved in female sexual development and function)<sup>6,15,16</sup>. EPHX1 has also been shown to regulate the endocannabinoid signaling pathway by metabolizing the endocannabinoid 2arachidonoylglycerol (2-AG) into free arachidonic acid (AA) and glycerol<sup>17</sup>. AA can then be further metabolized into eicosanoids, which are involved in processes such as inflammation, vasodilation, and cell growth<sup>18</sup>. EPHX1 knock-out mice, are generally phenotypically normal and do not display any obvious physical or behavioral abnormalities<sup>19</sup>. However, these enzymes are unable to metabolize some carcinogens, such as 7,12-dimethylbenz[a]anthracene, and therefore are resistant to some carcinogen-induced skin cancer<sup>19</sup>. This evidence corroborates the study that shows EPHX1 expression was found to be high in 89% of tumor samples in primary operable breast cancer<sup>20</sup>. On the other hand, mice carrying a gain-of-function variant of EPHX1 did not show any obvious physical or behavioral abnormalities<sup>21</sup>. However, they did show an increased rate of detoxification, and they metabolize endogenous EETs faster in different tissues.

Soluble epoxide hydrolase (sEH) is a 62 kDa homodimeric bifunctional enzyme encoded by the EPHX2 gene. It is in intracellular environments, including the cytosol and peroxisomes, and is highly expressed in the liver, kidney, and heart. sEH has a high catalytic rate for the hydrolysis of aliphatic epoxides, with an unknown role in xenobiotic metabolism<sup>5,6,22,23</sup>. Extensive details of sEH expression, function, and structure can be found in Chapter 1.

There are few studies on two others EH enzymes EH3 and EH4. EH3 is a 41 kDa (360 residues) protein encoded by the EPHX3 gene, and its microsomal properties have been identified by a related gene in insect cells<sup>5</sup>. The EPHX3 protein has a low level of similarity in its sequence compared to the EPHX1 and EPHX2 proteins, with protein sequence identities of 22% and 29% respectively<sup>6,24</sup>. However, it has a higher level of similarity in its sequence to the EPHX4 protein, with a protein sequence identity of 45%<sup>5</sup>. EPHX3 is localized to thean endoplasmic reticulum by an N-terminal transmembrane anchor.<sup>24,25</sup>. EPHX3 ccan catalyzes the hydrolysis of several EETs, EpOMEs, and leukotoxin with different regioselectivity as compared to EPHX1 and EPHX2<sup>24–26</sup>. While the in vivo test could not show the It has been shown that EPHX3 is capable of hydrolyzing both EETs and EpOMEs in *in vitro* tests. However, the authors did not observe the same results in vivo, suggesting that other metabolic pathways may be responsible for the metabolism of EpFAs in living organisms. In vitro tests have demonstrated that EPHX3 is capable of hydrolyzing both EETs and EpOMEs. However, in vivo tests confirm the enzyme's hydrolyzing capability only for EETs, not for EpOMEs<sup>24,25,27</sup>. This discrepancy between in vitro and in vivo finding could be be attributed to factors such as the enzyme location within cells or its binding to cellular membranes that may prevent it from effectively interacting with free epoxide substrates in the body, thereby hindering enzyme engagement with these substances in in vivo tests<sup>25,28</sup>. EPHX3 has also been shown to play a role in the formation of the water permeability barrier in the epidermis by catalyzing the hydrolysis of epoxide intermediates from the lipoxygenase pathway into linoleate triols, and its expression has been silenced in some types of cancer<sup>29–31</sup>. It can be inhibited by certain urea derivatives, which were originally developed as selective inhibitors of EPHX2<sup>24</sup>. On the other hand, EH4 is a 42 kDa (362 residue) protein encoded by the EPHX4 gene located on chromosome 1p22.1<sup>24</sup>. It is highly expressed in the brain, and its function is not well understood<sup>1,6</sup>.

However, it has been identified as a possible factor in various physiological activities. For example, EH4 is enriched in lipid droplets from sebaceous glands and the reduction of Ephx4 results in increased sebaceous lipids<sup>32</sup>. Additionally, the Ephx4 gene is among several genes that are modified in a rare tumor called Pseudomyxoma peritonei, while the specific role of Ephx4 in carcinogen is not understood<sup>33</sup>. its high homology with two EHs in *C. elegans* suggests that it may have important physiological activity in the brain<sup>34</sup>. Further information on epoxide hydrolase, their structure, mechanism, and expression levels can be found in chapter 1.

#### 1.2. Epoxide hydrolase as a therapeutic target for different diseases

There are two different types of inhibitors that target distinct activities of a bifunctional enzyme: one targets the C-terminus epoxide hydrolase activity, while the other targets the N-terminus phosphatase activity<sup>1,35</sup>. In this context, the primary focus is on inhibitors affecting the C-terminus, specifically those that interfere with epoxide hydrolase function. These inhibitors act on enzymes responsible for catalyzing the transformation of epoxides into diols, thus modulating their activity. These inhibitors have been studied for their potential therapeutic effects in a variety of diseases. In the first chapter the EH inhibition effects on different neurodegenerative diseases are explained in detail. The potential benefits of epoxide hydrolase inhibitors are summarized in **Table 1**.

Table 1. The potential benefits of epoxide hydrolase inhibitors in different disease

Disease Type	Treatment or Beneficial Effect	Explanation	Ref.		
Hypertension	Lowering blood pressure	This is based on the role of epoxides in the regulation of renal and vascular function, and on the fact that epoxide hydrolase inhibitors have beer shown to lower blood pressure in animal models of hypertension However, clinical trials have so far been inconclusive, and the effectiveness of epoxide hydrolase inhibitors in treating hypertension in humans remains uncertain.			
Atherosclerosis	Improving blood flow and reducing inflammation	sEH inhibitors are effective as an antiatherosclerosis therapy in murine models and for improving blood flow and reducing inflammation in models of stroke and myocardial infarction. This may be due to the ability of epoxides to dilate coronary arterioles and inhibit leukocyte adhesion to the vascular wall.	41– 44		
Pulmonary Diseases	Reducing lung inflammation	EETs elevation by EH inhibition have been reported to reduce bronchoconstriction and inflammation in murine models of asthma.	45– 49		
Diabetes	Reducing inflammation and improving insulin sensitivity	sEH inhibitors have shown promise in improving insulin sensitivity and reducing inflammation in murine models of diabetes.	50– 54		
Pain	Reducing inflammation and pain	sEH inhibitors have shown efficacy in reducing pain in various animal models of pain. Also shown to synergize activity of COX and 5-lipoxygenase (5-LOX) inhibitors.	55– 58		
Inflammation	Reducing inflammation and pain	sEH inhibitors have shown efficacy in reducing inflammation in various animal models of inflammation. This might be due to inhibition the expression of cytokines and adhesion molecules in endothelial cells by some epoxides.	5,59– 61		
Immunological Disorders	Treating immunological disorders	sEH inhibitors have shown promise in reducing inflammation in various animal models of immune disorders, such as allergies and asthma. This could be because of the ability of epoxides to modulate immune responses, including the production of cytokines and the activation of immune cells.	62– 65		
Smooth Muscle Disorders	Treating smooth muscle disorders	sEH inhibitors may have a role in the treatment of smooth muscle disorders through the modulation of EET levels.	41		
Renal disease	Reduced inflammation and improved kidney function	EETs inhibit inflammation and improve renal function by reducing leukocyte infiltration and decreasing the expression of adhesion molecules	66,67		
Neurodegeneratio n	Reduced inflammation and decrease neuronal defect	Soluble epoxide hydrolase deficiency or inhibition attenuates neurodegeneration induced by different toxicants such as MPTP in animal model; possibly through stabilizing Ep-PUFA level	68– 71		
Other Indications		sEH inhibitors have shown potential in a variety of different disease	3,5,7 2–74		

Several clinical trials using inhibitors of the EPHX2 enzyme have been conducted over the last decade<sup>75</sup>, and results from these trials have shown that pharmacological inhibition of EPHX2 is generally safe, with minimal serious adverse effects reported (See **Table 2**). Among them One

trial (NCT03486223) is investigating (i) whether a genetic variant in EPHX2 (p.Arg287Gln) is associated with insulin sensitivity and evaluating the effects of EPHX2 inhibition, by

**Table 2.** Some clinical trials studies related to epoxide hydrolase.

Case	Title	Conditions	Intervention s	Phases	Collaborators	Completion Date	Ref.
NCT05575713	The Effect of Soluble Epoxide Hydrolase (SEH) on Depression	Major Depressive Disorder	N/A	N/A	Nanfang Hospital of Southern Medical University	Jun-2023	76
NCT00654966	Evaluation of the Effects of Urotensin-II and Soluble Epoxide Hydrolase Inhibitors on Skin Microvessel Tone in Patients With Heart Failure, and in Healthy Volunteers	Heart Failure	Drug: Urotensine II Drug: Soluble epoxide hydrolase	2	Monash University, Australia	Dec-2010	77
NCT03486223	Soluble Epoxide Hydrolase Inhibition and Insulin Resistance	Diabetes Mellitus Endocrine System Diseases Glucose Metabolism Disorders PreDiabet es Obesity	Drug: GSK2256294  Drug: Placebo oral capsule	2	Vanderbilt University Medical Center, NIA, NIDDK	Nov-2021	78
NCT03318783	Subarachnoid Hemorrhage and Soluble Epoxide Hydrolase Inhibition Trial	Subarachnoid Hemorrhage, Aneurysmal Delaye d Cerebral Ischemia Vasospas m, Cerebral Endothelia I Dysfunction	Drug: GSK2256294  Drug: Placebo	1 and 2	-Oregon Health and Science University -FAER -GlaxoSmithKline	Jan-2020	79
NCT00847899	Evaluation of Soluble Epoxide Hydrolase (s-EH) Inhibitor in Patients With Mild to Moderate Hypertension and Impaired Glucose Tolerance	Hypertension Impaired Glucose Tolerance	Drug: AR9281 Drug: Placebo	2	Arete Therapeutics	Nov-09	80
NCT01762774	A Study to Assess the Safety, Tolerability, Pharmacokinetics and Pharmacodynamics of Single Doses of GSK2256294 in Healthy Volunteers, and Single and Repeat Doses of GSK2256294 in Adult Male Moderately Obese Smokers	Pulmonary Disease, Chronic Obstructive	Drug: GSK2256294  Drug: Placebo	1	GlaxoSmithKline	May-2014	81
NCT03100656	A Study to Investigate the Safety and Pharmacokinetics of a Single Dose of GSK2256294 in Healthy Young Males and Elderly Subjects	Pulmonary Disease, Chronic Obstructive	Drug: GSK2256294	1	UC, San Diego, UC Davis, University of Toronto	May-2014	82

GSK2256294 inhibitor, on type 2 diabetes<sup>78</sup>. The second trial (NCT03318783) is evaluating the efficacy of EPHX2 inhibition in patients with aneurysmal subarachnoid hemorrhage<sup>74,79</sup>. Furthermore, despite many examples of the therapeutic effect of EH inhibition, there have been challenges in translating these findings to the clinic, including lack of efficacy in a human clinical trial with clinical candidate AR9281. Besides, the influence of various factors such as dietary status and genetic variation on the effects of sEH inhibitors remains understudied despite the fact that

the epoxy fatty acid and dihydroxy fatty acid, the potential endogenous substrate and product of sEH respectively, are greatly affected by the dietary lipid level <sup>75,83–85</sup>.

#### 1.3. Epoxide hydrolase inhibitors:

Soluble epoxide hydrolase inhibitors are a class of compounds that have been investigated for their potential use in treating a variety of diseases, including hypertension, cancer, dyslipidemia, pain, immunological disorders, neurological diseases, diabetes, and eye diseases (**Table 1**). The most potent sEH inhibitors are urea, carbamate, and amide derivatives, which work by forming hydrogen bonds with specific amino acid residues in the enzyme(Figure 1)<sup>22,86–89</sup>.

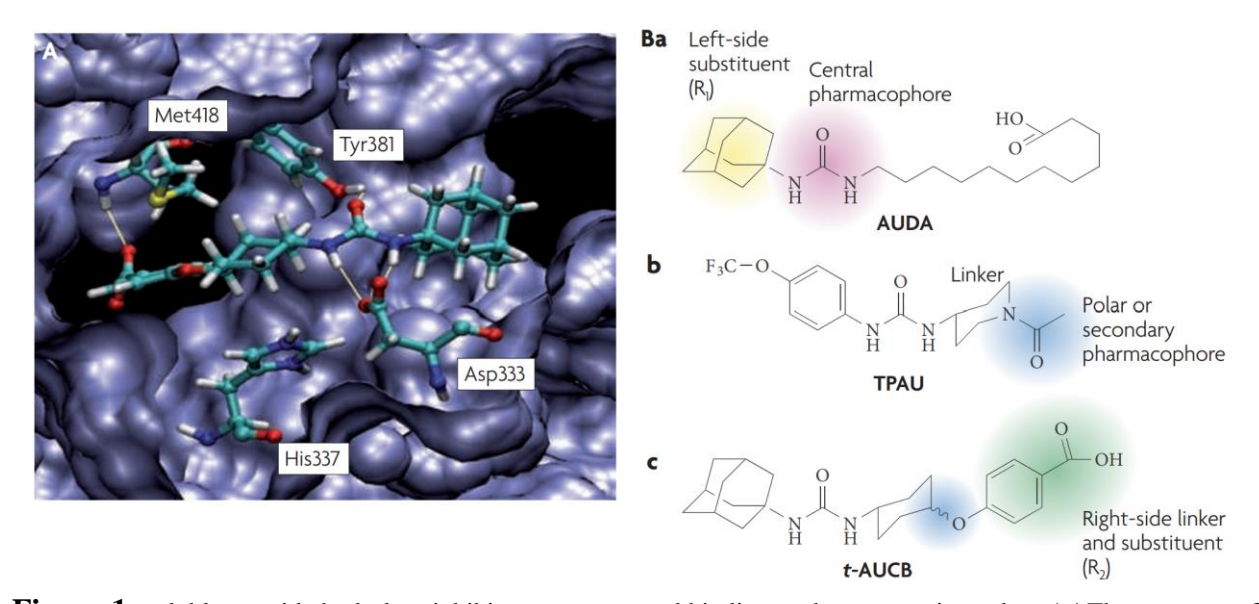


Figure 1. soluble epoxide hydrolase inhibitor structures and binding to the enzymatic pocket. A | The structure of the sEH enzymatic pocket with bound sEHI, trans-4-[4-(3-adamantan-1-yl-ureido)-cyclohexyloxy]-benzoic acid (t-AUCB). The residue Tyr465 is omitted for clarity. The structure was prepared using Scigress Explorer Standard version 7.7.0.49, the atomic coordinates of the human sEH were retrieved from the Protein Data Bank (PDB number 1VJ5) and the image was produced using freewares VMD 1.8.6 and POV-Ray 3.6. The key amino-acid residues that form the binding site for the sEHI are shown. Ba | The compound 12-(3-adamantan-1-yl-ureido) dodecanoic acid (AUDA) contains the central pharmacophore that forms multiple hydrogen bonds in the enzyme catalytic site. Urea, amide and carbamate substituents have been used for the central pharmacophore. The R1 or left side of the molecule rests in a hydrophobic pocket of the sEH catalytic tunnel. The hydrophobic right side of AUDA was designed to mimic 14,15-epoxyeicosatrienoic acid (EET). AUDA is a highly potent sEHI but must be formulated carefully for use in vivo. Bb | 1-trifluoromethoxyphenyl-3- (1-acetylpiperidin-4-yl)urea (TPAU) is a potent sEHI, illustrating that a polar secondary pharmacophore 7–8 Å from the central pharmacophore increases solubility while maintaining potency. It has a piperidine linker group between the central pharmacophore and secondary pharmacophore. Bc | t-AUCB has an ether as the secondary pharmacophore, with an R2 on the right side reaching towards the enzyme surface and mimicking the carboxylate of EETs. The cis isomer (not shown) is also an active sEHI. Both TPAU and t-AUCB are highly potent and have good oral availability and pharmacokinetic characteristics. t-AUCB is more broadly active across multiple species. Entire Figure is Taken from reference <sup>22</sup>.

A large number of urea derivatives have been shown to possess sEH inhibitory activity 89-93. For instance, N,N'-dicyclohexylurea (DCU) has shown significant inhibitory effect of sEH, however suffer from unfavorable pharmaceutical properties<sup>94</sup>. Likewise, 1-cyclohexyl-3-dodecylurea (CDU) shows a sufficient sEH inhibitory, has poor solubility and a high melting point that limit its uses in animal and clinical studies<sup>95–97</sup>. To address this issue, Dr. Hammock's group designed a sEH inhibitor that is an adamantine derivative that possesses increased water solubility compared with the cyclohexyl derivative in CDU<sup>98</sup>. AUDA (1-(1-adamantyl)-3-ureidopropan-2ol) which could be considered as a fatty acid analog, displayed excellent potency to sEH. Treatment with AUDA in a rat model of hypertension resulted in a higher accumulation of fatty acid epoxides and a relatively lower amount of the corresponding diol in the urine, representing the effectiveness of the drug in *in vivo* EH inhibition<sup>98</sup>. Also, several studies show that AUDA can lead to an increased level of specific epoxy-fatty acids such as EETs in the plasma and tissues that result various beneficial effects, including dilating coronary arterioles and inhibiting the leukocyte adhesion<sup>99–102</sup>. However, AUDA has some limitations as a potential therapeutic agent due to its metabolic liability resulting from the fatty acid β-oxidation and cytochrome P450 oxidation of the adamantane group<sup>3,103</sup>. In this regard, different strategies have been employed to improve the physical properties, pharmacokinetic properties, and potency of urea-based epoxide hydrolase inhibitors. These include, but not limited to, (i) substitution of an alkyl group in AUDA with a polar chain with ether group that improved the drug physical properties (i.e., AEPU)<sup>98</sup>; (ii) replacement of the ether group with conformationally restricted substituents which results in higher potency (i.e., TPPU, c-AUCB, t-AUCB, APAU, etc.)<sup>104–108</sup>; (iii) implementing fluorine and adamantane groups that increase the inhibitory effect <sup>109</sup>; and (iv) using natural bicyclic lipophilic groups which could increase the water solubility of compound 110. Research in this area is still ongoing in order to develop inhibitors with increased solubility, permeability, and stability, and nanomolar sEH inhibitory potency. It should be noted that there are several other non-urea based central pharmacophores that have shown promising sEH inhibitory activity including aminobenzisoxazole, acyl hydrazones, 4-benzamidobenzoic acid hydrazide, adamantly thioureas and sulphoxide derivatives<sup>111–116</sup>, which are out of scope of this chapter. Also, the focus in this chapter is (i) to study how a pharmacological inhibition using a EH inhibitor could affect the lifespan, healthspan, and the oxylipin profile *C. elegans* animal model; and (ii) to investigate if there is a different between pharmacological inhibition and genetic knock out of EH form lifespan, healthspan, and oxylipin profile perspective. To this end, we use AUDA, that has already been tested in different animal models, and its effect on *C. elegans* has previously shown by our group (see chapter 2 and 3).

## 1.4. Epoxide Hydrolase inhibitors in *C. elegans*

While there are four isoforms of epoxide hydrolase in humans, based on DNA sequence homology, *C. elegans* only has two isoforms, CEEH-1 and CEEH-1, which are most similar to the human EH3 and EH4 isoforms<sup>34</sup>. These isoforms are responsible for predominantly metabolizing Ep-PUFAs. The CEEH-1 and CEEH-2 enzymes in *C. elegans* have been shown to have both endobiotic and xenobiotic metabolizing activities, with CEEH-1 having higher activity towards Ep-PUFA substrates than CEEH-2<sup>34</sup>.

Harris et al examined the effect of four different urea-based mammalian sEH inhibitors on CEEH-1 extracted enzyme and found the AUDA to be the most effective one<sup>34</sup>. Furthermore, the *in vivo* study has shown that AUDA could inhibit the enzymes in a population of worms in liquid culture. When the worms were treated with the inhibitor at 24 and 36 hours after the larval stage, the levels of 9,10-EpOME and 12,13-EpOME increased by about 200% relative to the control

population, while the levels of 12,13-DiHOME decreased. The epoxide-to-diol ratio for 9,10-EpOME and 12,13-EpOME both increased significantly, with the 9,10-EpOME ratio increasing by 174% and the 12,13-EpOME ratio increasing tenfold, while changes in 9,10-DiHOME levels were not significantly different from the controls<sup>34</sup>. Our group also found that the AUDA could rescue neurodegeneration induced by dietary DGLA by inhibiting the epoxide hydrolase and decrease the level of DHEDs (See chapter 2). We also found that AUDA could modulate the neuronal deficient in C. elegans expressing human Aβ and tau (See chapter 3). Based on these findings, we recognized that AUDA ability to inhibit epoxide hydrolase (EH) and modulate neuronal deficiency might be crucial factors affecting the overall health and lifespan of *C. elegans*. Given the role of EH in the metabolism of bioactive lipid mediators, it is plausible that EH inhibition by AUDA could have a broader impact on the organism physiology and longevity. Therefore, we hypothesized that the EH inhibition by AUDA might play a significant role in the lifespan of C. elegans by promoting a healthier neuronal environment and potentially influencing other age-related processes. Thus, we aim to further explore the EH inhibition effect, by examining the effect of AUDA in the lifespan of C. elegans, and then compared it with genetic knock out of either CEEH-1 or CEEH-2.

## 2. Results and discussion

In this section the effect of epoxide hydrolase inhibition on the overall lifespan and healthspan of *C. elegans* is discussed. We first studied the effect of pharmacological inhibition of CEEHs using AUDA and compared it with vehicle (N2 wild type). Then, the strains with genetic knock out of either *ceeh-1* or *ceeh-2* are compared to vehicle or those treated with AUDA supplementation. The egg laying feature of the wild-type worm when supplemented with AUDA or vehicle, were also compared to *ceeh-1(ok3153)* and *ceeh-2 (tm3635)* strains. After that the

oxylipin profile of these four groups (N2, N2 supplemented with AUDA, *ceeh-1(ok3153)*, and *ceeh-2 (tm3635)* are discussed in detail. Finally, the future direction of this study has been discussed.

## 2.1. Epoxide hydrolase deficient and worm lifespan and healthspan

Lifespan is a measurable trait that refers to the length of time from birth until death. While aging and lifespan are related, they are not identical. It is because aging is a complex and multifaceted process that encompasses a wide range of changes that occur in the body over time. Studies in various species have shown that an increase in lifespan is often accompanied by slowing the onset of other aspects of aging. As a result, lifespan is often used as a measure for studying the aging process, but additional complementary measurements are needed. Lifespan can be measured in a variety of ways, including through lifespan assays in which the survival of a population is tracked from the onset of adulthood until the last member of the population dies <sup>117,118</sup>. In C. elegans, there are several methods for measuring lifespan, and the most common method is to use solid media plates <sup>117,118</sup>. In this method, worms are placed on plates containing food (such as the E. coli strain OP50) and their survival is monitored over time. The data collected from these experiments are used to plot a survival curve, which provides information about the lifespan of a population of tested *C. elegans*, including the mean, median, and maximal lifespan. It is important to note that the size of the population used in these experiments can impact the reliability of the lifespan data, with larger populations providing more reliable results 119. That is why we avoid using less than 100 worms per trial in each experiment. We also did not use more than 100 worms to avoid starvation from overcrowding which effects on lifespan<sup>117,120</sup>.

### 2.1.1. Lifespan study

To study the effect of AUDA on *C. elegans* lifespan, worms were transferred to an agar plate supplemented by AUDA at desired concentration (see the experimental section for further information) on L4 stage. Then the number of dead and alive worms were counted every other day. As the worms aged, their movement gets slower; thus, a gentle tap on the nose of worm was used to confirm their life status. Also, worms that lost or burrow into the medium, climb the plate walls and dry up, or injured during transfer are censored. Worms were transferred to the new plate every other day to provide fresh food/supplementation and remove the progeny contamination. Finally, survival data were plotted on a Kaplain-Meier curve using GraphPad Prism 9.5.

While the lifespan of wild-type worms treated with AUDA does not show difference compared to a vehicle control, both *ceeh-1(ok3153)* and *ceeh-2 (tm3635)* strains in which *ceeh-1* and *ceeh-2* are genetically knock out respectively, show shorter lifespan (Figure 2A-C) than the vehicle control. It is important to note that the *ok3153* and *tm3635* strains have partial deletions in their respective genes, which do not encompass the complete gene sequence. To further explore the impact of *ceeh-1* and *ceeh-2* genetic knockouts and investigate whether the complete deletion of the entire gene related to the enzyme might yield different results, we also examined another set of strains made by Dr. Pretrascheck's group at the Scripps Research Institute: *ceeh-1(vv228)* and *ceeh-2(vv226)*. These strains have the entire *ceeh-1* and *ceeh-2* genes deleted, potentially providing a more comprehensive understanding of the effects of EH gene knockout on *C. elegans* lifespan.

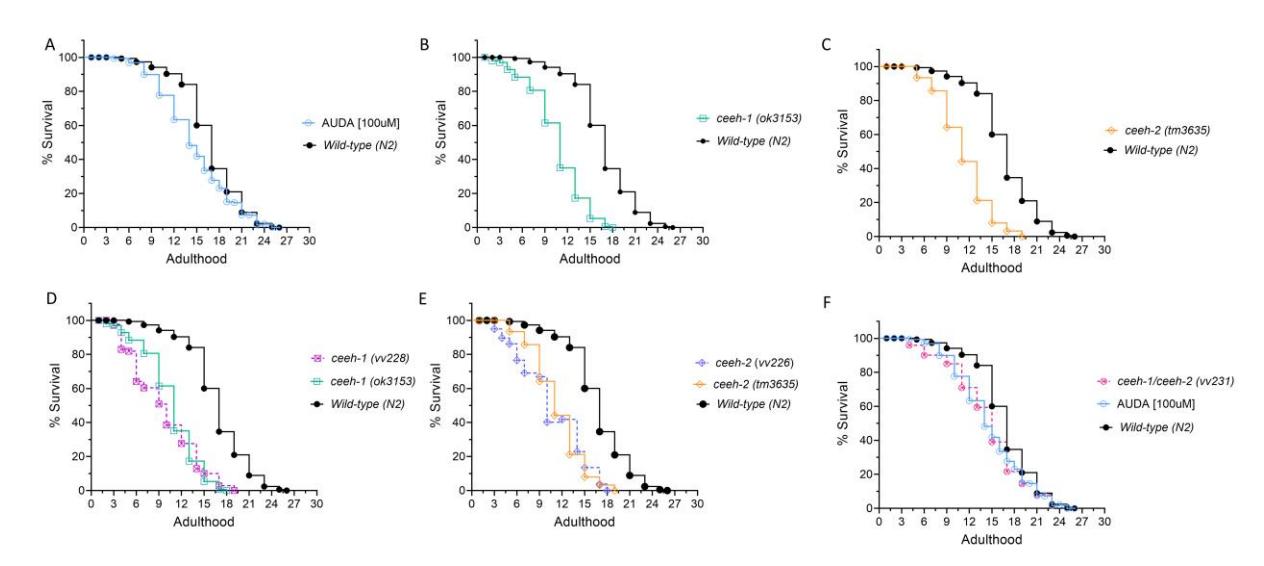


**Figure 2. Lifespan analysis.** (**A**) Lifespan of wildtype worm with and without supplementation with 100 μM AUDA. (**B**) Lifespan of *ceeh-1* (ok3153) compared to wildtype (**C**) Lifespan of *ceeh-2* (tm3635) compared to wildtype (**D**) Lifespan of *ceeh-1* (ok3153) and wildtype. (**E**) Lifespan of *ceeh-2* (vv228) compared to *ceeh-1* (ok3153) and wildtype (**F**) Lifespan of *ceeh-1/ceeh-2 hybrid* (vv231) compared to wildtype ±100 μM AUDA. Three replicates for each experiment have been done, and each trial started with 100 worms at L4 stage. For AUDA treatment, 100 larvae were grown on normal plate with OP50, and at L4 storage transferred to the plates supplemented with 100 μM AUDA.

Interestingly, Both *vv228* and *vv226* shows lifespan similar to other *ceeh-1(ok3153)* and *ceeh-2* (*tm3635*) strains, further confirm the effect of genetic knock out of *ceeh-1* and *ceeh-2* on worm lifespan is likely due to the absence of CEEH-1 and CEEH-2 activity in the worms (Figure 2D, and E). This is particularly interesting when studies on other mammalian models found that for instance, in mice either treatment with she inhibitor or genetic deletion of sEH gene (*Ephx2 KO*) significantly improved survival, preserved cardiac function, and maintained mitochondrial quality <sup>121,122</sup>. In addition, *Ephx1* and *Ephx2* knock-out mice are found to be viable, fertile, and normal in size with no obvious physical or behavioral abnormalities <sup>19</sup>. Also, mice with disruption in *Ephx3* did not show any changes in an overt phenotype. However, none of these studies investigate the overall lifespan of these genetic knockout mice. Our studies and the published report suggest EHs may play a critical role in the homeostatic state of the animals.

Interestingly, the strain with both ceeh-1 and ceeh-2 knocked out, named as *ceeh-1/ceeh-2* (*vv231*), exhibits a similar lifespan to that observed with AUDA supplementation (Figure 2F). This observation suggests that the shortened lifespan observed in either *ceeh-1* or *ceeh-2* strains could potentially be attributed to different substrate selectivity between these two enzymes for various epoxy-fatty acids. When one enzyme is eliminated, the other one may become dominant, leading to an increased production of specific oxylipins that could have toxic effects and accelerate the aging process. This will be further discussed in section 2.2.

#### 2.1.2. Egg production capacity

The reproductive organs of *C. elegans* are organized into two symmetrical gonad arms, each consisting of the somatic gonad and the germline (Figure 3). The germline is the tissue responsible for producing eggs and sperm and contains stem cells that give rise to all other germ cells. During the development stage, germline stem cells divide and migrate through the gonad arms, eventually undergoing meiosis and entering the spermatheca, where fertilization occurs. After fertilization, the resulting eggs are laid through the vulva and into the environment. *C. elegans* exhibit a characteristic pattern of egg production, with egg production peaking on the 2<sup>nd</sup> or 3<sup>rd</sup> day of adulthood. This peak is followed by a rapid decline in egg production until it ceases around the 6<sup>th</sup> day of adulthood. Researchers often use various statistical measures, such as timing of egg production and total number of eggs produced, to compare the egg production patterns of different *C. elegans* strains.

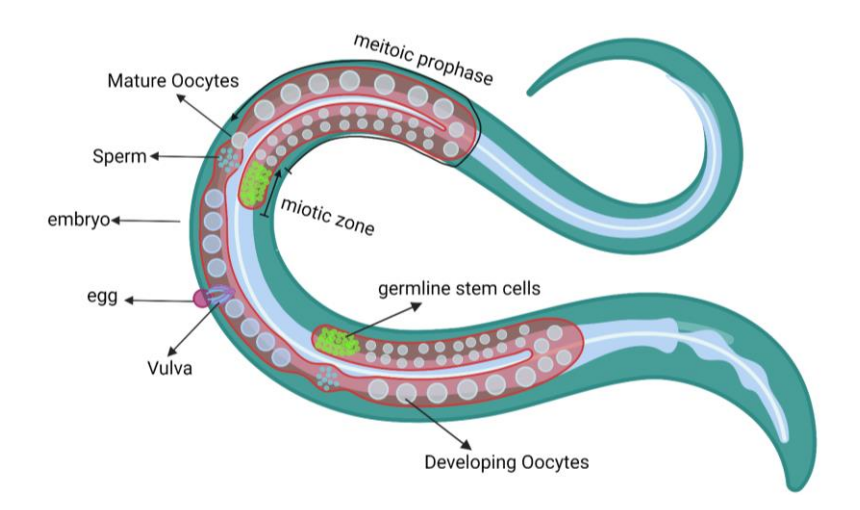


**Figure 3.** A schematic of an adult *C. elegans* hermaphrodite to show the bilaterally symmetrical U-shaped gonad arms (red). The germline stem cells (green) progress from the distal end of the gonad to the proximal end and formed immature oocytes. These immature oocytes then progress through the meiotic prophase, during which the process of meiosis takes place, resulting in the production of mature oocytes. The mature oocytes are then stored in the spermatheca, where they can be fertilized by sperm. Once fertilized, the oocytes exit the spermatheca as zygotes, which then form an eggshell and complete meiosis.

The egg-laying in *C. elegans* is regulated by a combination of cholinergic, serotonergic, GABAergic, and peptidergic signaling pathways  $^{123}$ . While the effects of age on reproductive function are yet to be well-known, previous research has shown that sacrificing fertility can extend lifespan in a range of species  $^{124,125}$ . In *C. elegans*, removing the germline not only increases the lifespan but also leads to an accumulation of fat, as demonstrated through the use of lipid-labeling dyes and gas chromatography  $^{126,127}$ . This link between reproductive deficiency and increased fat accumulation has been observed in a variety of other organisms, including invertebrates like Drosophila and vertebrates such as mice, rats, and monkeys  $^{128-132}$ . Furthermore, dietary restriction has been found to delay age-related degeneration of reproductive function and extends lifespan in *C. elegans*, while reducing the total number of progeny production per individual worm  $^{133,134}$ . Additionally, the *fat-3* mutant strain of *C. elegans*, which does not produce C-20  $\omega$ -6 and  $\omega$ -3 PUFAs, exhibits abnormal movement and defective egg-laying behavior, which are controlled by

motor neurons and specific serotonergic vulva neurons <sup>135–137</sup>. Egg laying deficient also was observed in The *fat-1* mutant and treatment with trilinolenin [D-TG(54:9)] could rescue the egglaying deficiency in this strain by preventing the propagation of damage caused by reactive oxygen species <sup>138</sup>. However, these studies have only partially explored the role of individual intact lipid molecules in regulating reproduction, and to the best of author knowledge there is no report on possible role the oxylipins could play on regulation of egg-laying in *C. elegans*.

Considering these and based on our above lifespan study, the egg-laying capacity of *ceeh-1* and *ceeh-2* strains were examined and compared to Wild-type with and without AUDA supplementation. As shown in Figure 4A, both *ceeh-1* and *ceeh-2* strains experienced significant egg laying deficiency, while simultaneous inhibition of EH enzymes using AUDA does not affect the overall egg laying capacity. Furthermore, the egg laying trend per day shows some differences in the egg laying patterns in *ceeh* knock out strains, and the high similarity between AUDA supplementation and Wildtype (Figure 4B).

The combination between shorter lifespan and lower number of progenies in *ceeh* knock out strain could suggest the possible aging and age-related decline of reproductive function. Reproductive aging is important for several reasons. It is likely to play a critical role in evolution, as the reproductive history of an individual involves the initiation of progeny production as a result of sexual maturity, some level of progeny production during the fertile period, and the cessation of progeny production as a result of reproductive aging or death <sup>139</sup>. These three processes

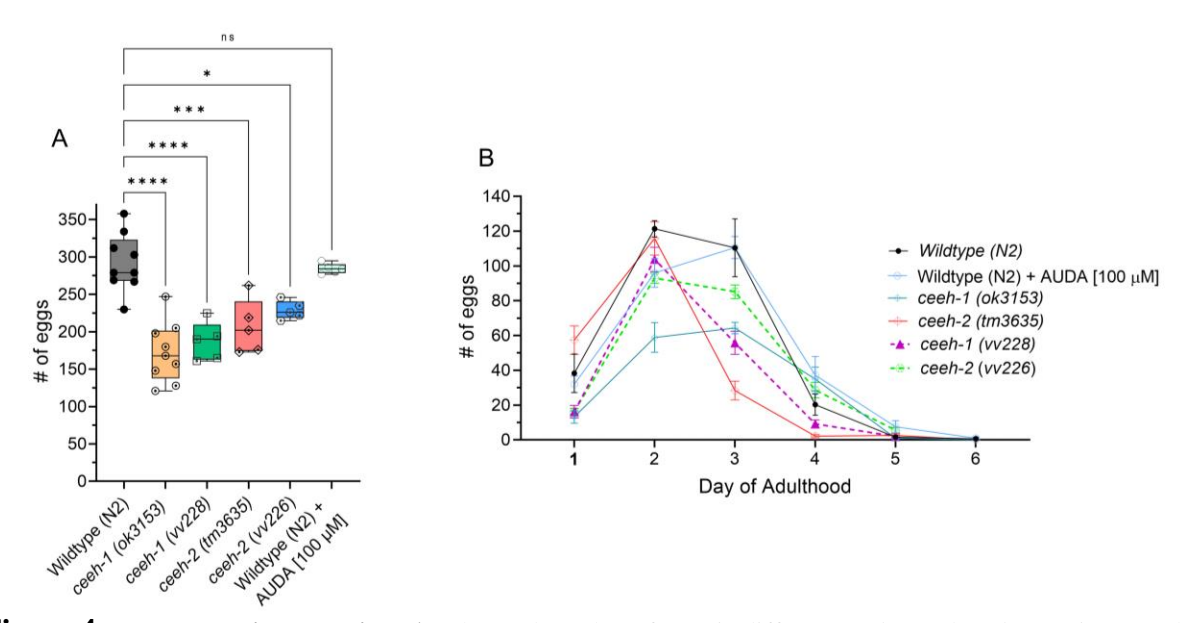


**Figure 4.** Egg production capacity. (A) The total number of eggs in different *ceeh-1* and *ceeh-2* strains as well as wildtype with and without supplementation with 100 μM AUDA. (B) The number of eggs laid per day of adulthood. The egg production capacity started at L4 stage, and Day 1 is the time after first egg is laid. Five trials have been done.

determine the rate of progeny production and the total number of progenies generated by an individual. Furthermore, these data suggest the possible involvement of CYP-EH metabolites on aging or age-related decline in reproduction (or egg-laying) and further analysis could reveal the possible signaling molecules involved in this process. Also, understanding reproductive aging could likely provide critical insights into the evolution of aging.

To further elucidate the observed phenotype and difference in lifespan of EH knock outs, the oxylipin profile of *ceeh-1(ok3153)* and *ceeh-2 (tm3635)* were analyzed and compared to wild-type with and without AUDA supplementation, which discussed in the next section.

## 2.2 Oxylipin profile of AUDA and EH KO

In order to further explore the possible effect of CYP-EH metabolites in aging (shortening lifespan) and reproduction decline in *C. elegans*, we used the LC-MS/MS technique established in our lab. The detailed experimental procedure including sample preparation and analysis is explained in Supporting Information (Appendix 4). First, two general groups of oxylipins related

to CYP-EH metabolites (i.e., epoxy PUFA, dihydroxy-PUFA) are discussed. Then, the overall impact of CEEH inhibition or knock out on epoxy- to dihydroxy-PUFA ratio, which is one of the criteria determining the effect of EH enzyme function will be discussed.

### 2.2.1. Epoxy PUFA level in CEEH genetic knock out and CEEH inhibition with AUDA

In this section we track the Ep-PUFAs level related to CYP-EH metabolism in *C. elegans* Wild-type and compared it with three different groups (i) AUDA supplementation, (ii) *ceeh-1(ok3153)* strain, and (iii) *ceeh-2 (tm3635)* strain. The overall oxylipin profile for all four groups is shown in Figure 5A and substantial changes in the oxylipin profile was observed among groups in which the CEEH enzymes are manipulated by either pharmacologically with the treatment of AUDA, or through genetic knock out of *ceeh-1* or *ceeh-2*. In regard to the endogenous level of Ep-PUFA metabolites that will be discussed here, we sub-categorized the oxylipin profiles based on their original fatty acid, including linoleic acid (LA), gama-dihomo linoleic acid (DGLA), arachidonic acid (AA),  $\alpha$ -linoleic acid ( $\alpha$ -LA), and eicosapentaenoic acid (EPA) and they will be discussed in the following paragraphs.

Our study shows that in *C. elegans*, the Ep-PUFA metabolites of LA are in the range of 10-1000 pmol/g of worms (Figure 5B). Interestingly, while *ceeh-1(ok3153)* shows a significant increase in both regioisomers of EpOME compared to vehicle, neither AUDA treatment nor *ceeh-2 (tm3635)* shows any substantial changes compared to the vehicle (Figure 5B). Furthermore, the *ceeh-1(ok3153)* shows an increase level of all EEDs regioisomers, while no significant change was found for wild-type strain treated with AUDA. The *ceeh-2 (tm3635)* does not produce any EEDs regioisomers (Figure 5C). On the other hand, the epoxy metabolites of arachidonic acid (EETs) have shown a mixed trend. While AUDA does not affect the 14,15-EET, 11,12-EET, and 8,9-EET level, it could completely block the production of 5,6-EET. The genetic knock out of CEEH-2

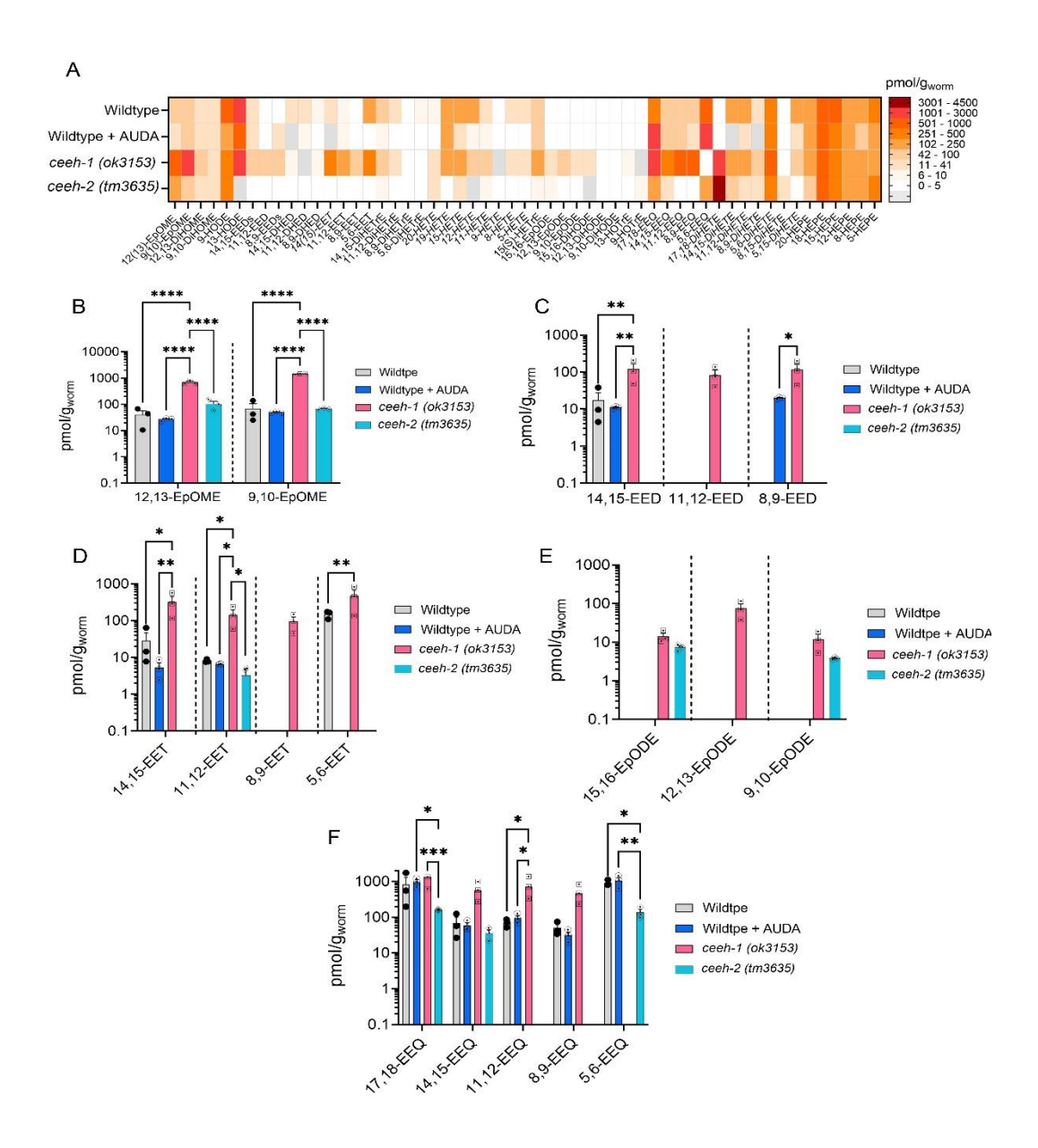


Figure 5. The oxylipin analysis and Ep-PUFA level in wildtype with and without AUDA supplementation, *ceeh-1(ok3153)*, and *ceeh-2 (tm3635)*. (A) The heatmap of overall oxylipin related to CYP-EH metabolites. (B) The level of different EpOME regioisomers (Ep-PUFA metabolites of LA). (C) The level of different EED regioisomers (Ep-PUFA metabolites of AA). (E) The level of different EpODE regioisomers (Ep-PUFA metabolites of α-LA). (F) The level of different EEQ regioisomers (Ep-PUFA metabolites of EPA). All experiments were done for three trials. All data are related to the worm at the first day adult. For AUDA treatment, 100 larvae were grown on normal plate with OP50, and at L4 storage transferred to the plates supplemented with 100 μM AUDA. Two-way analysis of variance (ANOVA), Tukey's multiple comparison test. K: \*P ≤ 0.05, \*\*P ≤ 0.01, \*\*\*P ≤ 0.001, \*\*\*\*P < 0.0001, non-significant is not shown.

enzyme could result in a complete depletion of 14,15-8,9-, and 5,6-EET, whereas no significant change was observed in 11,12-EET level when compared to vehicle (Figure 5D). Interestingly, the oxylipin profile of *ceeh-1(ok3153)* strain shows a similar trend observed for epoxy metabolites of

LA and DGLA, as all four different regioisomers of EETs were higher in *ceeh-1(ok3153)* strain compared to vehicle.

To further explore the effect of epoxide hydrolase manipulation on Ep-PUFA profiles, the epoxy metabolites of two  $\omega$ -3 PUFA, which are  $\alpha$ -LA and EPA, were studied. Interestingly, we could not detect any Ep-PUFA related to  $\alpha$ -linoleic acid in wild-type and treatment with AUDA also did not affect it (Figure 5E). However, *ceeh-1(ok3153)* could result in significant increase in all three regioisomers of EpODE compared to vehicle with the highest impact on 12,13-EpODE regioisomers. On the other hand, the CEEH-2 knock out did not affect the 12,13-EpODE regioisomers, while shows similar trend observed in ceeh-1(ok3153) for 9,10-EpODE and 15,16-EpODE (Figure 5E).

The oxylipin analysis for EPA metabolites shows a higher overall level of different Ep-PUFA of EPA (EEQs) compared to all other Ep-PUFA examined in this study (Figure 5F). This could be because of the higher level of EPA in *C. elegans* compared to other PUFAs as reported in pervious studies<sup>137</sup>. Furthermore, similar to other Ep-PUFA levels, AUDA treatment does not change the endogenous levels of EEQ regioisomers as compared to vehicle. On the other hand, CEEH-1 genetic knock out results a significant increase in 11,12-EEQ and a moderately enhancement in 8,9-EEQ, 14,15-EEQ, and 17,18-EEQ compared to vehicle. However, a complete depletion of 5,6-EEQ was observed in *ceeh-1(ok3153)* strain compared to wild-type. Intriguing, 5,6-EEQ level was significantly higher in *ceeh-2 (tm3635)* strain and a complete depletion in 11,12-EEQ and 8,9-EEQ, suggesting different substrate selectivity on CEEH-1 and CEEH-2 enzymes. No significant change was found for 14,15-EEQ and 17,18-EEQ in strain that has CEEH-2 knock out compared to wild-type (Figure 5F).

In general, our oxylipin analysis shows that (i) AUDA is not changing the individual Ep-PUFA regioisomers compared to vehicle (Figure 5). However, when considering the Ep-PUFA of each PUFA, AUDA could increase the overall level of Ep-PUFA for only EPA (Figure 6A and B). Furthermore, AUDA could cause a significant increase in overall  $\omega$ -3 Ep-PUFA level and a mild decrease in  $\omega$ -6 Ep-PUFA compared to vehicle (Figure 6C). Also, if consider the entire Ep-PUFA level of worm, no significant changed was found in AUDA treated worm with vehicle (Figure 6D). (ii) *ceeh-1* knock out causes an overall increase in regioisomers of Ep-PUFAs level when compared to the corresponding regioisomers in wild-type organisms (Figure 5). Also, genetic knock out of CEEH-1 has the most significant effect on Ep-PUFAs metabolites of EPA, LA, and AA, and less to no change observed for DGLA and  $\alpha$ -LA (Figure 6A and B). Moreover, in contrast to AUDA treatment, genetic knock out of CEEH-1 could increase the level of both  $\omega$ -6 and  $\omega$ -3

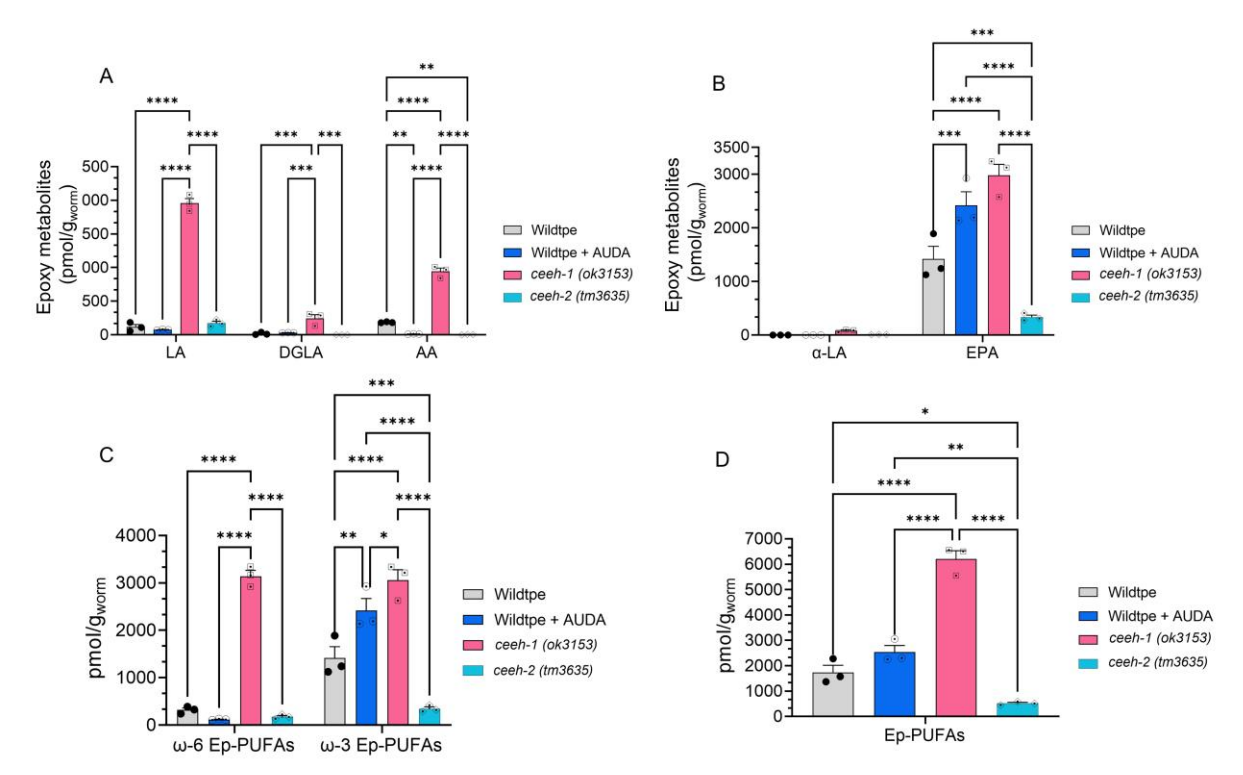


**Figure 6.** The Ep-PUFA level in wildtype with and without AUDA supplementation, *ceeh-1(ok3153)*, and *ceeh-2 (tm3635)*. (A) The overall level of Ep-PUFA related to LA, DGLA, and AA. (B) The overall level of Ep-PUFA related to α-LA, EPA. (C) The overall level of ω-3 and ω-6 Ep-PUFA (D) The overall level of Ep-PUFA in worm under different condition. All experiment were done for three trials. All data are related to the worm at the first day adult. For AUDA treatment, 100 larvae were grown on normal plate with OP50, and at L4 storage transferred to the plates supplemented with 100 μM AUDA. Two-way analysis of variance (ANOVA), Tukey's multiple comparison test. \*P  $\leq$  0.05, \*\*P  $\leq$  0.01, \*\*\*P  $\leq$  0.001, \*\*\*\*P < 0.0001, non-significant is not shown.

Ep-PUFA (Figure 6C). The *ceeh-1(ok3153)* worm also experiences an overall higher level of Ep-PUFA compared to wildtype (Figure 6D). (iii) *ceeh-2 (tm3635)* has shown moderate change compared to *ceeh-1(ok3153)*. Surprisingly, comparing each regioisomers of Ep-PUFAs in *ceeh-2 (tm3635)* and wild-type indicates an increase in none of the Ep-PUFAs level in *ceeh-2 (tm3635)* compared to the wildtype (Figure 5). Also, complete depletion in Ep-PUFAs such as EEDs, 11,12-EEQ, and 8,9-EEQ compared to wild-type was observed (Figure 5). Furthermore, by comparing the endogenous level of total Ep-PUFAs of each specific PUFA, our results show that genetic knock out of *ceeh-2* could significantly decrease the epoxy metabolites of EPA and AA (Figure 6A and B). The level of total amount of ω-3 Ep-PUFA in *ceeh-2 (tm3635)* strain was found to be

significantly lower than that of wild-type, while no significant difference was found for total amount of ω-6 Ep-PUFA level (Figure 6C). *ceeh-2 (tm3635)* strain also shows remarkable lower overall Ep-PUFA compared to wild-type (Figure 6D)

It is worth mentioning that interpreting the effect of EH inhibitor or genetic knock out of EH could not be done correctly by just tracking the Ep-PUFAs level as there is a physiological balance between different oxylipins. Thus, for instance, the inhibition of EH enzymes may cause stabilization in Ep-PUFAs while decreasing the dihydroxy-PUFA level. Therefore, to further explore the main effect of each CEEH knock out or inhibition, the dihydroxy-PUFA level was investigated as well, which is discussed in the next section.

## 2.2.2. Dihydroxy PUFA

As explained in detail in chapter 1, dihydroxy-PUFAs are the main product of EH enzymes and are more polar than their Ep-PUFA precursors, which means that they tend to reside in the extracellular fluid rather than inside cells. While it was originally thought that diols had little to no physiological activity, several studies have suggested that they may have certain functions in the body. For example, one study found that DiHOME has pro-inflammatory effects in a mouse model of asthma. Further studies suggested that diols can modulate blood vessel tone and cAMP production and may have a role in inflammation and vasodilation. Our pervious study has shown that the dihydroxy metabolites of DGLA (DHEDs) could induce neurodegeneration in dopaminergic neurons of *C. elegans* through ferroptosis mechanism. However, more research is needed to fully understand the physiological role of diols. Here we discuss the change in dihydroxy level PUFAs in *C. elegans* Wild-type and compared it with three different groups (i) AUDA supplementation, (ii) *ceeh-1(ok3153)* strain, and (iii) *ceeh-2 (tm3635)* strain. The overall oxylipin profile for all four groups is shown in Figure 5A, indicating the changes in the dihydroxy molecules

by manipulating the CEEH enzyme either pharmacologically by AUDA, or through the genetic knock out. Similar to Ep-PUFA metabolites that discussed in pervious section, the oxylipin profiles of Linoleic acid (LA), gama-dihomo Linoleic acid (DGLA), Arachidonic acid (AA),  $\alpha$ -Linoleic acid ( $\alpha$ -LA), and Eicosapentaenoic acid (EPA) will be discussed.

The oxylipin profile of LA metabolites shows an average level of each regioisomers of DiHOME around 30 pmol/gworm in wild-type strain (Figure 7A). While 9,10-DiHOME concertation does not change by AUDA supplementation or genetic knock out of CEEH-2, it does significantly increase by in *ceeh-1(ok3153)* strain (Figure 7A). The *ceeh-1(ok3153)* strain also shows a higher level of 12,13-DiHOME compared to wild-type. However, genetic knock out of CEEH-2 does not affect this regioisomer. Interestingly, AUDA treatment results in a significant decrease in 12,13-DiHOME level compared to vehicle (Figure 7A). AUDA treatment also causes a significant reduction in all regioisomers of DHEDs (Figure 7B). This was also found in the strain without CEEH-2 enzyme expression, where 14,15-DHED level was significantly reduced and 8,9-DHED and 11,12-DHED were depleted enough that was lower than the detection limit of our technique.

The *ceeh-1(ok3153)* strain shows a lower level of 11,12-DHED and 14,15-DHED compared to the wild-type, while no significant change was found for 8,9-DHED regioisomer. (Figure 7B). In case of AA-dihydroxy metabolites, worms treated with AUDA treatment have significantly lower levels of 11,12-DiHET and 14,15-DiHETs, while the 5,6-DiHET and 8,9-DiHET remain unchanged (Figure 7C). Similarly, the 8,9-DiHET regioisomer did not change in the *ceeh-2* (*tm3635*) strain, whereas all other three DiHETs regioisomers were decreased by genetic knock out of CEEH-2 enzyme. On the other hand, in *ceeh-1(ok3153)* strains the 11,12-DiHET

regioisomer level was significantly increased, while the other regioisomers did not considerably change (Figure 7C).

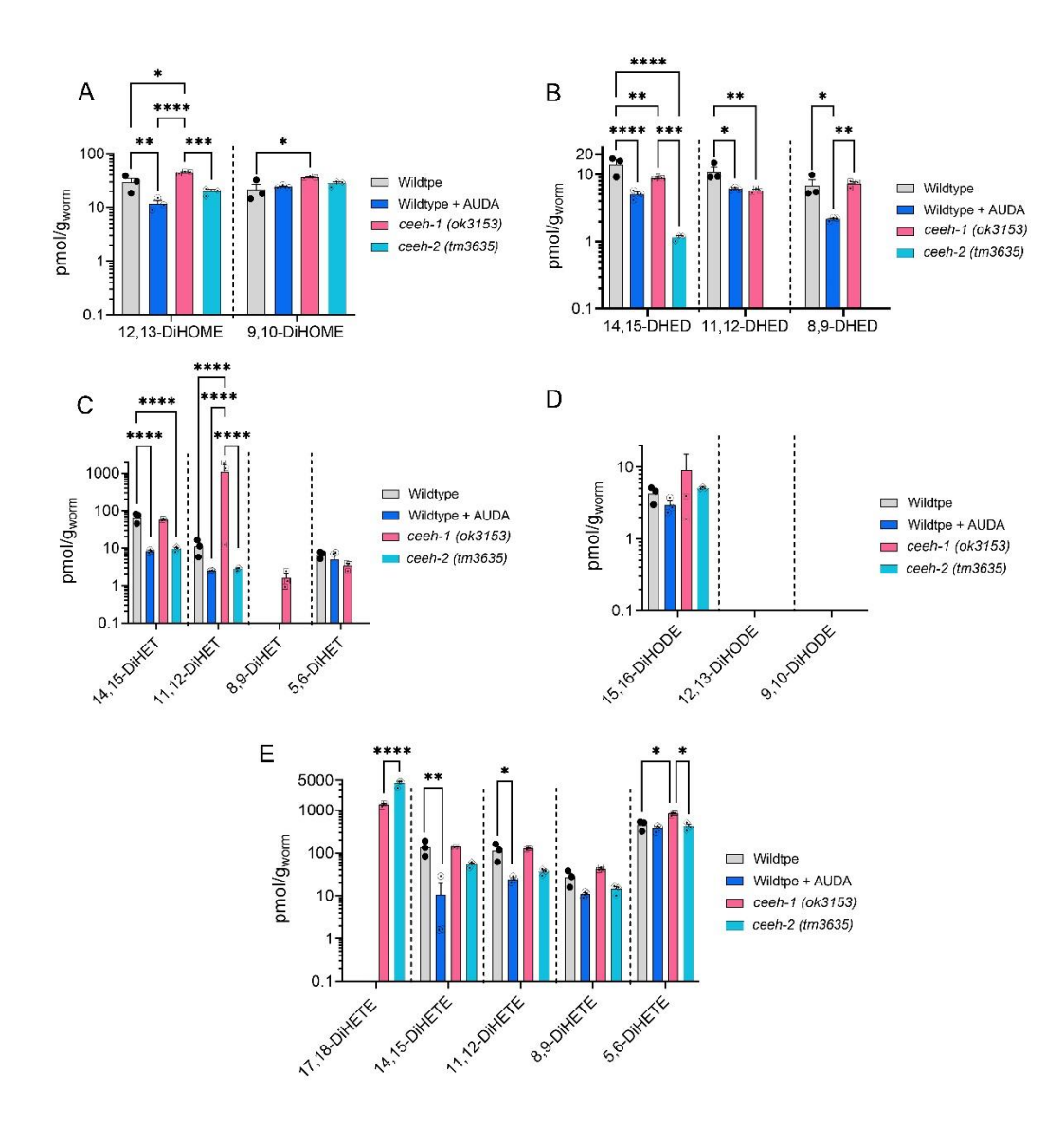


Figure 7. The Dihydroxy-PUFA level in wildtype with and without AUDA supplementation, *ceeh-l(ok3153)*, and *ceeh-2 (tm3635)*. (B) The level of different DiHOME regioisomers (Dihydroxy-PUFA metabolites of LA). (C) The level of different DiHED regioisomers (Dihydroxy-PUFA metabolites of DGLA). (D) The level of different DiHET regioisomers (Dihydroxy-PUFA metabolites of AA). (E) The level of different DiHODE regioisomers (Dihydroxy-PUFA metabolites of α-LA). (F) The level of different DiHETE regioisomers (Dihydroxy-PUFA metabolites of EPA). All experiments were done for three trials. All data are related to the worm at the first day adult. For AUDA treatment, 100 larvae were grown on normal plate with OP50, and at L4 storage transferred to the plates supplemented with 100 μM AUDA. Two-way analysis of variance (ANOVA), Tukey's multiple comparison test. \*P  $\leq$  0.05, \*\*P  $\leq$  0.01, \*\*\*P  $\leq$  0.001, \*\*\*\*P < 0.0001, non-significant is not shown.

To further explore the effect of epoxide hydrolase manipulation on Dihydroxy-PUFA, the epoxide metabolites of two  $\omega$ -3 PUFA, which are  $\alpha$ -LA and EPA, were studied. Interestingly, we could detect only one regioisomers of dihydroxy metabolites of α-LA, 15,16-DiHODE in all group tested in this study, and neither AUDA treatment nor genetic knock out of CEEH-1 or CEEH-2 causes change in its level (Figure 7D). Finally, we analyzed the dihydroxy metabolites of EPA, and found four of five DiHETE regioisomers, 5,6-DiHETE, 8,9- DiHETE, 11,12- DiHETE, and 14,15- DiHETE (Figure 7E). While AUDA treatment could decrease the level of all these four regioisomers, only the changes for 8,9- DiHETE, 11,12- DiHETE were significant. Furthermore, ceeh-2 (tm3635) strain shows a mild, yet insignificant decrease in the level of all these four regioisomers when compared to wild-type. Genetic knock out of CEEH-2 have similar level of 8,9- DiHETE, 11,12- DiHETE, and 14,15- DiHETE compared to wild-type, but 5,6-DiHETE increased level was observed in this strain (Figure 7E). Interestingly, while we could not detect any 17,18-DiHETE in Wilde-type strain with and without AUDA treatment, both *ceeh-1(ok3153)* and ceeh-2 (tm3635) showed a high level of this hydroxy metabolites of EPA with an average level of 1400 and 4200 pmol/gworm, respectively (Figure 7E).

In general, our oxylipin analysis of dihydroxy-PUFAs shows that (i) AUDA causes a decrease in most of dihydroxy-PUFA metabolites with the most significant effect observed in LA, AA, and EPA dihydroxy metabolites (Figure 7, 8A, and 8B). Furthermore, AUDA could cause a significant decrease in overall ω-6 Dihydroxy-PUFA level and a mild decrease in ω-3 Dihydroxy-PUFA compared to vehicle (Figure 8C and D). A mild, yet insignificant decrease in overalldihydroxy-PUFA was observed in worms treated with AUDA compared to vehicles (Figure 8E).

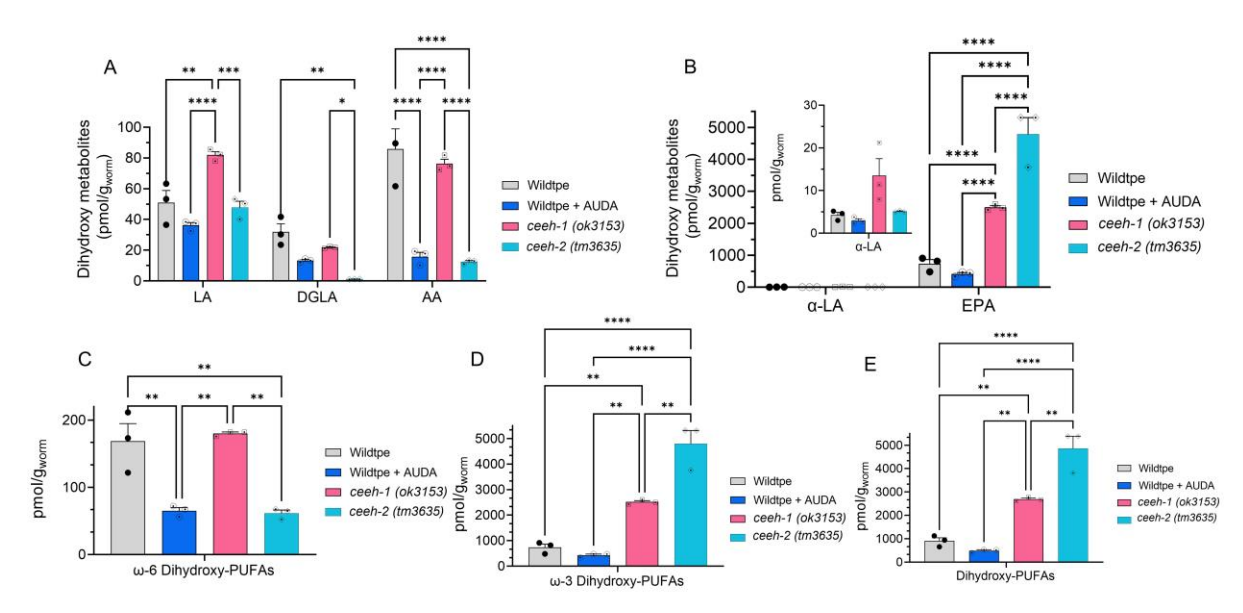


Figure 8. The Dihydroxy-PUFA level in wildtype with and without AUDA supplementation *ceeh-l(ok3153)*, and *ceeh-2 (tm3635)*. (A) The overall level of Dihydroxy-PUFA related to LA, DGLA, and AA. (B) The overall level of Dihydroxy-PUFA related to α-LA, EPA. (C) The overall level of ω-6 Dihydroxy-PUFA, (D) The overall level of ω-3 Dihydroxy-PUFA (E) The overall level of Dihydroxy-PUFA in worm under different condition. All experiment were done for three trials. All data are related to the worm at the first day adult. For AUDA treatment, 100 larvae were grown on normal plate with OP50, and at L4 storage transferred to the plates supplemented with 100 μM AUDA. Two-way analysis of variance (ANOVA), Tukey's multiple comparison test for (B) and (D); and t test for K: \*P ≤ 0.05, \*\*P ≤ 0.01, \*\*\*P ≤ 0.001, \*\*\*\*P < 0.0001, non-significant is not shown.

(ii) A mixed trend was observed in strain with genetic knock out of CEEH-1 enzyme when comparing each individual dihydroxy-PUFAs, as LA dihydroxy metabolites level are enhanced, DGLA dihydroxy metabolites level decreased, and most of dihydroxy-PUFA of AA (except 11,12 DiHET), α-LA, and EPA (except 5,6-DiHETE and 17,18-DiHETE) remains unchanged compared to wild-type (Figure 8A and B). Moreover, the general dihydroxy analysis shows that while overall ω-6 Dihydroxy-PUFA remained unchanged, the ω-3 Dihydroxy-PUFA level increased in *ceeh-1(ok3153)* strain compared to vehicle (Figure 8C and D). Furthermore, *ceeh-1(ok3153)* worms experience a significant higher level of Dihydroxy-PUFA compared to the wildtype (Figure 8E). (iii) Genetic knock out of CEEH-2 enzyme causes the DGLA and LA level significantly reduced, while EPA is level significantly increased. (Figure 8A and B). Likewise, while the total ω-6 Dihydroxy-PUFAs is decreased in *ceeh-2* (*tm3635*) strain, an increase in ω-3 Dihydroxy-PUFAs

was observed (Figure 8C and D). Finally, *ceeh-2* (*tm3635*) strain shows an overall increase of Dihydroxy-PUFAs compared to the wild-type (Figure 8E).

It is worth mentioning that interpreting the effect of EH inhibitor or genetic knock out of EH could not be done accurately by just tracking the Ep-PUFAs or Dihydroxy-PUFA level alone, as there is a physiological balance between different these two groups of compounds. Thus, for instance, the inhibition of EH enzymes may cause stabilization in Ep-PUFAs while decreasing the dihydroxy-PUFA level or may cause to increase of both for a specific strain or treatment. Therefore, to further explore the main effect of each CEEH knock out or inhibition, the epoxy to dihydroxy ratio of different PUFAs oxylipins metabolites should be considered as well, which is discussed in the next section.

## 2.2.4. Ep-PUFA to Dihydroxy-PUFA ratio as in indication of EH deficiency

To further explore the effect of CEEH inhibition/knock out on oxylipin profile of worms, the epoxy to dihydroxy PUFA ratio will be discussed as the indication of CEEH inhibition. In the previous section we found that the CEEH inhibition or knock out may not always result in an increase in Ep-PUFA and a decrease in dihydroxy-PUFA. For instance, our study shows that both EpOME regioisomers, and their relative dihydroxy (DiHOME) have higher levels in *ceeh-1(ok3153)* strain compared to wild-type. Similarly, Harris et al. also found that CEEH-1 inhibition using bacterially mediated RNAi can causes an increase in both 12,13-EpOME, 12,13-DiHOMEE <sup>34</sup>. We also found that CEEH inhibition using AUDA, does not change the level of different EED regioisomers compared to vehicle, but its effect could be seen by decreasing the level of related dihydroxy metabolites (DHEDs). Considering this, different studies have suggested an alternative comparison, which is epoxy/dihydroxy ratio to further validate the inhibition or knock out of epoxide hydrolase enzyme<sup>140,141</sup>. Therefore, we analyzed the epoxy to dihydroxy ratio of each

individual regioisomers, and then tracked the overall change of epoxy/dihydroxy ratio in each PUFA, and finally in each group of worms.

Worms treated with AUDA exhibit an overall increase in the epoxy/dihydroxy ratio compared to the vehicle control. Moreover, among various PUFAs, the metabolites of DGLA and EPA demonstrate a significant increase in this ratio. A detailed analysis of individual Ep-PUFA regioisomers reveals that inhibiting the CEEH enzyme with AUDA leads to a notable increase in the ratio of 8,9-EEDs, 11,12-EEQ, 15,16-EEQ, and 17,18-EEQ to their respective dihydroxy counterparts. This observation highlights the specific impact of AUDA on the metabolism of these Ep-PUFA regioisomers (Figure 9A-E). In addition, while *in vivo* study showed the increase in EpOME/DiHOME ratio by inhibiting CEEH-1 enzyme using AUDA<sup>34</sup>, we did not observe similar trend in our worm (Figure 9A). This could simply be because of the difference in physiological-condition and more complex behavior of enzyme *in vivo* is expected compared to extracted enzyme.

We also analyzed the epoxy to dihydroxy ratio of metabolites related to each group of PUFAs. For instance, we calculated the total ratio by taking all the epoxides associated with arachidonic acid and dividing it by all the dihydroxy PUFAs related to arachidonic acid. Our analysis showed an increased epoxy to dihydroxy ratio for EPA metabolites and a decreased ratio for AA metabolites, while the ratios for the remaining PUFA groups remained unchanged (Figure 9F). Intriguingly, AUDA treatment led to an overall increase in the epoxy to dihydroxy ratio in *C. elegans* (Figure 9G), calculated as the total epoxy content in the worm divided by the total dihydroxy content in the worm. Interestingly, AUDA treatment could increase the overall epoxy to dihydroxy ratio in *C. elegans* (Figure 9G).

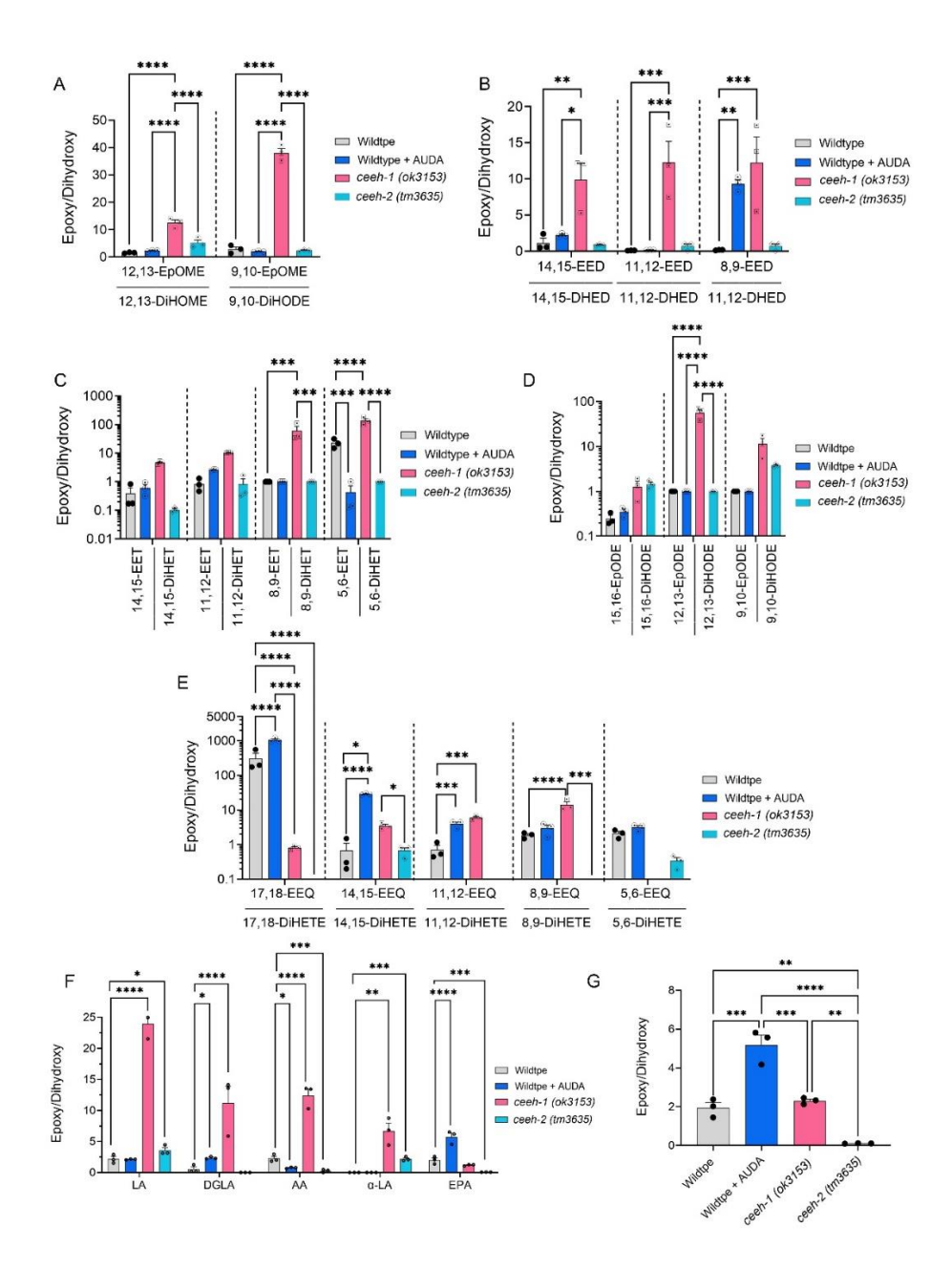


**Figure 9.** The Ep-PUFA to Dihydroxy-PUFA ratio in wildtype with and without AUDA supplementation, *ceeh-1(ok3153)*, and *ceeh-2 (tm3635)*. (A) The ratio of EpOME/DiHOME regioisomers (metabolites of LA). (B) The ratio of EED/DiHED regioisomers (metabolites of DGLA). (C) The ratio of EET/DiHET regioisomers (metabolites of AA). (D) The ratio of EpODE/DiHODE regioisomers (metabolites of α-LA). (E) The ratio of EEQ/DiHETE regioisomers (metabolites of EPA). All data are related to the worm at the first day adult. For AUDA treatment, 100 larvae were grown on normal plate with OP50, and at L4 storage transferred to the plates supplemented with 100 μM AUDA. Two-way analysis of variance (ANOVA), Tukey's multiple comparison test. K: \*P  $\leq$  0.05, \*\*P  $\leq$  0.01, \*\*\*P  $\leq$  0.001, \*\*\*\*P  $\leq$  0.001, non-significant is not shown.

While we did not observe an overall change in the ratio of ep-PUFA to dihydroxy-PUFA in the *ceeh-1(ok3153)* strain compared to wild-type (Figure 9G), the metabolites related to each group of PUFA, except EPA, exhibited a significant increase in the epoxy to dihydroxy ratio (Figure 9F). This trend was also observed in the epoxy to dihydroxy ratio for all regioisomers of EpOME, EEDs, EETs, EpODE, and their corresponding diols (Figure 9A-E). For EPA metabolites, the ratio of 5,6-EEQ and 17,18-EEQ to their corresponding diol decreased, whereas an increase was observed in three other regioisomer groups in the *ceeh-1(ok3153) strain* (Figure 7E).

In *ceeh-2* (*tm3635*) strain, tracking the individual regioisomers reveals a mild, yet insignificant increase in epoxy to dihydroxy ratio for 12,13-EpOME, 8,9-EEDs, 11,12-EEDs, and 9,10-DiHODE (Figure 9A, B, and D). On the other hand, we observed a significant decrease in the epoxy to dihydroxy ratio for 8,9-EEQ, 11,12-EEQ, and 17,18-EEQ (Figure 7E). Analyzing metabolites based on their parent PUFA, the epoxy to dihydroxy ratio increased for LA and α-LA metabolites, decreased for EPA and AA metabolites, and remained unchanged for DGLA metabolites (Figure 9F). Surprisingly, the genetic knockout of the CEEH-2 enzyme resulted in a significant decrease in the overall epoxy to dihydroxy ratio in the *ceeh-2* (*tm3635*) worm compared to wild-type (Figure 9G).

Comparing the epoxy to dihydroxy ratio of the ceeh-1(ok3153) and ceeh-2 (tm3635) strains suggests that CEEH-1 contributes more significantly to the CYP-EH metabolic pathway in *C. elegans*, which is consistent with previous reports<sup>34</sup>. Our results also indicate that an increase in Ep-PUFA levels and a decrease in Dihydroxy-PUFA levels upon inhibition or knockout of the CEEH enzyme may not always occur. This could be due to the existence of alternative pathways for diol production, and potential feedback regulation of enzymes involved in the formation or

elimination of epoxides and diols. For instance, a decrease in epoxide hydrolase activity might trigger the upregulation of other epoxide hydrolase, an increase in enzymes involved in epoxide production, the release of epoxides from lipid stores, upstream PUFA biosynthesis, or complementary metabolism of Ep-PUFA and dihydroxy-PUFA. Additionally, Ep-PUFAs are relatively lipophilic and tend to accumulate in tissues, while Dihydroxy-PUFAs are more polar and are rapidly eliminated from the body via the media or through conjugation. These factors, combined with compensatory mechanisms that may activate in response to a decrease in epoxide hydrolase activity, could result in relatively unchanged diol levels despite changes in epoxide levels. Thus, the impact of a decrease in epoxide hydrolase activity on epoxides and diols may depend on the specific pathways and regulatory mechanisms involved in their metabolism.

In summary, the significant increase in the epoxy to dihydroxy ratio observed for most individual PUFA metabolites in *ceeh-1(ok3153)* strains might contribute to the shortened lifespan of this strain. Conversely, a substantial decrease in the overall epoxy to hydroxy ratio in the ceeh-2 strain could also result in a shorter lifespan compared to wild-type. Additionally, AUDA-treated strains exhibited an overall increase in the epoxy to hydroxy ratio, particularly for EPA metabolites, which may enhance survival chances considering the beneficial effects of Ep-PUFAs (see Chapter 1). However, drawing more accurate conclusions requires further study. For example, examining the *ceeh-1/ceeh-2* double knockout strain for both lifespan and oxylipin analysis could help solve this puzzle and might lead to the discovery of another epoxide hydrolase in *C. elegans* or the identification of one or more specific epoxy or dihydroxy PUFAs responsible for the observed shortened lifespan.

## 2.3. FUDR effect in lifespan of strain with deficient epoxide hydrolase

In previous sections, we discovered that the inhibition or genetic knockout of epoxide hydrolase can lead to complex alterations in various epoxy- and dihydroxy-PUFAs. Each of these PUFA metabolites may have distinct signaling pathways, further complicating our understanding of the biological effects of each metabolite. For example, we observed that genetic knockout of either CEEH-1 or CEEH-2 enzyme results in a significantly shorter lifespan and reduced progeny production capacity compared to wild-type worms. However, we have not been able to identify which specific CYP-EH metabolites, or a combination of them, play a major role in the observed aging phenomena. One of the main experimental challenges in this regard is that the manual phenotypic and lifespan analysis in labor-intensive and required transferring the entire population every other day to avoid progeny contamination and to provide fresh food or supplementation for worms. Besides, this could result in mechanical damage during manual podding which interfere with final output <sup>142,143</sup>. To address these challenges, the scientific community are implementing at least two different approaches (i) reducing the progeny contamination by using chemical reproduction inhibitors, such 5-fluoro-2-deoxyuridine (FUDR) 144-146; and (ii) designing microfluidic device to automatically eliminate the produced progeny form the media<sup>147</sup>. In this section, we discuss both of these approaches and explore the potential of employing them to study CYP-EH metabolites in aging research using the *C. elegans* animal model.

#### 2.3.1. Using chemical reproduction inhibitor, 5-fluoro-2-deoxyuridine (FUDR)

In order to prevent overgrowth of progeny during *C. elegans* lifespan and aging, scientists often use 5-fluoro-2'-deoxyuridine (FUDR) for sterilization to eliminate progeny contamination<sup>146,148</sup>. FUDR is a chemical that is able to inhibit DNA and RNA synthesis, which leads to the death of mitotic cells and prevents progeny development in nematodes<sup>145,146</sup>. Adult

nematode cells are mostly post-mitotic; therefore, it is assumed that the effects of FUDR treatment on adult development are minimal. This in fact makes FUDR sterilization a popular technique for lifespan experiments with nematodes such as C. elegans 145,149,150. However, there are some important aspects that should be considered when using FUDR. One is that the effects of FUDR have mainly been studied in wild-type (N2) worms, and there are few studies that have confirmed that FUDR is not interfering with experimental conditions or specific mutant strains 145,149-151. However, some studies have found that FUDR could affect the aging process in mutants. For instance, Aitalhaj et al found that supplementing genetic knock out of tub-1, a homolog of the mammalian tubby family which involved with the modulation of fat storage, with FUDR could increase the lifespan of this strain<sup>152</sup>. A similar trend was found gas-1 strain, which is deficient in mitochondria complex I of the respiratory chain, where twofold increase in the lifespan was found with FUDR supplementation<sup>153</sup>. Another concern is that, while it is often assumed that the inhibition of DNA synthesis via FUDR is one-dimensional, and downstream effects are considered to be negligible, this may not be the case. Signals from the reproductive system can alter the lifespan of nematodes<sup>124</sup>, which means that there may be other effects of FUDR sterilization that have not yet been fully understood. These downstream effects may depend on different genetic backgrounds, or the specific behavior or physiology being studied. This means that researchers should be careful when using FUDR sterilization and make sure to control for any potential effects it may have on their experiment.

Considering these, we examined the effect of FUDR on C. elegans strain with pharmacological inhibition or genetic knock out of CEEH enzymes. In order to supplement worms with FUDR, we added FUDR to the agar solution to a final concentration of 50  $\mu$ M, and then make plate was made using the supplemented agar. Plates were subsequently seeded with a similar

quantity of bacteria as used for the standard plates. Worms were transferred to the supplemented plates at the L4 stage to prevent any potential interference from the supplementation during the developmental stage. The number of live and dead worms was recorded every other day. As the worms aged and their movement slowed, a gentle tap on the nose of the worm was used to verify their living status. Worms that were lost, burrowed into the medium, climbed the plate walls and dried up, or were injured during transfer were treated as censored. The worms were also moved to new plates to ensure fresh supplementation. Ultimately, survival data were plotted on a Kaplan-Meier curve using GraphPad Prism 9.5.

As shown in Figure 10A, FUDR supplementation does not affect the lifespan of wild-type animals, which corroborate with previous studies 145,149,150. However, supplementing *ceeh-1(ok3153)* worm with FUDR significantly increase the lifespan (Figure 10B). The *ceeh-1(vv228)* strain also shows similar trend in presence of FUDR (Figure 10C). Interestingly, similar extending lifespan was found for strains with genetic knock out of CEEH-2 enzyme supplemented with FUDR (Figure 10D and E). To further explore the effect of FUDR, the *ceeh-1/ceeh-2 (vv231)* lifespan was tested in presence of FUDR strain. However, supplementation of FUDR does not affect the life span of *ceeh-1/ceeh-2 (vv231)* strain (Figure 10F). These data suggest the possible intervention of FUDR with CYP-EH metabolic pathways. Pervious study also shows that the lifespan of strain with genetic knock out in *tub-1*, which exhibit fat accumulation,

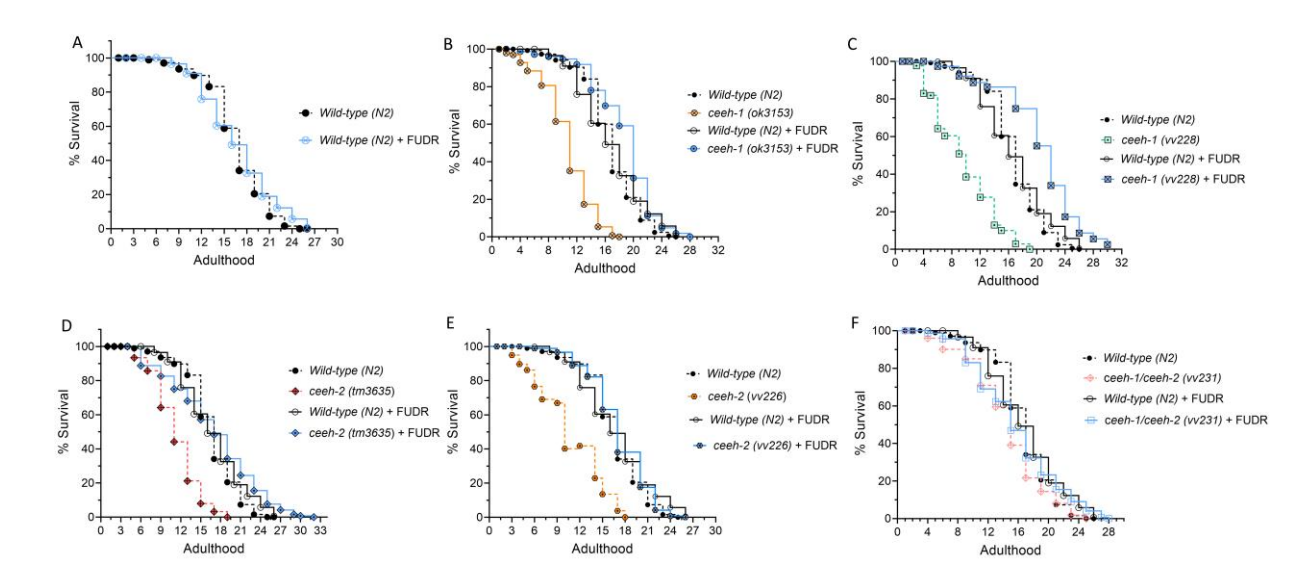


**Figure 10.** Lifespan analysis. (A) Lifespan of wildtype worm with and without supplementation with 50 μM FUDR. (B) Lifespan of *ceeh-1* (*ok3153*) with and without supplementation with 50 μM FUDR. (C) Lifespan of *ceeh-1* (*vv228*) with and without supplementation with 50 μM FUDR. (D) Lifespan of *ceeh-2* (*tm3635*) with and without supplementation with 50 μM FUDR. (E) Lifespan of *ceeh-2* (*vv228*) with and without supplementation with 50 μM FUDR. (F) Lifespan of *ceeh-1/ceeh-2 hybrid* (*vv231*) with and without supplementation with 50 μM FUDR. Three replicates for each experiment have been done, and each trial started with 100 worms at L4 stage. For FUDR treatment, 100 larvae were grown on normal plate with OP50, and at L4 storage transferred to the plates supplemented with 50 μM FUDR.

could be affected with FUDR supplementation. Furthermore, considering the decline of egg laying capacity in *ceeh-1* and *ceeh-2*, it could be suggested inhibition of reproduction by FUDR in these strains may increase some forms of stress resistance and synergize with genetic alterations to extend lifespan <sup>124,125,154</sup>. However, how FUDR is affecting the lifespan of some mutants with deficient fat metabolism, and how it is related to the reproductive system needs further investigation. On way to further explore the effect of FUDR in lipid metabolism and its possible mechanism that involved in the lifespan, is to use oxylipin analysis of mutant with and without supplementation with FUDR and track the change in different CYP-EH metabolites, which is an ongoing project of Dr. Lee and Dr. Alan's group in collaboration with Dr. Petrascheck.

Finally, one important consideration here is that the *C. elegans* scientific community studying lipid metabolism or oxylipin signaling molecule should consider the conferring effect of

FUDR and avoid using it. Even though this could result in higher accuracy, increased workload would be expected, in particular for studying the effect of lipid downstream metabolites on aging. One solution for this is to design a microfluidic device that can eliminate the progeny contamination and increase the number of tests or replicate that could be done in a short amount of time. In this regards, next section will summarize the efforts that have been done in Drs. Lee, Alan, and Johnson's group in designing a microfluidic system that could be used for aging study, in particular when the effect of lipid metabolites or hydrophobic compound is interested.

# 2.3. Microfluidic device, a possible solution for high-throughput analysis of lipid mediator effects on aging

In this section we discuss one possible solution in order to better understand the effect of fatty acids and their downstream metabolites in aging and age-related disease.

## 2.3.1. Challenge in studying the effect of oxylipins in aging study using C. elegans.

The studies provided in this dissertation clearly show that oxylipins metabolites, in particular CYP-EH metabolites, are involved in healthspan and lifespan. In chapter 2, we demonstrated that the Dihydroxy metabolites of DGLA could induce neurodegeneration. Also, in chapter 3, we suggested the potential rescuing effect of epoxide hydrolase inhibitors in strains expressing  $A\beta$  and tau, However, we could not identify a specific epoxy or dihydroxy-PUFA as major mediators, since there was alternation in many of these metabolite's levels in strains expressing either  $A\beta$  or tau. Furthermore, we found that deficiency in CEEH-1, CEEH-2, or both could result in different lifespan phenotype, and the oxylipin profiles are different between these different strains.

Further investigation on deciphering the effect of each epoxy or dihydroxy-PUFA metabolites could be done by supplementing ag-synchronized worm with specific epoxy or dihydroxy regioisomer, or a combination of them, and then examining their phenotypic and

lifespan. However, conducting manual screening in *C. elegans* is a repetitive and labor-intensive process, in which food and oxylipin compound must be added daily and extra care is required to prevent bacterial or fungal contamination<sup>142,155</sup>. In addition, manual screening requires larger quantities of molecular components that may not be available <sup>143</sup>. Progeny contamination is another challenge in the study of *C. elegans* and required moving animals on daily basis, which is time-consuming and limited the number of tests, and could result in mechanical damage during manual podding <sup>142,143</sup>. In this chapter, we showed that treatment of FUDR as the alternative way to reduce progeny contamination can interfere with CYP-EH metabolite study, those related to aging. Therefore, because of the above-mentioned limitation regarding the phenotypic screening assays, we designed a microfluidic device for high-throughput screening tools in C. elegans in collaboration with Dr. Johnson at Michigan State University.

The initial device design is inspired by published and commercially available microfluidic devices, such as WormFarm and NemaLife, which use size exclusion to separate progeny to produce a pool of age-synchronized worms <sup>156,157</sup>. Even though these commercial microfluidic worm chips are promising for life-span tracking of *C. elegans* and screening of some hydrophilic drugs, they have limited application for lipophilic molecules including PUFAs and their metabolites. All of these commercial microfluidic worm chips are made of polydimethylsiloxane (PDMS), which sequesters lipophilic molecules resulting a lower to no exposure of tested lipids to the worm and leads to the undesirable transfer of lipophilic molecules between adjacent microfluidic lines <sup>158</sup>. Thus, lipophilic lipid metabolites such as epoxy and dihydroxy-PUFAs cannot be accurately screened by these existing devices. Another major limitation of commercially available microfluidic worm chips is that they require specialized equipment and expertise that is not available to most *C. elegans* laboratories <sup>156,157</sup>. To address these drawbacks, we are designing

a plasma-treated polystyrene-based microfluidic device that can be used for all groups of hydrophilic and lipophilic drug/cellular metabolites. This automated phenotype screening assay offers several distinct benefits over both manual assays and commercial microfluidic assays, such as a broader range of the metabolites that can be tested, simplicity of technical analysis, and affordability.

2.3.2. WormPlate, an alternative solution for studying the oxylipins effect on aging using C. elegans.

In this part of the project, we will design the microfluidic device and show its ability for age-synchronizing of *C. elegans* and lipophilic compounds testing. The initial device design is inspired by published and commercially available PDMS microfluidic devices that use size exclusion to separate the *C. elegans* progeny<sup>156,157</sup>. These devices are not suitable for our studies and many other studies because they are fabricated using PDMS, which sequesters lipophilic molecules, and our preliminary data confirms this statement (Figure 9)<sup>159</sup>.

A novel micro-milling approach is used to create appropriate devices <sup>160</sup>. To ensure that the manufactured device is compatible across the variety of automated laboratory instruments used in high-throughput screening applications, we used a standard 48-well plate format approved by the Society for Laboratory Automation and Screening (SLAS) as well as the American National Standards Institute (ANSI)<sup>161</sup>. The devices are engineered and cut into 48-well (16 devices/plate) using computer-animated design (Solidworks, Dessault Systems, France). A computer numerical control (CNC) mill with appropriate endmills is used to mill the device directly into the bottom of a 48 well SLAS/ANSI compatible microplate and a 180 μm polystyrene sheet is secured via solvent bonding using acetonitrile. Figure 11A-C demonstrates the schematic and real image of

the designed device. The WormPlate devices are then treated with UV for 15 minutes to sterilize and be ready to use.

The design milling parameter and size of each chamber and arena were optimized to hold about 50 worms. We also found that the optimized size for the sieves to get the highest performance for excluding the progeny is a dimension of 35-40  $\mu$ m for sieves depth (Figure 11D). Our results demonstrated that the device could maintain  $79 \pm 7\%$  of adults after washing without retaining larvae or eggs, yet it could get better with further improvement. The food uptake (which is *E. coli*, OP50) is also optimized in order to have the minimum food aggregation in the device and to ensure that at no point in time during the lifespan assay food concentrations become too low and induce a dietary restriction effect. Thus, the optimized bacteria concentration was 6-10 mg/ml of OP50.

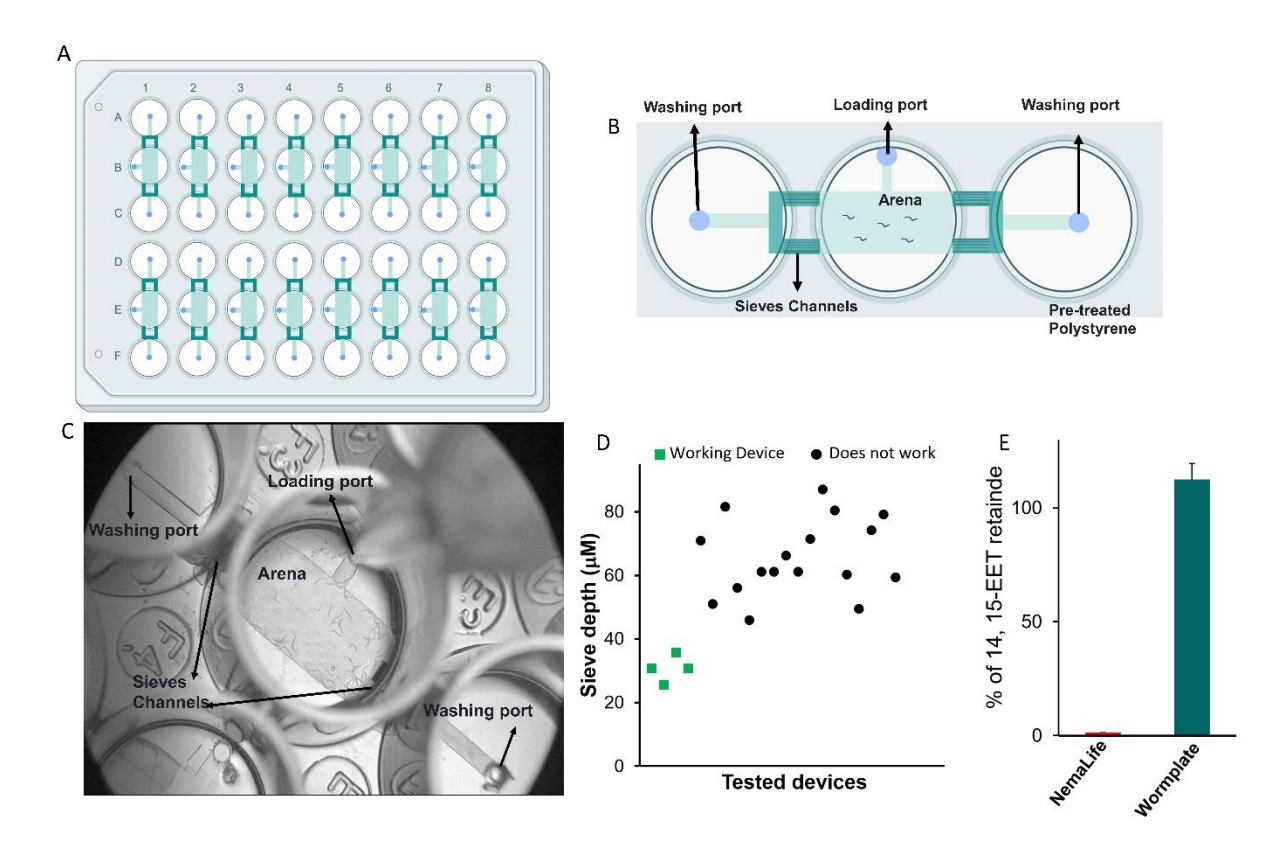


**Figure 11.** WormPlate microfluidic device. (A) a schematic representation of a WormPlate with 16 microfluidic chambers. (B) schematic representation of a single chamber, and (C) the manufactured device. (D) The egg and larva filtration by WormPlates with different Sieve depth. (E) Comparison of our WormPlate to NemaLife for retention of 14,15-epoxy-EET.

In order to evaluate the ability of the device to test lipophilic compound/drug, 14,15-epoxyeicosatrienoic acid (14,15-EET), which is an epoxide metabolite of arachidonic acid, was tested. In this regard, a solution of 100 µM of EET was incubated in both our designed (WormPlate) and the PDMS device manufactured by Nemalife company. The assessment of incubated solution by LC-MS/MS showed that lipophilic EET was completely absorbed by NemaLife device, while is largely intact in WormPlate; These data confirm the ability of our system to screen the lipophilic CYP-EH metabolites. (Figure 11E).

Besides these approaches, some other improvement is required to achieve the final design that could be used for high screen throughout of oxylipin metabolites. One main challenge that remained unsolved is leaking of solution from device from the bottom of polystyrene sheet. This sheet is secured via solvent bonding using acetonitrile to the bottom of WormPlate. This could be solved by using different bonding materials or increasing the bonding surface which is under investigation.

## 3. Conclusion:

In this chapter, we have thoroughly investigated the impact of epoxide hydrolase (EH) inhibition on the lifespan, healthspan, and reproductive capabilities of C. elegans. Our findings demonstrate that EH inhibition or genetic knockout leads to complex changes in the oxylipin profiles and the balance of Ep-PUFAs and dihydroxy-PUFAs. While the lifespan and reproduction remained unchanged in wild-type worms treated with the epoxide hydrolase inhibitor, AUDA, the genetic knockout of either *ceeh-1* or *ceeh-2* significantly shortened the lifespan and decreased egg production capacity. Interestingly, worms with double knockouts in both *ceeh-1* and *ceeh-2* displayed a similar lifespan as those treated with AUDA. Moreover, although we observed

significant alterations in CYP-EH metabolites in the experimental groups, the specific CYP-EH metabolites responsible for these effects remain elusive. One of the main reasons we could not test each individual metabolite is the high number of compounds (more than 50) and the possibility of synergistic effects among them, which necessitates testing different combinations during aging. This is almost impossible using conventional techniques (such as agar plates) due to challenges in manual phenotypic and lifespan analyses.

To overcome these challenges, we discussed the potential implementation of high-throughput assays to identify the specific CYP-EH metabolites involved in lifespan and aging of worms. We identified age-synchronization and progeny contamination as the main challenges in studying the effect of a large number of compounds, particularly CYP-EH metabolites, in aging. We also confirmed that the current approach techniques, which include (i) using FUDR and (ii) PDMS based microfluidic systems, are unsuitable for this type of study. For instance, while the administration of FUDR could solve the progeny contamination issue during aging studies, it may affect CYP-EH metabolites. When ceeh-1 knockout worms, which have a shorter lifespan compared to wild-type worms, were treated with FUDR, they displayed a similar lifespan as wildtype worms. This suggests that FUDR potentially rescues the shorter lifespan phenotype by altering CYP-EH metabolites. Furthermore, while the PDMS-based microfluidic system could resolve progeny contamination without needing FUDR and facilitate worm handling during aging, its material disadvantages make it unsuitable for studying CYP-EH metabolites (i.e., the hydrophobicity of CYP-EH metabolites causes them to be absorbed by PDMS, rendering the compound inaccessible to worms during aging studies). Thus, we designed a new microfluidic device made of styrene-based materials that could overcome these challenges, although the device still requires further improvement for high-throughput screening.

As we move forward, it will be crucial to identify the specific CYP-EH metabolites and their corresponding signaling pathways that play a major role in the observed aging phenomena. Unraveling these molecular mechanisms will enhance our understanding of the complex relationship between dietary PUFAs, their metabolites, and the aging process. Ultimately, this knowledge may pave the way for the development of novel therapeutic strategies to mitigate agerelated disorders and improve overall healthspan in humans.

#### **BIBLIOGRAPHY**

- (1) Sarparast, M.; Dattmore, D.; Alan, J.; Lee, K. S. S. Cytochrome P450 Metabolism of Polyunsaturated Fatty Acids and Neurodegeneration. *Nutrients* **2020**, *12* (11), 3523. https://doi.org/10.3390/nu12113523.
- (2) Morisseau, C.; Hammock, B. D. Epoxide Hydrolases: Mechanisms, Inhibitor Designs, and Biological Roles. *Annu. Rev. Pharmacol. Toxicol.* **2005**, *45*, 311–333. https://doi.org/10.1146/annurev.pharmtox.45.120403.095920.
- (3) Morisseau, C.; Hammock, B. D. Impact of Soluble Epoxide Hydrolase and Epoxyeicosanoids on Human Health. *Annu. Rev. Pharmacol. Toxicol.* **2013**, *53* (1), 37–58. https://doi.org/10.1146/annurev-pharmtox-011112-140244.
- (4) Schmelzer, K. R.; Kubala, L.; Newman, J. W.; Kim, I.-H.; Eiserich, J. P.; Hammock, B. D. Soluble Epoxide Hydrolase Is a Therapeutic Target for Acute Inflammation. *Proc. Natl. Acad. Sci. U. S. A.* **2005**, *102* (28), 9772–9777. https://doi.org/10.1073/pnas.0503279102.
- (5) Iyer, M. R.; Kundu, B.; Wood, C. M. Soluble Epoxide Hydrolase Inhibitors: An Overview and Patent Review from the Last Decade. *Expert Opin. Ther. Pat.* **2022**, *32* (6), 629–647. https://doi.org/10.1080/13543776.2022.2054329.
- (6) Gautheron, J.; Jéru, I. The Multifaceted Role of Epoxide Hydrolases in Human Health and Disease. *Int. J. Mol. Sci.* **2020**, 22 (1), 13. https://doi.org/10.3390/ijms22010013.
- (7) Arand, M.; Cronin, A.; Adamska, M.; Oesch, F. Epoxide Hydrolases: Structure, Function, Mechanism, and Assay. *Methods Enzymol.* **2005**, 400, 569–588. https://doi.org/10.1016/S0076-6879(05)00032-7.
- (8) Harris, T. R.; Hammock, B. D. Soluble Epoxide Hydrolase: Gene Structure, Expression and Deletion. *Gene* **2013**, *526* (2), 61–74. https://doi.org/10.1016/j.gene.2013.05.008.
- (9) Decker, M.; Arand, M.; Cronin, A. Mammalian Epoxide Hydrolases in Xenobiotic Metabolism and Signalling. *Arch. Toxicol.* **2009**, *83* (4), 297–318. https://doi.org/10.1007/s00204-009-0416-0.
- (10) Coller, J. K.; Fritz, P.; Zanger, U. M.; Siegle, I.; Eichelbaum, M.; Kroemer, H. K.; Mürdter, T. E. Distribution of Microsomal Epoxide Hydrolase in Humans: An Immunohistochemical Study in Normal Tissues, and Benign and Malignant Tumours. *Histochem. J.* **2001**, *33* (6), 329–336. https://doi.org/10.1023/a:1012414806166.
- (11) Václavíková, R.; Hughes, D. J.; Souček, P. Microsomal Epoxide Hydrolase 1 (EPHX1): Gene, Structure, Function, and Role in Human Disease. *Gene* **2015**, *571* (1), 1–8. https://doi.org/10.1016/j.gene.2015.07.071.
- (12) Nguyen, H. L.; Yang, X.; Omiecinski, C. J. Expression of a Novel MRNA Transcript for Human Microsomal Epoxide Hydrolase (EPHX1) Is Regulated by Short Open Reading

- Frames within Its 5'-Untranslated Region. *RNA* **2013**, *19* (6), 752–766. https://doi.org/10.1261/rna.037036.112.
- (13) Buterin, T.; Hess, M. T.; Luneva, N.; Geacintov, N. E.; Amin, S.; Kroth, H.; Seidel, A.; Naegeli, H. Unrepaired Fjord Region Polycyclic Aromatic Hydrocarbon-DNA Adducts in Ras Codon 61 Mutational Hot Spots. *Cancer Res.* **2000**, *60* (7), 1849–1856.
- (14) Lloyd, D. R.; Hanawalt, P. C. P53-Dependent Global Genomic Repair of Benzo[a]Pyrene-7,8-Diol-9,10-Epoxide Adducts in Human Cells. *Cancer Res.* **2000**, *60* (3), 517–521.
- (15) Fändrich, F.; Degiuli, B.; Vogel-Bindel, U.; Arand, M.; Oesch, F. Induction of Rat Liver Microsomal Epoxide Hydrolase by Its Endogenous Substrate 16 Alpha, 17 Alpha-Epoxyestra-1,3,5-Trien-3-Ol. *Xenobiotica* **1995**, 25 (3), 239–244. https://doi.org/10.3109/00498259509061848.
- (16) Hattori, N.; Fujiwara, H.; Maeda, M.; Fujii, S.; Ueda, M. Epoxide Hydrolase Affects Estrogen Production in the Human Ovary. *Endocrinology* **2000**, *141* (9), 3353–3365. https://doi.org/10.1210/endo.141.9.7682.
- (17) Nithipatikom, K.; Endsley, M. P.; Pfeiffer, A. W.; Falck, J. R.; Campbell, W. B. A Novel Activity of Microsomal Epoxide Hydrolase: Metabolism of the Endocannabinoid 2-Arachidonoylglycerol. *J. Lipid Res.* **2014**, *55* (10), 2093–2102. https://doi.org/10.1194/jlr.M051284.
- (18) Bosetti, F. Arachidonic Acid Metabolism in Brain Physiology and Pathology: Lessons from Genetically Altered Mouse Models. *J. Neurochem.* **2007**, *102* (3), 577–586. https://doi.org/10.1111/j.1471-4159.2007.04558.x.
- (19) Miyata, M.; Kudo, G.; Lee, Y.-H.; Fernandez-Salguero, P.; Kimura, S.; Gonzalez, F. J.; Yang, T. J.; Gelboin, H. V. Targeted Disruption of the Microsomal Epoxide Hydrolase Gene. *J. Biol. Chem.* **1999**, 274 (34), 23963–23968. https://doi.org/10.1074/jbc.274.34.23963.
- (20) Murray, G. I.; Weaver, R. J.; Paterson, P. J.; Ewen, S. W.; Melvin, W. T.; Burke, M. D. Expression of Xenobiotic Metabolizing Enzymes in Breast Cancer. *J. Pathol.* **1993**, *169* (3), 347–353. https://doi.org/10.1002/path.1711690312.
- (21) Marowsky, A.; Haenel, K.; Bockamp, E.; Heck, R.; Rutishauser, S.; Mule, N.; Kindler, D.; Rudin, M.; Arand, M. Genetic Enhancement of Microsomal Epoxide Hydrolase Improves Metabolic Detoxification but Impairs Cerebral Blood Flow Regulation. *Arch. Toxicol.* **2016**, 90 (12), 3017–3027. https://doi.org/10.1007/s00204-016-1666-2.
- (22) Imig, J. D.; Hammock, B. D. Soluble Epoxide Hydrolase as a Therapeutic Target for Cardiovascular Diseases. *Nat. Rev. Drug Discov.* **2009**, *8* (10), 794–805. https://doi.org/10.1038/nrd2875.
- (23) Ni, G.-H.; Chen, J.-F.; Chen, X.-P.; Yang, T.-L. Soluble Epoxide Hydrolase: A Promising Therapeutic Target for Cardiovascular Diseases. *Pharmazie* **2011**, *66* (3), 153–157.

- (24) Decker, M.; Adamska, M.; Cronin, A.; Di Giallonardo, F.; Burgener, J.; Marowsky, A.; Falck, J. R.; Morisseau, C.; Hammock, B. D.; Gruzdev, A.; Zeldin, D. C.; Arand, M. EH3 (ABHD9): The First Member of a New Epoxide Hydrolase Family with High Activity for Fatty Acid Epoxides. *J. Lipid Res.* **2012**, *53* (10), 2038–2045. https://doi.org/10.1194/jlr.M024448.
- (25) Edin, M. L.; Yamanashi, H.; Boeglin, W. E.; Graves, J. P.; DeGraff, L. M.; Lih, F. B.; Zeldin, D. C.; Brash, A. R. Epoxide Hydrolase 3 (Ephx3) Gene Disruption Reduces Ceramide Linoleate Epoxide Hydrolysis and Impairs Skin Barrier Function. *J. Biol. Chem.* **2021**, 296 (100198), 100198. https://doi.org/10.1074/jbc.RA120.016570.
- (26) Edin, M. L.; Hamedani, B. G.; Gruzdev, A.; Graves, J. P.; Lih, F. B.; Arbes, S. J., 3rd; Singh, R.; Orjuela Leon, A. C.; Bradbury, J. A.; DeGraff, L. M.; Hoopes, S. L.; Arand, M.; Zeldin, D. C. Epoxide Hydrolase 1 (EPHX1) Hydrolyzes Epoxyeicosanoids and Impairs Cardiac Recovery after Ischemia. *J. Biol. Chem.* **2018**, 293 (9), 3281–3292. https://doi.org/10.1074/jbc.RA117.000298.
- (27) Hoopes, S. L.; Gruzdev, A.; Edin, M. L.; Graves, J. P.; Bradbury, J. A.; Flake, G. P.; Lih, F. B.; DeGraff, L. M.; Zeldin, D. C. Generation and Characterization of Epoxide Hydrolase 3 (EPHX3)-Deficient Mice. *PLoS One* **2017**, *12* (4), e0175348. https://doi.org/10.1371/journal.pone.0175348.
- (28) Bononi, G.; Tuccinardi, T.; Rizzolio, F.; Granchi, C. A/β-Hydrolase Domain (ABHD) Inhibitors as New Potential Therapeutic Options against Lipid-Related Diseases. *J. Med. Chem.* **2021**, *64* (14), 9759–9785. https://doi.org/10.1021/acs.jmedchem.1c00624.
- (29) Yamanashi, H.; Boeglin, W. E.; Morisseau, C.; Davis, R. W.; Sulikowski, G. A.; Hammock, B. D.; Brash, A. R. Catalytic Activities of Mammalian Epoxide Hydrolases with Cis and Trans Fatty Acid Epoxides Relevant to Skin Barrier Function. *J. Lipid Res.* **2018**, *59* (4), 684–695. https://doi.org/10.1194/jlr.M082701.
- (30) Stott-Miller, M.; Zhao, S.; Wright, J. L.; Kolb, S.; Bibikova, M.; Klotzle, B.; Ostrander, E. A.; Fan, J.-B.; Feng, Z.; Stanford, J. L. Validation Study of Genes with Hypermethylated Promoter Regions Associated with Prostate Cancer Recurrence. *Cancer Epidemiol. Biomarkers Prev.* **2014**, *23* (7), 1331–1339. https://doi.org/10.1158/1055-9965.EPI-13-1000.
- (31) Bai, G.; Song, J.; Yuan, Y.; Chen, Z.; Tian, Y.; Yin, X.; Niu, Y.; Liu, J. Systematic Analysis of Differentially Methylated Expressed Genes and Site-Specific Methylation as Potential Prognostic Markers in Head and Neck Cancer. *J. Cell. Physiol.* **2019**, *234* (12), 22687–22702. https://doi.org/10.1002/jcp.28835.
- (32) Dahlhoff, M.; Fröhlich, T.; Arnold, G. J.; Müller, U.; Leonhardt, H.; Zouboulis, C. C.; Schneider, M. R. Characterization of the Sebocyte Lipid Droplet Proteome Reveals Novel Potential Regulators of Sebaceous Lipogenesis. *Exp. Cell Res.* **2015**, *332* (1), 146–155. https://doi.org/10.1016/j.yexcr.2014.12.004.
- (33) Roberts, D. L.; O'Dwyer, S. T.; Stern, P. L.; Renehan, A. G. Global Gene Expression in Pseudomyxoma Peritonei, with Parallel Development of Two Immortalized Cell Lines. *Oncotarget* **2015**, *6* (13), 10786–10800. https://doi.org/10.18632/oncotarget.3198.

- (34) Harris, T. R.; Aronov, P. A.; Jones, P. D.; Tanaka, H.; Arand, M.; Hammock, B. D. Identification of Two Epoxide Hydrolases in Caenorhabditis Elegans That Metabolize Mammalian Lipid Signaling Molecules. *Arch. Biochem. Biophys.* **2008**, *472* (2), 139–149. https://doi.org/10.1016/j.abb.2008.01.016.
- (35) Gomez, G. A.; Morisseau, C.; Hammock, B. D.; Christianson, D. W. Structure of Human Epoxide Hydrolase Reveals Mechanistic Inferences on Bifunctional Catalysis in Epoxide and Phosphate Ester Hydrolysis. *Biochemistry* **2004**, *43* (16), 4716–4723. https://doi.org/10.1021/bi036189j.
- (36) Ulu, A.; Harris, T. R.; Morisseau, C.; Miyabe, C.; Inoue, H.; Schuster, G.; Dong, H.; Iosif, A.-M.; Liu, J.-Y.; Weiss, R. H.; Chiamvimonvat, N.; Imig, J. D.; Hammock, B. D. Anti-Inflammatory Effects of ω-3 Polyunsaturated Fatty Acids and Soluble Epoxide Hydrolase Inhibitors in Angiotensin-II-Dependent Hypertension. *J. Cardiovasc. Pharmacol.* **2013**, *62* (3), 285–297. https://doi.org/10.1097/FJC.0b013e318298e460.
- (37) Ulu, A.; Stephen Lee, K. S.; Miyabe, C.; Yang, J.; Hammock, B. G.; Dong, H.; Hammock, B. D. An Omega-3 Epoxide of Docosahexaenoic Acid Lowers Blood Pressure in Angiotensin-II-Dependent Hypertension. *J. Cardiovasc. Pharmacol.* **2014**, *64* (1), 87–99. https://doi.org/10.1097/FJC.00000000000000094.
- (38) Manhiani, M.; Quigley, J. E.; Knight, S. F.; Tasoobshirazi, S.; Moore, T.; Brands, M. W.; Hammock, B. D.; Imig, J. D. Soluble Epoxide Hydrolase Gene Deletion Attenuates Renal Injury and Inflammation with DOCA-Salt Hypertension. *Am. J. Physiol. Renal Physiol.* **2009**, 297 (3), F740-8. https://doi.org/10.1152/ajprenal.00098.2009.
- (39) Luo, J.; Hu, S.; Fu, M.; Luo, L.; Li, Y.; Li, W.; Cai, Y.; Dong, R.; Yang, Y.; Tu, L.; Xu, X. Inhibition of Soluble Epoxide Hydrolase Alleviates Insulin Resistance and Hypertension via Downregulation of SGLT2 in the Mouse Kidney. *J. Biol. Chem.* **2021**, 296 (100667), 100667. https://doi.org/10.1016/j.jbc.2021.100667.
- (40) Xu, J.; Qiu, X.; Yu, G.; Ly, M.; Yang, J.; Silva, R. M.; Zhang, X.; Yu, M.; Wang, Y.; Hammock, B.; Pinkerton, K. E.; Zhao, D. Soluble Epoxide Hydrolase Inhibitor Can Protect the Femoral Head against Tobacco Smoke Exposure-Induced Osteonecrosis in Spontaneously Hypertensive Rats. *Toxicology* **2022**, *465* (153045), 153045. https://doi.org/10.1016/j.tox.2021.153045.
- (41) Kim, S. A.; Lee, A. S.; Lee, H. B.; Hur, H. J.; Lee, S. H.; Sung, M. J. Soluble Epoxide Hydrolase Inhibitor, TPPU, Attenuates Progression of Atherosclerotic Lesions and Vascular Smooth Muscle Cell Phenotypic Switching. *Vascul. Pharmacol.* **2022**, *145* (107086), 107086. https://doi.org/10.1016/j.vph.2022.107086.
- (42) Yu, W.; Li, S.; Wu, H.; Hu, P.; Chen, L.; Zeng, C.; Tong, X. Endothelial Nox4 Dysfunction Aggravates Atherosclerosis by Inducing Endoplasmic Reticulum Stress and Soluble Epoxide Hydrolase. *Free Radic. Biol. Med.* **2021**, *164*, 44–57. https://doi.org/10.1016/j.freeradbiomed.2020.12.450.

- (43) Demirdöğen, C. Missense Genetic Polymorphisms of Microsomal (EPHX1) and Soluble Epoxide Hydrolase (EPHX2) and Their Relation to the Risk of Large Artery Atherosclerotic Ischemic Stroke in a Turkish Population. *Neuropsychiatric disease and treatment* **2021**, 3251–3265.
- (44) Piper, K.; Garelnabi, M. Eicosanoids: Atherosclerosis and Cardiometabolic Health. *J. Clin. Transl. Endocrinol.* **2020**, *19* (100216), 100216. https://doi.org/10.1016/j.jcte.2020.100216.
- (45) Zhao, W.-Y.; Luan, Z.-L.; Liu, T.-T.; Ming, W.-H.; Huo, X.-K.; Huang, H.-L.; Sun, C.-P.; Zhang, B.-J.; Ma, X.-C. Inula Japonica Ameliorated Bleomycin-Induced Pulmonary Fibrosis via Inhibiting Soluble Epoxide Hydrolase. *Bioorg. Chem.* **2020**, *102* (104065), 104065. https://doi.org/10.1016/j.bioorg.2020.104065.
- (46) Wang, L.; Yang, J.; Guo, L.; Uyeminami, D.; Dong, H.; Hammock, B. D.; Pinkerton, K. E. Use of a Soluble Epoxide Hydrolase Inhibitor in Smoke-Induced Chronic Obstructive Pulmonary Disease. *Am. J. Respir. Cell Mol. Biol.* **2012**, *46* (5), 614–622. https://doi.org/10.1165/rcmb.2011-0359OC.
- (47) Smith, K. R.; Pinkerton, K. E.; Watanabe, T.; Pedersen, T. L.; Ma, S. J.; Hammock, B. D. Attenuation of Tobacco Smoke-Induced Lung Inflammation by Treatment with a Soluble Epoxide Hydrolase Inhibitor. *Proc. Natl. Acad. Sci. U. S. A.* **2005**, *102* (6), 2186–2191. https://doi.org/10.1073/pnas.0409591102.
- (48) Yang, L.; Cheriyan, J.; Gutterman, D. D.; Mayer, R. J.; Ament, Z.; Griffin, J. L.; Lazaar, A. L.; Newby, D. E.; Tal-Singer, R.; Wilkinson, I. B. Mechanisms of Vascular Dysfunction in COPD and Effects of a Novel Soluble Epoxide Hydrolase Inhibitor in Smokers. *Chest* **2017**, *151* (3), 555–563. https://doi.org/10.1016/j.chest.2016.10.058.
- (49) Revermann, M.; Barbosa-Sicard, E.; Dony, E.; Schermuly, R. T.; Morisseau, C.; Geisslinger, G.; Fleming, I.; Hammock, B. D.; Brandes, R. P. Inhibition of the Soluble Epoxide Hydrolase Attenuates Monocrotaline-Induced Pulmonary Hypertension in Rats. *J. Hypertens.* **2009**, *27* (2), 322–331. https://doi.org/10.1097/hjh.0b013e32831aedfa.
- (50) Hu, J.; Dziumbla, S.; Lin, J.; Bibli, S.-I.; Zukunft, S.; de Mos, J.; Awwad, K.; Frömel, T.; Jungmann, A.; Devraj, K.; Cheng, Z.; Wang, L.; Fauser, S.; Eberhart, C. G.; Sodhi, A.; Hammock, B. D.; Liebner, S.; Müller, O. J.; Glaubitz, C.; Hammes, H.-P.; Popp, R.; Fleming, I. Inhibition of Soluble Epoxide Hydrolase Prevents Diabetic Retinopathy. *Nature* **2017**, *552* (7684), 248–252. https://doi.org/10.1038/nature25013.
- (51) Fang, Q.; Liu, X.; Ding, J.; Zhang, Z.; Chen, G.; Du, T.; Wang, Y.; Xu, R. Soluble Epoxide Hydrolase Inhibition Protected against Diabetic Cardiomyopathy through Inducing Autophagy and Reducing Apoptosis Relying on Nrf2 Upregulation and Transcription Activation. *Oxid. Med. Cell. Longev.* **2022**, 2022, 3773415. https://doi.org/10.1155/2022/3773415.
- (52) Minaz, N.; Razdan, R.; Hammock, B. D.; Mujwar, S.; Goswami, S. K. Impact of Diabetes on Male Sexual Function in Streptozotocin-Induced Diabetic Rats: Protective Role of Soluble

- Epoxide Hydrolase Inhibitor. *Biomed. Pharmacother.* **2019**, *115* (108897), 108897. https://doi.org/10.1016/j.biopha.2019.108897.
- (53) Anita, N. Z.; Swardfager, W. Soluble Epoxide Hydrolase and Diabetes Complications. *Int. J. Mol. Sci.* **2022**, *23* (11), 6232. https://doi.org/10.3390/ijms23116232.
- (54) Lee, K. S. S.; Ng, J. C.; Yang, J.; Hwang, S.-H.; Morisseau, C.; Wagner, K.; Hammock, B. D. Preparation and Evaluation of Soluble Epoxide Hydrolase Inhibitors with Improved Physical Properties and Potencies for Treating Diabetic Neuropathic Pain. *Bioorg. Med. Chem.* **2020**, 28 (22), 115735. https://doi.org/10.1016/j.bmc.2020.115735.
- (55) Hammock, B. D.; McReynolds, C. B.; Wagner, K.; Buckpitt, A.; Cortes-Puch, I.; Croston, G.; Lee, K. S. S.; Yang, J.; Schmidt, W. K.; Hwang, S. H. Movement to the Clinic of Soluble Epoxide Hydrolase Inhibitor EC5026 as an Analgesic for Neuropathic Pain and for Use as a Nonaddictive Opioid Alternative. *J. Med. Chem.* **2021**, *64* (4), 1856–1872. https://doi.org/10.1021/acs.jmedchem.0c01886.
- (56) Wagner, K. M.; Gomes, A.; McReynolds, C. B.; Hammock, B. D. Soluble Epoxide Hydrolase Regulation of Lipid Mediators Limits Pain. *Neurotherapeutics* **2020**, *17* (3), 900–916. https://doi.org/10.1007/s13311-020-00916-4.
- (57) Gowler, P. R. W.; Turnbull, J.; Shahtaheri, M.; Gohir, S.; Kelly, T.; McReynolds, C.; Yang, J.; Jha, R. R.; Fernandes, G. S.; Zhang, W.; Doherty, M.; Walsh, D. A.; Hammock, B. D.; Valdes, A. M.; Barrett, D. A.; Chapman, V. Clinical and Preclinical Evidence for Roles of Soluble Epoxide Hydrolase in Osteoarthritis Knee Pain. *Arthritis Rheumatol.* **2022**, *74* (4), 623–633. https://doi.org/10.1002/art.42000.
- (58) Hammock, B. D.; Schmelzer, K.; Inceoglu, A. B. Use of Inhibitors of Soluble Epoxide Hydrolase to Synergize Activity of COX and 5-LOX Inhibitors. *U.S* **2011**.
- (59) Abdalla, H. B.; Alvarez, C.; Wu, Y.-C.; Rojas, P.; Hammock, B. D.; Maddipati, K. R.; Trindade-da-Silva, C. A.; Soares, M. Q. S.; Clemente-Napimoga, J. T.; Kantarci, A.; Napimoga, M. H.; Van Dyke, T. E. Soluble Epoxide Hydrolase Inhibition Enhances Specialized Pro-Resolving Lipid Mediator Production and Promotes Macrophage Plasticity. *Br. J. Pharmacol.* 2022. https://doi.org/10.1111/bph.16009.
- (60) Mashayekhi, M.; Wanjalla, C. N.; Warren, C. M.; Simmons, J. D.; Ghoshal, K.; Pilkinton, M.; Bailin, S. S.; Gabriel, C. L.; Pozzi, A.; Koethe, J. R.; Brown, N. J.; Kalams, S. A.; Luther, J. M. The Soluble Epoxide Hydrolase Inhibitor GSK2256294 Decreases the Proportion of Adipose Pro-Inflammatory T Cells. *Prostaglandins Other Lipid Mediat.* 2022, 158 (106604), 106604. https://doi.org/10.1016/j.prostaglandins.2021.106604.
- (61) Kodani, S. D.; Morisseau, C. Role of Epoxy-Fatty Acids and Epoxide Hydrolases in the Pathology of Neuro-Inflammation. *Biochimie* **2019**, *159*, 59–65. https://doi.org/10.1016/j.biochi.2019.01.020.
- (62) Trindade-da-Silva, C. A.; Clemente-Napimoga, J. T.; Abdalla, H. B.; Rosa, S. M.; Ueira-Vieira, C.; Morisseau, C.; Verri, W. A., Jr; Montalli, V. A. M.; Hammock, B. D.; Napimoga,

- M. H. Soluble Epoxide Hydrolase Inhibitor, TPPU, Increases Regulatory T Cells Pathway in an Arthritis Model. *FASEB J.* **2020**, *34* (7), 9074–9086. https://doi.org/10.1096/fj.202000415R.
- (63) Teixeira, J. M.; Abdalla, H. B.; Basting, R. T.; Hammock, B. D.; Napimoga, M. H.; Clemente-Napimoga, J. T. Peripheral Soluble Epoxide Hydrolase Inhibition Reduces Hypernociception and Inflammation in Albumin-Induced Arthritis in Temporomandibular Joint of Rats. *Int. Immunopharmacol.* **2020**, 87 (106841), 106841. https://doi.org/10.1016/j.intimp.2020.106841.
- (64) Biliktu, M. Pharmacological Inhibition of Soluble Epoxide Hydrolase Attenuates Chronic Experimental Autoimmune Encephalomyelitis by Modulating Inflammatory and Anti-Inflammatory Pathways in an Inflammasome-Dependent and-Independent Manner. *Inflammopharmacology* **2020**, 28, 1509–1524.
- (65) Jonnalagadda, D.; Wan, D.; Chun, J.; Hammock, B. D.; Kihara, Y. A Soluble Epoxide Hydrolase Inhibitor, 1-TrifluoromethoxyPhenyl-3-(1-Propionylpiperidin-4-Yl) Urea, Ameliorates Experimental Autoimmune Encephalomyelitis. *Int. J. Mol. Sci.* **2021**, 22 (9), 4650. https://doi.org/10.3390/ijms22094650.
- (66) Jung, O.; Jansen, F.; Mieth, A.; Barbosa-Sicard, E.; Pliquett, R. U.; Babelova, A.; Morisseau, C.; Hwang, S. H.; Tsai, C.; Hammock, B. D.; Schaefer, L.; Geisslinger, G.; Amann, K.; Brandes, R. P. Inhibition of the Soluble Epoxide Hydrolase Promotes Albuminuria in Mice with Progressive Renal Disease. *PLoS One* **2010**, *5* (8), e11979. https://doi.org/10.1371/journal.pone.0011979.
- (67) Liu, J.-Y. Inhibition of Soluble Epoxide Hydrolase for Renal Health. *Front. Pharmacol.* **2018**, 9, 1551. https://doi.org/10.3389/fphar.2018.01551.
- (68) Griñán-Ferré, C.; Codony, S.; Pujol, E.; Yang, J.; Leiva, R.; Escolano, C.; Puigoriol-Illamola, D.; Companys-Alemany, J.; Corpas, R.; Sanfeliu, C.; Pérez, B.; Loza, M. I.; Brea, J.; Morisseau, C.; Hammock, B. D.; Vázquez, S.; Pallàs, M.; Galdeano, C. Pharmacological Inhibition of Soluble Epoxide Hydrolase as a New Therapy for Alzheimer's Disease. *Neurotherapeutics* **2020**. https://doi.org/10.1007/s13311-020-00854-1.
- (69) Ghosh, A.; Comerota, M. M.; Wan, D.; Chen, F.; Propson, N. E.; Hwang, S. H.; Hammock, B. D.; Zheng, H. An Epoxide Hydrolase Inhibitor Reduces Neuroinflammation in a Mouse Model of Alzheimer's Disease. *Sci. Transl. Med.* **2020**, *12* (573), eabb1206. https://doi.org/10.1126/scitranslmed.abb1206.
- (70) Lee, H.-T.; Lee, K.-I.; Chen, C.-H.; Lee, T.-S. Genetic Deletion of Soluble Epoxide Hydrolase Delays the Progression of Alzheimer's Disease. *J. Neuroinflammation* **2019**, *16* (1), 267. https://doi.org/10.1186/s12974-019-1635-9.
- (71) Ghosh, A.; Comerota, M. E.; Wan, D.; Chen, F.; Propson, N. E.; Hwang, S. H.; Hammock, B. D.; Zheng, H. Epoxy Fatty Acid Dysregulation and Neuroinflammation in Alzheimer's Disease Is Resolved by a Soluble Epoxide Hydrolase Inhibitor. *bioRxiv*, 2020. https://doi.org/10.1101/2020.06.30.180984.

- (72) Manickam, M.; Meenakshisundaram, S.; Pillaiyar, T. Activating Endogenous Resolution Pathways by Soluble Epoxide Hydrolase Inhibitors for the Management of COVID-19. *Arch. Pharm.* (*Weinheim*) **2022**, *355* (3), e2100367. https://doi.org/10.1002/ardp.202100367.
- (73) Shan, J.; Hashimoto, K. Soluble Epoxide Hydrolase as a Therapeutic Target for Neuropsychiatric Disorders. *Int. J. Mol. Sci.* **2022**, 23 (9), 4951. https://doi.org/10.3390/ijms23094951.
- (74) Martini, R. P.; Siler, D.; Cetas, J.; Alkayed, N. J.; Allen, E.; Treggiari, M. M. A Double-Blind, Randomized, Placebo-Controlled Trial of Soluble Epoxide Hydrolase Inhibition in Patients with Aneurysmal Subarachnoid Hemorrhage. *Neurocrit. Care* **2022**, *36* (3), 905–915. https://doi.org/10.1007/s12028-021-01398-8.
- (75) Zarriello, S.; Tuazon, J. P.; Corey, S.; Schimmel, S.; Rajani, M.; Gorsky, A.; Incontri, D.; Hammock, B. D.; Borlongan, C. V. Humble Beginnings with Big Goals: Small Molecule Soluble Epoxide Hydrolase Inhibitors for Treating CNS Disorders. *Prog. Neurobiol.* **2019**, 172, 23–39. https://doi.org/10.1016/j.pneurobio.2018.11.001.
- (76) The Effect of Soluble Epoxide Hydrolase (SEH) on Depression. https://ClinicalTrials.gov/show/NCT05575713 (accessed 2023-04-15).
- (77) Evaluation of the Effects of Urotensin-II and Soluble Epoxide Hydrolase Inhibitors on Skin Microvessel Tone in Patients With Heart Failure, and in Healthy Volunteers. https://ClinicalTrials.gov/show/NCT00654966 (accessed 2023-04-15).
- (78) Soluble Epoxide Hydrolase Inhibition and Insulin Resistance. https://clinicaltrials.gov/ct2/show/NCT03486223 (accessed 2023-01-11).
- (79) Subarachnoid Hemorrhage and Soluble Epoxide Hydrolase Inhibition Trial Full Text View Clinicaltrials.gov. https://clinicaltrials.gov/ct2/show/NCT03318783 (accessed 2023-01-11).
- (80) Evaluation of Soluble Epoxide Hydrolase (s-EH) Inhibitor in Patients With Mild to Moderate Hypertension and Impaired Glucose Tolerance. https://ClinicalTrials.gov/show/NCT00847899 (accessed 2023-04-15).
- (81) A Study to Assess the Safety, Tolerability, Pharmacokinetics and Pharmacodynamics of Single Doses of GSK2256294 in Healthy Volunteers, and Single and Repeat Doses of GSK2256294 in Adult Male Moderately Obese Smokers. https://ClinicalTrials.gov/show/NCT01762774 (accessed 2023-04-15).
- (82) A Study to Investigate the Safety and Pharmacokinetics of a Single Dose of GSK2256294 in Healthy Young Males and Elderly Subjects. https://ClinicalTrials.gov/show/NCT02006537 (accessed 2023-04-15).
- (83) Wang, Y.; Wagner, K. M.; Morisseau, C.; Hammock, B. D. Inhibition of the Soluble Epoxide Hydrolase as an Analgesic Strategy: A Review of Preclinical Evidence. *J. Pain Res.* **2021**, *14*, 61–72. https://doi.org/10.2147/JPR.S241893.

- (84) Reisdorf, W. C.; Xie, Q.; Zeng, X.; Xie, W.; Rajpal, N.; Hoang, B.; Burgert, M. E.; Kumar, V.; Hurle, M. R.; Rajpal, D. K.; O'Donnell, S.; MacDonald, T. T.; Vossenkämper, A.; Wang, L.; Reilly, M.; Votta, B. J.; Sanchez, Y.; Agarwal, P. Preclinical Evaluation of EPHX2 Inhibition as a Novel Treatment for Inflammatory Bowel Disease. *PLoS One* **2019**, *14* (4), e0215033. https://doi.org/10.1371/journal.pone.0215033.
- (85) Burdon, K. P.; Lehtinen, A. B.; Langefeld, C. D.; Carr, J. J.; Rich, S. S.; Freedman, B. I.; Herrington, D.; Bowden, D. W. Genetic Analysis of the Soluble Epoxide Hydrolase Gene, EPHX2, in Subclinical Cardiovascular Disease in the Diabetes Heart Study. *Diab. Vasc. Dis. Res.* **2008**, *5* (2), 128–134. https://doi.org/10.3132/dvdr.2008.021.
- (86) Kim, I.-H. Structure— Activity Relationships of Cycloalkylamide Derivatives as Inhibitors of the Soluble Epoxide Hydrolase. *Journal of medicinal chemistry* **2011**, *54*, 1752–1761.
- (87) Gomez, G. A.; Morisseau, C.; Hammock, B. D.; Christianson, D. W. Human Soluble Epoxide Hydrolase: Structural Basis of Inhibition by 4-(3-Cyclohexylureido)-Carboxylic Acids. *Protein Sci.* **2006**, *15* (1), 58–64. https://doi.org/10.1110/ps.051720206.
- (88) Eldrup, A. B.; Soleymanzadeh, F.; Taylor, S. J.; Muegge, I.; Farrow, N. A.; Joseph, D.; McKellop, K.; Man, C. C.; Kukulka, A.; De Lombaert, S. Structure-Based Optimization of Arylamides as Inhibitors of Soluble Epoxide Hydrolase. *J. Med. Chem.* **2009**, *52* (19), 5880–5895. https://doi.org/10.1021/jm9005302.
- (89) Morisseau, C.; Goodrow, M. H.; Newman, J. W.; Wheelock, C. E.; Dowdy, D. L.; Hammock, B. D. Structural Refinement of Inhibitors of Urea-Based Soluble Epoxide Hydrolases. *Biochem. Pharmacol.* **2002**, *63* (9), 1599–1608. https://doi.org/10.1016/s0006-2952(02)00952-8.
- (90) Huang, S.-X.; Cao, B.; Morisseau, C.; Jin, Y.; Hammock, B. D.; Long, Y.-Q. Structure-Based Optimization of the Piperazino-Containing 1,3-Disubstituted Ureas Affording Sub-Nanomolar Inhibitors of Soluble Epoxide Hydrolase. *Medchemcomm* **2012**, *3* (3), 379–384. https://doi.org/10.1039/C2MD00288D.
- (91) Huang, S.-X.; Cao, B.; Morisseau, C.; Jin, Y.; Hammock, B. D.; Long, Y.-Q. Structure-Based Optimization of the Piperazino-Containing 1,3-Disubstituted Ureas Affording Sub-Nanomolar Inhibitors of Soluble Epoxide Hydrolase. *Medchemcomm* **2012**, *3* (3), 379. https://doi.org/10.1039/c2md00288d.
- (92) Jones, P. D.; Wolf, N. M.; Morisseau, C.; Whetstone, P.; Hock, B.; Hammock, B. D. Fluorescent Substrates for Soluble Epoxide Hydrolase and Application to Inhibition Studies. *Anal. Biochem.* **2005**, *343* (1), 66–75. https://doi.org/10.1016/j.ab.2005.03.041.
- (93) Ulu, A.; Appt, S. E.; Morisseau, C.; Hwang, S. H.; Jones, P. D.; Rose, T. E.; Dong, H.; Lango, J.; Yang, J.; Tsai, H. J.; Miyabe, C.; Fortenbach, C.; Adams, M. R.; Hammock, B. D. Pharmacokinetics and in Vivo Potency of Soluble Epoxide Hydrolase Inhibitors in Cynomolgus Monkeys. *Br. J. Pharmacol.* **2012**, *165* (5), 1401–1412. https://doi.org/10.1111/j.1476-5381.2011.01641.x.

- (94) Yu, Z.; Xu, F.; Huse, L. M.; Morisseau, C.; Draper, A. J.; Newman, J. W.; Parker, C.; Graham, L.; Engler, M. M.; Hammock, B. D.; Zeldin, D. C.; Kroetz, D. L. Soluble Epoxide Hydrolase Regulates Hydrolysis of Vasoactive Epoxyeicosatrienoic Acids. *Circ. Res.* **2000**, *87* (11), 992–998. https://doi.org/10.1161/01.res.87.11.992.
- (95) Watanabe, T.; Morisseau, C.; Newman, J. W.; Hammock, B. D. In Vitro Metabolism of the Mammalian Soluble Epoxide Hydrolase Inhibitor, 1-Cyclohexyl-3-Dodecyl-Urea. *Drug Metab. Dispos.* **2003**, *31* (7), 846–853. https://doi.org/10.1124/dmd.31.7.846.
- (96) Imig, J. D.; Zhao, X.; Capdevila, J. H.; Morisseau, C.; Hammock, B. D. Soluble Epoxide Hydrolase Inhibition Lowers Arterial Blood Pressure in Angiotensin II Hypertension. *Hypertension* **2002**, *39* (2 Pt 2), 690–694. https://doi.org/10.1161/hy0202.103788.
- (97) Muller, D. N.; Shagdarsuren, E.; Park, J.-K.; Dechend, R.; Mervaala, E.; Hampich, F.; Fiebeler, A.; Ju, X.; Finckenberg, P.; Theuer, J.; Viedt, C.; Kreuzer, J.; Heidecke, H.; Haller, H.; Zenke, M.; Luft, F. C. Immunosuppressive Treatment Protects against Angiotensin II-Induced Renal Damage. *Am. J. Pathol.* **2002**, *161* (5), 1679–1693. https://doi.org/10.1016/s0002-9440(10)64445-8.
- (98) Kim, I.-H.; Morisseau, C.; Watanabe, T.; Hammock, B. D. Design, Synthesis, and Biological Activity of 1,3-Disubstituted Ureas as Potent Inhibitors of the Soluble Epoxide Hydrolase of Increased Water Solubility. *J. Med. Chem.* **2004**, *47* (8), 2110–2122. https://doi.org/10.1021/jm030514j.
- (99) Olearczyk, J. J.; Field, M. B.; Kim, I.-H.; Morisseau, C.; Hammock, B. D.; Imig, J. D. Substituted Adamantyl-Urea Inhibitors of the Soluble Epoxide Hydrolase Dilate Mesenteric Resistance Vessels. *J. Pharmacol. Exp. Ther.* **2006**, *318* (3), 1307–1314. https://doi.org/10.1124/jpet.106.103556.
- (100) Imig, J. D.; Zhao, X.; Zaharis, C. Z.; Olearczyk, J. J.; Pollock, D. M.; Newman, J. W.; Kim, I.-H.; Watanabe, T.; Hammock, B. D. An Orally Active Epoxide Hydrolase Inhibitor Lowers Blood Pressure and Provides Renal Protection in Salt-Sensitive Hypertension. *Hypertension* **2005**, *46* (4), 975–981. https://doi.org/10.1161/01.HYP.0000176237.74820.75.
- (101) Merabet, N.; Bellien, J.; Glevarec, E.; Nicol, L.; Lucas, D.; Remy-Jouet, I.; Bounoure, F.; Dreano, Y.; Wecker, D.; Thuillez, C.; Mulder, P. Soluble Epoxide Hydrolase Inhibition Improves Myocardial Perfusion and Function in Experimental Heart Failure. *J. Mol. Cell. Cardiol.* **2012**, *52* (3), 660–666. https://doi.org/10.1016/j.yjmcc.2011.11.015.
- (102) Capozzi, M. E.; Penn, J. S. Epoxydocosapentaenoic Acid (EDP) and Epoxyeicosatrienoic Acid (EET) Affect TNFα Production and Leukocyte Adhesion in Diabetic Retinopathy. *Invest. Ophthalmol. Vis. Sci.* **2016**, *57* (12).
- (103) Inceoglu, B.; Wagner, K. M.; Yang, J.; Bettaieb, A.; Schebb, N. H.; Hwang, S. H.; Morisseau, C.; Haj, F. G.; Hammock, B. D. Acute Augmentation of Epoxygenated Fatty Acid Levels Rapidly Reduces Pain-Related Behavior in a Rat Model of Type I Diabetes. *Proc. Natl. Acad. Sci. U. S. A.* **2012**, *109* (28), 11390–11395. https://doi.org/10.1073/pnas.1208708109.

- (104) Chiamvimonvat, N.; Ho, C.-M.; Tsai, H.-J.; Hammock, B. D. The Soluble Epoxide Hydrolase as a Pharmaceutical Target for Hypertension. *J. Cardiovasc. Pharmacol.* **2007**, *50* (3), 225–237. https://doi.org/10.1097/FJC.0b013e3181506445.
- (105) Tsai, H.-J.; Hwang, S. H.; Morisseau, C.; Yang, J.; Jones, P. D.; Kasagami, T.; Kim, I.-H.; Hammock, B. D. Pharmacokinetic Screening of Soluble Epoxide Hydrolase Inhibitors in Dogs. *Eur. J. Pharm. Sci.* **2010**, *40* (3), 222–238. https://doi.org/10.1016/j.ejps.2010.03.018.
- (106) Chen, D.; Whitcomb, R.; MacIntyre, E.; Tran, V.; Do, Z. N.; Sabry, J.; Patel, D. V.; Anandan, S. K.; Gless, R.; Webb, H. K. Pharmacokinetics and Pharmacodynamics of AR9281, an Inhibitor of Soluble Epoxide Hydrolase, in Single- and Multiple-Dose Studies in Healthy Human Subjects. *J. Clin. Pharmacol.* **2012**, *52* (3), 319–328. https://doi.org/10.1177/0091270010397049.
- (107) Zhou, Y.; Yang, J.; Sun, G.-Y.; Liu, T.; Duan, J.-X.; Zhou, H.-F.; Lee, K. S.; Hammock, B. D.; Fang, X.; Jiang, J.-X.; Guan, C.-X. Erratum to: Soluble Epoxide Hydrolase Inhibitor 1-Trifluoromethoxyphenyl-3-(1-Propionylpiperidin-4-Yl) Urea Attenuates Bleomycin-Induced Pulmonary Fibrosis in Mice. *Cell Tissue Res.* **2016**, *364* (3), 675. https://doi.org/10.1007/s00441-016-2379-9.
- (108) Wan, D.; Yang, J.; McReynolds, C. B.; Barnych, B.; Wagner, K. M.; Morisseau, C.; Hwang, S. H.; Sun, J.; Blöcher, R.; Hammock, B. D. In Vitro and in Vivo Metabolism of a Potent Inhibitor of Soluble Epoxide Hydrolase, 1-(1-Propionylpiperidin-4-Yl)-3-(4-(Trifluoromethoxy)Phenyl)Urea. *Front. Pharmacol.* **2019**, *10*, 464. https://doi.org/10.3389/fphar.2019.00464.
- (109) Synthesis and Properties of N-[R-Adamantan-1(2)-Yl]- N'-(2-Fluorophenyl)Ureas-Target-Oriented Soluble Epoxide Hydrolase Inhibitors.
- (110) Burmistrov, V.; Morisseau, C.; Karlov, D.; Pitushkin, D.; Vernigora, A.; Rasskazova, E.; Butov, G. M.; Hammock, B. D. Bioisosteric Substitution of Adamantane with Bicyclic Lipophilic Groups Improves Water Solubility of Human Soluble Epoxide Hydrolase Inhibitors. *Bioorg. Med. Chem. Lett.* **2020**, *30* (18), 127430. https://doi.org/10.1016/j.bmcl.2020.127430.
- (111) Xing, L.; McDonald, J. J.; Kolodziej, S. A.; Kurumbail, R. G.; Williams, J. M.; Warren, C. J.; O'Neal, J. M.; Skepner, J. E.; Roberds, S. L. Discovery of Potent Inhibitors of Soluble Epoxide Hydrolase by Combinatorial Library Design and Structure-Based Virtual Screening. *J. Med. Chem.* **2011**, *54* (5), 1211–1222. https://doi.org/10.1021/jm101382t.
- (112) Shen, H. C. Soluble Epoxide Hydrolase Inhibitors: A Patent Review. *Expert Opin. Ther. Pat.* **2010**, *20* (7), 941–956. https://doi.org/10.1517/13543776.2010.484804.
- (113) Das Mahapatra, A.; Choubey, R.; Datta, B. Small Molecule Soluble Epoxide Hydrolase Inhibitors in Multitarget and Combination Therapies for Inflammation and Cancer. *Molecules* **2020**, *25* (23), 5488. https://doi.org/10.3390/molecules25235488.

- (114) Codony, S.; Calvó-Tusell, C.; Valverde, E.; Osuna, S.; Morisseau, C.; Loza, M. I.; Brea, J.; Pérez, C.; Rodríguez-Franco, M. I.; Pizarro-Delgado, J.; Corpas, R.; Griñán-Ferré, C.; Pallàs, M.; Sanfeliu, C.; Vázquez-Carrera, M.; Hammock, B. D.; Feixas, F.; Vázquez, S. From the Design to the in Vivo Evaluation of Benzohomoadamantane-Derived Soluble Epoxide Hydrolase Inhibitors for the Treatment of Acute Pancreatitis. *J. Med. Chem.* **2021**, 64 (9), 5429–5446. https://doi.org/10.1021/acs.jmedchem.0c01601.
- (115) Lee, K. S. S.; Liu, J.-Y.; Wagner, K. M.; Pakhomova, S.; Dong, H.; Morisseau, C.; Fu, S. H.; Yang, J.; Wang, P.; Ulu, A.; Mate, C. A.; Nguyen, L. V.; Hwang, S. H.; Edin, M. L.; Mara, A. A.; Wulff, H.; Newcomer, M. E.; Zeldin, D. C.; Hammock, B. D. Optimized Inhibitors of Soluble Epoxide Hydrolase Improve in Vitro Target Residence Time and in Vivo Efficacy. *J. Med. Chem.* **2014**, *57* (16), 7016–7030. https://doi.org/10.1021/jm500694p.
- (116) Sun, C.-P.; Zhang, X.-Y.; Morisseau, C.; Hwang, S. H.; Zhang, Z.-J.; Hammock, B. D.; Ma, X.-C. Discovery of Soluble Epoxide Hydrolase Inhibitors from Chemical Synthesis and Natural Products. *J. Med. Chem.* **2021**, *64* (1), 184–215. https://doi.org/10.1021/acs.jmedchem.0c01507.
- (117) Park, H.-E. H.; Jung, Y.; Lee, S.-J. V. Survival Assays Using Caenorhabditis Elegans. *Mol. Cells* **2017**, *40* (2), 90–99. https://doi.org/10.14348/molcells.2017.0017.
- (118) Cornwell, A. B.; Samuelson, A. V. Analysis of Lifespan in C. Elegans: Low- and High-Throughput Approaches. *Methods Mol. Biol.* **2020**, *2144*, 7–27. https://doi.org/10.1007/978-1-0716-0592-9\_2.
- (119) Chen, A. L.; Lum, K. M.; Lara-Gonzalez, P.; Ogasawara, D.; Cognetta, A. B., 3rd; To, A.; Parsons, W. H.; Simon, G. M.; Desai, A.; Petrascheck, M.; Bar-Peled, L.; Cravatt, B. F. Pharmacological Convergence Reveals a Lipid Pathway That Regulates C. Elegans Lifespan. *Nat. Chem. Biol.* **2019**, *15* (5), 453–462. https://doi.org/10.1038/s41589-019-0243-4.
- (120) Ludewig, A. H.; Gimond, C.; Judkins, J. C.; Thornton, S.; Pulido, D. C.; Micikas, R. J.; Döring, F.; Antebi, A.; Braendle, C.; Schroeder, F. C. Larval Crowding Accelerates C. Elegans Development and Reduces Lifespan. *PLoS Genet.* **2017**, *13* (4), e1006717. https://doi.org/10.1371/journal.pgen.1006717.
- (121) Jamieson, K. L.; Darwesh, A. M.; Sosnowski, D. K.; Zhang, H.; Shah, S.; Zhabyeyev, P.; Yang, J.; Hammock, B. D.; Edin, M. L.; Zeldin, D. C.; Oudit, G. Y.; Kassiri, Z.; Seubert, J. M. Soluble Epoxide Hydrolase in Aged Female Mice and Human Explanted Hearts Following Ischemic Injury. *Int. J. Mol. Sci.* 2021, 22 (4), 1691. https://doi.org/10.3390/ijms22041691.
- (122) Zuloaga, K. L.; Zhang, W.; Roese, N. E.; Alkayed, N. J. Soluble Epoxide Hydrolase Gene Deletion Improves Blood Flow and Reduces Infarct Size after Cerebral Ischemia in Reproductively Senescent Female Mice. *Front. Pharmacol.* **2014**, *5*, 290. https://doi.org/10.3389/fphar.2014.00290.
- (123) Schafer, W. F. Genetics of Egg-Laying in Worms. *Annu. Rev. Genet.* **2006**, *40* (1), 487–509. https://doi.org/10.1146/annurev.genet.40.110405.090527.

- (124) Hsin, H.; Kenyon, C. Signals from the Reproductive System Regulate the Lifespan of C. Elegans. *Nature* **1999**, *399* (6734), 362–366. https://doi.org/10.1038/20694.
- (125) Arantes-Oliveira, N.; Apfeld, J.; Dillin, A.; Kenyon, C. Regulation of Life-Span by Germ-Line Stem Cells in Caenorhabditis Elegans. *Science* **2002**, *295* (5554), 502–505. https://doi.org/10.1126/science.1065768.
- (126) Lapierre, L. R.; Gelino, S.; Meléndez, A.; Hansen, M. Autophagy and Lipid Metabolism Coordinately Modulate Life Span in Germline-Less C. Elegans. *Curr. Biol.* **2011**, *21* (18), 1507–1514. https://doi.org/10.1016/j.cub.2011.07.042.
- (127) Wang, M. C.; O'Rourke, E. J.; Ruvkun, G. Fat Metabolism Links Germline Stem Cells and Longevity in C. Elegans. *Science* **2008**, *322* (5903), 957–960. https://doi.org/10.1126/science.1162011.
- (128) Judd, E. T.; Wessels, F. J.; Drewry, M. D.; Grove, M.; Wright, K.; Hahn, D. A.; Hatle, J. D. Ovariectomy in Grasshoppers Increases Somatic Storage, but Proportional Allocation of Ingested Nutrients to Somatic Tissues Is Unchanged. *Aging Cell* 2011, 10 (6), 972–979. https://doi.org/10.1111/j.1474-9726.2011.00737.x.
- (129) Oxygen Consumption of Castrated Females of the Blow-Fly.
- (130) Pallier, E.; Aubert, R.; Lemonnier, D. Effect of Diet and Ovariectomy on Adipose Tissue Cellularity in Mice. *Reprod. Nutr. Dev.* **1980**, 20 (3A), 631–636. https://doi.org/10.1051/rnd:19800404.
- (131) Crane, S. W. Occurrence and Management of Obesity in Companion Animals. *J. Small Anim. Pract.* **1991**, *32* (6), 275–282. https://doi.org/10.1111/j.1748-5827.1991.tb00930.x.
- (132) Fettman, M. J.; Stanton, C. A.; Banks, L. L.; Hamar, D. W.; Johnson, D. E.; Hegstad, R. L.; Johnston, S. Effects of Neutering on Bodyweight, Metabolic Rate and Glucose Tolerance of Domestic Cats. *Res. Vet. Sci.* **1997**, *62* (2), 131–136. https://doi.org/10.1016/s0034-5288(97)90134-x.
- (133) Hughes, S. E.; Evason, K.; Xiong, C.; Kornfeld, K. Genetic and Pharmacological Factors That Influence Reproductive Aging in Nematodes. *PLoS Genet.* **2007**, *3* (2), e25. https://doi.org/10.1371/journal.pgen.0030025.
- (134) Hughes, S. E.; Evason, K.; Xiong, C.; Kornfeld, K. Genetic and Pharmacological Factors That Influence Reproductive Aging in Nematodes. *PLoS Genet.* **2005**, *preprint* (2006), e25. https://doi.org/10.1371/journal.pgen.0030025.eor.
- (135) Watts, J. L.; Phillips, E.; Griffing, K. R.; Browse, J. Deficiencies in C20 Polyunsaturated Fatty Acids Cause Behavioral and Developmental Defects in Caenorhabditis Elegans Fat-3 Mutants. *Genetics* **2003**, *163* (2), 581–589. https://doi.org/10.1093/genetics/163.2.581.
- (136) Lesa, G. M.; Palfreyman, M.; Hall, D. H.; Clandinin, M. T.; Rudolph, C.; Jorgensen, E. M.; Schiavo, G. Long Chain Polyunsaturated Fatty Acids Are Required for Efficient

- Neurotransmission in C. Elegans. *J. Cell Sci.* **2003**, *116* (Pt 24), 4965–4975. https://doi.org/10.1242/jcs.00918.
- (137) Watts, J. L. Using Caenorhabditis Elegans to Uncover Conserved Functions of Omega-3 and Omega-6 Fatty Acids. *J. Clin. Med.* **2016**, *5* (2), 19. https://doi.org/10.3390/jcm5020019.
- (138) Beaudoin-Chabot, C.; Wang, L.; Smarun, A. V.; Vidović, D.; Shchepinov, M. S.; Thibault, G. Deuterated Polyunsaturated Fatty Acids Reduce Oxidative Stress and Extend the Lifespan of C. Elegans. *Front. Physiol.* 2019, 10, 641. https://doi.org/10.3389/fphys.2019.00641.
- (139) Pickett, C. L.; Kornfeld, K. Age-Related Degeneration of the Egg-Laying System Promotes Matricidal Hatching in Caenorhabditis Elegans. *Aging Cell* **2013**, *12* (4), 544–553. https://doi.org/10.1111/acel.12079.
- (140) Inceoglu, B.; Wagner, K.; Schebb, N. H.; Morisseau, C.; Jinks, S. L.; Ulu, A.; Hegedus, C.; Rose, T.; Brosnan, R.; Hammock, B. D. Analgesia Mediated by Soluble Epoxide Hydrolase Inhibitors Is Dependent on CAMP. *Proc. Natl. Acad. Sci. U. S. A.* **2011**, *108* (12), 5093–5097. https://doi.org/10.1073/pnas.1101073108.
- (141) Inceoglu, B.; Zolkowska, D.; Yoo, H. J.; Wagner, K. M.; Yang, J.; Hackett, E.; Hwang, S. H.; Lee, K. S. S.; Rogawski, M. A.; Morisseau, C.; Hammock, B. D. Epoxy Fatty Acids and Inhibition of the Soluble Epoxide Hydrolase Selectively Modulate GABA Mediated Neurotransmission to Delay Onset of Seizures. *PLoS One* **2013**, 8 (12), e80922. https://doi.org/10.1371/journal.pone.0080922.
- (142) Stiernagle, T. Maintenance of C. Elegans. *WormBook* **2006**, 1–11. https://doi.org/10.1895/wormbook.1.101.1.
- (143) Clay, K. J.; Petrascheck, M. Design and Analysis of Pharmacological Studies in Aging. *Methods Mol. Biol.* **2020**, *2144*, 77–89. https://doi.org/10.1007/978-1-0716-0592-9\_7.
- (144) Wang, H.; Zhao, Y.; Zhang, Z. Age-Dependent Effects of Floxuridine (FUdR) on Senescent Pathology and Mortality in the Nematode Caenorhabditis Elegans. *Biochem. Biophys. Res. Commun.* **2019**, *509* (3), 694–699. https://doi.org/10.1016/j.bbrc.2018.12.161.
- (145) Gandhi, S.; Santelli, J.; Mitchell, D. H.; Wesley Stiles, J.; Rao Sanadi, D. A Simple Method for Maintaining Large, Aging Populations of Caenorhabditis Elegans. *Mech. Ageing Dev.* **1980**, *12* (2), 137–150. https://doi.org/10.1016/0047-6374(80)90090-1.
- (146) Mitchell, D. H.; Stiles, J. W.; Santelli, J.; Sanadi, D. R. Synchronous Growth and Aging of Caenorhabditis Elegans in the Presence of Fluorodeoxyuridine. *J. Gerontol.* **1979**, *34* (1), 28–36. https://doi.org/10.1093/geronj/34.1.28.
- (147) Rahman, M.; Edwards, H.; Birze, N.; Gabrilska, R.; Rumbaugh, K. P.; Blawzdziewicz, J.; Szewczyk, N. J.; Driscoll, M.; Vanapalli, S. A. NemaLife Chip: A Micropillar-Based Microfluidic Culture Device Optimized for Aging Studies in Crawling C. Elegans. *Sci. Rep.* **2020**, *10* (1), 16190. https://doi.org/10.1038/s41598-020-73002-6.

- (148) Bansal, A.; Zhu, L. J.; Yen, K.; Tissenbaum, H. A. Uncoupling Lifespan and Healthspan in Caenorhabditis Elegans Longevity Mutants. *Proc. Natl. Acad. Sci. U. S. A.* **2015**, *112* (3), E277-86. https://doi.org/10.1073/pnas.1412192112.
- (149) Hosono, R.; Mitsui, Y.; Sato, Y.; Aizawa, S.; Miwa, J. Life Span of the Wild and Mutant Nematode Caenorhabditis Elegans. Effects of Sex, Sterilization, and Temperature. *Exp. Gerontol.* **1982**, *17* (2), 163–172. https://doi.org/10.1016/0531-5565(82)90052-3.
- (150) Hosono, R. Sterilization and Growth Inhibition of Caenorhabditis Elegans by 5-Fluorodeoxyuridine. *Exp. Gerontol.* **1978**, *13* (5), 369–374. https://doi.org/10.1016/0531-5565(78)90047-5.
- (151) Greer, E. L.; Brunet, A. Different Dietary Restriction Regimens Extend Lifespan by Both Independent and Overlapping Genetic Pathways in C. Elegans. *Aging Cell* **2009**, 8 (2), 113–127. https://doi.org/10.1111/j.1474-9726.2009.00459.x.
- (152) Aitlhadj, L.; Stürzenbaum, S. R. The Use of FUdR Can Cause Prolonged Longevity in Mutant Nematodes. *Mech. Ageing Dev.* **2010**, *131* (5), 364–365. https://doi.org/10.1016/j.mad.2010.03.002.
- (153) Van Raamsdonk, J. M.; Hekimi, S. FUdR Causes a Twofold Increase in the Lifespan of the Mitochondrial Mutant Gas-1. *Mech. Ageing Dev.* **2011**, *132* (10), 519–521. https://doi.org/10.1016/j.mad.2011.08.006.
- (154) Anderson, E. N.; Corkins, M. E.; Li, J.-C.; Singh, K.; Parsons, S.; Tucey, T. M.; Sorkaç, A.; Huang, H.; Dimitriadi, M.; Sinclair, D. A.; Hart, A. C. C. Elegans Lifespan Extension by Osmotic Stress Requires FUdR, Base Excision Repair, FOXO, and Sirtuins. *Mech. Ageing Dev.* **2016**, *154*, 30–42. https://doi.org/10.1016/j.mad.2016.01.004.
- (155) Harris, T. W.; Chen, N.; Cunningham, F.; Tello-Ruiz, M.; Antoshechkin, I.; Bastiani, C.; Bieri, T.; Blasiar, D.; Bradnam, K.; Chan, J.; Chen, C.-K.; Chen, W. J.; Davis, P.; Kenny, E.; Kishore, R.; Lawson, D.; Lee, R.; Muller, H.-M.; Nakamura, C.; Ozersky, P.; Petcherski, A.; Rogers, A.; Sabo, A.; Schwarz, E. M.; Van Auken, K.; Wang, Q.; Durbin, R.; Spieth, J.; Sternberg, P. W.; Stein, L. D. WormBase: A Multi-Species Resource for Nematode Biology and Genomics. *Nucleic Acids Res.* **2004**, *32* (Database issue), D411-7. https://doi.org/10.1093/nar/gkh066.
- (156) Rahman, M.; Edwards, H.; Birze, N.; Gabrilska, R.; Rumbaugh, K. P.; Blawzdziewicz, J.; Szewczyk, N. J.; Driscoll, M.; Vanapalli, S. A. NemaLife: A Structured Microfluidic Culture Device Optimized for Aging Studies in Crawling C. Elegans. *bioRxiv*, 2019. https://doi.org/10.1101/675827.
- (157) Xian, B.; Shen, J.; Chen, W.; Sun, N.; Qiao, N.; Jiang, D.; Yu, T.; Men, Y.; Han, Z.; Pang, Y.; Kaeberlein, M.; Huang, Y.; Han, J.-D. J. WormFarm: A Quantitative Control and Measurement Device toward Automated Caenorhabditis Elegans Aging Analysis. *Aging Cell* **2013**, *12* (3), 398–409. https://doi.org/10.1111/acel.12063.

- (158) Shirure, V. S.; George, S. C. Design Considerations to Minimize the Impact of Drug Absorption in Polymer-Based Organ-on-a-Chip Platforms. *Lab Chip* **2017**, *17* (4), 681–690. https://doi.org/10.1039/c6lc01401a.
- (159) Regehr, K. J.; Domenech, M.; Koepsel, J. T.; Carver, K. C.; Ellison-Zelski, S. J.; Murphy, W. L.; Schuler, L. A.; Alarid, E. T.; Beebe, D. J. Biological Implications of Polydimethylsiloxane-Based Microfluidic Cell Culture. *Lab Chip* **2009**, *9* (15), 2132–2139. https://doi.org/10.1039/b903043c.
- (160) Guckenberger, D. J.; de Groot, T. E.; Wan, A. M. D.; Beebe, D. J.; Young, E. W. K. Micromilling: A Method for Ultra-Rapid Prototyping of Plastic Microfluidic Devices. *Lab Chip* **2015**, *15* (11), 2364–2378. https://doi.org/10.1039/c5lc00234f.
- (161) Jaquith, K. *ANSI/SLAS 1-2004 through 4-2004 microplate standards*. https://www.wellplate.com/ansi-slas-microplate-standards/ (accessed 2021-09-16).

# **APPENDIX 1:** SUPPORTING INFORMATION FOR CHAPTER 2

### TABLE OF CONTENTS

1. Supporting Figures and Tables (Figure S1-S8, and Table S)	218
2.Experimental Sections:	
3. Characterization of Synthesized compounds	248
BIBLIOGRAPHY	

### 1. Supporting Figures and Tables (Figure S1-S8, and Table S1):

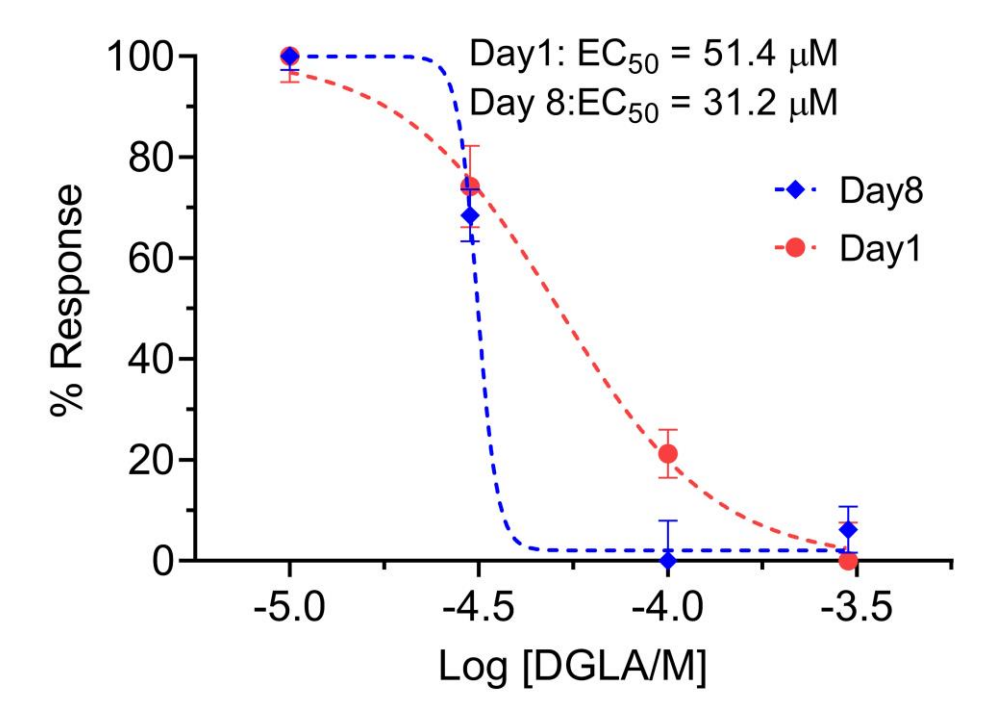


**Figure S1:** Dose response curve: the effect of different DGLA concentrations on degeneration of ADE neurons at Day 1 and Day 8 of adulthood. The slope for dose response curve on day 8 adulthood is significantly different compared to day1 adulthood, suggesting there may be different mechanism for neurodegeneration at these 2 timepoints.

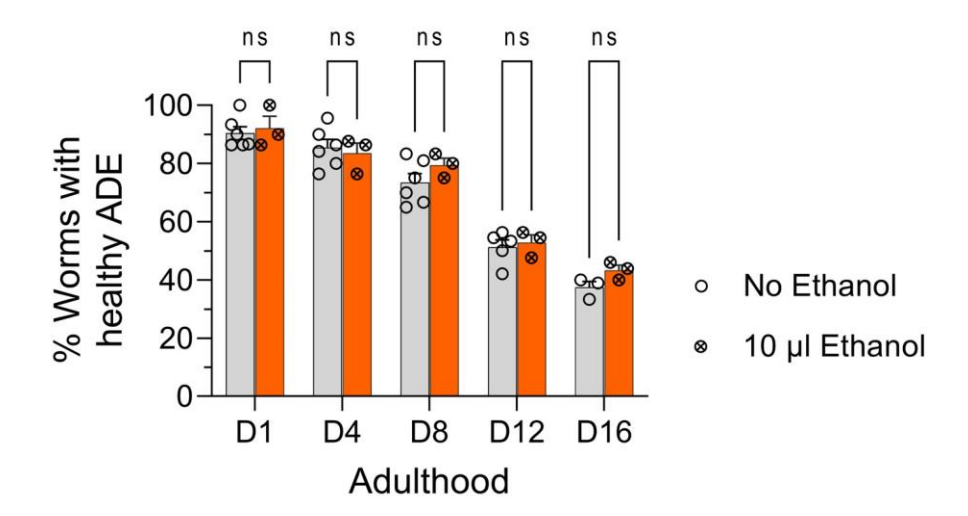


**Figure S2:** Ethanol does not alter ADE neuron phenotypes. Percentage (%) of worms with healthy ADE dopaminergic neurons in *dat-1::gfp* transgenic worms +/- supplementation with 10  $\mu$ l absolute ethanol. This test was done to determine whether ethanol in PUFA supplementation (which is 10  $\mu$ l) affects the overall healthspan of dopaminergic neurons. N=3, and about 20 worms were tested in each replicate. Two-way analysis of variance (ANOVA), Tukey's multiple comparison test, \*P  $\leq$  0.05, \*\*P  $\leq$  0.01, \*\*\*P  $\leq$  0.001, \*\*\*\*P  $\leq$  0.0001, ns: not significant.

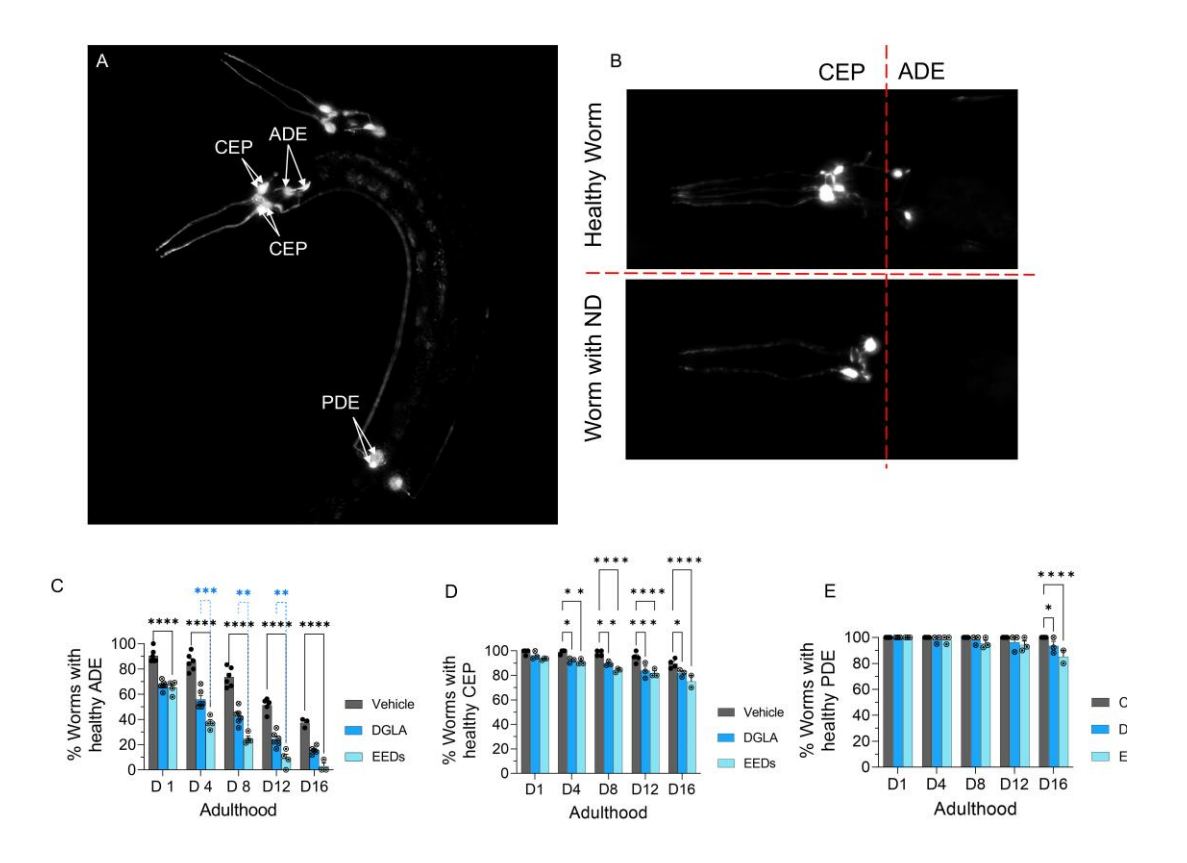


**Figure S3:** Different types of dopaminergic neurons in the hermaphrodite have varying sensitivity to the treatment with DGLA or EEDs. (A). Normal dopaminergic neurons in *C. elegans* labeled with *dat-1::gfp*, (B) Healthy worms (top) and degenerated dopaminergic neurons (bottom). (C) Percentage (%) of worms with healthy ADE dopaminergic neurons in *dat-1::gfp* transgenic +/- supplementation with 100 μM of DGLA or EEDs. (D) Percentage (%) of worms with healthy CEP dopaminergic neurons in *dat-1::gfp* transgenic worms +/1 supplementation with 100 μM of DGLA or EEDs. (E) Percentage (%) of worms with healthy PDE dopaminergic neurons in *dat-1::gfp* transgenic +/- supplementation with 100 μM of DGLA or EEDs. For all experiments N=3, and about 20 worms were tested for each replicate. A two-way analysis of variance (ANOVA), Tukey's multiple comparison test, \*P ≤ 0.05, \*\*P ≤ 0.01, \*\*\*P ≤ 0.001, \*\*\*\*P < 0.0001, ns: not significant.

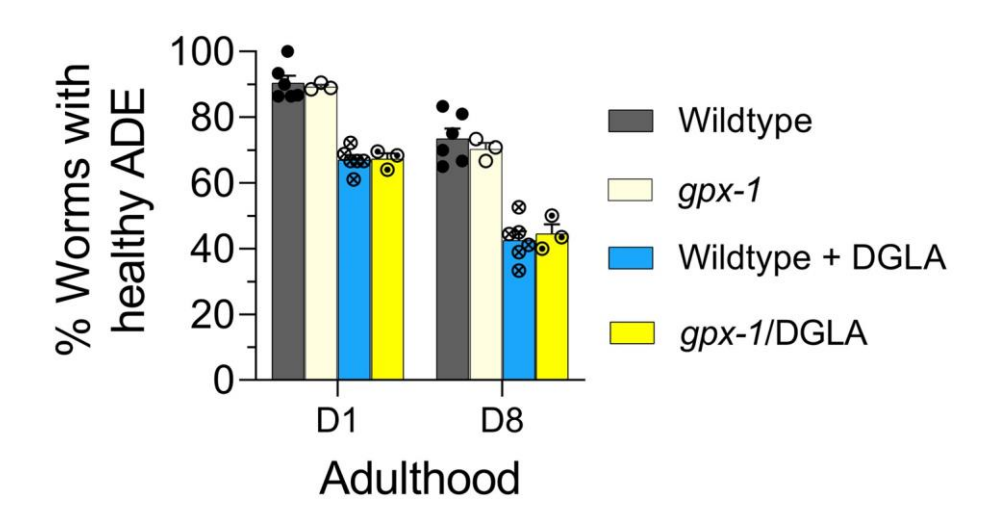


**Figure S4:** The genetic knockout of *gpx-1* does not result any observable changes of DGLA-induced neurodegeneration in dopaminergic neurons. Percentage (%) of worms with healthy ADE neurons for *dat-1::gfp* and *gpx-1;dat-1::gfp* worms treated with 100 μM DGLA were show. This result suggests that DGLA could trigger ferroptosis-mediated neurodegeneration independent of the GPX pathway, which is not without precedent.

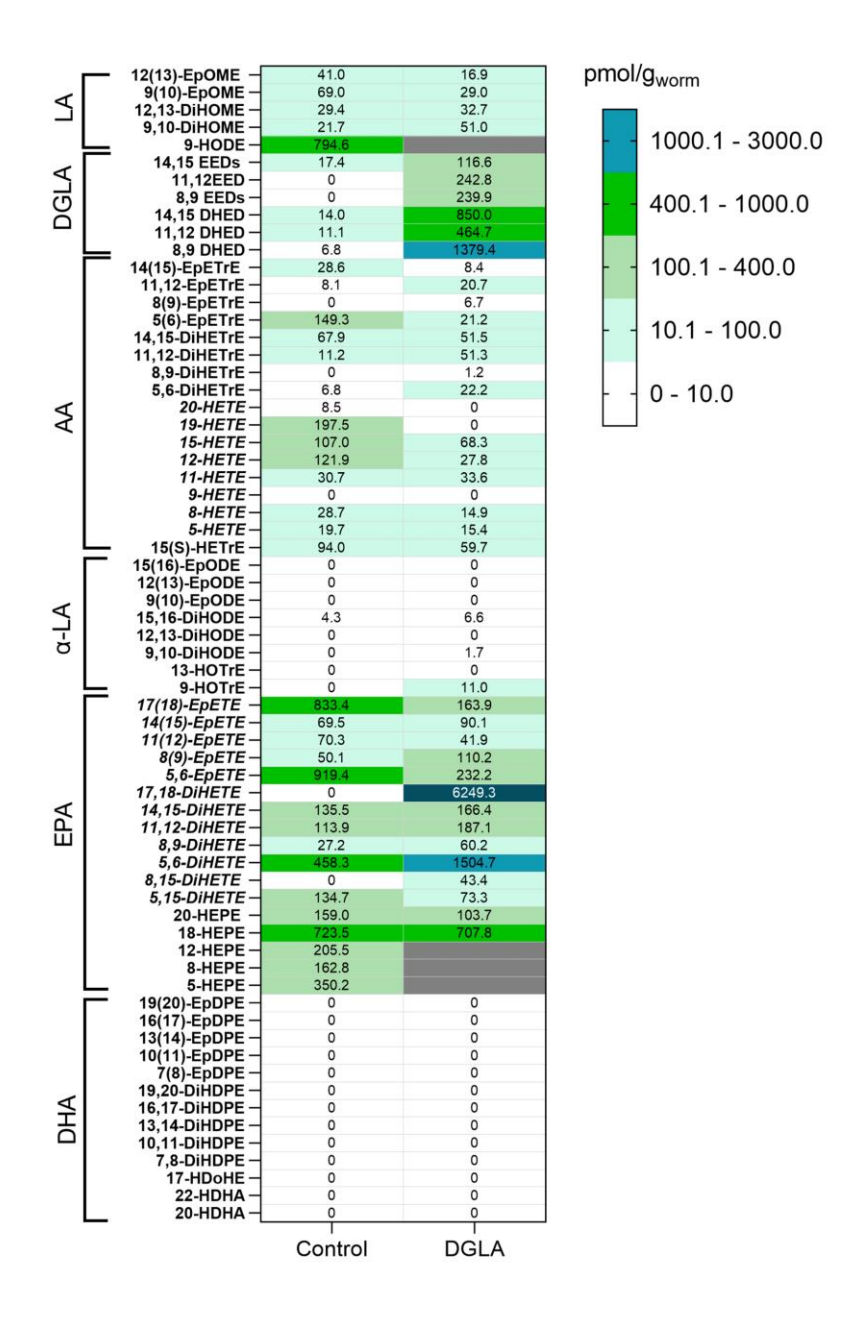


Figure S5: DGLA Supplementation significantly changes the EEDs and DHEDs levels in worm. Oxylipin profile representing the pmol/g of Epoxy- and dihydroxy- PUFA levels in worms treated with 100  $\mu$ M of DGLA compared to control. The worms were supplemented at the L4 stage and were tested at day 1 of adulthood. Black boxes represent the values are those that were inconsistent in different trials or were out of standard curve range.

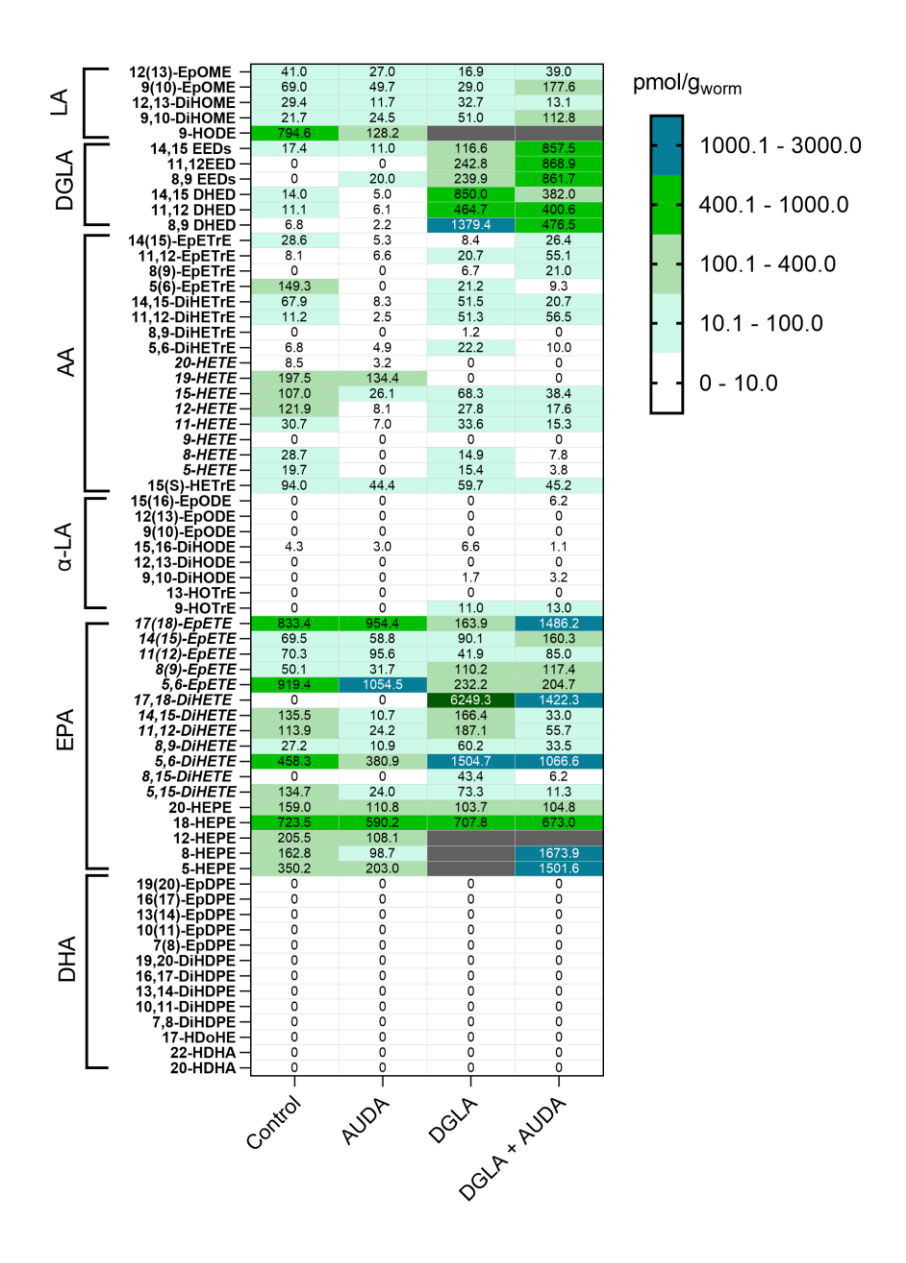


Figure S6: AUDA changes the EEDs and DHEDs levels in worm supplemented by DGLA, through inhibition of epoxide hydrolase enzyme. Oxylipin profile representing the pmol/g of Epoxy- and dihydroxy-PUFA level in worms treated with 100  $\mu$ M of DGLA  $\pm 100~\mu$ M AUDA compared to control. The worms were supplemented at the L4 stage and were tested at day 1 of adulthood. Black boxes represent the values are those that were inconsistent in different trials or were out of standard curve range.

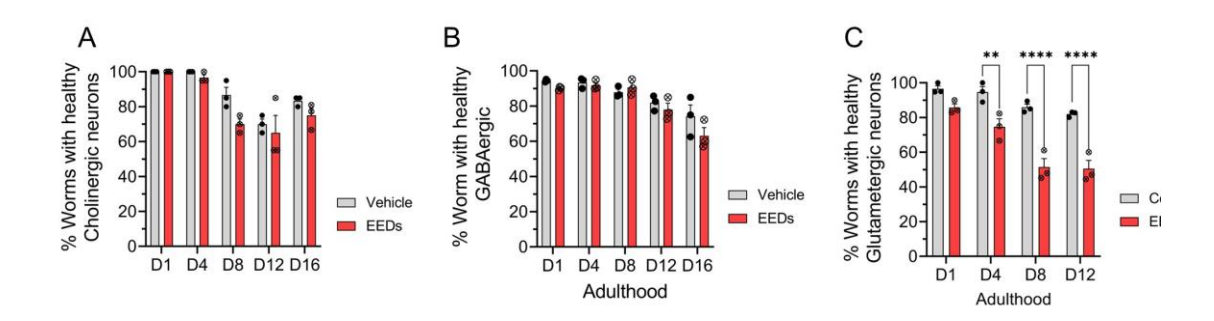


Figure S7: EEDs does not affect the neuronal healthspan of GABAergic and Cholinergic neurons, and its effect of glutamatergic neurons starts after day 4. The effect of 100  $\mu$ M of EEDs on various neuron types compared to vehicle. Percentage (%) of worms healthy (A) cholinergic neurons, (B) GABAergic neurons, and C) glutamatergic neurons. Worms are supplemented with 100  $\mu$ M of EEDs at the L4 stage. For all experiments N=3, and 20-30 worms were tested in each replicate. A two-way analysis of variance (ANOVA), Tukey's multiple comparison test, \*P  $\leq$  0.05, \*\*P  $\leq$  0.01, \*\*\*P  $\leq$  0.001, \*\*\*\*P < 0.0001, not significant is not shown.

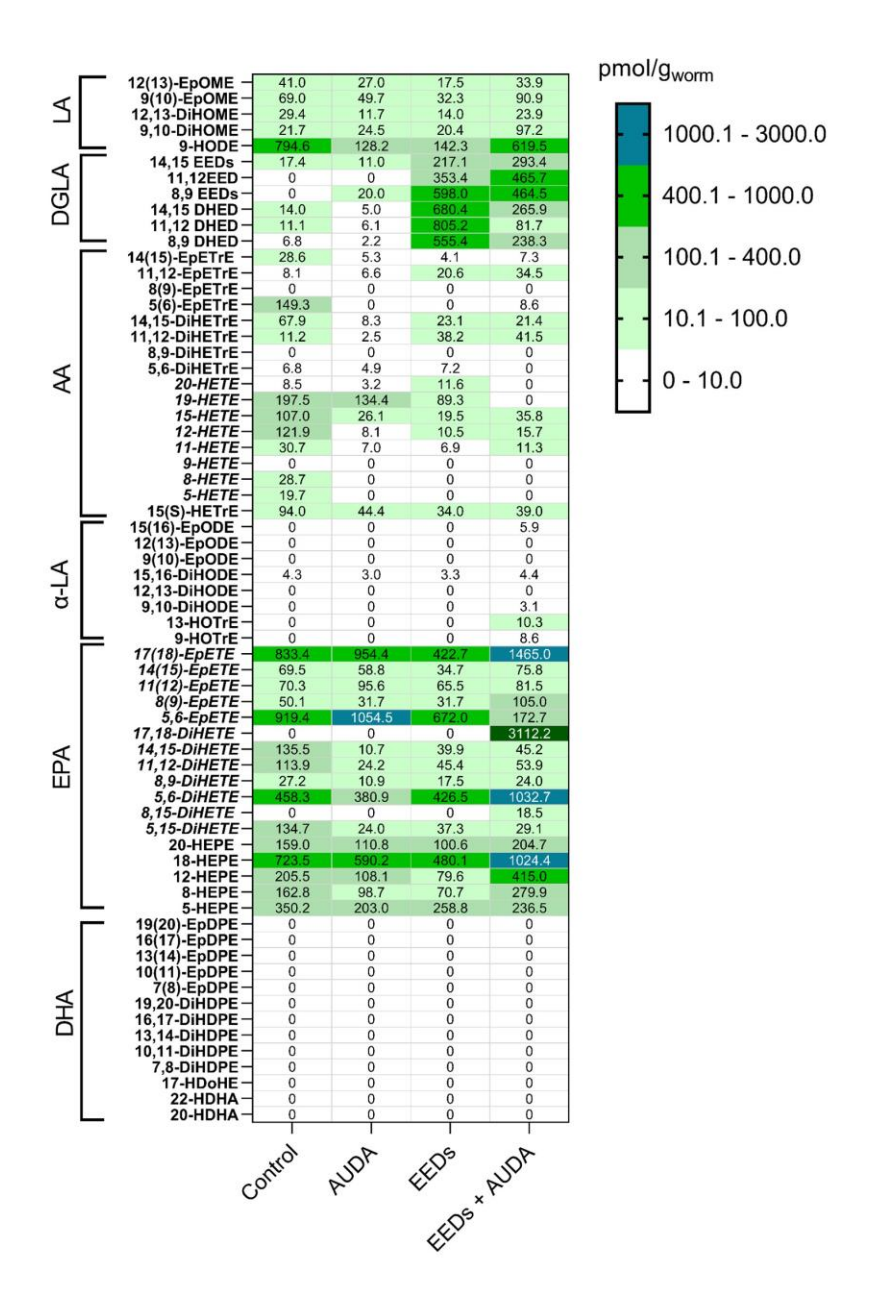
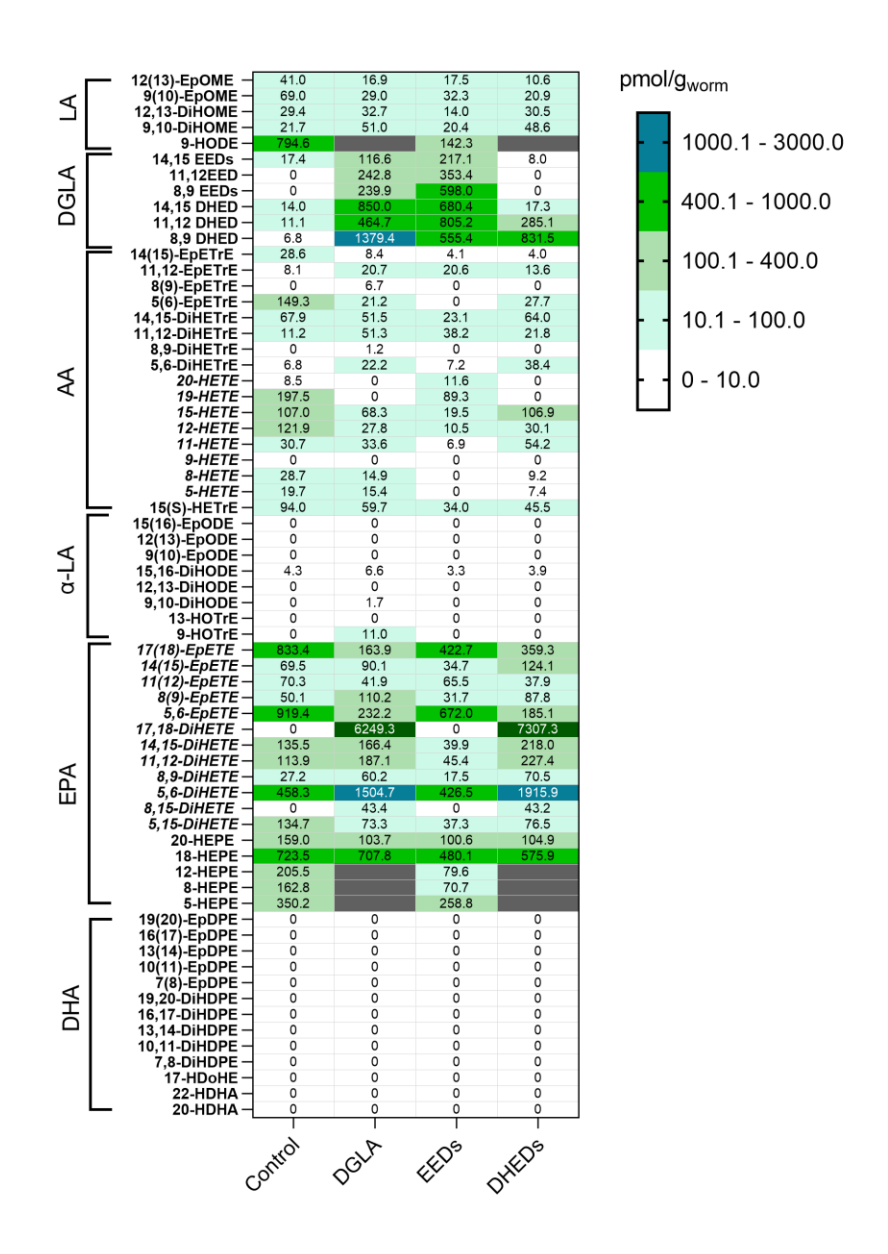


Figure S8: EEDs Supplementation significantly changes the EEDs and DHEDs levels in worm. AUDA changes the EEDs and DHEDs levels in worm supplemented by DGLA, through inhibition of epoxide hydrolase enzyme. Oxylipin profile representing the pmol/g of Epoxy- and dihydroxy- PUFA levels in worms treated with  $100~\mu M$  of EEDs  $\pm 100~\mu M$  AUDA compared to control. The worms were supplemented at the L4 stage, and were tested at day 1 of adulthood. Black boxes represent the values are those that were inconsistent in different trials or were out of standard curve range.



**Figure S9:** DGLA, EEDs, and DHEDs Supplementation alters the EEDs and DHEDs levels in worms. Oxylipin profile representing the pmol/g of Epoxy, hydroxy, and dihydroxy-PUFA regioisomers, CYP/EH metabolites in worms treated with  $100~\mu\text{M}$  of either DGLA or EEDs, or DHEDs compared to control. Worms were supplemented at the L4 stage and were tested at day 1 of adulthood. Black boxes represent the values those that were inconsistent in different trials or were out of standard curve range.

# 2. Experimental Sections:

## Reagent and resource

Table S1: Reagent and resource used in this study.

REAGENT or RESOURCE	SOURCE	IDENTIFIER
Trolox	Cayman Chemicals	Cat# 10011659; CAS: 53188-07-1
liproxstatin-1	BioVision	Cat#B2312-5,25;
2,2'-Bipyridine	Oakwood Chemical	Lot# 003434M03F; CAS: 366-18-7
Cholesterol	Alfa Aesar	Cat#A11470; CAS: 57-88-5
Agar	Fisher Bioreagents	Cat#BP9744-500; CAS: 9002-18-0
Bacto Agar	Becton, Dickinson, and Company	Cat# DIFCO 214010
Tryptone	Fisher Bioreagents	Cat#BP1421-500; CAS: 91079-40-2
Bacto Tryptone	Life Technologies Corporation	Cat# DIFCO 211705
Yeast Extract	Becton, Dickinson, and Company	Cat# DIFCO 212750
Sodium Chloride	VWR	Cat#BDH9286
Magnesium Sulfate heptahydrate	Fisher Chemical	Cat#M63-500; CAS: 10034-99-8
Potassium Phosphate, monobasic, crystal	Fisher Bioreagents	Cat#BP362-500; CAS: 7778-77-0
Potassium Phosphate, dibasic, powder	Fisher Chemical	Cat#P288-500; CAS: 7758-11-4
Calcium Chloride	Sigma-Aldrich	Cat#C1016-500; CAS: 10043-52-4
(anhydrous)		
Sodium Azide	Fisher Scientific	Cat#BP9221-500; CAS: 26628-22-8
Ethanol	Fisher Chemical	Cat#A409-4; CAS: 64-17-4
Arachidonic acid	NU-CHEK	Lot# U-71A-M31-B
DGLA	TCI Chemicals	Cat#E0640; CAS:1783-84-2
GLA	NU-CHEK	Lot#U-69A-D16-E
LA	NU-CHEK	Lot#U-62A-O21-E
EPA	NU-CHEK	Lot#U-99A-MA10-B
Hexane	Fisher Chemical	Lot#176581; CAS: 110-54-3
Acetic Acid	Fisher Scientific	Lot#193296; CAS: 64-19-7
Acetonitrile	Fisher Chemical	Lot#195771; CAS: 75-05-8
Chloroform	Acros Organic	Lot# B0541409A; CAS: 67-66-3
Methanol	Fisher Chemical	Lot#195771; CAS: 67-56-1
Acetone	Fisher Chemical	CAS: 67-64-1

## Deuterated standards used for oxylipin analysis

Table S2: Deuterated standards used in this study.

Oxylipin standard name	Oxylipin standard abbreviation
6-keto prostaglandin $F_{1\alpha}$ -d4	6-keto-PGF <sub>1α</sub> -d4
5(S)-hydroxyeicosatetrenoic-d8 acid	5(S)-HETE-d8
8,9-epoxyeicosatrienoic-d11 acid	8,9-EET-d11
Arachidonic-d8 acid	AA-d8
15(S)-hydroxyeicosatetraenoic-d8 acid	15(S)-HETE-d8
Prostaglandin B <sub>2</sub> -d4	PGB2-d4
8,9-dihydroxyeicosatrienoic-d11 acid	8,9-DiHETrE-d11
9(S)-hydroxyoctadecadienoic-d4 acid	9(S)-HODE-d4
Leukotriene B <sub>4</sub> -d <sup>4</sup>	LTB4-d4
Prostaglandin E <sub>2</sub> -d9	PGE2-d9

## Organisms/Strains

**Table S3:** *C. elegans* strains used in this study.

STRAIN	SOURCE	STRAIN
		NAME
N2 Bristol	Caenorhabditis Genetics Center	N2
CB767 <i>bli-3(e767)</i> I	Caenorhabditis Genetics Center	CB767
GA912 ftn-1(ok3625) V	David Gems (Jennifer watts)	GA912
MT1522 ced-3(n717) IV	Caenorhabditis Genetics Center	MT1522
FX2100 gpx-1(tm2100)	National Bioresource Project	FX2100
BZ555 [egls1 [Pdat-1:gfp)]	Caenorhabditis Genetics Center	BZ555
EM641 ( <i>Pcat-2::gfp</i> )	A gift from Scott W. Emmons	EM641
JKA76 [ced-3(n717); Pdat::gfp]	Generated in the lab of Jamie Alan	JKA76
JKA77 [bli-3(e767);Pdat-1::gfp]	Generated in the lab of Jamie Alan	JKA77
JKA78 [ftn-1(ok3625);Pdat-1::gfp]	Generated in the lab of Jamie Alan	JKA78
JKA79 [gpx-1(tm2100); Pdat::gfp]	Generated in the lab of Jamie Alan	JKA79

#### Software and Algorithms

**Table S4:** Software and Algorithms used in this study.

Microsoft Excel	Microsoft Corporation	N/A
ImageJ	Rasband, W.S.	https://imagej.nih.gov/ij/
BioRender	BioRender	https://biorender.com/
GraphPad Prism 6	GraphPad Software, Inc.	https://www.graphpad.com/

#### 2.1.C. elegans Strains and Maintenance

All nematode stocks were maintained on nematode growth media (NGM) plates seeded with bacteria (*E. coli* OP50) and maintained at 20°C unless otherwise noted. N2 Bristol (wild-type), MT1522 *ced-3(n717)*, and CB767 *bli-3(e767)*. The BY250 (P*dat-1::gfp*) was a gift form Dr. Randy Blakely (Florida Atlantic University). The EM641 (*cat-2::gfp*) strain was a gift from Dr. Scott W. Emmons (Albert Einstein College of Medicine, New York, United States). The GA912 *ftn-1(ok3625)* strain was a gift from Dr. David Gems (University College London, London, UK). Table S2 shows all the strains used in this study.

The JKA 76 [ced-3(n717); Pdat::gfp], JKA 77 [bli-3(e767);Pdat-1::gfp], and JKA 78 [ftn-1(ok3625);Pdat-1::gfp], and JKA 79 [gpx-1(tm2100); Pdat::gfp] strains were constructed using standard methods <sup>1</sup>.

#### 2.2.Age synchronized worms:

The age-synchronized population was prepared by transferring specific numbers (depending on the experiments and required number of progeny) of healthy and well-fed Day 1 adult worms to a fresh nematode growth media (NGM) with OP50, as described in previously published protocol <sup>2</sup>. The adult worms were allowed to lay eggs for 6-10 hours. The laid eggs were isolated and allowed to hatch. About 36-48 hours later, plates were washed off with s-basal

solution and transferred to a 40 µm cell strainer placed on top of a 50 mL centrifuge tube. The large sized L4 larvae stick to the filter, whereas eggs, larva, bacteria carryover or possible contamination were passed through the filter. L4 larvae were then washed with 75-100 µl of s-basal, transferred to a 1.7 ml centrifuge tube using a glass pipet, and spun at 325 x g on a table-top centrifuge for 30 s. The s-basal solution was removed by aspiration leaving behind a pellet of L4. Finally, L4 worms were resuspend in s-basal solution and transferred to the supplemented or control plates seeded with OP50.

During lifespan, every day the age synchronized population was filtered through a 40 µm cell strainer placed on top of a 50 mL centrifuge tube. The progeny was collected in the filtrate and removed. The age-synchronized adult worms were removed from the surface of the cell strainer and placed on a freshly seeded NGM/supplemented plate. The filtration process was repeated every day during early adulthood of the age synchronized population to avoid any contamination from the progeny, and to provide fresh supplementation for worm during their lifespan.

#### 2.3. Fatty acid supplementation:

In order to supplement worms with fatty acids and/or their downstream metabolites, 10 ul of each compound at desired concentration was spread on the NGM plate, and then immediately seeded with 250-400 µl E. *coli* OP50 (2.8 ×10<sup>8</sup> cell/ml). The seeded plates were sealed with parafilm? and kept for 2 days at room temperature (20-23°C) and then transferred to the refrigerator to be used later. In all experiments in this study, the NGM solution plates were made using standard methods<sup>3</sup>.

#### 2.4. Epoxide Hydrolase inhibitor supplementation:

For 12-(3-((3s,5s,7s)-adamantan-1-yl) ureido)dodecanoic acid (AUDA) supplementation, a 20 mM AUDA stock solution was prepared in ethanol, and then was added to NGM agar solution at 55-65 °C to reach the final concentration of 100  $\mu$ M before plating. Plates kept at room temperature for 1 day and then seeded by 250-400 ul *E. coli* OP50 (2.8 ×10<sup>8</sup> cell/ml).

#### 2.5. Supplementations for ferroptosis studies:

To study the possible role of DGLA and EEDs supplementation in ferroptosis, 10  $\mu$ l of 100  $\mu$ M of DGLA or EEDs was spread on NGM plates, followed by spreading 10  $\mu$ l of 100  $\mu$ M of liproxstatin-1 (Lip-1) solution in ethanol. Immediately after that, 250-400  $\mu$ l E. *coli* OP50 was plated and allowed to dry for two days. The plates were then either used immediately or kept in the fridge (4°C) for later use. The same procedure was used for the 2,2-bipyridine (BP) (100  $\mu$ M) and Trolox (500  $\mu$ M), For the control experiments, 10  $\mu$ l of ethanol solution was used.

#### 2.6. Fluorescence microscopy imaging for tracking dopaminergic neurons.

In order to track neurodegeneration, age-synchronized worms with *dat-1::gfp* transcriptional fusions were used. The age-synchronized worms were analyzed based on a previously published protocol with some modifications<sup>4</sup>. First agarose gel pad were prepared as previously described. (For quantitative analyses of changes in DAergic neuron cell morphology, 20-25 worms were mounted on the layer of the agar pad and paralyzed with 5 mM NaN<sub>3</sub> for 5 minutes (Fig.15). Finally, a coverslip was placed onto an agar pad containing worms. A fluorescent microscope (Eclipse Ti2-E–Nikon) was used to image the worms and NIS-Elements software was used to analyze the data. All 8 DAergic neurons were analyzed in each worm. The ADE neurons were the ones with significant neurodegeneration with the treatment of DGLA and its downstream metabolites. Therefore, in all microscopic tests in this study, neurodegeneration refers to the

absence of fluorescent signal in the ADE neurons. Worms with healthy ADE are those with both ADE cell bodies or processes that could be seen under fluorescent microscope. The same procedure was followed for dopaminergic neuron analyses using the *cat-2*::gfp (EM641).

#### 2.7.Oxylipin Analysis:

#### i. Step 1: Collecting and freezing worm samples for oxylipin analysis

Oxylipins are a class of bioactive oxidized lipid metabolites derived from PUFAs via cyclooxygenase (COX), lipoxygenase (LOX), and cytochrome P450 (CYP) enzymatic pathways. To investigate the oxylipin profile in C. elegans, we collected about 5 mg of worms per trial to ensure that the whole worm lysates contain a sufficient concentration of oxylipins for detection. A sufficiently sized population of worms was generated using a minimum of 7 P100 plates with a diameter of 100 mm?, per trial. To generate 5 mg of whole worm lysates, we prepared approximately 2000-3000 worms (300-400 worms per plate). The age-synchronized population of worms was generated and maintained using the filtration method illustrated and described above. When a population of worms was ready for isolation and collection, the entire population of seven plates per trial was transferred and filtered using s-basal solution and a cell strainer with a pore size of 40 µm. The worms that collected on the surface of the cell strainer were transferred using a Pasteur pipet to an Eppendorf vial to avoid C. elegans from sticking on the wall of the pipet. The worms were rinsed with s-basal medium and centrifuged. The supernatant was collected and discarded. The worms were then washed four more times with s-basal medium to ensure that all bacteria and PUFA supplements were removed. After the bacteria and supplements were removed, the Eppendorf vials containing each worm sample were transferred to a benchtop centrifuge. The vials were centrifuged for 10 minutes at 10,000 rpm at 4°C. The supernatant was removed using

100 µL and 10 mL pipets. A 20 mL pipet with a long tip was pushed to the bottom of the vial to remove the liquid between the worms. Lastly, the standard filter paper was cut and inserted into the Eppendorf vials to remove any remaining liquid within the worm sample. After all liquid was removed, the worm samples flash frozen using liquid nitrogen and stored in the -80°C freezer. Collection of worms for oxylipin and lipidomic analysis is illustrated in Figure S10.

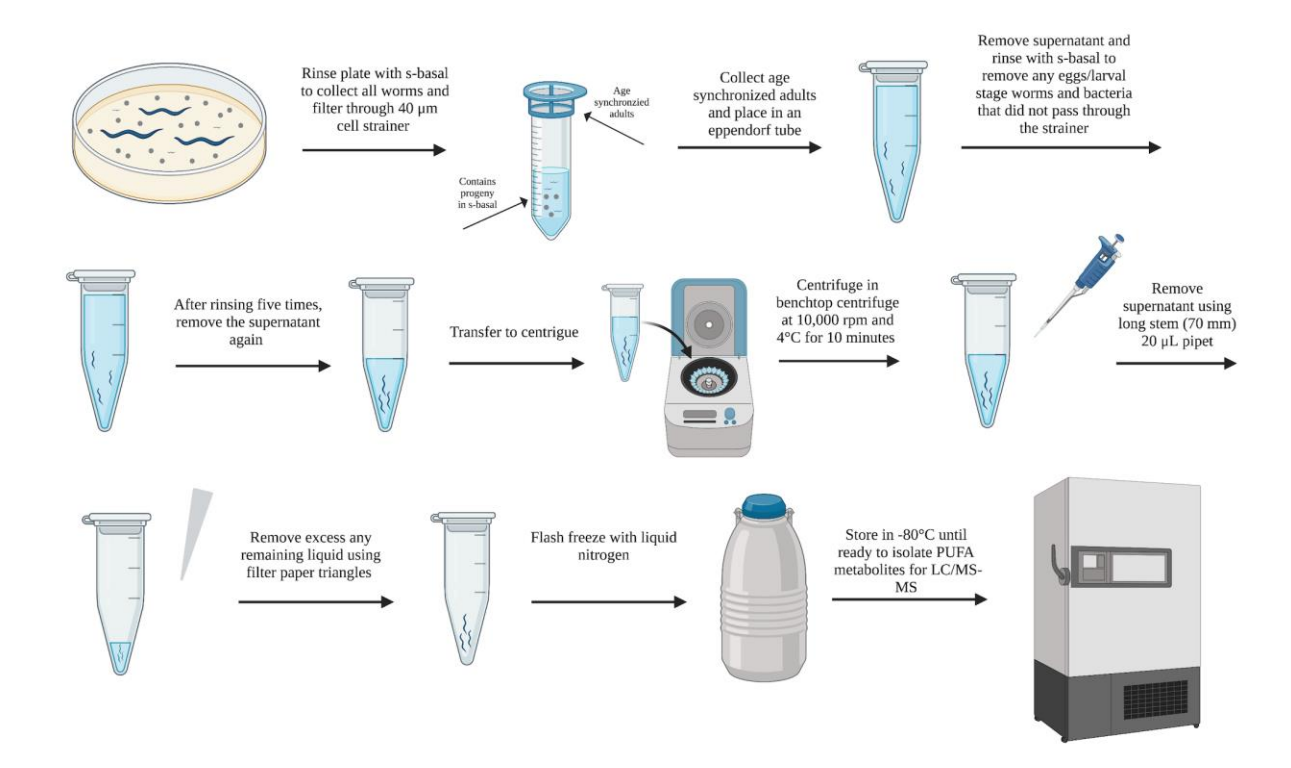
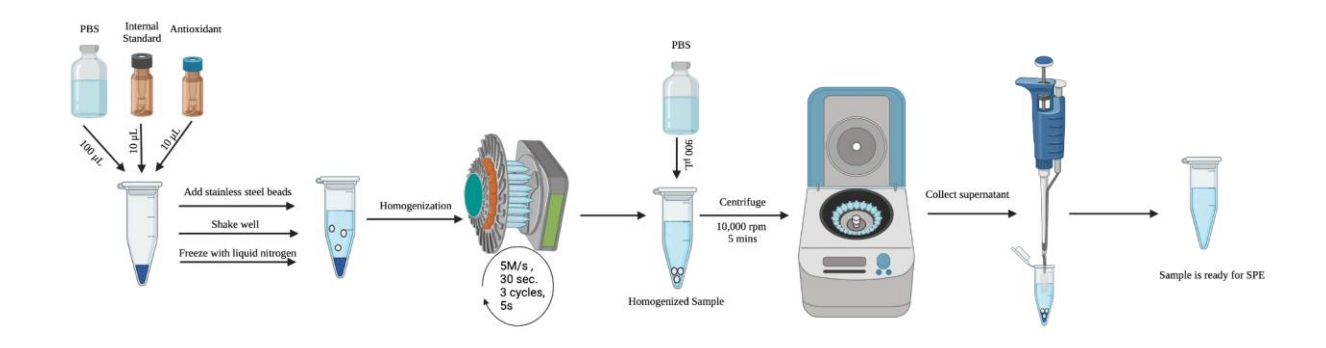


Figure S10. Worm sample preparation for oxylipin and analysis

#### ii. Step 2: Worm homogenization for oxylipin analysis

Eppendorf vials containing worms were removed from -80°C storage. The weight of one 2 mL cryogenic homogenizer vial per trial was recorded. The worm samples were flash frozen using liquid nitrogen, and the frozen worm samples were broken loose using a 0.7 mm needle. The worm samples were transferred to the homogenizer vial and the weight was recorded. The weight of each

vial with the worms was measured to determine the weight of worms used for each trial. Three homogenization beads were added to each homogenizer vial. Additionally, 100 μL phosphate-buffered saline (PBS), 10 μL of internal standard, consisting of 10 μL deuterated oxylipins, and 10μL of antioxidants, consisting of ethylenediamine tetraacetic acid (EDTA) (1 mg/ml in water), butylated hydroxytoluene (BHT) (0.2 mg/ml in methanol), and triphenylphosphine (TPP) (0.2 mg/ml in Ethanol). The details of the deuterated oxylipin standards are shown in Table S5. Each homogenizer vial containing the worm samples was flash frozen using liquid nitrogen and then homogenized for five 30-second cycles at 5 M/s using an Omni bead ruptor 24 homogenizers. After homogenization, an additional 900 μL of PBS was added to the homogenized sample. The sample was centrifuged using a benchtop centrifuge at 10,000 rpm for 5 minutes. The supernatant was collected and transferred to a new Eppendorf for solid phase extraction. The process of homogenization is illustrated in Figure S11.



**Figure S11.** Worm homogenization for oxylipin analysis

**Table S5**: Deuterated standards used for oxylipin analysis.

Oxylipin standard name	Oxylipin standard abbreviation
6-keto prostaglandin F <sub>1α</sub> -d4	$6$ -keto-PGF <sub>1<math>\alpha</math></sub> -d4
5(S)-hydroxyeicosatetrenoic-d8 acid	5(S)-HETE-d8
8,9-epoxyeicosatrienoic-d11 acid	8,9-EET-d11
Arachidonic-d8 acid	AA-d8
15(S)-hydroxyeicosatetraenoic-d8 acid	15(S)-HETE-d8
Prostaglandin B <sub>2</sub> -d4	PGB2-d4
8,9-dihydroxyeicosatrienoic-d11 acid	8,9-DiHETrE-d11
9(S)-hydroxyoctadecadienoic-d4 acid	9(S)-HODE-d4
Leukotriene B <sub>4</sub> -d4	LTB4-d4
Prostaglandin E <sub>2</sub> -d9	PGE2-d9

#### iii. Step 3: Solid phase extraction to isolate the oxylipins from the whole worm lysate

To isolate the oxylipins from the whole worm lysates solid phase extraction (SPE) (Waters Oasis-HLB cartridges, (Part No. WAT094226, Lot No. 176A30323A) was used. We used a polar stationary phase to trap the extremely polar biological material such as sugars. The oxylipins that we are isolating are significantly less polar in comparison. The SPE column was prepared by sequential washing with 2 mL ethyl acetate, 2 mL methanol twice, and 2 mL of 95:5 (v/v) mixture of water and methanol containing 0.1% acetic acid. The column was kept moist during preparation. The process of SPE column preparation is illustrated in Figure S12.

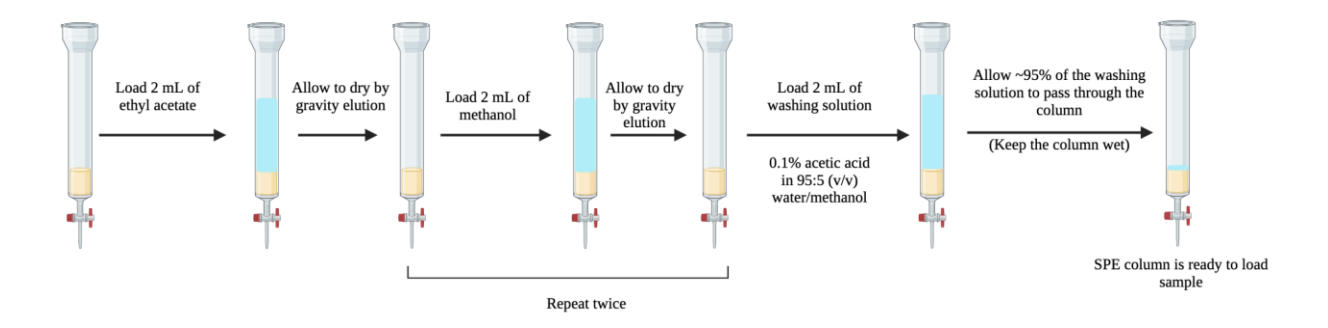


Figure S12. Solid phase extraction column preparation

After the SPE column was prepared, the Eppendorf vials containing the homogenized samples were loaded onto the SPE column. After the column was loaded with the sample by gravity, 1.5 mL of the washing solution, 95:5 (v/v) mixture of water and ethanol with 0.1% acetic acid, was added to the column. The column was dried by gravity. Next, the column was thoroughly dried with a vacuum pump for 20 minutes. After thorough drying, the column was ready for elution. The process of loading the sample to the SPE column is illustrated in the Figure S13.

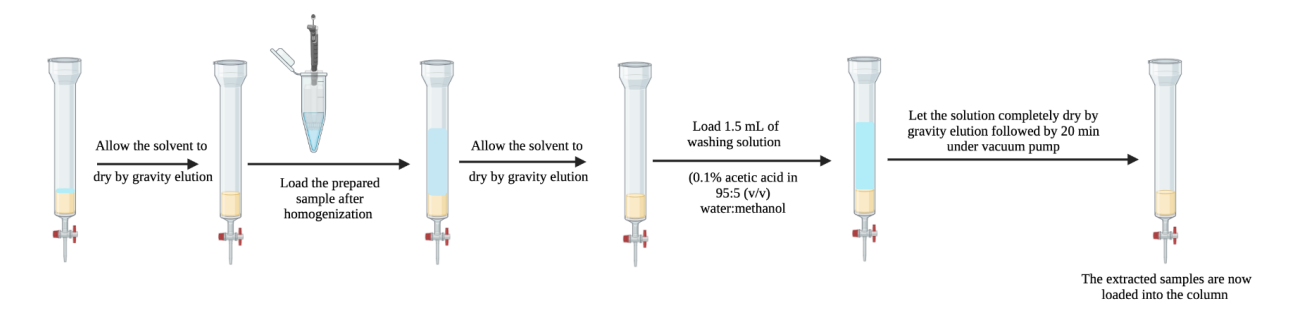
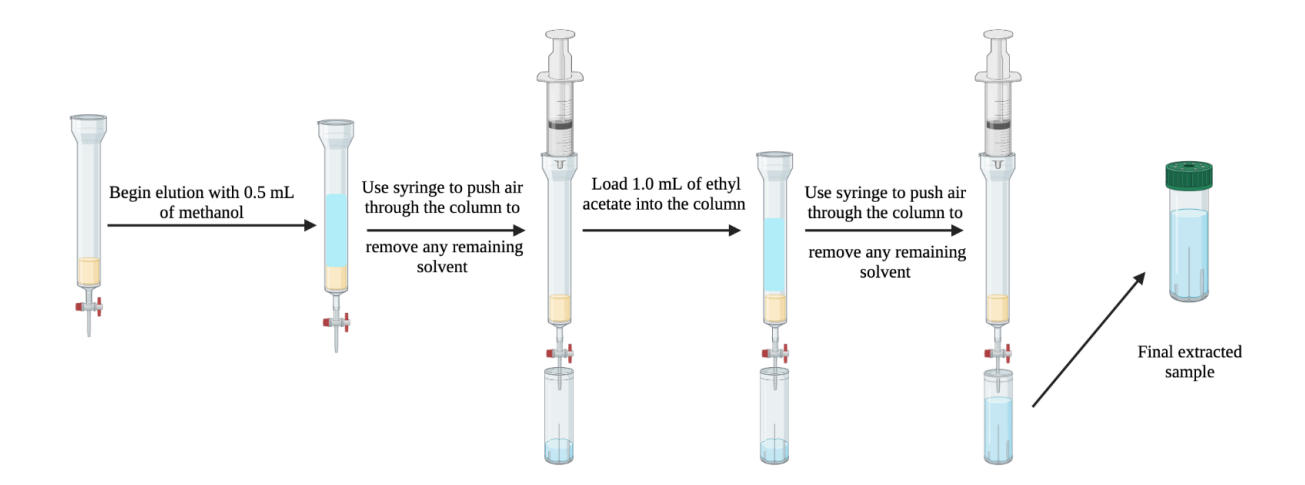


Figure S13. Loading the sample to the SPE column

After the column was loaded with the sample and completely dried, 0.5 mL of methanol was added to begin the elution step. Eluted compounds were collected to an Eppendorf vial containing 6 µL of 30% glycerol in methanol, which serves as a trap solution. The column was allowed to gravity elute until the column appeared dry. A 5 mL syringe was filled with air and placed on the top of the SPE column to gently push the remaining solvent out of the column with air. Once the column was completely dry, 1 mL of ethyl acetate was added to the column. The solvent was allowed to gravity elute until the column appeared dry to the eye. The remaining solvent was again removed using a 5 mL syringe and gently pushing air through the column. The process of eluting is illustrated in Figure S14.



**Figure S14.** Elution of oxylipins from SPE column.

Upon completion of SPE, the final extracted sample was dried using a speed-vac until the trap solution was all that remained. The residues were reconstituted with 100  $\mu$ L of 75% methanol/water containing 10 nM of internal standard, 12-[(cyclohexylcarbamoyl)amino]dodecanoic acid (CUDA). The samples were then mixed on a vortex for five minutes and filtered with a 0.45  $\mu$ m filter. Lastly, the samples were transferred to auto-sampler vials with salinized inserts, purged with argon gas, and stored at -80°C until injection.

#### iv. Step 4: Oxylipin analysis using LC/MS-MS

The LC conditions were optimized to separate all eicosanoids of interest with the desired peak shape and signal intensity using an XBridge BEH C18 2.1x150mm HPLC column. The mobile phase A comprised of 0.1% acetic acid in water. Mobile phase B consisted of acetonitrile: methanol (84:16) with 0.1% glacial acetic acid. Gradient elution was performed at a flow rate of 250 μL /min. Chromatography was optimized to separate all analytes in 20 min. The autosampler, Waters ACQUITY FTN, was kept at 10°C. The column was connected to a TQXS tandem mass spectrometer (Waters) equipped with Waters Acquity SDS pump and Waters Acquity CM detector. Electrospray was operated as ionization source for negative multiple reaction monitoring

(MRM) mode. To generate the best selectivity and sensitivity, each analyte standards were infused into the mass spectrometer and multiple reaction monitoring was used to analyze the desired compound.

#### 2.8. Synthesis of Diepoxyeicosaenoic acid (DiEEMe) and DLGA THF-diols

#### 1. General synthesis Methods

Reactions using air-sensitive reagents were conducted under an inert atmosphere of argon. All purchased chemicals were used as received (without further purification). Dihomo-gamma linoleic acid (DGLA) was purchased from Nu-Chek-Prep. SiliCycle irregular silica gel p60 (60, 230-400 mesh) was used for column chromatography and AnalTech 250 micron silica gel plates were used for analytical thin layer chromatography and visualized using either vanillin or KMnO<sub>4</sub> stain. <sup>1</sup>H and <sup>13</sup>C NMR spectra were collected at 25°C on Carian Inova 500 MHz instrument and reported in parts per million (ppm) relative to the solvent resonances ( $\delta$ ), with coupling constants (J) in Hertz (Hz). High-resolution mass spectroscopy (HRMS) data was collected on a Waters Xevo G2-XS UPLC/MS/MS Quadrupole/Time-of-Flight instrument. High-performance liquid chromatography (HPLC) was performed on a Rainin HPXL instrument with a Dynamax Absorbance Detector Model UV-D detection system with a Zorbax Sil 9.4 mm x 25 cm column (5 micron particle size, 100 Angstrom pore size). Gas-chromotography/mass spectroscopy (GC/MS) was performed on an Agilent Technologies 7890A GC system with an Agilent Technologies 5975C inert XL EI/CI MSD Triple-Axis Detector, and Agilent HP-5ms Fused Silica Capillary Column with 0.25 micron film thickness, 30 m long, and 0.25 mm inner diameter.

#### 2. Synthesis of Diepoxyeicosaenoic acid (DiEEMe) (1a - 1c):

**Scheme S1.** Synthesis of Diepoxyeicosaenoic acid (DiEEMe)

Methyl dihomo-gamma linoleate (1.569 mmol, 0.500 grams, 1 equiv.) was dissolved in 40 mL of dichloromethane (DCM). Meta-chloroperbenzoic acid (*m*-CPBA) (3.296 mmol, 0.813 grams, 2.1 equiv.) was added followed by saturated aqueous NaHCO<sub>3</sub> (40 mL) and the reaction was stirred vigorously under argon atmosphere at rt for 2 hours. Then, the organic layer was separated and collected. The aqueous phase was extracted with DCM (20 mL) for three times. The combined organic layers were washed with saturated aqueous NaHCO<sub>3</sub> (3 x 15 mL), brine (1 x 15 mL), dried over Na<sub>2</sub>SO<sub>4</sub>, and concentrated under reduced pressure to afford a clear oil. The crude product was purified with column chromatography (5–10% EtOAc/Hexanes) to afford 1a – 1c as a clear oil (mixture of regioisomers) (0.318 grams, 58% yield). HRMS (ES+): calculated C<sub>21</sub>H<sub>36</sub>O<sub>4</sub>Na+ [M+Na]+ 375.2506 observed 375.2519. For <sup>1</sup>H and <sup>13</sup>C NMR of mixture and separated fractions, see spectra below.† See characterization in Appendix.

#### 3. Synthesis of DLGA THF-diols (2-3):

**Scheme S2.** Synthesis of DLGA THF-diols

DGLA diepoxides (**1a** – **1c**) (0.902 mmol, 0.318 grams, 1 equiv.) was dissolved in 7.5 mL of aq. 5% HClO<sub>4</sub>, THF, and H<sub>2</sub>O (1:3:1) and stirred at rt under argon atmosphere overnight. Then, the reaction was cooled to 0°C and quenched with 15 mL of saturated aqueous NaHCO<sub>3</sub>. The reaction was diluted with 25 mL of EtOAc, the layers separated and the organic layer was collected. The aqueous phase was extracted with 3 x 10 mL of EtOAc. The combined organic layers were washed with saturated aqueous NaHCO<sub>3</sub> (3 x 15 mL), brine (1 x 15 mL), dried over Na<sub>2</sub>SO<sub>4</sub>, and concentrated under reduced pressure to afford the crude product as a clear oil. Purification via column chromatography (50% EtOAc/Hexanes) gave **2** – **3** as a clear oil (mixture of structural and stereoisomers) (0.109 grams, 33% yield). HRMS (ES+): calculated C<sub>21</sub>H<sub>38</sub>O<sub>5</sub>Na+ [M+Na]+ 393.2611 observed 393.2625. For <sup>1</sup>H and <sup>13</sup>C NMR of mixture, (See characterization section in APPENDIX1).

#### 4. Determination of Isomeric Ratios of DGLA THF-Diols:

**Scheme S3.** Isomeric structures of DGLA THF-Diols

Isomers of a mixture of DGLA diepoxides (1a–1c) were separated via HPLC (1% isopropanol/hexanes, 2 mL/min), giving 5 fractions (retention times, in minutes, were 18.6, 22.1, 23.8, 25.5, and 27.6 for fractions 1 – 5, respectively, see fFgure S35). Each fraction was subjected to <sup>1</sup>H and gCOSY NMR analysis (The <sup>1</sup>H NMR and gCOSY spectra of these fractions in Figures S36-S46.), leading to identification of isomer (4) and showing that the HPLC separation yielded two diastereomeric pairs of isomers 2 & 3. Following acid hydrolysis of each isolated fraction, isomer 4 was confirmed with low resolution mass spectroscopy (LRMS).

To prepare samples for GC/MS analysis, each of the other 4 fractions were individually dissolved **THF** mL of and incubated with 15 equivalents N.O-Bis(trimethylsilyl)trifluoroacetamide (BSTFA) and pyridine at 60°C for 30 minutes. The samples were dried under a stream of nitrogen, resuspended in DCM, and analyzed via GC/MS. Unique fragmentation patterns then successfully identified isomers 2 and 3 (GC/MS data, pages 62-70). Once the peaks (F1 – F5, see HPLC trace) were identified, relative ratios were determined by taking the total area of each diastereomeric isomer pair divided by the total area of all peaks (F1 – F5) obtained on HPLC trace.

#### 5. Synthesis of DGLA monoepoxide esters (5a - 5c):

**Scheme S4.** Synthesis of DGLA monoepoxide esters

Methyl dihomo-gamma linoleate (3.112 mmol, 1.000 grams, 1 equiv.) was dissolved in DCM (80 mL). Meta-chloroperbenzoic acid (*m*-CPBA) (3.423 mmol, 0.767 grams, 1.1 equiv.) was added followed by saturated aqueous NaHCO<sub>3</sub> (80 mL) and the reaction stirred vigorously under argon atmosphere at room temperature for 1 hour. Then, the layers were separated, and the aqueous phase extracted with DCM (3 x 20 mL). The combined organic layers were washed with saturated aqueous NaHCO<sub>3</sub> (3 x 15 mL), brine (1 x 15 mL), dried over Na<sub>2</sub>SO<sub>4</sub>, and concentrated under reduced pressure to afford a clear oil. The crude product was purified with column chromatography (5–10% EtOAc/Hexanes) to afford 5a – 5c as a clear oil (mixture of regioisomers,0.513 grams, 49% yield). Product 5a – 5 c was carried forward without further characterization.

#### 6. Synthesis of dihydroxyeicosadienoic acid (DHEDs) (6a - 6c):

COOMe COOMe 
$$O \oplus Cs$$
 (5 equiv.)

DMF, 120 °C, 3 days, then;
LiOH (5 equiv.), THF/H<sub>2</sub>O (4:1),  $0 \circ C \rightarrow rt$ , overnight

 $O \oplus Cs$  (5 equiv.)

 $O \oplus Cs$  (7 equiv.)

 $O \oplus Cs$  (8 equiv.)

 $O \oplus Cs$  (9 equiv.)

 $O \oplus Cs$  (9 equiv.)

 $O \oplus Cs$  (10 equiv.)

 $O \oplus Cs$  (10 equiv.)

 $O \oplus Cs$  (11 equiv.)

 $O \oplus Cs$  (12 equiv.)

 $O \oplus Cs$  (13 equiv.)

 $O \oplus Cs$  (14 equiv.)

 $O \oplus Cs$  (15 equiv.)

 $O \oplus Cs$  (17 equiv.)

 $O$ 

**Scheme S5.** Synthesis of dihydroxyeicosadienoic acid (DHEDs)

A mixture of **5a–5c** (0.200 g, 0.598 mmol) was diluted in anhydrous DMF (2 mL) and added to dry cesium propionate (0.621 g, 2.98 mmol) in DMF (5 mL) in a sealable tube. The tube was flushed with argon, sealed, and heated to 120 °C for 68 h. The mixture was cooled, poured into H<sub>2</sub>O (20 mL) and extracted with EtOAc (3 x 30 mL). The organic phase was washed with 5% NaCl (2 x 50 mL) and saturated aqueous NaCl (50 mL), dried over Na<sub>2</sub>SO<sub>4</sub>, and concentrated. The residue was purified by flash column chromatography (CombiFlash® Rf+ Lumen) (25 g SiO<sub>2</sub> cartridge, 0 – 50% EtOAc/Hexanes) to yield the EED propionate intermediate as a pale-yellow

syrup (0.220 g, 90%) after drying in vacuo (See Table S6 for solvent gradient used for EEDs Methyl ester).

**Table S6**. Solvent gradient for EEDs methyl ester separation.

Duration	%B	Solvent A	Solvent B
(minutes)			
0.0	0.0	Hexane	Ethyl Acetate
2.0	0.0	Hexane	Ethyl Acetate
7.0	5.0	Hexane	Ethyl Acetate
10.0	10.0	Hexane	Ethyl Acetate
5.0	12.0	Hexane	Ethyl Acetate
8.0	50.0	Hexane	Ethyl Acetate
3.0	0.0	Hexane	Ethyl Acetate

The mixture of EED propionates was then diluted in THF/H<sub>2</sub>O (5.5/1.4 mL) and cooled to 0°C under argon. LiOH (1.21 mL of a 2 M solution in H<sub>2</sub>O, 2.42 mmol) was added, and the mixture was warmed to rt and stirred overnight. The mixture was then quenched by the dropwise addition of formic acid, until the pH of the mixture was approximately 4. H<sub>2</sub>O and EtOAc (10 mL each) were then added, and the layers were separated. The aqueous layer was extracted with EtOAc (4 x 10 mL) and the organic phase was washed with saturated aqueous NaCl (40 mL), dried over Na<sub>2</sub>SO<sub>4</sub>, concentrated, and azeotroped with hexanes (3 x 20 mL) to remove residual formic acid. The residue was then purified by flash column chromatography (25 g SiO<sub>2</sub> cartridge, 40 – 75% EtOAc/Hexanes) to yield the DGLA diol mixture 6a - 6c (0.119 grams, 65% yield). Regioisomers were separated via HPLC with [CONDITIONS]. 6a; <sup>1</sup>H NMR (CDCl<sub>3</sub>, 500 MHz):  $\delta$  5.57 – 5.28 (m, 4H),  $\delta$  3.50 – 3.44 (m, 2H),  $\delta$  2.80 (t, J = 7.3 Hz, 2H),  $\delta$  2.84 – 2.29 (m, 2H),  $\delta$  2.04 (q, J = 7.2 Hz, 2H),  $\delta$  1.66 – 1.60 (m, 2H),  $\delta$  1.49 – 1.23 (m, 12H),  $\delta$  0.88 (t, J = 6.9 Hz, 3H). <sup>13</sup>C (CDCl<sub>3</sub>, 125 MHz):  $\delta$  179.4, 131.8, 130.9, 127.4, 125.1, 74.0, 74.0, 34.1, 33.6, 31.7, 31.6, 29.4, 29.3, 29.1, 27.4, 25.9, 25.5, 24.7, 22.7, 14.2. 6b; <sup>1</sup>H NMR (CDCl<sub>3</sub>, 500 MHz):  $\delta$  5.59 – 5.39 (m, 4H),  $\delta$  3.54

-3.51 (m, 2H),  $\delta 2.35 - 2.26$  (m, 6H),  $\delta 2.07 - 2.03$  (m, 4H),  $\delta 1.66 - 1.60$  (m, 2H),  $\delta 1.39 - 1.24$  (m, 12H), 0.88 (t, J = 6.8 Hz, 3H). <sup>13</sup>C (CDCl<sub>3</sub>, 125 MHz):  $\delta 179.2$ , 133.8, 133.4, 125.0, 124.7, 73.5, 73.4, 34.0, 31.9, 31.7, 29.4, 29.3, 28.9, 28.8, 27.5, 27.3, 24.7, 22.7, 14.2. **6c**: <sup>1</sup>H NMR (CDCl<sub>3</sub>, 500 MHz):  $\delta 5.57 - 5.31$  (m, 4H),  $\delta 3.52 - 3.47$  (m, 2H),  $\delta 2.82$  (t, J = 6.8 Hz, 2H),  $\delta 2.36 - 2.31$  (m, 4H),  $\delta 2.07 - 2.03$  (m, 2H),  $\delta 1.65 - 1.60$  (m, 2H),  $\delta 1.53 - 1.46$  (m, 2H),  $\delta 1.40 - 1.25$  (m, 12H),  $\delta 0.90$  (t, J = 7.0 Hz, 3H).

**Scheme S6.** Synthesis of epoxyeicosadienoic acid (EEDs)

## 7. Synthesis of epoxyeicosadienoic acid (EEDs)(7a-7c):

Each separated isomer 5a-5c was individually subjected to the following conditions: The methyl ester (0.0891 mmol, 0.0300 g, 1.00 equiv.) was added to a 5 mL round bottom flask with a stir bar and diluted with 0.750 mL of THF/H<sub>2</sub>O (5:1). To this solution was added LiOH • H<sub>2</sub>O (0.267 mmol, 0.00640 g, 3 equiv.) and allowed to stir under argon atmosphere overnight. Then, the pH was adjusted to 4 with formic acid, diluted with water and EtOAc, and added to a separatory funnel. The aqueous layer was extracted with 4 x 5 mL of EtOAc, the combined organic layer washed with brine, dried over Na<sub>2</sub>SO<sub>4</sub>, and concentrated. The residue was azeotroped with 4 x 10 mL of hexanes to remove any remaining formic acid. The crude product was purified via column chromatography (1/1 hexanes/EtOAc, 1% formic acid) to give the products as clear oils. **7a**; <sup>1</sup>H NMR (CDCl<sub>3</sub>, 500 MHz):  $\delta$  5.53 – 5.29 (m, 4H),  $\delta$  2.97 – 2.91 (m, 2H),  $\delta$  2.80 (t, J = 6.6 Hz, 2H),  $\delta$  2.43 – 2.34 (m, 3H),  $\delta$  2.24 – 2.19 (m, 1H), 2.05 (q, J = 7.1 Hz, 2H),  $\delta$  1.68 – 1.62 (m, 2H),  $\delta$ 

1.57 – 1.24 (m, 14H),  $\delta$  0.89 (t, J = 6.9 Hz, 3H). <sup>13</sup>C (CDCl<sub>3</sub>, 125 MHz):  $\delta$  179.4, 131.0, 130.9, 127.3, 124.2, 57.3, 56.6, 34.0, 31.7, 29.4, 29.3, 29.1, 27.8, 27.4, 26.6, 26.4, 26.0, 24.7, 22.7, 14.2. **7b**; <sup>1</sup>H NMR (CDCl<sub>3</sub>, 500 MHz):  $\delta$  5.56 – 5.39 (m, 4H),  $\delta$  2.97 – 2.93 (m, 2H),  $\delta$  2.44 – 2.38 (m, 2H),  $\delta$  2.34 (t, J = 7.5 Hz, 2H),  $\delta$  2.24 – 2.18 (m, 2H),  $\delta$  2.07 – 2.03 (m, 4H),  $\delta$  1.66 – 1.60 (m, 2H), 1.40 – 1.24 (m, 14H), 0.88 (t, J = 6.8 Hz, 3H). <sup>13</sup>C (CDCl<sub>3</sub>, 125 MHz):  $\delta$  179.5, 133.0, 132.7, 124.1, 123.8, 56.7, 56.7, 34.0, 31.6, 29.4, 29.4, 29.1, 29.0, 27.6, 27.5, 26.3, 24.7, 22.7, 14.2. **7c**; <sup>1</sup>H NMR (CDCl<sub>3</sub>, 500 MHz):  $\delta$  5.53 – 5.31 (m, 4H),  $\delta$  2.98 – 2.93 (m, 2H),  $\delta$  2.8 (t, J = 6.9 Hz, 2H),  $\delta$  2.44 – 2.39 (m, 1H),  $\delta$  2.35 (t, J = 7.6 Hz, 2H),  $\delta$  2.24 – 2.19 (m, 1H),  $\delta$  2.07 – 2.03 (m, 2H),  $\delta$  1.66 – 1.61 (m, 2H),  $\delta$  1.57 – 1.25 (m, 14H),  $\delta$  0.89 (t, J = 7.0 Hz, 3H). <sup>13</sup>C (CDCl<sub>3</sub>, 125 MHz):  $\delta$  179.0, 130.9, 130.6, 127.5, 124.3, 57.5, 56.7, 34.0, 31.9, 29.5, 29.0, 29.0, 27.8, 27.3, 26.4, 26.4, 26.0, 24.8, 22.7, 14.2.

† Compounds were used as mixtures for biological testing. The LC/UV-vis and LC/MS/MS oxylipin analysis was used to confirm the mixture of regioisomer and the purity of the compound Figure S16 shows the different regioisomers ratio in EEDs and DHEDs supplementation used in this study. Confirmation of desired structure was done by examining ratio of integrations of alkene protons (~5 – 6 ppm) to the methyl ester (~3.6 ppm) on <sup>1</sup>H NMR. HRMS was also done to ensure desired mass. Separations and characterization were performed to determine relative percentages of each isomer in mixture used for biological testing.

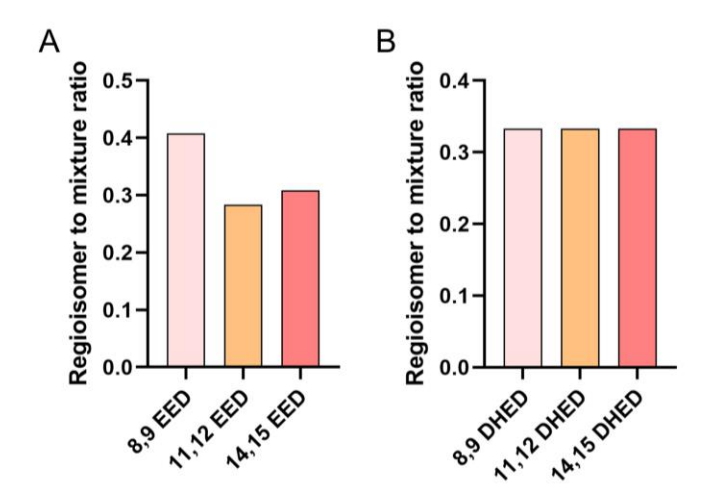


**Figure S16.** The different regioisomers ratio in EEDs and DHEDs supplementation used in this study.

## 8. Synthesis of 12-(3-((3s,5s,7s)-adamantan-1-yl)ureido)dodecanoic acid (AUDA):

## Scheme S7. Synthesis of AUDA

The synthesis followed published procedure <sup>5</sup>. To a suspension of 12-aminododecanoic acid (1g, FW = 215.33, 95% purity, 4.4 mmol) in 1,2-dichloroethane (100 mL), 1-adamantyl isocyanate (0.782 g, FW = 177.24, 97%, 4.28 mmol) was added. The reaction mixture was heated at 80 °C. The reaction was monitored by TLC until all the isocyanate is consumed. The reaction mixture was then cooled down to room temperature and the solid product was filtered. The solid paste was further triturated and washed with hexane (100 mL). The isolated solid product was dried in vacuum overnight to afford final compound as a white solid in 69 % yield (1.2 g, FW = 392.58, 3.1 mmol)

<sup>1</sup>H NMR (500 MHz, dmso-d<sub>6</sub>): δ 11.97 (br, 1H), 5.59 (t, J = 5 Hz, 1H), 5.43 (s, 1H), 2.89 (q, J = 5 Hz, 2H), 2.18 (t, J = 5 Hz, 2H), 1.95-2.00 (m, 3H), 1.80-1.86 (m, 6H), 1.54-1.63 (m, 6H), 1.43-1.52 (m, 2H), 1.25-1.35 (m, 2H), 1.17-1.27 (m, 14H)

<sup>13</sup>C NMR (125 MHz, dmso-d<sub>6</sub>): δ 174.53, 157.06, 49.32, 42.07, 38.76, 36.17, 33.69, 30.06, 29.08, 28.99, 28.97, 28.84, 28.81, 28.60, 26.46, 24.54

## 3. Characterization of Synthesized compounds

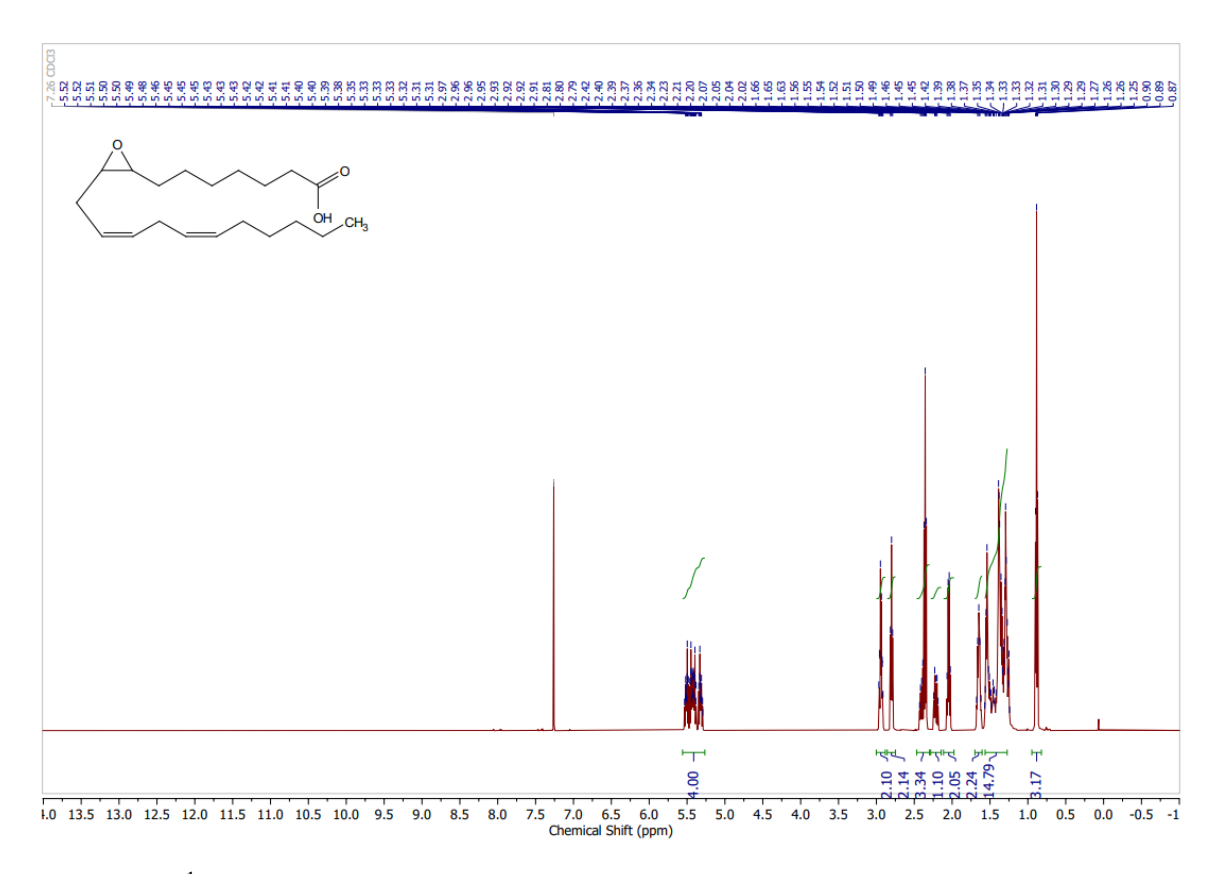


**Figure S17**: <sup>1</sup>H NMR of 8,9-epoxyeicosadienoic acid (8,9-EED)

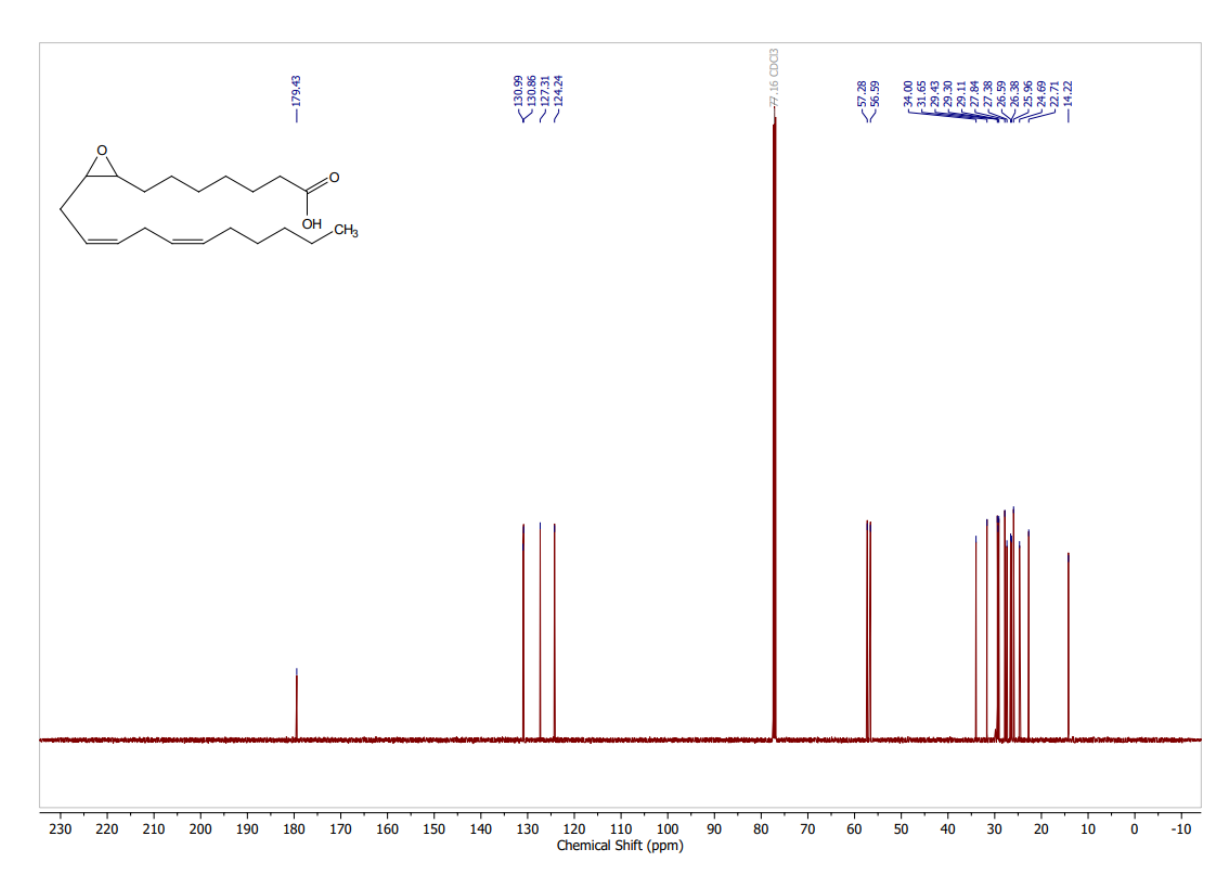


**Figure S18**:13C NMR of 8,9-epoxyeicosadienoic acid (8,9-EED)

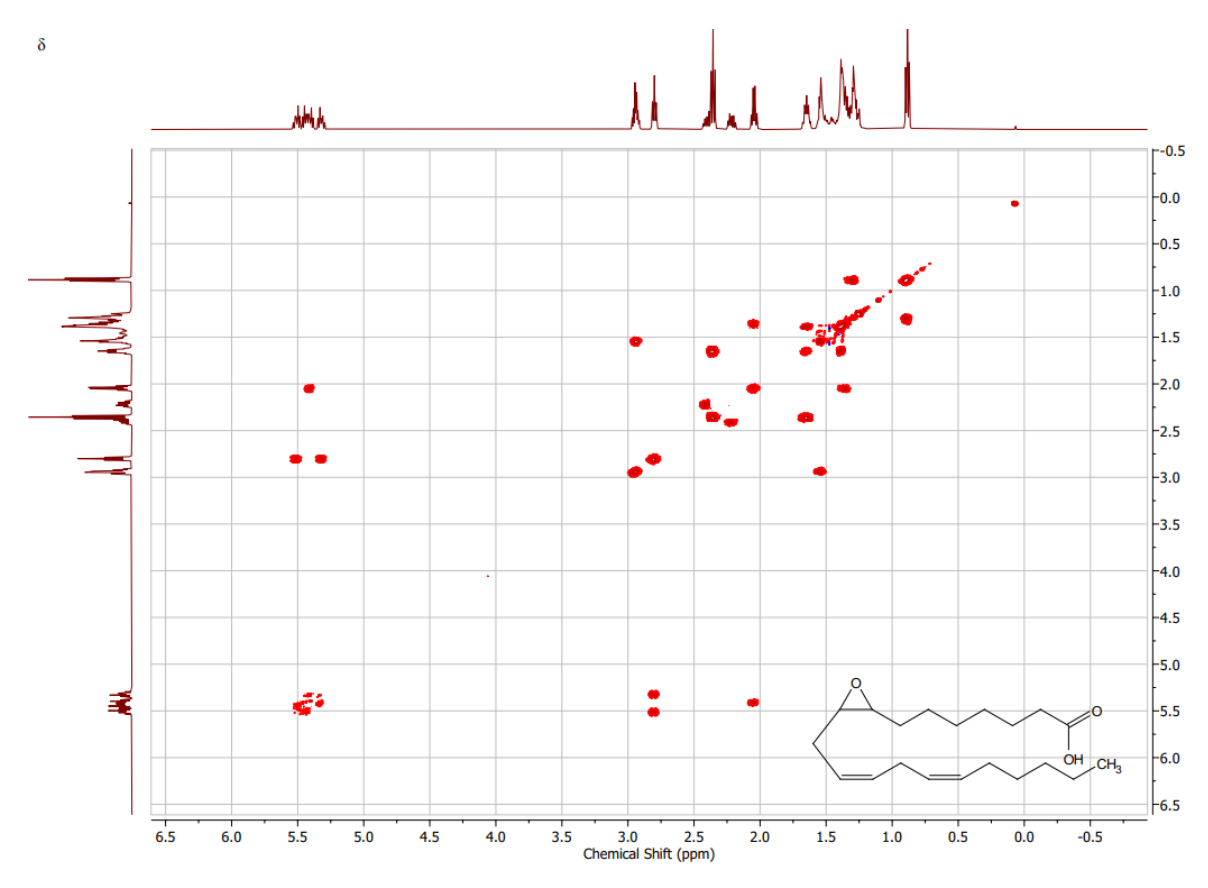
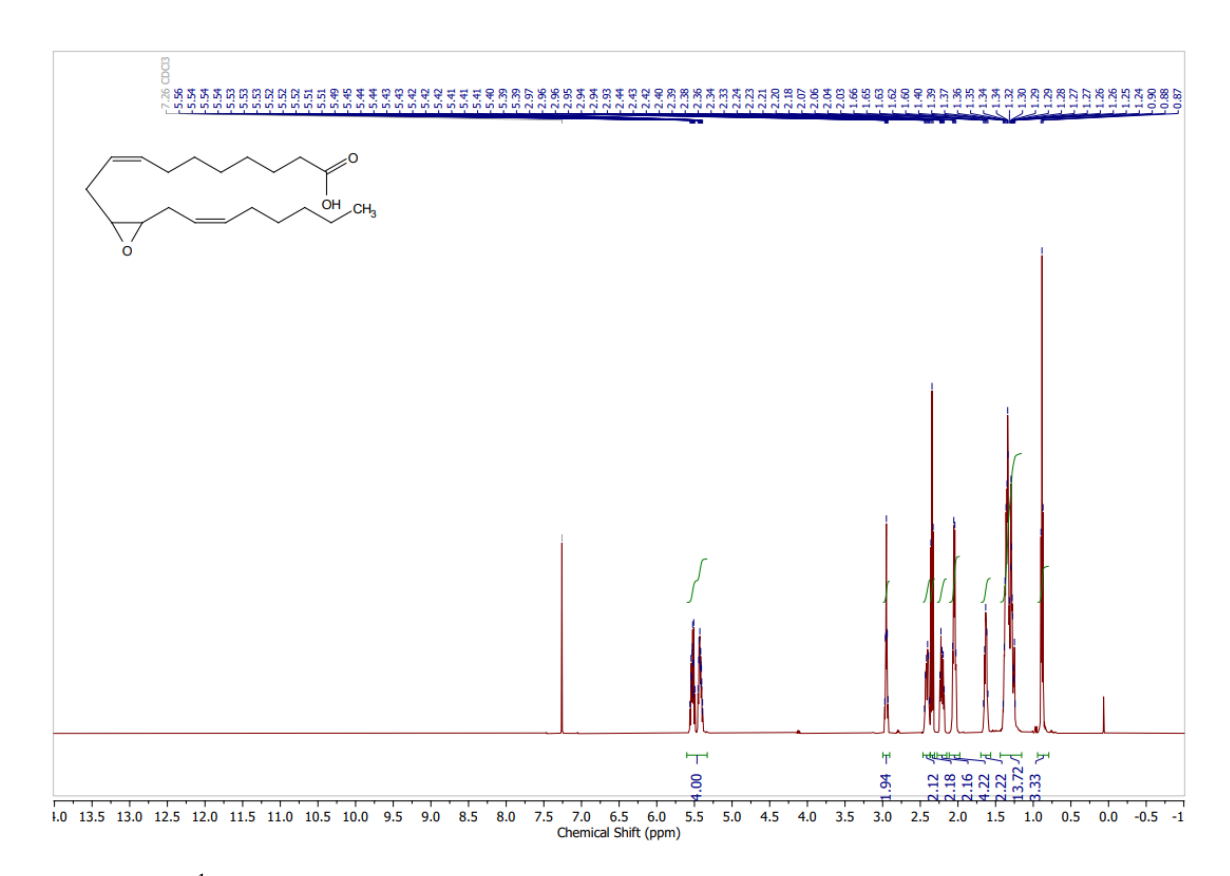
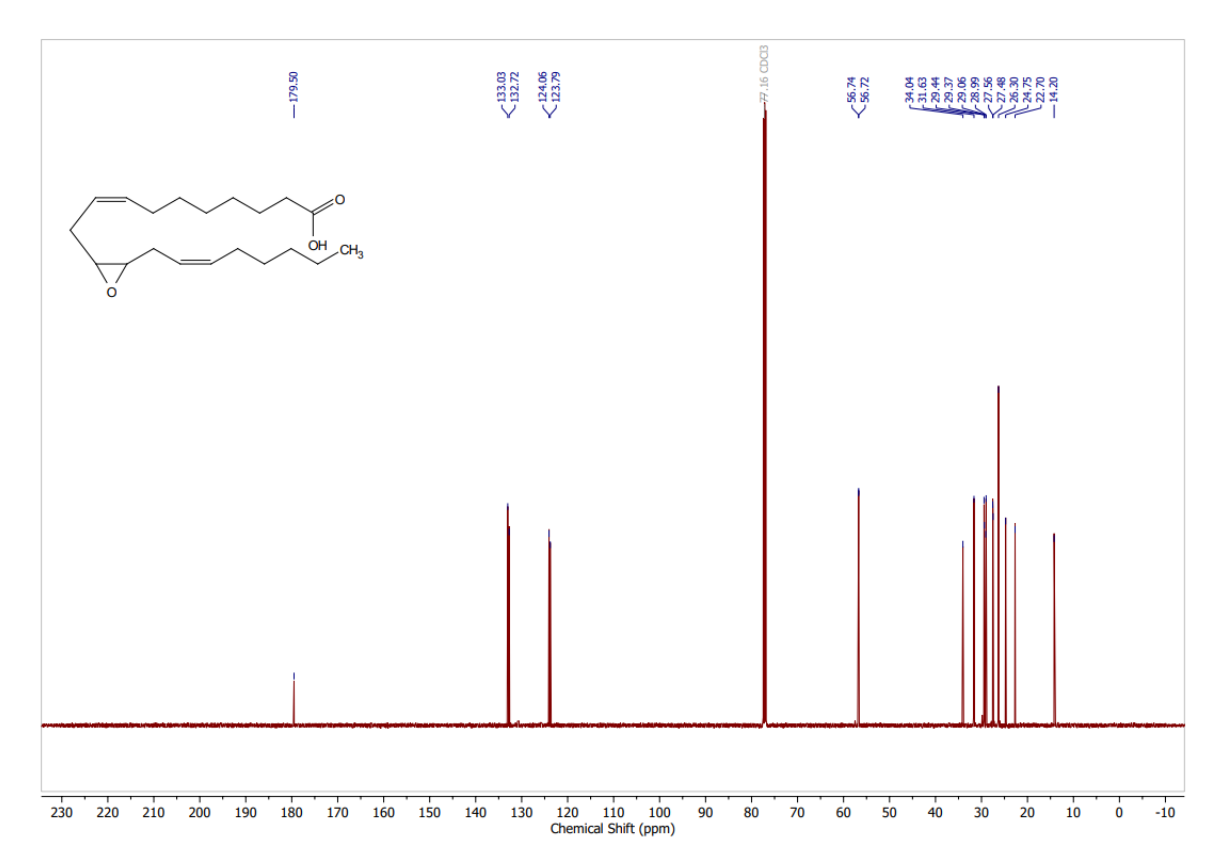


Figure S19: 2D NMR of 8,9-epoxyeicosadienoic acid (8,9-EED)



**Figure S20**: <sup>1</sup>H NMR of 11,12-epoxyeicosadienoic acid (11,12-EED)



**Figure S21**:<sup>13</sup>C NMR of 11,12-epoxyeicosadienoic acid (11,12-EED)

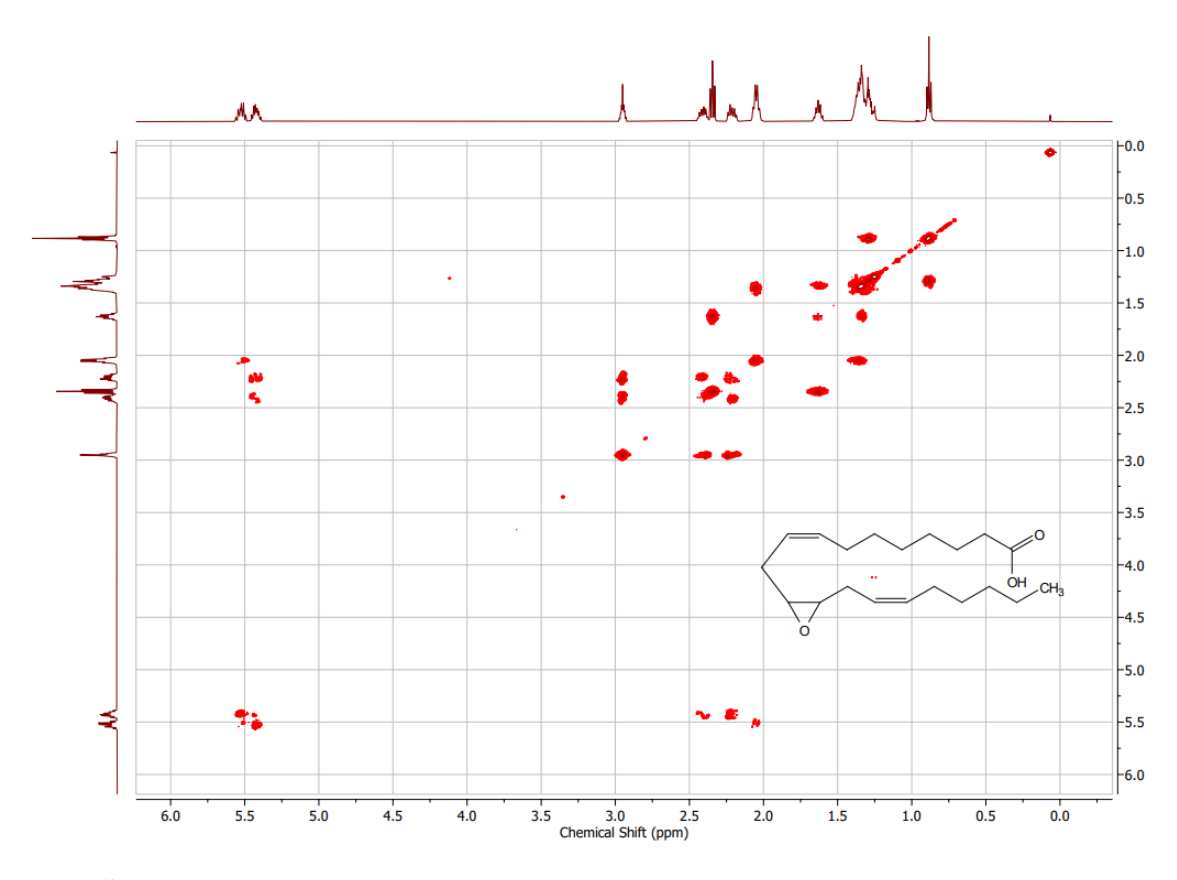
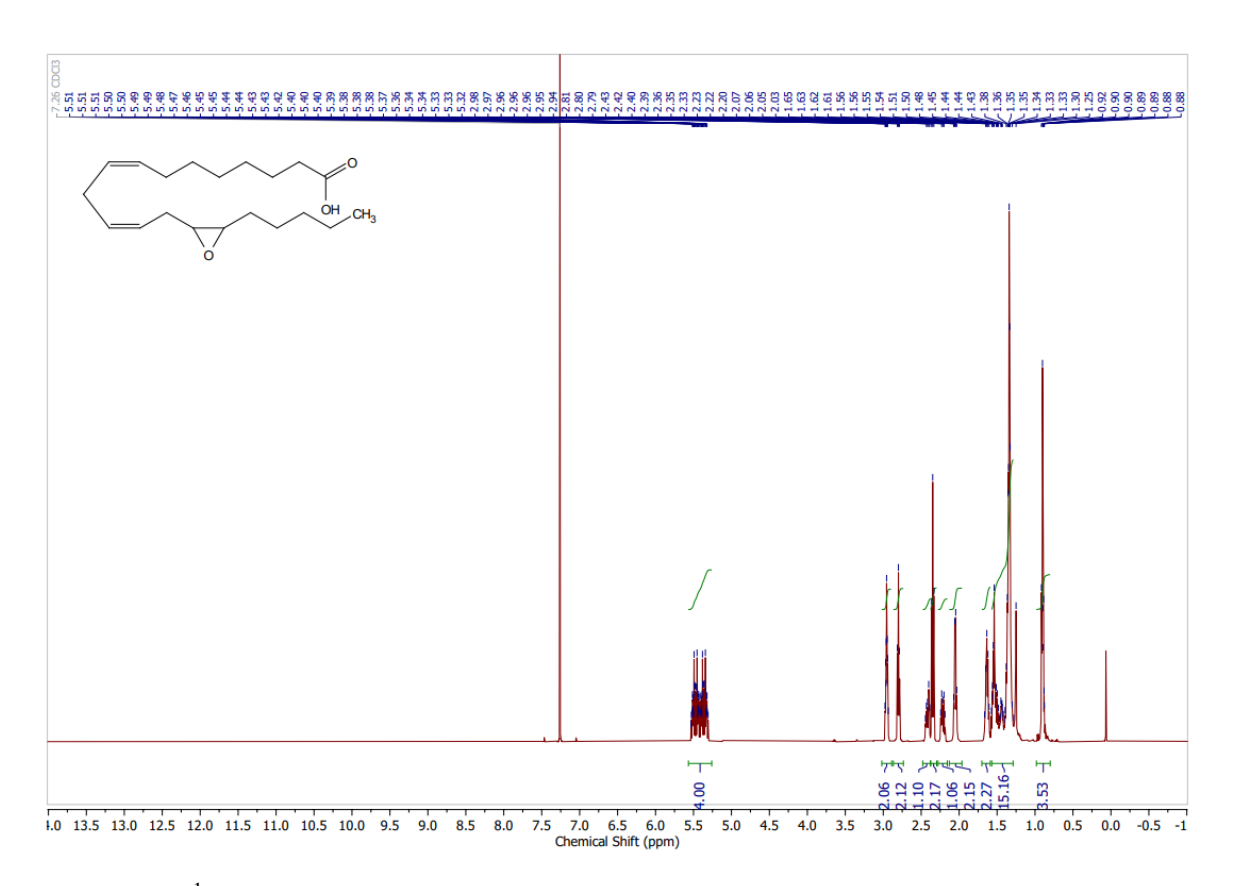
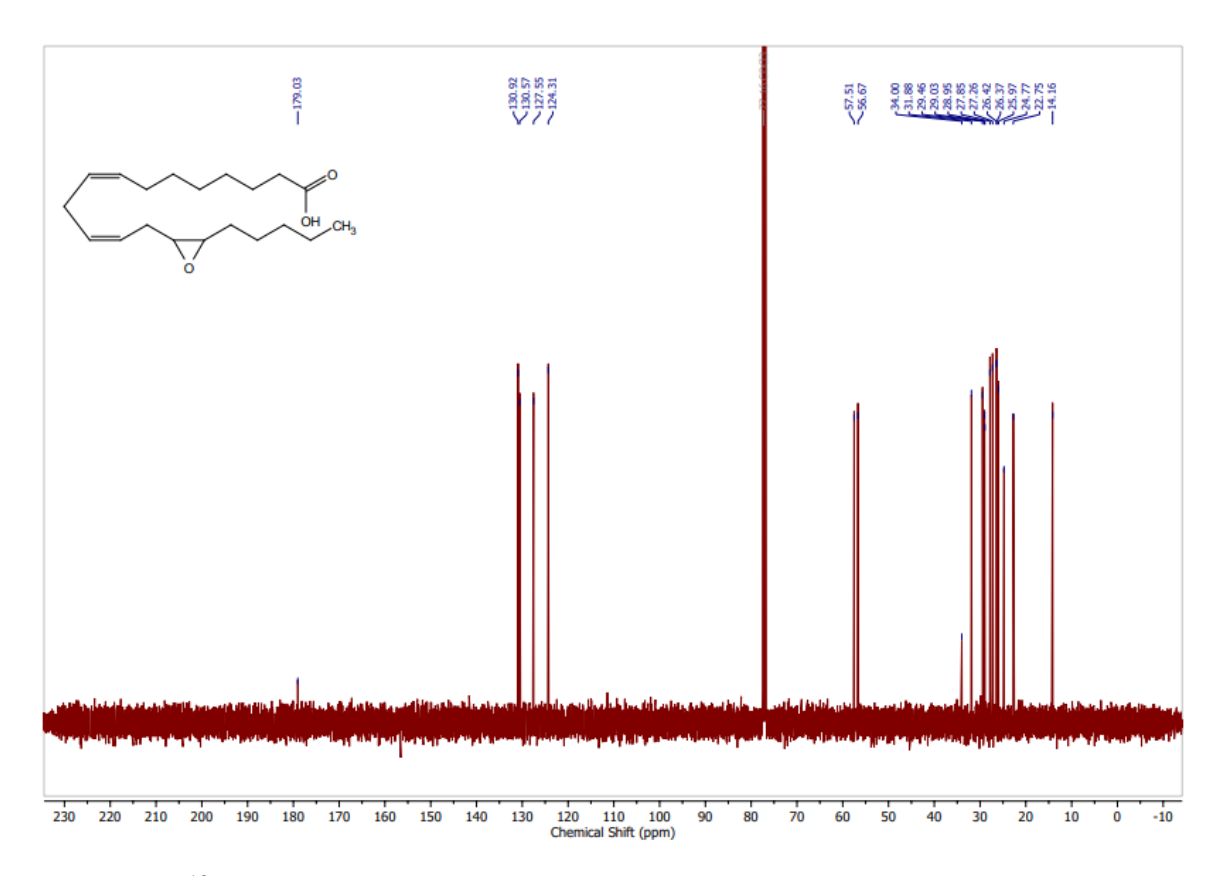


Figure S22: 2D NMR of 11,12-epoxyeicosadienoic acid (11,12-EED)



**Figure S23**: <sup>1</sup>H NMR of 14,15-epoxyeicosadienoic acid (14,15-EED)



**Figure S24**:<sup>13</sup>C NMR of 14,15-epoxyeicosadienoic acid (14,15-EED)

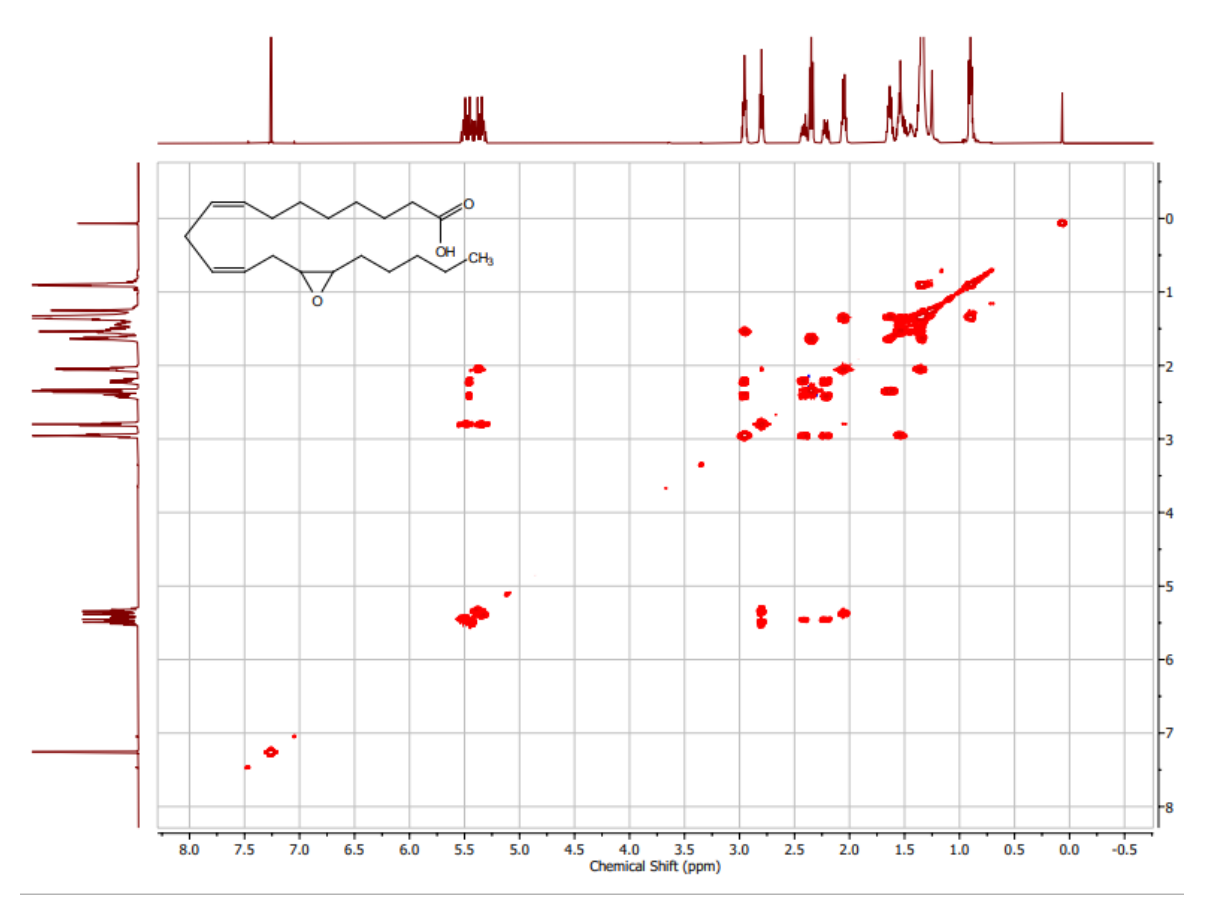


**Figure S25**:2D NMR of 14,15-epoxyeicosadienoic acid (14,15-EED)

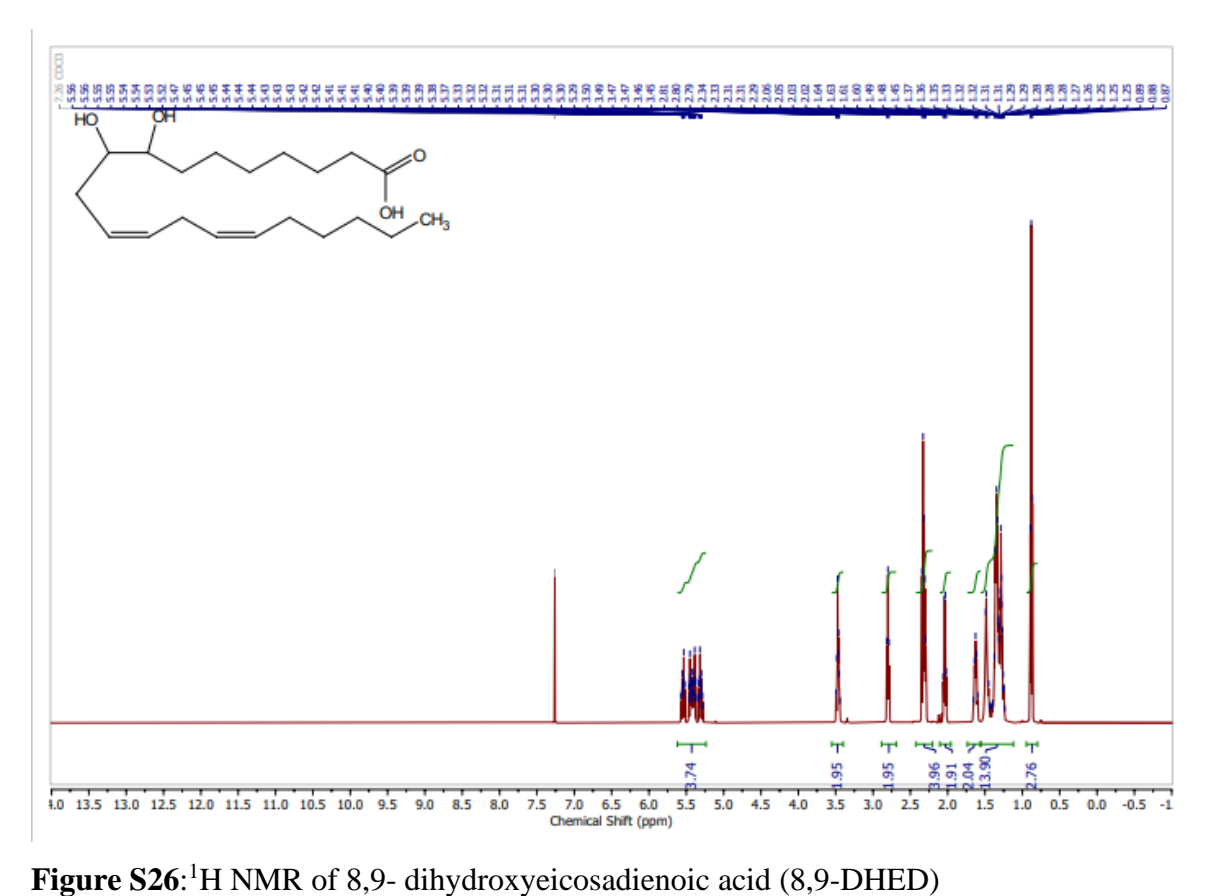


**Figure S26**: <sup>1</sup>H NMR of 8,9- dihydroxyeicosadienoic acid (8,9-DHED)

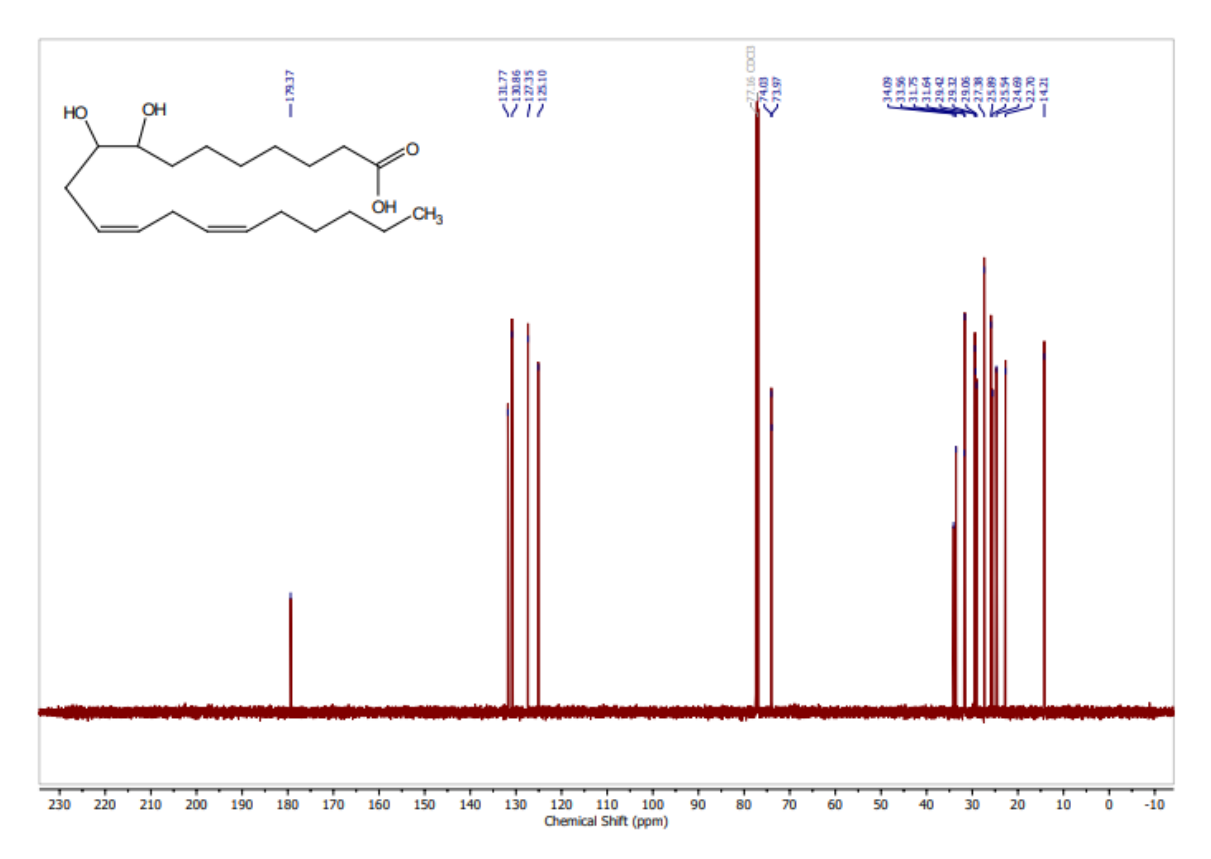


**Figure S27**:<sup>13</sup>C NMR of 8,9- dihydroxyeicosadienoic acid (8,9-DHED)

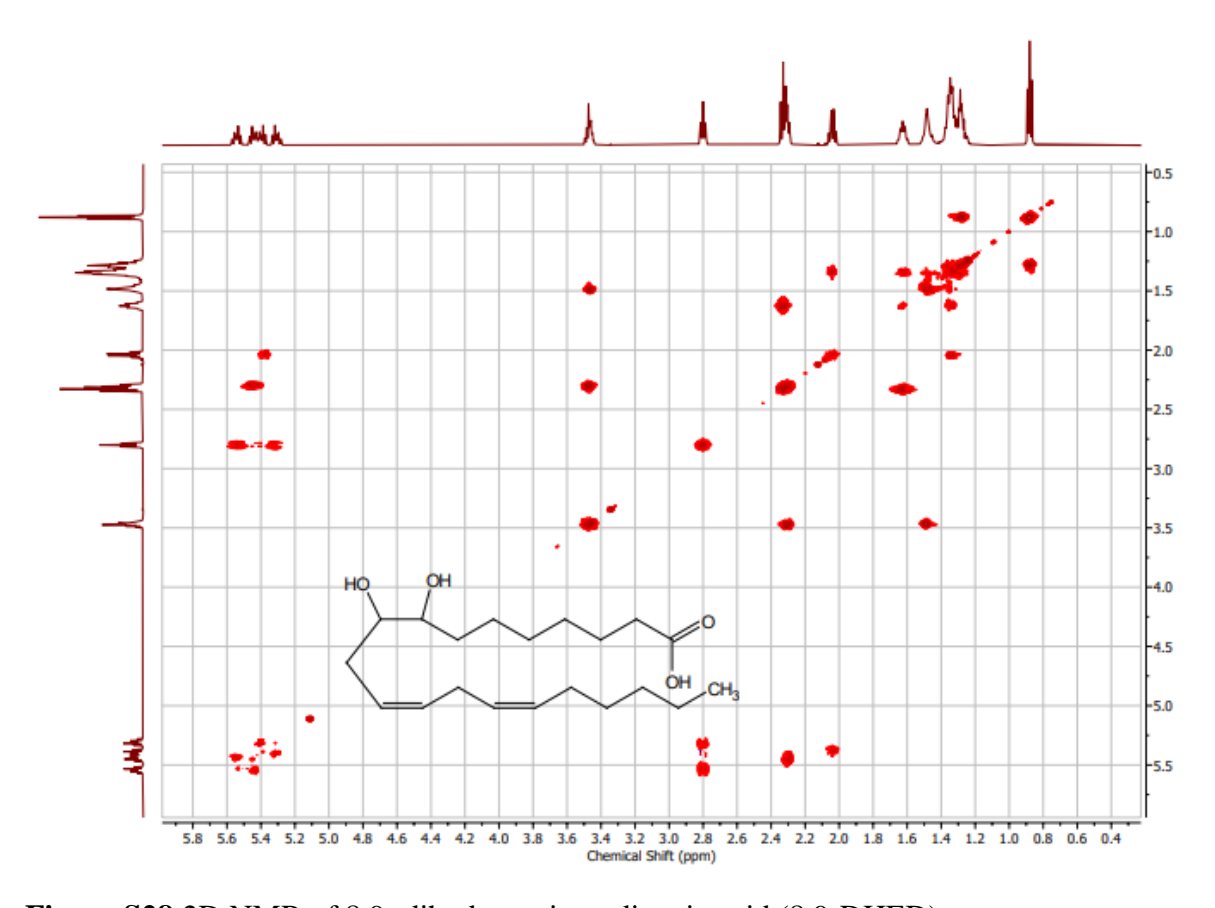


**Figure S28**:2D NMR of 8,9- dihydroxyeicosadienoic acid (8,9-DHED)

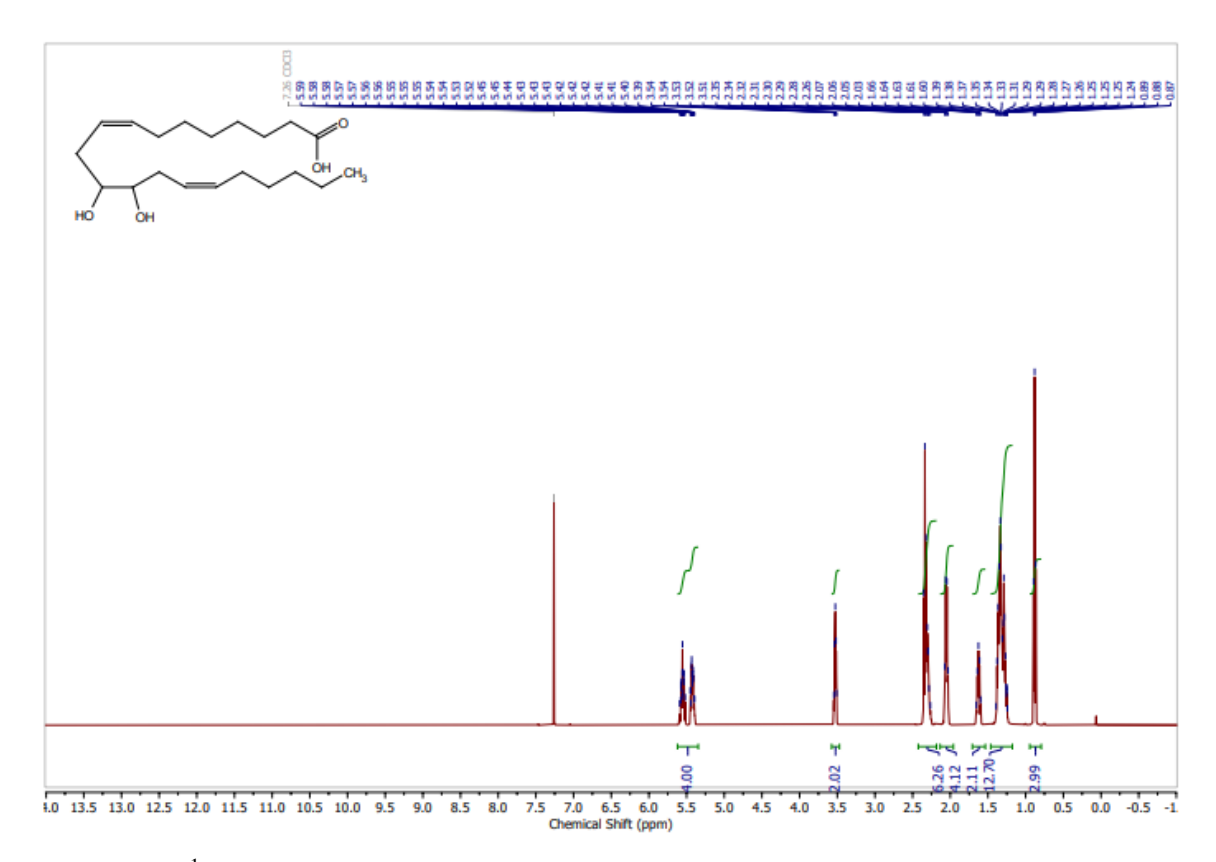


**Figure S29**: <sup>1</sup>H NMR of 11,12- dihydroxyeicosadienoic acid (11,12-DHED)

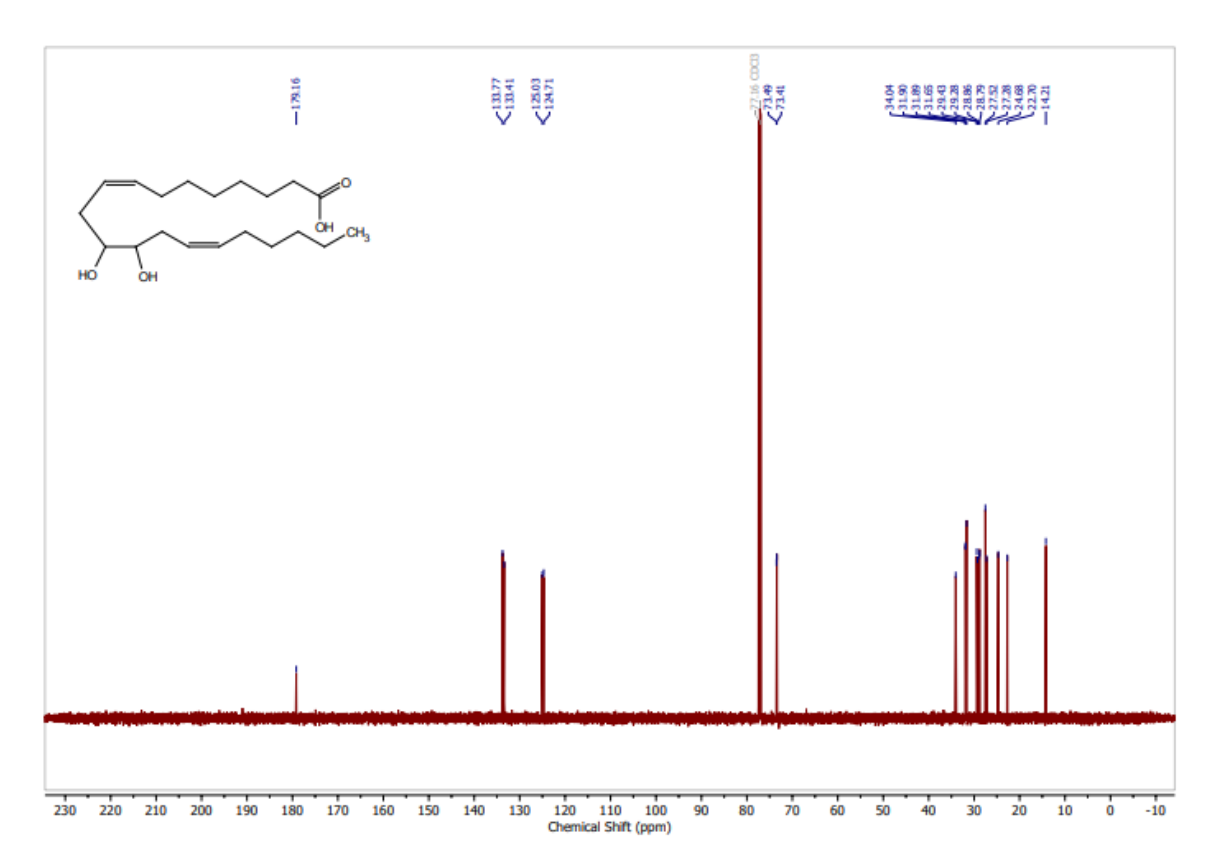


**Figure S30**:13C NMR of 11,12- dihydroxyeicosadienoic acid (11,12-DHED)

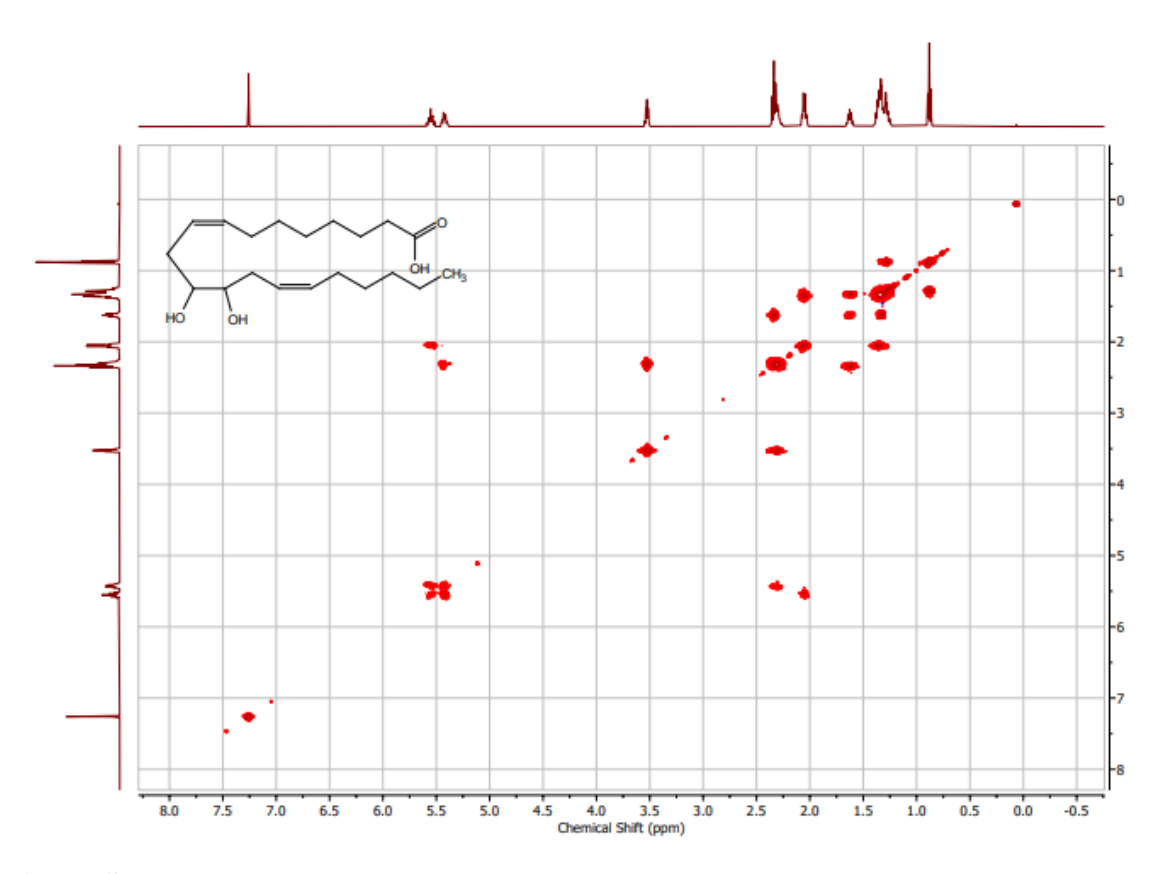
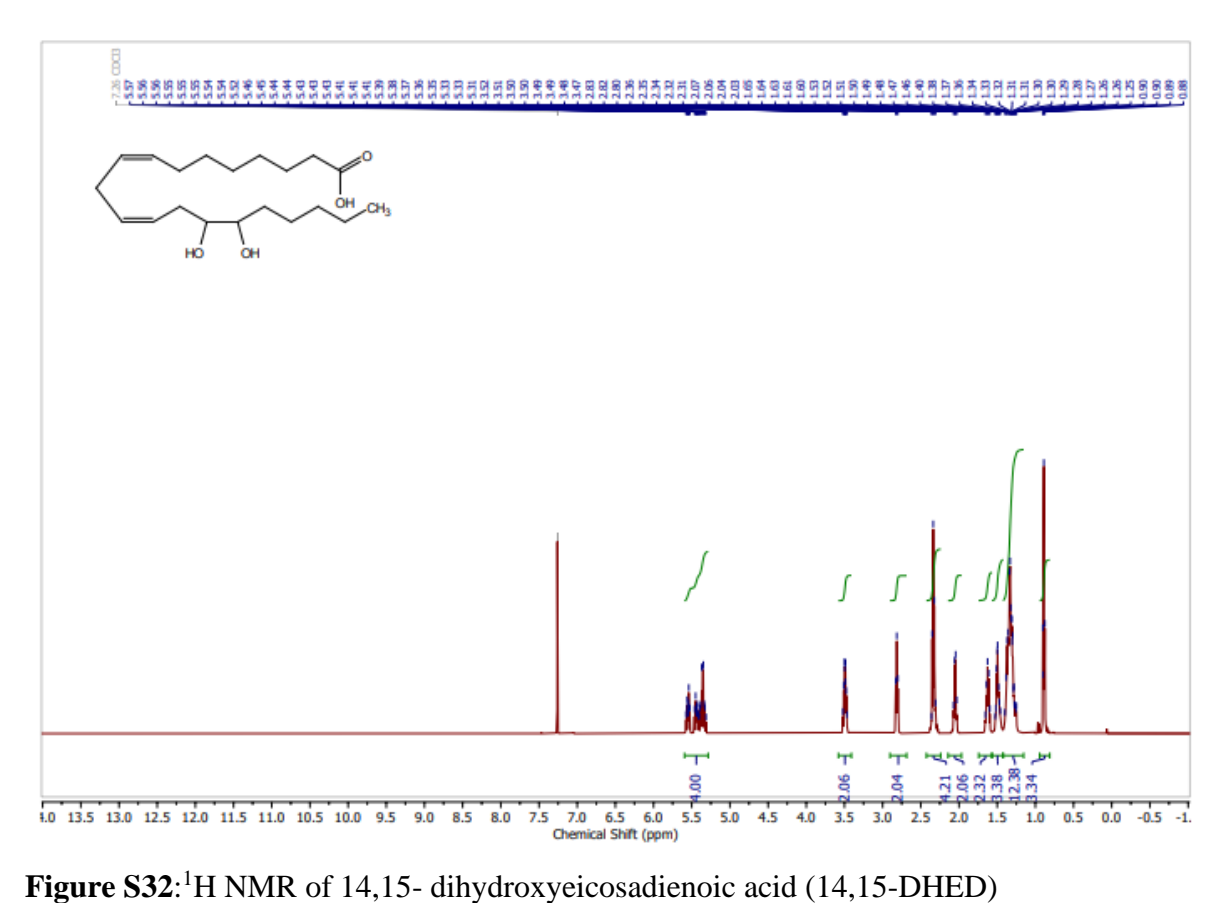
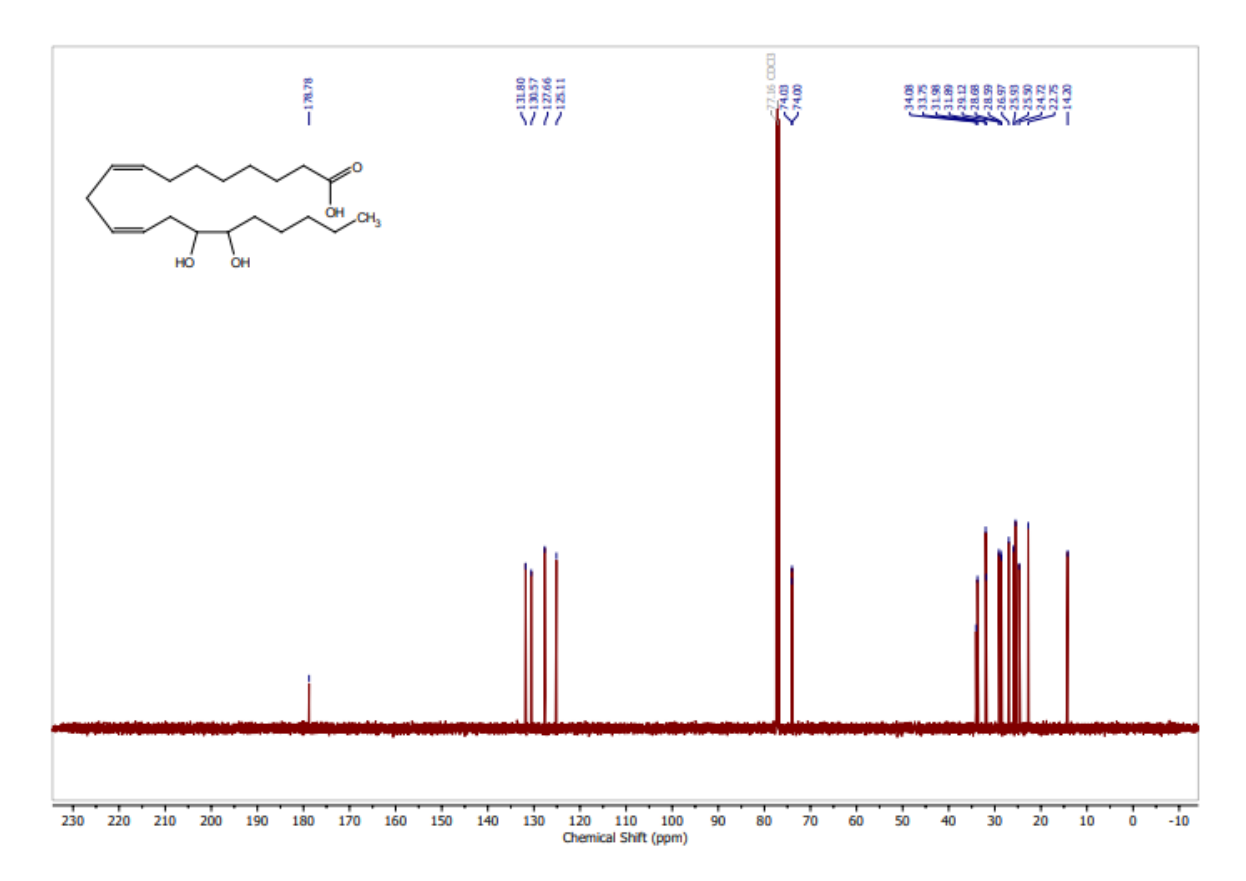


Figure S31:2D NMR of 11,12- dihydroxyeicosadienoic acid (11,12-DHED)



**Figure S32**: <sup>1</sup>H NMR of 14,15- dihydroxyeicosadienoic acid (14,15-DHED)



**Figure S33**:<sup>13</sup>C NMR of 14,15- dihydroxyeicosadienoic acid (14,15-DHED)

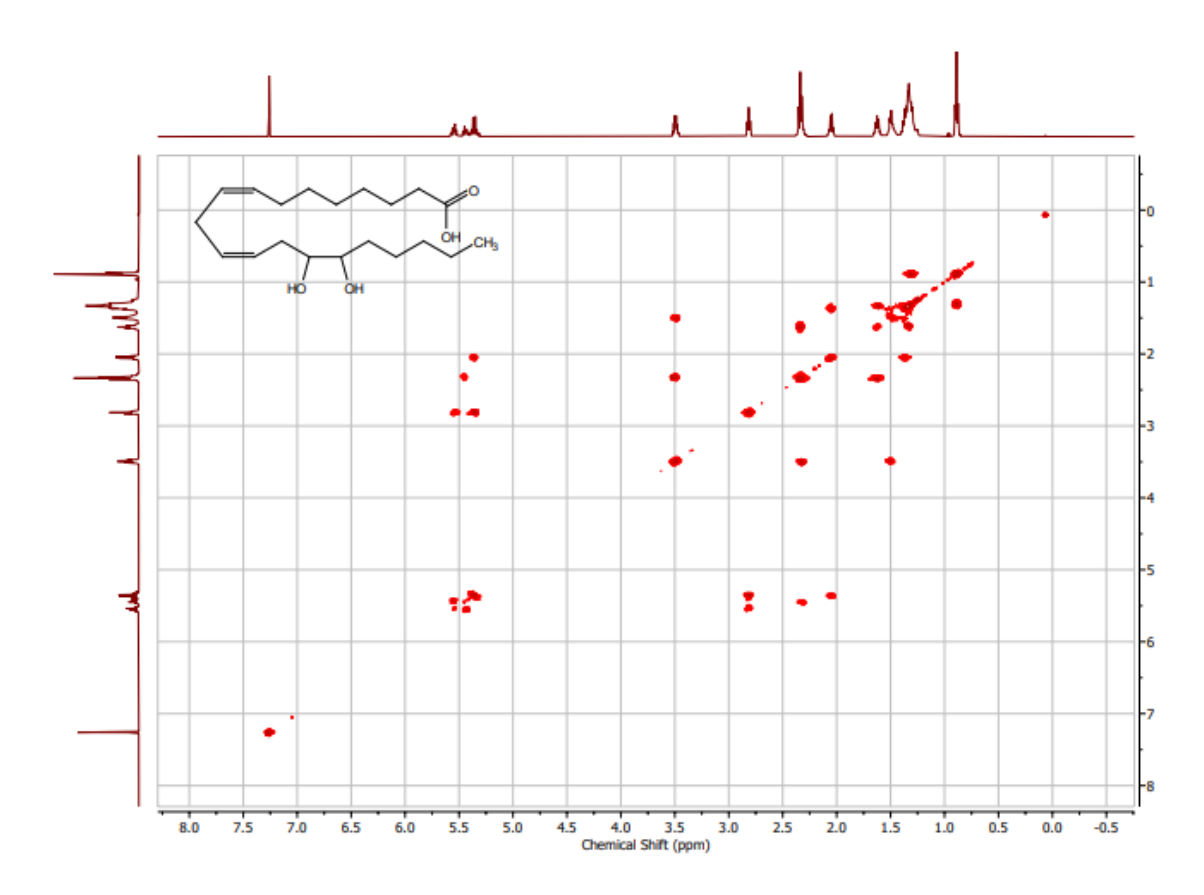


**Figure S34**:2D NMR of 14,15-dihydroxyeicosadienoic acid (14,15-DHED)

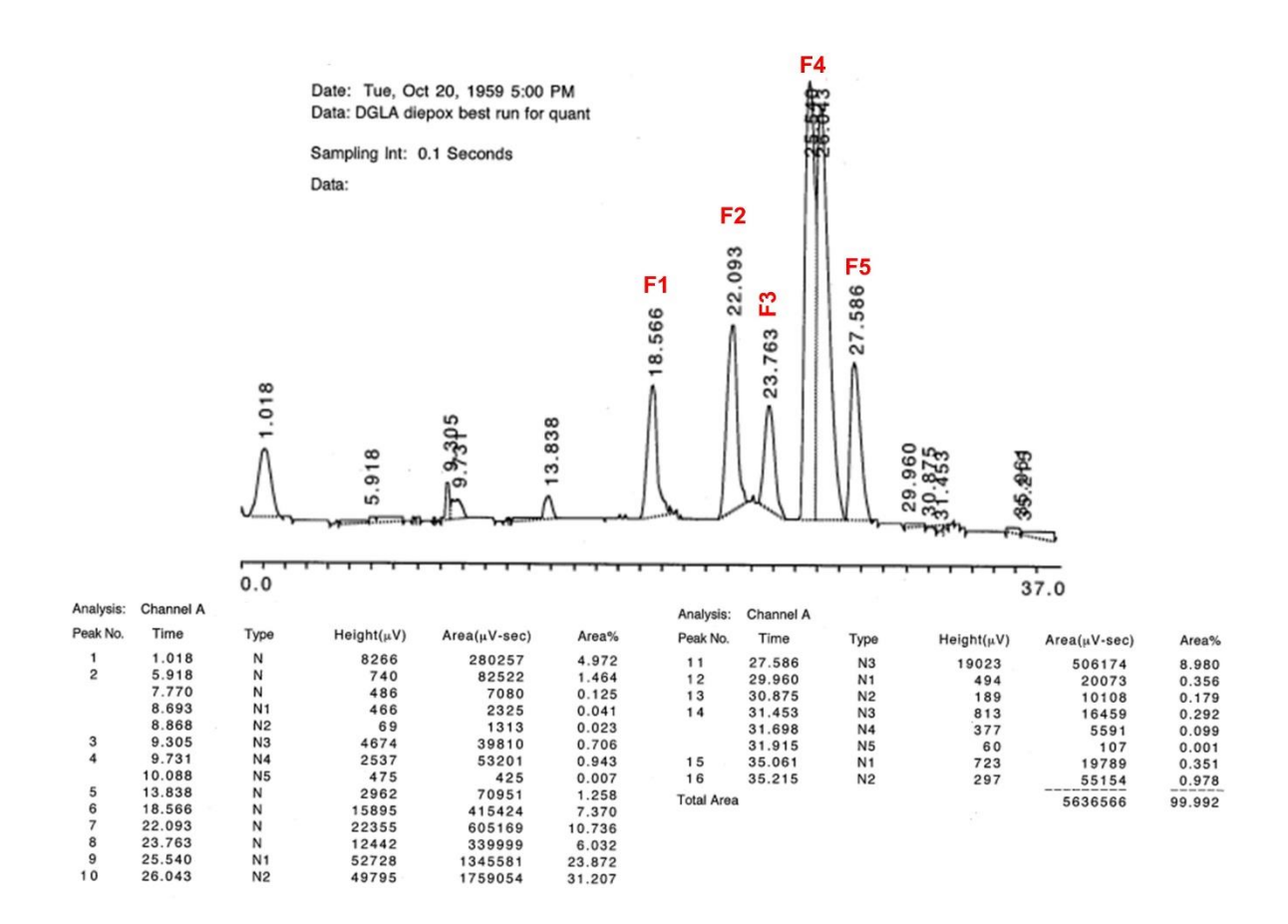


**Figure S35.** Isomers of a mixture of DGLA diepoxides were separated via HPLC (1% isopropanol/hexanes, 2 mL/min), giving 5 fractions (retention times, in minutes, were 18.6, 22.1, 23.8, 25.5, and 27.6 for fractions 1 - 5, respectively). The <sup>1</sup>H NMR and gCOSY spectra of these fractions are shown in Figures S36-S46.

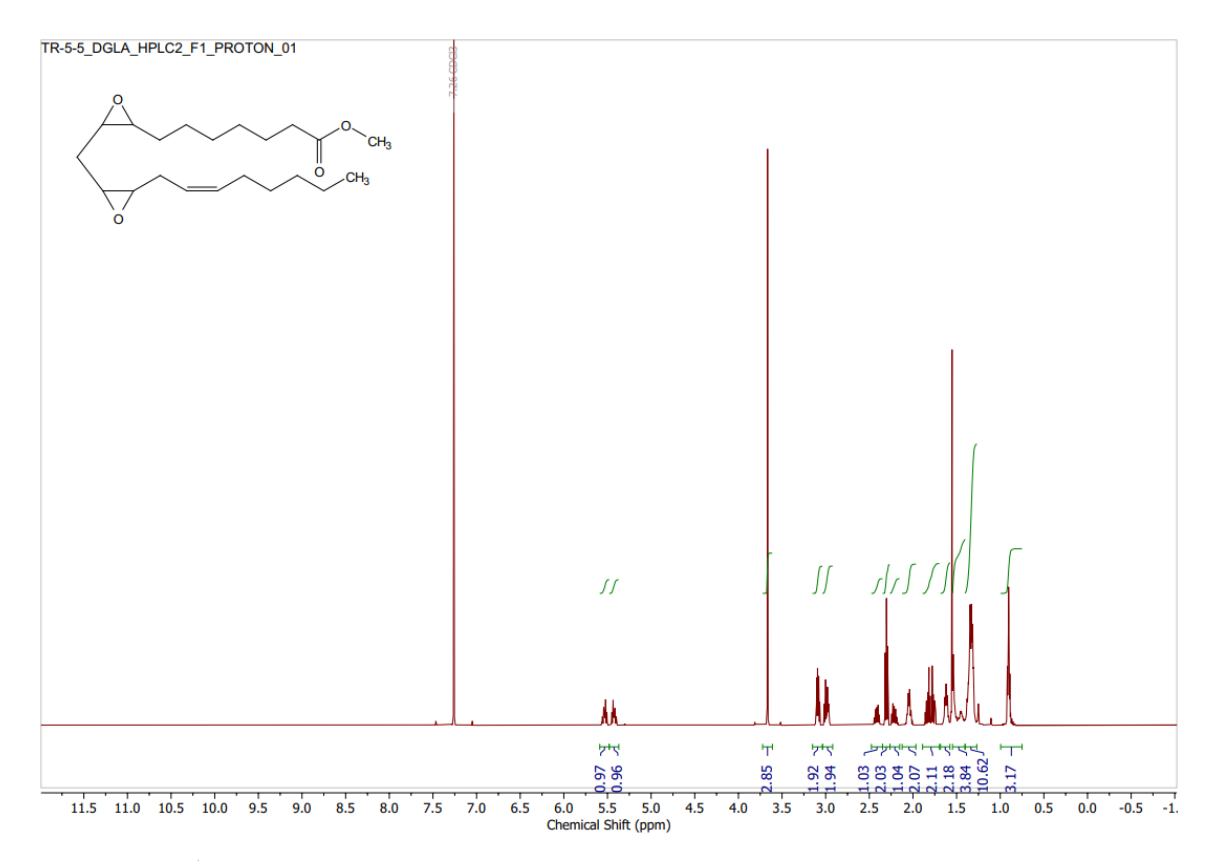


Figure S36: 1H NMR of the first fraction (F1) of DGLA diepoxides separated by HPLC.

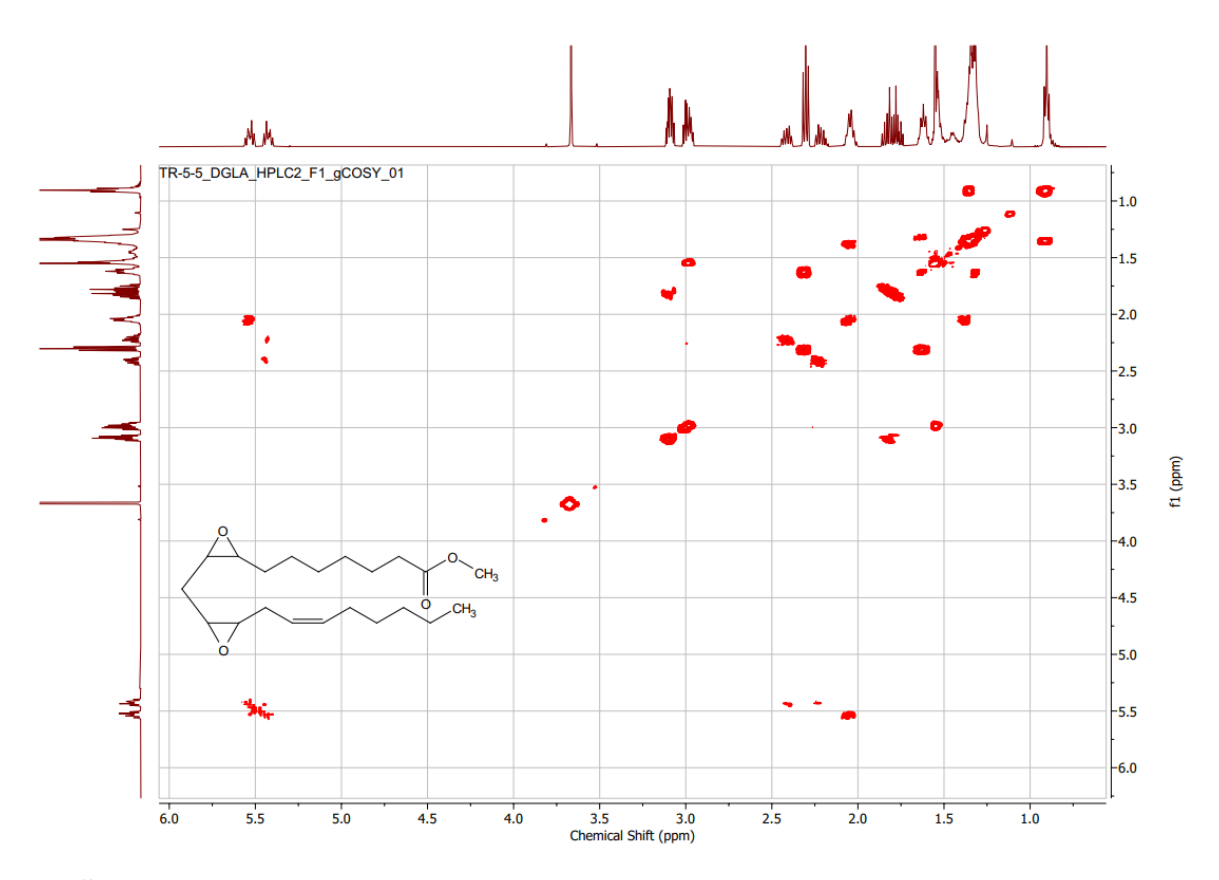


Figure S37: 2D NMR(gCOSY) of the first fraction (F1) of DGLA diepoxides separated by HPLC.

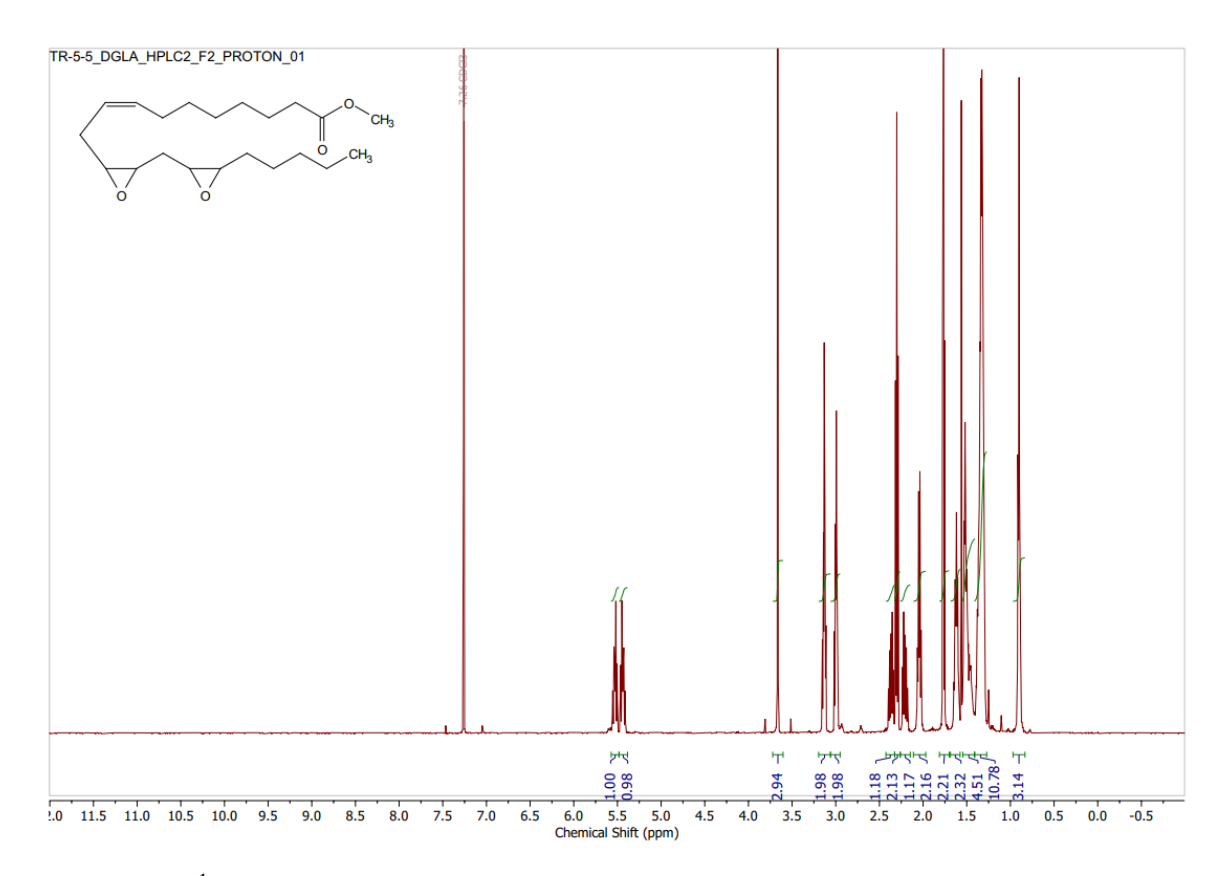


Figure S38: <sup>1</sup>H NMR of the 2nd fraction (F2) of DGLA diepoxides separated by HPLC.

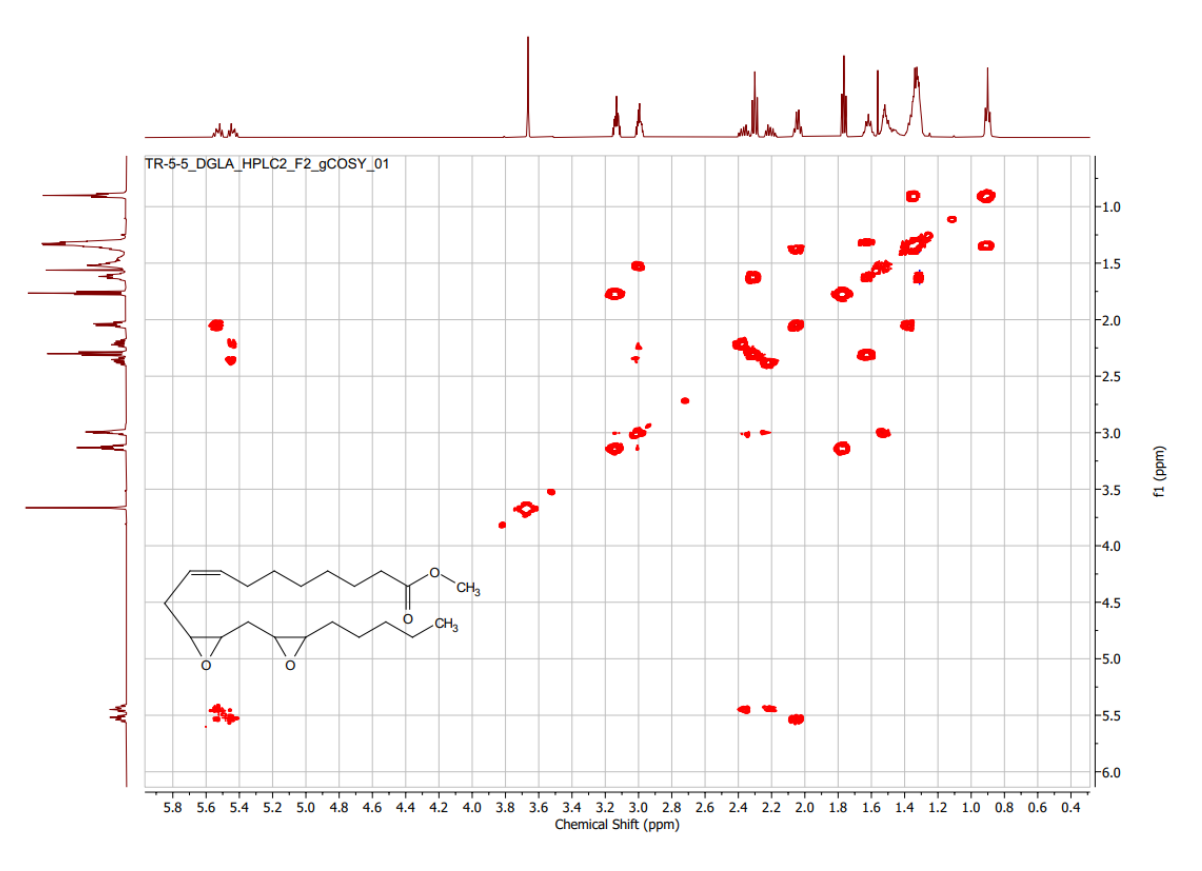


Figure S39. 2D NMR (gCOSY) of the first fraction (F1) of DGLA diepoxides seperated by HPLC.

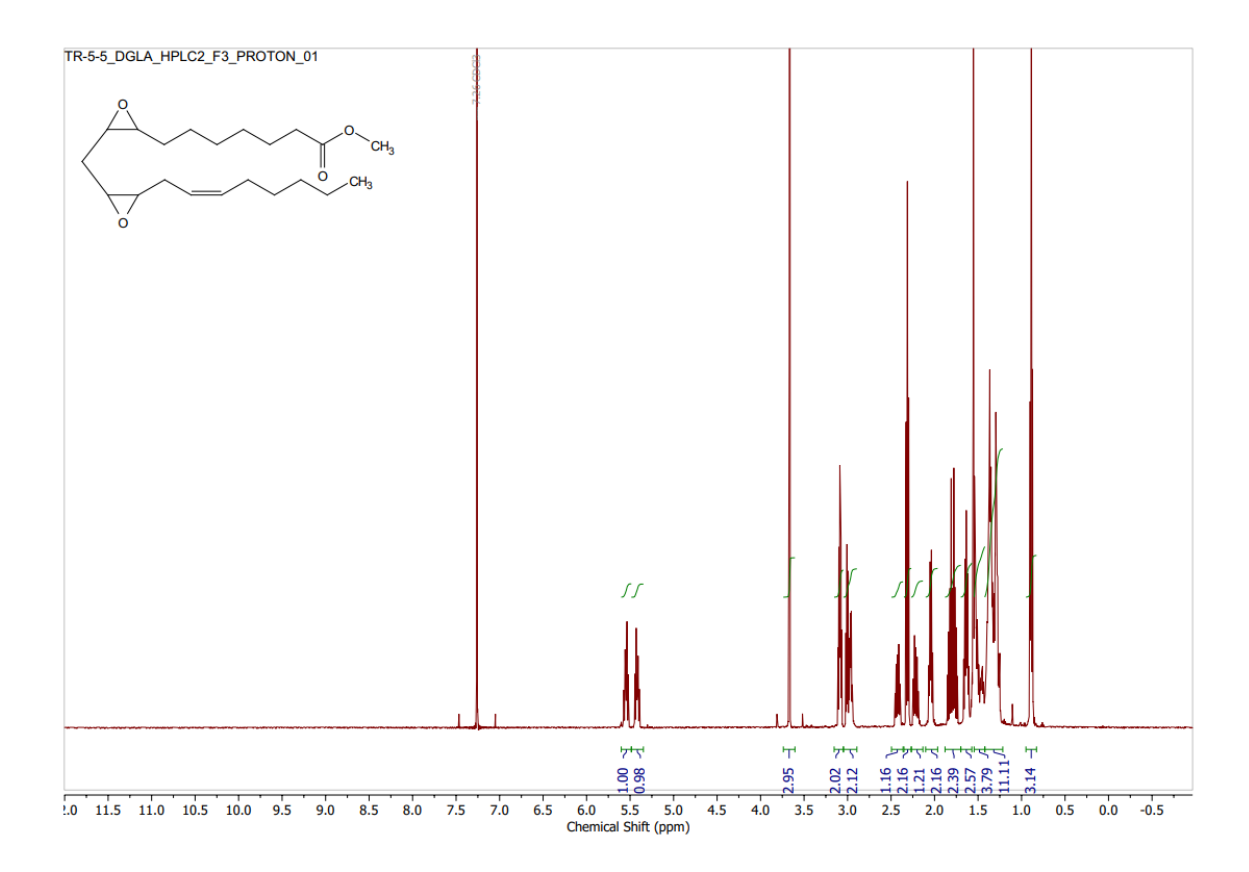


Figure S40: <sup>1</sup>H NMR of the 3rd fraction (F3) of DGLA diepoxides separated by HPLC.

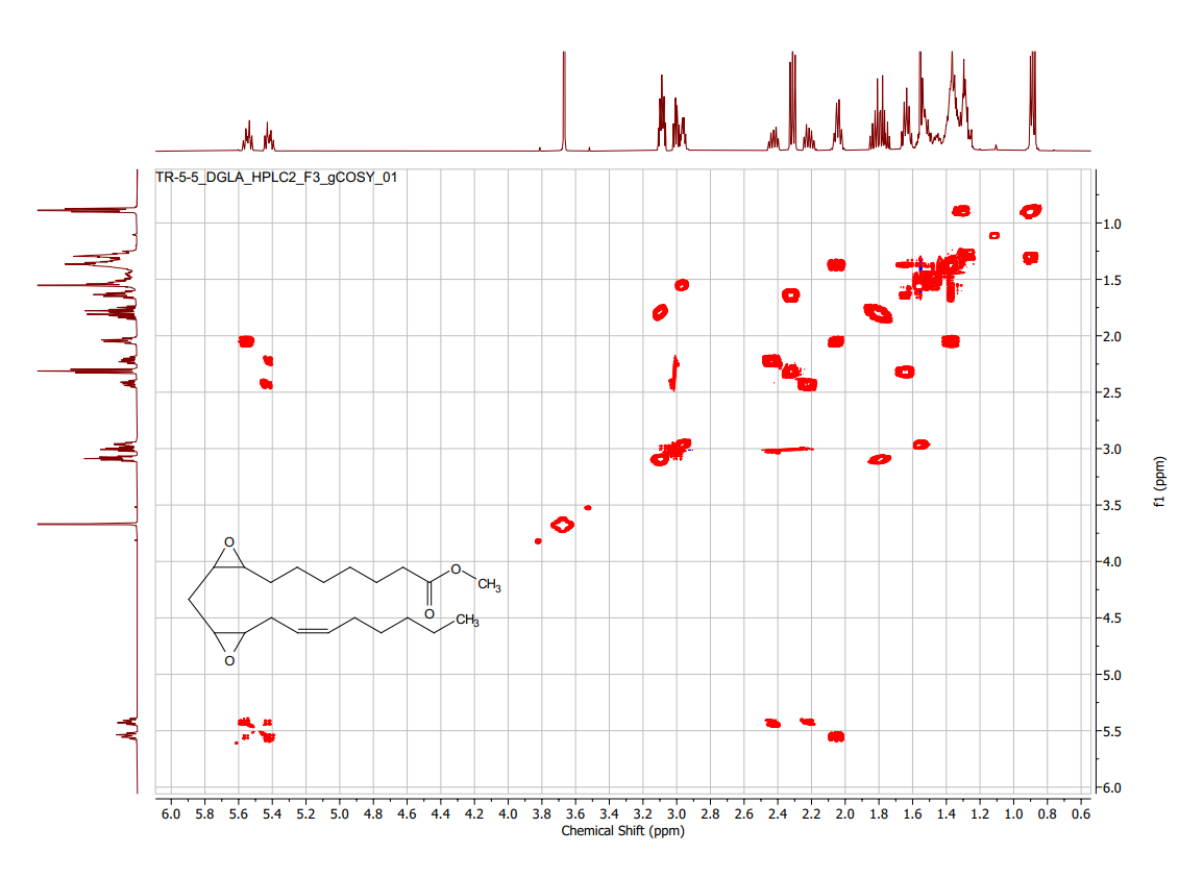


Figure S41: 2D NMR (gCOSY) of the 3rd fraction (F3) of DGLA diepoxides separated by HPLC.

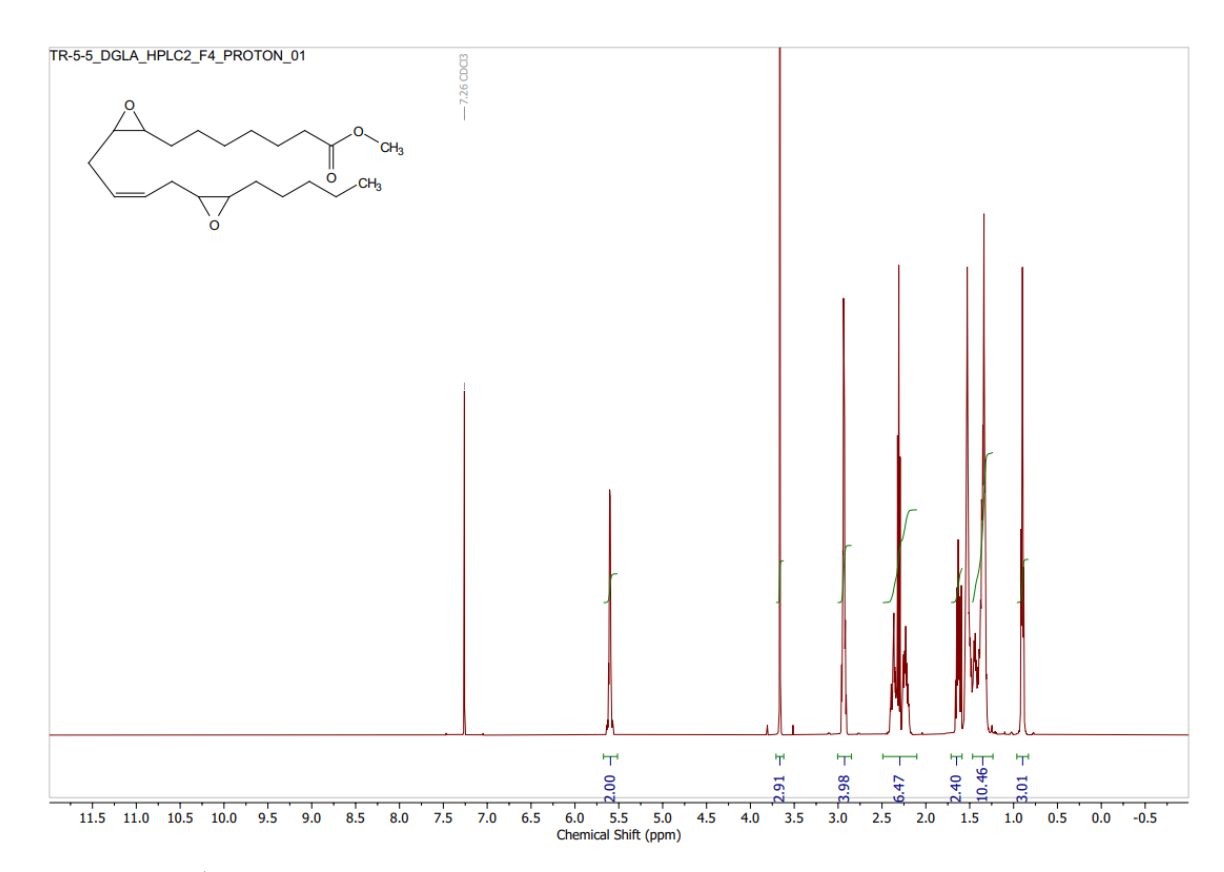


Figure S42: <sup>1</sup>H NMR of the 4th fraction (F4) of DGLA diepoxides separated by HPLC.

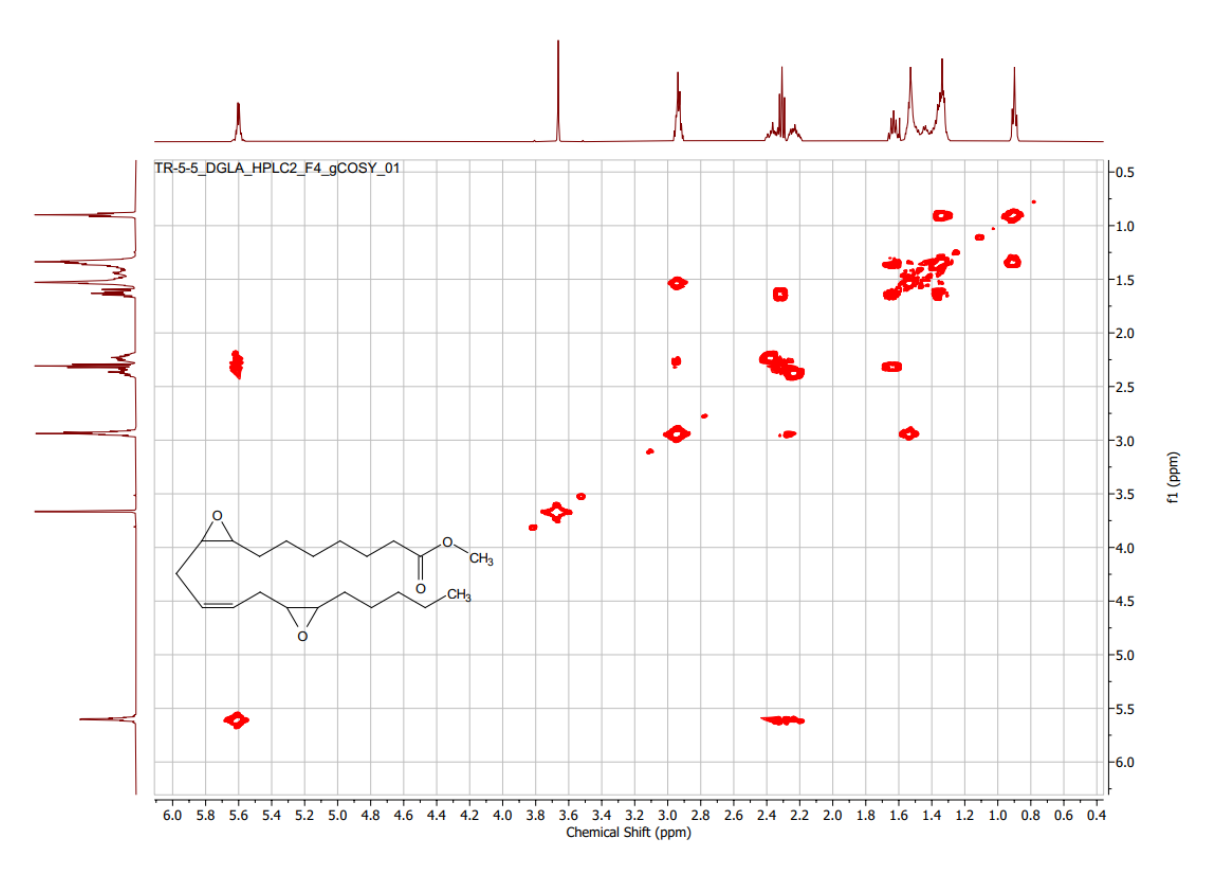


Figure S43: 2D NMR (gCOSY) of the 4th fraction (F4) of DGLA diepoxides separated by HPLC.

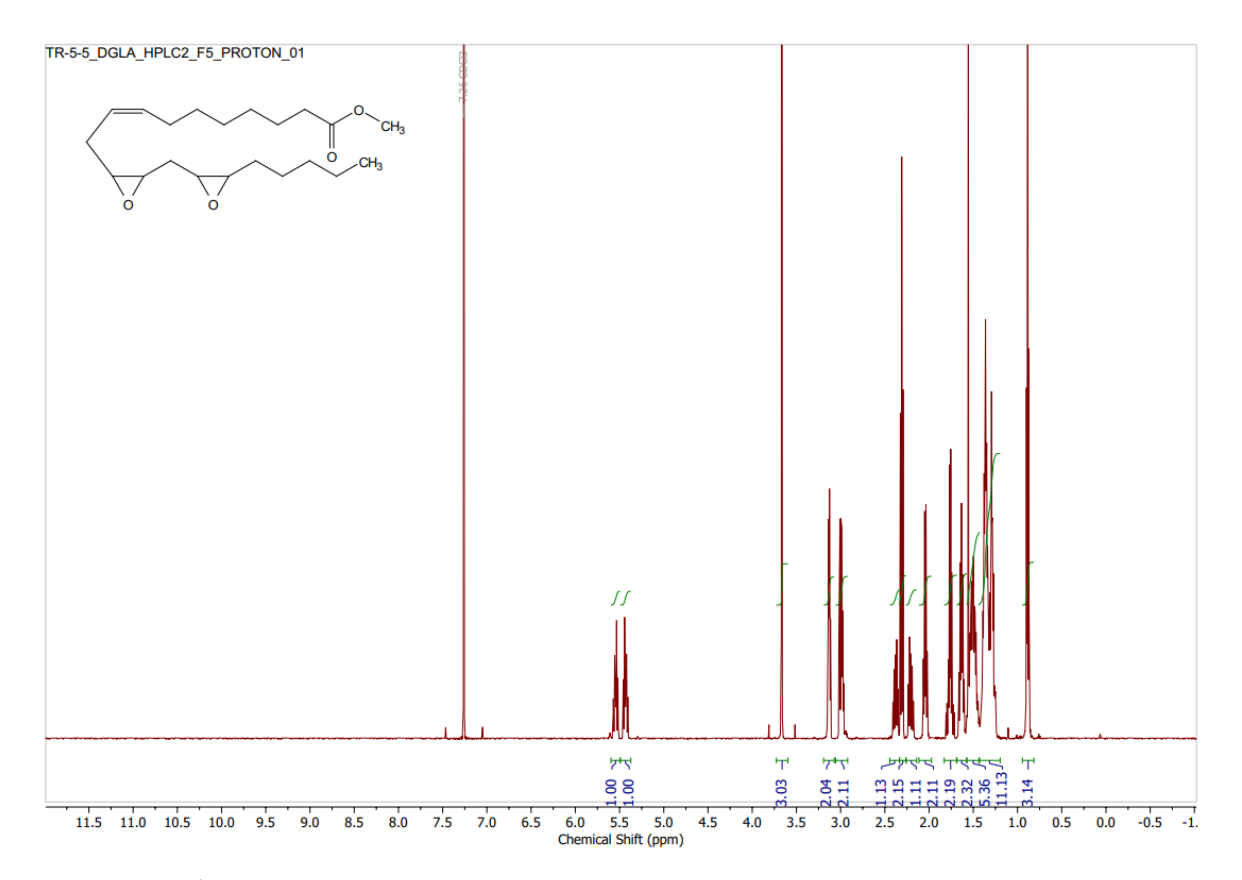


Figure S44: <sup>1</sup>H NMR of the 5th fraction (F5) of DGLA diepoxides separated by HPLC.

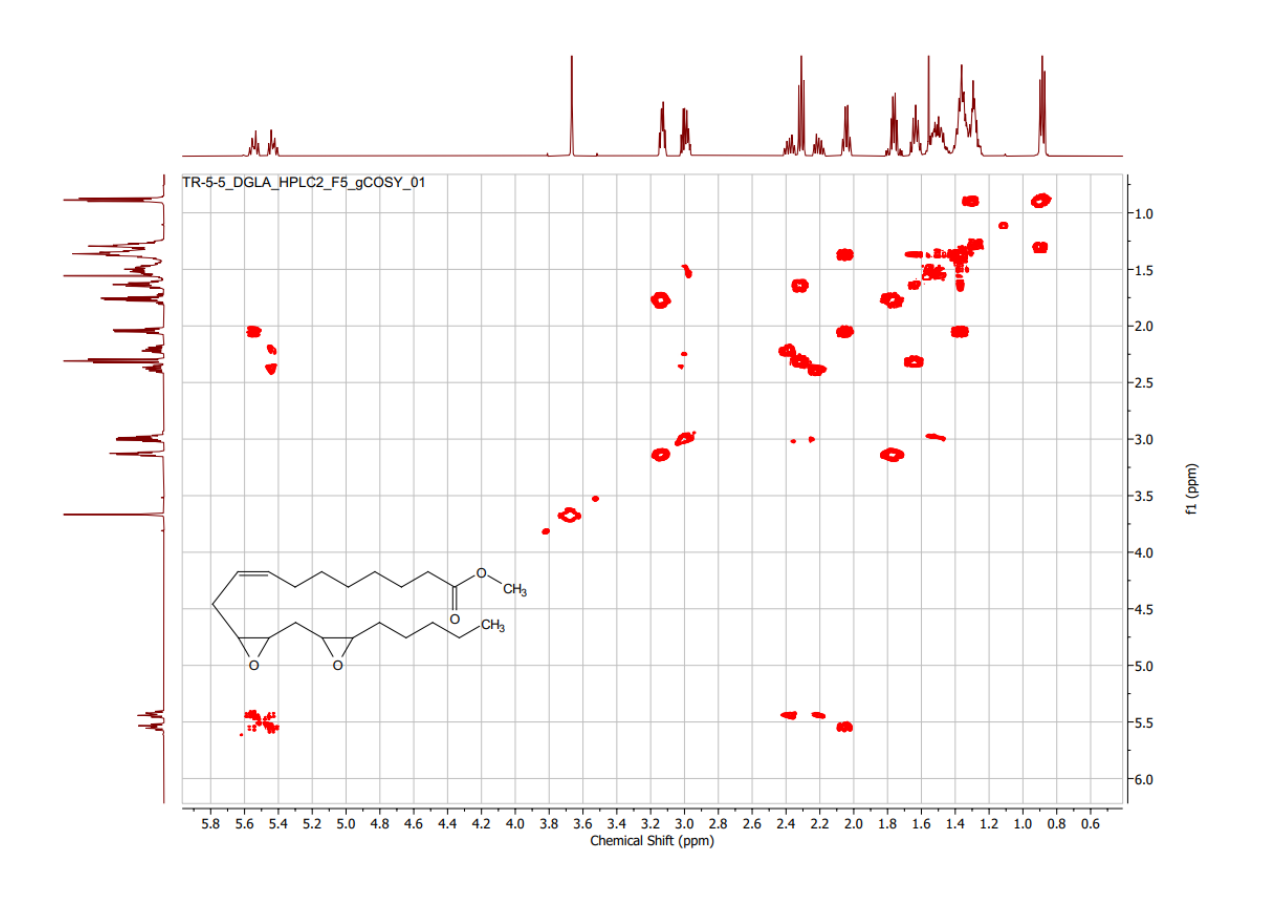
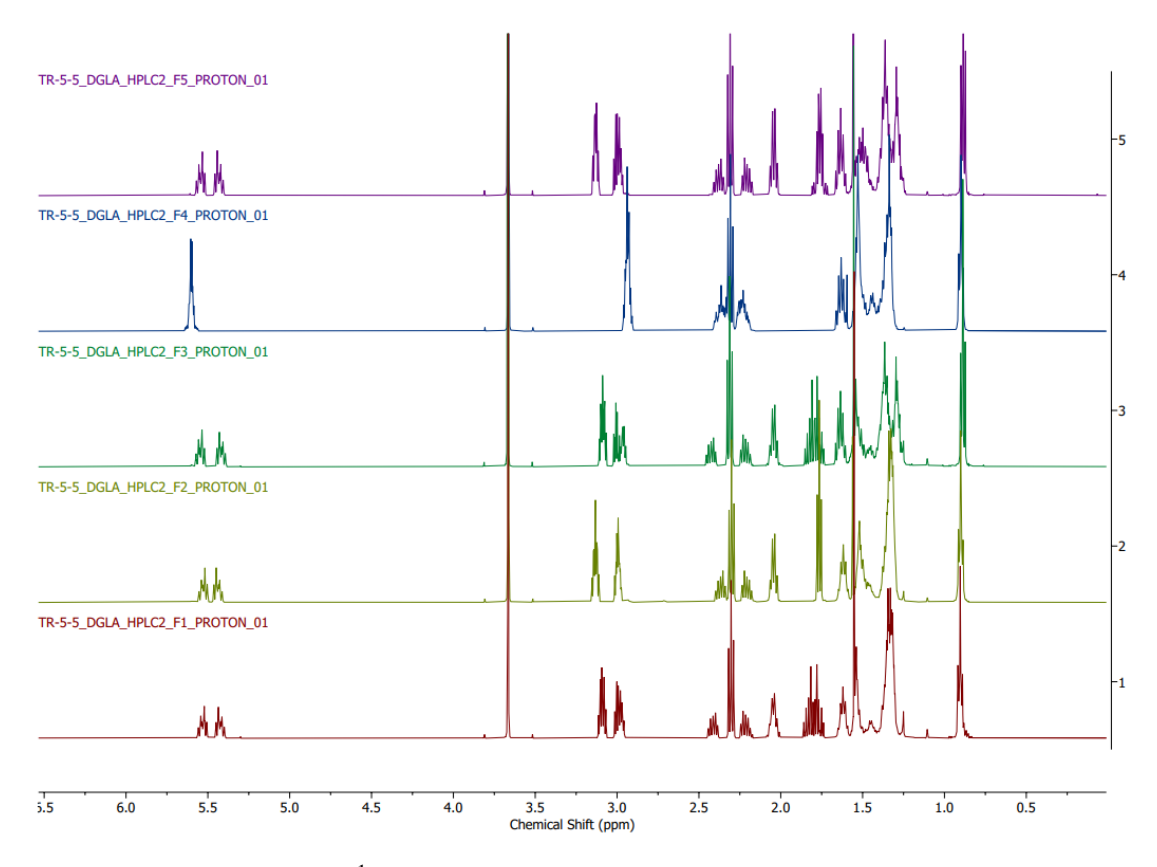
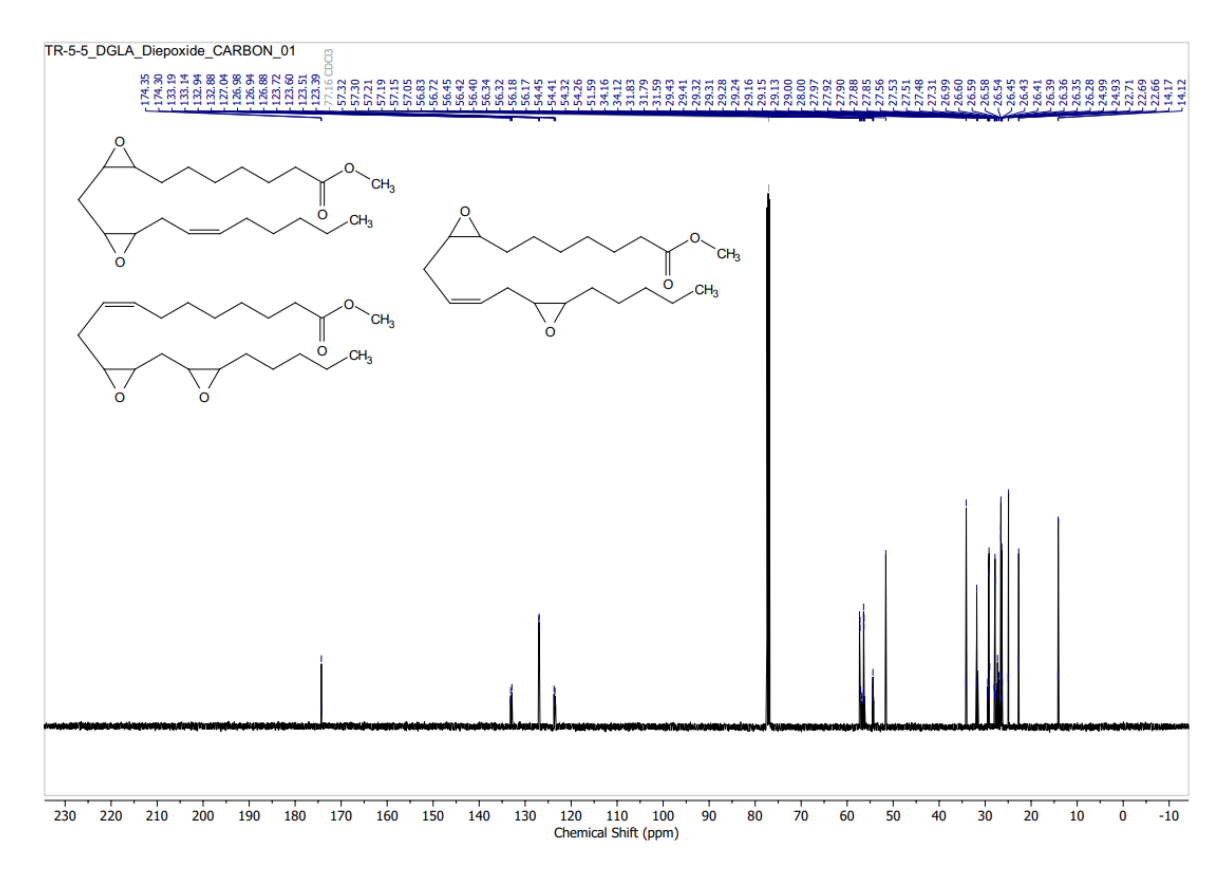


Figure S45: 2D NMR (gCOSY) of the 5th fraction (F5) of DGLA diepoxides separated by HPLC.



**Figure S46**: Comparing the <sup>1</sup>H NMR of different fractions of DGLA diepoxides separated by HPLC.



**Figure S47**: <sup>13</sup>C NMR of a mixture of different DGLA diepoxides regioisomers.

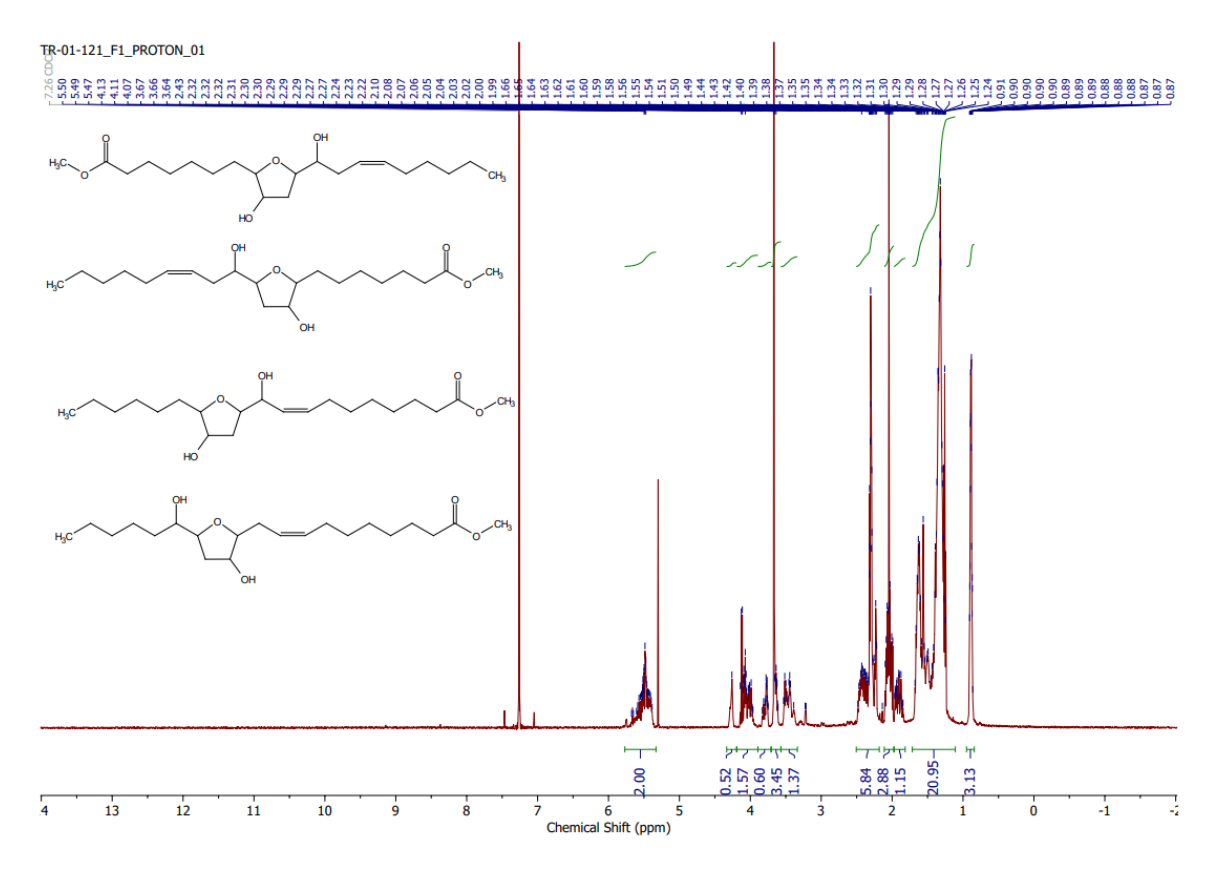


**Figure S48**: <sup>1</sup>H NMR of a mixture of different DGLA THF-diol regioisomers.

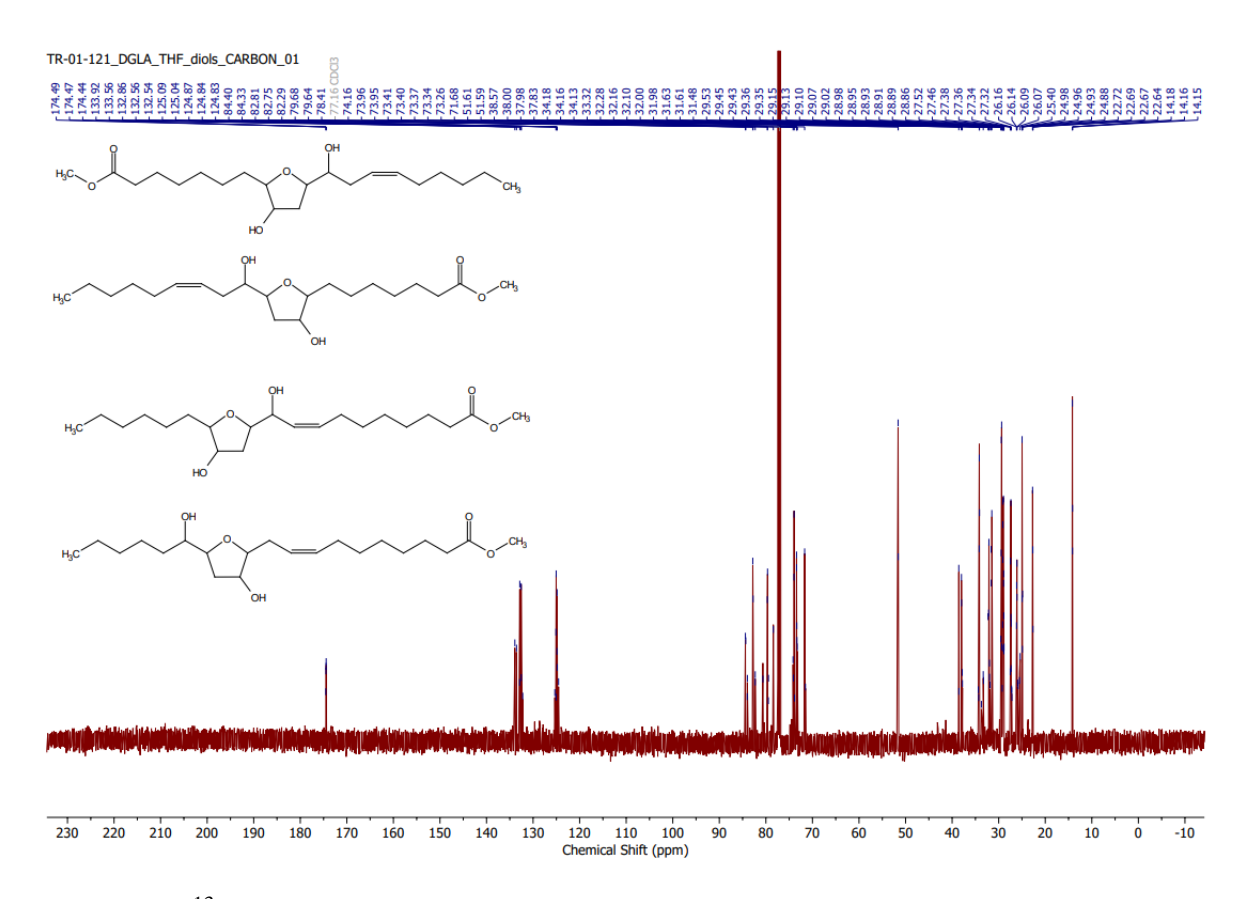


**Figure S49**: <sup>13</sup>C NMR of a mixture of different DGLA THF-diol regioisomers.

**Scheme S8**: Isomers of a mixture of DGLA diepoxides were separated via HPLC shown in Figure S35, representing relative ratio of each isomer.

```
File :C:\msdchem\1\data\Tommy\EI-AJ.M\TR-5-5 HPLC2 F5.D Operator : Jesus Acquired : 24 May 2022 14:34 using AcqMethod AJ_EI.M Instrument : 5975MSD Sample Name:
Misc Info : Vial Number: 0
```

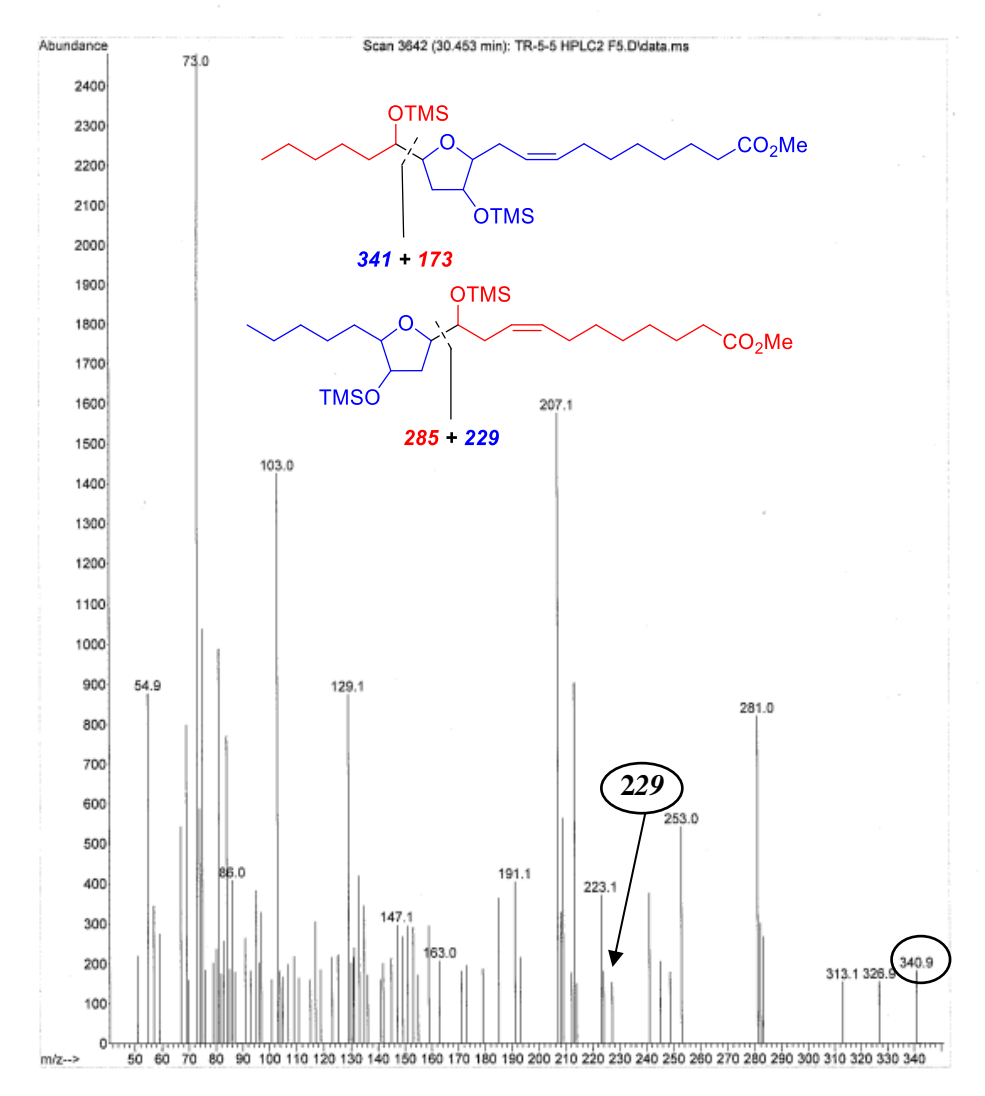


**Figure S50**: GC/MS spectrum of the derivatized isomer isolated from fraction 5 (F5), showing the structure 2 and 3 in fraction 5.

```
File :C:\msdchem\1\data\Tommy\EI-AJ.M\TR-5-5 HPLC2 F5.D
Operator : Jesus
Acquired : 24 May 2022 14:34 using AcqMethod AJ_EI.M
Instrument : 5975MSD
Sample Name:
Misc Info :
Vial Number: 0
```

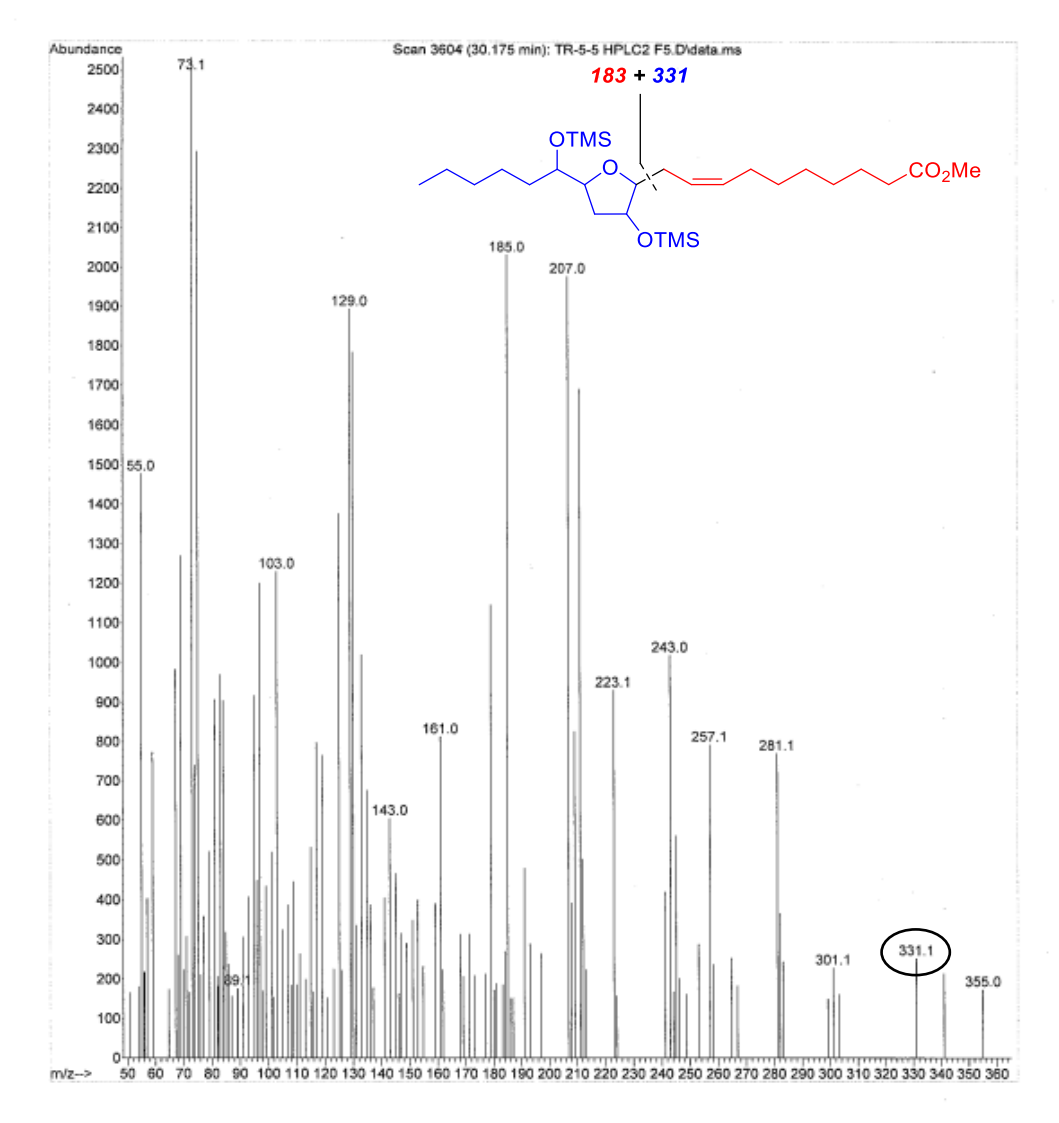


**Figure S51**: GC/MS spectrum of the derivatized isomer isolated from fraction 5 (F5), showing the structure 2 and 3 in fraction 5.

```
File :C:\msdchem\1\data\Tommy\EI-AJ.M\TR-5-5 HPLC2 F3.D
Operator : Jesus
Acquired : 24 May 2022 13:44 using AcqMethod AJ_EI.M
Instrument : 5975MSD
Sample Name:
Misc Info :
Vial Number: 0
```

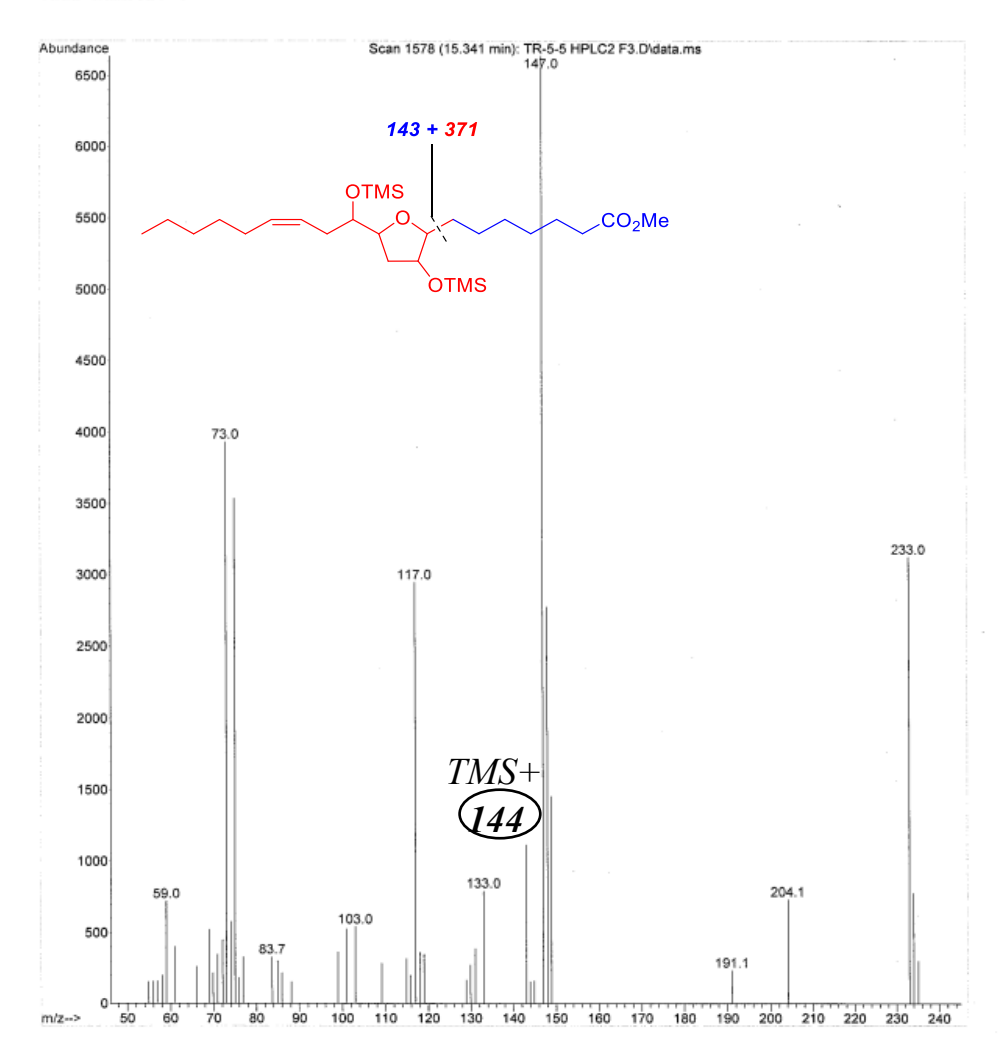


**Figure S52**: GC/MS spectrum of the derivatized isomer isolated from fraction 3 (F3), showing the presence of structure 2 and 3 in fraction 3.

```
File :C:\msdchem\l\data\Tommy\EI-AJ.M\TR-5-5 HPLC2 F3.D Operator : Jesus Acquired : 24 May 2022 13:44 using AcqMethod AJ_EI.M Instrument : 5975MSD Sample Name: Misc Info : Vial Number: 0
```

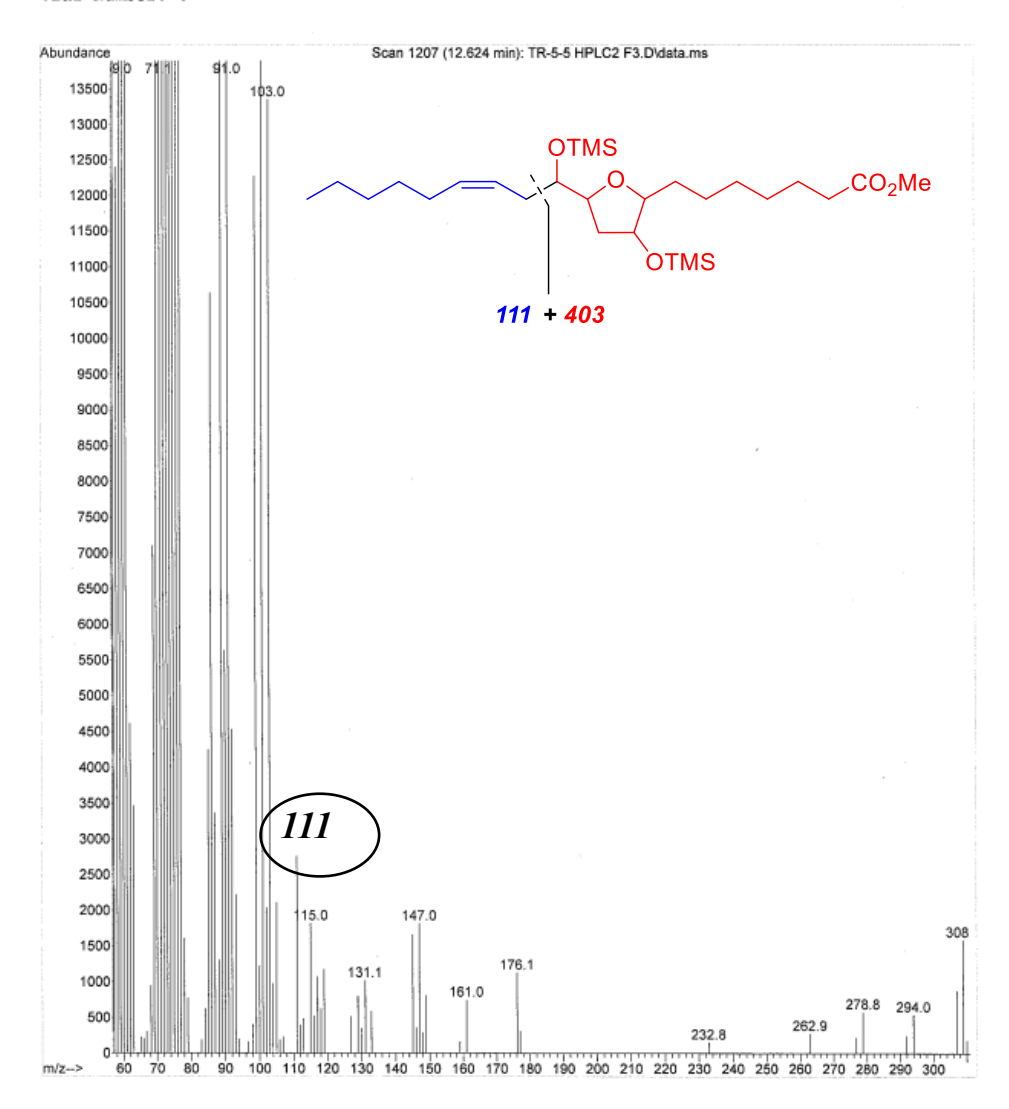


**Figure S53**: GC/MS spectrum of the derivatized isomer isolated from fraction 3 (F3), showing the presence of structure 2 and 3 in fraction 3.

#### **BIBLIOGRAPHY**

- (1) Fay, D. Genetic Mapping and Manipulation: Chapter 1--Introduction and Basics. *WormBook* **2006**, 1–12. https://doi.org/10.1895/wormbook.1.90.1.
- (2) Vladis, N. A.; Fischer, K. E.; Digalaki, E.; Marcu, D.-C.; Bimpos, M. N.; Greer, P.; Ayres, A.; Li, Q.; Busch, K. E. Gap Junctions in the C. Elegans Nervous System Regulate Ageing and Lifespan. *bioRxiv*, 2019, 657817. https://doi.org/10.1101/657817.
- (3) Stiernagle, T. Maintenance of C. Elegans. *WormBook* **2006**, 1–11. https://doi.org/10.1895/wormbook.1.101.1.
- (4) Tucci, M. L.; Harrington, A. J.; Caldwell, G. A.; Caldwell, K. A. Modeling Dopamine Neuron Degeneration in Caenorhabditis Elegans. *Methods Mol. Biol.* **2011**, *793*, 129–148. https://doi.org/10.1007/978-1-61779-328-8\_9.
- (5) Kim, I.-H.; Nishi, K.; Tsai, H.-J.; Bradford, T.; Koda, Y.; Watanabe, T.; Morisseau, C.; Blanchfield, J.; Toth, I.; Hammock, B. D. Design of Bioavailable Derivatives of 12-(3-Adamantan-1-Yl-Ureido)Dodecanoic Acid, a Potent Inhibitor of the Soluble Epoxide Hydrolase. *Bioorg. Med. Chem.* **2007**, *15* (1), 312–323. https://doi.org/10.1016/j.bmc.2006.09.057.

# **APPENDIX 2:** SUPPORTING INFORMATION FOR CHAPTER 3

### TABLE OF CONTENTS

1.	Supporting Figures (Figure S1-S16):	288
	Materials and strains:	
<i>3</i> .	Experimental procedure	306
	LIOGRAPHY Error! Bookmark not defin	

#### 1. Supporting Figures (Figure S1-S16):

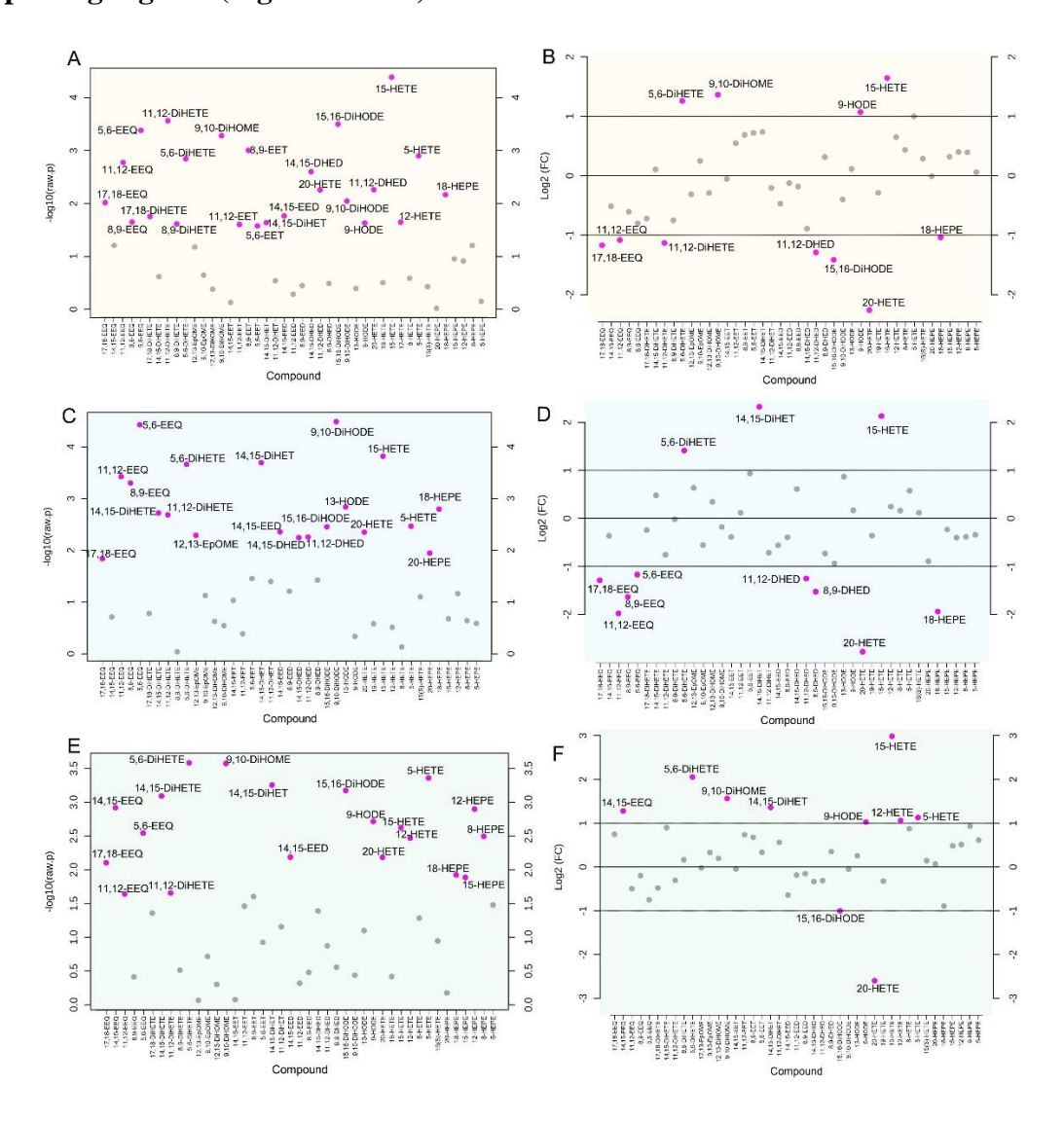


**Figure S1.** Oxylipin profile of *C. elegans* changes upon expression of  $A\beta$  and/or tau. (A) Unpaired T-test results for oxylipin change of *C. elegans* expressing tau compared to the wildtype. (B) Fold change analysis results for oxylipin change of *C. elegans* expressing tau compared to the wildtype. (C) Unpaired T-test results for oxylipin change of *C. elegans* expressing  $A\beta$  compared to the wildtype. (D) Fold change analysis results for oxylipin change of *C. elegans* coexpressing  $A\beta$  and tau compared to the wildtype. (E) Unpaired T-test results for oxylipin change of *C. elegans* coexpressing  $A\beta$  and tau compared to the wildtype. (F) Fold change analysis results for oxylipin change of *C. elegans* coexpressing  $A\beta$  and tau compared to the wildtype. Note that for A, C, and D, the raw p-value is shown here to the each oxylipin level in transgenic with its counterpart in wildtype. The results after applying multiple correction using the Benjamini-Hochberg procedure to control the false discovery rate (FDR 5%) are shown in chapter 3, Figure 1.

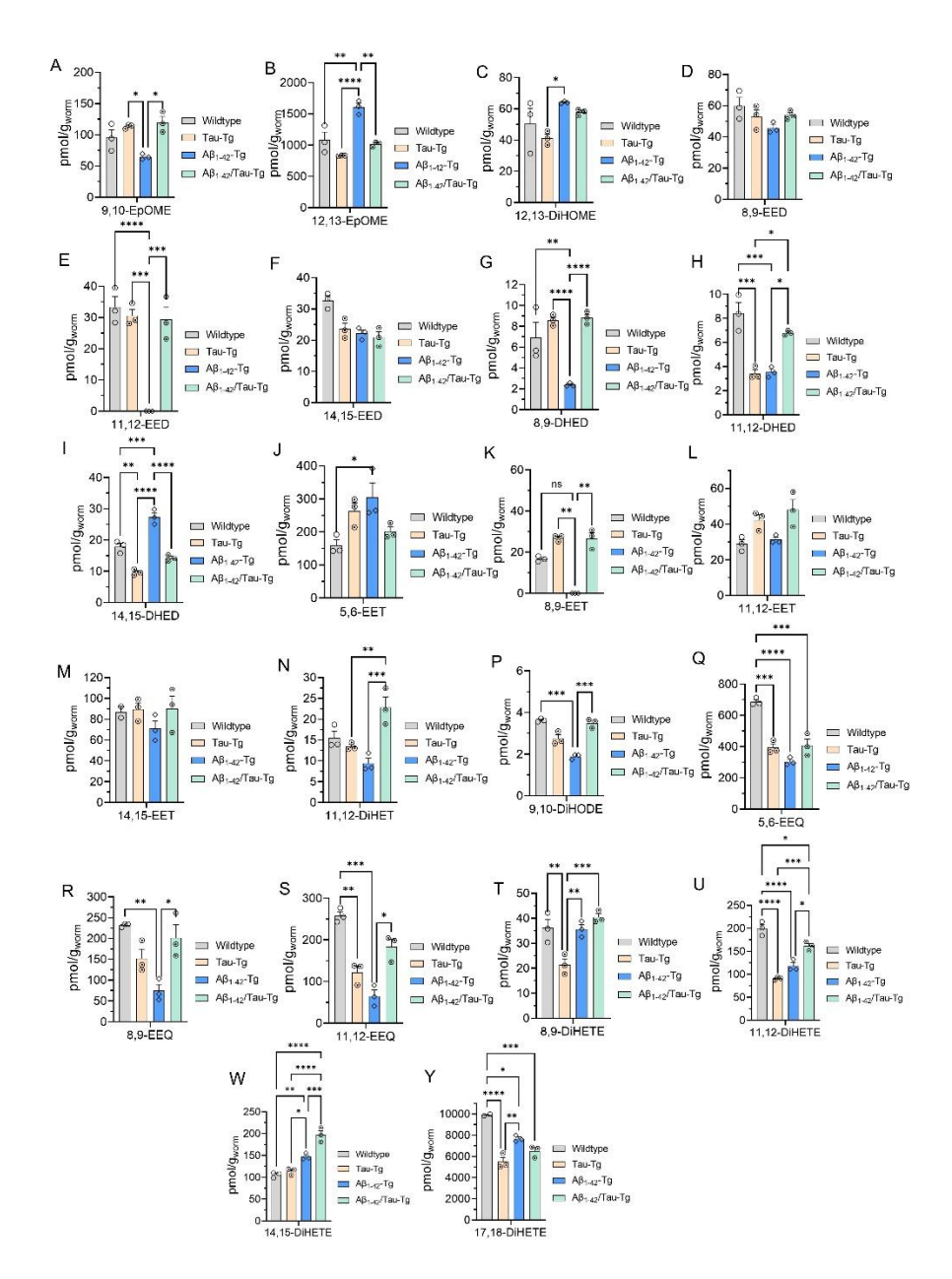


Figure S2. Ep-PUFA and dihydroxy-PUFA in C. elegans expressing Aβ and/or tau compared to wildtype. (A-C) linoleic acid epoxy and dihydroxy metabolites. (D-I) dihomo- $\gamma$  linoleic acid epoxy and dihydroxy metabolites. (J-N) Arachidonic acid epoxy and dihydroxy metabolites, (P) α-linoleic acid dihydroxy metabolite. (Q-Y) eicosapentaenoic acid epoxy and dihydroxy metabolites. In all experiments worms were grown at 16 degrees until L4; then transferred and kept at 25°C. age-synchronized worms were collected at day 3 for oxylipin analysis. Statistical analysis: One-way analysis of variance (ANOVA) with Tukey's multiple tests is used, where \*P  $\leq$  0.05, \*\*P  $\leq$  0.01, \*\*\*\*P  $\leq$  0.001, \*\*\*\*P  $\leq$  0.001, non-significant is not shown.

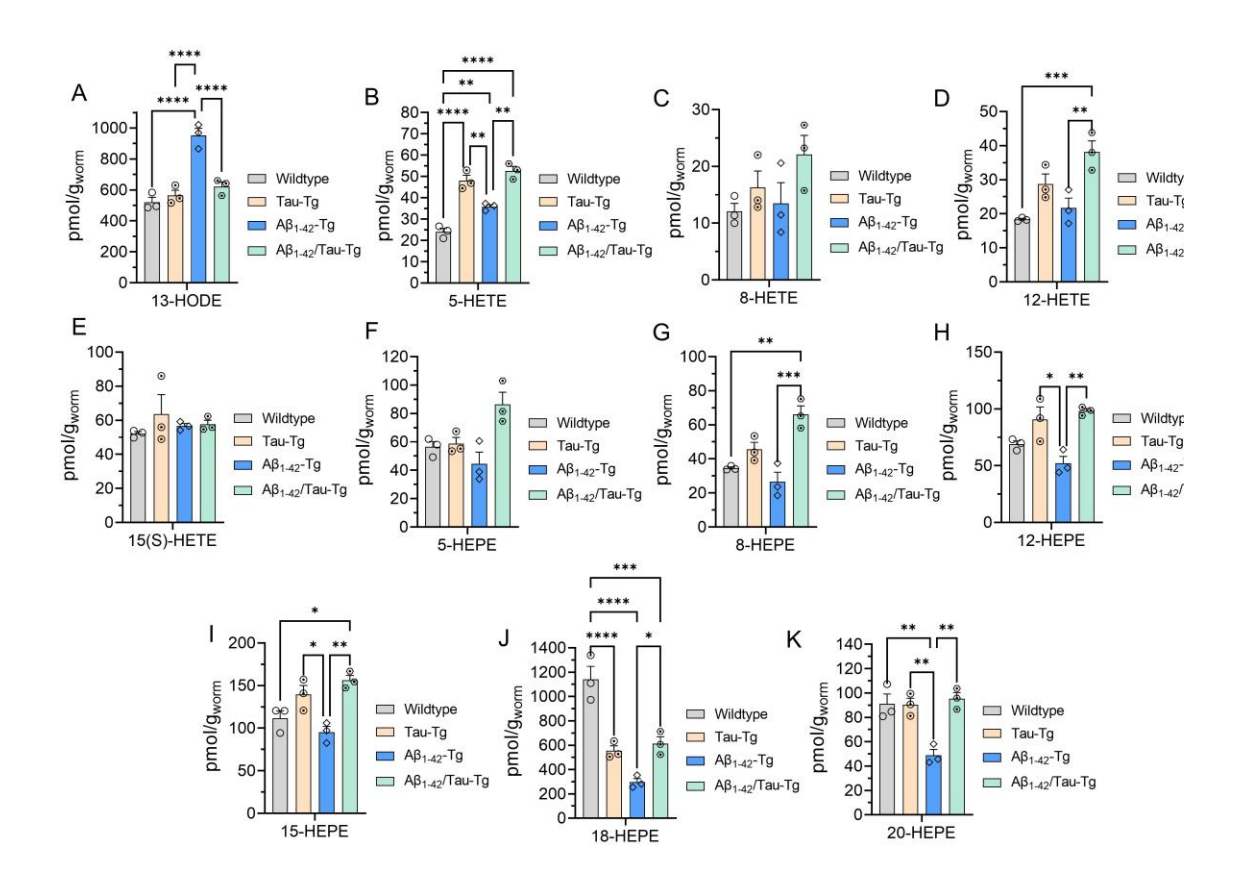
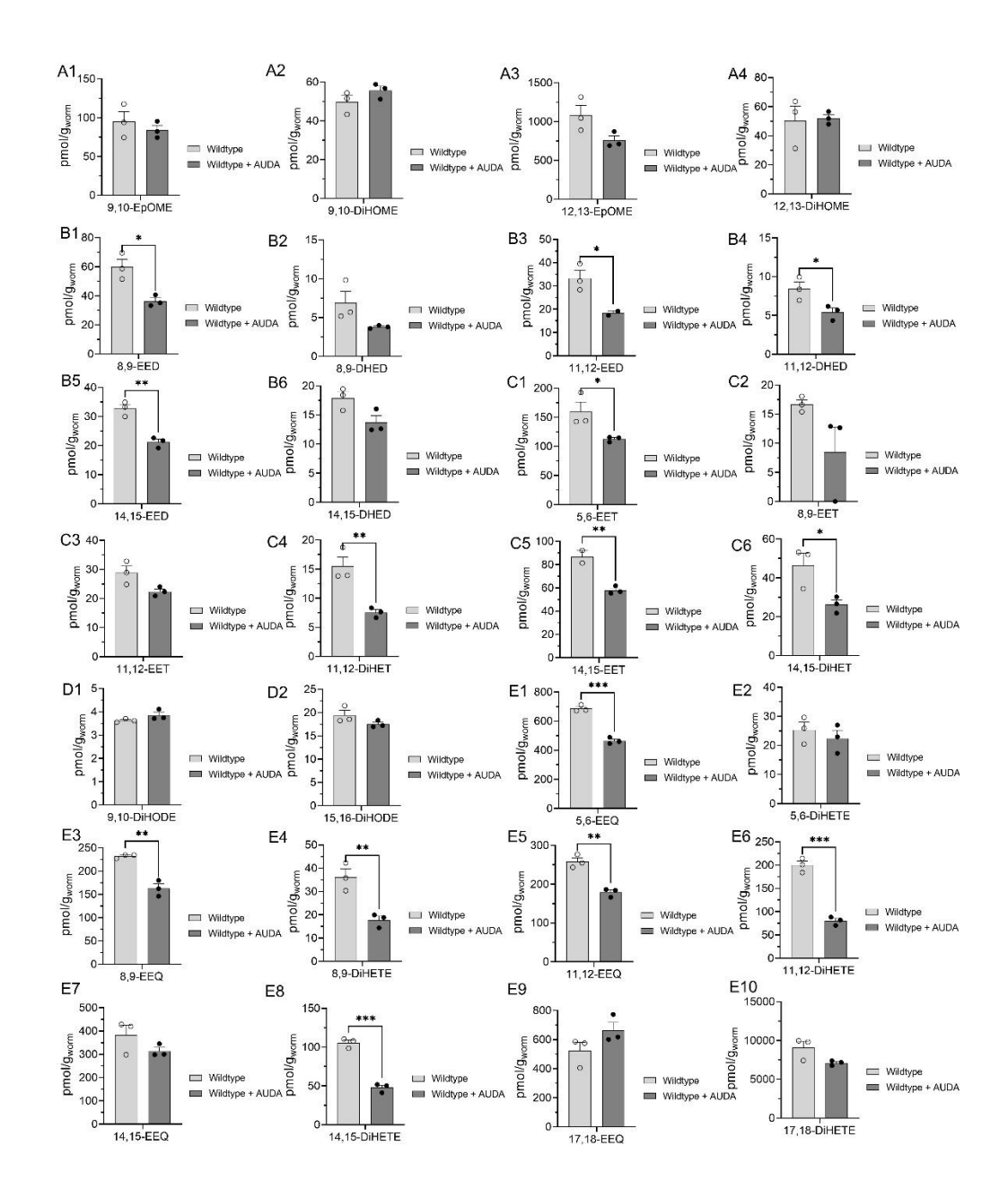
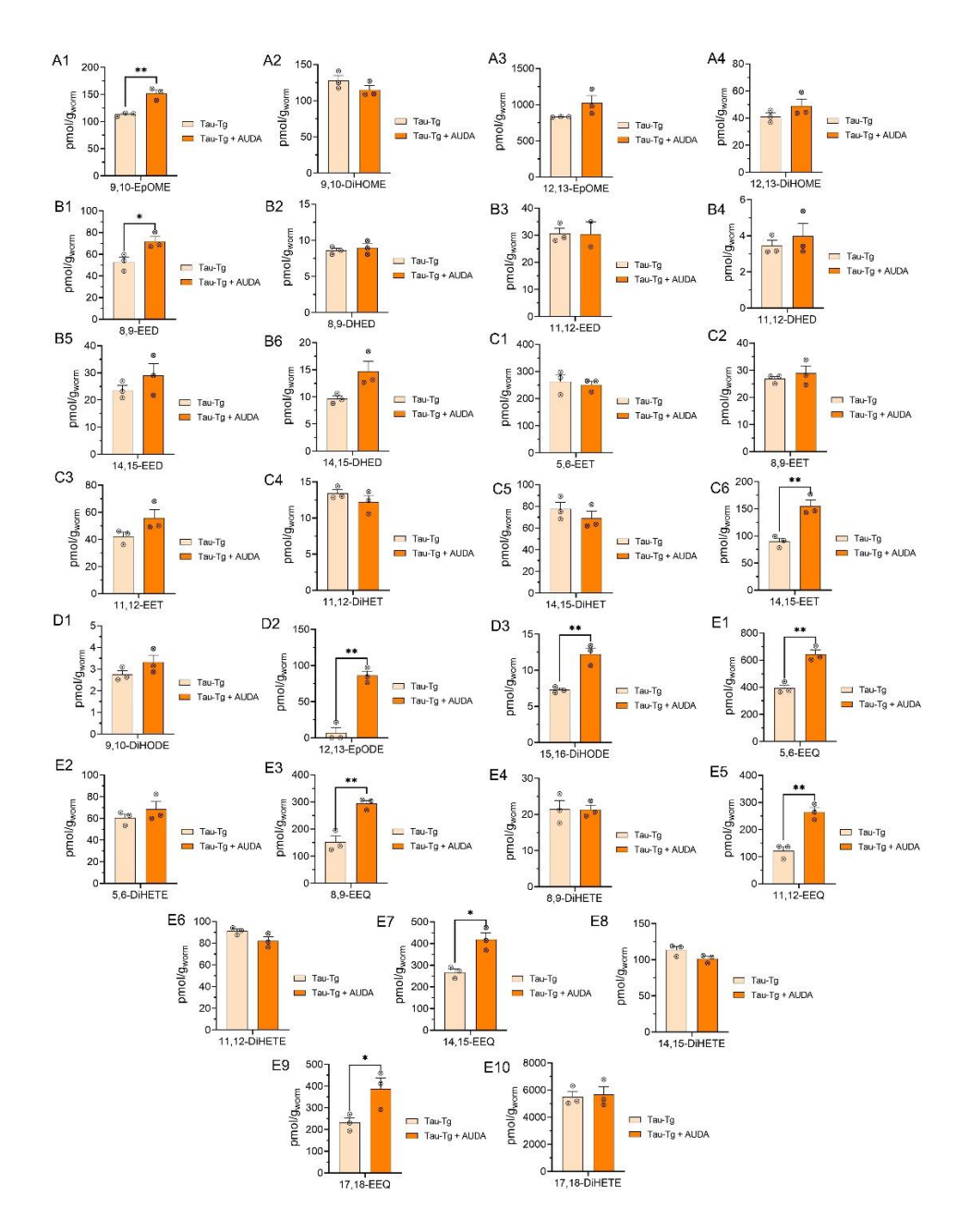


Figure S3. Hydroxy-PUFAs level comparison in *C. elegans* expressing Aβ and/or tau compared to wildtype. (A) linoleic acid hydroxy metabolites. (B-E) Arachidonic acid hydroxy metabolites. (F-K) eicosapentaenoic acid hydroxy metabolites. In all experiments worms were grown at 16 degrees till L4; then transferred and kept at 25°C. Age-synchronized worms were collected at day 3 for oxylipin analysis. Statistical analysis: One-way analysis of variance (ANOVA) with Tukey's multiple tests where \*P  $\leq$  0.05, \*\*P  $\leq$  0.01, \*\*\*\*P  $\leq$  0.001, \*\*\*\*P  $\leq$  0.001, non-significant is not shown.



**Figure S4.** AUDA effect on Ep-PUFA and dihydroxy-PUFA in wildtype *C. elegans* (A1-A4) linoleic acid epoxy and dihydroxy metabolites. (B1-B6) dihomo- $\gamma$  linoleic acid epoxy and dihydroxy metabolites. (C1-C6) Arachidonic acid epoxy and dihydroxy metabolites. (D1 and D2) α-linoleic acid dihydroxy metabolite. (E1-E10) eicosapentaenoic acid epoxy and dihydroxy metabolites. In all experiments worms were grown at 16 degrees until L4, then transferred to plates with or without AUDA (100 μM) and kept at 25°C. Age-synchronized worms were collected at day 3 for oxylipin analysis. Statistical analysis is based on unpaired t-test, where \*P  $\leq$  0.05, \*\*P  $\leq$  0.01, \*\*\*P  $\leq$  0.001, non-significant is not shown. The results after applying multiple correction using the Benjamini-Hochberg procedure to control the false discovery rate (FDR 5%) are shown in chapter 3, Figure 4B.



**Figure S5.** AUDA effect on Ep-PUFA and dihydroxy-PUFA in Tau-Tg strain (A1-A4) linoleic acid epoxy and dihydroxy metabolites. (B1-B6) dihomo- $\gamma$  linoleic acid epoxy and dihydroxy metabolites. (C1-C6) Arachidonic acid epoxy and dihydroxy metabolites. (D1-D3) α-linoleic acid dihydroxy metabolite. (E1-E10) eicosapentaenoic acid epoxy and dihydroxy metabolites. In all experiments worms were grown at 16 degrees until L4 then transferred to plates with or without AUDA (100 μM) and kept at 25°C. age-synchronized worms were collected at day 3 for oxylipin analysis. Statistical analysis is based on unpaired t-test, where  $*P \le 0.05$ ,  $**P \le 0.01$ ,  $***P \le 0.001$ , \*\*\*\*P < 0.0001, non-significant is not shown. The results after applying multiple correction using the Benjamini-Hochberg procedure to control the false discovery rate (FDR 5%) are shown in chapter 3, Figure 4C.

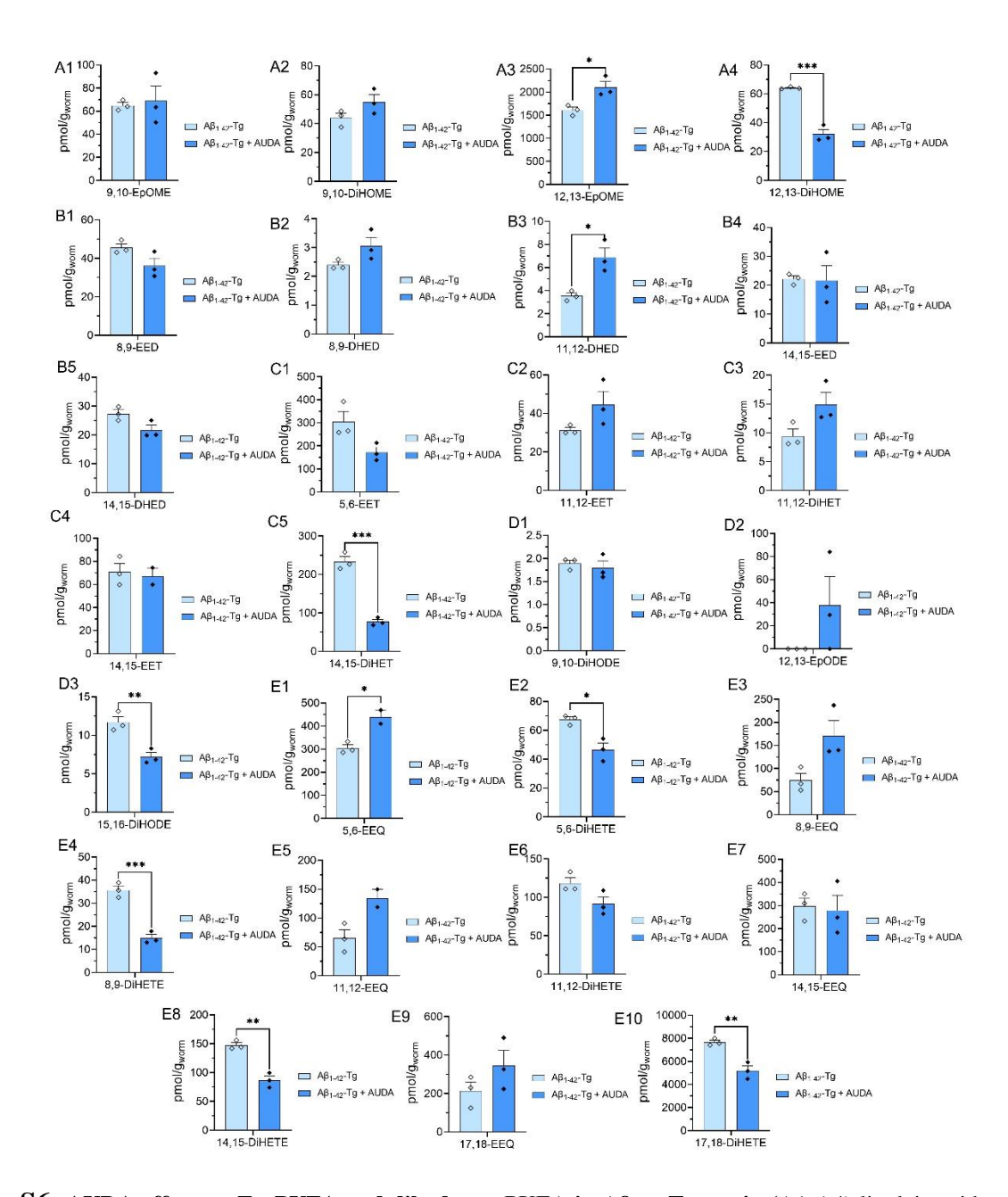


**Figure S6.** AUDA effect on Ep-PUFA and dihydroxy-PUFA in A $\beta_{1-42}$ -Tg strain (A1-A4) linoleic acid epoxy and dihydroxy metabolites. (B1-B5) dihomo- $\gamma$  linoleic acid epoxy and dihydroxy metabolites. (C1-C5) Arachidonic acid epoxy and dihydroxy metabolites. (D1-D3) α-linoleic acid dihydroxy metabolite. (E1-E10) eicosapentaenoic acid epoxy and dihydroxy metabolites. In all experiments worms were grown at 16 degrees until L4 then transferred to plates with or without AUDA (100 μM) and kept at 25°C. Age-synchronized worms were collected at day 3 for oxylipin analysis. Statistical analysis is based on unpaired t-test, where \*P  $\leq$  0.05, \*\*P  $\leq$  0.01, \*\*\*P  $\leq$  0.001, non-significant is not shown. The results after applying multiple correction using the Benjamini-Hochberg procedure to control the false discovery rate (FDR 5%) are shown in chapter 3, Figure 4D.

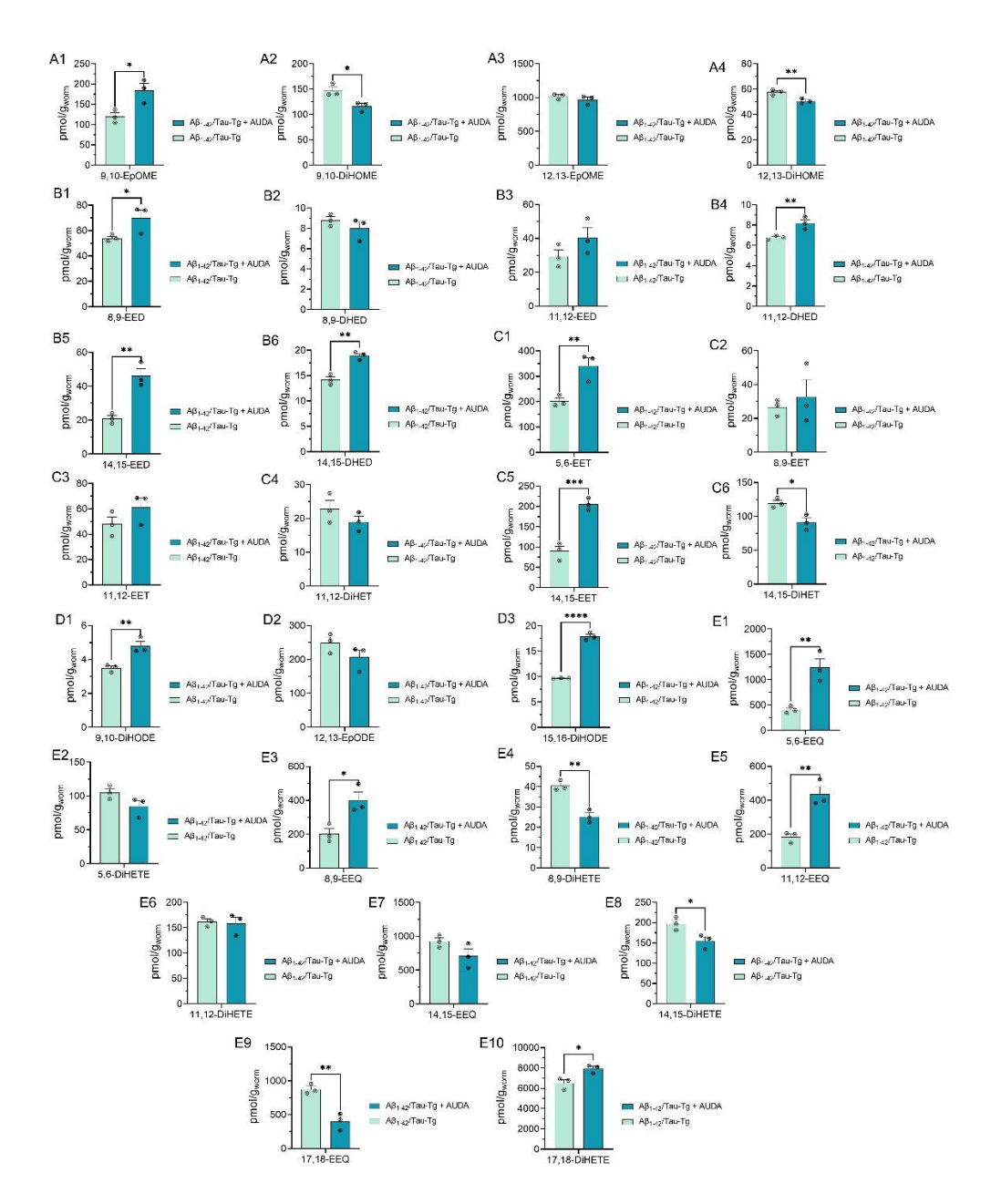
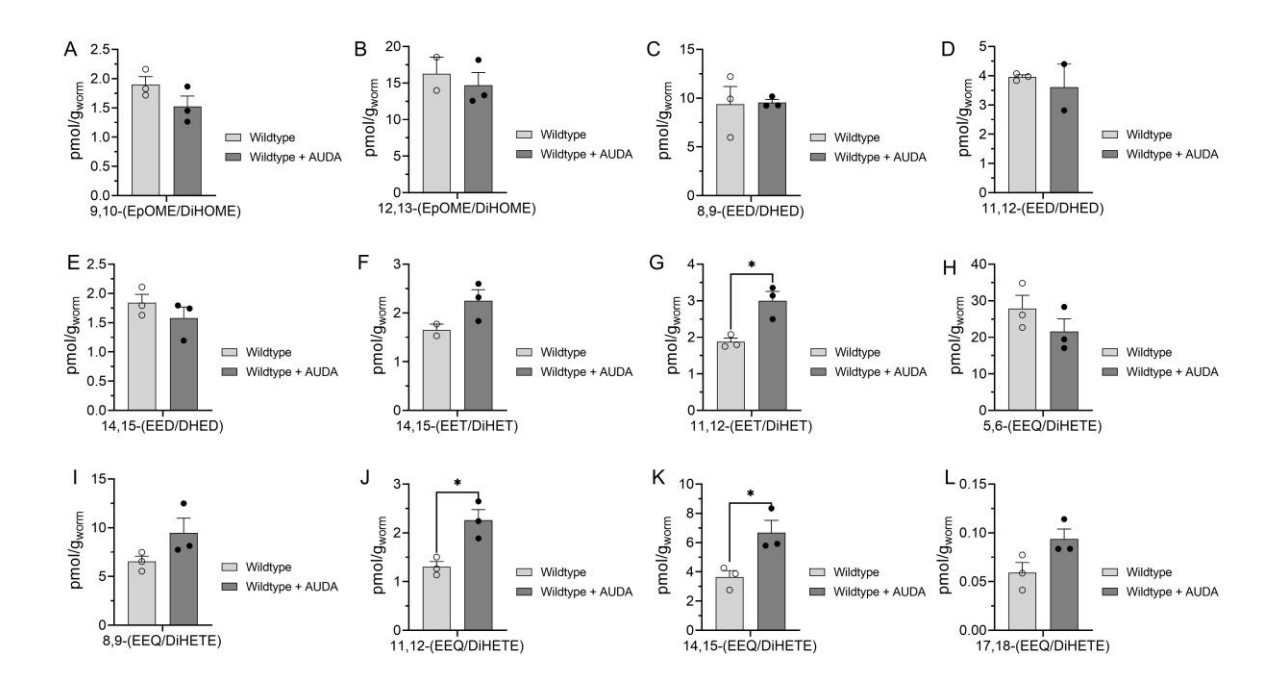
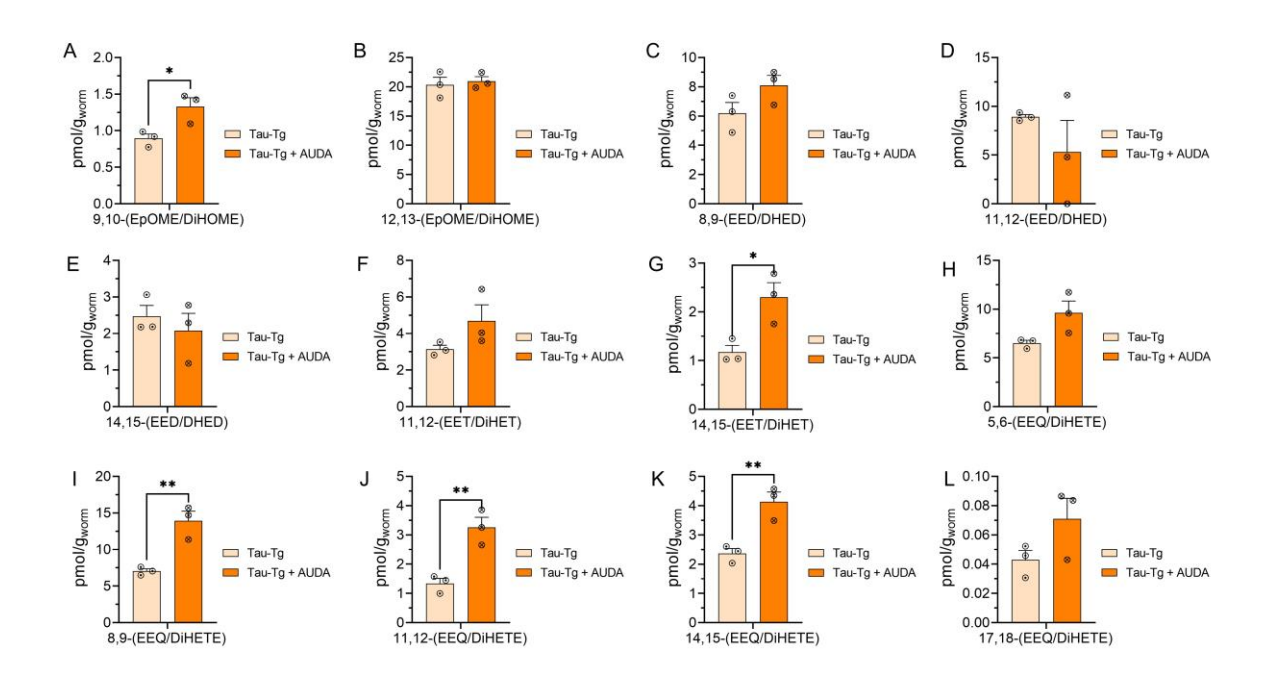


Figure S7. AUDA effect on Ep-PUFA and dihydroxy-PUFA in A $\beta_{1-42}$ /Tau-Tg strain (A1-A4) linoleic acid epoxy and dihydroxy metabolites. (B1-B6) dihomo- $\gamma$  linoleic acid epoxy and dihydroxy metabolites. (C1-C6) Arachidonic acid epoxy and dihydroxy metabolites. (D1-D3) α-linoleic acid dihydroxy metabolite. (E1-E10) eicosapentaenoic acid epoxy and dihydroxy metabolites. In all experiments worms were grown at 16 degrees until L4 then transferred to plates with or without AUDA (100 μM) and kept at 25°C. age-synchronized worms were collected at day 3 for oxylipin analysis. Statistical analysis is based on unpaired t-test, where \*P  $\leq$  0.05, \*\*P  $\leq$  0.01, \*\*\*P  $\leq$  0.001, \*\*\*\*P < 0.0001, non-significant is not shown. The results after applying multiple correction using the Benjamini-Hochberg procedure to control the false discovery rate (FDR 5%) are shown in chapter 3 Figure 4E.



**Figure S8.** AUDA effect on epoxy to dihydroxy ratio in wildtype worm. (A and B) linoleic acid epoxy and dihydroxy metabolites. (C-E) dihomo- $\gamma$  linoleic acid epoxy and dihydroxy metabolites. (F and G) Arachidonic acid epoxy and dihydroxy metabolites. (H-L) eicosapentaenoic acid epoxy and dihydroxy metabolites. In all experiments worms were grown at 16 degrees until L4 then transferred to plates with or without AUDA (100 μM) and kept at 25°C. Age-synchronized worms were collected at day 3 for oxylipin analysis. Statistical analysis is based on unpaired t-test, where \*P ≤ 0.05, \*\*P ≤ 0.01, \*\*\*P ≤ 0.001, \*\*\*\*P < 0.0001, non-significant is not shown. The results after applying multiple correction using the Benjamini-Hochberg procedure to control the false discovery rate (FDR 5%) were used for volcano plot in chapter 3, Figure 4F.



**Figure S9.** AUDA effect on epoxy to dihydroxy ratio in Tau-Tg strain. (A and B) linoleic acid epoxy and dihydroxy metabolites. (C-E) dihomo- $\gamma$  linoleic acid epoxy and dihydroxy metabolites. (F and G) Arachidonic acid epoxy and dihydroxy metabolites. (H-L) eicosapentaenoic acid epoxy and dihydroxy metabolites. In all experiments worms were grown at 16 degrees until L4 then transferred to plates with or without AUDA (100 μM) and kept at 25°C. Age-synchronized worms were collected at day 3 for oxylipin analysis. Statistical analysis is based on unpaired t-test, where \*P ≤ 0.05, \*\*P ≤ 0.01, \*\*\*\*P ≤ 0.001, \*\*\*\*P < 0.0001, non-significant is not shown. The results after applying multiple correction using the Benjamini-Hochberg procedure to control the false discovery rate (FDR 5%) were used for volcano plot in chapter 3, Figure 4G.

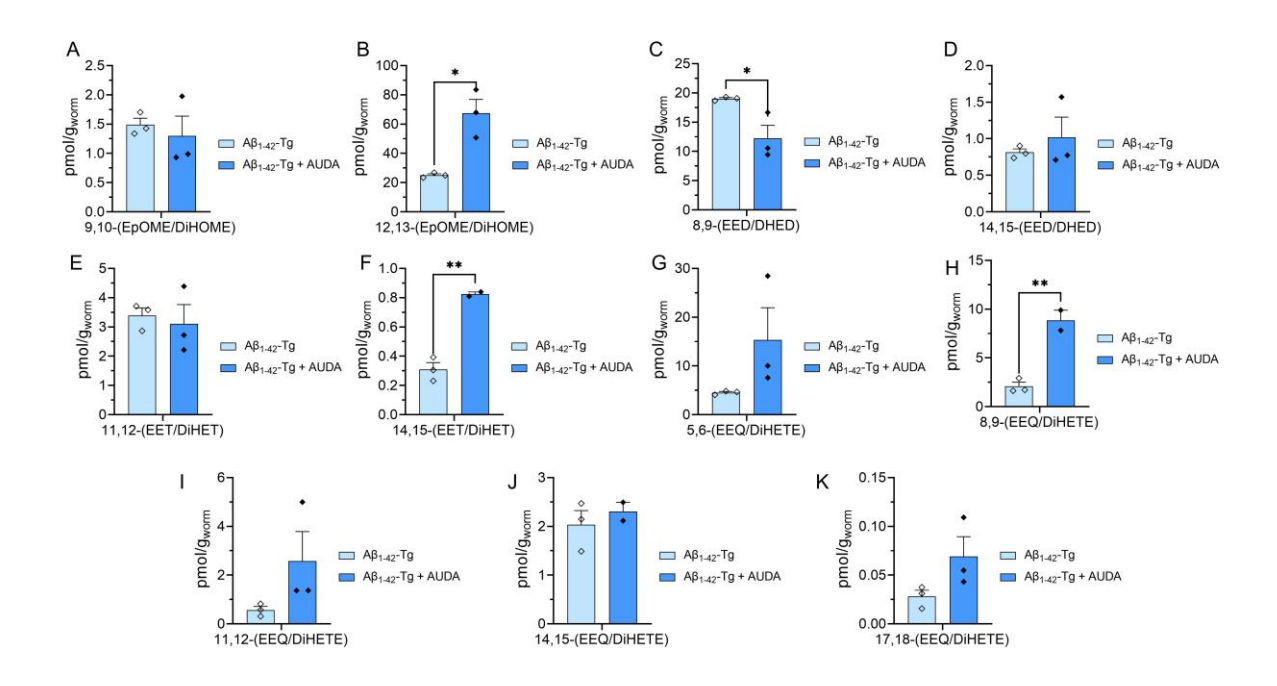


**Figure S10.** AUDA effect on epoxy to dihydroxy ratio in Aβ<sub>1-42</sub>-Tg strain. (A and B) linoleic acid epoxy and dihydroxy metabolites. (C and D) dihomo- $\gamma$  linoleic acid epoxy and dihydroxy metabolites. (E and F) Arachidonic acid epoxy and dihydroxy metabolites. (G-K) eicosapentaenoic acid epoxy and dihydroxy metabolites. In all experiments worms were grown at 16 degrees until L4 then transferred to plates with or without AUDA (100 μM) and kept at 25°C. Age-synchronized worms were collected at day 3 for oxylipin analysis. Statistical analysis is based on unpaired t-test, where \*P  $\leq$  0.05, \*\*P  $\leq$  0.01, \*\*\*P  $\leq$  0.001, \*\*\*\*P < 0.0001, non-significant is not shown. The results after applying multiple correction using the Benjamini-Hochberg procedure to control the false discovery rate (FDR 5%) were used for volcano plot in chapter 3, Figure 4H.

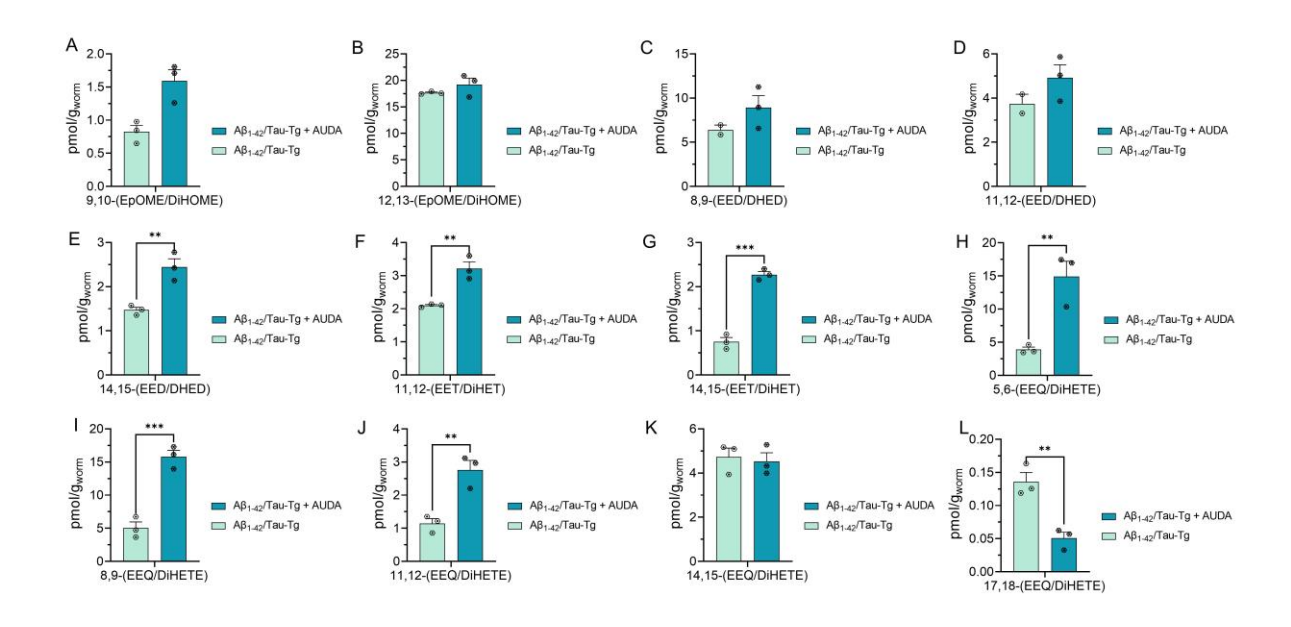


**Figure S11.** AUDA effect on epoxy to dihydroxy ratio in A $β_{1-42}$ /Tau-Tg strain. (A and B) linoleic acid epoxy and dihydroxy metabolites. (C-E) dihomo-γ linoleic acid epoxy and dihydroxy metabolites. (F and G) Arachidonic acid epoxy and dihydroxy metabolites. (H-L) eicosapentaenoic acid epoxy and dihydroxy metabolites. In all experiments worms were grown at 16 degrees until L4 then transferred to plates with or without AUDA (100 μM) and kept at 25°C. Age-synchronized worms were collected at day 3 for oxylipin analysis. Statistical analysis is based on unpaired t-test, where \*P  $\le 0.05$ , \*\*P  $\le 0.01$ , \*\*\*P  $\le 0.001$ , \*\*\*\*P < 0.0001, non-significant is not shown. The results after applying multiple correction using the Benjamini-Hochberg procedure to control the false discovery rate (FDR 5%) were used for volcano plot in chapter 3, Figure 4I.

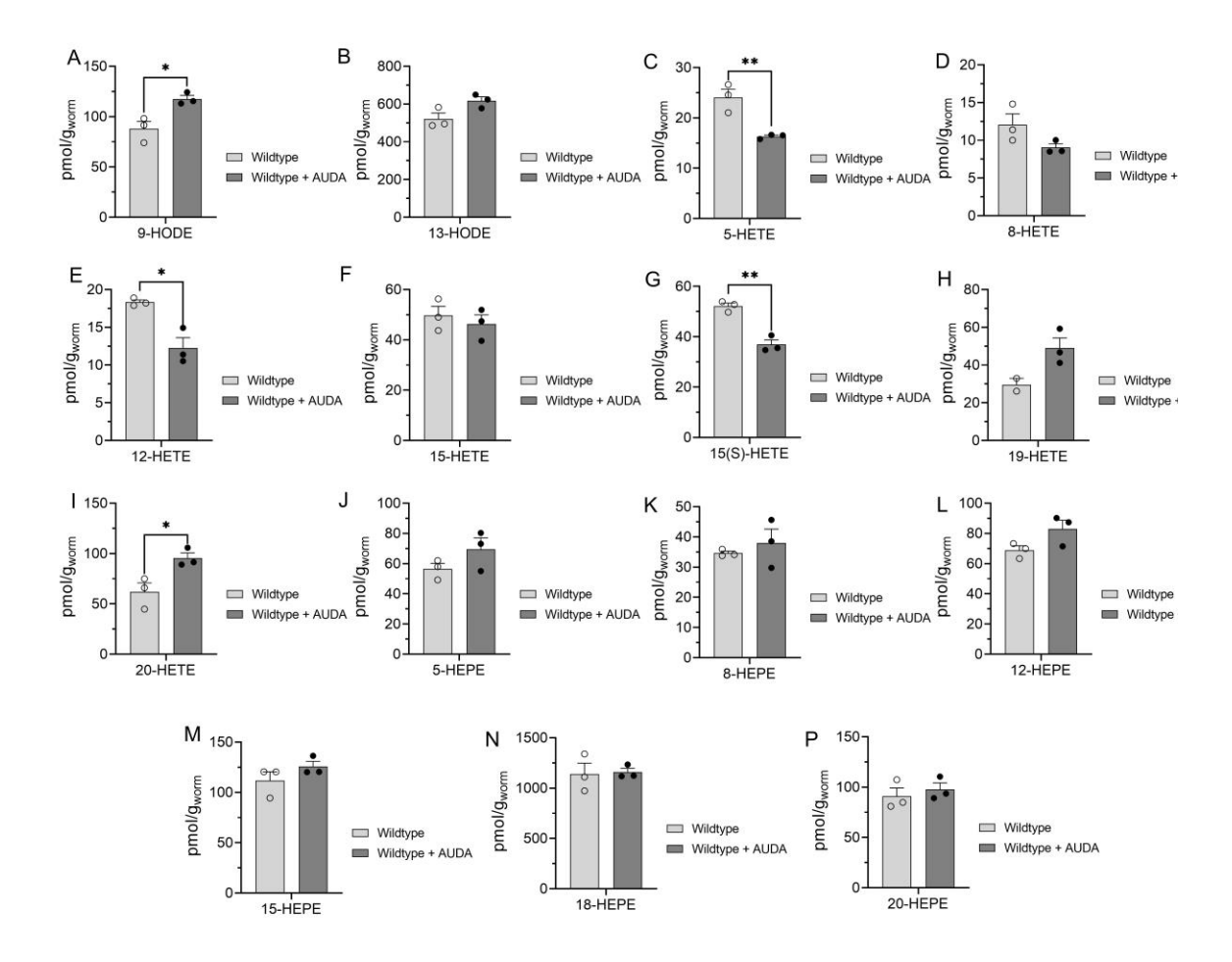


**Figure S12.** AUDA effect on hydroxy-PUFA in wildtype *C. elegans* (A1 and B) linoleic acid hydroxy metabolites. (C-I) Arachidonic acid hydroxy metabolites. (J-P) eicosapentaenoic acid hydroxy metabolites. In all experiments worms were grown at 16 degrees until L4, then transferred to plates with or without AUDA (100  $\mu$ M) and kept at 25°C. Age-synchronized worms were collected at day 3 for oxylipin analysis. Statistical analysis is based on unpaired t-test, where \*P  $\leq$  0.05, \*\*P  $\leq$  0.01, \*\*\*P  $\leq$  0.001, \*\*\*P < 0.0001, non-significant is not shown. The results after applying multiple correction using the Benjamini-Hochberg procedure to control the false discovery rate (FDR 5%) were used for volcano plot in chapter 3, Figure 4J.

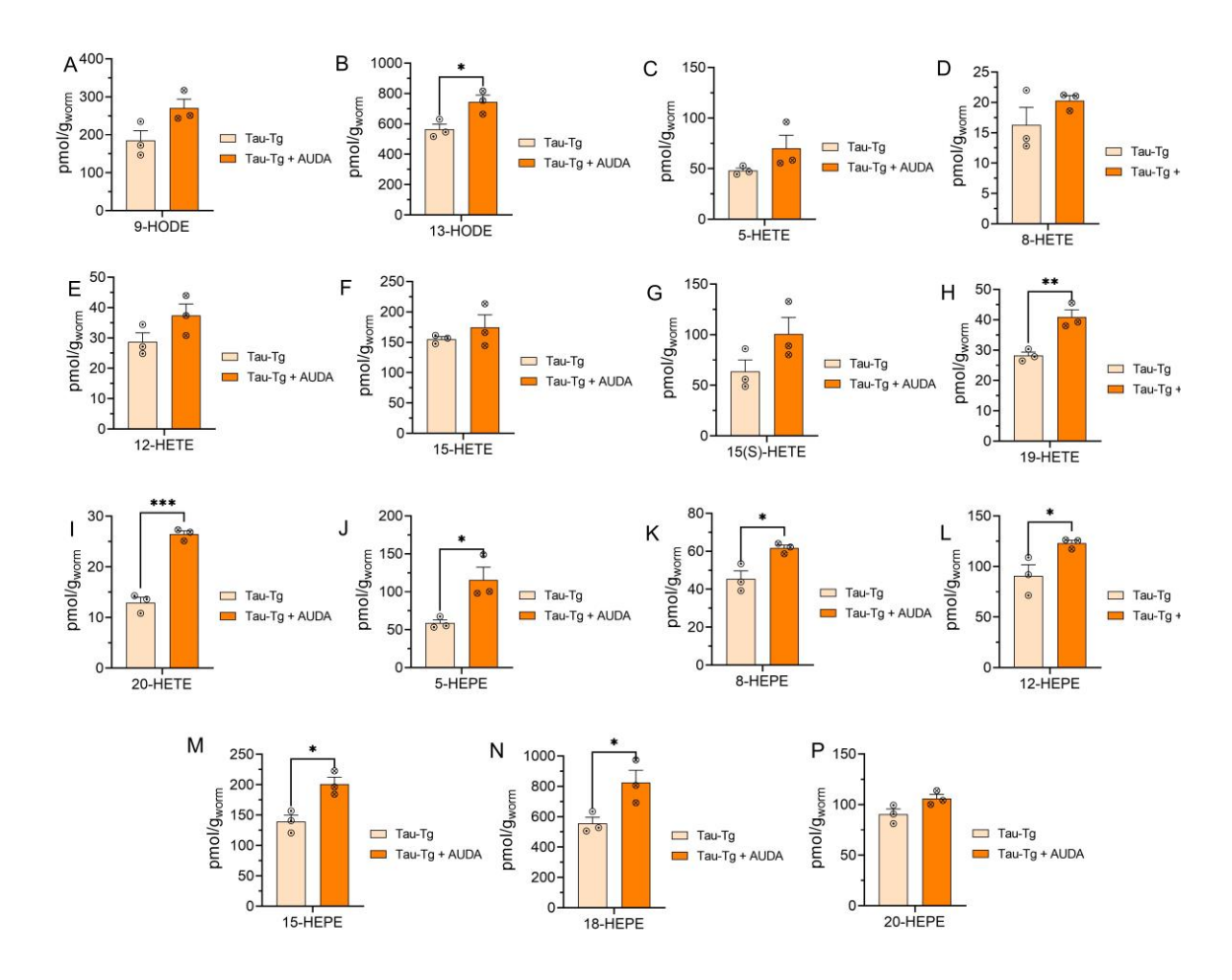


**Figure S13.** AUDA effect on hydroxy-PUFA in Tau-Tg strain (A1 and B) linoleic acid hydroxy metabolites. (C-I) Arachidonic acid hydroxy metabolites. (J-P) eicosapentaenoic acid hydroxy metabolites. In all experiments worms were grown at 16 degrees until L4, then transferred to plates with or without AUDA (100  $\mu$ M) and kept at 25°C. Age-synchronized worms were collected at day 3 for oxylipin analysis. Statistical analysis is based on unpaired t-test, where \*P  $\leq$  0.05, \*\*P  $\leq$  0.01, \*\*\*P  $\leq$  0.001, \*\*\*\*P < 0.0001, non-significant is not shown. The results after applying multiple correction using the Benjamini-Hochberg procedure to control the false discovery rate (FDR 5%) were used for volcano plot in chapter 3, Figure 4K.

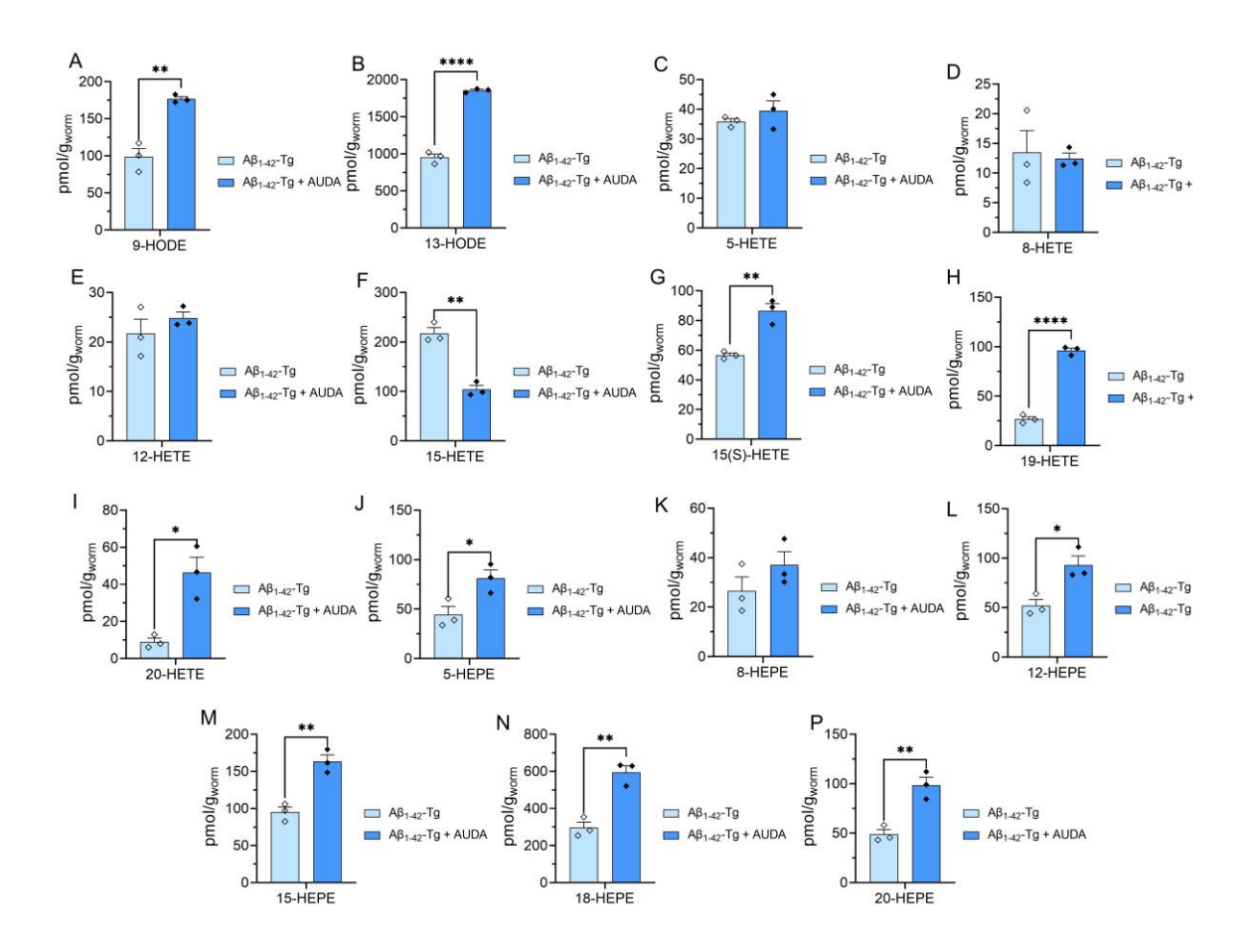


**Figure S14.** AUDA effect on hydroxy-PUFA in A $β_{1-42}$ -Tg strain (A1 and B) linoleic acid hydroxy metabolites. (C-I) Arachidonic acid hydroxy metabolites. (J-P) eicosapentaenoic acid hydroxy metabolites. In all experiments worms were grown at 16 degrees until L4, then transferred to plates with or without AUDA (100 μM) and kept at 25°C. Age-synchronized worms were collected at day 3 for oxylipin analysis. Statistical analysis is based on unpaired t-test, where \*P ≤ 0.05, \*\*P ≤ 0.01, \*\*\*P ≤ 0.001, \*\*\*P < 0.0001, non-significant is not shown. The results after applying multiple correction using the Benjamini-Hochberg procedure to control the false discovery rate (FDR 5%) were used for volcano plot in chapter 3, Figure 4L.

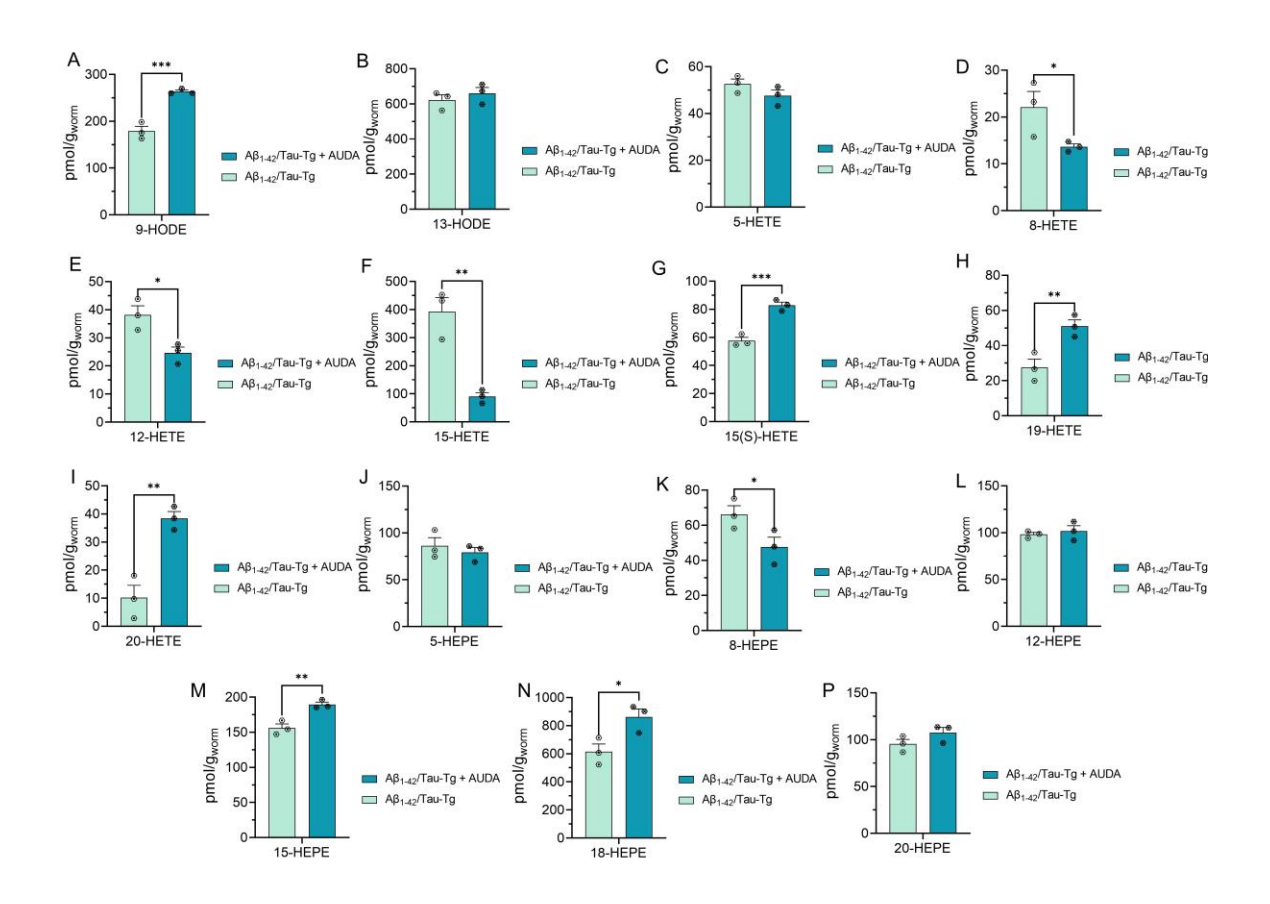
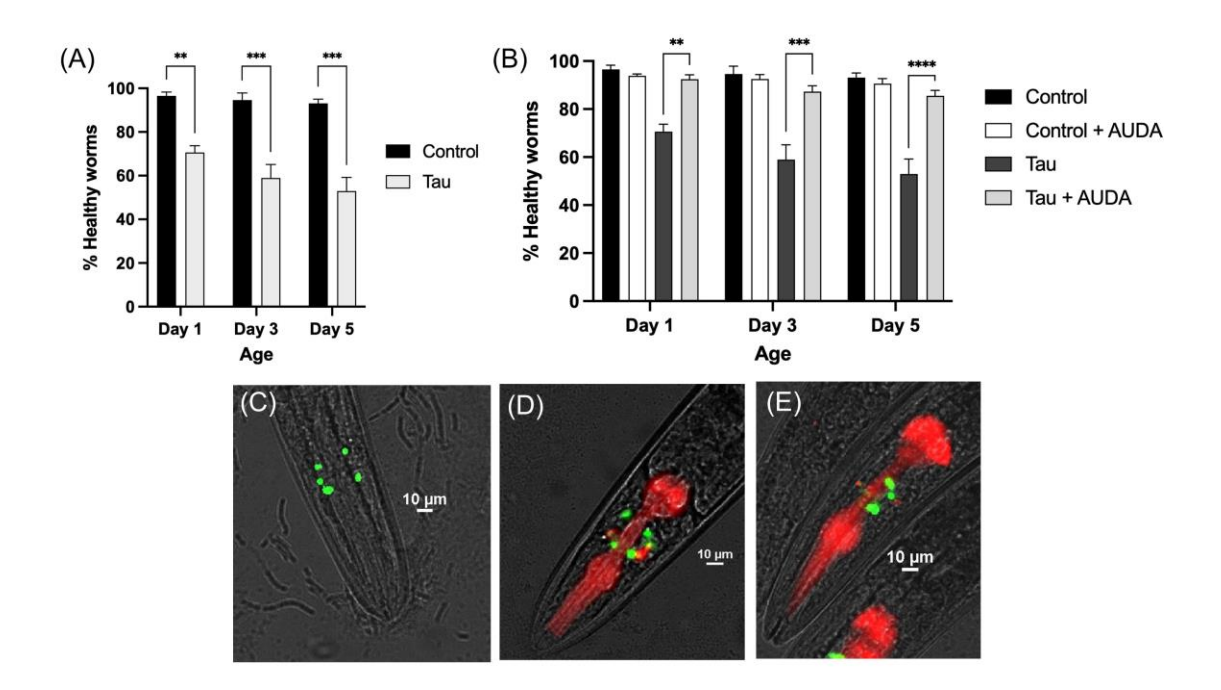


Figure S15. AUDA effect on hydroxy-PUFA in A $β_{1-42}$ /Tau-Tg strain (A1 and B) linoleic acid hydroxy metabolites. (C-I) Arachidonic acid hydroxy metabolites. (J-P) eicosapentaenoic acid hydroxy metabolites. In all experiments worms were grown at 16 degrees until L4, then transferred to plates with or without AUDA (100 μM) and kept at 25°C. Age-synchronized worms were collected at day 3 for oxylipin analysis. Statistical analysis is based on unpaired t-test, where \*P ≤ 0.05, \*\*P ≤ 0.01, \*\*\*P ≤ 0.001, \*\*\*P < 0.0001, non-significant is not shown. The results after applying multiple correction using the Benjamini-Hochberg procedure to control the false discovery rate (FDR 5%) were used for volcano plot in chapter 3, Figure 4M.



**Figure S16.** AUDA rescues neurodegeneration induced by tau expression in glutamatergic neurons. (A) Quantified glutamatergic neural health in *eat-4::GFP* (Control) and *eat-4::GFP*; *aex-3:tau* (Tau-Tg). (B) Quantified glutamatergic neural health in *eat-4::GFP* (Control) and *eat-4::GFP*; *aex-3:tau* (Tau-Tg) in presence and absence of AUDA. (C) fluorescence image of *eat-4::GFP*, (D) fluorescence image of *eat-4::GFP* in worm expressing tau. (E) fluorescence image of *eat-4::GFP* in worm expressing tau in presence of AUDA. Three trials of 20 worms each were performed for each strain at each time point. The % healthy worms for each time point is the average of the triplicate. Error bars are standard error (SEM). Two-way analysis of variance (ANOVA) and Tukey's multiple comparison test was used to analyze the statistical significance of this results. (\*P< 0.05, \*\*P< 0.01, \*\*\*P< 0.001, \*\*\*\*P< 0.001, \*\*\*\*P< 0.0001).

# 2. Materials and strains:

# 2.1. Reagent and resource:

 $\label{eq:Table S1} \textbf{Table S1}. \ \textbf{Reagents and resources used in this study}.$ 

REAGENT or RESOURCE	SOURCE	IDENTIFIER
Cholesterol	Alfa Aesar	Cat#A11470; CAS: 57-88-5
Agar	Fisher Bioreagents	Cat#BP9744-500; CAS: 9002- 18-0
Bacto Agar	Becton, Dickinson, and Company	Cat# DIFCO 214010
Tryptone	Fisher Bioreagents	Cat#BP1421-500; CAS: 91079-40-2
Bacto Tryptone	Life Technologies Corporation	Cat# DIFCO 211705
Yeast Extract	Becton, Dickinson, and Company	Cat# DIFCO 212750
Sodium Chloride	VWR	Cat#BDH9286
Magnesium Sulfate heptahydrate	Fisher Chemical	Cat#M63-500; CAS: 10034-99-8
Potassium Phosphate, monobasic, crystal	Fisher Bioreagents	Cat#BP362-500; CAS: 7778-77-0
Potassium Phosphate, dibasic, powder	Fisher Chemical	Cat#P288-500; CAS: 7758-11-4
Calcium Chloride (anhydrous)	Sigma-Aldrich	Cat#C1016-500; CAS: 10043- 52-4
Sodium Azide	Fisher Scientific	Cat#BP9221-500; CAS: 26628- 22-8
Ethanol	Fisher Chemical	Cat#A409-4; CAS: 64-17-4
Hexane	Fisher Chemical	Lot#176581; CAS: 110-54-3
Acetic Acid	Fisher Scientific	Lot#193296; CAS: 64-19-7
Acetonitrile	Fisher Chemical	Lot#195771; CAS: 75-05-8
Chloroform	Acros Organic	Lot# B0541409A; CAS: 67-66-3
Methanol	Fisher Chemical	Lot#195771; CAS: 67-56-1
Acetone	Fisher Chemical	CAS: 67-64-1

# 2.2.Deuterated standards used for oxylipin analysis.

Table S2. Deuterated standards used in this study.

Oxylipin standard name	Oxylipin standard abbreviation
6-keto prostaglandin $F_{1\alpha}$ -d4	6-keto-PGF <sub>1α</sub> -d4
5(S)-hydroxyeicosatetrenoic-d8 acid	5(S)-HETE-d8
8,9-epoxyeicosatrienoic-d11 acid	8,9-EET-d11
Arachidonic-d8 acid	AA-d8
15(S)-hydroxyeicosatetraenoic-d8 acid	15(S)-HETE-d8
Prostaglandin B <sub>2</sub> -d4	PGB2-d4
8,9-dihydroxyeicosatrienoic-d11 acid	8,9-DiHETrE-d11
9(S)-hydroxyoctadecadienoic-d4 acid	9(S)-HODE-d4
Leukotriene B <sub>4</sub> -d4	LTB4-d4
Prostaglandin E <sub>2</sub> -d9	PGE2-d9

## 2.3.Organisms/Strains

**Table S3**. *C. elegans* strains used in this study.

STRAIN	SOURCE	STRAIN NAME
N2 Bristol	Caenorhabditis Genetics Center	N2
CK1441 (Paex-3::Tau WT (4R1N); Pmyo-2::dsRED)	Caenorhabditis Genetics Center	CK1441
CL2355 ( <i>smg-1ts</i> ( <i>snb-1</i> /Aβ1–42/long 3'-UTR; Pmlt-2::GFP)	David Gems (Jennifer watts)	CL2355
CK1609 [(Paex-3::Tau WT (4R1N); Pmyo-2::dsRED); (smg-1ts (snb-1/Aβ1–42/long 3'-UTR; Pmlt-2::GFP)]	Caenorhabditis Genetics Center	CK1609
OH11152 (eat-4::GFP; ttx-3::DsRed)	Caenorhabditis Genetics Center	OH11152
JKA71 [(eat-4::GFP; ttx-3::DsRed); (Paex-3::Tau WT (4R1N); Pmyo-2::dsRED)]	Generated in the lab of Jamie Alan	JKA71

### 2.4. Software and Algorithms

**Table S4**. Software and Algorithms used in this study.

Microsoft Excel	Microsoft Corporation	N/A
ImageJ	Rasband, W.S.	https://imagej.nih.gov/ij/
BioRender	BioRender	https://biorender.com/
GraphPad Prism 9	GraphPad Software, Inc.	https://www.graphpad.com/
MetaboAnalyst	Open source	https://www.metaboanalyst.ca/
NIS Element	Nikon	Nikon

### 3. Experimental procedure

#### 3.1. Worm maintenance

Worms were maintained at  $16^{\circ}$ C until they reached the L4 stage, at which they were transferred to  $25^{\circ}$ C to induce the appropriate expression of human amyloid-beta (A $\beta$ ) and/or tau. This approach enabled us to maintain worms under conditions with lower A $\beta$  and/or tau expression during development, and to increase A $\beta$  and/or tau accumulation upon reaching the L4 stage, where the nervous system is fully developed. We employed this method to more closely mimic the temporal changes associated with Alzheimer's disease (AD), which is believed to manifest in adulthood within a developed nervous system. A similar procedure was utilized for the control (wildtype) worms.

#### 3.2.Age-synchronized worm:

The age-synchronized population was prepared by transferring specific numbers of healthy and well-fed Day 1 adult worms to a fresh nematode growth media (NGM) with OP50, *E. coli* OP50 (2.8 ×10<sup>8</sup> cell/ml), as described in previously published protocol<sup>1,2</sup>. The adult worms were allowed to lay eggs for 6-10 hours (at 16°C.) The laid eggs were isolated either by filtration or directly taking out adult worms depending on the number worms<sup>2</sup>. Eggs are then allowed to hatch

at 16°C. About 36-48 hours later, plates were washed off with s-basal solution and transferred to a 40 µm cell strainer placed on top of a 50 mL centrifuge tube. The large sized L4 larvae were retained on the filter, whereas eggs, larva, bacteria were passed through the filter. L4 larvae were then transferred to a 1.7 ml centrifuge tube using a glass pipet and spun at 325 x g on a table-top centrifuge for 30 s. The s-basal solution was removed by aspiration leaving behind a pellet of L4. Finally, L4 worms were resuspend in s-basal solution and transferred to the supplemented or control plates seeded with OP50, then kept at 25°C. During experiment, the age synchronized population was filtered on daily basis, through a 40 µm cell strainer placed on top of a 50 mL centrifuge tube in order to remove progeny. The age-synchronized adult worms were then collected and transferred to a freshly seeded NGM/supplemented plate.

### **3.3.**Epoxide Hydrolase inhibitor supplementation:

To supplement with 12-(3-((3s,5s,7s)-adamantan-1-yl) ureido) dodecanoic acid (AUDA), a 20 mM solution of AUDA in ethanol was made and added to 1 Liter NGM agar solution at 55-65 °C to reach a final concentration of 100  $\mu$ M for preparing the treatment plates for the experiments. The plates were left at room temperature for one day, then seeded with 250-400  $\mu$ l of *E. coli* OP50 (2.8 ×108 cell/ml).

#### 3.4.5-HT SENSITIVITY ASSAY.

Synchronized transgenic and the control worms that were grown according to above protocol were collected at days 3 and day 5 adulthood. We then assessed serotonin hypersensitivity by placing 20-30 age-synchronized worms in 1 mM serotonin solution dissolved in s-basal and scoring worms that remained mobile after 10 minutes exposure <sup>3</sup>.

#### 3.5. Thrashing Assay:

Age-synchronized transgenic strain and the control worm that grown according to the protocol mentioned above. For thrashing assays, 20 age synchronized worms of a at day 3 and day 5 adulthood were transferred by a worm pick to the s-basal solution on a NGM agar plate at room temperature. The worms were allotted 30 seconds to adapt to the new environment. Then, the worm's movement "thrashing" was recorded using a camera for 30 seconds. Finally, the number of "thrashes" were counted (each thrash is when the worms head and body moved from their starting position to the other side of a vertical axis and back to the starting position)<sup>4</sup>.

#### 3.6. Radian locomotion:

Synchronized transgenic strain and the control worm that grown according to the protocol mentioned above. To do radian locomotion assay, 30-50 age synchronized worms at day 3 and day 5 adulthood were transferred to the center of a NGM plate that covered with a thin layer of OP50. Worm were allowed for 30 minutes to move, then the distance each worm traveled from the center of plate during 30 mins was measured using a microscope image of plate at the end of experiment and ImageJ software to measure the position of worm compare to the center of plat. Finally, the radian locomotion was calculated for each worm as  $R = \frac{Distance\ of\ worm\ from\ center(um)}{time\ (sec.)}$ .

### 3.7. Cold tolerance:

Age-synchronized worms, at day 5 adulthood that grown at 25 degrees were transferred to a 4°C fridge, to cause a cold shock. The worms were left at 4°C for 48 hours, and then removed from the refrigerator and allotted approximately 2-4 hour to equilibrate to room temperature. The worms were then assayed for viability by gently tapping each worm with a pick and observing movement or lack thereof<sup>5,6</sup>.

#### 3.8. Oxylipin Analysis:

To examine the oxylipin profile across various *C. elegans* strains, approximately 5-10 mg of synchronized day 3 adult worms which are equivalent to approximately 5000 to 10000 worms gathered per trial, ensuring that adequate oxylipin concentrations were present in the whole worm lysates<sup>2</sup>. To generate a sufficient population, a minimum of seven P100 plates, each 100 mm in diameter, were used per trial. Approximately 2000-3000 worms were prepared for each 5 mg whole worm lysate sample (300-400 worms per plate). The age-synchronized worm populations were established and maintained using the previously mentioned filtration method.

Once the worm populations were ready for collection, they were transferred from the seven plates per trial and filtered using s-basal solution and a 40 µm pore size cell strainer. The worms that accumulated on the cell strainer's surface were moved to an Eppendorf vial using a Pasteur pipet to prevent the worms from sticking inside pipet wall. The worms were then rinsed with s-basal medium, centrifuged, and the supernatant was discarded. The worms underwent four additional washes with s-basal medium to remove bacteria and PUFA supplements.

After removal of bacteria and supplements, the worm samples in the Eppendorf vials were centrifuged at 10,000 rpm and 4°C for 10 minutes. Supernatant was removed using pipets of 100 μL and 10 mL. A 20 mL pipet featuring a long tip was employed to extract liquid from between the worms. Finally, standard filter paper was cut and placed into the Eppendorf vials to eliminate any remaining liquid in the worm samples. The worm samples were then flash-frozen with liquid nitrogen and stored at -80°C. Upon removal from -80°C storage, the weight of a 2 mL cryogenic homogenizer vial per trial was recorded. Worm samples were flash-frozen with liquid nitrogen, loosened using a 0.7 mm needle, and transferred to the homogenizer vial, the weight of which was recorded. The weight of each vial containing worms determined the amount of worms used in each

trial. Three homogenization beads were added to every homogenizer vial, along with 100  $\mu$ L phosphate-buffered saline (PBS), 10  $\mu$ L internal standard (deuterated oxylipins), and 10  $\mu$ L antioxidants, including ethylenediamine tetraacetic acid (EDTA), butylated hydroxytoluene (BHT), and triphenylphosphine (TPP). Table S4 provides further details on deuterated oxylipin standards.

Each homogenizer vial containing worm samples was flash-frozen with liquid nitrogen and then homogenized for five 30-second cycles at 5 M/s using an Omni bead ruptor 24 homogenizer. An additional 900 μL of PBS was added to the homogenized samples, which were then centrifuged at 10,000 rpm for 5 minutes. Supernatant was collected and transferred to a new Eppendorf vial for solid-phase extraction (SPE). SPE, using Waters Oasis-HLB cartridges, isolated oxylipins from whole worm lysates. A polar stationary phase trapped highly polar biological materials like sugars, while the targeted oxylipins were considerably less polar. SPE column preparation involved sequential washing with 2 mL ethyl acetate, 2 mL methanol (twice), and 2 mL of a 95:5 (v/v) water and methanol mixture containing 0.1% acetic acid, ensuring the column remained moist.

Once the SPE column was prepared, the Eppendorf vials containing the homogenized samples were loaded onto the SPE column. After the sample was loaded onto the column by gravity, 1.5 mL of washing solution (95:5 v/v mixture of water and ethanol with 0.1% acetic acid) was added to the column. The column was then dried by gravity. Next, the column was thoroughly dried using a vacuum pump for 20 minutes. Upon completion of drying, the column was ready for elution.

During the elution step, 0.5 mL of methanol was added to the column. The eluted compounds were collected in an Eppendorf vial containing 6  $\mu$ L of 30% glycerol in methanol, acting as a trap solution. The column was allowed to gravity elute until it appeared dry. A 5 mL syringe filled with air was placed at the top of the SPE column to gently push out any remaining

solvent with air. Once the column was completely dry, 1 mL of ethyl acetate was added to the column. The solvent was allowed to gravity elute until the column appeared dry to the eye. The remaining solvent was again removed using a 5 mL syringe and gently pushing air through the column.

After completing SPE, the final extracted sample was dried using a speed-vac until only the trap solution remained. The residues were reconstituted with 100  $\mu$ L of 75% ethanol/water containing 10 nM of internal standard, 12-[(cyclohexylcarbamoyl)amino]dodecanoic acid (CUDA). The samples were then mixed on a vortex for five minutes and filtered with a 0.45  $\mu$ m filter. Finally, the samples were transferred to auto-sampler vials with salinized inserts, purged with argon gas, and stored at -80°C until injection.

The liquid chromatography (LC) conditions were optimized to separate all eicosanoids of interest with the desired peak shape and signal intensity using an XBridge BEH C18 2.1x150mm HPLC column. Mobile phase A consisted of 0.1% acetic acid in water, while mobile phase B comprised acetonitrile: methanol (84:16) with 0.1% glacial acetic acid. Gradient elution was performed at a flow rate of 250 μL/min, and chromatography was optimized to separate all analytes in 20 minutes. The autosampler, Waters ACQUITY FTN, was maintained at 10°C. The column was connected to a TQXS tandem mass spectrometer (Waters) equipped with Waters Acquity SDS pump and Waters Acquity CM detector. Electrospray was used as the ionization source for negative multiple reaction monitoring (MRM) mode. To achieve the best selectivity and sensitivity, each analyte standard was infused into the mass spectrometer, and multiple reaction monitoring was employed to analyze the desired compound.

### 3.9. Fluorescence microscopy imaging for tracking glutamatergic neurons:

To investigate the effect of tau on glutamatergic neurons, a eat-4::GFP; ttx-3::DsRed (expresses GFP in five glutamatergic neurons) was crossed with tau transgenic worms, (CK1441). Worms were grown at 16 °C until L4, then placed on new OP50 plate with or without AUDA supplementation, and transferred to 25 °C. At day 1, day 3, and day 5 adulthood, the GFP-tagged glutamatergic neurons were tracked using Nikon Ti-2 inverted microscope. To do so, Sufficient sodium azide was added to generate a 2 mM NaN3 solution mixed in the 1% agarose solution. Approximately 200 μL agarose/sodium azide solution was placed on a microcopy slide. Another slide was placed on top of agarose/sodium azide droplet to generate a smooth pad that the worms can be placed. Once the agar pad is sufficiently dry, the second slide was removed. Then, 10 μL of 5 mM sodium azide was placed on top of the pad, and approximately 20 worms were placed into the droplet of sodium azide, which functioned to paralyze the worms for imaging. The worms were observed until all were fully paralyzed. Lastly, a microscopy slide cover was placed on top of the paralyzed worms. The microcopy slide containing the paralyzed worms was then placed under a Nikon Ti-2 inverted microscope for analysis of neuronal GFP in the paralyzed worms.

#### 3.10. Statistical Analysis:

Statistical analysis was performed using GraphPad Prism version 9.00 for Windows (GraphPad Software; <a href="www.graphpad.com">www.graphpad.com</a>). For phenotypic assays, One-way analysis of variance (ANOVA) with Tukey's multiple tests is used. For oxylipin analysis, an initial evaluation was conducted using the student's unpaired t-test to identify changes in each oxylipin compared to their counterparts (these data are provided in the supporting information figures). Subsequently, a multiple unpaired t-test with corrections using the Benjamini and Hochberg method at a false discovery rate (FDR) of 0.05 was employed to determine the most significant changes while

accounting for multiple comparison errors. The results of this analysis are presented in the main manuscript and serve as the primary statistical method for comparing differences between groups. We also use MetaboAnalyst 5.0 (<a href="https://www.metaboanalyst.ca/">https://www.metaboanalyst.ca/</a>) to normalize oxylipin data and obtain the heatmap and correlation coefficient.

#### **BIBLIOGRAPHY**

- (1) Vladis, N. A.; Fischer, K. E.; Digalaki, E.; Marcu, D.-C.; Bimpos, M. N.; Greer, P.; Ayres, A.; Li, Q.; Busch, K. E. Gap Junctions in the C. Elegans Nervous System Regulate Ageing and Lifespan. *bioRxiv*, **2019**, 657817. https://doi.org/10.1101/657817.
- (2) Sarparast, M.; Pourmand, E.; Hinman, J.; Vonarx, D.; Reason, T.; Zhang, F.; Paithankar, S.; Chen, B.; Borhan, B.; Watts, J. L.; Alan, J.; Lee, K. S. S. Dihydroxy-Metabolites of Dihomo-γ-Linolenic Acid Drive Ferroptosis-Mediated Neurodegeneration. *ACS Cent. Sci.* **2023**. https://doi.org/10.1021/acscentsci.3c00052.
- (3) Law, W.; Wuescher, L. M.; Ortega, A.; Hapiak, V. M.; Komuniecki, P. R.; Komuniecki, R. Heterologous Expression in Remodeled C. Elegans: A Platform for Monoaminergic Agonist Identification and Anthelmintic Screening. *PLoS Pathog.* **2015**, *11* (4), e1004794. https://doi.org/10.1371/journal.ppat.1004794.
- (4) Gallrein, C.; Iburg, M.; Michelberger, T.; Koçak, A.; Puchkov, D.; Liu, F.; Ayala Mariscal, S. M.; Nayak, T.; Kaminski Schierle, G. S.; Kirstein, J. Novel Amyloid-Beta Pathology C. Elegans Model Reveals Distinct Neurons as Seeds of Pathogenicity. *Prog. Neurobiol.* **2021**, *198* (101907), 101907. https://doi.org/10.1016/j.pneurobio.2020.101907.
- (5) Ohta, A.; Ujisawa, T.; Sonoda, S.; Kuhara, A. Light and Pheromone-Sensing Neurons Regulates Cold Habituation through Insulin Signalling in Caenorhabditis Elegans. *Nat. Commun.* **2014**, *5* (1), 4412. https://doi.org/10.1038/ncomms5412.
- (6) Liachko, N. *Cold-tolerance is a fast and easy method to identify neuronal dysfunction in C. elegans*. The WBG. http://wbg.wormbook.org/2016/07/05/cold-tolerance-is-a-fast-and-easy-method-to-identify-neuronal-dysfunction-in-c-elegans/ (accessed 2023-03-22).

# **APPENDIX 3: SUPPORTING INFORMATION FOR CHAPTER 4**

### TABLE OF CONTENTS

1.Materials and strains:	317
2.Experimental procedure	319
BIBLIOGRAPHY	319

# 1. Materials and strains:

# 1.1. Reagent and resource:

 $\label{eq:Table S1} \textbf{Table S1}. \ \textbf{Reagents and resources used in this study}.$ 

REAGENT or RESOURCE	SOURCE	IDENTIFIER
Cholesterol	Alfa Aesar	Cat#A11470; CAS: 57-88-5
Agar	Fisher Bioreagents	Cat#BP9744-500; CAS: 9002- 18-0
Bacto Agar	Becton, Dickinson, and Company	Cat# DIFCO 214010
Tryptone	Fisher Bioreagents	Cat#BP1421-500; CAS: 91079-40-2
Bacto Tryptone	Life Technologies Corporation	Cat# DIFCO 211705
Yeast Extract	Becton, Dickinson, and Company	Cat# DIFCO 212750
Sodium Chloride	VWR	Cat#BDH9286
Magnesium Sulfate heptahydrate	Fisher Chemical	Cat#M63-500; CAS: 10034-99-8
Potassium Phosphate, monobasic, crystal	Fisher Bioreagents	Cat#BP362-500; CAS: 7778-77-0
Potassium Phosphate, dibasic, powder	Fisher Chemical	Cat#P288-500; CAS: 7758-11-4
Calcium Chloride (anhydrous)	Sigma-Aldrich	Cat#C1016-500; CAS: 10043-52-4
Sodium Azide	Fisher Scientific	Cat#BP9221-500; CAS: 26628- 22-8
Ethanol	Fisher Chemical	Cat#A409-4; CAS: 64-17-4
Hexane	Fisher Chemical	Lot#176581; CAS: 110-54-3
Acetic Acid	Fisher Scientific	Lot#193296; CAS: 64-19-7
Acetonitrile	Fisher Chemical	Lot#195771; CAS: 75-05-8
Chloroform	Acros Organic	Lot# B0541409A; CAS: 67-66-3
Methanol	Fisher Chemical	Lot#195771; CAS: 67-56-1
Acetone	Fisher Chemical	CAS: 67-64-1

# 1.2. Deuterated standards used for oxylipin analysis.

 $\label{eq:Table S2} \textbf{Table S2}. \ \ \textbf{Deuterated standards used in this study}.$ 

Oxylipin standard name	Oxylipin standard abbreviation
6-keto prostaglandin F <sub>1α</sub> -d4	6-keto-PGF <sub>1α</sub> -d4
5(S)-hydroxyeicosatetrenoic-d8 acid	5(S)-HETE-d8
8,9-epoxyeicosatrienoic-d11 acid	8,9-EET-d11
Arachidonic-d8 acid	AA-d8
15(S)-hydroxyeicosatetraenoic-d8 acid	15(S)-HETE-d8
Prostaglandin B <sub>2</sub> -d4	PGB2-d4
8,9-dihydroxyeicosatrienoic-d11 acid	8,9-DiHETrE-d11
9(S)-hydroxyoctadecadienoic-d4 acid	9(S)-HODE-d4
Leukotriene B <sub>4</sub> -d4	LTB4-d4
Prostaglandin E <sub>2</sub> -d9	PGE2-d9

## 1.3. Organisms/Strains

**Table S3**. *C. elegans* strains used in this study.

STRAIN	SOURCE	STRAIN NAME
N2 Bristol	Caenorhabditis Genetics Center	N2
ceeh-1(ok3153)	Caenorhabditis Genetics Center	ok3153
ceeh-2 (tm3635)	National BioResource Project, Japan	tm3635
ceeh-1(vv228)	Gifted from Dr. Pretrascheck's group at the Scripps Research Institute	vv228
ceeh-2(vv226)	Gifted from Dr. Pretrascheck's group at the Scripps Research Institute	vv226
ceeh-2/ceeh-1(vv231)	Gifted from Dr. Pretrascheck's group at the Scripps Research Institute	vv231

#### 1.4. Software and Algorithms

**Table S4**. Software and Algorithms used in this study.

Microsoft Excel	Microsoft Corporation	N/A
ImageJ	Rasband, W.S.	https://imagej.nih.gov/ij/
BioRender	BioRender	https://biorender.com/
GraphPad Prism 9	GraphPad Software, Inc.	https://www.graphpad.com/
NIS Element	Nikon	Nikon

### 2. Experimental procedure

#### 2.1. Worm maintenance

All nematode stocks were maintained on nematode growth media (NGM) plates seeded with bacteria (E. coli OP50) with 2.8 ×108 cell/ml and maintained at 20°C unless otherwise noted.

#### 2.2. Age-synchronized worm

To obtain an age-synchronized population, a specific number of healthy and well-fed Day 1 adult worms (determined by the experiment and the desired progeny count) were transferred to fresh nematode growth media (NGM) with OP50, as outlined in the previously published protocol <sup>1</sup>. The adult worms were allowed to lay eggs for a period of 6-10 hours. The deposited eggs were then separated and allowed to hatch. Approximately 36-48 hours later, the plates were rinsed with s-basal solution, and the contents were transferred to a 40 µm cell strainer placed atop a 50 mL centrifuge tube. The larger L4 larvae remained on the filter, while eggs, other larval stages, bacteria, and potential contaminants passed through. The L4 larvae were washed with 75-100 µl of s-basal and moved to a 1.7 ml centrifuge tube using a glass pipette, followed by a 30-second spin at 325 x g in a tabletop centrifuge. The s-basal was carefully aspirated, leaving a pellet of L4 larvae. Lastly, the L4 worms were resuspended in s-basal solution and transferred to either supplemented or control plates containing OP50.

#### 2.3. C. elegans longevity assessment:

The longevity assays are conducted by placing 100 L4 *C. elegans* (obtained during egg production following the previously mentioned procedure) on fresh NGM plates inoculated with OP50. These specimens are then relocated daily or every two days to a new NGM + OP50 plate, while keeping track of living (transferred), deceased, and censored (wounded or killed during transfer, misplaced/buried in agar, or desiccated on the plate wall) worms. This process is carried out until the entire sample population has perished. Older worms generally exhibit reduced mobility; therefore, a gentle prod on the worm's anterior end may be employed if necessary to verify their vitality. This assay is conducted in triplicate.

#### 2.4. Supplementing plates with drugs (AUDA and FUDR)

For supplementation with 12-(3-((3s,5s,7s)-adamantan-1-yl) ureido) dodecanoic acid (AUDA), a 20 mM AUDA solution was prepared in ethanol and incorporated into 1 Liter of NGM agar solution, maintaining a temperature of 55-65 °C, until achieving a final concentration of 100 μM before plating<sup>2</sup>. The plates were allowed to sit at room temperature for a day and then inoculated with 250-400 μl of E. coli OP50 (2.8 ×108 cells/ml). Similar procedure was followed for making 5-fluoro-2-deoxyuridine FUDR supplementation, where a final concentration of 50 μM was made in 1 Liter of NGM agar solution and followed by making plate and seeding them with similar amount of OP50.

### 2.5. Oxylipin Analysis:

The detailed experimental method for oxylipin analysis, including specific techniques, equipment, and reagents used, can be found in Chapter 2, Appendix 1. Briefly, Oxylipins, were investigated in *C. elegans* using whole worm lysates. The D1 adulthood of different strains were generated and maintained as previously described. Worms were collected, filtered, rinsed, and

centrifuged to create worm samples, which were then flash frozen and stored at -80°C. To analyze the oxylipins, the samples were prepared, homogenized, and subjected to solid phase extraction (SPE) using a polar stationary phase. After the elution step, the extracted samples were dried, reconstituted, filtered, and transferred to auto-sampler vials for storage. The LC conditions were optimized for peak shape and signal intensity, and the samples were analyzed using a TQXS tandem mass spectrometer.

### 2.6. Egg production assessment.

The egg-laying capacity assay is conducted by placing a single L4 worm on a fresh NGM plate inoculated with OP50. After 24 hours, the worm is relocated to a new NGM + OP50 plate (with or without supplementation) and the eggs/larvae generated by the worm are enumerated. This process is carried out daily until the worm ceases to produce progeny, usually around adult day 5 or 6. This experiment is performed with a minimum of three replicates.

#### **BIBLIOGRAPHY**

- (1) Vladis, N. A.; Fischer, K. E.; Digalaki, E.; Marcu, D.-C.; Bimpos, M. N.; Greer, P.; Ayres, A.; Li, Q.; Busch, K. E. Gap Junctions in the C. Elegans Nervous System Regulate Ageing and Lifespan. *bioRxiv*, **2019**, 657817. https://doi.org/10.1101/657817.
- (2) Sarparast, M.; Pourmand, E.; Hinman, J.; Vonarx, D.; Reason, T.; Zhang, F.; Paithankar, S.; Chen, B.; Borhan, B.; Watts, J. L.; Alan, J.; Lee, K. S. S. Dihydroxy-Metabolites of Dihomo-γ-Linolenic Acid Drive Ferroptosis-Mediated Neurodegeneration. *ACS Cent. Sci.* **2023**. https://doi.org/10.1021/acscentsci.3c00052.